frontiers | Research Topics

Molecular diagnostics for infectious diseases: Novel approaches, clinical applications and future challenges

Edited by
Xiaogang Xu, Chao Zhuo, Bing Gu and Kamal El Bissati

Published in
Frontiers in Microbiology

ISSN 1664-8714
ISBN 978-2-83251-949-3
DOI 10.3389/978-2-83251-949-3

About Frontiers

Frontiers is more than just an open access publisher of scholarly articles: it is a pioneering approach to the world of academia, radically improving the way scholarly research is managed. The grand vision of Frontiers is a world where all people have an equal opportunity to seek, share and generate knowledge. Frontiers provides immediate and permanent online open access to all its publications, but this alone is not enough to realize our grand goals.

Frontiers journal series

The Frontiers journal series is a multi-tier and interdisciplinary set of open-access, online journals, promising a paradigm shift from the current review, selection and dissemination processes in academic publishing. All Frontiers journals are driven by researchers for researchers; therefore, they constitute a service to the scholarly community. At the same time, the *Frontiers journal series* operates on a revolutionary invention, the tiered publishing system, initially addressing specific communities of scholars, and gradually climbing up to broader public understanding, thus serving the interests of the lay society, too.

Dedication to quality

Each Frontiers article is a landmark of the highest quality, thanks to genuinely collaborative interactions between authors and review editors, who include some of the world's best academicians. Research must be certified by peers before entering a stream of knowledge that may eventually reach the public - and shape society; therefore, Frontiers only applies the most rigorous and unbiased reviews. Frontiers revolutionizes research publishing by freely delivering the most outstanding research, evaluated with no bias from both the academic and social point of view. By applying the most advanced information technologies, Frontiers is catapulting scholarly publishing into a new generation.

What are Frontiers Research Topics?

Frontiers Research Topics are very popular trademarks of the *Frontiers journals series*: they are collections of at least ten articles, all centered on a particular subject. With their unique mix of varied contributions from Original Research to Review Articles, Frontiers Research Topics unify the most influential researchers, the latest key findings and historical advances in a hot research area.

Find out more on how to host your own Frontiers Research Topic or contribute to one as an author by contacting the Frontiers editorial office: frontiersin.org/about/contact

Molecular diagnostics for infectious diseases: Novel approaches, clinical applications and future challenges

Topic editors

Xiaogang Xu — Fudan University, China
Chao Zhuo — Guangzhou Medical University, China
Bing Gu — Guangdong Provincial People's Hospital, China
Kamal El Bissati — The University of Chicago, United States

Citation

Xu, X., Zhuo, C., Gu, B., El Bissati, K., eds. (2023). *Molecular diagnostics for infectious diseases: Novel approaches, clinical applications and future challenges.* Lausanne: Frontiers Media SA. doi: 10.3389/978-2-83251-949-3

Table of contents

frontiers | Frontiers in Microbiology

TYPE Editorial
PUBLISHED 03 March 2023
DOI 10.3389/fmicb.2023.1153827

OPEN ACCESS

EDITED AND REVIEWED BY
Axel Cloeckaert,
Institut National de recherche pour l'agriculture, l'alimentation et l'environnement (INRAE), France

*CORRESPONDENCE
Xiaogang Xu
✉ xuxiaogang@fudan.edu
Kamal El Bissati
✉ kelbissati@uchicago.edu

†These authors share first authorship

SPECIALTY SECTION
This article was submitted to Infectious Agents and Disease, a section of the journal Frontiers in Microbiology

RECEIVED 30 January 2023
ACCEPTED 21 February 2023
PUBLISHED 03 March 2023

CITATION
Gu B, Zhuo C, Xu X and El Bissati K (2023) Editorial: Molecular diagnostics for infectious diseases: Novel approaches, clinical applications and future challenges. *Front. Microbiol.* 14:1153827. doi: 10.3389/fmicb.2023.1153827

Editorial: Molecular diagnostics for infectious diseases: Novel approaches, clinical applications and future challenges

Bing Gu[1†], Chao Zhuo[2†], Xiaogang Xu[3*] and Kamal El Bissati[4*]

[1]Division of Laboratory Medicine, Guangdong Provincial People's Hospital, Guangzhou, China, [2]Guangzhou Institute of Respiratory Health, First Affiliated Hospital of Guangzhou Medical University, Guangzhou, China, [3]Institute of Antibiotics, Huashan Hospital, Fudan University, Shanghai, China, [4]Institute for Molecular Engineering, University of Chicago Medical Center, Chicago, IL, United States

KEYWORDS

infectious diseases, molecular diagnostics, mNGS, CRISPR-Cas based assay, POCT

Editorial on the Research Topic
Molecular diagnostics for infectious diseases: Novel approaches, clinical applications and future challenges

In this Research Topic of Frontiers in Microbiology, we assembled a collection of 12 original research articles and 2 reviews within the theme "*Molecular Diagnostics for Infectious Diseases: Novel approaches, Clinical Applications and Future Challenges*." The intended goal of this Research Topic was to present an updated view of current innovations in molecular diagnostics and challenges against clinical pathogens. The incidence of infectious diseases is high and often causes critical illness, which seriously threatens human life and health. The diagnosis and treatment depend on etiological detection techniques. Therefore, etiological detection technology is required to achieve timely, accurate, and comprehensive detection of pathogens. The traditional etiological diagnosis methods of infection mainly include morphological identification, microbial culture, smear microscopic examination, antigen and antibody detection, nucleic acid detection, etc. However, these methods have many limitations, such as long detection cycles, low sensitivity, and narrow detection spectrum of pathogens, especially for infections caused by rare or new pathogens. Traditional detection methods cannot effectively address them. Therefore, there is an urgent need for a series of more powerful pathogen detection tools. Metagenomic next-generation sequencing (mNGS) is a powerful pathogen detection approach that can potentially diagnose nucleic acids (DNA and RNA) of all infectious diseases, including bacteria, fungi, viruses, and parasites, in a single test. It has been recognized as a subversive technique for pathogen detection, especially for rare and complex infectious diseases. Specific High Sensitivity Enzymatic Reporter UnLOCKing (SHERLOCK) is a platform molecular diagnostic based on CRISPR-Cas enzymology for specific recognition of desired DNA or RNA sequences. It has been used to detect viruses such as Zika, dengue, and African classical swine fever virus. Although mNGS and SHERLOCK have played an active role in diagnosing clinical infection, they still face many limitations and challenges in clinical applications (e.g., quality control and standardization, distinguishing pathogenic pathogens from colonized pathogens, stability, simplicity, and diversity of targets). In light of these challenges, new research strategies have appeared that enhance the possibility of traditional pathogen detection methods. This Research Topic evaluates these new possibilities and brings together authorities in this field

and experiences that will focus on the clinical applications, advantages, and challenges of all aspects of molecular approaches for pathogen diagnostics. This Research Topic includes but is not limited to (i) progression of methodology for pathogen diagnostics, (ii) sequencing-based applications in diagnostics of clinical infection, (iii) progression of databases and analysis procedures for clinical application of metagenomics, (iv) CRISPR-Cas based pathogen identification, and (v) discovery of candidate biomarkers for infection diagnostics.

The paper of Lin Z. et al. reported the development of the visual method, dRAA-CRISPR/Cas12a, in detecting the expression of the virulent genes *aerA* and/or *hlyA* of *Aeromonas hydrophila*. *A. hydrophila* is a re-emerging aquaculture and waterborne/foodborne pathogen to humans. This method is rapid and highly sensitive. The results of the expression of the genes can be read using a UV flashlight. The authors showed the prospect of this promising method in the early diagnosis of *A. hydrophila* infection and on-site detection, especially in resource-poor areas of this pathogen in food and aquaculture. In another earlier study, Wang et al. used a similar technique to accurately identify and detect *Staphylococcus aureus* in clinical samples. Ummarino et al. describe a novel PCR-based method for the diagnosis of *Enterobius vermicularis* in stool samples, specifically designed for clinical application. This is the first time that such a technique has been used to detect these nematodes in fecal samples. The advantages of this method can help in the identification and molecular characterization of parasite species. However, parasitological methods and coprological analysis (especially eggs) in feces remain the gold standard for this detection.

In addition, Chen W. et al. reviewed current knowledge about the current molecular diagnostic methods of swine vesicular diseases, such as Foot-and-Mouth Disease Virus (FMDV), SenecaVirus A (SVA), and Swine Vesicular Disease Virus (SVDV). All these viruses are members of the family Picornaviridae, which can cause vesicular lesions in the tissues of the mouth, nose, feet, skin, and mucous membrane of animals. RT-PCR and real-time RT-PCR are still the most reliable and gold standard methods for detecting viruses, including FMDV, SVA, and SVDV. The authors illustrate novel molecular diagnostics of vesicular diseases. These include loop-mediated isothermal amplification (LAMP), recombinase polymerase amplification (RPA), Luminex, and CRISPR-Cas technology. Luminex technology has been developed for the differential diagnosis of FMDV, SVDV, and other vesicular disease pathogens. In addition, the PCR-based fluorescent Luminex assay was suitable for human papillomavirus (HPV) genotyping. The assay may be used to provide critical clinical information for the early detection of HPV.

Havasi et al. reviewed the similarities and differences in the diagnosis of influenza A, influenza B, and SARS-CoV-2. They discussed the clinical presentation of influenza and SARS-CoV-2 and techniques available for diagnosis. Furthermore, they summarized available data regarding the multiplex diagnostic assay of both viral infections. Lin Y. et al. developed a rapid PCR-based nanopore adaptive sequencing method (RPNAS) to enrich the viral genome directly from respiratory samples. The same method was further applied successfully for the enrichment of SARS-CoV-2. These findings promise to improve viral clinical detection and genome surveillance sensitivity and timeliness.

Porcine circovirus (PCV) type 2 has been identified as a causative agent of post-weaning multisystem wasting syndrome (PMWS), an economically important multifactorial disease in the swine industry worldwide. Li et al. developed a dual nested PCR detection method to monitor PCV types 2 and 3 simultaneously. This method provides an effective tool for molecular epidemiological studies and blood sample detection of PCV.

Zhang et al. chose to focus their work on the molecular characteristics, susceptibility, and prevalence of infection of *Cryptococcus* spp. to understand the epidemiology of this disease in a province of China. They generated a large amount of data from 180 strains of *Cryptococcus* using the WGS method. These data will lay a good foundation for the subsequent development of molecular detection methods for *Cryptococcus* spp.

Chlamydia trachomatis is one of the most common pathogens causing sexually transmitted infections. In their study, Zhao et al. used next-generation high-throughput sequencing (NGHTS) to determine *C. trachomatis* genotypes, particularly mixed-genotype infections, and their association with clinical manifestations. The results indicated that NGHTS is suitable for identifying *C. trachomatis* mixed-genotype infections. In another study, Chen X. et al. integrated nanoparticle-based lateral flow biosensors with LAMP for rapid and visual identification of *C. trachomatis* for point-of-care, which may provide a convenient testing tool for chlamydial infection screening.

Haemophilus influenzae is a common human pathogen that causes a range of infectious diseases in children and adults. Cheng et al. reported the clinical application of the LAMP method to rapidly detect *H. influenzae*. The assay provides rapid, accurate, and sensitive detection, making it a promising screening strategy in clinical laboratory settings. In another paper, Slotved et al. evaluated the use of whole genome sequencing (WGS) in national surveillance and characterization of *H. influenza* clinical isolates in Denmark. Their results show 100% concordance between phenotypic serotyping methods and WGS-based approaches.

Cutaneous leishmaniasis is a disease caused by protozoan parasites of the genus *Leishmania* and is a major public health problem in many parts of Latin America. Dueñas et al. developed CRISPR-based molecular tools to diagnose *Leishmania* infections at the genus and *L.* (*Viannia*) subgenus levels. Visceral leishmaniasis (Kala-Azar) is uncommon in China. Gao et al. reported two Kala-Azar cases in China diagnosed by mNGS. Their reports suggest that mNGS detection is beneficial for diagnosing and treating infectious diseases with unknown causes.

In conclusion, this collection includes several excellent studies summarizing the latest advances in pathogenic molecular detection technology and accumulating a large amount of pathogenic genomic data. This collection will promote the integration and utilization of molecular detection technology and pathogens genomic data in the future and establish simpler, faster, and more accurate infection pathogen detection methods. Creating a system that integrates pathogen genomic sequences from numerous ongoing surveillance efforts, such as foodborne and hospital-acquired, would allow for automated real-time analyses (Jackson et al., 2016; Stevens et al., 2022). This can rapidly identify cluster-related pathogen genome sequences, potential transmission chains, and alerts

for disease outbreaks. Finally, developing new detection methods should consider the economic component of low and middle-income countries for universal equality and one health world.

Author contributions

KE, XX, CZ, and BG drafted and edited the editorial. All authors contributed to the article and approved the submitted version.

Acknowledgments

We are grateful to Dr. Hassan Ghazal for critical reading of the manuscript.

Conflict of interest

The authors declare that the research was conducted in the absence of any commercial or financial relationships that could be construed as a potential conflict of interest.

Publisher's note

References

Jackson, B. R., Tarr, C., Strain, E., Jackson, K. A., Conrad, A., Carleton, H., et al. (2016). Implementation of nationwide real-time whole-genome sequencing to enhance listeriosis outbreak detection and investigation. *Clin. Infect. Dis.* 63, 380–386. doi: 10.1093/cid/ciw242

Stevens, E. L., Carleton, H. A., Beal, J., Tillman, G. E., Lindsey, R. L., Lauer, A. C., et al. (2022). Use of whole genome sequencing by the federal interagency collaboration for genomics for food and feed safety in the United States. *J. Food Prot.* 85, 755–772. doi: 10.4315/JFP-21-437

frontiers | Frontiers in Microbiology

ORIGINAL RESEARCH
published: 03 June 2022
doi: 10.3389/fmicb.2022.903298

Rapid and Ultrasensitive Detection of Methicillin-Resistant *Staphylococcus aureus* Based on CRISPR-Cas12a Combined With Recombinase-Aided Amplification

Ying Wang[1], *Xuan Liang*[1], *Jie Xu*[1], *Lan Nan*[2], *Fang Liu*[1], *Guangcai Duan*[1] *and Haiyan Yang*[1]*

[1] Department of Epidemiology, College of Public Health, Zhengzhou University, Zhengzhou, China, [2] Yusuf Hamied Department of Chemistry, University of Cambridge, Cambridge, United Kingdom

OPEN ACCESS

Edited by:
Bing Gu,
Guangdong Provincial People's Hospital, China

Reviewed by:
Rory Joseph Cave,
University of East London, United Kingdom
Long Ma,
Tianjin University of Science and Technology, China
Qiuchun Li,
Yangzhou University, China
Peter Kinnevey,
Dublin Dental University Hospital, Ireland

***Correspondence:**
Haiyan Yang
yhy@zzu.edu.cn

Specialty section:
This article was submitted to Infectious Agents and Disease, a section of the journal Frontiers in Microbiology

Received: 24 March 2022
Accepted: 09 May 2022
Published: 03 June 2022

Citation:
Wang Y, Liang X, Xu J, Nan L, Liu F, Duan G and Yang H (2022) Rapid and Ultrasensitive Detection of Methicillin-Resistant Staphylococcus aureus Based on CRISPR-Cas12a Combined With Recombinase-Aided Amplification. Front. Microbiol. 13:903298. doi: 10.3389/fmicb.2022.903298

Staphylococcus aureus is one of the main pathogens causing hospital and community-acquired infections, in particular, infections caused by methicillin-resistant *Staphylococcus aureus* (MRSA) cause a higher mortality rate than those caused by methicillin-sensitive strains, which poses a serious global public health problem. Therefore, rapid and ultrasensitive detection of patients with clinical MRSA infection and timely control of infection are essential. Clustered regularly interspaced short palindromic repeats (CRISPR) and CRISPR-associated proteins (Cas) based on nucleic acid detection methods are well-known for its high specificity and sensitivity and programmability. Here, we successfully proposed a method based on CRISPR-Cas12a combined with recombinase-aided amplification (RAA) through fluorescent readout to achieve accurate identification and highly sensitive detection of MRSA in clinical samples. Results showed that the limit of detection (LoD) of the RAA-Cas12a method could reach 10 copies/μl at 60 min of reaction. Specificity tests showed that the method could distinguish MRSA from clinically common bacteria. The results of RAA-Cas12a were consistent with that of antimicrobial susceptibility tests (AST) and polymerase chain reaction (PCR) in 83 clinical samples. These results indicated that the detection method based on RAA-Cas12a has high sensitivity and specificity, and provides important value for rapid detection of MRSA.

Keywords: ***Staphylococcus aureus*, MRSA, CRISPR-Cas12a, RAA, detection**

INTRODUCTION

Staphylococcus aureus (*S. aureus*) is an opportunistic pathogen capable of adapting to different hosts and environmental conditions, and is one of the main causes of various infectious diseases (Antonelli et al., 2019; He and Wunderink, 2020). With the emergence of antibiotics, *S. aureus* infection has been well treated (Lindsay, 2014). However, due to the large-scale and high-frequency use of antibiotics and the impact of various human activities, such as agricultural fertilization and intensive animal feedlots, a major problem associated with *S. aureus* is the significant resistance to various antibiotics, among which methicillin-resistant *S. aureus* (MRSA) is one of the major strains of refractory bacterial infections (Turner et al., 2019). MRSA is defined by the presence

of the staphylococcal cassette chromosome *mec* (SCC*mec*) element inserted within the *orfX* gene of *S. aureus* (Ito et al., 2001; Malachowa and DeLeo, 2010). SCC*mec* contains the *mecA* gene complex (responsible for methicillin resistance) and a set of site-specific recombinase genes that are responsible for its mobility (Liu et al., 2016). *mecA* gene encodes an alternative penicillin-binding protein (PBP2a or PBP2′) that has a low affinity for most semisynthetic penicillins, which prevents the β-lactam antibiotics from destroying the bacterial cell wall and thus showing resistance (Pinho et al., 2001; Peacock and Paterson, 2015). The remaining portions of SCC*mec* also carry additional metal and antibiotic resistance genes carried by transposons and plasmids (Miragaia, 2018). SCC*mec* can be frequently transferred between *Staphylococci*, causing more bacteria to develop broad-spectrum resistance (Shore et al., 2011). In addition, among the various MGEs within the MRSA genome, a variety of other toxins that are effective against the human host have been reported (Malachowa and DeLeo, 2010). The gain and loss of virulence determinants carried on MGEs have a vital role in bacterial adaptability, virulence, and survival (Turner et al., 2019). Overall, resistance to widespread antibiotics and carrying a wide variety of virulence factors may make MRSA infections difficult to treat and even have more severe outcomes. Hospital-associated MRSA (HA-MRSA) strains are prevalent in many health care facilities worldwide and are among the most common cause of intravenous-catheter associated infections, ventilator-associated pneumonias, and nosocomial infective endocarditis (Álvarez et al., 2019). Studies have shown that MRSA accounts for 26–60% of clinical infections caused by *S. aureus* (Hu et al., 2016; Di Ruscio et al., 2017). In the meantime, MRSA infection has a higher mortality rate than MSSA (methicillin-sensitive *S. aureus*). Meta-analyses show that MRSA bacteremia is twice as likely to prove fatal as MSSA bacteremia, resulting in longer hospital stays, increased utilization of hospital resources, and a three-fold increase in treatment costs (Lakhundi and Zhang, 2018).

For more effective treatment of MRSA patients, it is very important for clinical workers to select a rapid detection method to accurately and quickly detect patients infected with MRSA. Ideally, it is of great clinical significance to rapidly downgrade from broad-spectrum therapy to targeted antibiotics shortly after or on the same day as patient samples are collected. The most traditional method of bacterial detection in clinical and experimental laboratories is phenotypic methods for antimicrobial resistance detection such as chromogenic media, broth microdilution method (BMD), disk diffusion method, and gradient diffusion methods (Sanchini, 2022). Although these methods can provide accurate identification report, they also have the disadvantages of long culture time (2–4 days), high labor intensity, and being influenced by factors such as culture conditions, inducers, and genetic background. The others are based on molecular methods such as polymerase chain reaction (PCR), nucleic acid sequence-based amplification (NASBA), loop-mediated isothermal amplification (LAMP), and Real-Time quantitative PCR (qPCR) (van Belkum and Rochas, 2018; Chen et al., 2020b; Palavecino, 2020). These methods can effectively improve the detection sensitivity but need professional detection personnel and special equipment.

Recently, great progress has been made in the research on clustered regularly interspaced short palindromic repeats (CRISPR) and CRISPR-associated proteins (Cas) which provides a revolutionary development for nucleic acid molecular diagnosis (Horvath and Barrangou, 2010; Jinek et al., 2012). CRISPR-Cas is an RNA-guided adaptive immune platform for cleaving foreign genetic components of invading viruses and phages (Jinek et al., 2012). An effective CRISPR-Cas system needs two compositions, CRISPR RNAs (crRNAs) or single-guide RNA (sgRNA), and Cas effectors, to form RNP complexes (Jinek et al., 2012). CRISPR systems are classified into two categories based on the composition of Cas effectors. Class 1 systems consist of multiple Cas effectors, while class 2 systems are characterized by only one effector protein. Interestingly, several effectors (Cas12, Cas13, and Cas14) in class 2 systems have not only cis cleavage but also trans cleavage (Swarts and Jinek, 2019). For Cas12a, more specifically, crRNA is employed to recognize the target sequence by a short protospacer-adjacent motif (PAM) sequence (Collias and Beisel, 2021). After the Cas12a-crRNA complex binding with target sequence, the cis cleavage for both strands of double-stranded DNA (dsDNA) target occurs (Chen et al., 2018). And then, non-specific cleavage (trans cleavage) of Cas12a effector was activated to cleave non-specific single-stranded DNA (ssDNA) (Chen et al., 2018). Particularly, the PAM sequence is essential for target sequence recognition but not for non-specific ssDNA (Chen et al., 2018). Based on this property, the CRISPR-Cas system can be developed to detect pathogens, proteins, and biomarkers. At present, SHERLOCK, an RNA targeting method based on Cas13, has been applied to detect viruses such as HBV, ZIKA, and SARS-CoV-2 (Gootenberg et al., 2017; Myhrvold et al., 2018; Joung et al., 2020). This method establishes a complete diagnostic program, which can achieve highly specific and sensitive detection of nucleic acid. However, using Cas13a as an RNase requires a processing step that first converts the amplified DNA into RNA. Instead, Cas12a targets dsDNA and does not require a transcription step (Chen et al., 2018).

Here, we propose a novel MRSA detection strategy that could accurately and sensitively identify MRSA under clinical and experimental conditions. We selected adhesin clumping factor (*clfA*) and thermostable nuclease (*nuc*) genes that have been confirmed by laboratory studies in all *S. aureus* chromosomes as candidates for specific detection of *S. aureus* (Smeltzer et al., 1997; Chen et al., 2020a). Meanwhile, we selected the *mecA* gene as the specific gene of methicillin resistance. The detection process and principle based on RAA-Cas12a are shown in **Figure 1**. In this study, the MRSA detection method based on RAA-Cas12a is of great significance for the rapid and accurate detection of MRSA infected patients.

MATERIALS AND METHODS

Materials

In this study, all strains were from laboratory preserved strains (Molecular Epidemiology Group, School of Public Health,

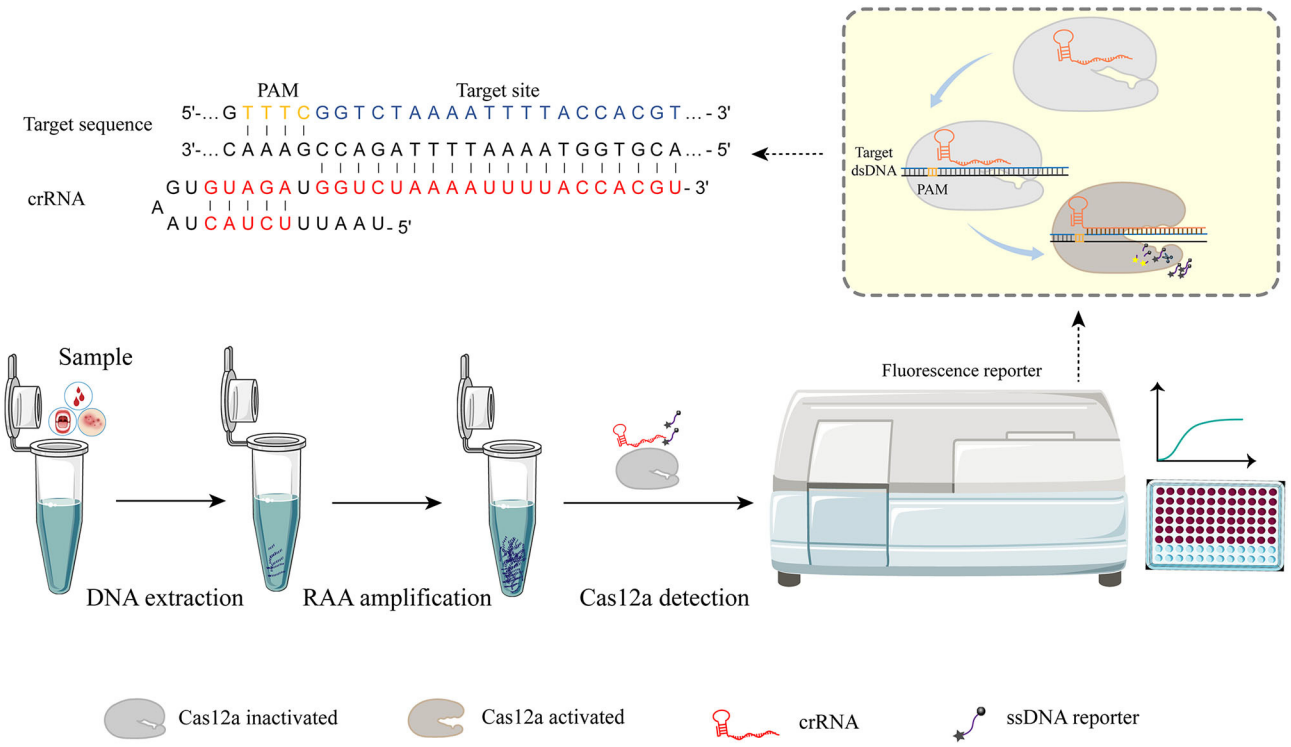

FIGURE 1 | RAA-Cas12a detection system. The detection process can be roughly divided into three parts. Step I, the sample was pretreated and DNA was extracted as the substrate for the next step. Step II, nucleic acid was amplified by recombinase-aided amplification (RAA). Step III, Cas-based signal generation. Cas12a-crRNA complex is activated when crRNA is employed to recognize the target sequence by a short protospacer-adjacent motif (PAM) sequence. After the Cas12a-crRNA complex binding with the target sequence, the cis cleavage for both strands of the dsDNA target occurs. The activated Cas12a-crRNA complex possesses non-specific cleavage (trans cleavage) activity that can cleave non-specific ssDNA reporters to generate fluorescence signals that are captured by the instrument.

Zhengzhou University, Zhengzhou, Henan, China), including *S. aureus*, *Escherichia coli* (*E. coli*), *Staphylococcus epidermidis* (*S. epidermidis*), *Helicobacter pylori* (*H. pylori*), *Shigella sonnei* (*S. sonnei*), *Klebsiella pneumoniae* (*K. pneumoniae*), and *Salmonella typhimurium* (*S. typhimurium*). All synthetic plasmids, DNA fragments [crRNA, primers, and fluorescent probe ssDNA] were synthesized by Sangon Biotech (Shanghai, China). RAA test kit purchased from Hangzhou ZC Bio-Sci&Tech Co. Ltd (Hangzhou, China). CRISPR-Cas12a (Cpf1) (1 μM) was purchased from Bio-lifesci (Guangzhou, China). HiScribe T7 Quick High Yield RNA Synthesis Kit and Monarch® RNA Cleanup Kit were purchased from New England Biolabs (Beijing, China).

Nucleic Acids Preparation

The strains isolated from the hospital were inoculated on the Columbia blood plate and cultured in 37°C incubator for 18–24 h. Morphological characteristics and hemolysis of the colony were observed. The colonies with morphological characteristics of *Staphylococcus* and hemolytic ring were selected for further identification by Gram staining and slide coagulase test. The DNA extraction used in this paper by bacterial genome DNA extraction kit was purchased from LifeFeng (Shanghai, China). The plasmid was extracted and purified using a plasmid extraction kit (Biomed, Beijing, China).

crRNA, RPA Primer, and ssDNA Preparation

All *clfA*, *nuc*, and *mec* (*mecA* and *mecC*) gene sequences of *S. aureus* were obtained from the NCBI database (https://www.ncbi.nlm.nih.gov/) and sequence alignment was performed by using Mega10.1.6 software. Then, conserved sequences matching the PAM of Cas12a (5'-TTTN) were screened, and the corresponding crRNAs were designed as the gRNAs for subsequent detection (**Supplementary Table S1**). In this process, we did not find a universal crRNA that could simultaneously recognize *mecA* and *mecC*. Therefore, we chose the *mecA* gene, which has a relatively high prevalence, to design the crRNA. To prepare crRNAs, a single-stranded cognate DNA oligonucleotide with a T7 promoter sequence was annealed with a primer sequence having a complementary T7 primer sequence (**Supplementary Table S1**). It was then transcribed into crRNA using the HiScribe T7 Quick High Yield RNA Synthesis Kit. Subsequently, the product crRNA was purified using Monarch® RNA Cleanup Kit. The optimal crRNA was screened through experiments. Based on the screened optimal crRNA, the corresponding RPA amplification primers and

PCR amplification primers were designed by Primer 5 and Oligo 7 software (**Supplementary Table S2**). Fluorescence probe ssDNA with sequence 5′-6-FAM-TTTT TTTT TTTT-BHQ1 was retrieved in the literature (Ai et al., 2019).

RAA-Cas12a Detection Method

The whole detection process is divided into two parts: the first part is RAA amplification, and the second part is Cas12a detection. The RAA reaction system was operated strictly according to the instructions. The RAA system consisted of 50 μl: add 38.5 μl A Buffer, 2.0 μl forward primers (10 μM), 2.0 μl reverse primers (10 μM), and 2.0 μl template DNA into the detection unit tube containing the detection dry enzyme preparation, then add 2.5 μl B Buffer into the detection unit tube. Mix thoroughly upside down, centrifuge at low speed for 10 s. The tube was placed in 37°C constant temperature incubators for 30 min to obtain the amplification products. The Cas12a detection system consisted of 50 μl, including 5 μl of RAA amplification products (above products), 5 μl of Cas12a (1 μM), 5 μl of Buffer, 5 μl of fluorescent probe (10 μM), 2.5 μl of crRNA (above crRNA), and 27.5 μl of enzyme-free water. The detection system was placed in a fluorescence reader (microplate reader), and fluorescence intensity was detected with excitation light of 494 nm and emission light of 521 nm, once every 2 min. Continuous fluorescence value reports were obtained at 37°C for 60 min. For the definition of positive results for the fluorescence reader, we set the signal-to-noise ratio parameter (the ratio of the fluorescence value of the detected object to the negative control, S/N) to S/N $>$ 3 after 60 min of Cas12a reaction, which was considered positive results.

Evaluation of LoD (Limit of Detection)

The synthetic plasmid was obtained by cloning *clfA*, *nuc*, *mecA* fragments into pUC57 (**Supplementary Table S3**) (Liu et al., 2021). After the plasmid was extracted and purified, the concentration was determined using Nanodrop 2000 spectrophotometer (Thermo Scientific, Massachusetts, USA). Copies number was determined following formula copies/μl = $(6.02 \times 10^{23}) \times (\text{ng}/\mu\text{l} \times 10^{-9})$ / (DNA length × 660) (Ai et al., 2019). The solution was diluted to a concentration of 10^9-10^0 copies per μl in TE buffer, from which a 10-fold dilution series was made to serve as the LoD.

Specificity Determination Experiments

Based on our previous studies and other published literature (Mao et al., 2019; Wei, 2021), we selected bacteria that are more commonly found in clinical infections for specificity experiments. The nucleic acid of *S. aureus*, *E. coli*, *S. epidermidis*, *H. pylori*, *S. sonnei*, *K. pneumoniae*, and *S. typhimurium* was extracted, and Cas12a was detected by RAA amplification. Our previous study found that common drug resistance genes in *S. aureus* were *ermC*, *msrA*, *tetK*, *acc(6')-aph(2")*, *ant(4',4")*, and *aph(3')-III* (Luo et al., 2018). Strains containing the above resistance genes were selected, and RAA amplification and Cas12a detection were performed using the extracted DNAs as the templates.

Detection of Clinical Samples

A total of 83 clinical patient samples, including 21 from secretions, 20 from fester, 19 from drainage fluid or indwelling catheters, 14 from sputum, 7 from blood, and 2 from urine, were provided by the hospital in Zhengzhou. Samples were detected by three different methods, including bacterial culture and antimicrobial susceptibility tests (AST), PCR, and RAA-Cas12a detection, among them, using AST as the gold standard, which is commonly used in clinical practice. AST was performed using the broth dilution method according to the recommendations of the Clinical and Laboratory Standards Institute 29th edition (CLSI, 29th ed). The tests were controlled using *S. aureus* ATCC 29213. *S. aureus* with MIC $\geq$ 4 μg/ml to oxacillin was determined as MRSA. A PCR assay was carried out in a 50 μl reaction mixture, including 25 μl of 2 × Taq PCR Master Mix (purchased from CWBIO, Jiangsu, China), 2 μl of forward primers (10 μM), 2 μl of reverse primers (10 μM), 2 μl of extracted template DNA, and 19 μl of ddH_2O. A PCR assay was carried out with the following thermal-cycled process: pre-denaturation at 94°C for 2 min, 30 cycles with the following parameters: denaturation at 94°C for 30 s, annealing at 56°C for 30 s, extension at 72°C for 30 s and final extension at 72°C for 5 min. The above experiments were repeated twice to avoid experimental error and ensure the effectiveness of the experiment. S/N $>$ 3 was considered positive results. In addition, the effectiveness of RAA-Cas12a detection was evaluated by sensitivity, specificity, positive predictive value (PPV), negative predictive value (NPV), and Youden's index.

Statistical Analysis

Data were analyzed using SPSS 21.0 (IBM Crop., Chicago, USA) and GraphPad Prism 8.0.2 (GraphPad Software Inc., Chicago, USA). Fluorescence values were expressed as mean ± SD. The average fluorescence value was obtained by three parallel experiments. Multiple groups were compared with one-way ANOVA method, and differences were considered significant at values of $P < 0.05$.

RESULTS

Design and Construction of RAA-Cas12a System

Cas12a detection system was used to detect clinical MRSA strains, and sequence alignment of *clfA*, *nuc*, and *mecA* sequences was conducted to screen out conserved target regions, and different crRNAs were designed (**Supplementary Table S1**). Then, we constructed a system, consisting of Cas12a, Buffer, probe, MRSA genomic DNA, and different crRNAs designed, to screen the optimal crRNA. Our experimental results showed that *clfA*-crRNA3 and *mecA*-crRNA2 combined with Cas12a had a better shear effect on ssDNA (**Figures 2A,B**). Therefore, *clfA*-crRNA3 and *mecA*-crRNA2 were selected for subsequent experiments.

As shown in **Figures 2C,D**, we successfully constructed the RAA-Cas12a detection system. Only if the Cas12a protein, crRNA, probe, and target gene were present in one system simultaneously, can the Cas12a protein bind the crRNA and target gene to form a complex that plays the role of shearing the

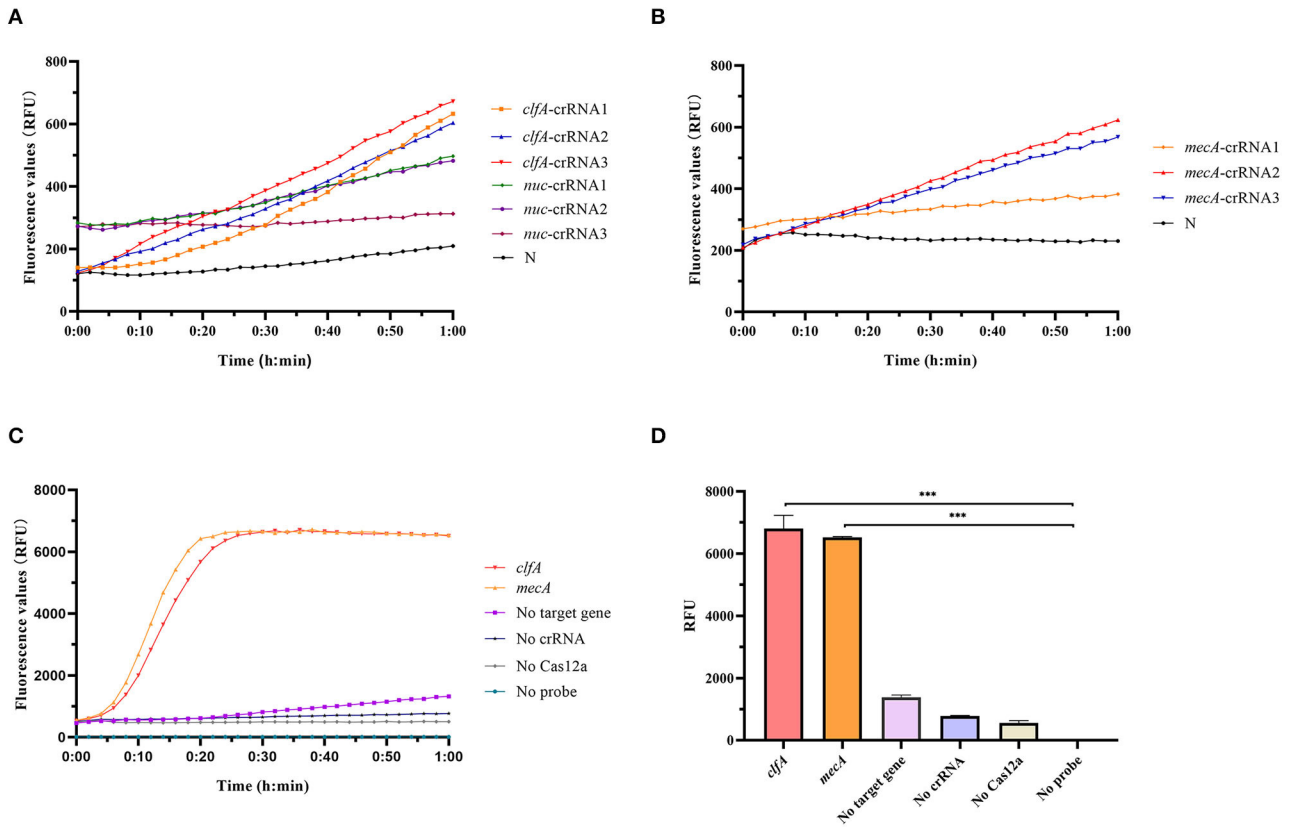

FIGURE 2 | Preparation of Cas12a detection system. **(A)** To screen for optimal crRNA that specifically identify *S. aureus*, we designed different crRNAs for *nuc* and *clfA* genes and simultaneously performed Cas12a detection for *S. aureus* with the same concentration without amplification. **(B)** Different crRNAs were designed for the *mecA* gene, and Cas12a detection was performed on unamplified MRSA DNA to screen out crRNA with better specificity to recognize MRSA. **(C)** Cas12a detection system fluorescence report curve. **(D)** Comparison of fluorescence values generated after 60 min of Cas12a reaction, $^{***}p < 0.0001$. Data were expressed as mean ± SD ($n = 3$).

ssDNA probe, thus producing a fluorescent signal that is captured by the instrument.

Evaluation of LoD of RAA-Cas12a Detection System

A series of gradient dilutions of the synthetic plasmid containing *clfA* as a template was amplified using RAA for 30 min and detected using the Cas12a system. The results showed that the fluorescence intensity of the products at 10^5 and 10^4 copies/μl concentration reached its peak within 30 min of incubation at 37°C. The fluorescence intensity at 10^3-10^0 copies/μl concentration was significantly higher than that in the negative control group, and the difference was statistically significant ($P < 0.0001$; **Figures 3A,B**). The RAA-Cas12a system was used to detect synthetic plasmids containing *mecA* using the same method. The results showed that the fluorescence intensity at 10^5-10^3 copies/μl concentration reached the peak within 30 min of incubation at 37°C, and the fluorescence intensity at 10^2 to 10^0 copies/μl concentration was significantly higher than that of the negative control group, the difference was statistically significant ($P < 0.0001$; **Figures 3C,D**). However, the results of the fluorescence values at 10^0 copy/μl did not meet our predefined criteria for positive results S/N > 3. Therefore, the LoD of this detection method could reach 10 copies/μl at 60 min of reaction.

After gradient dilution of the synthetic plasmid containing *clfA* gene, PCR amplification was performed, and the results of agarose gel electrophoresis experiments showed there was no obvious band when the concentration was below 10^5 copies/μl (**Supplementary Figures S1, S2**). This indicates that RAA-Cas12a method had higher sensitivity than PCR method.

Specificity of RAA-Cas12a Detection System

Different strains were detected by RAA-Cas12a, and the results showed that only *S. aureus* had an amplification curve after detection. There were no amplification curves for *E. coli*, *S. epidermidis*, *H. pylori*, *S. sonnei*, *K. pneumoniae*, and *S. typhimurium*, indicating that the RAA-Cas12a detection system had high specificity for *S. aureus* (**Figures 4A,B**).

RAA-Cas12a was used to detect common resistance genes in bacteria, and the results showed that only the strains containing

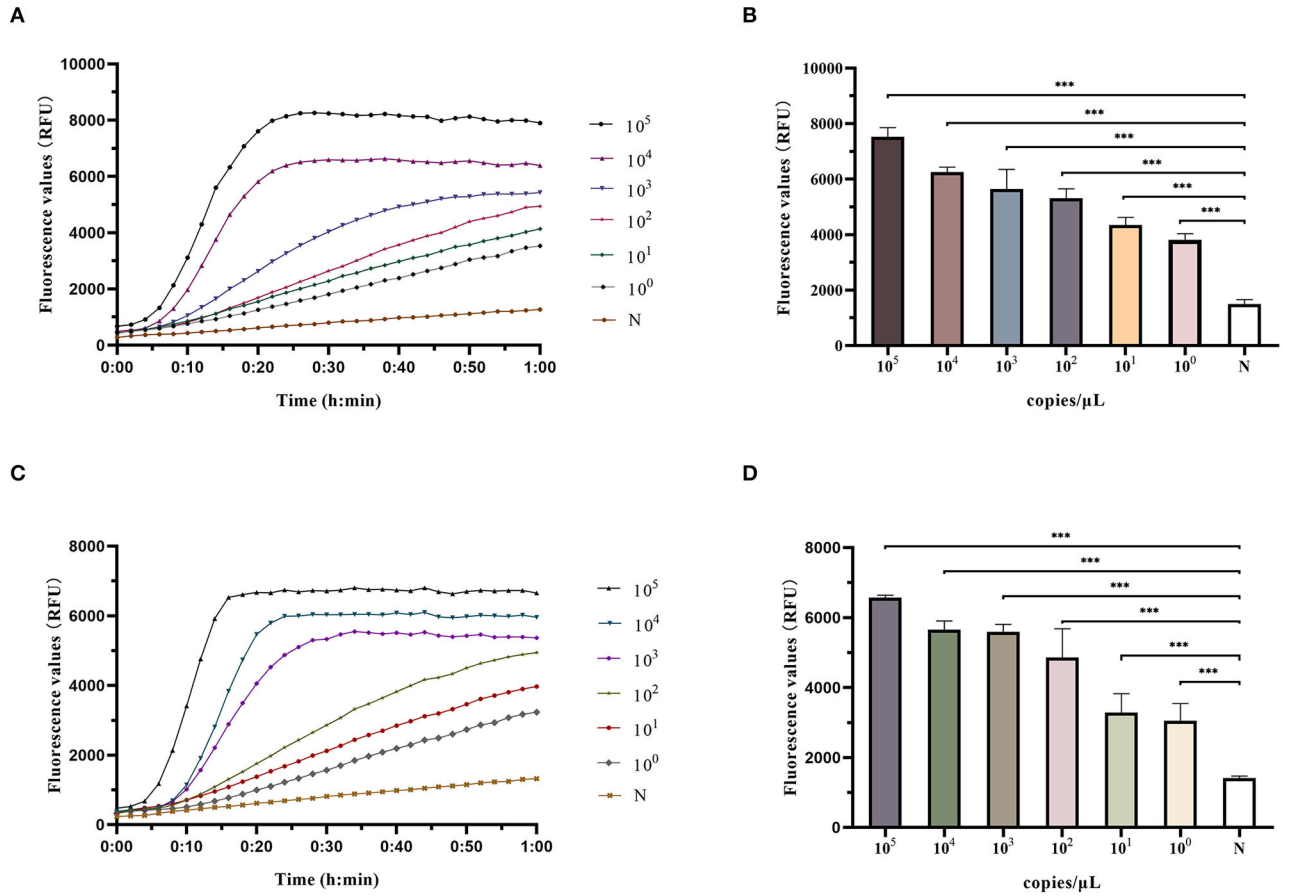

FIGURE 3 | Determination of LoD (limit of detection) of RAA-Cas12a detection system. Data were expressed as mean ± SD ($n = 3$). Negative control (N) utilized RNase-free water as input instead of DNA dilutions. ***$p < 0.0001$. **(A)** Fluorescence curves were generated when Cas12a reacts with the *clfA* target at each dilution. **(B)** Comparison of fluorescence values generated after 60 min of Cas12a reaction (*clfA* target). **(C)** Fluorescence curves were generated when Cas12a reacts with the *mecA* target at each dilution. **(D)** Comparison of fluorescence values generated after 60 min of Cas12a reaction (*mecA* target).

mecA had amplification curves. Whereas, the strains, containing *ermC*, *msrA*, *tetK*, *acc(6')-aph(2")*, *ant(4',4")* and/or *aph(3')-III*, had no amplification curve, indicating that the RAA-Cas12a detection system had high specificity for *mecA* (**Figures 4C,D**).

Clinical Samples Detection by the RAA-Cas12a System

To evaluate the effectiveness of the RAA-Cas12a detection system in clinical samples, 83 clinically isolated *S. aureus* strains were assayed using AST, PCR, and RAA-Cas12a detection system. The results of AST are shown in **Supplementary Table S4**, we found that 41 isolates were phenotypically classed as MRSA. And then PCR method was used to detect *mecA* of these 83 strains (**Supplementary Figure S3**). The results of agarose gel electrophoresis experiments showed that 41 strains of *S. aureus* contained the 500 bp gene. The amplified products were sent for sequencing, and the BLAST sequence indicated that the gene amplified was *mecA*, proving that all 41 strains were MRSA. At the same time, these 83 strains were detected by the RAA-Cas12a detection system. All 83 strains were *S. aureus*, among which 41 strains of MRSA samples were detected (**Figure 5**). The results showed that MRSA detection based on RAA-Cas12a was consistent with AST and PCR. The results of sensitivity, specificity, PPA, NPA, and Youden's index are shown in **Table 1**, indicating that this method was fully comparable with AST and PCR.

DISCUSSION

MRSA, due to its wide antibiotic resistance spectrum, fast transmission speed, and easy to cause outbreaks, is one of the typical representatives of multi-drug resistant bacteria (Lindsay, 2013). Therefore, the sensitive, specific, and rapid detection of MRSA strains is the key from broad-spectrum antibiotic treatment to specific antibiotic treatment. As we know, genetic information is contained in the nucleotide sequence of DNA (and sometimes RNA), therefore, in molecular diagnostics, the detection of DNA is crucial for the identification of microorganisms of interest, and PCR is a mature nucleic acid amplification technology (Matsuda, 2017). It has been applied

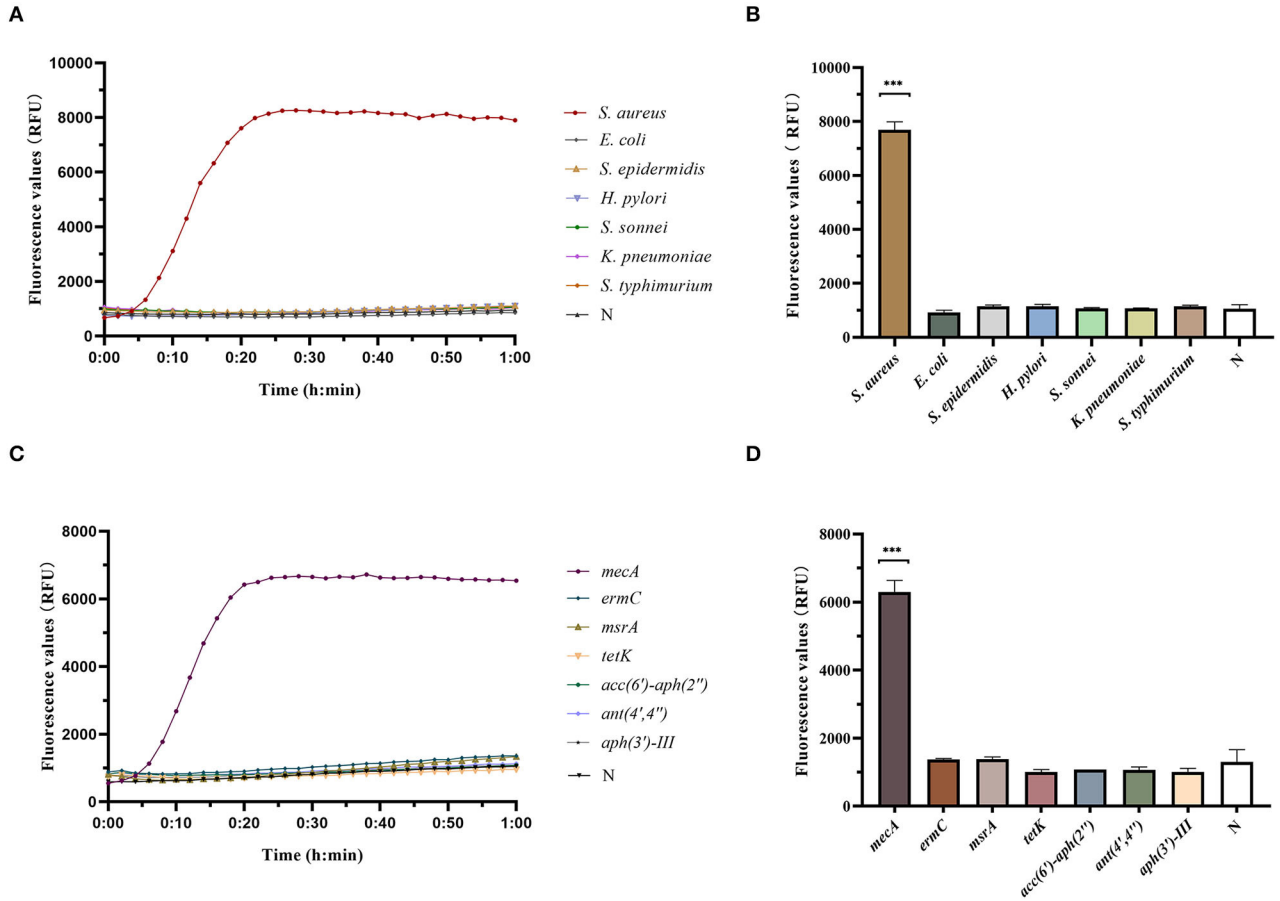

FIGURE 4 | Determination of specificity of RAA-Cas12a detection system. Data were expressed as mean ± SD ($n = 3$). Negative control (N) utilized RNase-free water as input instead of DNA dilutions. ***$p < 0.0001$. **(A)** Fluorescence curves were generated when different clinical strain samples were detected by the RAA-Cas12a detection system. **(B)** Cas12a reaction was performed after 60 min to compare the fluorescence values of different clinical strain samples. **(C)** Fluorescence curves were generated when different antibiotic resistance genes were detected by the RAA-Cas12a detection system. **(D)** Cas12a reaction was performed after 60 min to compare the fluorescence values of different antibiotic resistance genes.

to microbial detection in a variety of fields, including clinical, food, and environmental. However, the PCR-based methods are faced with some inevitable shortcomings, such as complex trained personnel, thermal cycling procedures, the accuracy of reaction steps, and the bulky experimental equipment (Maurer, 2011; Chen et al., 2019; Qian et al., 2022). Compared to PCR, the RAA technique is an alternative method that uses different mechanisms throughout the reaction process at a constant temperature and does not require complex thermal cycles, making it ideal for point-of-care detection (Fan et al., 2020). In this study, gel electrophoresis results after PCR amplification showed that the *mecA* gene could not be observed at the dilution concentration of 10^5 copies/μl. However, the detection results of the RAA-Cas12a system showed that the LoD of this detection method could reach 10 copies/μl at 60 min of reaction. These results indicate that the established RAA-Cas12a method has a high sensitivity. In addition, because both RAA amplification and Cas12a reactions can function at 37°C, a complex thermal cycling process is avoided, a small incubator or water bath can meet the testing needs, and can be used in primary health care institutions.

In recent years, emerging nucleic acid detection technologies based on CRISPR-Cas developments have opened up new opportunities for pathogen detection (Peng et al., 2020; Zhou et al., 2020; Yin et al., 2021). Compared to traditional assays, the CRISPR-Cas system has low requirements on sample quality and strong anti-interference ability and can be combined with rapid sample pretreatment technology to extract nucleic acids in the field without relying on professional equipment (Ding et al., 2021a). It has been shown that a visualized and rapid detection technology of CRISPR-Cas13a nucleic acid suitable for the lateral flow test strip technology was established by modifying biotin and small molecule antigen FAM at both ends of the reporter RNA (Gootenberg et al., 2018; Ding et al., 2021b). Gootenberg et al. have successfully applied the technology to rapid tests for ZIKA (Gootenberg et al., 2018). Compared with traditional methods, the lateral flow test strip technology is portable and fast, enabling rapid and visual detection with the naked eye in the field.

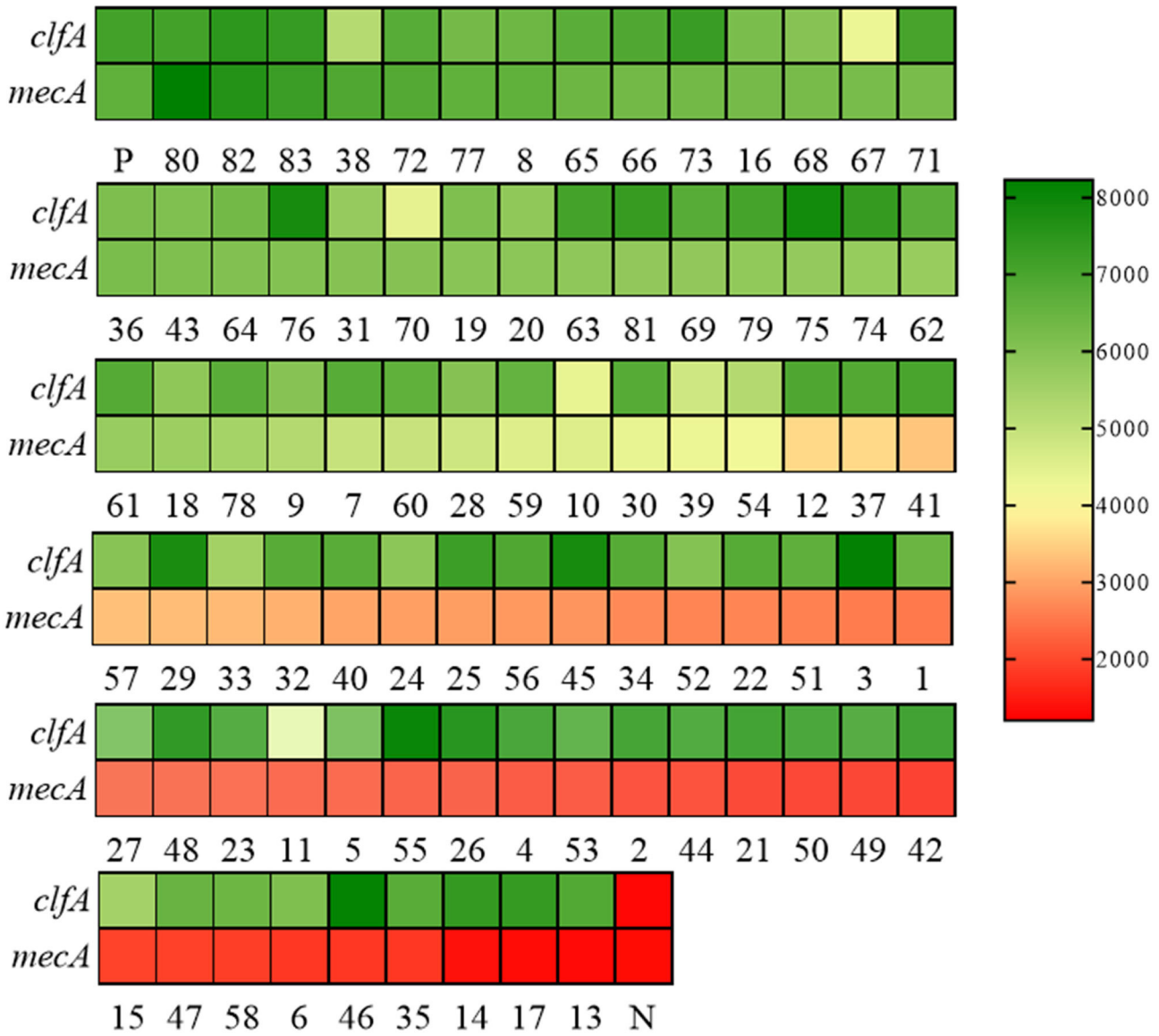

FIGURE 5 | RAA-Cas12a detection system for MRSA in 83 clinical samples. Green indicates that the gene detected in the sample is positive, and the shade of the color is positively correlated with the fluorescence value. Red indicates that the gene tested in the sample is negative, and the depth of red is negatively correlated with the fluorescence value. Positive control (P) and negative control (N). Both *clfA* and *mecA* tests are positive, indicating that the sample is MRSA.

The detection system can realize convenient visual detection of specific nucleic acid (pathogen, gene mutation, etc.). However, the sensitivity of the lateral flow test strip technology based on the RAA-Cas12a system for MRSA detection in this study is not particularly ideal. After the development and improvement of lateral flow test strip technology, RAA-Cas12a technology can be transformed into a convenient visual test paper, which can further simplify the detection process and reduce the detection time (Arizti-Sanz et al., 2020).

Although the RAA-Cas12a method we established has high sensitivity and specificity, it still has several weaknesses. First, our method does not detect the few MRSA strains containing the *mecA*-like gene (*mecC*) (Lakhundi and Zhang, 2018), which has also been observed in other molecular strategies (Buchan et al., 2015; Xu et al., 2020; Suea-Ngam et al., 2021). *mecC* is a new resistance gene recently discovered and identified in MRSA isolated from animals. Although *mecA*- and *mecC*-encoded proteins possess different biochemical properties, *mecC* nevertheless confers methicillin resistance (García-Garrote et al., 2014). Because the Cas effector's recognition requirements for PAM lead to the narrowing of the range of recognizable sequences, we did not find a target sequence for simultaneous recognition of *mec*. Second, due to the limitations of current basic research, we only used Cas12 for detection. Gootenberg et al. revealed that different Cas effectors with unique cleavage preferences for different dinucleotide motifs, and multiple

TABLE 1 | RAA-Cas12a, AST and PCR for clinical samples detection.

		AST		Total	Sensitivity	Specificity	PPA	NPA	YI
		MRSA	MSSA		(95% CI)	(95% CI)	(95% CI)	(95% CI)	(95% CI)
PCR	MRSA	41	0	41	100%	100%	100%	100%	100%
	MSSA	0	42	42	(89.3–100%)	(89.6–100%)	(89.3-100%)	(89.6–100%)	(78.9–100%)
	Total	41	42	83					
RAA-Cas12a	MRSA	41	0	41	100%	100%	100%	100%	100%
	MSSA	0	42	42	(89.3–100%)	(89.6–100%)	(89.3–100%)	(89.6–100%)	(78.9–100%)
	Total	41	42	83					

AST, antimicrobial susceptibility tests; PCR, polymerase chain reaction; MRSA, methicillin-resistant Staphylococcus aureus; MSSA, methicillin-sensitive Staphylococcus aureus; RAA, recombinase-aided amplification; PPA, positive predictive agreement; NPA, negative predictive agreement; YI, Youden's index. The gold standard for MRSA is AST.

sensing of different targets can be achieved (Gootenberg et al., 2018). However, multiplex detection is still a challenge for CRISPR-Cas (Li et al., 2019), with the development of CRISPR-Cas technology, the functions of Cas effectors have become clearer, and in the coming years it is possible to combine different Cas effectors simultaneously for purpose of simultaneous detection of different target genes.

CONCLUSION

In this study, we successfully constructed the CRISPR-Cas12a combined with the RAA method based on fluorescence readout, realizing the accurate identification and high sensitivity detection of MRSA in clinical samples. The results of RAA-Cas12a were consistent with AST and PCR results of 83 clinical samples. Although the clinical application of the CRISPR-Cas system is still in its infancy and has some shortcomings, its emergence opens up many possibilities for the biomedical field. With the deepening of research and clinical verification, we believe that the application of the CRISPR-Cas system will play an irreplaceable role in pathogen detection, drug resistance gene detection, and other aspects.

DATA AVAILABILITY STATEMENT

The original contributions presented in the study are included in the article/**Supplementary Material**, further inquiries can be directed to the corresponding author.

ETHICS STATEMENT

The use of clinical samples has been reviewed by the Life Sciences Ethics Review Committee of Zhengzhou University (ZZUIRB 2019-003).

AUTHOR CONTRIBUTIONS

YW designed this study. YW and XL finished the experiments and wrote the manuscripts together. YW, XL, JX, LN, FL, GD, and HY revised the manuscript critically for important intellectual content. All authors read and approved the final manuscript.

FUNDING

This work was funded by the National Natural Science Foundation of China (No. 81973105). The funder had no role in the study design, data collection, and analysis, decision to publish, or preparation of the manuscript.

SUPPLEMENTARY MATERIAL

The Supplementary Material for this article can be found online at: https://www.frontiersin.org/articles/10.3389/fmicb.2022.903298/full#supplementary-material

REFERENCES

Ai, J. W., Zhou, X., Xu, T., Yang, M., Chen, Y., He, G. Q., et al. (2019). CRISPR-based rapid and ultra-sensitive diagnostic test for Mycobacterium tuberculosis. *Emerg. Microbes. Infect.* 8, 1361–1369. doi: 10.1080/22221751.2019.1664939

Álvarez, A., Fernández, L., Gutiérrez, D., Iglesias, B., Rodríguez, A., and García, P. (2019). Methicillin-resistant *Staphylococcus aureus* in Hospitals: latest trends and treatments based on bacteriophages. *J. Clin. Microbiol.* 57, e01006–19. doi: 10.1128/JCM.01006-19

Antonelli, A., Giani, T., Coppi, M., Di Pilato, V., Arena, F., Colavecchio, O. L., et al. (2019). *Staphylococcus aureus* from hospital-acquired pneumonia from an Italian nationwide survey: activity of ceftobiprole and other anti-staphylococcal agents, and molecular epidemiology of methicillin-resistant isolates. *J. Antimicrob. Chemother.* 74, 3453–3461. doi: 10.1093/jac/dkz371

Arizti-Sanz, J., Freije, C. A., Stanton, A. C., Petros, B. A., Boehm, C. K., Siddiqui, S., et al. (2020). Streamlined inactivation, amplification, and Cas13-based detection of SARS-CoV-2. *Nat. Commun.* 11, 5921. doi: 10.1038/s41467-020-19097-x

Buchan, B. W., Allen, S., Burnham, C. A., McElvania TeKippe, E., Davis, T., Levi, M., et al. (2015). Comparison of the next-generation Xpert MRSA/SA BC assay and the GeneOhm StaphSR assay to routine culture for identification of *Staphylococcus aureus* and methicillin-resistant *S. aureus* in positive-blood-culture broths. *J. Clin. Microbiol.* 53, 804–809. doi: 10.1128/JCM.03108-14

Chen, J. S., Ma, E., Harrington, L. B., Da Costa, M., Tian, X., Palefsky, J. M., et al. (2018). CRISPR-Cas12a target binding unleashes indiscriminate single-stranded DNase activity. *Science* 360, 436–439. doi: 10.1126/science.aar6245

Chen, Q., Xie, S., Lou, X., Cheng, S., Liu, X., Zheng, W., et al. (2020a). Biofilm formation and prevalence of adhesion genes among *Staphylococcus aureus* isolates from different food sources. *Microbiologyopen* 9, e00946. doi: 10.1002/mbo3.946

Chen, R., Lu, X., Li, M., Chen, G., Deng, Y., Du, F., et al. (2019). Polymerase chain reaction using "V" shape thermal cycling program. *Theranostics* 9, 1572–1579. doi: 10.7150/thno.31986

Chen, X., Ma, K., Yi, X., Xiong, L., Wang, Y., and Li, S. (2020b). The rapid and visual detection of methicillin-susceptible and methicillin-resistant *Staphylococcus aureus* using multiplex loop-mediated isothermal amplification linked to a nanoparticle-based lateral flow biosensor. *Antimicrob. Resist. Infect. Control* 9, 111. doi: 10.1186/s13756-020-00774-x

Collias, D., and Beisel, C. L. (2021). CRISPR technologies and the search for the PAM-free nuclease. *Nat. Commun.* 12, 555. doi: 10.1038/s41467-020-20633-y

Di Ruscio, F., Bjørnholt, J. V., Leegaard, T. M., Moen, A. E. F., and de Blasio, B. F. (2017). MRSA infections in Norway: a study of the temporal evolution, 2006-2015. *PLoS ONE* 12, e0179771. doi: 10.1371/journal.pone.0179771

Ding, R., Long, J., Yuan, M., Jin, Y., Yang, H., Chen, M., et al. (2021a). CRISPR/Cas system: a potential technology for the prevention and control of COVID-19 and emerging infectious diseases. *Front. Cell Infect. Microbiol.* 11, 639108. doi: 10.3389/fcimb.2021.639108

Ding, R., Long, J., Yuan, M., Zheng, X., Shen, Y., Jin, Y., et al. (2021b). CRISPR/Cas12-based ultra-sensitive and specific point-of-care detection of HBV. *Int. J. Mol. Sci.* 22, 842. doi: 10.3390/ijms22094842

Fan, X., Li, L., Zhao, Y., Liu, Y., Liu, C., Wang, Q., et al. (2020). Clinical validation of two recombinase-based isothermal amplification assays (RPA/RAA) for the rapid detection of african swine fever virus. *Front. Microbiol.* 11, 1696. doi: 10.3389/fmicb.2020.01696

García-Garrote, F., Cercenado, E., Marín, M., Bal, M., Trincado, P., Corredoira, J., et al. (2014). Methicillin-resistant *Staphylococcus aureus* carrying the mecC gene: emergence in Spain and report of a fatal case of bacteraemia. *J. Antimicrob. Chemother.* 69, 45–50. doi: 10.1093/jac/dkt327

Gootenberg, J. S., Abudayyeh, O. O., Kellner, M. J., Joung, J., Collins, J. J., and Zhang, F. (2018). Multiplexed and portable nucleic acid detection platform with Cas13, Cas12a, and Csm6. *Science* 360, 439–444. doi: 10.1126/science.aaq0179

Gootenberg, J. S., Abudayyeh, O. O., Lee, J. W., Essletzbichler, P., Dy, A. J., Joung, J., et al. (2017). Nucleic acid detection with CRISPR-Cas13a/C2c2. *Science* 356, 438–442. doi: 10.1126/science.aam9321

He, H., and Wunderink, R. G. (2020). *Staphylococcus aureus* pneumonia in the community. *Semin. Respir. Crit. Care. Med.* 41, 470–479. doi: 10.1055/s-0040-1709992

Horvath, P., and Barrangou, R. (2010). CRISPR/Cas, the immune system of bacteria and archaea. *Science* 327, 167–170. doi: 10.1126/science.1179555

Hu, F. P., Guo, Y., Zhu, D. M., Wang, F., Jiang, X. F., Xu, Y. C., et al. (2016). Resistance trends among clinical isolates in China reported from CHINET surveillance of bacterial resistance, 2005-2014. *Clin. Microbiol. Infect.* 22(Suppl. 1), S9–14. doi: 10.1016/j.cmi.2016.01.001

Ito, T., Katayama, Y., Asada, K., Mori, N., Tsutsumimoto, K., Tiensasitorn, C., et al. (2001). Structural comparison of three types of staphylococcal cassette chromosome mec integrated in the chromosome in methicillin-resistant *Staphylococcus aureus*. *Antimicrob. Agents Chemother.* 45, 1323–1336. doi: 10.1128/AAC.45.5.1323-1336.2001

Jinek, M., Chylinski, K., Fonfara, I., Hauer, M., Doudna, J. A., and Charpentier, E. (2012). A programmable dual-RNA-guided DNA endonuclease in adaptive bacterial immunity. *Science* 337, 816–821. doi: 10.1126/science.1225829

Joung, J., Ladha, A., Saito, M., Kim, N. G., Woolley, A. E., Segel, M., et al. (2020). Detection of SARS-CoV-2 with SHERLOCK one-pot testing. *N. Engl. J. Med.* 383, 1492–1494. doi: 10.1056/NEJMc2026172

Lakhundi, S., and Zhang, K. (2018). Methicillin-resistant *Staphylococcus aureus*: molecular characterization, evolution, and epidemiology. *Clin. Microbiol. Rev.* 31, e00020–18. doi: 10.1128/CMR.00020-18

Li, Y., Liu, L., and Liu, G. (2019). CRISPR/Cas multiplexed biosensing: a challenge or an insurmountable obstacle? *Trends Biotechnol.* 37, 792–795. doi: 10.1016/j.tibtech.2019.04.012

Lindsay, J. A. (2013). Hospital-associated MRSA and antibiotic resistance-what have we learned from genomics? *Int. J. Med. Microbiol.* 303, 318–323. doi: 10.1016/j.ijmm.2013.02.005

Lindsay, J. A. (2014). *Staphylococcus aureus* genomics and the impact of horizontal gene transfer. *Int. J. Med. Microbiol.* 304, 103–109. doi: 10.1016/j.ijmm.2013.11.010

Liu, H., Wang, J., Zeng, H., Liu, X., Jiang, W., Wang, Y., et al. (2021). RPA-Cas12a-FS: a frontline nucleic acid rapid detection system for food safety based on CRISPR-Cas12a combined with recombinase polymerase amplification. *Food Chem.* 334, 127608. doi: 10.1016/j.foodchem.2020.127608

Liu, J., Chen, D., Peters, B. M., Li, L., Li, B., Xu, Z., et al. (2016). Staphylococcal chromosomal cassettes mec (SCCmec): a mobile genetic element in methicillin-resistant *Staphylococcus aureus*. *Microb. Pathog.* 101, 56–67. doi: 10.1016/j.micpath.2016.10.028

Luo, K., Shao, F., Kamara, K. N., Chen, S., Zhang, R., Duan, G., et al. (2018). Molecular characteristics of antimicrobial resistance and virulence determinants of *Staphylococcus aureus* isolates derived from clinical infection and food. *J. Clin. Lab. Anal.* 32, e22456. doi: 10.1002/jcla.22456

Malachowa, N., and DeLeo, F. R. (2010). Mobile genetic elements of *Staphylococcus aureus*. *Cell Mol. Life Sci.* 67, 3057–3071. doi: 10.1007/s00018-010-0389-4

Mao, T., Zhai, H., Duan, G., and Yang, H. (2019). Patterns of drug-resistant bacteria in a general hospital, China, 2011-2016. *Pol. J. Microbiol.* 68, 225–232. doi: 10.33073/pjm-2019-024

Matsuda, K. (2017). PCR-based detection methods for single-nucleotide polymorphism or mutation: real-time PCR and its substantial contribution toward technological refinement. *Adv. Clin. Chem.* 80, 45–72. doi: 10.1016/bs.acc.2016.11.002

Maurer, J. J. (2011). Rapid detection and limitations of molecular techniques. *Annu. Rev. Food Sci. Technol.* 2, 259–279. doi: 10.1146/annurev.food.080708.100730

Miragaia, M. (2018). Factors contributing to the evolution of mecA-mediated β-lactam resistance in staphylococci: update and new insights from whole genome sequencing (WGS). *Front. Microbiol.* 9, 2723. doi: 10.3389/fmicb.2018.02723

Myhrvold, C., Freije, C. A., Gootenberg, J. S., Abudayyeh, O. O., Metsky, H. C., Durbin, A. F., et al. (2018). Field-deployable viral diagnostics using CRISPR-Cas13. *Science* 360, 444–448. doi: 10.1126/science.aas8836

Palavecino, E. L. (2020). Rapid methods for detection of MRSA in clinical specimens. *Methods Mol. Biol.* 2069, 29–45. doi: 10.1007/978-1-4939-9849-4_2

Peacock, S. J., and Paterson, G. K. (2015). Mechanisms of methicillin resistance in *Staphylococcus aureus*. *Annu. Rev. Biochem.* 84, 577–601. doi: 10.1146/annurev-biochem-060614-034516

Peng, L., Zhou, J., Yin, L., Man, S., and Ma, L. (2020). Integration of logic gates to CRISPR/Cas12a system for rapid and sensitive detection of pathogenic bacterial genes. *Anal. Chim. Acta* 1125, 162–168. doi: 10.1016/j.aca.2020.05.017

Pinho, M. G., de Lencastre, H., and Tomasz, A. (2001). An acquired and a native penicillin-binding protein cooperate in building the cell wall of drug-resistant staphylococci. *Proc. Natl. Acad. Sci. U. S. A.* 98, 10886–10891. doi: 10.1073/pnas.191260798

Qian, S., Chen, Y., Xu, X., Peng, C., Wang, X., Wu, H., et al. (2022). Advances in amplification-free detection of nucleic acid: CRISPR/Cas system as a powerful tool. *Anal. Biochem.* 643, 114593. doi: 10.1016/j.ab.2022.114593

Sanchini, A. (2022). Recent developments in phenotypic and molecular diagnostic methods for antimicrobial resistance detection in *Staphylococcus aureus*: a narrative review. *Diagnostics.* 12, 208. doi: 10.3390/diagnostics12010208

Shore, A. C., Rossney, A. S., Brennan, O. M., Kinnevey, P. M., Humphreys, H., Sullivan, D. J., et al. (2011). Characterization of a novel arginine catabolic mobile element (ACME) and staphylococcal chromosomal cassette mec composite island with significant homology to Staphylococcus epidermidis ACME type II in methicillin-resistant *Staphylococcus aureus* genotype ST22-MRSA-IV. *Antimicrob. Agents Che Mother.* 55, 1896–1905. doi: 10.1128/AAC.01756-10

Smeltzer, M. S., Gillaspy, A. F., Pratt, F. L., Jr., Thames, M. D., and Iandolo, J. J. (1997). Prevalence and chromosomal map location of *Staphylococcus aureus* adhesin genes. *Gene* 196, 249–259. doi: 10.1016/S0378-1119(97)00237-0

Suea-Ngam, A., Howes, P. D., and deMello, A. J. (2021). An amplification-free ultra-sensitive electrochemical CRISPR/Cas biosensor for drug-resistant bacteria detection. *Chem. Sci.* 12, 12733–12743. doi: 10.1039/D1SC02197D

Swarts, D. C., and Jinek, M. (2019). Mechanistic insights into the cis- and trans-acting DNase activities of Cas12a. *Mol. Cell* 73, 589–600.e584. doi: 10.1016/j.molcel.2018.11.021

Turner, N. A., Sharma-Kuinkel, B. K., Maskarinec, S. A., Eichenberger, E. M., Shah, P. P., Carugati, M., et al. (2019). Methicillin-resistant *Staphylococcus aureus*: an overview of basic and clinical research. *Nat. Rev. Microbiol.* 17, 203–218. doi: 10.1038/s41579-018-0147-4

van Belkum, A., and Rochas, O. (2018). Laboratory-based and point-of-care testing for MSSA/MRSA detection in the age of whole genome sequencing. *Front. Microbiol.* 9, 1437. doi: 10.3389/fmicb.2018.01437

Wei, J. (2021). Accurate and sensitive analysis of *Staphylococcus aureus* through CRISPR-Cas12a based recycling signal amplification cascades for early diagnosis of skin and soft tissue infections. *J. Microbiol. Methods* 183, 106167. doi: 10.1016/j.mimet.2021.106167

Xu, L., Dai, Q., Shi, Z., Liu, X., Gao, L., Wang, Z., et al. (2020). Accurate MRSA identification through dual-functional aptamer and CRISPR-Cas12a assisted rolling circle amplification. *J. Microbiol. Methods* 173, 105917. doi: 10.1016/j.mimet.2020.105917

Yin, L., Man, S., Ye, S., Liu, G., and Ma, L. (2021). CRISPR-Cas based virus detection: recent advances and perspectives. *Biosens. Bioelectron.* 193, 113541. doi: 10.1016/j.bios.2021.113541

Zhou, J., Yin, L., Dong, Y., Peng, L., Liu, G., Man, S., et al. (2020). CRISPR-Cas13a based bacterial detection platform: sensing pathogen *Staphylococcus aureus* in food samples. *Anal. Chim. Acta* 1127, 225–233. doi: 10.1016/j.aca.2020.06.041

Conflict of Interest: The authors declare that the research was conducted in the absence of any commercial or financial relationships that could be construed as a potential conflict of interest.

frontiers | Frontiers in Microbiology

ORIGINAL RESEARCH
published: 16 June 2022
doi: 10.3389/fmicb.2022.929241

Rapid PCR-Based Nanopore Adaptive Sequencing Improves Sensitivity and Timeliness of Viral Clinical Detection and Genome Surveillance

Yanfeng Lin[1,2†], Yan Dai[3†], Yuqi Liu[1,2†], Zhuli Ren[4†], Hao Guo[3,5†], Zhenzhong Li[3], Jinhui Li[2], Kaiying Wang[2], Lang Yang[2], Shuang Zhang[1,6], Hongbo Liu[2], Leili Jia[2], Ming Ni[1,6], Peng Li[2]* and Hongbin Song[1,2]**

[1] Academy of Military Medical Sciences, Academy of Military Sciences, Beijing, China, [2] Chinese PLA Center for Disease Control and Prevention, Beijing, China, [3] State Key Laboratory of Translational Medicine and Innovative Drug Development, Jiangsu Simcere Diagnostics Co., Ltd., Nanjing, China, [4] Changchun Veterinary Research Institute, Chinese Academy of Agricultural Sciences, Changchun, China, [5] Nanjing Simcere Medical Laboratory Science Co., Ltd., Nanjing, China, [6] Institute of Health Service and Transfusion Medicine, Beijing, China

Nanopore sequencing has been widely used for the real-time detection and surveillance of pathogens with portable MinION. Nanopore adaptive sequencing can enrich on-target sequences without additional pretreatment. In this study, the performance of adaptive sequencing was evaluated for viral genome enrichment of clinical respiratory samples. Ligation-based nanopore adaptive sequencing (LNAS) and rapid PCR-based nanopore adaptive sequencing (RPNAS) workflows were performed to assess the effects of enrichment on nasopharyngeal swab samples from human adenovirus (HAdV) outbreaks. RPNAS was further applied for the enrichment of severe acute respiratory syndrome coronavirus 2 (SARS-CoV-2) from nasopharyngeal swab samples to evaluate sensitivity and timeliness. The RPNAS increased both the relative abundance (7.87–12.86-fold) and data yield (1.27–2.15-fold) of HAdV samples, whereas the LNAS increased only the relative abundance but had no obvious enrichment on the data yield. Compared with standard nanopore sequencing, RPNAS detected the SARS-CoV-2 reads from two low-abundance samples, increased the coverage of SARS-CoV-2 by 36.68–98.92%, and reduced the time to achieve the same coverage. Our study highlights the utility of RPNAS for virus enrichment directly from clinical samples, with more on-target data and a shorter sequencing time to recover viral genomes. These findings promise to improve the sensitivity and timeliness of rapid identification and genomic surveillance of infectious diseases.

Keywords: nanopore sequencing, adaptive sequencing, human adenovirus, SARS-CoV-2, pathogen detection

OPEN ACCESS

Edited by:
Chao Zhuo,
Guangzhou Medical University, China

Reviewed by:
Qiao Fei,
Medical University of South Carolina, United States
Quanyi Wang,
Beijing Center for Disease Prevention and Control, China

***Correspondence:**
Ming Ni
niming@bmi.ac.cn
Peng Li
jiekenlee@126.com
Hongbin Song
hongbinsong@263.net

† These authors have contributed equally to this work

Specialty section:
This article was submitted to Infectious Agents and Disease, a section of the journal Frontiers in Microbiology

Received: *26 April 2022*
Accepted: *16 May 2022*
Published: *16 June 2022*

Citation:
Lin Y, Dai Y, Liu Y, Ren Z, Guo H, Li Z, Li J, Wang K, Yang L, Zhang S, Liu H, Jia L, Ni M, Li P and Song H (2022) Rapid PCR-Based Nanopore Adaptive Sequencing Improves Sensitivity and Timeliness of Viral Clinical Detection and Genome Surveillance. Front. Microbiol. 13:929241. doi: 10.3389/fmicb.2022.929241

INTRODUCTION

Infectious diseases have posed a major challenge to public health for centuries (Morens et al., 2004). Rapid and accurate pathogen detection represents the primary step of disease prevention and control. Compared with traditional next-generation sequencing (NGS), nanopore sequencing has the advantages of real-time, long read length, and portability, making it suitable for rapid

pathogen detection (Lewandowski et al., 2019). Recently, nanopore sequencing has been widely used in the field of outbreak investigations and genome surveillance [e.g., Ebola (Quick et al., 2016), Zika (Faria et al., 2016), and SARS-CoV-2 (Meredith et al., 2020)], as well as clinical infections (Gu et al., 2021). However, the high host background and low microbial content limited the application of nanopore sequencing of the clinical samples (Greninger et al., 2015). The low throughput of nanopore sequencing reduces the sensitivity of pathogen detection, making it more difficult for pathogen traceability and typing. The enrichment of target pathogens is particularly important for nanopore sequencing, and thus, a series of enrichment methods have been developed. Saponin-based removal of host nucleic acid can achieve a median 600-fold depletion of human DNA from respiratory samples, but it is only applicable to bacteria with intact cell walls (Charalampous et al., 2019). The probe hybridization capture approach (Schuele et al., 2020) and multiplex PCR amplification (Quick et al., 2017) have been applied to viral enrichment but have been restricted to certain known types of pathogens. Moreover, these methods require complicated pretreatment of the samples, which cannot meet the demands of point-of-care sequencing.

Oxford Nanopore Technologies recently launched an adaptive sequencing function by aligning the reads to the references and ejecting uninterested reads by reversing the voltage across individually selected nanopores in real-time, which could achieve a computational enrichment of on-target sequences without an additional pretreatment process (Loose et al., 2016; Bao et al., 2021). Previous studies have developed adaptive sequencing tools using a graphical processing unit base-calling (readfish) (Payne et al., 2021) or raw electrical signal mapping (UNCALLED) (Kovaka et al., 2021). Sequencing enrichment of the human genome, tumor genes, or specific species in a mock microbial community has been observed by adaptive sequencing. For human genetic diagnosis, adaptive sequencing has been used to accurately identify pathogenic structural variants (Miller et al., 2021; Stevanovski et al., 2022) and determine the structure of the small supernumerary marker chromosomes (Mariya et al., 2022). Combined with the enzymatic removal of the host background, adaptive sequencing obtained a 113.41-fold enrichment of microbial DNA in respiratory tract samples (Gan et al., 2021). Through the direct depletion of host DNA using adaptive sequencing, Marquet et al. (2022) achieved a 1.70-fold (±0.27-fold) enrichment without changing the microbial composition ratio of the samples. However, the application of adaptive sequencing for the rapid pathogen detection of infectious disease outbreaks remains lacking and requires further evaluation.

In the present study, we first performed adaptive sequencing of samples from a human adenovirus (HAdV) outbreak and evaluated the enrichment efficiency of two different workflows. The rapid PCR-based nanopore adaptive sequencing (RPNAS) workflow, which showed a better enrichment effect than the ligation-based nanopore adaptive sequencing (LNAS) workflow, was further applied to enrich severe acute respiratory syndrome coronavirus 2 (SARS-CoV-2) from respiratory samples. Our study aimed to evaluate the utility of adaptive sequencing for virus detection and genome enrichment from clinical samples.

MATERIALS AND METHODS

Sample Collection, Nucleic Acid Extraction, and Real-Time PCR Assay

The nasopharyngeal swab specimens used in this study were from the 2019 outbreak of HAdV in Hubei province, China. The nucleic acid of 10 HAdV-positive specimens was extracted and the Ct values were determined by real-time PCR (RT-PCR) in our previous study (Li et al., 2021). A total of 10 nasopharyngeal swab specimens from case-patients with COVID-19 were collected in January 2021 through routine surveillance. A 200 μl sample of each specimen was used for nucleic acid extraction using a LabServ Prefill Viral Total NA Kit (Fisher Scientific, Waltham, MA, United States) following the manufacturer's instructions. A commercial RT-PCR assay kit (BioGerm, Shanghai, China) was used to determine the SARS-CoV-2 Ct values by targeting ORF1ab and N genes, with the human RNaseP gene used as a control. All of the clinical samples used in this study were collected through routine surveillance, as no personally identifiable data were included. The ethics of the study were reviewed and supervised by the Chinese PLA Center for Disease Control and Prevention.

Nanopore Library Preparation and Sequencing of the Clinical Samples

The remnant nucleic acid of HAdV samples was used for adaptive sequencing. Two nanopore adaptive sequencing workflows were used in this study (**Supplementary Figure 1**). Samples M9 and HB204 with higher DNA concentrations were first selected for pilot evaluation. For the LNAS workflow, approximately 10–30 ng DNA was used for library preparation with a Ligation Sequencing Kit (Oxford Nanopore Technologies, Cambridge, United Kingdom). Barcodes were added with a Native Barcoding Expansion kit for each sample. The adaptor-ligated library was cleaned up with 0.8× AMPure XP beads (Beckman Coulter, Indianapolis, IN, United States). For the RPNAS workflow, approximately 3 ng DNA was used for library preparation with a Rapid PCR Barcoding Kit (Oxford Nanopore Technologies, Cambridge, United Kingdom) with the number of PCR cycles set at 25.

The prepared libraries were sequenced on a MinION with an R9.4.1 flow cell (FLO-MIN106). A desktop computer with an Intel Core i7-10700F CPU and NVIDIA GeForce RTX 2070 SUPER GPU was used, and adaptive sequencing was performed using MinKNOW (v21.05.20) with a fast-basecalling model and set as an enrichment mode with the whole HAdV-55 genome (Genbank accession number: MT806175.1) used as the reference. The channels in the flow cell were separated into two groups: channel 1–256 was set as the enriched group (adaptive sequencing) and channel 257–512 as the control group (standard sequencing). Reads were mapped to the reference genome of HAdV-55 using an in-built minimap2 (Li, 2018).

For the SARS-CoV-2 samples, reverse transcription and second-strand cDNA synthesis were performed prior to library preparation using the NEBNext Ultra II RNA First-Strand Synthesis Module and the NEBNext Ultra II Non-directional

RNA Second Strand Synthesis Module (New England BioLabs, Ipswich, MA, United States) with both random hexamers and oligo-dT primers. Synthesis products were cleaned using a 1:1 ratio of AMPure XP beads and quantified using the Qubit dsDNA HS kit (Thermo Fisher Scientific, Waltham, MA, United States). The samples were sequenced with the RPNAS workflow as described above using the SARS-CoV-2 reference genome (Genbank accession number: MN908947.3).

Bioinformatics and Statistical Analysis

For the assessment of adaptive sequencing performance, the log files for adaptive sequencing were used to discriminate the signal sent to the pore for each read in the enriched group, which included three decisions: the reserved target reads (stop receiving), the ejected non-target reads (unblock), and the reads that were aligned but could not be classified (no decision). In addition, reads generated by channels corresponding to the enriched group but not recorded in the log file were defined as non-adaptive reads. The classification of decisions was then merged with more read details, such as read-id, sequencing time, read length, and channel location in the sequencing-summary files, followed by a comparison between the enriched and control groups. The read length distributions of different decisions were visualized using a violin plot, and *p*-values were calculated with Student's *t*-test. Channels in which sequencing occurred between the intervals of adjacent time were defined as active. BAM files were processed to calculate the depth and coverage using minimap2 v2.21 and SAMtools v1.13 (Li et al., 2009) with default parameters. Statistics of the total yield, mean depth, coverage, and active channels over time were calculated in sliding windows for every 15 min. A comparison of mean depth between two groups was performed using the Wilcoxon signed-rank test. All plots and tables were created in R 4.1.2.

RESULTS

Performance of Adaptive Sequencing With the Ligation-Based Nanopore Adaptive Sequencing and Rapid PCR-Based Nanopore Adaptive Sequencing Workflows

To evaluate the effect of different workflows on adaptive sequencing, we first used sample M9 from an HAdV outbreak to enrich HAdV genomes with the LNAS workflow. Channels on the flow cell were divided into the enriched group with adaptive sequencing (channel 1–256) and the control group with standard sequencing (channel 257–512). In the 24 h sequencing of M9, MinION generated 381 MB of data with 489,633 reads. The enriched group obtained fewer data and a lower increase rate of the bases than that of the control group (9.00×10^7 vs. 2.91×10^8 bases) (**Figure 1A** and **Supplementary Table 1**). The median read length of the enriched and control groups was 417 and 596 bp ($p < 0.001$), respectively, and most of the reads were shorter than 1 kb. In the enriched group, 78.42% of reads were identified as unblocked reads with a median length of 441 bp. Non-adaptive and no decision reads constituted 20.44% and 1.09%, respectively, with shorter fragments (median length of 278 and 346 bp, respectively), and only 0.05% reads were identified as stop receiving reads with a median length of 840 bp (**Figure 1B**). A total of 142 reads were mapped to HAdV in the enriched group, whereas there were 156 reads in the control group. However, adaptive sequencing obtained an increased relative abundance of HAdV bases (0.21% in the enriched group and 0.08% in the control group). There was no promotion of the total HAdV base yield (1.90×10^5 bases in the enriched group and 2.28×10^5 bases in the control group). The mean depth of HAdV in the enriched group was slightly higher than that in the control group during the early stages of sequencing (approximately 8 h); however, no significant differences were observed after approximately 10 h of sequencing (**Figure 1C**). In addition, adaptive sequencing generated additional HAdV reads in the enriched group than that in the control group in the first 12 h, which suggested the potential for rapid pathogen detection (**Supplementary Figure 2**).

Sample HB204 was further used to evaluate the enrichment performance of the RPNAS workflow, which generated 1.09×10^6 reads with 1.95×10^9 bases in 24 h. Adaptive sequencing generated more reads in the enriched group (6.08×10^5 reads) than that in the control group (4.85×10^5 reads), but the total bases in the enriched group were much lower than that of the control group (2.11×10^8 vs. 1.74×10^9 bases) (**Figure 1D** and **Supplementary Table 1**). The median read length of the enriched group (307 bp) was much shorter than that of the control group (3,607 bp) ($p < 0.001$) due to the ejection of unwanted sequences, which lead to additional reads with a short length (**Figure 1E**).

In 24 h of sequencing, 4,397 reads (1.72×10^6 bases) and 3,411 reads (1.35×10^6 bases) were identified as HAdV in the enriched and control groups, respectively, which showed both the enrichment of relative abundance (10.48-fold) and data yield (1.27-fold) of HAdV. Moreover, the mean depth of HAdV in the enriched group was significantly higher than that in the control group through all timestamps ($p < 0.05$). However, the increasing rate of the mean depth in the enriched group decreased rapidly along the sequencing time (**Figure 1F**).

Validation of the Enrichment Effect of Nanopore Adaptive Sequencing With Nine Human Adenovirus Samples

The above results showed that the RPNAS workflow had a better enrichment effect on adaptive sequencing than the LNAS workflow. To verify the repeatability, another nine samples with different Ct values were pooled and sequenced by the LNAS and RPNAS workflow on two flow cells, which generated 3.58 and 2.70 M reads within 24 h, respectively (**Supplementary Table 1**). The median read length of the control group in the RPNAS workflow (3,415 bp) was much higher than that in the LNAS workflow (346 bp) ($p < 0.001$), whereas the read length of the enriched groups

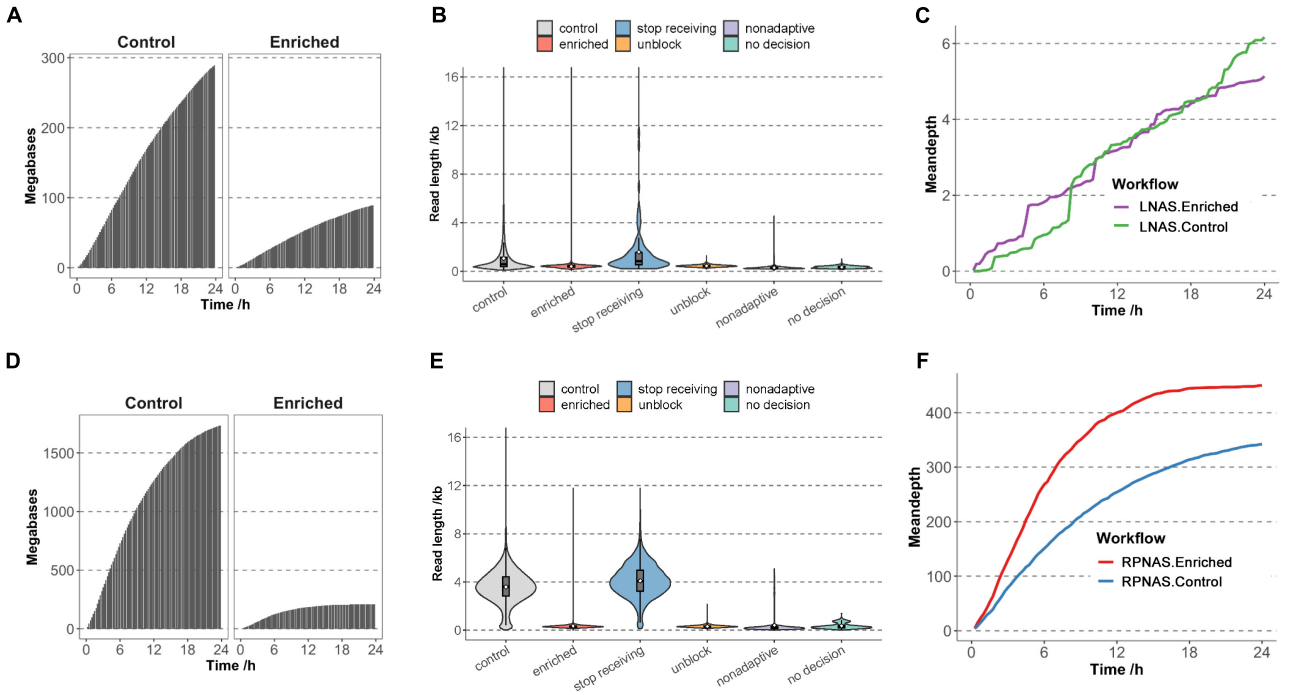

FIGURE 1 | Adaptive sequencing performance of the ligation-based nanopore adaptive sequencing (LNAS) and rapid PCR-based nanopore adaptive sequencing (RPNAS) workflows. The cumulative total base yield in the enriched and control groups over 24 h sequencing of sample M9 with the LNAS workflow **(A)** and sample HB204 with the RPNAS workflow **(D)**. The read length distribution of sample M9 with the LNAS workflow **(B)** and sample HB204 with the RPNAS workflow **(E)**. Reads in both the enriched and control groups were represented with red and gray colors, separately. Blue, orange, purple, and green colors represent stop receiving, unblock, non-adaptive, and no decision, respectively. The white dot represents the mean read length of each decision. The mean depth of human adenovirus (HAdV) in both the enriched and control groups over 24 h sequencing of sample M9 with LNAS workflow **(C)** and sample HB204 with RPNAS workflow **(F)**.

in both workflows was short (median read length < 400 bp), which was consistent with the above results in a single sample (**Figure 2A**). Furthermore, channel attrition rates were estimated by calculating changes in the active channel numbers, and the channel attrition rates of the enriched group were similar to that of the control group in the LNAS workflow but higher than the control group in the RPNAS workflow (**Figure 2B**).

Subsequently, the HAdV reads from each sample were analyzed. Sample HB205 was not included, with only one read detected in both the LNAS and RPNAS workflows. The mean depth in the enriched group increased faster than that of the control group in the RPNAS workflow, and the RPNAS workflow had a much higher mean depth of HAdV than the LNAS workflow (**Figure 3A**). Comparing the coverage of the HAdV genome at each of the different timestamps (0.25, 2, 8, and 24 h), all samples gradually approached 100% coverage over the reference, and a higher depth was observed in samples with lower Ct values for the same timestamp. A higher coverage was always observed in the enriched group in the RPNAS workflow (**Figure 3B**). The RPNAS workflow obtained a 1.50–2.15-fold enrichment of HAdV data yield and a 7.87–12.86-fold enrichment of HAdV relative abundance (**Supplementary Table 2**). However, inconspicuous enrichment was observed in the LNAS workflow with 0.24–7.08-fold enrichment of the HAdV data yield and 0.22–7.87-fold enrichment of HAdV relative abundance (**Supplementary Table 2**).

Enrichment of SARS-CoV-2 Genomes From Nasopharyngeal Swab Samples by Adaptive Sequencing

To evaluate the potential utility of adaptive sequencing on viral sequencing, 10 SARS-CoV-2 positive samples were collected and the viral genome was enriched using the RPNAS workflow. Nanopore sequencing generated 3.9×10^5–1.1×10^6 total reads per sample. In all samples, SARS-CoV-2 reads were detected in a 24 h sequencing period. Adaptive sequencing detected SARS-CoV-2 in samples S46 and S45 with 1 and 2 reads from the enriched group, whereas no SARS-CoV-2 read was detected in the control group. In sample S41, the first SARS-CoV-2 read (1 h 58 min) was detected much earlier in the enriched group compared with the control group (9 h 22 min). This finding indicated that adaptive sequencing could detect pathogens with greater sensitivity from low-abundance samples compared with standard metagenomic sequencing. The other seven samples generated 10 to 37,733 SARS-CoV-2 reads, and the enriched group obtained 1.52–2.90-fold enrichment in the data yield and 4.02–9.35-fold enrichment in the relative abundance of SARS-CoV-2 compared with the control group

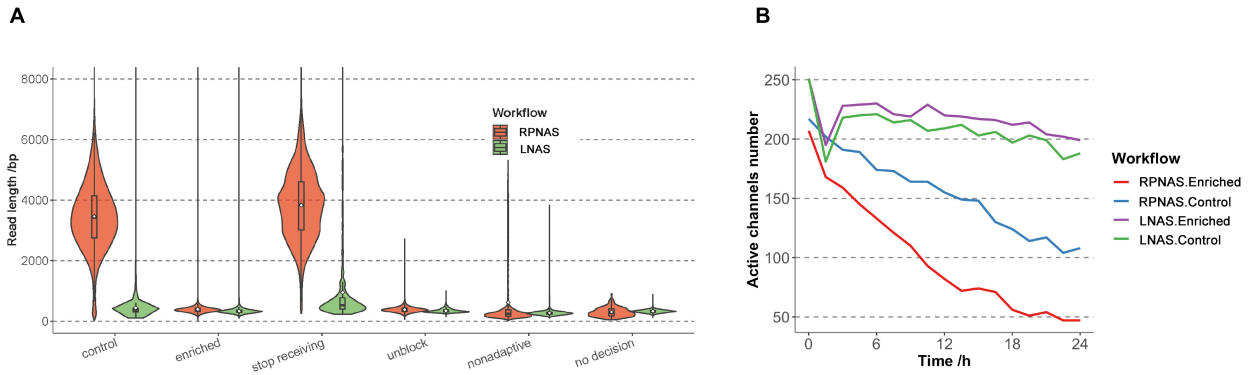

FIGURE 2 | Sequencing performance of the RPNAS and LNAS workflows with pooled samples. **(A)** Read length distributions with different decisions in two workflows. Reads in RPNAS and LNAS workflow were indicated in red and green, respectively. **(B)** Changes in the active channel numbers over 24 h of sequencing in different workflows.

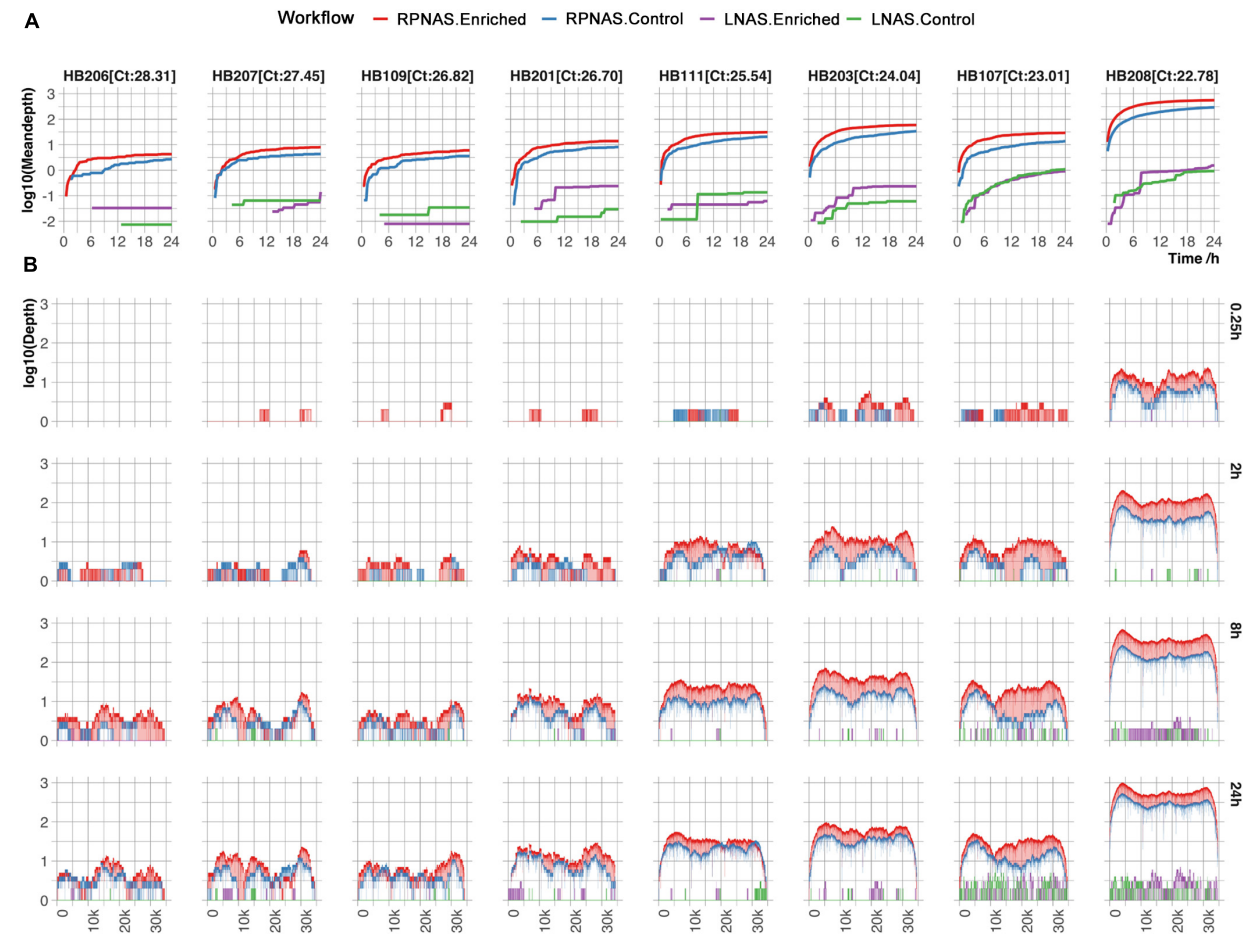

FIGURE 3 | Comparison of HAdV enrichment in eight samples with different workflows. **(A)** The mean depth of the HAdV genomes changed over 24 h of sequencing. **(B)** Coverage of HAdV genomes at the different timestamps (0.25, 2, 8, and 24 h). Red, blue, purple, and green lines represent the enriched group in RPNAS workflow, the control group in RPNAS workflow, the enriched group in LNAS workflow, and the control group in LNAS workflow, respectively.

(**Supplementary Table 3**). We further calculated the time taken to reach the maximum coverage of each sample. In samples S30, S44, S43, and S35, we observed that SARS-CoV-2 coverage in the enriched group was increased by 36.68–98.92% compared with the control group after 24 h. In samples S42, S27, and S38, the coverage of SARS-CoV-2 exceeded 95% in both the

enriched and control groups. However, the enriched group took less time to achieve the same coverage of SARS-CoV-2 compared with the control group (3.14 vs. 16.10 h on average) (**Figure 4**).

DISCUSSION

In the present study, we evaluated the utility of nanopore adaptive sequencing to enrich the viral genome directly from respiratory samples. First, we performed adaptive sequencing on HAdV positive samples to evaluate the enrichment performance of two different workflows. The LNAS workflow increased the relative abundance of HAdV, indicating a certain enrichment effect. However, adaptive sequencing only slightly increased the mean depth in the enriched group during the early stage and failed to improve the data yield. The RPNAS workflow increased both the relative abundance and data yield of HAdV. The effective enrichment of SARS-CoV-2 suggested that RPNAS could achieve rapid pathogen detection with higher sensitivity and reduce the sequencing time to recover the genome sequences of the pathogen compared with standard nanopore sequencing.

The length of DNA fragments from the samples is an important factor affecting the enrichment effect of adaptive sequencing, and libraries with longer fragment lengths showed better enrichment performance (Zhao et al., 2021; Martin et al., 2022). In this study, the RPNAS workflow, which generated a longer length of library fragments, also showed better enrichment performance than that of the LNAS workflow. This finding was likely due to long fragment PCR amplification, and size selection with magnetic beads increased the proportion of longer DNA fragments. In contrast, the low concentration of the sequencing library and short DNA fragments in the LNAS workflow may lead to inconspicuous enrichment. For RNA viruses (e.g., SARS-CoV-2), it is challenging to synthesize full-length cDNA before sequencing, which is critical for enrichment performance. Therefore, maintaining the integrity and avoiding nucleic acid degradation during sample processing may improve the enrichment effects of adaptive sequencing. Extraction of high molecular weight DNA can help obtain longer DNA fragments as much as possible, to improve the enrichment performance of adaptive sequencing (Mayjonade et al., 2016; Angthong et al., 2020; Penouilh-Suzette et al., 2020; Boughattas et al., 2021; Jones et al., 2021). Previous studies have found that the loss of active channels was faster during adaptive sequencing (Payne et al., 2021), and read rejections lead to a reduction of the overall data throughput (Martin et al., 2022; Sun et al., 2022), which may decrease the enrichment effect of adaptive sequencing. We also observed a decline in the overall data yield during adaptive sequencing. Therefore, increasing the enrichment efficiency is a key factor for the application of adaptive sequencing, which requires further optimization. The existing adaptive sequencing methods are primarily based on the alignment of nucleotide sequences or raw electrical signals, which could achieve approximately a 5-fold maximum enrichment of target genome data (Gan et al., 2021; Kipp et al., 2021; Kovaka et al., 2021; Payne et al., 2021; Wanner et al., 2021; Martin et al., 2022). A deep-learning model distinguishes human DNA from bacterial DNA with over 90% accuracy and is faster than alignment-based approaches, which could represent an

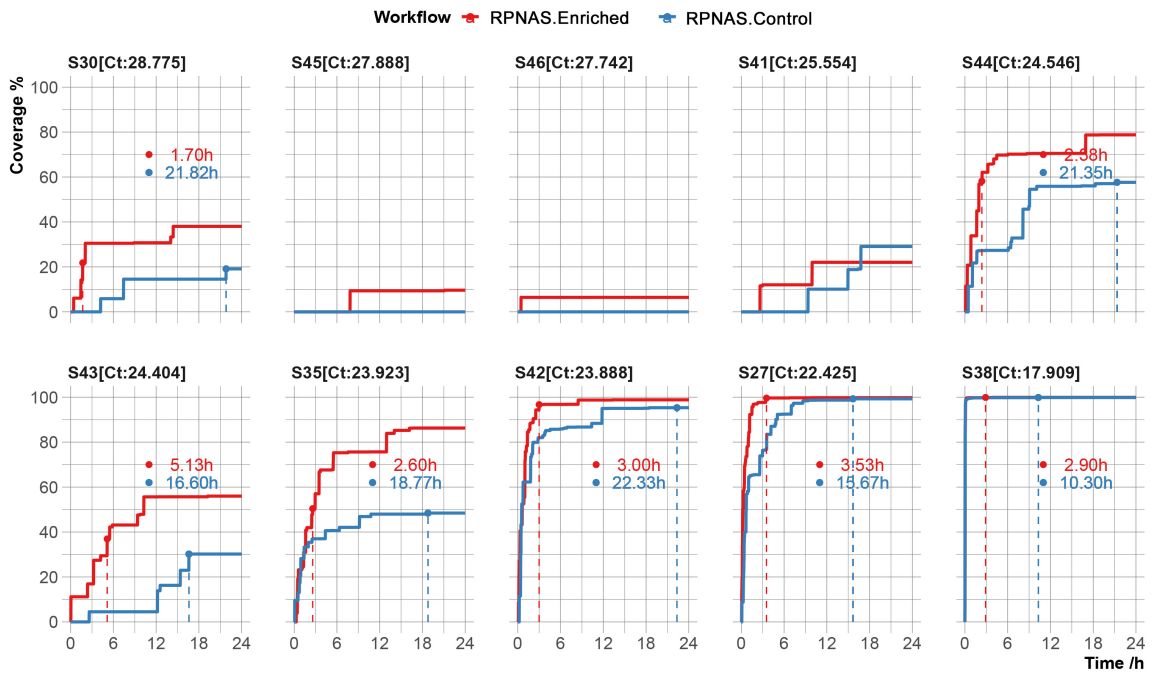

FIGURE 4 | Genome coverage of the severe acute respiratory syndrome coronavirus 2 (SARS-CoV-2) reference over 24 h in 10 samples. The time to reach the max coverage of the control group is indicated by the dotted lines.

alternative option for adaptive sequencing to increase enrichment efficiency (Bao et al., 2021).

There were some limitations associated with this study. The amount and remaining DNA in the samples used in this study were limited. Sample M9 was exhausted during the LNAS workflow, and another sample HB204 was selected for an evaluation of the RPNAS workflow. Moreover, the pathogen in all of the samples was identified and the specific reference genomes of HAdV or SARS-CoV-2 could be selected in advance. However, it is often difficult to know which pathogen is present in the samples prior to detection and makes it impossible for pathogen enrichment. A panel of multi-reference genomes could be established for the detection and enrichment of different concerned pathogens. Meanwhile, depleting the reads of the host with the human genome as the reference is an alternative strategy, which can increase microbial data output without changing the microbial composition in the sample (Marquet et al., 2022).

In conclusion, our study highlighted the utility of RPNAS for the enrichment of viral genomes from clinical samples. Adaptive sequencing could obtain more targeted genome data and shorten the time to recover viral genomes, which holds promise as an application as a point-of-care assay for pathogen detection and surveillance of infectious diseases with higher sensitivity and shorter timeliness.

DATA AVAILABILITY STATEMENT

The datasets presented in this study can be found in online repositories. The names of the repository/repositories and accession number(s) can be found below: https://www.ncbi.nlm.nih.gov/, PRJNA816258.

ETHICS STATEMENT

The studies involving human participants were reviewed and approved by the Chinese PLA Center for Disease Control and Prevention. Written informed consent for participation was not required for this study in accordance with the national legislation and the institutional requirements.

AUTHOR CONTRIBUTIONS

YFL, JL, and KW performed the experiment. YD, YQL, ZR, ZL, LY, and SZ performed the formal analysis. HL and LJ collected the samples. YFL, YD, and ZR wrote and revised the draft of the manuscript. HG, MN, PL, and HS designed the study and revised the manuscript. All authors contributed to the article and approved the submitted version.

FUNDING

This study was supported by grants from the National Major Science and Technology Project (Nos. 2021YFC2301002, 2018YFE0102100, and 2018ZX10305410-004) and the UK-China Collaboration Fund to tackle AMR [Innovate UK (TS/S00887X/1)].

SUPPLEMENTARY MATERIAL

The Supplementary Material for this article can be found online at: https://www.frontiersin.org/articles/10.3389/fmicb.2022.929241/full#supplementary-material

REFERENCES

Angthong, P., Uengwetwanit, T., Pootakham, W., Sittikankaew, K., Sonthirod, C., Sangsrakru, D., et al. (2020). Optimization of high molecular weight DNA extraction methods in shrimp for a long-read sequencing platform. *PeerJ* 8:e10340. doi: 10.7717/peerj.10340

Bao, Y., Wadden, J., Erb-Downward, J. R., Ranjan, P., Zhou, W., McDonald, T. L., et al. (2021). Squiggle net: real-time, direct classification of nanopore signals. *Genome Biol.* 22:298. doi: 10.1186/s13059-021-02511-y

Boughattas, S., Albatesh, D., Al-Khater, A., Giraldes, B. W., Althani, A. A., and Benslimane, F. M. (2021). Whole genome sequencing of marine organisms by oxford nanopore technologies: assessment and optimization of HMW-DNA extraction protocols. *Ecol. Evol.* 11, 18505–18513. doi: 10.1002/ece3.8447

Charalampous, T., Kay, G. L., Richardson, H., Aydin, A., Baldan, R., Jeanes, C., et al. (2019). Nanopore metagenomics enables rapid clinical diagnosis of bacterial lower respiratory infection. *Nat. Biotechnol.* 37, 783–792. doi: 10.1038/s41587-019-0156-5

Faria, N. R., Sabino, E. C., Nunes, M. R., Alcantara, L. C., Loman, N. J., and Pybus, O. G. (2016). Mobile real-time surveillance of Zika virus in Brazil. *Geno. Med.* 8:97. doi: 10.1186/s13073-016-0356-2

Gan, M., Wu, B., Yan, G., Li, G., Sun, L., Lu, G., et al. (2021). Combined nanopore adaptive sequencing and enzyme-based host depletion efficiently enriched microbial sequences and identified missing respiratory pathogens. *BMC Geno.* 22:732. doi: 10.1186/s12864-021-08023-0

Greninger, A. L., Naccache, S. N., Federman, S., Yu, G., Mbala, P., Bres, V., et al. (2015). Rapid metagenomic identification of viral pathogens in clinical samples by real-time nanopore sequencing analysis. *Geno. Med.* 7:99. doi: 10.1186/s13073-015-0220-9

Gu, W., Deng, X., Lee, M., Sucu, Y. D., Arevalo, S., Stryke, D., et al. (2021). Rapid pathogen detection by metagenomic next-generation sequencing of infected body fluids. *Nat. Med.* 27, 115–124. doi: 10.1038/s41591-020-1105-z

Jones, A., Torkel, C., Stanley, D., Nasim, J., Borevitz, J., and Schwessinger, B. (2021). High-molecular weight DNA extraction, clean-up and size selection for long-read sequencing. *PLoS One* 16:e0253830. doi: 10.1371/journal.pone.0253830

Kipp, E. J., Lindsey, L. L., Khoo, B. S., Faulk, C., Oliver, J. D., and Larsen, P. A. (2021). Enabling metagenomic surveillance for bacterial tick-borne pathogens using nanopore sequencing with adaptive sampling. *bioRxiv* [preprint]. doi: 10.1101/2021.08.17.456696

Kovaka, S., Fan, Y., Ni, B., Timp, W., and Schatz, M. C. (2021). Targeted nanopore sequencing by real-time mapping of raw electrical signal with UNCALLED. *Nat. Biotechnol.* 39, 431–441. doi: 10.1038/s41587-020-0731-9

Lewandowski, K., Xu, Y., Pullan, S. T., Lumley, S. F., Foster, D., Sanderson, N., et al. (2019). Metagenomic nanopore sequencing of influenza virus direct from clinical respiratory samples. *J. Clin. Microbiol.* 58:19. doi: 10.1128/jcm.00963-19

Li, H. (2018). Minimap2: pairwise alignment for nucleotide sequences. *Bioinformatics* 34, 3094–3100. doi: 10.1093/bioinformatics/bty191

Li, H., Handsaker, B., Wysoker, A., Fennell, T., Ruan, J., Homer, N., et al. (2009). The sequence alignment/map format and samtools. *Bioinformatics* 25, 2078–2079. doi: 10.1093/bioinformatics/btp352

Li, P., Wang, K., Qiu, S., Lin, Y., Xie, J., Li, J., et al. (2021). Rapid identification and metagenomics analysis of the adenovirus type 55 outbreak in hubei using real-time and high-throughput sequencing platforms. *Infect. Genet. Evol.* 93:104939. doi: 10.1016/j.meegid.2021.104939

Loose, M., Malla, S., and Stout, M. (2016). Real-time selective sequencing using nanopore technology. *Nat. Methods* 13, 751–754. doi: 10.1038/nmeth.3930

Mariya, T., Kato, T., Sugimoto, T., Miyai, S., Inagaki, H., Ohye, T., et al. (2022). Target enrichment long-read sequencing with adaptive sampling can determine the structure of the small supernumerary marker chromosomes. *J. Hum. Genet.* 67, 363–368. doi: 10.1038/s10038-021-01004-x

Marquet, M., Zöllkau, J., Pastuschek, J., Viehweger, A., Schleußner, E., Makarewicz, O., et al. (2022). Evaluation of microbiome enrichment and host DNA depletion in human vaginal samples using oxford nanopore's adaptive sequencing. *Sci. Rep.* 12:4000. doi: 10.1038/s41598-022-08003-8

Martin, S., Heavens, D., Lan, Y., Horsfield, S., Clark, M. D., and Leggett, R. M. (2022). Nanopore adaptive sampling: a tool for enrichment of low abundance species in metagenomic samples. *Genome Biol.* 23:11. doi: 10.1186/s13059-021-02582-x

Mayjonade, B., Gouzy, J., Donnadieu, C., Pouilly, N., Marande, W., Callot, C., et al. (2016). Extraction of high-molecular-weight genomic DNA for long-read sequencing of single molecules. *Biotechniques* 61, 203–205. doi: 10.2144/000114460

Meredith, L. W., Hamilton, W. L., Warne, B., Houldcroft, C. J., Hosmillo, M., Jahun, A. S., et al. (2020). Rapid implementation of SARS-CoV-2 sequencing to investigate cases of health-care associated COVID-19: a prospective genomic surveillance study. *Lancet Infect. Dis.* 20, 1263–1272. doi: 10.1016/s1473-3099(20)30562-4

Miller, D. E., Sulovari, A., Wang, T., Loucks, H., Hoekzema, K., Munson, K. M., et al. (2021). Targeted long-read sequencing identifies missing disease-causing variation. *Am. J. Hum. Genet.* 108, 1436–1449. doi: 10.1016/j.ajhg.2021.06.006

Morens, D. M., Folkers, G. K., and Fauci, A. S. (2004). The challenge of emerging and re-emerging infectious diseases. *Nature* 430, 242–249. doi: 10.1038/nature02759

Payne, A., Holmes, N., Clarke, T., Munro, R., Debebe, B. J., and Loose, M. (2021). Readfish enables targeted nanopore sequencing of gigabase-sized genomes. *Nat. Biotechno.l* 39, 442–450. doi: 10.1038/s41587-020-00746-x

Penouilh-Suzette, C., Fourré, S., Besnard, G., Godiard, L., and Pecrix, Y. (2020). A simple method for high molecular-weight genomic DNA extraction suitable for long-read sequencing from spores of an obligate biotroph oomycete. *J. Microbiol. Methods* 178:106054. doi: 10.1016/j.mimet.2020.106054

Quick, J., Grubaugh, N. D., Pullan, S. T., Claro, I. M., Smith, A. D., Gangavarapu, K., et al. (2017). Multiplex PCR method for MinION and Illumina sequencing of Zika and other virus genomes directly from clinical samples. *Nat. Protoc.* 12, 1261–1276. doi: 10.1038/nprot.2017.066

Quick, J., Loman, N. J., Duraffour, S., Simpson, J. T., Severi, E., Cowley, L., et al. (2016). Real-time, portable genome sequencing for ebola surveillance. *Nature* 530, 228–232. doi: 10.1038/nature16996

Schuele, L., Cassidy, H., Lizarazo, E., Strutzberg-Minder, K., Schuetze, S., Loebert, S., et al. (2020). Assessment of viral targeted sequence capture using nanopore sequencing directly from clinical samples. *Viruses* 12:58. doi: 10.3390/v12121358

Stevanovski, I., Chintalaphani, S. R., Gamaarachchi, H., Ferguson, J. M., Pineda, S. S., Scriba, C. K., et al. (2022). Comprehensive genetic diagnosis of tandem repeat expansion disorders with programmable targeted nanopore sequencing. *Sci. Adv.* 8:eabm5386. doi: 10.1126/sciadv.abm5386

Sun, Y., Li, X., Yang, Q., Zhao, B., Wu, Z., and Xia, Y. (2022). Genome enrichment of rare, unknown species from complicated microbiome by nanopore selective sequencing. *bioRxiv* [preprint]. doi: 10.1101/2022.02.13.480078

Wanner, N., Larsen, P. A., McLain, A., and Faulk, C. (2021). The mitochondrial genome and epigenome of the golden lion tamarin from fecal DNA using nanopore adaptive sequencing. *BMC Genom.* 22:726. doi: 10.1186/s12864-021-08046-7

Zhao, N., Cao, J., Xu, J., Liu, B., Liu, B., Chen, D., et al. (2021). Targeting RNA with next- and third-generation sequencing improves pathogen identification in clinical samples. *Adv. Sci.* 8:e2102593. doi: 10.1002/advs.202102593

Conflict of Interest: YD, HG, and ZL were employed by Jiangsu Simcere Diagnostics Co., Ltd. HG was employed by Nanjing Simcere Medical Laboratory Science Co., Ltd.

The remaining authors declare that the research was conducted in the absence of any commercial or financial relationships that could be construed as a potential conflict of interest.

Publisher's Note: All claims expressed in this article are solely those of the authors and do not necessarily represent those of their affiliated organizations, or those of the publisher, the editors and the reviewers. Any product that may be evaluated in this article, or claim that may be made by its manufacturer, is not guaranteed or endorsed by the publisher.

frontiers | Frontiers in Microbiology

REVIEW
published: 20 June 2022
doi: 10.3389/fmicb.2022.908525

Influenza A, Influenza B, and SARS-CoV-2 Similarities and Differences – A Focus on Diagnosis

Andrei Havasi[1,2], Simona Visan[3], Calin Cainap[1,2], Simona Sorana Cainap[4,5], Alin Adrian Mihaila[6] and Laura-Ancuta Pop[7]*

[1] Department of Oncology, "Iuliu Hatieganu" University of Medicine and Pharmacy, Cluj-Napoca, Romania, [2] Department of Medical Oncology, The Oncology Institute "Prof. Dr. Ion Chiricuta", Cluj-Napoca, Romania, [3] Department of Genetics, Genomics and Experimental Pathology, The Oncology Institute "Prof. Dr. Ion Chiricuta", Cluj-Napoca, Romania, [4] Pediatric Clinic No. 2, Department of Pediatric Cardiology, Emergency County Hospital for Children, Cluj-Napoca, Romania, [5] Department of Mother and Child, "Iuliu Hatieganu" University of Medicine and Pharmacy, Cluj-Napoca, Romania, [6] Faculty of Economics and Business Administration, Babes-Bolyai University, Cluj-Napoca, Romania, [7] Research Center for Functional Genomics, Biomedicine and Translational Medicine, "Iuliu Hatieganu" University of Medicine and Pharmacy, Cluj-Napoca, Romania

OPEN ACCESS

Edited by:
Bing Gu, Guangdong Provincial People's Hospital, China

Reviewed by:
Hin Fung Tsang, Hong Kong Adventist Hospital, Hong Kong SAR, China
Silvia Spoto, Policlinico Universitario Campus Bio-Medico, Italy
Israel Parra-Ortega, Federico Gómez Children's Hospital, Mexico
Lalit Batra, University of Louisville, United States

***Correspondence:**
Simona Sorana Cainap
cainap.simona@umfcluj.ro;
cainap.simona@gmail.com

Specialty section:
This article was submitted to Infectious Agents and Disease, a section of the journal Frontiers in Microbiology

Received: *30 March 2022*
Accepted: *23 May 2022*
Published: *20 June 2022*

Citation:
Havasi A, Visan S, Cainap C, Cainap SS, Mihaila AA and Pop LA (2022) Influenza A, Influenza B, and SARS-CoV-2 Similarities and Differences – A Focus on Diagnosis. Front. Microbiol. 13:908525. doi: 10.3389/fmicb.2022.908525

In late December 2019, the first cases of viral pneumonia caused by an unidentified pathogen were reported in China. Two years later, SARS-CoV-2 was responsible for almost 450 million cases, claiming more than 6 million lives. The COVID-19 pandemic strained the limits of healthcare systems all across the world. Identifying viral RNA through real-time reverse transcription-polymerase chain reaction remains the gold standard in diagnosing SARS-CoV-2 infection. However, equipment cost, availability, and the need for trained personnel limited testing capacity. Through an unprecedented research effort, new diagnostic techniques such as rapid diagnostic testing, isothermal amplification techniques, and next-generation sequencing were developed, enabling accurate and accessible diagnosis. Influenza viruses are responsible for seasonal outbreaks infecting up to a quarter of the human population worldwide. Influenza and SARS-CoV-2 present with flu-like symptoms, making the differential diagnosis challenging solely on clinical presentation. Healthcare systems are likely to be faced with overlapping SARS-CoV-2 and Influenza outbreaks. This review aims to present the similarities and differences of both infections while focusing on the diagnosis. We discuss the clinical presentation of Influenza and SARS-CoV-2 and techniques available for diagnosis. Furthermore, we summarize available data regarding the multiplex diagnostic assay of both viral infections.

Keywords: SARS-CoV-2, influenza, diagnosis, PCR diagnosis, COVID-19 influenza coinfection

INTRODUCTION

Influenza are negative-sense single-stranded RNA viruses, members of the Orthomyxoviridae family. Four influenza viruses are acknowledged within this family. Influenza A (IVA) and B (IVB) represent significant morbidity, and mortality causes in humans of all age groups and are responsible for local outbreaks and seasonal epidemics. Influenza infections are accountable

for ∼500,000 deaths yearly and infect up to a quarter of the human population worldwide (Petrova and Russell, 2018). Influenza C viruses (IVC) can infect humans but usually cause mild disease in healthy adults; however, they may cause severe lower respiratory infections in children under 2 years old. In 2011, Influenza D viruses were identified as the newest members of the Orthomyxoviridae family, and the bovine species have been identified as a reservoir of infection. Several studies demonstrated that IDV could infect and spread among humans (Liu et al., 2020). Infection-associated symptoms may vary from mild upper respiratory tract involvement characterized by fever, rhinorrhea, cough, sore throat, muscle pain, headache, and fatigue to severe, potentially lethal pneumonia and non-respiratory complications involving the heart, central nervous system, and other organs leading to multiorgan failure or exacerbation of underlying conditions (Paules and Subbarao, 2017).

Human coronaviruses (HCoV) cause various respiratory conditions such as the common cold, bronchiolitis, and pneumonia (Pene et al., 2003). Additionally, HCoVs are associated with rapid disease progression due to increased proliferation rate via nucleotide substitution and recombination (Vijgen et al., 2005). Throughout the 21st century, HCoV's have been identified in various locations worldwide and were correlated with outbreaks of deadly human pneumonia (Wu et al., 2020). The first CoV outbreak was reported in November 2002 in Foshan, China, causing severe acute respiratory syndrome (SARS-CoV) (Banerjee et al., 2019). In 2003, the outbreak spread into a global infection with a 10% mortality rate (Lee et al., 2003). In June 2012, the second pandemic caused by coronaviruses responsible for the Middle East Respiratory Syndrome (MERS-CoV) spread from Jeddah, Saudi Arabia, with a global mortality rate of 35% (de Groot et al., 2013). The third major pandemic caused by HCoV broke out in December 2019 in China's Wuhan Province. It was caused by a new homologous strain of coronavirus (CoV-2) responsible for the severe acute respiratory syndrome (SARS-CoV-2), thus causing the Coronavirus disease (COVID-19) at a global level (Zhu et al., 2020). The pandemics caused by human coronaviruses are a continuous threat to human health and the world economy due to the high and unpredictable proliferation rate, leading to catastrophic consequences (Kirtipal et al., 2020).

The evolution of the current ongoing COVID-19 pandemic shows that SARS-CoV-2 is expected to continue to pose a critical healthcare concern in the years to come. Healthcare systems are likely to confront the overlapping of SARS-CoV-2 and influenza outbreaks.

The current review aims to underline the differences and similarities that these viruses share to provide a better understanding of pathogenesis, clinical manifestations, and treatment, focusing on the diagnosis of these infections.

VIROLOGY

Influenza

Influenza viruses are 80–120 nm enveloped filamentous or spherical, negative-sense single-stranded RNA viruses with a segmented genome containing eight RNA segments that encode several proteins, including the viral surface glycoproteins, which enable cellular entry – hemagglutinins (HA) and the release of new virions from the infected cells – neuraminidase (NA) (Cohen et al., 2013). The main three RNA segments encode the viral RNA-dependent RNA polymerase responsible for RNA synthesis and replication in the infected cells. RNA segment 5 encodes the viral nucleoprotein, which binds the RNA genome. The remaining segments encode several proteins: membrane protein (M1), non-structural protein (NS1), nuclear export protein (NEP), and several accessory viral proteins. Together these proteins regulate essential processes such as RNA segment rearrangement, viral entry and exit, virion genesis, and immune response evasion (Krammer et al., 2018). HA and NA viral proteins are located on the surface of the virus. They are the primary targets for the immune response. In the case of IVA, they allow classification in several antigenically diverse subtypes based on 16 distinct HA and nine different NA with the addition of two HA and NA identified in bats (Tong et al., 2013). However, just three HA subtypes of IVA (H1N1, H2N2, and H3N2) have caused pandemics in humans in the last century. Influenza B and C viruses do not display the same antigenic and genetic heterogeneity; IVB was recently classified into two distinct antigenic and genetic lineages, B/Victoria/2/1987 and B/Yamagata/16/1988 (Shaw et al., 2002).

Influenza viruses can spread from person to person through three mechanisms – aerosols, droplets, and contact transmission. Coughing and sneezing generate small aerosol particles that remain suspended in the air for various times ranging from minutes to hours, depending on changes in temperature and humidity. Currently, aerosol's involvement in disease spreading is controversial, but the influenza genome has been identified in aerosols through polymerase chain reactions (PCR). Therefore it is safe to assume that aerosols from infected individuals may be inhaled and deposited in the upper or lower respiratory tract leading to disease transmission (Nikitin et al., 2014). Larger droplets usually fall within 3 m of the infected individual, infecting subjects situated in this range, and are generally deposited in the upper respiratory tract. Contact transmission may also occur. The virus can remain viable for various amounts of time depending on viral concentration, surface type, and environmental factors. Particles are then transferred to the mucous membranes of the upper respiratory tract leading to infection (Killingley and Nguyen-Van-Tam, 2013).

Upon contact, the virus targets the epithelial cells of the respiratory tract and initiates viral replication. The virus binds with the epithelial cells via HA and is internalized in an endosome, leading to conformational changes in HA that eventually cause the release of viral genetic material into the cellular cytoplasm. The genetic material is then imported into the nucleus, where transcription and viral RNA replication are initiated, resulting in positive mRNA strands exported to the cytoplasm, where viral protein translation occurs with the generation of novel virions. NA enables the newly formed virions to leave the infected cell. Viral replication ends in cell death which, in conjunction with viral antigens, induces an

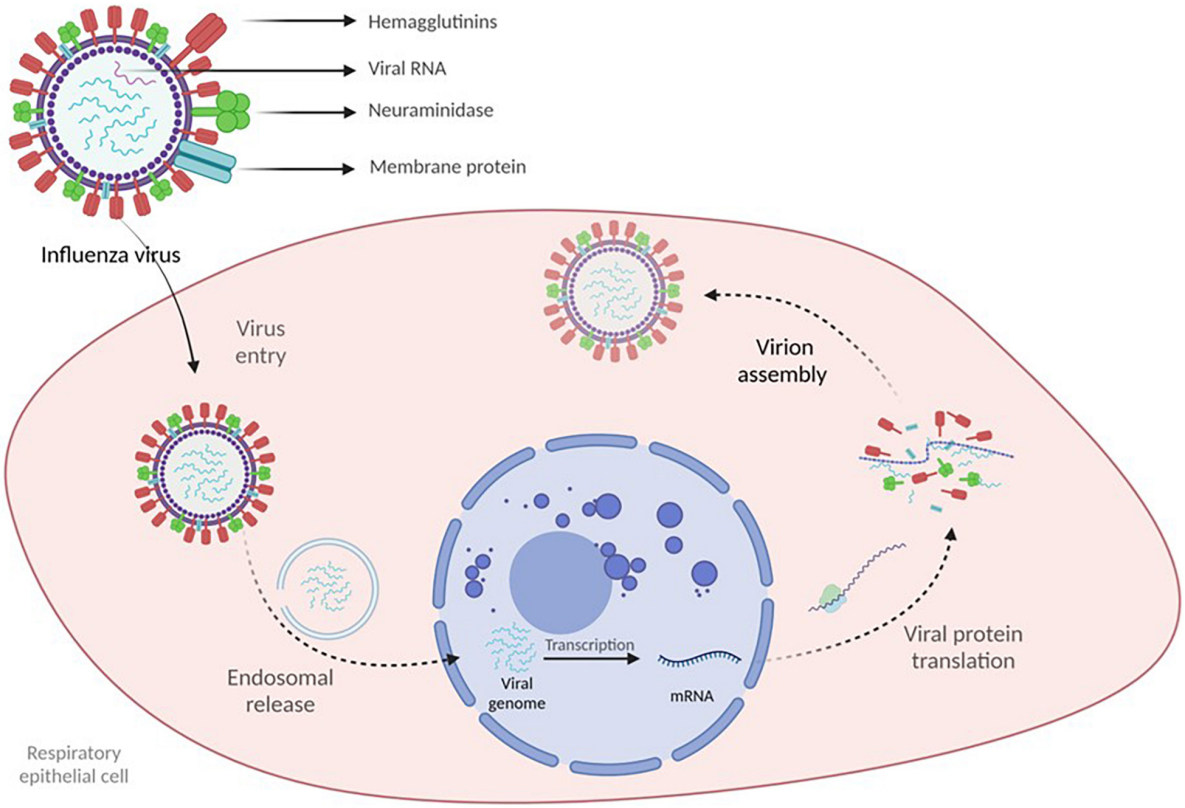

FIGURE 1 | Influenza virus structure and viral genome synthesis.

inflammatory response aiming to eliminate the virus (**Figure 1**) (Krammer et al., 2018).

Influenza viruses possess two key traits that enable immune evasion: antigenic drift and antigenic shift. Antigenic drift refers to minor antigenic changes in viral HA and NA. Point mutations result in the accumulation of amino acid alterations in the antigenic sites of HA and NA surface glycoproteins. Antibodies generated by exposure to previous antigenic variants are unable to effectively neutralize the newly formed variant leading to the immunologic selection of a new predominant virus strain (Webster and Govorkova, 2014). At arbitrary time intervals, radical changes in the influenza virus antigenicity cause widespread disease and pandemics. These significant antigenic changes are called antigenic shifts and generate a viral strain toward which the population has little or no immunity. The segmented nature of the influenza genome allows the acquirement of HA or NA segments from various animal strains of Influenza through reassortment resulting in novel virus variants that encode completely different HA or NA, causing pandemic outbreaks responsible for substantial morbidity and mortality (Bouvier and Palese, 2008; Webster and Govorkova, 2014).

SARS-CoV-2

The Coronaviridae family includes viruses with 80–220 nm length, a spherical or elliptical shape, enveloped, with peduncular prominences and rounded extremities arranged in a crown shape. The nucleocapsid has a helical symmetry with large spire loops and a monopartite genome organized in a linear mRNA, oriented in a positive sense and 27–32 kb in length (**Figure 1**). This family includes four genera: Alpha-, Beta-, Delta-, Gamma-coronavirus, and comprises more than 60 species with several viruses ranging from human to bovine, porcine, canine, feline, murine, leporid, and avian species of coronaviruses. However, a substantial number is found in bats. Members of this family of viruses infect various species, causing respiratory and digestive symptoms. Birds and bats play an essential role in spreading the coronaviruses. Some coronaviruses may cause zoonotic diseases responsible for largescale outbreaks (Perlman and Netland, 2009).

The diversity of the coronaviruses is the result of RNA polymerase inconsistency which is RNA-dependent polymerase, the increased frequency of homologous RNA recombination, and the size of the viral genome, the latter being the largest of all viral genomes with an RNA length of 27–32 kb. Due to the increasing number of coronaviruses, their adaptability to several host species, as well as the similarities between the viral genomes of a diverse range of species, it is worth considering that these viruses could be the cause of spreading zoonotic diseases such as SARS (Severe Acute Respiratory Syndrome) and MERS (Middle Eastern Respiratory Syndrome), which have recently evolved into human species (Woo et al., 2009; Rapuntean, 2019).

The SARS-CoV-2 virion contains several structural proteins such as the spike (S) protein, membrane (M) protein, envelope (E) protein, and the nucleocapsid (N) protein that binds the genome RNA into a long helical ribonucleocapside. Upon contact with the target cell, viral entry is mediated via the interaction between the S protein and the angiotensin-converting enzyme 2 (ACE2) receptors. To enter the cell, the S protein must undergo a conformational transition that is enabled through the cleaving action of 2 proteases: cathepsin L and transmembrane protease, serine 2 (TMPRSS2). TMPRSS2 is expressed on the cell membrane while cathepsin L activation occurs in the endolysosome. Thus, based on the target-cell protease location, there are two cell entry pathways for SARS-CoV-2. If the target cell displays low TMPRSS2 expression, the virus-ACE2 complex is internalized through clathrin-mediated endocytosis into endolysosomes where S-protein cleavage occurs *via* cathepsin L. If the ACE2-virus complex is formed in the presence of TMPRSS2, cleavage occurs at the cell's surface. S-protein cleavage leads to the fusion of cellular and viral membranes forming a fusion pore that enables viral RNA release into the target cell, thus enabling further RNA uncoating and replication (**Figure 2**) (Bai et al., 2021; Jackson et al., 2022).

CLINICAL PRESENTATION

Influenza

Depending on both virus and host characteristics, the clinical presentation of Influenza ranges from asymptomatic infections to a fulminant illness. Typical Influenza usually begins with a sudden onset after an incubation period of 1–2 days. Systemic symptoms dominate the initial presentation and typically consist of fever, chills, headache, myalgia, malaise, and anorexia. Headache and myalgia involving extremities or back muscles are frequently the most troublesome symptoms, and their severity often correlates with the height of the fever. Ocular symptoms consisting of ocular muscle pain caused by lateral eye movement, tearing, lacrimation, and burning sensation are often present. Respiratory symptoms are also present at disease onset and consist of dry cough, pharyngeal pain, nasal discharge, and obstruction; however, they are often overshadowed by the systemic manifestations that distinguish Influenza from other upper respiratory tract infections. Children and older adults have different initial presentations. Children and infants have a higher fever, may present with febrile seizures, severe myalgia involving calf muscles, and often display gastrointestinal symptoms. Older adults present with high fever, fatigue, and confusion, sometimes without respiratory symptoms. Fever is the main finding at physical examination, and it can be as high as 4°C within 24 h of onset. Usually, fever is continuous and lasts for three days, but it may maintain high for up to 8 days. Upon fever remission, systemic symptoms diminish. Additional findings on physical examination are flushed facies, hot, moist skin, clear nasal discharge, hyperaemic nasal and throat mucosa, and small tender cervical lymphadenopathies (Cox and Subbarao, 1999; Rothberg et al., 2008; Paules and Subbarao, 2017; Bennett et al., 2019).

SARS-CoV-2

SARS-CoV-2 infection exhibits a wide range of clinical presentations, often characterized by fever, dyspnea, lymphopenia, and lower respiratory tract infection (Nie et al., 2003). Although COVID-19 is considered mainly a viral pneumonia, the patients may also present gastrointestinal involvement such as diarrhea (30–40% of patients) caused by the active replication of SARS-CoV-2 in enterocytes (Leung et al., 2003), splenic atrophy, and gastrointestinal lymphadenopathy (To et al., 2004). In addition, infected individuals present slightly decreased platelet counts, prolonged coagulation profiles, and mildly elevated serum liver enzymes. The respiratory involvement caused by SARS-CoV-2 infection has been associated with diffuse alveolar lesions, epithelial cells proliferation, and increased macrophage infiltration. Multinucleate giant-cell infiltrates of macrophagic or epithelial origin have been associated with putative syncytium-like formation specific to most coronavirus infections. Symptoms like lymphopenia, hemophagocytosis, and white-pulp atrophy of the spleen observed in SARS-CoV-2 patients were reported to be similar to those identified in 1997 caused by the H5N1 influenza virus subtype outbreak (To et al., 2001). Although the disease may present with a wide array of clinical manifestations, some are more frequent than others. da Rosa Mesquita et al. performed a systematic review on the clinical manifestation of COVID-19 in the general population; it comprised data from 152 studies and over 41,000 patients. Six symptoms displayed higher prevalence: fever (58.66%), cough (54.52%), dyspnea (30.82%), malaise (29.75%), fatigue (28.16%), and sputum (25.33%). Neurological, dermatological manifestations, and anorexia were present in ∼20% of patients, while ∼10% had diarrhea, headache, and chest pain. Hemoptysis was the least reported symptom, only 1.65% of patients reporting hemoptysis (da Rosa Mesquita et al., 2021).

COMPLICATIONS

Influenza

The leading cause of influenza-associated mortality is the possible complications associated with infection. Two pulmonary complications are frequently associated with Influenza – primary Influenza viral pneumonia and secondary bacterial pneumonia. Primary, Influenza viral pneumonia starts with typical influenza symptoms followed in the first 24 h by rapid respiratory decompensation with severe dyspnoea, cyanosis, and hypoxemia. Critically diseased patients often develop adult respiratory distress syndrome and multiorgan dysfunction with increased mortality up to 80% of the cases (Rothberg et al., 2008; Bennett et al., 2019). Secondary, bacterial pneumonia evolves biphasic; symptoms resolve after the initial typical influenza presentation; however, fever recurs 4–14 days later and is usually associated with dyspnoea, productive cough, and consolidation on chest imaging. *Streptococcus pneumoniae, Staphylococcus aureus, Haemophilus influenzae,* other *Streptococcus* species, and other Gram-negative bacilli are the most commonly isolated pathogens from Influenza infection (Cox and Subbarao, 1999; Rothberg et al., 2008; Bennett et al., 2019). The

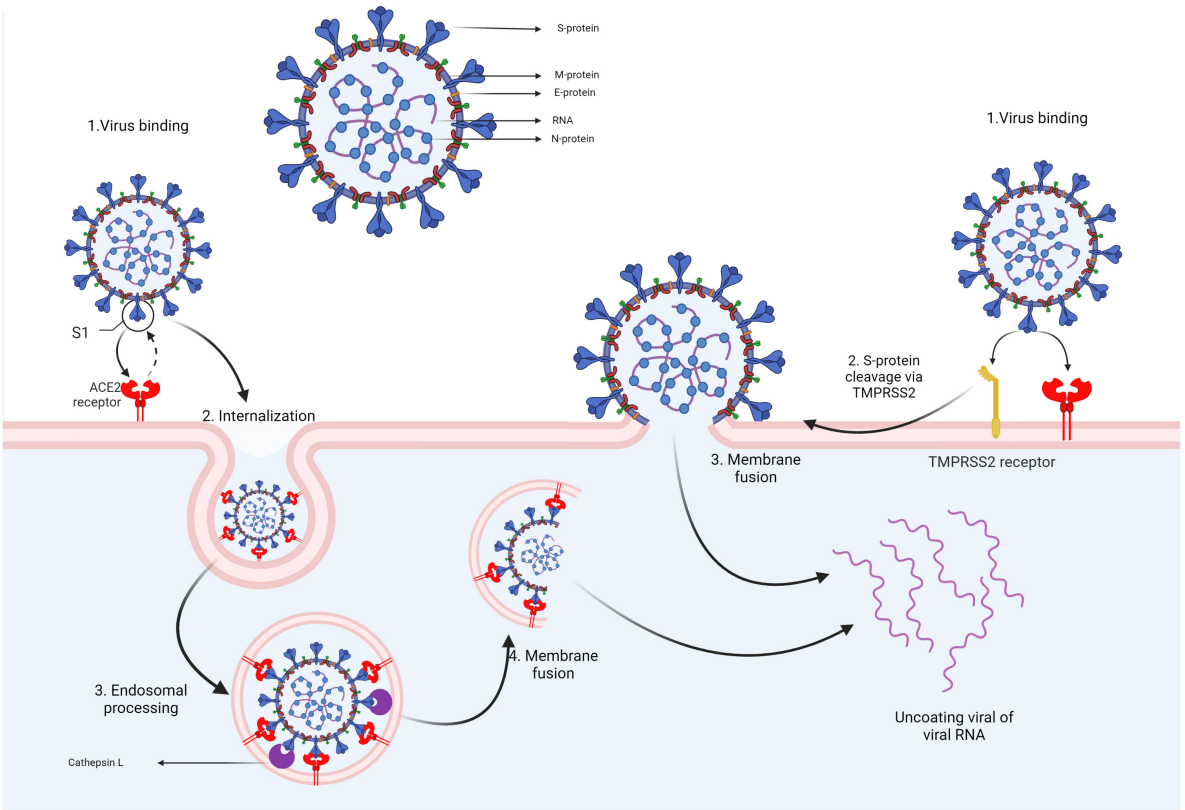

FIGURE 2 | Coronavirus structure and cell entry mechanism.

incidence of bacterial coinfection of influenza varies across studies. One metanalysis and systematic review, including 3,215 patients across 27 studies, found high heterogeneity in bacterial coinfection rates ranging from 2 to 65%; however, in 64% of all patients, bacterial coinfection incidence ranged from 11 to 35%. *S. pneumoniae* and *S. aureus* were most frequently responsible, accounting for 35% respectively, 28% of all pathogens responsible for coinfection (Klein et al., 2016). Other pulmonary complications associated with Influenza are represented by bronchiolitis, exacerbation of asthma, and chronic bronchitis. One study found influenza accountable for 25% of all underlying chronic obstructive pulmonary disease exacerbations related to upper or lower inspiratory tract infections (Rohde et al., 2003). Besides pulmonary complications, the involvement of other organs and systems has been linked with flu. Myositis occurs more frequently in children than adults and is often associated with IVB infections. Most patients will have transiently elevated serum creatine phosphokinase, but some may present with important myoglobinuria and renal failure. More than 50% of hospitalized Influenza A patients presented elevated creatine phosphokinase in one study symptoms generally resolve after 4–6 weeks (Cox and Subbarao, 1999; Rothberg et al., 2008). Several neurologic manifestations that are associated with influenza infections include Reyes syndrome, Guillain-Barre syndrome, transverse myelitis, encephalomyelitis, aseptic meningitis, and encephalitis. Central nervous involvement is more frequent in children but causes a higher morbidity rate up to 30% in adult patients (Studahl, 2003; Tsai and Baker, 2013). Influenza can also be complicated with altered renal function. Renal influenza complications include acute kidney injury, acute glomerulonephritis, minimal change disease, and acute tubulointerstitial nephritis. Acute kidney injury may occur in 18–66% of intensive care unit patients leading to renal replacement therapy in up to 22% of cases. Liver injury has also been associated with influenza as up to 1/4 of patients may present with elevated AST and ALT (Sellers et al., 2017). Influenza more commonly causes exacerbation of underlying cardiac disorders; however, both pericarditis and myocarditis have been linked to Influenza (Bennett et al., 2019; Baral et al., 2020). Influenza-associated myocarditis has been reported in 0.4–13% of critically ill patients; disease severity ranges from asymptomatic to severe disease, with most patients presenting with cardiac symptoms rather than respiratory ones (Kodama, 2010; Sellers et al., 2017). Several reports also confirmed Influenza B-associated pericarditis (Horai et al., 2010; Spoto et al., 2019).

SARS-CoV-2

Acute respiratory distress syndrome (ARDS) is one of the most frequent and potentially severe complications of SARS-CoV-2. A meta-analysis including 50,000 COVID-19 patients reported that 28.8% developed ARDS (Cao et al., 2020). ARDS causes diffuse alveolar damage responsible for hypoxemia, lung

infiltrates, and fibrosis as the disease progresses. A prolonged inflammatory response and consequent epithelial damage are responsible for reducing the diffusing capacity of the lungs present in 30% of the patients one year after moderate SARS-CoV-2 infection. Lung fibrosis has also been associated with COVID-19. Although a more extended follow-up period is necessary, based on observational data from SARS, post-COVID lung fibrosis may be estimated at 2–6% for moderate to severe illness (Gibson et al., 2020; Bazdyrev et al., 2021). Other respiratory complications are secondary bacterial and fungal coinfections and sepsis which may be present in 8% of the cases (Rawson et al., 2020).

COVID-19 is also associated with several cardiovascular complications: myocardial injury and myocarditis, acute myocardial infarction, heart failure and cardiomyopathy, arrhythmias, and thromboembolic events. Myocarditis and myocardial injury may occur in 7–17% of hospitalized COVID-19 patients and up to 1/3 of those requiring intensive care. Heart failure may be present in 24% of patients; however, more data is necessary to distinguish if this is secondary to a SARS-CoV-2 induced cardiomyopathy or is caused by exacerbation of a previously undiagnosed heart condition. Arrhythmias are present in up to 44% of intensive care patients. These symptoms are frequently secondary to hypoxia, dyselectrolytemia, and inflammatory stress (Long B. et al., 2020). COVID-19 is also associated with an increased risk for thrombotic and thromboembolic events in up to 40% of patients. SARS-CoV-2 associated thrombosis is caused by several factors such as inflammatory response leading to endothelial dysfunction, sepsis, liver injury, intravascular coagulopathy, and bedridden stasis. These lead to venous thromboembolism, myocardial infarction, and disseminated intravascular coagulation (Bikdeli et al., 2020; Long B. et al., 2020).

Neurological complications associated with COVID-19 have been reported in numerous studies. Hematogenous spread and retrograde neuronal dissemination are the primary mechanisms through which SARS-CoV-2 targets the neuronal cell leading to neurological manifestation that involve the central and peripheral nervous systems. Acute ischemic stroke has been reported in 2.1% of COVID-19 cases, followed by hemorrhagic stroke 0.4% and cerebral venous thrombosis 0.3%. Other severe neurologic complications associated with COVID-19 are meningitis, encephalitis, Guillain-Barre syndrome, Miller-Fisher syndrome, acute myelitis, and posterior reversible encephalitis syndrome. However, mild neurologic manifestations including gustatory, olfactory impairment, headache, myalgia, dizziness, and confusion were present in up to 82% of patients throughout the disease (**Figure 3**) (Favas et al., 2020; Harapan and Yoo, 2021).

Kidney involvement has been reported in COVID-19 patients. The incidence varies greatly across studies ranging from 0.5 to 46%, depending on the prevalence of preexisting chronic kidney disease and disease severity, with critically ill patients reporting a high incidence of kidney injury (Minami et al., 2020; Chan et al., 2021). A meta-analysis of 22 observational cohort studies encompassing over 17,000 COVID-19 patients found that 12.5% presented electrolyte imbalance, particularly hyperkalemia, 11% acute kidney injury, and 6.8% required renal replacement therapy (Kunutsor and Laukkanen, 2020). Acute kidney injury developed on average after nine days after admission. Age, diabetes, heart failure, and body mass index were associated with the risk and severity of acute kidney injury (Fanelli et al., 2020). Acute tubular necrosis is the most frequent histopathological finding associated whit SARS-CoV-2-related kidney involvement. Other possible mechanisms involved in COVID-19-associated kidney involvement are renal ischemia, cytokine storm, thrombotic complications, and rhabdomyolysis (Minami et al., 2020; Migliaccio et al., 2021).

DIAGNOSIS

Influenza

In most cases, diagnosis is based on clinical presentation and epidemiological probability. Clinical diagnosis provides acceptable accuracy in healthy young and middle-aged adults presenting with acute influenza-like symptoms throughout seasonal epidemics. Several studies demonstrated an 80–90% accuracy of clinical diagnosis during influenza outbreaks (Boivin et al., 2000; Monto et al., 2000; Zambon et al., 2001). The diagnostic accuracy decreases in hospitalized, older patients and children due to atypical presentations and a higher probability of infection with other pathogens (Drinka et al., 2003; Ruest et al., 2003). The symptoms of Influenza are similar to the clinical presentation of other respiratory pathogens such as adenoviruses, coronaviruses, rhinoviruses, parainfluenza virus, respiratory syncytial virus, and specific laboratory diagnostic tests are needed to confirm influenza infection. Additionally, confirmation is essential for public health policies and epidemiologic surveillance (Newton et al., 2000; Petric et al., 2006).

There is a wide array of diagnostic tests available: rapid Influenza diagnostic tests, rapid molecular assay, immunofluorescence, direct or indirect fluorescent antibody staining, RT-PCR, rapid cell culture, and viral tissue cell culture [Information on Rapid Molecular Assays, RT-PCR, and other Molecular Assays for Diagnosis of Influenza Virus Infection CDC (Centers for Disease Control and Prevention [CDC], 2021b)].

In patients with influenza-like symptoms, samples should be ideally collected within 12–36 h from disease onset, allowing antiviral treatment initiation within the recommended 48-h timeline. Viral diagnostic testing has evolved considerably from the traditional viral cell cultures that rendered results in 10–14 days to rapid diagnostic tests that can confirm the diagnosis accurately in less than 30 min (Peaper and Landry, 2014; Bennett et al., 2019).

Several factors may influence results such as antigen variations, inadequate specimen – nasopharyngeal swabs, nasal aspirates, or lower respiratory samples are recommended while others may be suboptimal (sputum, throat, and nares swabs); improper timing – collecting too early (<12 h) or too late (>72 h) from symptom onset. Transport or storage may alter testing accuracy – improper storage – freezing, or prolonged storing can reduce viral titers or promote viral degradation. Excessive dilution in the transport media can alter rapid influenza test

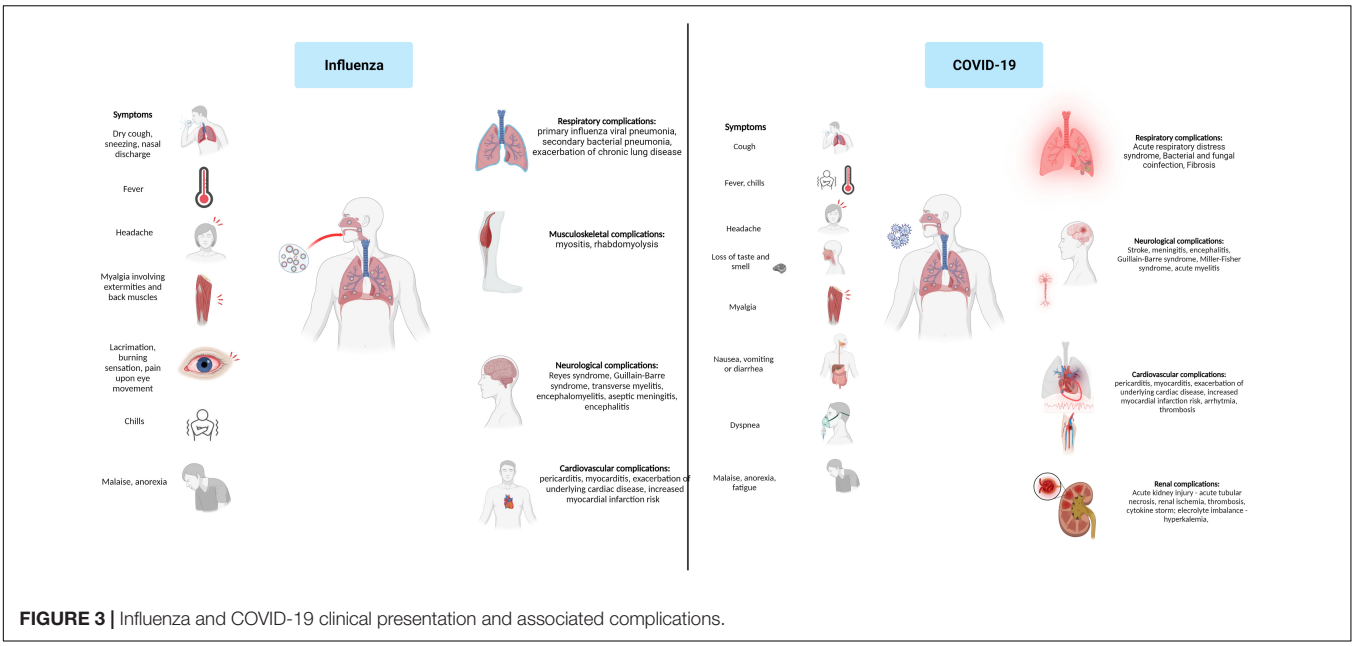

FIGURE 3 | Influenza and COVID-19 clinical presentation and associated complications.

results. Other factors that may influence the accuracy of Influenza diagnostic tests are the different sensitivity and specificity of the chosen testing method test interpretation as rapid tests require reading at a specific time, and the direct fluorescence assays require subjective assessment [Rapid Influenza Diagnostic Tests | CDC (Peaper and Landry, 2014; Uyeki et al., 2019; Centers for Disease Control and Prevention [CDC], 2021c)].

SARS-CoV-2

The management of the ongoing COVID-19 pandemic depends on providing accurate, accessible, time and cost-efficient testing. Currently, nucleic acid-based molecular diagnosis *via* real-time reverse transcription-polymerase chain reaction (RT-PCR) test is considered the golden standard for the early diagnosis of SARS-CoV-2 infection. However, this method requires adequate viral RNA concentrations in patient samples because of its high specificity. Research in qRT-PCR is focused on improving sensitivity, handling, time, and cost-efficiency (Benzigar et al., 2021). Sample source selection is a matter of debate as it may improve diagnostic efficiency. Lin et al. demonstrated higher detection rates in sputum samples than from throat swabs, 76.9% compared to 44.2% positive rates ($p = 0.001$). The SARS-CoV-2 ORF1b, E, and N genes were found to be specific to samples of human origin (Chu et al., 2020). Several laboratories developed qRT-PCR assays to detect the ORF1b and N gene and distributed these assays to improve SARS-CoV-2 detection worldwide (Sheridan, 2020). However, the fluctuations of mRNA levels in different tissues may lead to false-negative results (Feng et al., 2020). Suo et al. demonstrated that digital PCR might overcome the limitations of performing the assay in a low viral concentration setting. Nevertheless, this method has limitations regarding accessibility, cost, and lack of practical reliability (Suo et al., 2020). Alongside RT-PCR, antigen and antibody rapid testing is used to increase the current testing capacity. These rapid tests are readily available, cheap, can be used in a point of care setting, and render quick results but lack the sensitivity and specificity of nucleic acid amplification-based methods.

Sample quality is fundamental for the effective detection of SARS-CoV-2. The sample type, collection, and preprocessing play a vital part regardless of the technique. Nasopharyngeal and oropharyngeal swabs are frequently used for sample collection from the upper respiratory tract. However, these samples most often require a trained healthcare worker for specimen collection, increasing exposure risk. Saliva sampling is an alternative method because the patient can easily collect at home and provide higher detection rates compared to throat and nasal swabs (Fakheran et al., 2020). In addition, saliva sampling may facilitate the detection of both SARS-CoV-2 antigens and antibodies. One study found that saliva specimens contained more SARS-CoV-2 RNA copies than nasopharyngeal swabs, and there was less variation in nucleic acid levels throughout the clinical course of the disease. Furthermore, saliva specimens displayed higher sensitivity for SARS-CoV-2 detection in asymptomatic patients (Wyllie et al., 2020).

Sputum and bronchoalveolar lavage can also be used as samples for COVID-19 detection, with high detection rates. Blood and serum are most often used in antibody tests and tracking patients' immune responses. Timing also plays a crucial role in sample source selection, with peak viral load from symptom onset in 0–7 days for nasopharyngeal swabs and 3–7 days for sputum and saliva (Jayamohan et al., 2021).

DIAGNOSTIC METHODS

Rapid Influenza Diagnostic Tests

Rapid diagnostic tests are based on the immunologic identification of viral nucleoprotein antigens in respiratory secretions. Monoclonal antibodies target viral antigens using immunochromatographic or immunoassay techniques ensuing

visual changes that allow the qualitative diagnosis of Influenza. RIDT can distinguish influenza type A and B, however, they cannot identify specific subtypes [Rapid Influenza Diagnostic Tests | CDC (Dziąbowska et al., 2018; Centers for Disease Control and Prevention [CDC], 2021c)]. The main advantage of RIDT is that they are easy to use and provide diagnostic in a point of care setting with a sensitivity ranging from 50 to 80% across studies and a specificity of 90% (McMullen et al., 2016; Dziąbowska et al., 2018). The number of viral antigens influences the sensitivity of RIDT. Up to 104–106 infectious particles are frequently required to ensure adequate sensitivity. RIDT sensitivity is highly dependent on viral shedding and is increased in children compared to adults (Casiano-Colón et al., 2003; Sakai-Tagawa et al., 2010). Another significant limitation to RIDT performance is antigenic variation. Several studies reported a considerable drop in sensitivity (40–60%) compared to circulating strains during the 2009 H1N1 influenza A virus outbreak (Centers for Disease Control and Prevention [CDC], 2021a). The variable performance of different manufacturers and the widespread use of RIDT has led to the reclassification of RIDT by the FDA as Class II *in vitro* devices and imposed specific performance criteria for all RIDT manufacturers. Currently, rapid influenza diagnostic tests must achieve minimum standards of 80% sensitivity for Influenza A and B compared to RT-PCR. Compared to viral cultures, a 90% sensitivity for influenza A and 80% for influenza B must be reached. Furthermore, the novel FDA classification requires manufacturers to test novel emerging strains within 30 days in the case of a public health emergency (Green and StGeorge, 2018).

Rapid SARS-CoV-2 Diagnostic Tests

Antigen SARS-CoV-2 Testing

Rapid antigen diagnostic tests detect SARS-CoV-2 antigens in clinical samples collected from the respiratory tract of infected individuals. This testing method is based on the antibodies' immune response against specific SARS-CoV-2 antigens found in the specimen. Testing kits utilize various immunological detection technologies such as lateral flow sandwich immunoassay, paramagnetic microbead-based immunoassay, and chromatographic digital immunoassay (Food and Drug Administration [FDA], 2022). The viral nucleocapsid is most often used as the target antigen due to its size, abundance in infected cells, and role as an immunodominant antigen in host response (Bai et al., 2021).

The optic lateral-flow immunochromatographic assay uses gold nanoparticles (AuNPs) and colorimetric labeling to provide a rapid platform for serologic testing in a point of care setting (Parolo et al., 2013). Specific SARS-CoV-2 antigens are conjugated to AuNPs, forming anti-human IgM and IgG conjugates that can detect human SARS-CoV-2 IgG and IgM from blood or saliva samples through colorimetric labeling. The assay renders results in 20 min with 100% sensitivity and 93.3% specificity compared to RT-PCR (Huang et al., 2020). Brümmer et al. analyzed data from 133 studies evaluating 61 different rapid antigen tests pooling a sensitivity and specificity of 71.2% (95% CI 68.2–74.0) and 98.9% (95% CI 98.6–99.1); however, when considering only manufacturer's instructions conforming studies sensitivity increased to 76.3% (95% CI 73.1–79.2) (Brümmer et al., 2021). The World Health Organization (WHO) established a minimum performance requirement of $\geq$80% sensitivity and $\geq$97% specificity for antigen tests for SARS-CoV-2 diagnosis when RT-PCR testing is unavailable. Antigen testing is recommended for symptomatic individuals in the first 5–7 days after symptom onset. Their use in presymptomatic and asymptomatic cases is not recommended due to their low performance (World Health Organization [WHO], 2021).

Antibody SARS-CoV-2 Testing

Antibody synthesis against SARS-CoV-2 is the primary immune response to infection. Neutralizing antibodies are present in up to 50% of infected people by day 7 and in all infected people by day 14. Serological studies are an alternative to the diagnosis of SARS-CoV-2 by RT-PCR. Combining the RT-PCR technique with the serological testing significantly enhanced SARS-CoV-2 diagnosis. IgM levels increase in the first week after SARS-CoV-2 infection and peak after two weeks. IgG levels are detectable after one week and remain elevated for an extended time, sometimes over 48 days, and can serve as protection against reinfection (Hou et al., 2020). IgA responses occur 4 to 10 days after infection. Thus, serum IgA along with IgG and IgM, are considered COVID-19 diagnostic markers (Long Q. X. et al., 2020; Padoan et al., 2020). Antibody titers may decrease after seven days of illness. Recent studies have identified SARS-CoV-2 antibodies in saliva (Pisanic et al., 2020). Multiplex immunoassays for detecting SARS-CoV-2 antibodies have been used to determine the differences between antibody levels in saliva and serum. The simultaneous presence of antibodies in saliva and serum suggests a humoral-mediated immune response (Mahalingam et al., 2021).

Antibody testing differs concerning the types of antibodies measured: IgG, IgM, IgA, total immunoglobulins, or various combinations of the previously mentioned. Antibody assays generally target the SARS-CoV-2 nucleocapsid or spike protein. The most frequently used techniques for antibody detection are enzyme-linked immunosorbent assay (ELISA), chemiluminescence immunoassay (CLIA), and lateral flow immunoassays (Lai and Lam, 2021). Results are available in 13–45 min, depending on manufacturer and technique (Kevadiya et al., 2021). Although antibody testing provides good sensitivity and specificity, they have limited use in an acute infection setting. However, antibody testing can be used in conjuncture with antigen and nucleic acid testing to confirm the diagnosis when nucleic acid amplification and antigen tests have limited sensitivity. Antibody tests may also be used in seroprevalence studies to determine past SARS-CoV-2 exposures [Interim Guidelines for COVID-19 Antibody Testing | CDC (Safiabadi Tali et al., 2021; Centers for Disease Control and Prevention [CDC], 2022)].

Real-Time Reverse Transcriptase PCR

Influenza Reverse Transcriptase-PCR Testing

Reverse transcriptase-PCR is regarded as the current gold standard for influenza diagnosis in most countries. RT-PCR

is based on the simple principle of base pairing described by Watson and Crick. Firstly, viral RNA is reverse transcribed into complementary DNA, then the target gene is amplified using specific DNA primers and DNA polymerase. Finally, intercalating dyes or fluorescently labeled probes are added and detected by the equipment (Walper et al., 2018). Intercalating dyes bind to the amplified DNA and emit a fluorescent signal detected by the device. The main advantage of intercalating dyes is cost efficiency, however, this process has limited specificity and may lead to false-positive results (Courtney et al., 2021). Two fluorescent probes are most frequently used to diagnose Influenza: hydrolysis probes and molecular beacons. Both probes bind only specific DNA sequences allowing for increased accuracy, but they are more expensive than intercalating dyes. Hydrolysis probes are composed of a fluorophore and a quencher, which are detached *via* degradation during amplification. They have high specificity, reduced background fluorescence, and grant multiplex possibilities by using various fluorophores (Smith and Osborn, 2009). Molecular beacons consist of a fluorophore and a quencher, which are separated during amplification *via* displacement. Molecular beacons offer the same advantages as hydrolysis probes.

Additionally, they may allow allelic discrimination (Courtney et al., 2021). Time and cost are the main limitations associated with RT-PCR. In order to bypass these limitations, microwell PCR systems were designed to reduce reagent volumes from 20 to 5 μL (Ahrberg et al., 2019), and multiplex assays were developed to enable testing for multiple viruses or viral subtypes from a single sample (Dong et al., 2010).

Real-time reverse transcription-polymerase chain reaction (rRT-PCR) testing enables the detection and subtyping of influenza viral RNA from respiratory specimens *via* specific primers with high specificity and sensitivity, making it the current gold standard in influenza diagnosis (Gavin and Thomson, 2004). Several target genes are most commonly used for proper influenza virus identification *via* PCR, including but not limited to influenza type A matrix gene, hemagglutinin gene-specific for Influenza A subtypes A(H1N1)pdm09 virus, A(H3N2), former seasonal A(H1N1), the highly pathogenic avian influenza A (H5N1) virus, the avian influenza A(H7N9) virus, and other subtypes associated with zoonotic events (e.g., H9N2, H7Nx, H5Nx, and H10N8), type B influenza targeting the matrix, NP or NS genes of influenza B type-specific hemagglutinin genes. The accurate detection of Influenza *via* PCR is highly dependent on primer selection. To enable the amplification of the desired DNA region, a set of two primers are required; one primer is oriented in the $5' \rightarrow 3'$ direction, the sense strand, and the other primer should complement the minus strand, which is oriented in the $3' \rightarrow 5'$ direction, the antisense strand (Li and Brownley, 2010).

SARS-CoV-2 Reverse Transcriptase-PCR Testing

Currently, the diagnosis of SARS-CoV-2 is based on the detection of viral nucleic acids, antibodies, and proteins. Still, the real-time polymerase chain reaction (RT-PCR) remains the gold standard in diagnosing COVID-19 (Banerjee et al., 2019). Diagnosis based on nucleic acid detection is more sensitive and specific than currently available serological tests.

Nevertheless, RT-PCR testing for SARS-CoV-2 has some pitfalls that need improvement. A systematic review comprising 34 studies collecting data from 12,057 confirmed COVID-19 cases found a false-negative rate of 0.13 (95% CI 0.09–0.19); however, there was high heterogenicity between the included studies, with false-negative rates ranging from 0.018 to 0.58 (Arevalo-Rodriguez et al., 2020). Sampling timing is one of the key factors influencing false-negative results. Kucirka et al. found a false-negative rate one day before symptom onset of 67% (CI, 27–94%); this decreased to 20% (CI, 12–30%) 3 days after symptom manifestation, then started to rise again (Kucirka et al., 2020). Sample viral load also influences false-negative rates, with lower respiratory tract samples featuring higher loads than other sample sources (Abbasi-Oshaghi et al., 2020). Viral RNA denaturation or degradation may also occur due to improper sample manipulation or storage. False-negative rates can be lowered by considering clinical presentation and associating antibody testing (Teymouri et al., 2021). Additionally, to limit false-negative results, particularly in the setting of low viral loads, current guidelines recommend the simultaneous detection of at least two target SARS-CoV-2 genes (World Health Organization [WHO], 2020; Tombuloglu et al., 2022). Virus mutation rates also influence false-negative rates. Data from sequencing studies showed that SARS-CoV-2 has a moderate mutation rate of ∼two nucleotides/month. However, despite the low mutation rate, over 12,000 mutations in the SARS-CoV-2 genome have been identified (Callaway, 2020). Mutations in the primer binding site for nucleic acid amplification may hinder assay sensitivity. Several reports found that mutations in the E or N SARS-CoV-2 gene interfered with virus detection leading to false-negative results (Artesi et al., 2020; Ziegler et al., 2020; Hasan et al., 2021). To overcome this limitation, the use of primers directed at multiple target genes is recommended by current guidelines (Food and Drug Administration [FDA], 2021). Other ways to surpass the impact of new mutation reside in better primer design. Dong et al. developed a primer design strategy based on nucleic acid sequence and the three-dimensional structure of the encoded protein. Using this principle, they designed primer pairs that targeted the nucleocapsid (N) gene. Their design rendered similar sensitivity and specificity to the US and Chinese CDC-validated primers, but more importantly, performance was not influenced by frequently occurring mutations (Dong et al., 2021).

False-positive results can also decrease RT-PCR diagnostic accuracy. Misleading results may occur due to cross-contamination, inactive viral RNA remnants, detection of other coronaviruses, or technical reasons relating to primers, probes, or procedures (Mouliou and Gourgoulianis, 2021). After patient discharge, a positive RT-PCR assay is challenging in differentiating between a false-positive assay due to the shedding of inactive SARS-CoV-2 remnants, reinfection, or reactivation. Multiple studies underlined the possibility of SARS-Cov-2 reinfection or reactivation however, there is little data on accurately distinguishing the two scenarios. Tang et al. performed a systematic review that included data from studies analyzing more than 113,715 patients to solve this conundrum. They observed that if the interval between discharge and positivity is $\leq$28 days, reinfection or relapse is more plausible-

with reactivation generally occurring ≤15 days; if the time interval is 2 months, it is more likely to be reinfection, and if the time from discharge is longer than 3 months then reinfection is very likely to be the cause. Nevertheless, the most reliable way to distinguish reinfection from reactivation is to perform whole-genome sequencing to assess if the newly detected SARS-CoV-2 is a different strain (Siqueira et al., 2021; Tang et al., 2021). It has been shown that viral shedding can continue long after the immune system neutralizes the virus and is no longer infectious. Shedding duration varies across reports; one meta-analysis investigating data from 79 studies reported a mean shedding duration of 17 days with a maximum shedding in the upper respiratory tract of 83 days. No study managed to find a live virus beyond day 9 of illness despite high viral loads (Cevik et al., 2021). However, RT-PCR may detect viral RNA remnants rendering false-positive results. Thus, a differential diagnosis between reinfection and viral shedding is needed. Several approaches are available to distinguish the two: genome sequencing may be employed, a distinct SARS-CoV-2 variant would provide a definitive diagnosis of reinfection, while the identification of the same variant requires additional testing if clinical suspicion of reinfection is high. Viral load quantification – one study found that viral loads below 6.6310RNA copies/mL are associated with a less than 5% probability of isolating infectious virus (van Kampen et al., 2021). Viral cultures can also provide information in this regard – if viral cultures are negative, then viral shedding is more likely while identifying viable viruses argues for reinfection or reactivation. Clinical features may also aid in the differential diagnosis: the elapsed time from the first RT-PCR confirmation – longer time intervals being associated with a higher probability of reinfection; the presence of symptoms is also likely to suggest reinfection most patients with prolonged viral shedding are asymptomatic (European Centre for Disease Prevention and Control [ECDC], 2020; Tuan et al., 2021).

PCR virus detection is performed based on a known and relatively efficient protocol with high accuracy. However, increased mutation rates are responsible for major viral nucleic acid structure changes, thus lowering the PCR-based test's diagnostic power. In order to surpass this limitation, the use of specific primers and probes is recommended. A variety of RT-PCR assays using various primers and probes have been developed. A report by Anantharajah et al. compared the clinical performance of the primer/probe sets recommended by the WHO. A significant difference was found in SARS-CoV-2 detection between different primer/probes (Anantharajah et al., 2021). Mollaei et al. compared five primer sets' accuracy in SARS-CoV-2 detection *via* RT-PCR. Primers targeting ORF1ab, nucleocapsid (N), and RNA-dependent RNA polymerase (RdRp) genes had higher sensitivity, specificity, and positive predictive value compared to those aimed at the spike protein (S) and envelope (E) genes (Mollaei et al., 2020). Another study performed by the University of Washington Clinical Virology Lab analyzed seven different primer/probe sets. They found the primers targeting the E gene proposed by Corman et al. (2020) to be the most sensitive (Nalla et al., 2020).

Isothermic amplification techniques are an alternative to cyclic nucleic acid amplification. Simplified RT-PCR testing is available for different regions of the SARS-CoV-2 genome. The RdRp, helicase (Hel), and nucleocapsid genes are commonly targeted *via* RT-PCR, with RdRp/Hel diagnostic tests rendering higher viral RNA detection sensitivity. High-output platforms such as Cobas 6800, alongside proper sample manipulation, ensure quick and accurate COVID-19 diagnosis (Eigner et al., 2019; Zhang W. et al., 2020).

RT-PCR testing remains the gold standard for SARS-CoV-2 diagnosis. Despite high accuracy, the assay is limited by equipment and personnel requirements and prolonged procedure time. Depending on the protocol, the process is completed in 4–8 h. To overcome this limitation, automated or semi-automated high throughput platforms have been developed to analyze a large number of samples while also limiting reagents costs (Falzone et al., 2021). A different approach to overcoming RT-PCR testing limitations was the development of rapid diagnostic tests based on the RT-PCR principles. These assays provide an accurate diagnosis with minimal hands-on time in less than 1 h, thus enabling their use in a point-of-care setting. The Xpert Xpress SARS-CoV-2 assay on the Cepheid GeneXpert platform renders results in <45 min with minimal hands-on time while providing an accurate and sensitive diagnosis. One systematic review encompassing data from 14 studies and 1,647 samples found a sensitivity and specificity of 0.97 (0.96–0.98) and 0.97 (0.96–0.98) and an AUC of 0.9926 for the Xpert Xpress SARS-CoV-2 (Cao et al., 2022). Loeffelholz et al. performed a multicenter evaluation of Xpert Xpress SARS-CoV-2 accuracy compared to standard of care RT-PCR testing using 483 clinical samples. The positive agreement rate was 99.5%, while the negative agreement was 95.8%. A third nucleic acid amplification test was used to analyze the discordant results, all in favor of the Xpert assay (Loeffelholz et al., 2020). Similarly, Roche's cobas Liat SARS-CoV-2 assay provides accurate diagnosis in 20 min with high accuracy when compared to standard of care RT-PCR assays. A multicentric analysis of cobas Liat SARS-CoV-2 performance using samples from 444 patients demonstrated a 100% positive agreement rate and 97.4% negative agreement rate (Hansen et al., 2021).

However, despite promising high accuracy and significantly lower assay time, these findings need further validation in a real-world clinical practice setting. Most of these results are primarily based on remnant laboratory samples, and there is little data on their accuracy in relation to sample collection timing or patient symptom status. Prospective and comparative analysis in clinically relevant settings is needed in order to validate these assays properly. Until then, they can be considered when there is a need to make a quick decision about the patient or in situations where RT-PCR cannot be performed in a timely manner.

Multiplex Reverse Transcriptase-PCR Diagnosis of Influenza and SARS-CoV-2

Patients infected with SARS-CoV-2 can display various clinical presentations ranging from asymptomatic to severe acute respiratory distress syndrome. However, most patients present with influenza-like symptoms such as fever (99%), chills, dry cough (59%), fatigue (70%), lethargy, arthralgia, myalgia

TABLE 1 | Data on current RT-PCR multiplex detection of SARS-CoV-2, Influenza A, B, and Respiratory syncytial virus.

References	Assay	Platform	Target virus	Limit of detection	Sensitivity (%)	Specificity	Clinical sample size
Chung et al. (2021a)	BD MAX dual multiplex real-time RT-PCR panel	BD MAX	SC2	50 copies/PCR	100%	100%	205
			IFV A	100–200 copies/PCR	N/A	N/A	
			IFV B	100 copies/PCR	N/A	N/A	
			RSV	100 copies/PCR	N/A	N/A	
Kim et al. (2022)	PowerChek SARS-CoV-2, Influenza A & B Multiplex Real-time PCR Kit	PowerChek	SC2	0.16 copies/μL	97.5%	100%	147
			IFV A	0.14 copies/μL	100%	100%	
			IFV B	0.034 copies/μL	100%	100%	
Nörz et al. (2021)	SC2/InflA/InflB-UCT	Cobas6800	SC2	94.9 copies/mL^{-1}	98.1%	N/A	164
			IFV A	14.57 copies/mL	97.7%	N/A	
			IFV B	422.3 copies/mL^{-1}	100%	N/A	
Pabbaraju et al. (2021)	SC2/Flu (SARS-CoV-2/influenza A and B) assay	easyMAG, MagMAX Express 96, Hamilton STARlet	SC2	3 copies/PCR	100%	99.83%	128
			IFV A	2 copies/PCR	100%	100%	
			IFV B	2 copies/PCR	100%	98.86%	
Chung et al. (2021b)	SARS-CoV-2, influenza A/B, RSV in multiplex RT-PCR	LabTurbo AIO 48	SC2	9.4 copies/PCR	N/A	N/A	652
			IFV A	24 copies/PCR	N/A	N/A	
			IFV B	24 copies/PCR	N/A	N/A	
			RSV	24 copies/PCR	N/A	N/A	
Kim et al. (2021)	PowerChek SARS-CoV-2, Influenza A&B, RSV Multiplex Real-time PCR Kit	PowerChek	SC2	0.36 copies/μL	100%	100%	175
			IFV A	1.24 copies/μL	100%	100%	
			IFV B	0.09 copies/μL	100%	100%	
			RSV	0.63 copies/μL	93.1%	100%	
Kim et al. (2021)	Allplex™ SARS-CoV-2/FluA/FluB/RSV Assay	Allplex	SC2 -N gene	1,649.6 copies/mL	95.9%	100.0%	403
			SC2 - RdRp gene	283.5 copies/mL			
			SC2 -S gene	361.0 copies/mL			
			IFV A	4,917.3 copies/mL	100%	99.7%	
			IFV B	248.9 copies/mL	100%	100%	
			RSV	282.48 copies/mL	94.0%	100%	
	STANDARD M Flu/SARS-CoV-2 Real-time Detection Kit	STANDARD M	SC2 – E gene	1,176.4 copies/mL	95.9%	100.0%	
			SC2 - ORF1ab gene	259.7 copies/mL			
			IFV A	11,205 copies/mL	100%	99.7%	
			IFV B	578.0 copies/mL	100%	100%	
	PowerChek SARS-CoV-2, Influenza A&B Multiplex Real-time PCR Kit	PowerChek	SC2 – E gene	212.1 copies/mL	92.8%	100%	
			SC2 - ORF1ab gene	402.3 copies/mL			
			IFV A	5,661.8 copies/mL	100%	100%	
			IFV B	88.8 copies/mL	100%	100%	
Paradis et al. (2021)	MAX SARS-CoV-2/Flu	BD MAX	SC2	N/A	96.2%	100%	

(Continued)

TABLE 1 | (Continued)

References	Assay	Platform	Target virus	Limit of detection	Sensitivity (%)	Specificity	Clinical sample size
			IFV A	N/A	100%	98.9%	235
			IFV B	N/A	98.3%	100%	
Trick et al. (2021)	Rapid multiplexed screening of SARS-CoV-2/Flu	Magnetofluidic cartridge platform for automated PCR	SC2	2 copies/μL	98.1%	95.2%	130
			IFV A	2 copies/μL	87.5%	100%	
			IFV B	24 copies/μL	100%	98.2%	
Mboumba Bouassa et al. (2022)	AMPLIQUICK® Respiratory Triplex	AMPLIQUICK	SC2	N/A	97.6%	100%	442
			IFV A	N/A	97.9%	100%	
			IFV B	N/A	89.5%	100%	
			RSV	N/A	100%	100%	
Shu et al. (2021)	Influenza SARS-CoV-2 Multiplex Assay	Thermo Fisher	SC2	5 copies/PCR	100%	100%	104
			IFV A	5 copies/PCR	100%	100%	
			IFV B	5 copies/PCR	100%	100%	
Cheng et al. (2022)	Abbott Alinity m Resp-4-Plex assay	Alinity m	SC2	≤25 copies per mL	N/A	N/A	72
			IFV A	47 copies/mL	N/A	N/A	
			IFV B	36 copies/mL	N/A	N/A	
			RSV	39.8 copies/mL	N/A	N/A	
Mancini et al. (2021)	Multiplex rtRT-PCR for SC2 and seasonal flu	Roche BioRad Stratagene Rotor Gene Q Applied Biosystems Bioline	SC2	N/A	98.8%	100%	1000
			IFV A	N/A	100%	100%	
			IFV B	N/A	100%	100%	
Zhen et al. (2022)	Alinity m Resp-4-Plex Assay	Alinity m	SC2	26 copies/mL	95%	100%	100
			IFV A	36 copies/mL	100%	100%	
			IFV B	22 copies/mL	95%	100%	
			RSV	22 copies/mL	100%	100%	
	Xpert Xpress SARS-CoV-2, flu A/B, and RSV	GeneXpert Xpress	SC2	83 copies/mL	100%	100%	
			IFV A	32 copies/mL	100%	100%	
			IFV B	38 copies/mL	95%	100%	
			RSV	326 copies/mL	95%	100%	
	Cobas Liat SARS-CoV-2 and flu A/B	Cobas Liat	SC2	58 copies/mL	95%	100%	
			IFV A	77 copies/mL	100%	100%	
			IFV B	122 copies/mL	95%	100%	
Wolters et al. (2021)	Xpert Xpress SARS-CoV-2/Flu/RSV	GeneXpert Xpress	SC2	N/A	97.2%	100%	295
			IFV A	N/A	95.3%	100%	
			IFV B	N/A	95.6%	100%	
			RSV	N/A	96.1%	96.8%	

SC2, SARS-CoV-2; IFV A, Influenza A; IFV B, Influenza B; RSV, Respiratory syncytial virus.

(35%), headache, dyspnea (31%), anorexia (40%), thus making a differential diagnosis, solely based on clinical presentation, challenging (Liu and Pan, 2020; Song et al., 2020). Infection confirmation is necessary *via* real-time reverse transcription-polymerase chain reaction to establish an accurate diagnosis and ensure proper therapeutic management (Valencia, 2020).

Shu et al. developed the Centers for Disease Control and Prevention (CDC) Influenza SARS-CoV-2 Multiplex Assay to address this issue, enabling the simultaneous detection of influenza A, B, and SARS-CoV-2 from upper and lower respiratory samples. The primers used for influenza detection were identical to those used in the singleplex assays of the US Food and Drug Administration (FDA)–approved CDC Human Influenza Virus Real-Time RT-PCR Detection and Characterization Panel. The assay rendered high sensitivity and specificity; it detected Influenza A virus at 102.0, influenza B virus at 102.2, and SARS-CoV-2 at 100.3 50% tissue culture or egg infectious dose, or as few as 5 RNA copies/reaction. The assay was evaluated with viral RNA from 13 influenza A and two influenza B isolate to assess primer specificity. No cross-reactivity could be observed. Additionally, assay performance was evaluated using nucleic acids from 104 clinical samples. In all instances, the results agreed with the expected value for each specimen (Shu et al., 2021). Minjun et al. also evaluated a one-step quadruplex rRT-PCR assay to detect and differentiate SARS-CoV-2 ORF1ab and N genes, influenza type A and B. Primers targeting the matrix protein gene and the neuraminidase gene were designed to enable the detection of influenza A and B viral RNA (**Table 2**). The assay's performance was assessed using 312 clinical samples consisting of 110 nasopharyngeal swabs, 186 oropharyngeal swabs, and 16 sputum samples. Results were compared to singleplex rRT-PCR assays. Only four tested clinical samples displayed inconsistent results with the singleplex rRT-PCR assays. However, the quadruplex detected Influenza A and B RNA with 100% sensitivity and specificity, and all the results agreed with the expected outcome (Ni et al., 2021).

One study adapted a laboratory-developed multiplex RT-PCR assay for simultaneous detection of SARS-CoV-2, influenza A and influenza B on a fully automated high-throughput system, Cobas 6800 system, a fully automated sample-to-result high-throughput platform, requiring minimal hands-on time and able to perform up to 384-tests in an 8-h shift. Assay performance was assessed *via* serial dilution of quantified reference material and cell culture stocks in transport medium and evaluation of predetermined clinical samples. Custom-made primers were used for the detection of influenza A and B RNA. The assay enabled the detection of Influenza nucleic acids with 97.7% sensitivity for influenza A and 100% sensitivity for influenza B. In cross-reactivity experiments, there were no false-positive results. The assay was able to detect Influenza A H1N1 pdm09 (A/Michigan/45/2015), Influenza A H7N9 (A/Anhui/1/2013), Influenza A H5N8 (A/DE-SH/Reiherente/AR8444/2016), Influenza B Yamagata (B/Phuket/3073/2013), and Influenza B Victoria (B/Colorado/06/2017) strains (Nörz et al., 2021). A similar study also evaluated a high-throughput platform multiplex rRT-PCR for the simultaneous detection of SARS-CoV-2, influenza A, B, and respiratory syncytial virus. The BD MAX platform multiplex was validated using 205 pretested clinical samples. Results were consistent with the gold standard approved singleplex assay and accurately detected influenza A and B infections. Furthermore, the BD MAX platform shortened turnaround time to 2.5 h by running 24 samples per batch and 192–216 samples in 11 h (Chung et al., 2021a). Similarly, Pabbaraju et al. validated a multiplex rRT-PCR assay for the simultaneous detection of SARS-CoV-2, influenza A and influenza B. Detection of Influenza A and B was performed using rtRT-PCR assays targeting the matrix (M) and non-structural protein 1 (NS1) genes of influenza A and B, respectively. The assays have been developed by the CDC and approved by the FDA to diagnose seasonal Influenza A, B, H1, H3, and avian H5 serotypes. Multiplex sensitivity and specificity were evaluated in comparison to gold standard singleplex assay using 128 clinical samples and rendered a sensitivity and specificity of 100% (95% CI: 90.8–100%), (95%CI: 94.03–99.97%) for influenza A; for influenza B 100% sensitivity (95%CI: 91.96–100%) and 98.9% (95%CI: 93.8–99.97%) specificity; while for SARS-Cov-2 the multiplex assay assured a 100% (95%CI: 93.3–100%) sensitivity and 99.83% (95%CI: 99.1–100%) specificity(Pabbaraju et al., 2021).

In order to analyze currently available data on multiplex RT-PCR detection of Influenza and SARS-CoV-2, we performed a PubMed database search using [(Influenza) AND (SARS-CoV-2)] AND (Multiplex PCR). We selected articles in English. Of the initial 64 results, we selected 15 studies. We summarized the findings regarding assay limit of detection (LoD), sensitivity, specificity, target virus, and clinical validation sample data in **Table 1**.

ISOTHERMAL AMPLIFICATION TECHNIQUES

Isothermal amplification techniques are performed at a single reaction temperature under simple conditions, and therefore, they are more cost-efficient, quicker, and more energy-efficient than the classic thermal cycling procedure. Several isothermal amplification techniques have been applied in diagnosing Influenza and SARS-CoV-2, allowing an accurate diagnosis in a point of care setting and resource-limited settings.

Loop-Mediated Isothermal Amplification – Influenza

Loop-Mediated Isothermal Amplification (LAMP) uses inner and outer loop primer pairs to hybridize and amplify a specific cDNA sequence. The primer pairs amplify the target sequence through self-hybridization within the newly amplified strands resulting in dumbbell-shaped amplicons, which provide loop primer binding sites. Reverse transcriptase and DNA polymerase are contained within the reaction mixture for influenza viruses. Amplified DNA is quantified *via* fluorescent signals emitting intercalating dyes. LAMP is cost-effective; using isothermal conditions only requires a heating block for amplification, offers high sensitivity and specificity >95%, and can be used in multiplex panels. However, the main limitation associated with LAMP is primer design, a time-consuming, complex process requiring high expertise (Kubo et al., 2010; Abe et al., 2011; Mahony et al., 2013).

Loop-Mediated Isothermal Amplification – SARS-CoV-2

Loop-mediated isothermal amplification, in association with reverse transcription (RT-LAMP), is the most frequently used isothermal amplification technique for SARS-CoV-2 detection. RT-LAMP targets specific regions of the viral genome by using 4–6 primers and DNA polymerase, thus enabling the detection of ORF1ab, S, E, and N genes of the SARS-CoV-2. RT-LAMP amplifies target DNA isothermally, and results are measured photometrically using fluorescent or colorimetric dyes. Turnaround time is ∼1 h, and the limited equipment requirements alongside higher cost-efficiency make it a good candidate for accurate point of care testing (Mardian et al., 2021). Furthermore, RT-LAMP may also be performed at home. The Accessible LAMP-Enabled Rapid Test (ALERT) for SARS-CoV-2 detection is an affordable (<5 $), five-stage assay that enables viral nucleic acid detection with high sensitivity (LoD as low as 0.1–2 copies/μL) and specificity (97%). In addition, results are available in 60 min, and the flexible nature of ALERT allows the co-detection of other respiratory viruses while the easy workflow enables wide use (Bektaş et al., 2021). A meta-analysis of 33 studies encompassing 9,360-suspected SARS-CoV-2 cases compared the screening value of RT-PCR and RT-LAMP. Overall pooled sensitivity was 96% for RT-PCR and 92% for RT-LAMP. RT-PCR specificity was 100%, while RT-LAMP had a 99% specificity for the diagnosis of SARS-CoV-2. False-negative and false-positive rates for RT-LAMP were 12 and 1%, respectively (Pu et al., 2022).

Loop-Mediated Isothermal Amplification Multiplex for SARS-CoV-2 and Influenza

Lee et al. developed an RT-LAMP-based multiplex assay aiming to detect SARS-CoV-2, Influenza A, and B in a point of care setting. The assay detected viral RNA reliably with a LoD of 50 copies/μL. Saliva samples analyzed through qRT-PCR confirmed COVID-19 diagnosis in the patients that were used to validate the assay clinically. The multiplex panel was in 100% concordance with PCR testing (Lee et al., 2021). Similarly, Zhang et al. also described an RT-LAMP-based method for the multiplex detection of SARS-CoV-2 and Influenza. The assay was not only able to identify the presence of each viral RNA but managed to distinguish coinfection with multiple viruses (Zhang and Tanner, 2021).

CRISPR – Influenza

Recombinase polymerase amplification (RPA) and CRISPR-based diagnostics clustered regularly interspaced short palindromic repeats (CRISPR)-Cas (CRISPR-associated proteins) systems have been recently developed to detect influenza infections. The specific high-sensitivity enzymatic reporter unlocking (SHERLOCK) consists of isothermal RPA followed by transcription and detection of the target RNA using the Cas13 nuclease and was shown to detect the Influenza A virus with high accuracy (Freije et al., 2019). An additional CRISPR-Cas13 technique labeled Combinational Arrayed Reactions for Multiplexed Evaluation of Nucleic Acids-Cas13 (CARMEN-Cas13) was able to detect 169 human viruses simultaneously with attomolar sensitivity. Furthermore, CARMEN-Cas13 was able to identify the Influenza A virus and enable subtyping for H1–H16 and N1–N9. It also detected several drug resistance mutations in HIV and swiftly incorporated CRISP RNA to detect the causative agent of the COVID-19 pandemic; due to its highly multiplex characteristics, including high specificity and accuracy, this technique leads to a 300 fold decrease in reagent cost (Ackerman et al., 2020).

CRISPR – SARS-CoV-2

CRISPR- based detection methods have been developed for the diagnosis of SARS-CoV-2. Chen et al. combined the activation of Cas12a single-stranded deoxyribonuclease with isothermal amplification to create the DNA endonuclease-targeted CRISPR trans reporter (DETECTR) technique. DETECTR quickly and accurately detected human papillomavirus in human samples (Chen et al., 2018). Mammoth Biosciences adapted this technique to enable accurate and specific SARS-CoV-2 detection in response to the ongoing pandemic. DETECTR coupled with RT-LAMP provided high-precision results in a low-resource setting within 30 min (Ali et al., 2020). Broughton et al. compared the DETECTR RT-LAMP assay with the CDC qRT-PCR assay for SARS-CoV-2 detection; results were validated using samples from 36 COVID-19 patients and 42 samples with other respiratory viruses. DETECTR RT-LAMP rendered results in 45 min vs. 4 h for RT-PCR with a detection limit of 10 copies/μl compared to 1 copies/μl for PCR, a 95% predictive agreement and 100% negative predictive agreement (Broughton et al., 2020). The specific high-sensitivity enzymatic reporter unlocking (SHERLOCK) technique has also been adapted for SARS-CoV-2 detection (Zhang F. et al., 2020). SHERLOCK-based SARS-CoV-2 diagnosis was clinically validated using 534 nasopharyngeal and throat samples. Lateral flow and fluorescence readout SHERLOCK were compared to qRT–PCR. LoD was 42 copies/reaction. The assay was 100% specific and 96% sensitive with the fluorescence readout, while the lateral-flow readout had 86% sensitivity (Patchsung et al., 2020). Compared to the DETECTR technique, SHERLOCK has higher detection sensitivity of 10–100 copies/μl compared to the 70–300 copies/μl of the input sample. Additionally, unlike DETECTR, SHERLOCK can regulate the expression profile of genes without modifying the genome. Therefore, the flexibility, robustness and sensitivity provide an advantage for SHERLOCK (Gupta et al., 2021). A third assay developed by Azhar et al. identifies viral RNA using the Cas9 nuclease. FNCAS9 Editor Linked Uniform Detection Assay (FELUDA) combined with lateral flow readout provided accurate SARS-CoV-2 diagnosis with a 100% sensitivity and 96.7% specificity compared to qRT-PCR on 473 clinical samples (Azhar et al., 2021).

CRISPR Multiplex for SARS-CoV-2 and Influenza

Furthermore, Welch et al. developed a multiplexed microfluidic CRISPR-based platform, mCARMEN, which enabled the

TABLE 2 | SARS-CoV-2 diagnostic assays advantages and limitations.

Assay technique	Advantages	Limitations
Rapid antigen test	Assay time – min; Suitable for point of care setting use; Easy to use, visual readout; Cost-efficient;	Lower specificity and sensitivity compared to RT-PCR Low performance in asymptomatic and presymptomatic patients
Rapid antibody test	Assay time – min; Easy to use;	Not suitable for diagnosis; Can be used retrospectively; Cross-reactivity;
RT-PCR	High sensitivity & sensitivity; Capable of high throughput through designated platforms; Current gold standard; Multiplexing	Requires equipment, trained personnel, and reagents cost; Hard to implement in a point of care setting; Assay time – hours;
LAMP	High sensitivity & specificity; Suitable for point of care use; Assay time ∼1 h; Cost-efficient; Multiplexing;	Complex primer design; Higher false-positive rate compared to RT-PCR;
CRISPR	High sensitivity & specificity; Assay time < 1 h; Cost-efficient; Multiplexing;	Laks extensive validation for SARS-CoV-2;
NGS	Viral strain identification and characterization; Phylogenetic tracing; Information regarding treatment resistance, vaccine efficiency;	Requires complex equipment, highly trained personnel; Expensive; Long assay time;

diagnosis of 21 respiratory viruses, including SARS-CoV-2 and Influenza. mCARMEN was further enhanced to identify six SARS-CoV-2 variants, including Delta and Omicron. mCARMEN variant identification panel provided similarly valuable data regarding SARS-CoV-2 key mutations as next-generation sequencing (NGS) but at 5–10 times cheaper and identified the rapid emergence of Omicron variant in Massachusetts 8 days before NGS. Five hundred twenty-five clinical samples were used to assess mCARMEN performance compared to qRT-PCR. The assay was able to identify 100% of qRT-PCR positive samples and even outperformed PCR in samples exposed to RNA degradation rendering a 100% sensitivity for mCARMEN and 88% for PCR. In addition, unlike other CRISPR assays, mCARMEN was able to identify and quantify Influenza and SARS-CoV-2 copies in samples by using a combined Cas13 and Cas12 approach (Welch et al., 2022).

NEXT-GENERATION SEQUENCING

Next-Generation Sequencing of Influenza

Numerous commonly found infectious diseases are managed without ever finding the causative pathogen. One study found that in 2,259 hospitalized patients with community-acquired pneumonia, an etiologic pathogen could be identified in only 38% of cases (Jain et al., 2015). NGS may represent the key to overcoming this limitation as it has been proven to identify bacteria, viruses, fungi, and parasites directly from clinical samples, thus allowing an accurate diagnosis. Additionally, NGS was also proven to find and characterize novel pathogens (Li et al., 2021).

Next-generation sequencing (NGS) enables the simultaneous analysis of multiple samples and can be used to detect and characterize multiple agents in a single specimen. NGS eliminates the need for prior knowledge of the viral genome and has an advantage over traditional nucleic acid detection methods that require target-specific primers (Kustin et al., 2019). Additionally, NGS identifies novel viruses in the characterization of genetic variants and offers critical information regarding mutations associated with increased virulence or treatment resistance, thus improving epidemiologic surveillance and guiding treatment decisions (Graf et al., 2016; Vemula et al., 2016; O'Flaherty et al., 2018).

Zhao et al. developed a RT-PCR-NGS platform that enabled the simultaneous detection of unknown influenza infections and coinfections in a single tube assay. Assay performance was tested using 162 influenza-positive archived clinical samples. The assay was not only able to identify the influenza virus in 99.4% of the samples but also provided accurate genotyping. NGS enabled the simultaneous identification of specific influenza subtypes and provided information regarding specific mutations such as the E627K mutation in the PB2 protein of influenza A(H3N2) linked to increased virulence the S31N mutation in the M2 protein associated with treatment resistance (Zhao et al., 2016). Furthermore, Next-generation sequencing-based metagenomics and deep sequencing strategies were proven able to detect, identify, and characterize the 2009 pandemic H1N1 influenza A virus. Using the Virochip array, Greninger et al. detected the novel virus without any prior information at concentrations close to RT-PCR detection limits. The assay also enabled the *de novo* assembly of the whole 2009 H1N1 genome using 17 clinical samples (Greninger et al., 2010).

Next-generation sequencing has several drawbacks that limit its widespread use. NGS is time-consuming and requires expensive equipment and highly trained personnel (Courtney et al., 2021). However, the main limitation hindering NGS efficiency in influenza diagnosis is the low amount of viral RNA related to host and commensal nucleic acids present in the clinical sample. To bypass this limit, target-based enrichment probes have been designed, thus providing improved NGS sensitivity in viral RNA identification and analysis (O'Flaherty et al., 2018). NGS can be accomplished with several methodologies, namely sequencing-by-ligation (SOLiD technology), sequencing-by-hybridization (resequencing microarray), and sequencing-by-synthesis (Illumina, Ion Torrent) (Slatko et al., 2018). Despite limitations, NGS is the most promising approach to Influenza genome sequencing, thus enabling new pathways in understanding treatment resistance, identifying novel therapeutics, and assuring epidemiological

surveillance through the accurate identification of novel variants (Van Poelvoorde et al., 2020).

Next-Generation Sequencing of SARS-CoV-2

In late December 2019, reports of viral pneumonia caused by an unidentified pathogen were reported in Wuhan, China. NGS was employed for the identification and characterization of the novel pathogen. NGS enabled the phylogenetic analysis, revealing that the virus belongs to the subgenus Sarbecovirus, a member of the Betacoronavirus genus. Furthermore, genomic analyses led to the revelation that although SARS-CoV-2 displays high similarities to bat-SL-CoVZC45 and bat-SL-CoVZXC21, the receptor-binding domain (S1) sequence of the spike protein (S) was more similar to that of SARS-CoV, thus suggesting that SARS-CoV-2 gains entry into cells *via* the ACE-2 receptor (Lu R. et al., 2020; Zhou et al., 2020; Zhu et al., 2020). Sequencing also demonstrated the presence of a furin-like cleavage in the spike protein of SARS-CoV-2. This cleavage site, absent in other coronaviruses, mimics the furin cleavable peptide on the epithelial sodium channel α-subunit (ENaC-α). Thus SARS-CoV-2 activates the ENaC-α causing cellular electrolyte imbalance responsible for fluid accumulation in COVID-19 patients (Anand et al., 2020; Coutard et al., 2020).

Next-generation sequencing can also be applied to the patient's genome to underline particularities that may pertain to particular disease susceptibility. Ellinghaus et al. performed a genome-wide analysis on 1,610 patients with COVID-19 associated respiratory failure and found a higher risk for respiratory failure in patients with the rs11385942 insertion-deletion GA/A SNP at chromosome 3p21.31 and the rs657152 A/C SNP at chromosome 9q34.2. The association signal in chromosome 9q34.2 was located in the ABO blood group's locus and demonstrated a higher risk for A-positive and a protective effect for group O. The mutated region in chromosome 3 comprises a gene encoding Sodium/Imino-acid Transporter 1 (SIT1) which interacts with ACE-2 and the CC-motif chemokine receptor 9 (CCR9) and the C-X-C motif chemokine receptor 6 (CXCR6) that regulate pulmonary CD8 memory T-cells immune response to airway pathogens (Severe Covid-19 GWAS Group et al., 2020). The GenOMICC (Genetics of Mortality in Critical Care) study performed genome-wide associations in 2,244 critically ill COVID-19 patients. They found a significant association between low expression of interferon receptor gene IFNAR2 or high expression of tyrosine kinase 2 and severe disease. Additionally, transcriptome-wide analysis revealed that monocyte-macrophage chemotactic receptor CCR2 high expression in lung tissue was also linked to severe COVID-19 disease (Pairo-Castineira et al., 2021). The same working group later performed genome sequencing on 7,491 COVID-19 patients compared to 48,400 controls and found 22 independent variants associated with a life-threatening disease form. Variants included genes involved in interferon signaling – IL10RB, PLSCR1, myeloid cells differentiation – BCL11A, TAC4, CSF2, and mucin expression -MUC1. The group also reported the protective effect of a stop-gain mutation in chromosome 19:48703417:G:A, leading to a non-secretor FUT2 phenotype (Kousathanas et al., 2021).

Next-generation sequencing may also be employed in public health surveillance and disease control. SARS-CoV-2 genetic sequencing provides data on disease origin, global transmission, and epidemiological history. A metagenomic NGS study performed on ten newly sequenced SARS-CoV-2 genomes obtained from COVID-19 patients in Hubei combined with 136 genomes from the GISAID database could trace the virus sample's origin to the original SARS-CoV-2 haplotype found in patients living near the Huanan Seafood Wholesale Market (Chen et al., 2021). Meanwhile, Lu et al. generated 53 genomes from infected patients in the Guangdong region and demonstrated that the infections were likely to be related to travel and not local communities (Lu J. et al., 2020). Similarly, Lorruso et al. used NGS to trace infections from the Abruzzo region to a sequence originating in a sample from Northern Europe with a travel history to Italy based on the presence of the R203K and G204R mutations in the N protein (Lorusso et al., 2020).

Next-generation sequencing has been widely used to monitor the emergence of mutations and new variants (John et al., 2021). The COVID-19 Genomics United Kingdom (COG-UK) group performs periodic whole SARS-CoV-2 genome sequencing. As a result of this surveillance using NGS, they quickly identified and characterized the B.1.1.7 variant responsible for more than half of COVID-19 cases in southeast England. Genomic surveillance was also able to detect the delta variant responsible for 90% of cases in the United Kingdom. Thus, efficient genomic surveillance enables the prompt identification of new variants enabling proper public health measures and assessment of treatment efficiency (Robishaw et al., 2021). NGS also identified co-infection with other pathogens as up to 19% of COVID-19 patients may present coinfection (Moore et al., 2020; Musuuza et al., 2021). The advantages and limitations of previously discussed SARS-CoV-2 diagnostic assays are summarized in **Table 2**.

CONCLUSION

Influenza viruses infect almost a quarter of the world population worldwide. Periodic antigenic shits are responsible for the upsurge of novel variants that elude preexisting immunity and are responsible for pandemic outbreaks. Systemic and upper respiratory symptoms dominate influenza clinical presentation. Although most infections are mild, some patients develop complications that are the leading cause of death associated with influenza. Most frequently, Influenza infections are complicated with viral or bacterial pneumonia that in some patients leads to ARDS. Influenza may also cause exacerbation of underlying respiratory or cardiac disease leading to significant morbidity. Neurologic complications are rare in adults but more frequent in pediatric patients, where they are responsible for high mortality.

SARS-CoV-2 infection most often presents with flu-like symptoms, but it may display various clinical presentations often involving gastrointestinal and neurological symptoms. However, unlike influenza, a higher percentage of cases develop severe disease with high morbidity and mortality. Across reports, up

to one-third of the cases may develop ARDS. The increased and prolonged inflammatory response is responsible for late complications such as fibrosis and reduced oxygen diffusion capacity. Some degree of neurological involvement is also present in more than 80% of cases, while the prothrombotic status causes thromboembolic events in 40% of the patients.

After 2 years of an ongoing pandemic responsible for more than 6 million deaths worldwide, SARS-CoV-2 is here to stay. Despite vaccination and the ever-evolving therapeutic landscape, the high mutation rate responsible for the emergence of new variants limiting vaccine and treatment efficiency makes SARS-CoV-2 a significant public health concern. Meanwhile, lockdowns, restrictions, and the wide use of face masks limited the spread of seasonal Influenza. However, as restrictions are being lifted, influenza outbreaks will likely overlap with COVID-19, thus posing a diagnostic challenge. In this review, we covered Influenza and SARS-CoV-2 characteristics, clinical presentation while focusing on the diagnosis. RT-PCR remains the gold standard for the diagnosis of both infections. RT-PCR multiplexing panels that enable the diagnosis of Influenza and SARS-COV-2 are being developed, allowing an accurate diagnosis for patients presenting with flu-like symptoms. However, RT-PCR has several limitations. Equipment requirements and reagents cost limit their use in point-of-care settings and low-income countries. In addition, RT-PCR requires trained personnel for both sample collection and performing the procedure. Furthermore, primer selection and genetic material in clinical samples limit its accuracy. Isothermal amplification techniques like LAMP and CRISPR are being developed to answer these limitations. They promise an accurate diagnosis in a point of care setting without the need for trained personnel or expensive equipment. Rapid diagnostic tests also ease the healthcare system's strain, allowing a quick and inexpensive population screening. Novel technologies such as NGS provide insight into the virus pathogenesis and discover novel variants offering information that may guide new therapeutics and the development of more effective vaccines.

AUTHOR CONTRIBUTIONS

AH, SV, and L-AP: conceptualization and writing (original draft preparation). CC, L-AP, and AH: methodology. SV, L-AP, AH, and SC: data curation. CC, SC, and L-AP: writing (review and editing) and supervision. AH and SV: visualization. AM and CC: project administration. CC, SC, and AM: funding acquisition. All authors contributed to the article and approved the submitted version.

FUNDING

This work was supported by the grant partnership for the transfer of knowledge in biogenomics applications in oncology and related fields – BIOGENONCO, Project co-financed by FEDR through Competitiveness Operational Programme 2014–2020, contract no. 10/01.09.2016, Code: ID P_40_318, MySMIS 105774.

ACKNOWLEDGMENTS

We would like to thank the company Resident Laboratory SRL for their help with this manuscript.

REFERENCES

Abbasi-Oshaghi, E., Mirzaei, F., Farahani, F., Khodadadi, I., and Tayebinia, H. (2020). Diagnosis and treatment of coronavirus disease 2019 (COVID-19): laboratory, PCR, and chest CT imaging findings. *Int. J. Surg.* 79, 143–153. doi: 10.1016/j.ijsu.2020.05.018

Abe, T., Segawa, Y., Watanabe, H., Yotoriyama, T., Kai, S., Yasuda, A., et al. (2011). Point-of-care testing system enabling 30 min detection of influenza genes. *Lab Chip* 11:1166. doi: 10.1039/c0lc00519c

Ackerman, C. M., Myhrvold, C., Thakku, S. G., Freije, C. A., Metsky, H. C., Yang, D. K., et al. (2020). Massively multiplexed nucleic acid detection with Cas13. *Nature* 582, 277–282. doi: 10.1038/s41586-020-2279-8

Ahrberg, C. D., Lee, J. M., and Chung, B. G. (2019). Microwell array-based digital PCR for influenza virus detection. *Biochip J.* 13, 269–276. doi: 10.1007/s13206-019-3302-8

Ali, Z., Aman, R., Mahas, A., Rao, G. S., Tehseen, M., Marsic, T., et al. (2020). iSCAN: an RT-LAMP-coupled CRISPR-Cas12 module for rapid, sensitive detection of SARS-CoV-2. *Virus Res.* 288:198129. doi: 10.1016/j.virusres.2020.198129

Anand, P., Puranik, A., Aravamudan, M., Venkatakrishnan, A. J., and Soundararajan, V. (2020). SARS-CoV-2 strategically mimics proteolytic activation of human ENaC. *Elife* 9:e58603. doi: 10.7554/eLife.58603

Anantharajah, A., Helaers, R., Defour, J.-P., Olive, N., Kabera, F., Croonen, L., et al. (2021). How to choose the right real-time RT-PCR primer sets for the SARS-CoV-2 genome detection? *J. Virol. Methods* 295:114197. doi: 10.1016/j.jviromet.2021.114197

Arevalo-Rodriguez, I., Buitrago-Garcia, D., Simancas-Racines, D., Zambrano-Achig, P., Del Campo, R., Ciapponi, A., et al. (2020). False-negative results of initial RT-PCR assays for COVID-19: a systematic review. *PLoS One* 15:e0242958. doi: 10.1371/journal.pone.0242958

Artesi, M., Bontems, S., Göbbels, P., Franckh, M., Maes, P., Boreux, R., et al. (2020). A recurrent mutation at position 26340 of SARS-CoV-2 is associated with failure of the E gene quantitative reverse transcription-PCR utilized in a commercial dual-target diagnostic assay. *J. Clin. Microbiol.* 58, e01598-20. doi: 10.1128/JCM.01598-20

Azhar, M., Phutela, R., Kumar, M., Ansari, A. H., Rauthan, R., Gulati, S., et al. (2021). Rapid and accurate nucleobase detection using FnCas9 and its application in COVID-19 diagnosis. *Biosens. Bioelectron.* 183:113207. doi: 10.1016/j.bios.2021.113207

Bai, Z., Cao, Y., Liu, W., and Li, J. (2021). The SARS-CoV-2 nucleocapsid protein and its role in viral structure, biological functions, and a potential target for drug or vaccine mitigation. *Viruses* 13:1115. doi: 10.3390/v13061115

Banerjee, A., Kulcsar, K., Misra, V., Frieman, M., and Mossman, K. (2019). Bats and coronaviruses. *Viruses* 11:41. doi: 10.3390/v11010041

Baral, N., Adhikari, P., Adhikari, G., and Karki, S. (2020). Influenza myocarditis: a literature review. *Cureus* 12:e12007. doi: 10.7759/cureus.12007

Bazdyrev, E., Rusina, P., Panova, M., Novikov, F., Grishagin, I., and Nebolsin, V. (2021). Lung fibrosis after COVID-19: treatment prospects. *Pharmaceuticals* 14:807. doi: 10.3390/ph14080807

Bektaş, A., Covington, M. F., Aidelberg, G., Arce, A., Matute, T., Núñez, I., et al. (2021). Accessible LAMP-Enabled Rapid Test (ALERT) for Detecting SARS-CoV-2. *Viruses* 13:742. doi: 10.3390/v13050742

Bennett, J. E., Blaser, M. J., and Dolin, R. (2019). *Mandell, Douglas, and Bennett's Principles and Practice of Infectious Diseases*. Edn.9 Philadelphia, PA: Elsevier/Saunders.

Benzigar, M. R., Bhattacharjee, R., Baharfar, M., and Liu, G. (2021). Current methods for diagnosis of human coronaviruses: pros and cons. *Anal. Bioanal. Chem.* 413, 2311–2330. doi: 10.1007/s00216-020-03046-0

Bikdeli, B., Madhavan, M. V., Jimenez, D., Chuich, T., Dreyfus, I., Driggin, E., et al. (2020). COVID-19 and thrombotic or thromboembolic disease: implications for prevention, antithrombotic therapy, and follow-up: JACC state-of-the-art review. *J. Am. Coll. Cardiol.* 75, 2950–2973. doi: 10.1016/j.jacc.2020.04.031

Boivin, G., Hardy, I., Tellier, G., and Maziade, J. (2000). Predicting influenza infections during epidemics with use of a clinical case definition. *Clin. Infect. Dis.* 31, 1166–1169. doi: 10.1086/317425

Bouvier, N. M., and Palese, P. (2008). The biology of influenza viruses. *Vaccine* 26(Suppl. 4), D49–D53. doi: 10.1016/j.vaccine.2008.07.039

Broughton, J. P., Deng, X., Yu, G., Fasching, C. L., Servellita, V., Singh, J., et al. (2020). CRISPR-Cas12-based detection of SARS-CoV-2. *Nat. Biotechnol.* 38, 870–874. doi: 10.1038/s41587-020-0513-4

Brümmer, L. E., Katzenschlager, S., Gaeddert, M., Erdmann, C., Schmitz, S., Bota, M., et al. (2021). Accuracy of novel antigen rapid diagnostics for SARS-CoV-2: a living systematic review and meta-analysis. *PLoS Med.* 18:e1003735. doi: 10.1371/journal.pmed.1003735

Callaway, E. (2020). The coronavirus is mutating - does it matter? *Nature* 585, 174–177. doi: 10.1038/d41586-020-02544-6

Cao, X., Fang, K., Li, Y., Zhou, J., and Guo, X. (2022). The diagnostic accuracy of Xpert Xpress to SARS-CoV-2: a systematic review. *J. Virol. Methods* 301:114460. doi: 10.1016/j.jviromet.2022.114460

Cao, Y., Liu, X., Xiong, L., and Cai, K. (2020). Imaging and clinical features of patients with 2019 novel coronavirus SARS-CoV-2: a systematic review and meta-analysis. *J. Med. Virol.* 92, 1449–1459. doi: 10.1002/jmv.25822

Casiano-Colón, A. E., Hulbert, B. B., Mayer, T. K., Walsh, E. E., and Falsey, A. R. (2003). Lack of sensitivity of rapid antigen tests for the diagnosis of respiratory syncytial virus infection in adults. *J. Clin. Virol.* 28, 169–174. doi: 10.1016/S1386-6532(03)00002-7

Centers for Disease Control and Prevention [CDC] (2021a). *Evaluation of Rapid Influenza Diagnostic Tests for Detection of Novel Influenza A (H1N1) Virus — United States, 2009*. Available online at: https://www.cdc.gov/mmwr/preview/mmwrhtml/mm5830a2.htm (Accessed June 11, 2021)

Centers for Disease Control and Prevention [CDC] (2021b). *Information on Rapid Molecular Assays, RT-PCR, and other Molecular Assays for Diagnosis of Influenza Virus Infection | CDC*. Available online at: https://www.cdc.gov/flu/professionals/diagnosis/molecular-assays.htm (Accessed May 20, 2021)

Centers for Disease Control and Prevention [CDC] (2021c). *Rapid Influenza Diagnostic Tests | CDC*. Available online at: https://www.cdc.gov/flu/professionals/diagnosis/clinician_guidance_ridt.htm (Accessed June 10, 2021)

Centers for Disease Control and Prevention [CDC] (2022). *Interim Guidelines for COVID-19 Antibody Testing | CDC*. Available online at: https://www.cdc.gov/coronavirus/2019-ncov/lab/resources/antibody-tests-guidelines.html (Accessed February 17, 2022)

Cevik, M., Tate, M., Lloyd, O., Maraolo, A. E., Schafers, J., and Ho, A. (2021). SARS-CoV-2, SARS-CoV, and MERS-CoV viral load dynamics, duration of viral shedding, and infectiousness: a systematic review and meta-analysis. *Lancet. Microbe* 2, e13–e22. doi: 10.1016/S2666-5247(20)30172-5

Chan, L., Chaudhary, K., Saha, A., Chauhan, K., Vaid, A., Zhao, S., et al. (2021). AKI in hospitalized patients with COVID-19. *J. Am. Soc. Nephrol.* 32, 151–160. doi: 10.1681/ASN.2020050615

Chen, J. S., Ma, E., Harrington, L. B., Da Costa, M., Tian, X., Palefsky, J. M., et al. (2018). CRISPR-Cas12a target binding unleashes indiscriminate single-stranded DNase activity. *Science* 360, 436–439. doi: 10.1126/science.aar6245

Chen, X., Kang, Y., Luo, J., Pang, K., Xu, X., Wu, J., et al. (2021). Next-generation sequencing reveals the progression of COVID-19. *Front. Cell. Infect. Microbiol.* 11:632490. doi: 10.3389/fcimb.2021.632490

Cheng, A., Riedel, S., Arnaout, R., and Kirby, J. E. (2022). Verification of the Abbott Alinity m Resp-4-Plex assay for detection of SARS-CoV-2, influenza A/B, and respiratory syncytial virus. *Diagn. Microbiol. Infect. Dis.* 102:115575. doi: 10.1016/j.diagmicrobio.2021.115575

Chu, D. K. W., Pan, Y., Cheng, S. M. S., Hui, K. P. Y., Krishnan, P., Liu, Y., et al. (2020). Molecular diagnosis of a novel coronavirus (2019-nCoV) causing an outbreak of pneumonia. *Clin. Chem.* 66, 549–555. doi: 10.1093/clinchem/hvaa029

Chung, H.-Y., Jian, M.-J., Chang, C.-K., Lin, J.-C., Yeh, K.-M., Chen, C.-W., et al. (2021a). Novel dual multiplex real-time RT-PCR assays for the rapid detection of SARS-CoV-2, influenza A/B, and respiratory syncytial virus using the BD MAX open system. *Emerg. Microbes Infect.* 10, 161–166. doi: 10.1080/22221751.2021.1873073

Chung, H.-Y., Jian, M.-J., Chang, C.-K., Lin, J.-C., Yeh, K.-M., Yang, Y.-S., et al. (2021b). Multicenter study evaluating one multiplex RT-PCR assay to detect SARS-CoV-2, influenza A/B, and respiratory syncytia virus using the LabTurbo AIO open platform: epidemiological features, automated sample-to-result, and high-throughput testing. *Aging* 13, 24931–24942. doi: 10.18632/aging.203761

Cohen, M., Zhang, X., Senaati, H. P., Chen, H., Varki, N. M., Schooley, R. T., et al. (2013). Influenza A penetrates host mucus by cleaving sialic acids with neuraminidase. *Virol. J.* 10:321. doi: 10.1186/1743-422X-10-321

Corman, V. M., Landt, O., Kaiser, M., Molenkamp, R., Meijer, A., Chu, D. K., et al. (2020). Detection of 2019 novel coronavirus (2019-nCoV) by real-time RT-PCR. *Eurosurveillance* 25, 185–193. doi: 10.2807/1560-7917.ES.2020.25.3.2000045

Courtney, S. J., Stromberg, Z. R., and Kubicek-Sutherland, J. Z. (2021). Nucleic acid-based sensing techniques for diagnostics and surveillance of influenza. *Biosensors* 11:47. doi: 10.3390/bios11020047

Coutard, B., Valle, C., de Lamballerie, X., Canard, B., Seidah, N. G., and Decroly, E. (2020). The spike glycoprotein of the new coronavirus 2019-nCoV contains a furin-like cleavage site absent in CoV of the same clade. *Antiviral Res.* 176:104742. doi: 10.1016/j.antiviral.2020.104742

Cox, N. J., and Subbarao, K. (1999). Influenza. *Lancet* 354, 1277–1282. doi: 10.1016/S0140-6736(99)01241-6

da Rosa Mesquita, R., Francelino Silva Junior, L. C., Santos Santana, F. M., Farias de Oliveira, T., Campos Alcântara, R., Monteiro Arnozo, G., et al. (2021). Clinical manifestations of COVID-19 in the general population: systematic review. *Wien. Klin. Wochenschr.* 133, 377–382. doi: 10.1007/s00508-020-01760-4

de Groot, R. J., Baker, S. C., Baric, R. S., Brown, C. S., Drosten, C., Enjuanes, L., et al. (2013). Middle East respiratory syndrome coronavirus (MERS-CoV): announcement of the Coronavirus Study Group. *J. Virol.* 87, 7790–7792. doi: 10.1128/JVI.01244-13

Dong, H., Wang, S., Zhang, J., Zhang, K., Zhang, F., Wang, H., et al. (2021). Structure-based primer design minimizes the risk of PCR failure caused by SARS-CoV-2 mutations. *Front. Cell. Infect. Microbiol.* 11:741147. doi: 10.3389/fcimb.2021.741147

Dong, H., Zhang, Y., Xiong, H., Yan, A., Ding, G., Chen, Y., et al. (2010). Detection of human novel influenza A (H1N1) viruses using multi-fluorescent real-time RT-PCR. *Virus Res.* 147, 85–90. doi: 10.1016/j.virusres.2009.10.011

Drinka, P. J., Krause, P., and Nest, L. (2003). Clinical features of influenza a virus infection in older hospitalized persons. *J. Am. Geriatr. Soc.* 51, 1184–1184. doi: 10.1046/j.1532-5415.2003.51374.x

Dziąbowska, K., Czaczyk, E., and Nidzworski, D. (2018). Detection methods of human and animal influenza virus—current trends. *Biosensors* 8:94. doi: 10.3390/bios8040094

Eigner, U., Reucher, S., Hefner, N., Staffa-Peichl, S., Kolb, M., Betz, U., et al. (2019). Clinical evaluation of multiplex RT-PCR assays for the detection of influenza A/B and respiratory syncytial virus using a high throughput system. *J. Virol. Methods* 269, 49–54. doi: 10.1016/j.jviromet.2019.03.015

European Centre for Disease Prevention and Control [ECDC] (2020). *European Centre for Disease Prevention and Control. Reinfection with SARS-CoV: Considerations for Public Health Response*. Solna: ECDC.

Fakheran, O., Dehghannejad, M., and Khademi, A. (2020). Saliva as a diagnostic specimen for detection of SARS-CoV-2 in suspected patients: a scoping review. *Infect. Dis. poverty* 9:100. doi: 10.1186/s40249-020-00728-w

Falzone, L., Gattuso, G., Tsatsakis, A., Spandidos, D. A., and Libra, M. (2021). Current and innovative methods for the diagnosis of COVID-19 infection (Review). *Int. J. Mol. Med.* 47:100. doi: 10.3892/ijmm.2021.4933

Fanelli, V., Fiorentino, M., Cantaluppi, V., Gesualdo, L., Stallone, G., Ronco, C., et al. (2020). Acute kidney injury in SARS-CoV-2 infected patients. *Crit. Care* 24:155. doi: 10.1186/s13054-020-02872-z

Favas, T. T., Dev, P., Chaurasia, R. N., Chakravarty, K., Mishra, R., Joshi, D., et al. (2020). Neurological manifestations of COVID-19: a systematic review and meta-analysis of proportions. *Neurol. Sci.* 41, 3437–3470. doi: 10.1007/s10072-020-04801-y

Feng, H., Liu, Y., Lv, M., and Zhong, J. (2020). A case report of COVID-19 with false negative RT-PCR test: necessity of chest CT. *Jpn. J. Radiol.* 38, 409–410. doi: 10.1007/s11604-020-00967-9

Food and Drug Administration [FDA] (2021). *SARS-CoV-2 Viral Mutations: Impact on COVID-19 Tests On this page: Genetic Variations: Background and Considerations General Information for Clinical Laboratory Staff and Healthcare Providers. U.S. Food Drug Adm., 1–6*. Silver Spring: Food and Drug Administration.

Food and Drug Administration [FDA] (2022). *In Vitro Diagnostics EUAs - Antigen Diagnostic Tests for SARS-CoV-2 | FDA*. Available online at: https://www.fda.gov/medical-devices/coronavirus-disease-2019-covid-19-emergency-use-authorizations-medical-devices/in-vitro-diagnostics-euas-antigen-diagnostic-tests-sars-cov-2 (Accessed February 17, 2022)

Freije, C. A., Myhrvold, C., Boehm, C. K., Lin, A. E., Welch, N. L., Carter, A., et al. (2019). Programmable Inhibition and Detection of RNA viruses using Cas13. *Mol. Cell* 76, 826–837.e11. doi: 10.1016/j.molcel.2019.09.013

Gavin, P. J., and Thomson, R. B. (2004). Review of rapid diagnostic tests for influenza. *Clin. Appl. Immunol. Rev.* 4, 151–172. doi: 10.1016/S1529-1049(03)00064-3

Gibson, P. G., Qin, L., and Puah, S. H. (2020). COVID-19 acute respiratory distress syndrome (ARDS): clinical features and differences from typical pre-COVID-19 ARDS. *Med. J. Aust.* 213, 54–56.e1. doi: 10.5694/mja2.50674

Graf, E. H., Simmon, K. E., Tardif, K. D., Hymas, W., Flygare, S., Eilbeck, K., et al. (2016). Unbiased detection of respiratory viruses by use of RNA sequencing-based metagenomics: a systematic comparison to a commercial PCR panel. *J. Clin. Microbiol.* 54, 1000–1007. doi: 10.1128/JCM.03060-15

Green, D. A., and StGeorge, K. (2018). Rapid antigen tests for influenza: rationale and significance of the FDA reclassification. *J. Clin. Microbiol.* 56:e00711-18. doi: 10.1128/JCM.00711-18

Greninger, A. L., Chen, E. C., Sittler, T., Scheinerman, A., Roubinian, N., Yu, G., et al. (2010). A metagenomic analysis of pandemic influenza A (2009 H1N1) infection in patients from North America. *PLoS One* 5:e13381. doi: 10.1371/journal.pone.0013381

Gupta, R., Kazi, T. A., Dey, D., Ghosh, A., Ravichandiran, V., Swarnakar, S., et al. (2021). CRISPR detectives against SARS-CoV-2: a major setback against COVID-19 blowout. *Appl. Microbiol. Biotechnol.* 105, 7593–7605. doi: 10.1007/s00253-021-11583-6

Hansen, G., Marino, J., Wang, Z.-X., Beavis, K. G., Rodrigo, J., Labog, K., et al. (2021). Clinical performance of the point-of-care cobas liat for detection of SARS-CoV-2 in 20 minutes: a multicenter study. *J. Clin. Microbiol.* 59, e02811-20. doi: 10.1128/JCM.02811-20

Harapan, B. N., and Yoo, H. J. (2021). Neurological symptoms, manifestations, and complications associated with severe acute respiratory syndrome coronavirus 2 (SARS-CoV-2) and coronavirus disease 19 (COVID-19). *J. Neurol.* 268, 3059–3071. doi: 10.1007/s00415-021-10406-y

Hasan, M. R., Sundararaju, S., Manickam, C., Mirza, F., Al-Hail, H., Lorenz, S., et al. (2021). A novel point mutation in the N gene of SARS-CoV-2 may affect the detection of the virus by reverse transcription-quantitative PCR. *J. Clin. Microbiol.* 59, 19–21. doi: 10.1128/JCM.03278-20

Horai, Y., Miyamura, T., Takahama, S., Sonomoto, K., Nakamura, M., Ando, H., et al. (2010). Influenza virus B-associated hemophagocytic syndrome and recurrent pericarditis in a patient with systemic lupus erythematosus. *Mod. Rheumatol.* 20, 178–182. doi: 10.1007/s10165-009-0241-6

Hou, H., Wang, T., Zhang, B., Luo, Y., Mao, L., Wang, F., et al. (2020). Detection of IgM and IgG antibodies in patients with coronavirus disease 2019. *Clin. Transl. Immunol.* 9:e01136. doi: 10.1002/cti2.1136

Huang, C., Wen, T., Shi, F.-J., Zeng, X.-Y., and Jiao, Y.-J. (2020). Rapid detection of IgM antibodies against the SARS-CoV-2 virus *via* colloidal gold nanoparticle-based lateral-flow assay. *ACS Omega* 5, 12550–12556. doi: 10.1021/acsomega.0c01554

Jackson, C. B., Farzan, M., Chen, B., and Choe, H. (2022). Mechanisms of SARS-CoV-2 entry into cells. *Nat. Rev. Mol. Cell Biol.* 23, 3–20. doi: 10.1038/s41580-021-00418-x

Jain, S., Self, W. H., Wunderink, R. G., Fakhran, S., Balk, R., Bramley, A. M., et al. (2015). Community-acquired pneumonia requiring hospitalization among U.S. *Adults. N. Engl. J. Med.* 373, 415–427. doi: 10.1056/NEJMoa1500245

Jayamohan, H., Lambert, C. J., Sant, H. J., Jafek, A., Patel, D., Feng, H., et al. (2021). SARS-CoV-2 pandemic: a review of molecular diagnostic tools including sample collection and commercial response with associated advantages and limitations. *Anal. Bioanal. Chem.* 413, 49–71. doi: 10.1007/s00216-020-02958-1

John, G., Sahajpal, N. S., Mondal, A. K., Ananth, S., Williams, C., Chaubey, A., et al. (2021). Next-Generation Sequencing (NGS) in COVID-19: a tool for SARS-CoV-2 diagnosis, monitoring new strains and phylodynamic modeling in molecular epidemiology. *Curr. Issues Mol. Biol.* 43, 845–867. doi: 10.3390/cimb43020061

Kevadiya, B. D., Machhi, J., Herskovitz, J., Oleynikov, M. D., Blomberg, W. R., Bajwa, N., et al. (2021). Diagnostics for SARS-CoV-2 infections. *Nat. Mater.* 20, 593–605. doi: 10.1038/s41563-020-00906-z

Killingley, B., and Nguyen-Van-Tam, J. (2013). Routes of influenza transmission. *Influenza Other Respir. Viruses* 7, 42–51. doi: 10.1111/irv.12080

Kim, T. Y., Kim, J.-Y., Shim, H. J., Yun, S. A., Jang, J., Huh, H. J., et al. (2021). Comparison of the PowerChek SARS-CoV-2, Influenza A&B, RSV multiplex real-time PCR Kit and BioFire Respiratory Panel 2.1 for simultaneous detection of SARS-CoV-2, influenza A and B, and respiratory syncytial virus. *J. Virol. Methods* 298:114304. doi: 10.1016/j.jviromet.2021.114304

Kim, T. Y., Kim, J.-Y., Shim, H. J., Yun, S. A., Jang, J., Huh, H. J., et al. (2022). Performance evaluation of the PowerChek SARS-CoV-2, Influenza A & B Multiplex Real-Time PCR Kit in Comparison with the BioFire respiratory panel. *Ann. Lab. Med.* 42, 473–477. doi: 10.3343/alm.2022.42.4.473

Kirtipal, N., Bharadwaj, S., and Kang, S. G. (2020). From SARS to SARS-CoV-2, insights on structure, pathogenicity and immunity aspects of pandemic human coronaviruses. *Infect. Genet. Evol.* 85:104502. doi: 10.1016/j.meegid.2020.104502

Klein, E. Y., Monteforte, B., Gupta, A., Jiang, W., May, L., Hsieh, Y.-H., et al. (2016). The frequency of influenza and bacterial coinfection: a systematic review and meta-analysis. *Influenza Other Respir. Viruses* 10, 394–403. doi: 10.1111/irv.12398

Kodama, M. (2010). Influenza myocarditis. *Circ. J.* 74, 2060–2061. doi: 10.1253/circj.cj-10-0833

Kousathanas, A., Pairo-Castineira, E., Rawlik, K., Stuckey, A., Odhams, C. A., Walker, S., et al. (2021). Whole genome sequencing identifies multiple loci for critical illness caused by COVID-19. *medRxiv [Preprint]* doi: 10.1101/2021.09.02.21262965

Krammer, F., Smith, G. J. D., Fouchier, R. A. M., Peiris, M., Kedzierska, K., Doherty, P. C., et al. (2018). Influenza. *Nat. Rev. Dis. Prim.* 4:3. doi: 10.1038/s41572-018-0002-y

Kubo, T., Agoh, M., Mai, L. Q., Fukushima, K., Nishimura, H., Yamaguchi, A., et al. (2010). Development of a reverse transcription-loop-mediated isothermal amplification assay for detection of pandemic (H1N1) 2009 virus as a novel molecular method for diagnosis of pandemic influenza in resource-limited settings. *J. Clin. Microbiol.* 48, 728–735. doi: 10.1128/JCM.01481-09

Kucirka, L. M., Lauer, S. A., Laeyendecker, O., Boon, D., and Lessler, J. (2020). Variation in false-negative rate of reverse transcriptase polymerase chain reaction-based SARS-CoV-2 tests by time since exposure. *Ann. Intern. Med.* 173, 262–267. doi: 10.7326/M20-1495

Kunutsor, S. K., and Laukkanen, J. A. (2020). Renal complications in COVID-19: a systematic review and meta-analysis. *Ann. Med.* 52, 345–353. doi: 10.1080/07853890.2020.1790643

Kustin, T., Ling, G., Sharabi, S., Ram, D., Friedman, N., Zuckerman, N., et al. (2019). A method to identify respiratory virus infections in clinical samples using next-generation sequencing. *Sci. Rep.* 9:2606. doi: 10.1038/s41598-018-37483-w

Lai, C. K. C., and Lam, W. (2021). Laboratory testing for the diagnosis of COVID-19. *Biochem. Biophys. Res. Commun.* 538, 226–230. doi: 10.1016/j.bbrc.2020.10.069

Lee, D., Chu, C.-H., and Sarioglu, A. F. (2021). Point-of-care toolkit for multiplex molecular diagnosis of SARS-CoV-2 and influenza A and B viruses. *ACS Sensors* 6, 3204–3213. doi: 10.1021/acssensors.1c00702

Lee, N., Hui, D., Wu, A., Chan, P., Cameron, P., Joynt, G. M., et al. (2003). A major outbreak of severe acute respiratory syndrome in Hong Kong. *N. Engl. J. Med.* 348, 1986–1994. doi: 10.1056/NEJMoa030685

Leung, W. K., To, K.-F., Chan, P. K. S., Chan, H. L. Y., Wu, A. K. L., Lee, N., et al. (2003). Enteric involvement of severe acute respiratory syndrome-associated coronavirus infection. *Gastroenterology* 125, 1011–1017. doi: 10.1016/s0016-5085(03)01215-0

Li, K., and Brownley, A. (2010). "Primer design for RT-PCR," in *Methods in Molecular Biology (Clifton, N.J.) Methods in Molecular Biology*, ed. N. King (Totowa, NJ: Humana Press), 271–299. doi: 10.1007/978-1-60761-629-0_18

Li, N., Cai, Q., Miao, Q., Song, Z., Fang, Y., and Hu, B. (2021). High-throughput metagenomics for identification of pathogens in the clinical settings. *Small Methods* 5:2000792. doi: 10.1002/smtd.202000792

Liu, R., Sheng, Z., Huang, C., Wang, D., and Li, F. (2020). Influenza D virus. *Curr. Opin. Virol.* 44, 154–161. doi: 10.1016/j.coviro.2020.08.004

Liu, S., and Pan, C. (2020). Differentiating diagnosis of COVID-19 or influenza in patients based on laboratory data during flu season. *EClinicalMedicine* 26:100511. doi: 10.1016/j.eclinm.2020.100511

Loeffelholz, M. J., Alland, D., Butler-Wu, S. M., Pandey, U., Perno, C. F., Nava, A., et al. (2020). Multicenter evaluation of the cepheid xpert Xpress SARS-CoV-2 Test. *J. Clin. Microbiol.* 58, e00926-20. doi: 10.1128/JCM.00926-20

Long, B., Brady, W. J., Koyfman, A., and Gottlieb, M. (2020). Cardiovascular complications in COVID-19. *Am. J. Emerg. Med.* 38, 1504–1507. doi: 10.1016/j.ajem.2020.04.048

Long, Q.-X., Liu, B.-Z., Deng, H.-J., Wu, G.-C., Deng, K., Chen, Y.-K., et al. (2020). Antibody responses to SARS-CoV-2 in patients with COVID-19. *Nat. Med.* 26, 845–848. doi: 10.1038/s41591-020-0897-1

Lorusso, A., Calistri, P., Mercante, M. T., Monaco, F., Portanti, O., Marcacci, M., et al. (2020). A "One-Health" approach for diagnosis and molecular characterization of SARS-CoV-2 in Italy. *One Heal.* 10:100135. doi: 10.1016/j.onehlt.2020.100135

Lu, J., du Plessis, L., Liu, Z., Hill, V., Kang, M., Lin, H., et al. (2020). Genomic epidemiology of SARS-CoV-2 in guangdong province, China. *Cell* 181, 997–1003.e9. doi: 10.1016/j.cell.2020.04.023

Lu, R., Zhao, X., Li, J., Niu, P., Yang, B., Wu, H., et al. (2020). Genomic characterisation and epidemiology of 2019 novel coronavirus: implications for virus origins and receptor binding. *Lancet* 395, 565–574. doi: 10.1016/S0140-6736(20)30251-8

Mahalingam, S., Peter, J., Xu, Z., Bordoloi, D., Ho, M., Kalyanaraman, V. S., et al. (2021). Landscape of humoral immune responses against SARS-CoV-2 in patients with COVID-19 disease and the value of antibody testing. *Heliyon* 7:e06836. doi: 10.1016/j.heliyon.2021.e06836

Mahony, J., Chong, S., Bulir, D., Ruyter, A., Mwawasi, K., and Waltho, D. (2013). Multiplex loop-mediated isothermal amplification (M-LAMP) assay for the detection of influenza A/H1, A/H3 and influenza B can provide a specimen-to-result diagnosis in 40min with single genome copy sensitivity. *J. Clin. Virol.* 58, 127–131. doi: 10.1016/j.jcv.2013.06.006

Mancini, F., Barbanti, F., Scaturro, M., Fontana, S., Di Martino, A., Marsili, G., et al. (2021). Multiplex real-time reverse-transcription polymerase chain reaction assays for diagnostic testing of severe acute respiratory syndrome coronavirus 2 and seasonal influenza viruses: a challenge of the phase 3 pandemic setting. *J. Infect. Dis.* 223, 765–774. doi: 10.1093/infdis/jiaa658

Mardian, Y., Kosasih, H., Karyana, M., Neal, A., and Lau, C.-Y. (2021). Review of current COVID-19 diagnostics and opportunities for further development. *Front. Med.* 8:615099. doi: 10.3389/fmed.2021.615099

Mboumba Bouassa, R.-S., Tonen-Wolyec, S., Veyer, D., Péré, H., and Bélec, L. (2022). Analytical performances of the AMPLIQUICK® Respiratory Triplex assay for simultaneous detection and differentiation of SARS-CoV-2, influenza A/B and respiratory syncytial viruses in respiratory specimens. *PLoS One* 17:e0262258. doi: 10.1371/journal.pone.0262258

McMullen, A. R., Anderson, N. W., and Burnham, C.-A. D. (2016). Pathology consultation on influenza diagnostics. *Am. J. Clin. Pathol.* 145, 440–448. doi: 10.1093/ajcp/aqw039

Migliaccio, M. G., Di Mauro, M., Ricciolino, R., Spiniello, G., Carfora, V., Verde, N., et al. (2021). Renal involvement in COVID-19: a review of the literature. *Infect. Drug Resist.* 14, 895–903. doi: 10.2147/IDR.S288869

Minami, T., Iwata, Y., and Wada, T. (2020). Renal complications in coronavirus disease 2019: a systematic review. *Inflamm. Regen.* 40:31. doi: 10.1186/s41232-020-00140-9

Mollaei, H. R., Afshar, A. A., Kalantar-Neyestanaki, D., Fazlalipour, M., and Aflatoonian, B. (2020). Comparison five primer sets from different genome region of COVID-19 for detection of virus infection by conventional RT-PCR. *Iran. J. Microbiol.* 12, 185–193. doi: 10.18502/ijm.v12i3.3234

Monto, A. S., Gravenstein, S., Elliott, M., Colopy, M., and Schweinle, J. (2000). Clinical signs and symptoms predicting influenza infection. *Arch. Intern. Med.* 160:3243. doi: 10.1001/archinte.160.21.3243

Moore, S. C., Penrice-Randal, R., Alruwaili, M., Randle, N., Armstrong, S., Hartley, C., et al. (2020). Amplicon-based detection and sequencing of SARS-CoV-2 in nasopharyngeal swabs from patients With COVID-19 and identification of deletions in the viral genome that encode proteins involved in interferon antagonism. *Viruses* 12:1164. doi: 10.3390/v12101164

Mouliou, D. S., and Gourgoulianis, K. I. (2021). False-positive and false-negative COVID-19 cases: respiratory prevention and management strategies, vaccination, and further perspectives. *Expert Rev. Respir. Med.* 15, 993–1002. doi: 10.1080/17476348.2021.1917389

Musuuza, J. S., Watson, L., Parmasad, V., Putman-Buehler, N., Christensen, L., and Safdar, N. (2021). Prevalence and outcomes of co-infection and superinfection with SARS-CoV-2 and other pathogens: a systematic review and meta-analysis. *PLoS One* 16:e0251170. doi: 10.1371/journal.pone.0251170

Nalla, A. K., Casto, A. M., Huang, M.-L. W., Perchetti, G. A., Sampoleo, R., Shrestha, L., et al. (2020). Comparative performance of SARS-CoV-2 detection assays using seven different primer-probe sets and one assay kit. *J. Clin. Microbiol.* 58:e00557-20. doi: 10.1128/JCM.00557-20

Newton, D. W., Treanor, J. J., and Menegus, M. A. (2000). Clinical and laboratory diagnosis of influenza virus infections. *Am. J. Manag. Care* 6, S265–S275.

Ni, M., Xu, H., Luo, J., Liu, W., and Zhou, D. (2021). Simultaneous detection and differentiation of SARS-CoV-2, influenza A virus and influenza B virus by one-step quadruplex real-time RT-PCR in patients with clinical manifestations. *Int. J. Infect. Dis.* 103, 517–524. doi: 10.1016/j.ijid.2020.12.027

Nie, Q.-H., Luo, X.-D., Zhang, J.-Z., and Su, Q. (2003). Current status of severe acute respiratory syndrome in China. *World J. Gastroenterol.* 9, 1635–1645. doi: 10.3748/wjg.v9.i8.1635

Nikitin, N., Petrova, E., Trifonova, E., and Karpova, O. (2014). Influenza virus aerosols in the air and their infectiousness. *Adv. Virol.* 2014, 859090. doi: 10.1155/2014/859090

Nörz, D., Hoffmann, A., Aepfelbacher, M., Pfefferle, S., and Lütgehetmann, M. (2021). Clinical evaluation of a fully automated, laboratory-developed multiplex RT-PCR assay integrating dual-target SARS-CoV-2 and influenza A/B detection on a high-throughput platform. *J. Med. Microbiol.* 70:001295. doi: 10.1099/jmm.0.001295

O'Flaherty, B. M., Li, Y., Tao, Y., Paden, C. R., Queen, K., Zhang, J., et al. (2018). Comprehensive viral enrichment enables sensitive respiratory virus genomic identification and analysis by next generation sequencing. *Genome Res.* 28, 869–877. doi: 10.1101/gr.226316.117

Pabbaraju, K., Wong, A. A., Ma, R., Zelyas, N., and Tipples, G. A. (2021). Development and validation of a multiplex reverse transcriptase-PCR assay for simultaneous testing of influenza A, influenza B and SARS-CoV-2. *J. Virol. Methods* 293:114151. doi: 10.1016/j.jviromet.2021.114151

Padoan, A., Sciacovelli, L., Basso, D., Negrini, D., Zuin, S., Cosma, C., et al. (2020). IgA-Ab response to spike glycoprotein of SARS-CoV-2 in patients with COVID-19: a longitudinal study. *Clin. Chim. Acta* 507, 164–166. doi: 10.1016/j.cca.2020.04.026

Pairo-Castineira, E., Clohisey, S., Klaric, L., Bretherick, A. D., Rawlik, K., Pasko, D., et al. (2021). Genetic mechanisms of critical illness in COVID-19. *Nature* 591, 92–98. doi: 10.1038/s41586-020-03065-y

Paradis, S., Lockamy, E., Cooper, C. K., and Young, S. (2021). Clinical evaluation of the molecular-based BD SARS-CoV-2/Flu for the BD MAXTM system. *J. Clin. Virol.* 143:104946. doi: 10.1016/j.jcv.2021.104946

Parolo, C., de la Escosura-Muñiz, A., and Merkoçi, A. (2013). Enhanced lateral flow immunoassay using gold nanoparticles loaded with enzymes. *Biosens. Bioelectron.* 40, 412–416. doi: 10.1016/j.bios.2012.06.049

Patchsung, M., Jantarug, K., Pattama, A., Aphicho, K., Suraritdechachai, S., Meesawat, P., et al. (2020). Clinical validation of a Cas13-based assay for the detection of SARS-CoV-2 RNA. *Nat. Biomed. Eng.* 4, 1140–1149. doi: 10.1038/s41551-020-00603-x

Paules, C., and Subbarao, K. (2017). Influenza. *Lancet* 390, 697–708. doi: 10.1016/S0140-6736(17)30129-0

Peaper, D. R., and Landry, M. L. (2014). Rapid diagnosis of influenza: state of the art. *Clin. Lab. Med.* 34, 365–385. doi: 10.1016/j.cll.2014.02.009

Pene, F., Merlat, A., Vabret, A., Rozenberg, F., Buzyn, A., Dreyfus, F., et al. (2003). Coronavirus 229E-related pneumonia in immunocompromised patients. *Clin. Infect. Dis.* 37, 929–932. doi: 10.1086/377612

Perlman, S., and Netland, J. (2009). Coronaviruses post-SARS: update on replication and pathogenesis. *Nat. Rev. Microbiol.* 7, 439–450. doi: 10.1038/nrmicro2147

Petric, M., Comanor, L., and Petti, C. A. (2006). Role of the laboratory in diagnosis of influenza during seasonal epidemics and potential pandemics. *J. Infect. Dis.* 194, S98–S110. doi: 10.1086/507554

Petrova, V. N., and Russell, C. A. (2018). The evolution of seasonal influenza viruses. *Nat. Rev. Microbiol.* 16, 47–60. doi: 10.1038/nrmicro.2017.118

Pisanic, N., Randad, P. R., Kruczynski, K., Manabe, Y. C., Thomas, D. L., Pekosz, A., et al. (2020). COVID-19 Serology at Population Scale: SARS-CoV-2-Specific Antibody Responses in Saliva. *J. Clin. Microbiol.* 59, e02204-20. doi: 10.1128/JCM.02204-20

Pu, R., Liu, S., Ren, X., Shi, D., Ba, Y., Huo, Y., et al. (2022). The screening value of RT-LAMP and RT-PCR in the diagnosis of COVID-19: systematic review and meta-analysis. *J. Virol. Methods* 300:114392. doi: 10.1016/j.jviromet.2021.114392

Rapuntean, S. (2019). *Special Veterinary Virology*. Cluj-Napoca: AcademicPres Publishing House.

Rawson, T. M., Moore, L. S. P., Zhu, N., Ranganathan, N., Skolimowska, K., Gilchrist, M., et al. (2020). Bacterial and fungal coinfection in individuals with coronavirus: a rapid review to support COVID-19 antimicrobial prescribing. *Clin. Infect. Dis.* 71, 2459–2468. doi: 10.1093/cid/ciaa530

Robishaw, J. D., Alter, S. M., Solano, J. J., Shih, R. D., DeMets, D. L., Maki, D. G., et al. (2021). Genomic surveillance to combat COVID-19: challenges and opportunities. *Lancet Microbe* 2, e481–e484. doi: 10.1016/S2666-5247(21)00121-X

Rohde, G., Wiethege, A., Borg, I., Kauth, M., Bauer, T. T., Gillissen, A., et al. (2003). Respiratory viruses in exacerbations of chronic obstructive pulmonary disease requiring hospitalisation: a case-control study. *Thorax* 58, 37–42. doi: 10.1136/thorax.58.1.37

Rothberg, M. B., Haessler, S. D., and Brown, R. B. (2008). Complications of viral influenza. *Am. J. Med.* 121, 258–264. doi: 10.1016/j.amjmed.2007.10.040

Ruest, A., Michaud, S., Deslandes, S., and Frost, E. H. (2003). Comparison of the directigen Flu A+B Test, the QuickVue influenza test, and clinical case definition to viral culture and reverse transcription-PCR for rapid diagnosis of influenza virus infection. *J. Clin. Microbiol.* 41, 3487–3493. doi: 10.1128/JCM.41.8.3487-3493.2003

Safiabadi Tali, S. H., LeBlanc, J. J., Sadiq, Z., Oyewunmi, O. D., Camargo, C., Nikpour, B., et al. (2021). Tools and techniques for severe acute respiratory syndrome coronavirus 2 (SARS-CoV-2)/COVID-19 detection. *Clin. Microbiol. Rev.* 34, 1–63. doi: 10.1128/CMR.00228-20

Sakai-Tagawa, Y., Ozawa, M., Tamura, D., Le, M. T. Q., Nidom, C. A., Sugaya, N., et al. (2010). Sensitivity of influenza rapid diagnostic tests to H5N1 and 2009 pandemic H1N1 viruses. *J. Clin. Microbiol.* 48, 2872–2877. doi: 10.1128/JCM.00439-10

Sellers, S. A., Hagan, R. S., Hayden, F. G., and Fischer, W. A. (2017). The hidden burden of influenza: a review of the extra-pulmonary complications of influenza infection. *Influenza Other Respir. Viruses* 11, 372–393. doi: 10.1111/irv.12470

Severe Covid-19 GWAS Group, Ellinghaus, D., Degenhardt, F., Bujanda, L., Buti, M., Albillos, A., et al. (2020). Genomewide association study of severe covid-19 with respiratory failure. *N. Engl. J. Med.* 383, 1522–1534. doi: 10.1056/NEJMoa2020283

Shaw, M. W., Xu, X., Li, Y., Normand, S., Ueki, R. T., Kunimoto, G. Y., et al. (2002). Reappearance and global spread of variants of influenza B/Victoria/2/87 lineage viruses in the 2000–2001 and 2001–2002 seasons. *Virology* 303, 1–8. doi: 10.1006/viro.2002.1719

Sheridan, C. (2020). Coronavirus and the race to distribute reliable diagnostics. *Nat. Biotechnol.* 38, 382–384. doi: 10.1038/d41587-020-00002-2

Shu, B., Kirby, M. K., Davis, W. G., Warnes, C., Liddell, J., Liu, J., et al. (2021). Multiplex real-time reverse transcription PCR for influenza A virus, influenza B Virus, and severe acute respiratory syndrome coronavirus 2. *Emerg. Infect. Dis.* 27, 1821–1830. doi: 10.3201/eid2707.210462

Siqueira, J. D., Goes, L. R., Alves, B. M., da Silva, A. C. P., de Carvalho, P. S., Cicala, C., et al. (2021). Distinguishing SARS-CoV-2 bonafide re-infection from pre-existing minor variant reactivation. *Infect. Genet. Evol.* 90:104772. doi: 10.1016/J.MEEGID.2021.104772

Slatko, B. E., Gardner, A. F., and Ausubel, F. M. (2018). Overview of next-generation sequencing technologies. *Curr. Protoc. Mol. Biol.* 122, 1–15. doi: 10.1002/cpmb.59

Smith, C. J., and Osborn, A. M. (2009). Advantages and limitations of quantitative PCR (Q-PCR)-based approaches in microbial ecology. *FEMS Microbiol. Ecol.* 67, 6–20. doi: 10.1111/j.1574-6941.2008.00629.x

Song, X., Delaney, M., Shah, R. K., Campos, J. M., Wessel, D. L., and DeBiasi, R. L. (2020). Comparison of clinical features of COVID-19 vs seasonal influenza A and B in US children. *JAMA Netw. Open* 3:e2020495. doi: 10.1001/jamanetworkopen.2020.20495

Spoto, S., Valeriani, E., Locorriere, L., Anguissola, G. B., Pantano, A. L., Terracciani, F., et al. (2019). Influenza B virus infection complicated by life-threatening pericarditis: a unique case-report and literature review. *BMC Infect. Dis.* 19:40. doi: 10.1186/s12879-018-3606-7

Studahl, M. (2003). Influenza virus and CNS manifestations. *J. Clin. Virol.* 28, 225–232. doi: 10.1016/S1386-6532(03)00119-7

Suo, T., Liu, X., Feng, J., Guo, M., Hu, W., Guo, D., et al. (2020). ddPCR: a more accurate tool for SARS-CoV-2 detection in low viral load specimens. *Emerg. Microbes Infect.* 9, 1259–1268. doi: 10.1080/22221751.2020.1772678

Tang, X., Musa, S. S., Zhao, S., and He, D. (2021). Reinfection or reactivation of severe acute respiratory syndrome coronavirus 2: a systematic review. *Front. Public Heal.* 9:663045. doi: 10.3389/fpubh.2021.663045

Teymouri, M., Mollazadeh, S., Mortazavi, H., Naderi Ghale-Noie, Z., Keyvani, V., Aghababaei, F., et al. (2021). Recent advances and challenges of RT-PCR tests for the diagnosis of COVID-19. *Pathol. Res. Pract.* 221:153443. doi: 10.1016/j.prp.2021.153443

To, K. F., Chan, P. K., Chan, K. F., Lee, W. K., Lam, W. Y., Wong, K. F., et al. (2001). Pathology of fatal human infection associated with avian influenza A H5N1 virus. *J. Med. Virol.* 63, 242–246. doi: 10.1002/1096-9071(200103)63:3<242::aid-jmv1007<3.0.co;2-n

To, K. F., Tong, J. H. M., Chan, P. K. S., Au, F. W. L., Chim, S. S. C., Chan, K. C. A., et al. (2004). Tissue and cellular tropism of the coronavirus associated with severe acute respiratory syndrome: an in-situ hybridization study of fatal cases. *J. Pathol.* 202, 157–163. doi: 10.1002/path.1510

Tombuloglu, H., Sabit, H., Al-Khallaf, H., Kabanja, J. H., Alsaeed, M., Al-Saleh, N., et al. (2022). Multiplex real-time RT-PCR method for the diagnosis of SARS-CoV-2 by targeting viral N, RdRP and human RP genes. *Sci. Rep.* 12:2853. doi: 10.1038/s41598-022-06977-z

Tong, S., Zhu, X., Li, Y., Shi, M., Zhang, J., Bourgeois, M., et al. (2013). New world bats harbor diverse influenza A viruses. *PLoS Pathog.* 9:e1003657. doi: 10.1371/journal.ppat.1003657

Trick, A. Y., Chen, F.-E., Chen, L., Lee, P.-W., Hasnain, A. C., Mostafa, H. H., et al. (2021). Magnetofluidic platform for rapid multiplexed screening of SARS-CoV-2 variants and respiratory pathogens. *medRxiv [Preprint]*. doi: 10.1101/2021.05.10.21256995

Tsai, J. P., and Baker, A. J. (2013). Influenza-associated neurological complications. *Neurocrit. Care* 18, 118–130. doi: 10.1007/s12028-012-9796-8

Tuan, J., Spichler-Moffarah, A., and Ogbuagu, O. (2021). A new positive SARS-CoV-2 test months after severe COVID-19 illness: reinfection or intermittent viral shedding? *BMJ Case Rep.* 14:e240531. doi: 10.1136/bcr-2020-240531

Uyeki, T. M., Bernstein, H. H., Bradley, J. S., Englund, J. A., File, T. M., Fry, A. M., et al. (2019). Clinical practice guidelines by the infectious diseases society of America: 2018 update on diagnosis, treatment, chemoprophylaxis, and institutional outbreak management of seasonal influenzaa. *Clin. Infect. Dis.* 68, e1–e47. doi: 10.1093/cid/ciy866

Valencia, D. N. (2020). Brief review on COVID-19: the 2020 pandemic caused by SARS-CoV-2. *Cureus* 12:e7386. doi: 10.7759/cureus.7386

van Kampen, J. J. A., van de Vijver, D. A. M. C., Fraaij, P. L. A., Haagmans, B. L., Lamers, M. M., Okba, N., et al. (2021). Duration and key determinants of infectious virus shedding in hospitalized patients with coronavirus disease-2019 (COVID-19). *Nat. Commun.* 12:267. doi: 10.1038/s41467-020-20568-4

Van Poelvoorde, L. A. E., Saelens, X., Thomas, I., and Roosens, N. H. (2020). Next-generation sequencing: an eye-opener for the surveillance of antiviral resistance in influenza. *Trends Biotechnol.* 38, 360–367. doi: 10.1016/j.tibtech.2019.09.009

Vemula, S., Zhao, J., Liu, J., Wang, X., Biswas, S., and Hewlett, I. (2016). Current approaches for diagnosis of influenza virus infections in humans. *Viruses* 8:96. doi: 10.3390/v8040096

Vijgen, L., Keyaerts, E., Moës, E., Maes, P., Duson, G., and Van Ranst, M. (2005). Development of one-step, real-time, quantitative reverse transcriptase PCR assays for absolute quantitation of human coronaviruses OC43 and 229E. *J. Clin. Microbiol.* 43, 5452–5456. doi: 10.1128/JCM.43.11.5452-5456.2005

Walper, S. A., Lasarte Aragonés, G., Sapsford, K. E., Brown, C. W., Rowland, C. E., Breger, J. C., et al. (2018). Detecting biothreat agents: from current diagnostics to developing sensor technologies. *ACS Sensors* 3, 1894–2024. doi: 10.1021/acssensors.8b00420

Webster, R. G., and Govorkova, E. A. (2014). Continuing challenges in influenza. *Ann. N. Y. Acad. Sci.* 1323, 115–139. doi: 10.1111/nyas.12462

Welch, N. L., Zhu, M., Hua, C., Weller, J., Mirhashemi, M. E., Nguyen, T. G., et al. (2022). Multiplexed CRISPR-based microfluidic platform for clinical testing of respiratory viruses and identification of SARS-CoV-2 variants. *Nat. Med.* 28, 1083–1094. doi: 10.1038/s41591-022-01734-1

Wolters, F., Grünberg, M., Huber, M., Kessler, H. H., Prüller, F., Saleh, L., et al. (2021). European multicenter evaluation of Xpert® Xpress SARS-CoV-2/Flu/RSV test. *J. Med. Virol.* 93, 5798–5804. doi: 10.1002/jmv.27111

Woo, P. C. Y., Lau, S. K. P., Lam, C. S. F., Lai, K. K. Y., Huang, Y., Lee, P., et al. (2009). Comparative analysis of complete genome sequences of three avian coronaviruses reveals a novel group 3c coronavirus. *J. Virol.* 83, 908–917. doi: 10.1128/JVI.01977-08

World Health Organization [WHO] (2020). *Laboratory Testing for Coronavirus Disease 2019 (COVID-19) in Suspected Human Cases*. 1–7. Geneva: World Health Organization.

World Health Organization [WHO] (2021). *WHO/2019-nCoV/Antigen_Detection/2021.1*. Geneva: World Health Organization

Wu, C., Liu, Y., Yang, Y., Zhang, P., Zhong, W., Wang, Y., et al. (2020). Analysis of therapeutic targets for SARS-CoV-2 and discovery of potential drugs by computational methods. *Acta Pharm. Sin. B* 10, 766–788. doi: 10.1016/j.apsb.2020.02.008

Wyllie, A. L., Fournier, J., Casanovas-Massana, A., Campbell, M., Tokuyama, M., Vijayakumar, P., et al. (2020). Saliva or nasopharyngeal swab specimens for detection of SARS-CoV-2. *N. Engl. J. Med.* 383, 1283–1286. doi: 10.1056/NEJMc2016359

Zambon, M., Hays, J., Webster, A., Newman, R., and Keene, O. (2001). Diagnosis of influenza in the community. *Arch. Intern. Med.* 161:2116. doi: 10.1001/archinte.161.17.2116

Zhang, F., Abudayyeh, O. O., and Gootenberg, J. S. (2022). *A Protocol for Detection of COVID-19 Using CRISPR Diagnostics*. Available online at: https://www.broadinstitute.org/files/publications/special/COVID-19detection(updated).pdf (accessed February 28, 2022).

Zhang, W., Du, R.-H., Li, B., Zheng, X.-S., Yang, X.-L., Hu, B., et al. (2020). Molecular and serological investigation of 2019-nCoV infected patients: implication of multiple shedding routes. *Emerg. Microbes Infect.* 9, 386–389. doi: 10.1080/22221751.2020.1729071

Zhang, Y., and Tanner, N. A. (2021). Development of multiplexed reverse-transcription loop-mediated isothermal amplification for detection of SARS-CoV-2 and influenza viral RNA. *Biotechniques* 70, 167–174. doi: 10.2144/btn-2020-0157

Zhao, J., Liu, J., Vemula, S. V., Lin, C., Tan, J., Ragupathy, V., et al. (2016). Sensitive detection and simultaneous discrimination of influenza A and B viruses in nasopharyngeal swabs in a single assay using next-generation sequencing-based diagnostics. *PLoS One* 11:e0163175. doi: 10.1371/journal.pone.0163175

Zhen, W., Manji, R., Smith, E., Wuitschick, J., Lucic, D., and Berry, G. J. (2022). Evaluation of the Alinity m Resp-4-Plex assay for the detection of severe acute respiratory syndrome coronavirus 2, Influenza A Virus, Influenza B virus, and respiratory syncytial virus. *Microbiol. Spectr.* 10:e0109021. doi: 10.1128/spectrum.01090-21

Zhou, P., Yang, X.-L., Wang, X.-G., Hu, B., Zhang, L., Zhang, W., et al. (2020). A pneumonia outbreak associated with a new coronavirus of probable bat origin. *Nature* 579, 270–273. doi: 10.1038/s41586-020-2012-7

Zhu, N., Zhang, D., Wang, W., Li, X., Yang, B., Song, J., et al. (2020). A novel coronavirus from patients with pneumonia in China, 2019. *N. Engl. J. Med.* 382, 727–733. doi: 10.1056/NEJMoa2001017

Ziegler, K., Steininger, P., Ziegler, R., Steinmann, J., Korn, K., and Ensser, A. (2020). SARS-CoV-2 samples may escape detection because of a single point mutation in the N gene. *Euro Surveill.* 25:2001650. doi: 10.2807/1560-7917.ES.2020.25.39.2001650

Conflict of Interest: The authors declare that the research was conducted in the absence of any commercial or financial relationships that could be construed as a potential conflict of interest.

Publisher's Note: All claims expressed in this article are solely those of the authors and do not necessarily represent those of their affiliated organizations, or those of the publisher, the editors and the reviewers. Any product that may be evaluated in this article, or claim that may be made by its manufacturer, is not guaranteed or endorsed by the publisher.

frontiers | Frontiers in Microbiology

ORIGINAL RESEARCH
published: 12 July 2022
doi: 10.3389/fmicb.2022.914620

Nanoparticle-Based Lateral Flow Biosensor Integrated With Loop-Mediated Isothermal Amplification for Rapid and Visual Identification of *Chlamydia trachomatis* for Point-of-Care Use

OPEN ACCESS

Edited by:
Bing Gu,
Guangdong Provincial People's Hospital, China

Reviewed by:
Margaret Hammerschlag, SUNY Downstate Medical Center, United States
Subash C. Sonkar, Maulana Azad Medical College and Associated Hospitals, India

***Correspondence:**
Shilei Dong
dsl166@126.com

Specialty section:
This article was submitted to Infectious Agents and Disease, a section of the journal Frontiers in Microbiology

Received: *07 April 2022*
Accepted: *09 June 2022*
Published: *12 July 2022*

Citation:
Chen X, Zhou Q, Tan Y, Wang R, Wu X, Liu J, Liu R, Wang S and Dong S (2022) Nanoparticle-Based Lateral Flow Biosensor Integrated With Loop-Mediated Isothermal Amplification for Rapid and Visual Identification of Chlamydia trachomatis for Point-of-Care Use. Front. Microbiol. 13:914620. doi: 10.3389/fmicb.2022.914620

Xu Chen*[1,2], *Qingxue Zhou*[3], *Yan Tan*[4], *Ronghua Wang*[5], *Xueli Wu*[2], *Jiangli Liu*[2], *Rui Liu*[2], *Shuoshi Wang*[2] *and Shilei Dong*[6]

[1] *The Second Clinical College, Guizhou University of Traditional Chinese Medicine, Guiyang, China,* [2] *Clinical Medical Laboratory of the Second Affiliated Hospital, Guizhou University of Traditional Chinese Medicine, Guiyang, China,* [3] *Clinical Laboratory, Hangzhou Women's Hospital, Hangzhou, China,* [4] *Guizhou Provincial Center for Clinical Laboratory, Guiyang, China,* [5] *Department of Clinical Laboratory, Longli People's Hospital, Qiannan Buyi and Miao Autonomous Prefecture, China,* [6] *Department of Clinical Laboratory, Zhejiang Hospital, Hangzhou, China*

Chlamydial infection, caused by *Chlamydia trachomatis*, is the most common bacterial sexually transmitted infection and remains a major public health problem worldwide, particularly in underdeveloped regions. Developing a rapid and sensitive point-of-care (POC) testing for accurate screening of *C. trachomatis* infection is critical for earlier treatment to prevent transmission. In this study, a novel diagnostic assay, loop-mediated isothermal amplification integrated with gold nanoparticle-based lateral flow biosensor (LAMP-LFB), was devised and applied for diagnosis of *C. trachomatis* in clinical samples. A set of LAMP primers based on the *ompA* gene from 14 *C. trachomatis* serological variants (serovar A-K, L1, L2, L3) was successfully designed and used for the development of *C. trachomatis*-LAMP-LFB assay. The optimal reaction system can be performed at a constant temperature of 67°C for 35 min. The total assay process, including genomic DNA extraction (~15 min), LAMP reaction (35 min), and LFB readout (~2 min), could be finished within 60 min. The *C. trachomatis*-LAMP-LFB could detect down to 50 copies/ml, and the specificity was 100%, no cross-reactions with other pathogens were observed. Hence, our *C. trachomatis*-LAMP-LFB was a rapid, reliable, sensitive, cost-effective, and easy-to-operate assay, which could offer an attractive POC testing tool for chlamydial infection screening, especially in resource starvation settings.

Keywords: *Chlamydia trachomatis*, loop-mediated isothermal amplification, gold nanoparticle-based lateral flow biosensor, limit of detection, point-of-care testing

INTRODUCTION

Chlamydia trachomatis is a Gram-negative, obligate intracellular pathogen that causes the most common bacterial sexually transmitted infections (STIs) (Woodhall et al., 2018; Murray and McKay, 2021), with an estimated ∼130 million new cases worldwide each year, thereby remaining a major global health challenge, particularly in underdeveloped regions (World Health Organization, 2016). *C. trachomatis* infection in women can cause pelvic inflammatory disease, including salpingitis, tubo-ovarian abscesses, endometritis, pelvic peritonitis, and cervical carcinoma (Cooksey et al., 2010; Di Pietro et al., 2019). Also, chlamydial infections during pregnancy can lead to adverse outcomes, such as premature rupture of membranes, stillbirth, miscarriages, and preterm labor with low birth weight (Adachi et al., 2016). Maternal transmission to neonate during birth may also cause infant pneumonia, otitis media, and inclusion conjunctivitis (Wise et al., 2015). Chlamydial infection in men can lead to orchitis, epididymitis, and urethritis (Dukers-Muijrers et al., 2016; Rowley et al., 2019). Furthermore, *C. trachomatis* infection is related to an increased risk of human immunodeficiency virus (HIV) infection and transmission (Khosropour et al., 2021). In addition, ocular infection with *C. trachomatis* can bring about trachoma, which is the leading cause of blindness worldwide (Pourabbas et al., 2018; Khosropour et al., 2021). Owing to the majority of patients being asymptomatic, making early diagnosis is difficult (Park et al., 2021). Developing a rapid and sensitive point-of-care (POC) testing for accurate screening of *C. trachomatis* infection is critical for earlier treatment to prevent transmission.

Traditional laboratory-based diagnosis of urogenital *C. trachomatis* infection was based on cell cultivation (Meyer, 2016). Isolating pathogens from cell cultures was considered as the initial gold standard for diagnosis of *C. trachomatis* (Meyer, 2016; Kelly et al., 2017). However, the sensitivity was low (ranging from 60 to 80%) and requires stringent conditions in specimen collection, transport, and cultivation (Peng et al., 2020). In addition, cell culture is labor-intensive and time-consuming (48–72 h). Hence, it is rarely performed in routine clinical diagnostic application. Nucleic acid amplification technologies (NAATs), including polymerase chain reaction (PCR) and ligase chain reaction, have been considered as a major breakthrough and have been regarded as the new gold standard for the detection of *C. trachomatis* infection for high sensitivity, specificity, and automation (Gaydos et al., 2013; Safarkar et al., 2017). Nevertheless, NAATs are often unaffordable and inaccessible in resource-limited regions due to requiring skilled technicians and expensive analytical instruments. Therefore, devising a cheap, rapid, simple, and accurate assay is critical to making an early diagnosis and follow-up antibiotic use during the initial stage of *C. trachomatis* infection.

Loop-mediated isothermal amplification (LAMP), an innovative nucleic acid isothermal amplification technique, was considered as an attractive alternative to traditional NAATs, which has potential applications as a POC testing for its simplicity, rapidity, and easy-to-operate (Notomi et al., 2000; Sahoo et al., 2016; Shirato, 2019). More importantly, it has been widely applied to diagnosis of various pathogens, such as SARS-CoV-2, *Neisseria gonorrhoeae*, and HIV (Rudolph et al., 2015; Chen et al., 2021a,b). LAMP amplicons can be analyzed with electrophoresis, turbidity, fluorescent dye, and colorimetric indicators (Li et al., 2017; Shirato, 2019). Nevertheless, all of these techniques require special facilities and reagents. To conveniently detect the LAMP products, gold nanoparticle-based lateral flow biosensor (LFB) is used as a paper-based and POC testing platform, which is currently of enormous potential for clinical applications due to its rapidness, visualization, simplicity, cost-saving, and portability of detection of molecular markers (Anfossi et al., 2019; Ye et al., 2020).

In this study, LAMP integrated with gold nanoparticle-based LFB (LAMP-LFB) was first developed for visual, rapid, specific, sensitive, portable, identification of *C. trachomatis* by targeting the *ompA* gene (Molano et al., 2018; Somboonna et al., 2018). The principle of *C. trachomatis*-LAMP-LFB is illustrated in **Figure 1**, and its feasibility was confirmed with clinical samples. The assay was completed with a high accuracy within 60 min. Therefore, the LAMP-LFB method can be regarded as a valuable POC assay for the detection of *C. trachomatis* infection, particularly in resource-scarce regions.

MATERIALS AND METHODS

Reagents

The LAMP kits and visual detection reagents (Malachite Green, MG) were obtained from HuiDeXin Bio-technology (Tianjin, China). Nucleic acid-releasing agents were purchased from Sansure Biotech Inc. (Changsha, China). Dye streptavidin-coated gold nanoparticles (size: 35 ± 5 nm; crimson red) were obtained from Bangs Laboratories, Inc. (Indiana, USA). Rabbit anti-fluorescein antibody (anti-FAM) and biotinylated bovine serum albumin (biotin-BSA) were purchased from Abcam Co., Ltd. (Shanghai, China). Gold nanoparticle-based biosensor materials, including sample pad, conjugate pad, nitrocellulose (NC) membrane, and absorbent pad were manufactured and assembled by HuiDeXing Biotech. Co., Ltd. (Tianjing, China) according to the design instructions of this study (**Figure 2**).

Clinical Specimens and Target Genes Preparation

A total of 87 clinical genital secretion samples were collected from suspected *C. trachomatis*-infected patients at the Hangzhou Women's Hospital between July 2021 and December 2021. The genomic DNA was obtained using nucleic acid-releasing agents (Sansure Biotech, Changsha, China) in accordance with the instructions of the manufacturer. Briefly, the collected genital secretion samples were centrifuged at 12,000 rpm for 5 min.

Abbreviations: STIs, sexually transmitted infections; LAMP, loop-mediated isothermal amplification; LFB, gold nanoparticle-based lateral flow biosensor; WHO, World Health Organization; PCR, polymerase chain reaction; MG, malachite green; LoD, limit of detection; 2nd GZUTCM, Second Affiliated Hospital, Guizhou University of Traditional Chinese Medicine; GZCCL, Guizhou Provincial Center for Clinical Laboratory; POC, Point of care; nt, nucleotide; mer, monomeric unit; FAM, carboxyfluorescein; TL, test line; CL, control line; DW, distilled water; BC, blank control.

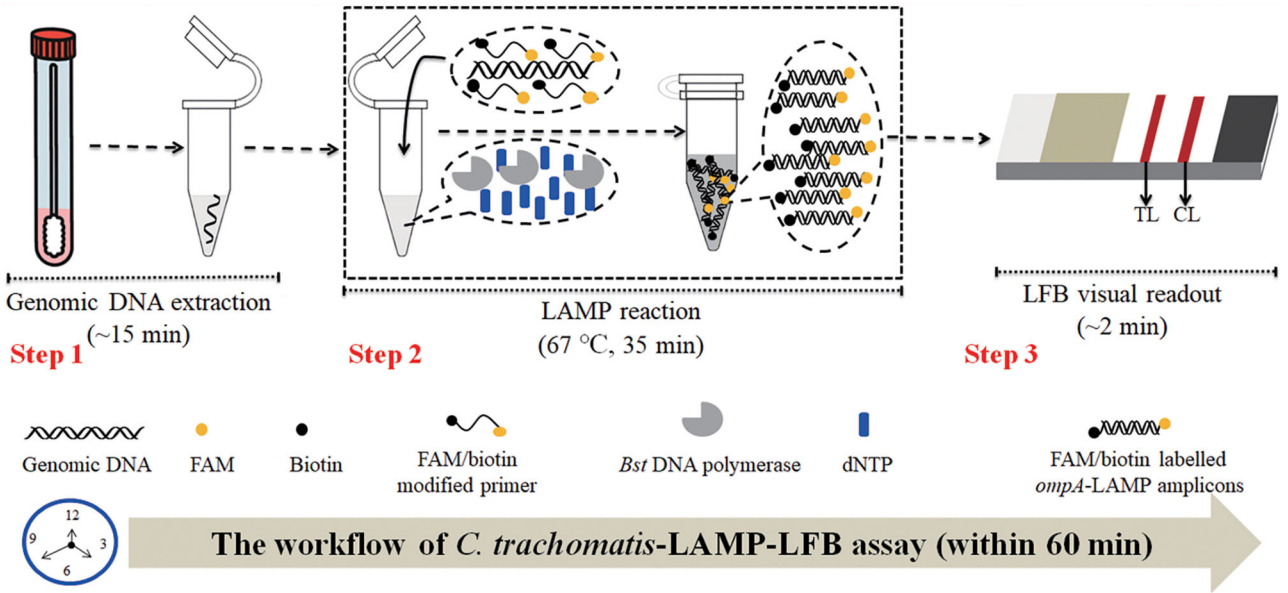

FIGURE 1 | *C. trachomatis*-LAMP-LFB workflow. *C. trachomatis*-LAMP-LFB assay contains three steps: genomic DNA preparation (step 1), LAMP reaction (step 2), and LFB visually readout (step 3). The whole diagnosis procedure can be completed within 60 min.

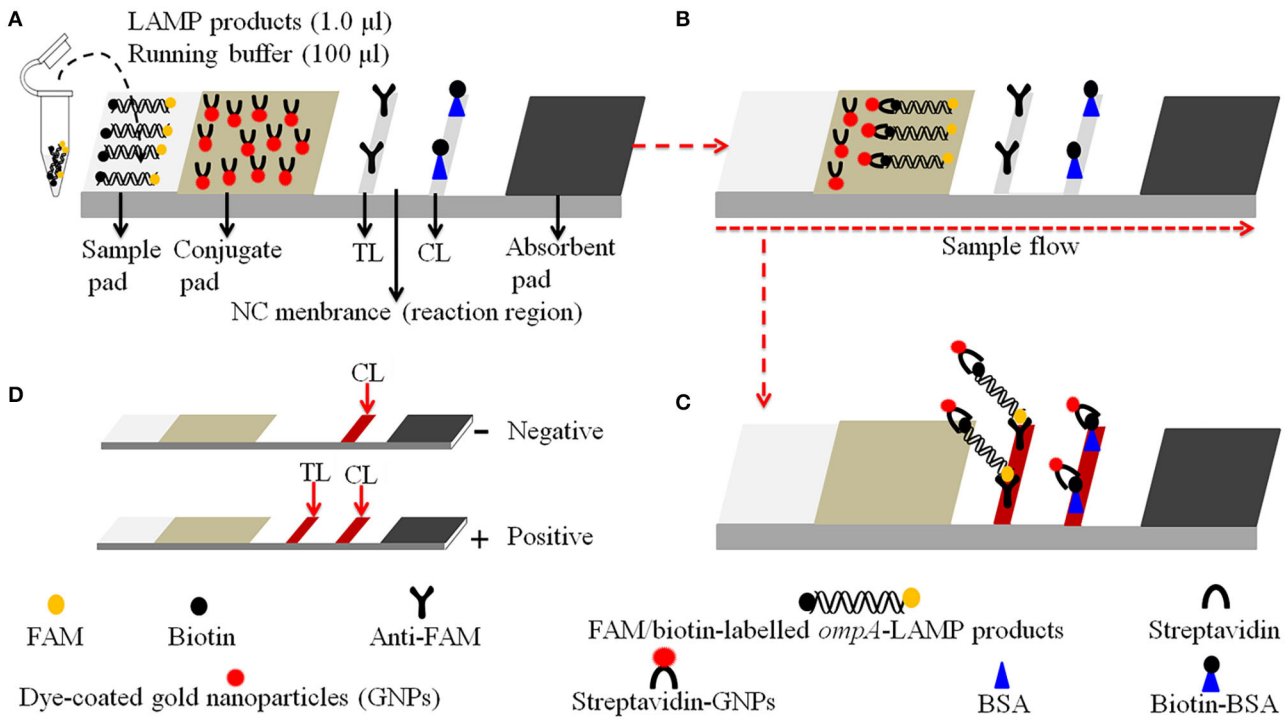

FIGURE 2 | Schematic diagram of the principle of LFB for visually readout *C. trachomatis*-LAMP products. **(A)** *C. trachomatis*-LAMP products and (1.0 μl) and running buffer (100 μl) were simultaneously added to the sample pad. **(B)** The running buffer and *C. trachomatis*-LAMP products move forward to conjugate pad and reaction region due to capillary action. **(C)** For positive results, the FAM/biotin-labeled *ompA*-LAMP products are arrested by anti-FAM at TL strip, and the streptavidin-DPNs are arrested through biotin-BSA at CL strip. For negative results, only the streptavidin-DPNs flow to reaction region and arrested by biotin-BSA at CL strip. **(D)** Interpretation of the *C. trachomatis*-LAMP-LFB assay results: negative—only the CL appears on the LFB; positive—CL and TL appear on biosensor.

The pellet was suspended in 50 μl nucleic acid-releasing agents and incubated at room temperature (25°C) for 10 min, and the supernatant was used as templates for assay. The concentration of nucleic acid was measured using Nano-Drop ND-2000 (Beijing, China) at A260/280.

The full-length DNA sequences of *ompA* gene for *C. trachomatis* serological variants A-K, L1, L2, L3 (serovar A: GenBank Accession No. JX548318.1; serovar B: GenBank Accession No. JX559518.1; serovar C: GenBank Accession No. JX559519.1; serovar D: GenBank Accession No. KP164991.1; serovar E: GenBank Accession No. JX559522.1; serovar F: GenBank Accession No. JX564244.1; serovar G: GenBank Accession No. JX564245.1; serovar H: GenBank Accession No. JX564246.1; serovar I: GenBank Accession No. JX564247.1; serovar J: GenBank Accession No. JX648604.1; serovar K: GenBank Accession No. JX564248.1; serovar L1: GenBank Accession No. JX569832.1; serovar L2: GenBank Accession No. KP120855.1; serovar L3: GenBank Accession No. JX569834.1) were synthesized and cloned in pUC57 vector through Tsingke Biotech (Beijing, China), respectively. The initial concentration of each plasmid was 1×10^8 copies/ml, and the *C. trachomatis* serovar A-plasmid was used as a positive control.

TABLE 1 | *C. trachomatis*-LAMP primers used in this study.

Primer name	Sequence and modifications	Length	Gene
F3	5′-GT(A/T)TTTGCCGCTTTGAGTTCTG-3′	22 nt	*ompA*
B3	5′-AAAC(A/G)CGGTCGAAAACAAAGTC-3′	22 nt	
FIP*	5′-FAM- ATTCCGTCGATC ATAAGGCTTGGTCTTCCTCCTTGCA AGCTCTG-3′	44 mer	
BIP	5′-TGGGAAGGTTT(C/T)GG (C/T)GGAGAT(A/T)CC(A/G) TAGTAACC(A/C)A(C/T)(A/G) CGCATG-3′	43 mer	
LF*	5′-Biotin-CAGCAGGATT CCCCACA-3′	17 nt	
LB	5′-ATCCTTGC(A/G)CCACTTGGTG-3′	19 nt	

FIP, 5′-labeled with FAM when applied for LAMP-LFB detection; LF*, 5′-labeled with biotin when applied for LAMP-LFB detection; FAM, 6-carboxy-fluorescein; nt, nucleotide; mer, monomeric unit.*

Gold Nanoparticle-Based Biosensor Preparation

The schematic design of gold nanoparticle-based LFB is shown in **Figure 2**. Briefly, the LFB consisted of four sections, namely, sample pad, conjugate pad, NC membrane with immobilized anti-FAM and biotin-BSA, and an absorbent pad, all of them were assembled on a plastic adhesive backing card (HuiDeXin Bio-technology, Tianjin, China). Dye streptavidin-coated gold nanoparticles (GNPs) were deposited on the conjugate pad, the size of GNPs was 35 ± 5 nm, and the concentration was 10 mg/ml. Rabbit anti-FAM antibody (0.2 mg/ml; Abcam) and biotin-BSA (4 mg/ml; Abcam) were fixed onto the NC membrane as test line (TL) and control line (CL), respectively. Each line was separated by 5 mm. Hence, the LFB can detect two targets, including *C. trachomatis* LAMP amplicons (TL) and a chromatography control (CL).

Chlamydia trachomatis-LAMP Primers Design and Screening

The *ompA* genes from 14 *C. trachomatis* serological variants (serovar A, B, C, D, E, F, G, H, I, J, K, L1, L2, L3) were aligned with MEGA-X (https://www.megasoftware.net/), and then the conserved sequences were selected for designing of *C. trachomatis*-LAMP primers. A total of three sets of LAMP primers were designed by Primer Explorer V5 (http://primerexplorer.jp/e/) according to the LAMP reaction mechanisms. Each set of LAMP primers includes outer primers F3 and B3, loop primers LF and LB, and inner primers FIP and BIP. The screening of primers was performed with standard *C. trachomatis*-LAMP reaction system, and LAMP amplicons were monitored using real-time turbidity (LA-500). The first set of LAMP primers showed better outcome in amplification efficiency (data not shown), which was used for the establishment of the *C. trachomatis*-LAMP assay. The schematic design of *C. trachomatis*-LAMP primers is demonstrated in **Supplementary Figure 1**, and the sequences and modifications are shown in **Table 1**. All LAMP primers were synthesized and purified by Tsingke Biotech (Beijing, China) at high-performance liquid chromatography purification grade.

Chlamydia trachomatis-LAMP Reaction and Detection

The standard LAMP reaction was performed with an isothermal amplification kit (HuiDeXing Biotech. Co., Ltd. Tianjing, China). Briefly, a 25 μl reaction mixture contained 12.5 μl 2× reaction buffer [16 mM $MgSO_4$, 2 M betaine, 40 mM Tris–HCl (pH 8.8), 40 mM KCl, 20 mM $(NH_4)_2SO_4$, and 0.2% Tween-20]; 1 μl of standard plasmid template (5 μl of clinical sample template); 0.4 μM each outer primer, F3 and B3; 0.8 μM each loop primer, LF* and LB; 1.6 μM each inner primer, FIP* and BIP; 8 U of *Bst* 2.0 DNA polymerase; and double-distilled water (DW) was added to 25 μl. The reaction was carried out in a heat block at constant temperature (optimization outlined later).

Real-time turbidity (LA-500), visual detection reagents (Malachite Green, MG), and LFB were applied to analyze the LAMP products and confirm the optimal *C. trachomatis*-LAMP-LFB reaction system. For the real-time turbidity detection, turbidity > 0.1 was considered as a positive result. For visual MG reagent analysis, the reaction mixtures changed to light green, indicating a positive outcome, and remained colorless, suggesting a negative result. For the LFB method, CL and TL were observed simultaneously, indicating a positive outcome, and only the CL appeared, suggesting a negative result.

Chlamydia trachomatis-LAMP Reaction Temperature Optimization

Temperature is important for LAMP reaction. An optimal amplification temperature of *C. trachomatis*-LAMP ranging from 63 to 70°C (with 1°C intervals) was evaluated with *ompA*-plasmids (5.0×10^3 copies/ml). The LAMP products were monitored with real-time turbidity (LA-500). The examinations were conducted independently in triplicate.

Sensitivity of the *C. trachomatis*-LAMP-LFB Assay

The initial concentrations of *ompA* standard plasmids were 1×10^8 copies/ml. Then, 10-fold serial diluted from 5.0×10^4 to 5.0×10^{-1} copies/ml were used to evaluate the limit of detection (LoD) of the *C. trachomatis*-LAMP-LFB. The reactions were carried out under optimal reaction temperature, and the outcomes were analyzed simultaneously with MG and LFB. The LoD of *C. trachomatis*-LAMP was verified as the lowest dilution for which all three replicates were positive. Next, the concentration of *ompA*-plasmids at the LoD level was applied for identifying the optimal reaction times (15, 25, 35, and 45 min) of the *C. trachomatis*-LAMP assay.

Specificity of the *C. trachomatis*-LAMP-LFB Assay

The analytical specificity of the *C. trachomatis*-LAMP-LFB was estimated by comparing *C. trachomatis* DNA templates (serovar A-K, L1, L2, L3) with the nucleic acid (at least 1.0×10^4/test) extracted from various pathogens (**Table 2**), and DW was used as a blank control. The results were analyzed with LFB, and each test was performed in triplicate.

Validating the Feasibility of *C. trachomatis*-LAMP-LFB Using Clinical Samples

For confirming assay feasibility, the optimized diagnostic system was verified with clinical specimens. A total of 87 suspected *C. trachomatis*-infected genital secretion samples were collected from Hangzhou Women's Hospital (Hangzhou, China). Specimens were simultaneously detected using real-time quantitative PCR (qPCR) and LAMP-LFB assays. qPCR diagnosis was performed with a commercial *C. trachomatis* nucleic acid assay kit (DaAn Gene Co., Ltd. China), and the amplification and detection were performed using Applied Biosystems™ 7500 Real-Time PCR System (Life Technologies, Singapore). The concentration of more than 500 copies/ml of *C. trachomatis* is regarded as a positive outcome according to the instructions of the manufacturer. The *C. trachomatis*-LAMP-LFB process is described above. The whole process was carried out at biosafety level 2 according to the *WHO Laboratory Biosafety Manual*, 3rd edition.

RESULTS

Schematic Mechanism of the *C. trachomatis*-LAMP-LFB Assay

The *C. trachomatis*-LAMP-LFB schematic mechanism and workflow are shown in **Figure 1**. In brief, the *C. trachomatis* genomic DNA was released by nucleic acid releasing agents (**Step 1**), and then was pre-amplified through LAMP at a constant temperature of 67°C for 35 min, two core primers, including FIP and LF, were labeled at the 5′-end with FAM and biotin, respectively. As a result, plenty of detectable double-labeled products are formed with *ompA*-LAMP amplicons simultaneously labeled with FAM and biotin (**Step 2**). Finally, the LAMP amplicons are visually analyzed using LFB within 2 min (**Step 3**).

The Principle of Visual Detection of *C. trachomatis*-LAMP Products Using LFB

Details of the visual detection of *C. trachomatis*-LAMP products through nanoparticle-based LFB are shown in **Figure 2**. Notably, 1.0 μl of *C. trachomatis*-LAMP products and 100 μl of running buffer (100 mM PBS, pH 7.4 with 1% Tween 20) were deposited on the sample pad (**Figure 2A**). The running buffer containing *C. trachomatis*-LAMP products can move along the LFB with capillary action, and rehydrate the immobilized streptavidin-GNPs in conjugate pad (**Figure 2B**). Positive amplicons were specifically captured by anti-FAM and Biotin-BSA at TL and CL in reaction region, respectively (**Figure 2C**). For negative results, only streptavidin-DPNs were captured by biotin-BSA at the CL. The interpretation of *C. trachomatis*-LAMP-LFB assay readout is shown in **Figure 2D**.

Confirmation and Analysis of *C. trachomatis*-LAMP Products

For validating the *C. trachomatis*-LAMP system, LAMP amplification was performed at a constant temperature of 65°C for 1 h using *ompA* standard plasmids. Using visual MG reagent analysis, the *C. trachomatis*-LAMP tube was visualized by the naked eye as bright green, while the negative controls (*Neisseria gonorrhoeae* and *Ureaplasma urealyticum*) and blank control remained colorless (**Figure 3A**). In the LFB, two red bands appeared in TL and CL in positive *C. trachomatis*-LAMP amplification. Only a red band presented in CL represents negative and blank controls (**Figure 3B**). These data demonstrated that the *C. trachomatis*-LAMP primer set and reaction system are valid for target gene detection.

Confirmation of the Optimal Amplification Temperature for *C. trachomatis*-LAMP-LFB Assay

For optimization of the reaction temperature at the *C. trachomatis*-LAMP pre-amplification stage, temperature from 63 to 70°C with 5.0×10^3 copies/ml of *C. trachomatis* DNA template was investigated (**Figures 4A–H**). Utilizing real-time turbidity (LA-500), the robust amplification of *C. trachomatis*-LAMP was observed at 67°C (**Figure 4E**).

TABLE 2 | Pathogens used in this study.

No.	Pathogen	Source of pathogens[a]	No. of strains	*C. trachomatis*-LAMP-LFB result[b]
1	*C. trachomatis* serovar A *ompA*-plasmids	Constructed by Tsingke Biotech (Beijing, China)	1	P
2	*C. trachomatis* serovar B *ompA*-plasmids	Constructed by Tsingke Biotech (Beijing, China)	1	P
3	*C. trachomatis* serovar C *ompA*-plasmids	Constructed by Tsingke Biotech (Beijing, China)	1	P
4	*C. trachomatis* serovar D *ompA*-plasmids	Constructed by Tsingke Biotech (Beijing, China)	1	P
5	*C. trachomatis* serovar E *ompA*-plasmids	Constructed by Tsingke Biotech (Beijing, China)	1	P
6	*C. trachomatis* serovar F *ompA*-plasmids	Constructed by Tsingke Biotech (Beijing, China)	1	P
7	*C. trachomatis* serovar G *ompA*-plasmids	Constructed by Tsingke Biotech (Beijing, China)	1	P
8	*C. trachomatis* serovar H *ompA*-plasmids	Constructed by Tsingke Biotech (Beijing, China)	1	P
9	*C. trachomatis* serovar I *ompA*-plasmids	Constructed by Tsingke Biotech (Beijing, China)	1	P
10	*C. trachomatis* serovar J *ompA*-plasmids	Constructed by Tsingke Biotech (Beijing, China)	1	P
11	*C. trachomatis* serovar K *ompA*-plasmids	Constructed by Tsingke Biotech (Beijing, China)	1	P
12	*C. trachomatis* serovar L1 *ompA*-plasmids	Constructed by Tsingke Biotech (Beijing, China)	1	P
13	*C. trachomatis* serovar L2 *ompA*-plasmids	Constructed by Tsingke Biotech (Beijing, China)	1	P
14	*C. trachomatis* serovar L3 *ompA*-plasmids	Constructed by Tsingke Biotech (Beijing, China)	1	P
15	*C. trachomatis* (clinical samples)	Hangzhou Women's Hospital	5	P
16	*Neisseria gonorrhoeae*	Hangzhou Women's Hospital	1	N
17	*Ureaplasma urealyticum*	Hangzhou Women's Hospital	1	N
18	*Mycobacterium tuberculosis* (nucleic acid samples)	GZCDC	1	N
19	*Escherichia coli*	2nd GZUTCM	1	N
20	*Haemophilus influenza*	ATCC49247	1	N
21	*Cryptococcus neoformans*	ATCC13690	1	N
22	*Streptococcus pyogenes*	2nd GZUTCM	1	N
23	*Pseudomonas aeruginosa*	2nd GZUTCM	1	N
24	*Staphylococcus aureus*	2nd GZUTCM	1	N
25	*Candida glabrata*	2nd GZUTCM	1	N
26	*Bordetella pertussis*	GZCCL	1	N
27	*Hemophililus parainfluenza*	GZCCL	1	N
28	*Klebsiella pneumoniae*	GZCCL	1	N
29	*Mycoplasma pneumoniae*	Hangzhou Women's Hospital	1	N
30	*Shigella flexneri*	Hangzhou Women's Hospital	1	N
31	*Listeria monocytogenes*	GZCCL	1	N
32	Human enterovirus EV71	GZCCL	1	N
33	Coxsackie virus CAV16	GZCCL	1	N
34	Human rhinovirus	GZCCL	1	N
35	Human papilloma virus	GZCCL	1	N

[a] *2nd GZUTCM, the Second Affiliated Hospital, Guizhou University of Traditional Chinese Medicine; ATCC, American Type Culture Collection; GZCCL, Guizhou Provincial Center for Clinical Laboratory; GZCDC, Guizhou Provincial Center for Disease Control and Prevention.*

[b] *P, positive; N, negative.*

Hence, 67°C was used as the optimal amplification for *C. trachomatis*-LAMP-LFB assay.

Sensitivity of the *C. trachomatis*-LAMP-LFB Assay

As shown in **Figure 5**, the *C. trachomatis*-LAMP-LFB assay can detect as few as 50 copies/ml of *ompA* standard plasmids in a vessel. The *C. trachomatis*-LAMP amplification was operated as described above, and the results were obtained using LFB and MG visual reagent. The results obtained *via* LFB were consistent with MG reagent (**Figures 5A,B**).

Optimal Amplification Times for the *C. trachomatis*-LAMP-LFB Assay

The reaction time for the *C. trachomatis*-LAMP-LFB assay during the amplification stage was optimized. As shown in **Figure 6**, the lowest template level of *ompA* standard plasmid (50 copies/ml) was tested when the reaction time lasted for 35 and 45 min at 67°C, and a reaction time of 35 min was recommended during the LAMP pre-amplification stage. Hence, the whole diagnostic procedure of the *C. trachomatis*-LAMP-LFB technique, including rapid genomic DNA preparation (15 min), LAMP reaction (35 min), and result readout (<2 min), can be completed within 1 h.

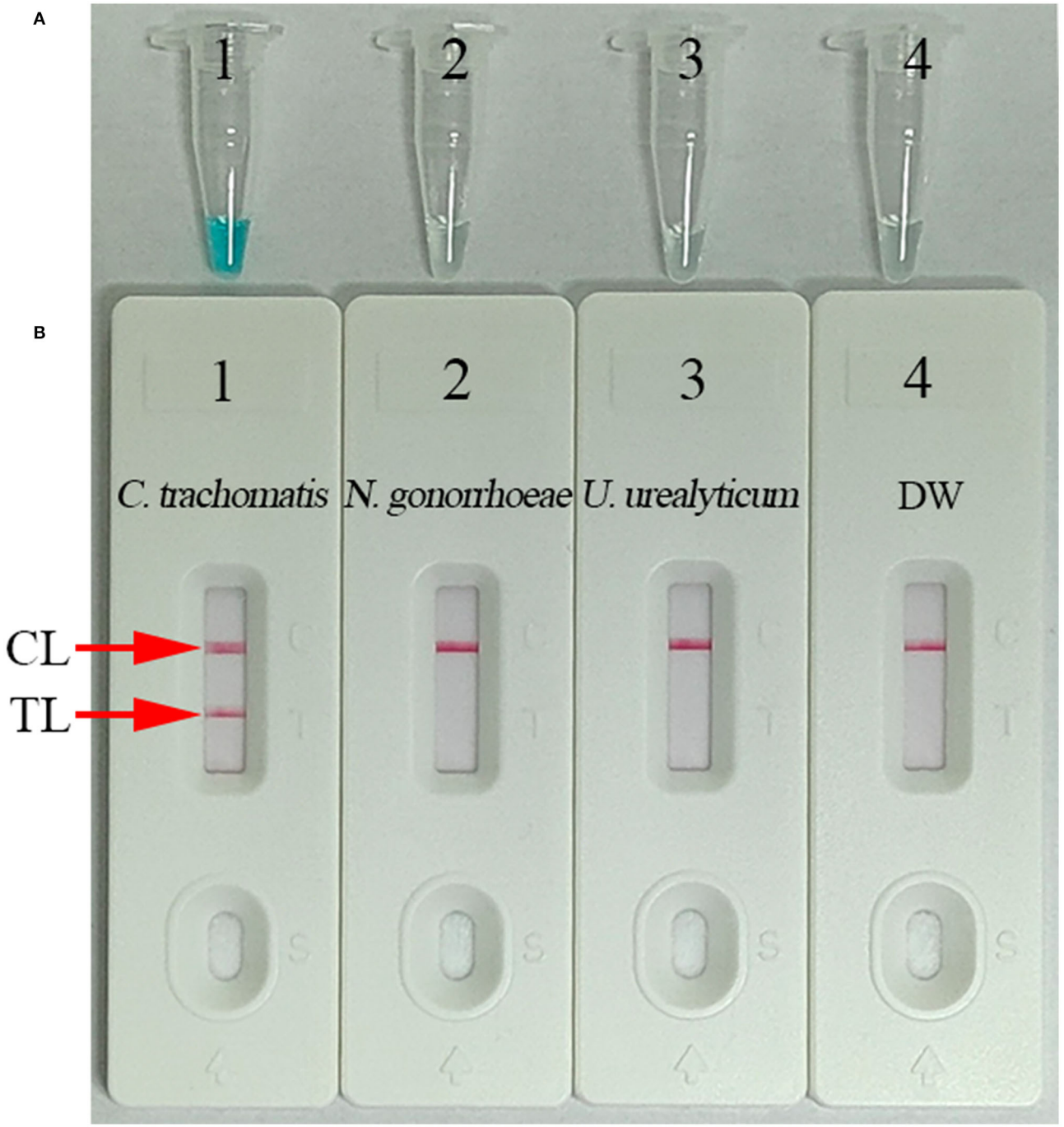

FIGURE 3 | Confirmation and verification of *C. trachomatis*-LAMP products. *C. trachomatis*-LAMP products were measured simultaneously through MG regents **(A)** and LFB **(B)**. Tube 1/biosensor 1: positive result for the *C. trachomatis ompA* standard plasmids; tube 2/biosensor 2: negative result for *Neisseria gonorrhoeae*; tube 3/biosensor 3: negative result for *Ureaplasma urealyticum*; tube 4/biosensor 4: blank control (distilled water, DW). TL, test line; CL, control line.

Specificity of the *C. trachomatis*-LAMP-LFB Assay

The specificity estimation of the *C. trachomatis*-LAMP-LFB assay was tested using synthesized templates (*omp A* sequences from serovar A-K, L1, L2, and L3, respectively), *C. trachomatis*-positive clinical samples (confirmed with qPCR), and various non-*C. trachomatis* pathogens (**Table 2**; **Supplementary Figure 2**). The positive results were observed when the templates were extracted from *C. trachomatis* species. While no positive results were detected from non-*C. trachomatis* pathogens and

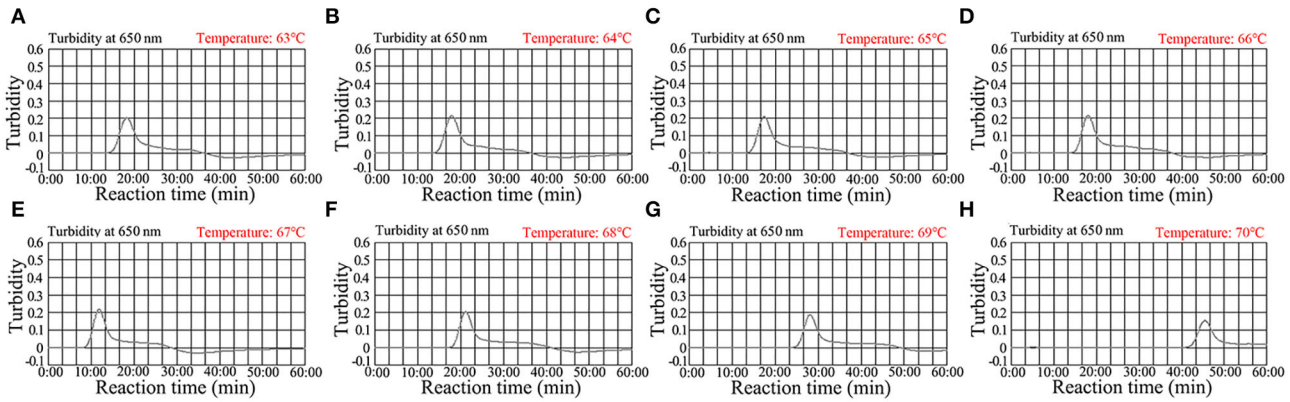

FIGURE 4 | Optimization of the temperature for *C. trachomatis*-LAMP reactions. *C. trachomatis*-LAMP reaction process was monitored using real-time turbidity (LA-500). The threshold value was 0.1, and the turbidity >0.1 was regarded as positive. Eight kinetic graphs **(A–H)** were yielded at various amplification temperatures (63–70°C at 1°C intervals) with *C. trachomatis ompA*-plasmids at the level of 5×10^3 copies/ml. The graphs at 67°C showed robust amplification.

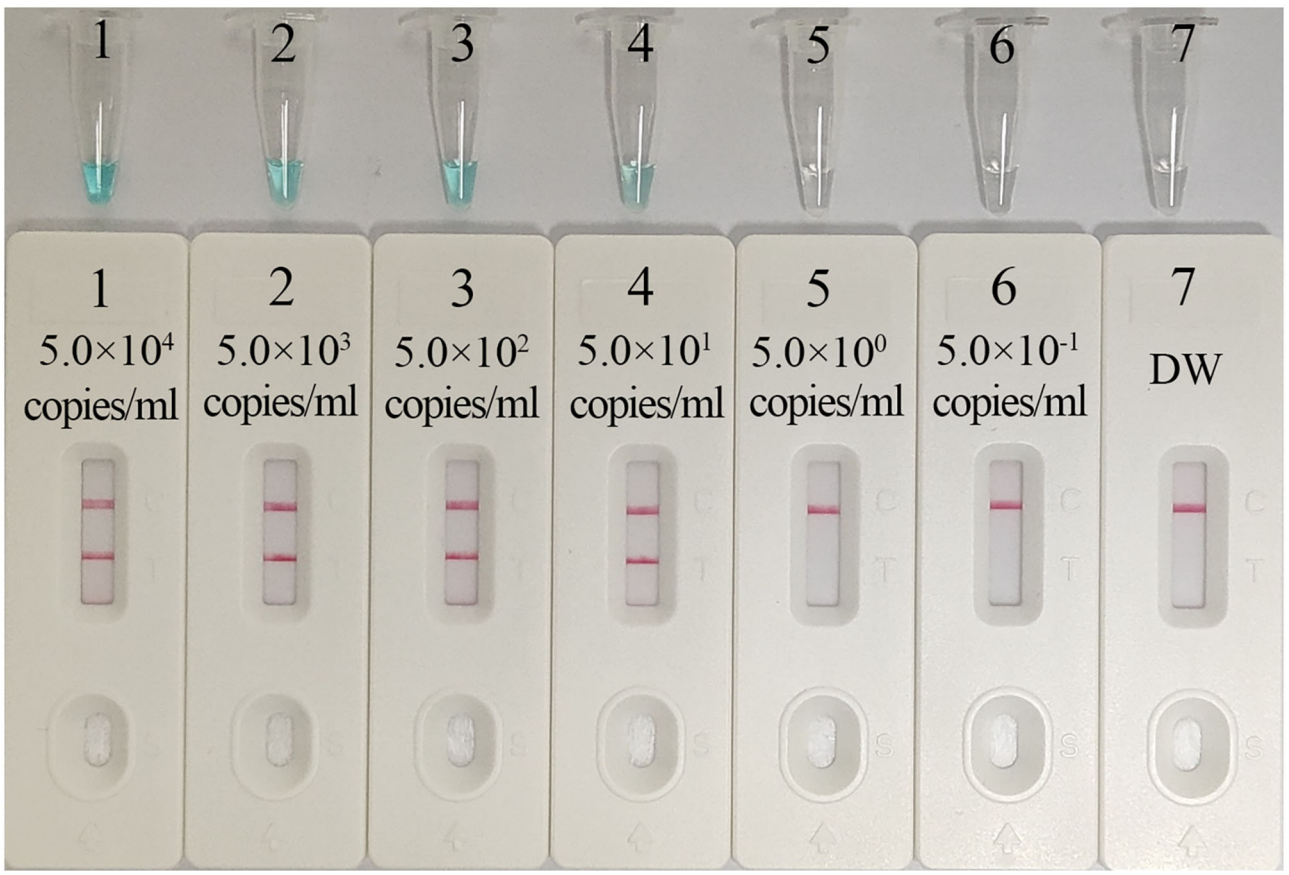

FIGURE 5 | Assay sensitivity using serially diluted *C. trachomatis ompA*-plasmid templates. **(A)** Visual MG regents used for detecting the results; **(B)** LFB used for detecting the results. Tubes A1–A7 (biosensors B1–B7) represent the *C. trachomatis ompA*-plasmid levels of 5.0×10^4, 5.0×10^3, 5.0×10^2, 5.0×10^1, 5.0×10^0, 5.0×10^{-1}, and 5.0×10^{-2} copies/ml and blank control (distilled water). The template levels from 5.0×10^4 to 5.0×10^1 copies/ml showed positive results. CL, control line; TL, test line.

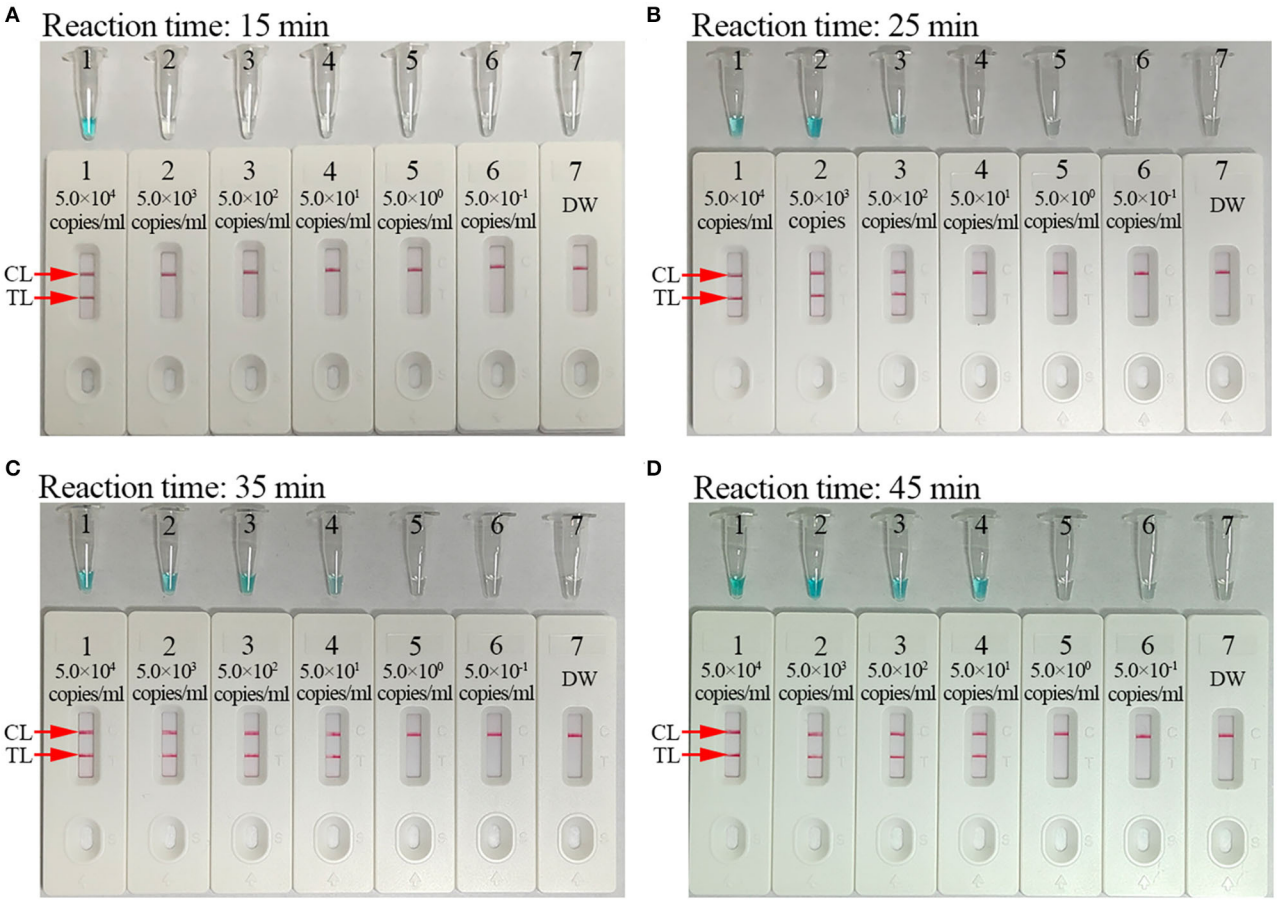

FIGURE 6 | Optimization of reaction time for *C. trachomatis*-LAMP-LFB assay. Reaction times (**A**, 15 min; **B**, 25 min; **C**, 35 min; **D**, 45 min) were tested at optimal reaction temperature of 67°C. Tube/biosensors B1–B7 represent plasmid levels of 5.0×10^4, 5.0×10^3, 5.0×10^2, 5.0×10^1, 5.0×10^0, 5.0×10^{-1}, and 5.0×10^{-2} copies/ml and blank control (distilled water). The LoD of plasmid template could be detected when the reaction lasted for 35 min (C). CL, control line; TL, test line.

blank control (**Table 2**; **Supplementary Figure 2**). These data suggested that the *C. trachomatis*-LAMP-LFB assay has an excellent specificity.

Evaluation of the *C. trachomatis*-LAMP-LFB Assay Using Clinical Samples

A total of 87 suspected *C. trachomatis*-infection genital secretion samples detected were simultaneously using qPCR and *C. trachomatis*-LAMP-LFB assay. A total of 37 (42.5%) were detected as positive outcomes using qPCR (>500 copies/ml); these *C. trachomatis*-positive samples have also been confirmed through *C. trachomatis*-LAMP-LFB. Besides, 3 of the 50 "negative samples" (range from 300 to 500 copies/ml) were detected as positive outcomes through *C. trachomatis*-LAMP-LFB (**Table 3**; **Supplementary Table 1**). These results indicated that our *C. trachomatis*-LAMP-LFB assay is an advanced diagnostic tool for suspected *C. trachomatis*-infected patients, especially for those with low bacterial loads.

TABLE 3 | Comparison of qPCR and LAMP-LFB for detection of *C. trachomatis* in clinical samples.

Detection method	Clinical samples ($n = 87$)	
	Positive	Negative
qPCR	37 (>500 copies/ml)	50 (47, undetected; 3, range from 300 to 500 copies/ml)
LAMP-LFB	40	47

DISCUSSION

Genital infection with *C. trachomatis* is considered to be one of the most common bacterial STIs worldwide (Ramadhani et al., 2019; La Rosa et al., 2021). A distinguishing feature of *C. trachomatis* infection is that the patients are asymptomatic at the early stage of infection and usually delay or do not seek medical treatment, especially in less-developed regions,

which brings about the continued transmission (Tadele et al., 2019; Caven and Carabeo, 2020). Hence, a rapid, accurate, cost-saving, and easy-to-operate assay for early diagnosis of *C. trachomatis* is critical for addressing ever-increasing *C. trachomatis* infection transmission rates. Here, a novel *C. trachomatis*-LAMP-LFB assay, which combined LAMP amplification with gold nanoparticle-based biosensor, was devised and applied successfully to the visual and rapid testing of *C. trachomatis* in clinical samples.

Traditional diagnostic techniques, including cell culture, enzyme immunoassay, and direct fluorescence assay, were used to diagnose *C. trachomatis* infection (Kelly et al., 2017; Peng et al., 2020). However, all of these tools cannot meet fully the requirement of early and easy-to-operate diagnosis in clinical application. Cell culture was regarded as the initial gold standard for *C. trachomatis* detection, but *C. trachomatis* require fastidious and demanding cultivation conditions, and the procedure of cell culture is time-consuming and labor-intensive (Herbst De Cortina et al., 2016). Therefore, it is now seldom utilized in clinical laboratory. Compared with cell cultivation, enzyme immunoassay and direct fluorescence assay are relatively simple and rapid, but are not recommended as routine diagnostic methods due to low diagnostic accuracy (Peng et al., 2020). Nucleic acid amplification tests are more sensitive and have an excellent specificity, which is recommended as the new gold diagnostic method for *C. trachomatis* detection (Herbst De Cortina et al., 2016; Safarkar et al., 2017). However, their use is confined due to requiring complicated laboratory facilities and trained technicians in resource-impoverished regions. In this study, the *C. trachomatis*-LAMP-LFB method only requires simple instruments, such as water bath, heating block, or even a thermos cup that can maintain a constant temperature (67°C). More importantly, the detection results can be visually read out with LFB. The whole diagnosis procedure, including genomic DNA releasing (∼15 min), LAMP amplification (35 min), and result visual interpretation (<2 min), can be completed within 60 min.

In this study, LAMP was applied to amplify the target gene of *C. trachomatis*, which is a novel nucleic acid amplification technique devised by Notomi et al., usually 100-fold higher sensitivity than traditional PCR (Notomi et al., 2000; Avendaño and Patarroyo, 2020; Chaouch, 2021). A set of four or six primers spanning six or eight different regions of the target gene makes the amplification results highly specific. The primer set contains two outer primers (F3 and B3), two inner primers (FIP and BIP), and two loop primers (LF and LB) (Panno et al., 2020). Typically, four primers (F3, B3, FIP, and BIP) are enough to amplify a target fragment and improve its efficiency and specificity, while the two loop primers are added to the LAMP amplification system (Augustine et al., 2020; García-Bernalt Diego et al., 2021). In addition, a *Bst* DNA polymerase with chain displacement capability is critical for LAMP amplification at a fixed temperature (Notomi et al., 2000). Here, a set of *C. trachomatis*-LAMP primers were successfully designed for targeting 8 regions of *ompA* gene from 14 *C. trachomatis* serological variants (serovar A, B, C, D, E, F, G, H, I, J, K, L1, L2, L3). The specificity analysis confirmed that the *C. trachomatis*-LAMP-LFB assay can correctly identify the target pathogens and have no cross-reactions with no-*C. trachomatis* templates (**Table 2**; **Supplementary Figure 2**). Furthermore, the LoD of *C. trachomatis*-LAMP-LFB assay is as low as 50 copies/ml. To further confirm the feasibility of the assay in clinical application, 87 genomic DNA samples isolated from suspected *C. trachomatis*-infected patients were tested simultaneously with *C. trachomatis*-LAMP-LFB and qPCR. The data indicated that our assay is strengthened in detecting *C. trachomatis*-infected genital secretion samples (**Table 3**; **Supplementar Table 1**). To further verify its feasibility, much more low copy number of clinical samples should be collected and tested in the subsequent study. The lower detection rate of qPCR may be attributed to low copy number of the *C. trachomatis* DNA templates, and the qPCR detection was performed with a commercial real-time TaqMan PCR Kit (Da An Gene Co., Ltd. China). The concentrations of *C. trachomatis* < 500 copies/ml will be regarded as a negative outcome according to the illustrations of the manufacturer. In this study, three "negative" clinical specimens (*C. trachomatis* concentrations ranging from 300 to 500 copies/ml) presented positive results using *C. trachomatis*-LAMP-LFB, which further verified that the sensitivity of our assay is higher than the traditional PCR technique.

For visual and rapid presentation of *C. trachomatis*-LAMP results, gold nanoparticle-based LFB was used in this assay system. LFB is a paper-based device that has been extensively used in the diagnosis of infectious diseases, foodborne pathogens, cancer biomarkers, and cardiovascular disease, owing to its low-cost, rapid detection with good robustness, specificity, sensitivity, and easy-to-operate (Hsieh et al., 2017; Huang et al., 2020; Wang et al., 2021). Here, the LFB strips were immobilized with anti-FAM and BSA-biotin on TL and CL, respectively. For positive outcomes, the FAM/biotin-labeled *C. trachomatis*-LAMP amplicons were arrested by anti-FAM at the TL and the streptavidin-DPNs were captured by biotin-BSA at the CL, respectively. For negative results, only the streptavidin-DPNs were arrested by biotin-BSA at the CL. Although the MG regents and real-time turbidity were able to test the *C. trachomatis*-LAMP results in this study, the former is ambiguous when LAMP amplicon concentrations were low (**Figure 6C**), and the latter technique requires expensive apparatus. The LFB method is simple and cost-effective (∼US$2.0 for each strip). Hence, the overall cost of each *C. trachomatis*-LAMP-LFB test, including DNA template extraction (∼US$1.0), LAMP reaction (∼US$3.0), and LFB readout (∼US$2.0), was calculated at US$6.0. In previous studies, LAMP has already been used to identify *C. trachomatis*. Choopara et al. (2017) and Somboonna and Choopara (2019) combined LAMP with hydroxynaphthol blue for visual color detection of *C. trachomatis* by the naked eye, but the results of this assay were ambiguous when LAMP product concentrations were low. Dean et al. (2021) have also utilized the LAMP assay for testing *C. trachomatis*, and the *C. trachomatis*-LAMP amplification products were examined with colorimetric chemistry, which must rely on optical detection instrumentation. In this study, we first combined LAMP amplification with LFB for the identification of *C. trachomatis*, which is more convenient and rapid than other methods.

The *C. trachomatis*-LAMP-LFB also has some shortcomings. First, there is a risk of carryover contamination; the LAMP reaction tube must be taken off for LFB identification. Spraying a 10–15% sodium hypochlorite solution and 70% ethanol after LFB detection is an effective way of avoiding nucleic acid contamination in laboratory. In this study, no false-positive outcomes were observed in non-*C. trachomatis* templates. It is indicated that the cross-contamination can be effectively controlled in our laboratory. Secondly, our assay can be used for qualitative detection of *C. trachomatis*, but not measurement of the concentrations of *C. trachomatis* in sample; the quantitative determination of LAMP-LFB could be considered for further study in the future. Thirdly, the *C. trachomatis*-LAMP-LFB system just detected the *ompA* gene from 14 *C. trachomatis* serological variants (serovar A-K, L1, L2, L3) and neglected the internal control gene. For better fitting the clinical application, the *C. trachomatis*-LAMP amplification system should add a set of LAMP primers based on the internal control gene (human gene) for avoiding false-negative results. The LFB has designed three lines, including CL, internal control line, and TL, which can effectively avoid false-positive results.

In conclusion, we combined a LAMP reaction with LFB readout platform for successfully devising a novel *C. trachomatis*-LAMP-LFB for the rapid, visual, cost-effective, specific, and sensitive identification of *C. trachomatis* agent in clinical samples. The LoD of our assay was 50 copies/ml and had no cross-reaction with non-*C. trachomatis* pathogens. The whole assay process can be completed within 60 min without any special instrument. Therefore, the *C. trachomatis*-LAMP-LFB shows great potential as POC testing for *C. trachomatis* screening and detection in clinical settings, especially in resource-starved regions.

DATA AVAILABILITY STATEMENT

The datasets presented in this study can be found in online repositories. The names of the repository/repositories and accession number(s) can be found in the article/**Supplementary Material**.

ETHICS STATEMENT

The study was approved by the Human Ethics Committee of Hangzhou Women's Hospital (Approval No. [2021]-K (2)-8) and complied with the Declaration of Helsinki. Before clinical samples/isolates were obtained, all personal patient identifiers were removed. Patients' informed consent was waived by the committee.

AUTHOR CONTRIBUTIONS

XC and SD designed and conceived this study and drafted and revised the manuscript. XC, QZ, YT, RW, XW, JL, RL, SW, and SD collected clinical samples and performed the experiments. XC, QZ, and SD analyzed the data. All authors read and approved the final manuscript.

FUNDING

This study was funded by the Program of Scientific and Technological Project in Guizhou Province (Grant No. Qian Ke He [2020]4Y184), the Scientific and Technological in Guiyang City (Grant No. Zhu Ke He [2020]-10-5), and the Public Welfare Technology Research Program in Zhejiang Province (Grant No. LGF21H190001).

ACKNOWLEDGMENTS

We thank the medical personnel in the Hangzhou Women's Hospital, 2nd GZUTCM, and GZCCL for their cooperation in this study, and we also thank all of the patients who provided the clinical specimens.

SUPPLEMENTARY MATERIAL

The Supplementary Material for this article can be found online at: https://www.frontiersin.org/articles/10.3389/fmicb.2022.914620/full#supplementary-material

REFERENCES

Adachi, K., Nielsen-Saines, K., and Klausner, J. D. (2016). *Chlamydia trachomatis* infection in pregnancy: the global challenge of preventing adverse pregnancy and infant outcomes in Sub-Saharan Africa and Asia. *Biomed Res. Int.* 2016, 1–21. doi: 10.1155/2016/9315757

Anfossi, L., Di Nardo, F., Cavalera, S., Giovannoli, C., and Baggiani, C. (2019). Multiplex lateral flow immunoassay: an overview of strategies towards high-throughput point-of-need testing. *Biosensors* 9, 2. doi: 10.3390/bios9010002

Augustine, R., Hasan, A., Das, S., Ahmed, R., Mori, Y., Notomi, T., et al. (2020). Loop-mediated isothermal amplification (LAMP): a rapid, sensitive, specific, and cost-effective point-of-care test for coronaviruses in the context of COVID-19 pandemic. *Biology* 9, 182. doi: 10.3390/biology9080182

Avendaño, C., and Patarroyo, M. A. (2020). Loop-mediated isothermal amplification as point-of-care diagnosis for neglected parasitic infections. *Int. J. Mol. Sci.* 21, 7981. doi: 10.3390/ijms21217981

Caven, L., and Carabeo, R. A. (2020). Pathogenic puppetry: manipulation of the host actin cytoskeleton by *Chlamydia trachomatis*. *Int. J. Mol. Sci.* 21, 90. doi: 10.3390/ijms21010090

Chaouch, M. (2021). Loop-mediated isothermal amplification (LAMP): an effective molecular point-of-care technique for the rapid diagnosis of coronavirus SARS-CoV-2. *Rev. Med. Virol.* 31, e2215. doi: 10.1002/rmv.2215

Chen, X., Zhou, Q., Li, S., Yan, H., Chang, B., Wang, Y., et al. (2021a). Rapid and visual detection of SARS-CoV-2 using multiplex reverse transcription Loop-mediated isothermal amplification linked with gold nanoparticle-based lateral flow biosensor. *Front. Cell. Infect. Microbiol.* 11, 581239. doi: 10.3389/fcimb.2021.581239

Chen, X., Zhou, Q., Wu, X., Wang, S., Liu, R., Dong, S., et al. (2021b). Visual and rapid diagnosis of *Neisseria gonorrhoeae* using Loop-mediated isothermal amplification combined with a polymer nanoparticle–based biosensor in clinical application. *Front. Mol. Biosci.* 8, 702134. doi: 10.3389/fmolb.2021.702134

Choopara, I., Arunrut, N., Kiatpathomchai, W., Dean, D., and Somboonna, N. (2017). Rapid and visual *Chlamydia trachomatis* detection using loop-mediated isothermal amplification and hydroxynaphthol blue. *Lett. Appl. Microbiol.* 64, 51–56. doi: 10.1111/lam.12675

Cooksey, C. M. J. L., Berggren, E. K., and Lee, J. (2010). *Chlamydia trachomatis* infection in minority adolescent women: a public health challenge. *Obstet. Gynecol. Surv.* 65, 729–735. doi: 10.1097/OGX.0b013e3182110204

Dean, D., Swaminathan, S., Kama, M., Goemans, S., Faktaufon, D., Alnabelseya, N., et al. (2021). Development and evaluation of a point-of-Care test in a low-resource setting with high rates of *Chlamydia trachomatis* urogenital infections in Fiji. *J. Clin. Microbiol.* 59, e0018221. doi: 10.1128/JCM.00182-21

Di Pietro, M., Filardo, S., Romano, S., and Sessa, R. (2019). *Chlamydia trachomatis* and *Chlamydia pneumoniae* interaction with the host: latest advances and future prospective. *Microorganisms* 7, 140. doi: 10.3390/microorganisms7050140

Dukers-Muijrers, N. H., Wolffs, P. F., Eppings, L., Gotz, H. M., Bruisten, S. M., Schim, V. D. L. M., et al. (2016). Design of the FemCure study: prospective multicentre study on the transmission of genital and extra-genital *Chlamydia trachomatis* infections in women receiving routine care. *BMC Infect. Dis.* 16, 381. doi: 10.1186/s12879-016-1721-x

García-Bernalt Diego, J., Fernández-Soto, P., and Muro, A. (2021). LAMP in neglected tropical diseases: a focus on parasites. *Diagnostics* 11, 521. doi: 10.3390/diagnostics11030521

Gaydos, C. A., Van Der Pol, B., Jett-Goheen, M., Barnes, M., Quinn, N., Clark, C., et al. (2013). Performance of the cepheid CT/NG Xpert rapid PCR test for detection of *Chlamydia trachomatis* and *Neisseria gonorrhoeae*. *J. Clin. Microbiol.* 51, 1666–1672. doi: 10.1128/JCM.03461-12

Herbst De Cortina, S., Bristow, C. C., Joseph Davey, D., and Klausner, J. D. (2016). A systematic review of point of care testing for *Chlamydia trachomatis*, *Neisseria gonorrhoeae*, and *Trichomonas vaginalis*. *Infect. Dis. Obstet. Gynecol.* 2016, 4386127. doi: 10.1155/2016/4386127

Hsieh, H., Dantzler, J., and Weigl, B. (2017). Analytical tools to improve optimization procedures for lateral flow assays. *Diagnostics* 7, 29. doi: 10.3390/diagnostics7020029

Huang, Y., Xu, T., Wang, W., Wen, Y., Li, K., Qian, L., et al. (2020). Lateral flow biosensors based on the use of micro- and nanomaterials: a review on recent developments. *Microchim. Acta.* 187, 70. doi: 10.1007/s00604-019-3822-x

Kelly, H., Coltart, C. E. M., Pant Pai, N., Klausner, J. D., Unemo, M., Toskin, I., et al. (2017). Systematic reviews of point-of-care tests for the diagnosis of urogenital *Chlamydia trachomatis* infections. *Sex. Transm. Infect.* 93, S22–S30. doi: 10.1136/sextrans-2016-053067

Khosropour, C. M., Dombrowski, J. C., Vojtech, L., Patton, D. L., Campbell, L. A., Barbee, L. A., et al. (2021). Rectal chlamydia trachomatis infection: a narrative review of the state of the science and research priorities. *Sex. Transm. Dis.* 48, e223–e227. doi: 10.1097/OLQ.0000000000001549

La Rosa, L., Svidler, L. L., Entrocassi, A. C., Lopez, A. D., Caffarena, D., Buttner, K. A., et al. (2021). *Chlamydia trachomatis* anorectal infections by LGV (L1, L2 and L2b) and non-LGV serotypes in symptomatic patients in Buenos Aires, Argentina. *Int. J. STD AIDS* 32, 1318–1325. doi: 10.1177/09564624211038384

Li, Y., Fan, P., Zhou, S., and Zhang, L. (2017). Loop-mediated isothermal amplification (LAMP): a novel rapid detection platform for pathogens. *Microb. Pathogenesis* 107, 54–61. doi: 10.1016/j.micpath.2017.03.016

Meyer, T. (2016). Diagnostic procedures to detect *Chlamydia trachomatis* infections. *Microorganisms* 4, 25. doi: 10.3390/microorganisms4030025

Molano, M., Tabrizi, S. N., Phillips, S., Danielewski, J., Cornall, A., Morre, S. A., et al. (2018). Development of a rapid colorimetric multiplex PCR-reverse line blot for the detection and typing of 14 *Chlamydia trachomatis* genovars. *J. Med. Microbiol.* 67, 1560–1570. doi: 10.1099/jmm.0.000836

Murray, S. M., and McKay, P. F. (2021). *Chlamydia trachomatis*: cell biology, immunology and vaccination. *Vaccine* 39, 2965–2975. doi: 10.1016/j.vaccine.2021.03.043

Notomi, T., Okayama, H., Masubuchi, H., Yonekawa, T., Watanabe, K., Amino, N., et al. (2000). Loop-mediated isothermal amplification of DNA. *Nucleic Acids Res.* 28, E63. doi: 10.1093/nar/28.12.e63

Panno, S., Matic, S., Tiberini, A., Caruso, A. G., Bella, P., Torta, L., et al. (2020). Loop mediated isothermal amplification: principles and applications in plant virology. *Plants* 9, 461. doi: 10.3390/plants9040461

Park, J. J., Stafylis, C., Pearce, D. D., Taylor, J., Little, S. J., Kojima, N., et al. (2021). Interest, concerns, and attitudes among men who have sex with men and health care providers toward prophylactic use of doxycycline against *Chlamydia trachomatis* infections and syphilis. *Sex. Transm. Dis.* 48, 615–619. doi: 10.1097/OLQ.0000000000001395

Peng, L., Chen, J., and Wang, D. (2020). Progress and perspectives in point of care testing for urogenital *Chlamydia trachomatis* infection: a review. *Med. Sci. Monitor.* 26, e920873. doi: 10.12659/MSM.920873

Pourabbas, B., Rezaei, Z., Mardaneh, J., Shahian, M., and Alborzi, A. (2018). Prevalence of *Chlamydia trachomatis* and *Neisseria gonorrhoeae* infections among pregnant women and eye colonization of their neonates at birth time, Shiraz, Southern Iran. *BMC Infect. Dis.* 18, 477. doi: 10.1186/s12879-018-3382-4

Ramadhani, A. M., Derrick, T., Macleod, D., Massae, P., Malisa, A., Mbuya, K., et al. (2019). Ocular immune responses, *Chlamydia trachomatis* infection and clinical signs of trachoma before and after azithromycin mass drug administration in a treatment naive trachoma-endemic Tanzanian community. *PLoS Negl Trop Dis.* 13, e7559. doi: 10.1371/journal.pntd.0007559

Rowley, J., Vander Hoorn, S., Korenromp, E., Low, N., Unemo, M., Abu-Raddad, L. J., et al. (2019). Chlamydia, gonorrhoea, trichomoniasis and syphilis: global prevalence and incidence estimates, 2016. *Bull. World Health Organ.* 97, 548–562P. doi: 10.2471/BLT.18.228486

Rudolph, D. L., Sullivan, V., Owen, S. M., and Curtis, K. A. (2015). Detection of acute HIV-1 infection by RT-LAMP. *PLoS ONE* 10, e126609. doi: 10.1371/journal.pone.0126609

Safarkar, R., Mehrabadi, J. F., Noormohammadi, Z., and Mirnejad, R. (2017). Development a rapid and accurate multiplex real time PCR method for the detection *Chlamydia trachomatis* and *Mycoplasma hominis*. *J. Clin. Lab. Anal.* 31, e22126. doi: 10.1002/jcla.22126

Sahoo, P. R., Sethy, K., Mohapatra, S., and Panda, D. (2016). Loop mediated isothermal amplification: an innovative gene amplification technique for animal diseases. *Vet. World* 9, 465–469. doi: 10.14202/vetworld.2016.465-469

Shirato, K. (2019). Detecting amplicons of loop-mediated isothermal amplification. *Microbiol. Immunol.* 63, 407–412. doi: 10.1111/1348-0421.12734

Somboonna, N., and Choopara, I. (2019). Point-of-care *Chlamydia trachomatis* detection using loop-mediated isothermal amplification and hydroxynaphthol blue. *Methods Mol. Biol.* 2042, 11–17. doi: 10.1007/978-1-4939-9694-0_2

Somboonna, N., Choopara, I., Arunrut, N., Sukhonpan, K., Sayasathid, J., Dean, D., et al. (2018). Rapid and sensitive detection of *Chlamydia trachomatis* sexually transmitted infections in resource-constrained settings in Thailand at the point-of-care. *PLoS Negl. Trop. Dis.* 12, e6900. doi: 10.1371/journal.pntd.0006900

Tadele, A., Hussen, S., and Shimelis, T. (2019). Prevalence and associated factors of *Chlamydia trachomatis* and *Neisseria gonorrhoeae* among female commercial sex workers in Hawassa City, Southern Ethiopia. *BMC Infect. Dis.* 19, 61. doi: 10.1186/s12879-019-3698-8

Wang, T., Chen, L., Chikkanna, A., Chen, S., Brusius, I., Sbuh, N., et al. (2021). Development of nucleic acid aptamer-based lateral flow assays: a robust platform for cost-effective point-of-care diagnosis. *Theranostics* 11, 5174–5196. doi: 10.7150/thno.56471

Wise, M. R., Sadler, L., and Ekeroma, A. (2015). *Chlamydia trachomatis* screening in pregnancy in New Zealand: translation of national guidelines into practice. *J. Prim. Health Care* 7, 65–70. doi: 10.1071/HC15065

Woodhall, S. C., Gorwitz, R. J., Migchelsen, S. J., Gottlieb, S. L., Horner, P. J., Geisler, W. M., et al. (2018). Advancing the public health applications of *Chlamydia trachomatis* serology. *Lancet Infect. Dis.* 18, e399–e407. doi: 10.1016/S1473-3099(18)30159-2

World Health Organization (2016). *WHO Guidelines for the Treatment of Chlamydia trachomatis*. Geneva: World Health Organization.

Ye, H., Liu, Y., Zhan, L., Liu, Y., and Qin, Z. (2020). Signal amplification and quantification on lateral flow assays by laser excitation of plasmonic nanomaterials. *Theranostics* 10, 4359–4373. doi: 10.7150/thno.44298

Conflict of Interest: The authors declare that the research was conducted in the absence of any commercial or financial relationships that could be construed as a potential conflict of interest.

Publisher's Note: All claims expressed in this article are solely those of the authors and do not necessarily represent those of their affiliated organizations, or those of the publisher, the editors and the reviewers. Any product that may be evaluated in this article, or claim that may be made by its manufacturer, is not guaranteed or endorsed by the publisher.

frontiers | Frontiers in Microbiology

PERSPECTIVE
published: 30 August 2022
doi: 10.3389/fmicb.2022.922894

A Case Report of Two Kala-Azar Cases in China Diagnosed by Metagenomic Next-Generation Sequencing

Hongguang Gao[1], *Jing Wang*[2], *Shu Zhang*[1]* *and Tian Li*[3]

[1] Department of Emergency Medicine, West China Hospital, Sichuan University, Chengdu, China, [2] Precision Medicine Center, Precision Medicine Key Laboratory of Sichuan Province, West China Hospital, Sichuan University, Chengdu, China, [3] School of Basic Medicine, Fourth Military Medical University, Xi'an, China

Background: Leishmaniasis being a local disease, as kala-azar this particular form is a visceral form. It is transmitted by sandflies, and is a parasitic disease involving the reticuloendothelial system of mononuclear macrophages. Due to its poor prognosis and high fatality rate, the fatality rate of patients without effective treatment can exceed 95%. Thereby, early diagnosis and treatment can significantly improve its prognosis. The metagenomic next-generation sequencing (mNGS) has the advantage of being able to find pathogens that cannot be detected by traditional methods. More importantly, it can conduct nucleic acid detection of pathogens covering a wide range in a short time. For infectious diseases like kala-azar, which is clinically complicated and difficult, mNGS detection provides a basis for accurate etiological diagnosis.

Case Report: We report 2 cases of kala-azar in West China Hospital, Chengdu, China. The first case is a 47-year-old male patient who had recurrent fever for 4 months, accompanied by reduction of red blood cell, white blood cell, and blood platelet. He was detected by mNGS and clinically diagnosed as kala-azar (*Leishmania* detection), finally died of multiple organ failure. The second patient was a 15-year-old male who had fever for more than 10 days. He was detected by mNGS and clinically diagnosed as kala-azar (*Leishmania* detection). He recovered and discharged quickly after treatment with sodium stibogluconate.

Conclusion: Efforts should be made to improve early etiological diagnosis in order to improve patient prognosis. mNGS detection is beneficial to the diagnosis and treatment of infectious diseases with unknown causes in the early stage of emergency treatment.

Keywords: kala-azar, *Leishmania*, mNGS, fever, diagnosis

OPEN ACCESS

Edited by:
Bing Gu,
Guangdong Provincial People's Hospital, China

Reviewed by:
Sarfaraz Ahmad Ejazi,
Indian Institute of Chemical Biology (CSIR), India
Manas R. Dikhit,
Rajendra Memorial Research Institute of Medical Sciences, India
Shibabrata Mukherjee,
BD Biosciences, United States

***Correspondence:**
Shu Zhang
zhangs@wchscu.cn

Specialty section:
This article was submitted to Infectious Agents and Disease, a section of the journal Frontiers in Microbiology

Received: *18 April 2022*
Accepted: *20 June 2022*
Published: *30 August 2022*

Citation:
Gao H, Wang J, Zhang S and Li T (2022) A Case Report of Two Kala-Azar Cases in China Diagnosed by Metagenomic Next-Generation Sequencing. Front. Microbiol. 13:922894. doi: 10.3389/fmicb.2022.922894

BACKGROUND

Visceral leishmaniasis (VL) is caused by *Leishmania* protozoa. The parasite is spread by sandflies. It is commonly known as kala-azar (Lun et al., 2015). Kala-azar is a parasitic disease involving the reticuloendothelial system of mononuclear macrophages (Martins-Melo et al., 2014). At present, the incidence of leishmaniasis has been significantly reduced in China, whereas some provinces

in northwest/southwest China are still leishmaniasis endemic areas (The Editorial Committee of Chinese Journal of Infectious Diseases, 2017). Visceral leishmaniasis remains endemic in the Mediterranean basin, East Africa, the Indian subcontinent, Rahman et al. (2021). Visceral leishmaniasis is considered to be an emerging disease in Europe (Dujardin et al., 2008). The clinical manifestations of kala-azar are complex, characterized by long-term irregular fever, progressive splenomegaly, emaciation, anemia, pancytopenia, and increased plasma globulin (Lun et al., 2015). Due to its poor prognosis and high fatality rate, the fatality rate of patients without effective treatment can exceed 95% (Martins-Melo et al., 2014). Thereby, early diagnosis and treatment can significantly improve its prognosis.

Clinical emergency doctors lack sufficient understanding and attention to kala-azar, and insufficient epidemiological history data have been collected so far. Therefore, it is difficult to distinguish kala-azar from hematological and other infectious diseases; and a misdiagnose or missed diagnosis can easily occur. At present, the clinical diagnosis of kala-azar is mainly achieved through bone marrow smear, histopathological biopsy etiology, or rK39 immunochromatographic strip test, among which the discovery of *Leishmania* parasite in bone marrow, lymph nodes, spleen, and other tissues is considered the golden criterion of diagnosis (The Editorial Committee of Chinese Journal of Infectious Diseases, 2017). However, the histopathological examination requires a long operation period, which might delay diagnosis and treatment. The rK39 immunochromatographic strip detection is an unconventional detection method that can only be performed in specific institutions. The PCR detection has high specificity and can improve the detection level of *Leishmania,* but it has not been widely used in China (Guo et al., 2020). Metagenomic second-generation sequencing is unbiased, high-coverage, accurate, and reliable; thus, it has been gradually applied to parasitic infectious diseases (Wang et al., 2018). Metagenomic sequencing can effectively detect parasite sequences that cannot be detected by conventional methods, and has been widely applied to clinical practice.

In the emergency department of our hospital, two male patients with fever of unknown cause were not clearly diagnosed by conventional etiological tests. The mNGS has the advantage of being able to find pathogens that cannot be detected by traditional methods. More importantly, it can conduct nucleic acid detection of pathogens covering a wide range in a short time (Brown et al., 2018). The diagnosis was confirmed by the next-generation metagenomic sequencing (mNGS) detection of *Leishmania* protozoa in the early emergency treatment, providing suggestions for accurate diagnosis and treatment of clinical infectious diseases at an early stage.

METAGENOMIC NEXT-GENERATION SEQUENCING DATA ANALYSIS AND CASE REPORTS

Metagenomic Next-Generation Sequencing Methods and Data Analysis

A total of 5–10 ml of whole blood was collected from each patient and stored in an EDTA tube at 4°C. Samples were centrifuged within 1 h after collection for 10 min at 1,600 × *g* at 4°C. Plasma samples were transferred to 1.5-ml microcentrifuge tubes and stored at −80°C until DNA extraction. Nucleic acids were extracted from 0.3 ml plasma, and DNA libraries were established by shearing, end repair, A-tailing, adapter ligation, and PCR amplification. DNA libraries were denatured and circularized. DNA nanoballs were generated with the ssDNA circle by rolling circle replication. Finally, sequencing was performed on a BGI MGISEQ-2000 platform in the SE50 format for 12 h. The sequencing raw data were preprocessed by removing contained adapter sequences, reads with high N base and low-complexity reads based on in-house software. Human reads and reads of internal reference were computationally extracted using Burrows–Wheeler Alignment (Li, 2013). Subsequently, the remaining data were identified through BWA alignment to the pathogen sequence database (PMDB). Finally, pathogens were annotated with all classified mapped reads. The total reads number and the reads number of internal reference for each sample were counted to control the sample quality, and the draft reports were generated automatically by interpretation logic. Draft reports were reviewed and revised by infectious disease physicians according to patients' clinical symptoms and other laboratory test results to generate the final reports.

Case I of a 47-Year-Old Male Patient

Patient 1: Male, 47 years old, technical staff. He came to our hospital for emergency treatment in December 28, 2020 due to "recurrent fever for 4 months with aggravation accompanied with diarrhea for 1 month." About 4 months ago, the patient suddenly developed fever without an evident cause, with the highest temperature of 39.9°C. The fever usually occurred in the afternoon and dropped to normal temperature after several hours, accompanied by headache, muscle pain, and nausea. The patient took "antipyretics and artemisinin" orally; however, the temperature did not come down significantly. He was referred to multiple hospitals for treatment but ended with no definite diagnosis.

In October 2020, he was discharged from a local hospital after his body temperature returned to normal. One month after discharge, the fever reoccurred with a temperature of 39°C, which appeared as a persistent high fever and endured significantly longer than before. The high fever was accompanied by diarrhea for more than 10 times per day, which appeared as yellow liquid stool. The past medical history: 6 years ago, the patient was diagnosed with malaria in Africa and was treated with oral Quinine. Examination results after admission: Novel Coronavirus nucleic acid test: negative, blood cell analysis (five categories): Hb 83 g/L, Plt count 16 × 10^9/L, WBC count 2.82 × 10^9/L, NE percentage 84.0%, lymphocyte percentage 8.0%, and procalcitonin 0.87 ng/ml. Blood culture: methicillin-resistant coagulase-negative Staphylococci. The patient was hypersensitive to all quinolones, such as moxifloxacin. The cryptococcus antigen test, fungal G test, and GM test were negative. The schistosoma japonicum IgG antibody, echinococcus granulosus antibody, liver fluke antibody test, plasmodium antigen test, and blood smear test were all negative. Other tests such as hepatitis A virus and hepatitis B virus were also negative. Autoimmune liver, alpha fetoprotein (AFP), and carcinoembryonic antigen

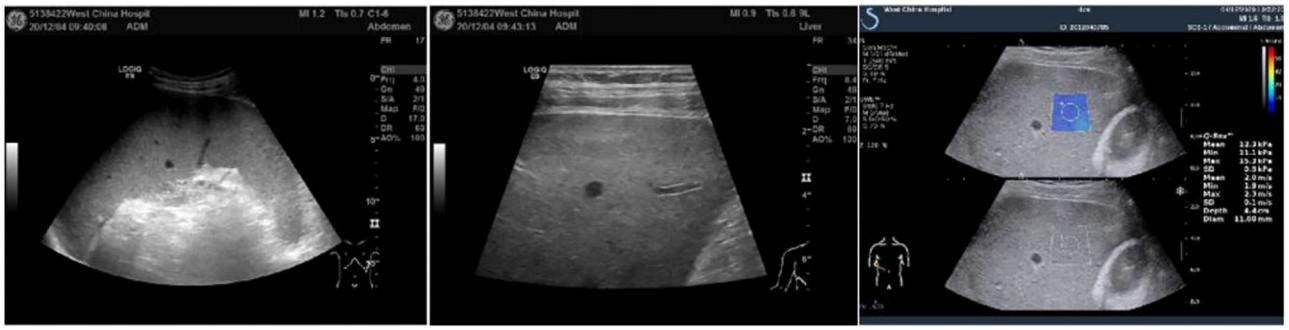

FIGURE 1 | Abdominal ultrasound image of the 47-year-old at 2020.12.04. **(A)** Intercostal spleen thickness was ~7.0 cm and parenchymal echo was uniform; **(B)** Hepatomegaly with liver parenchymal damage; **(C)** Liver hardness measurement: 12.3 kpa.

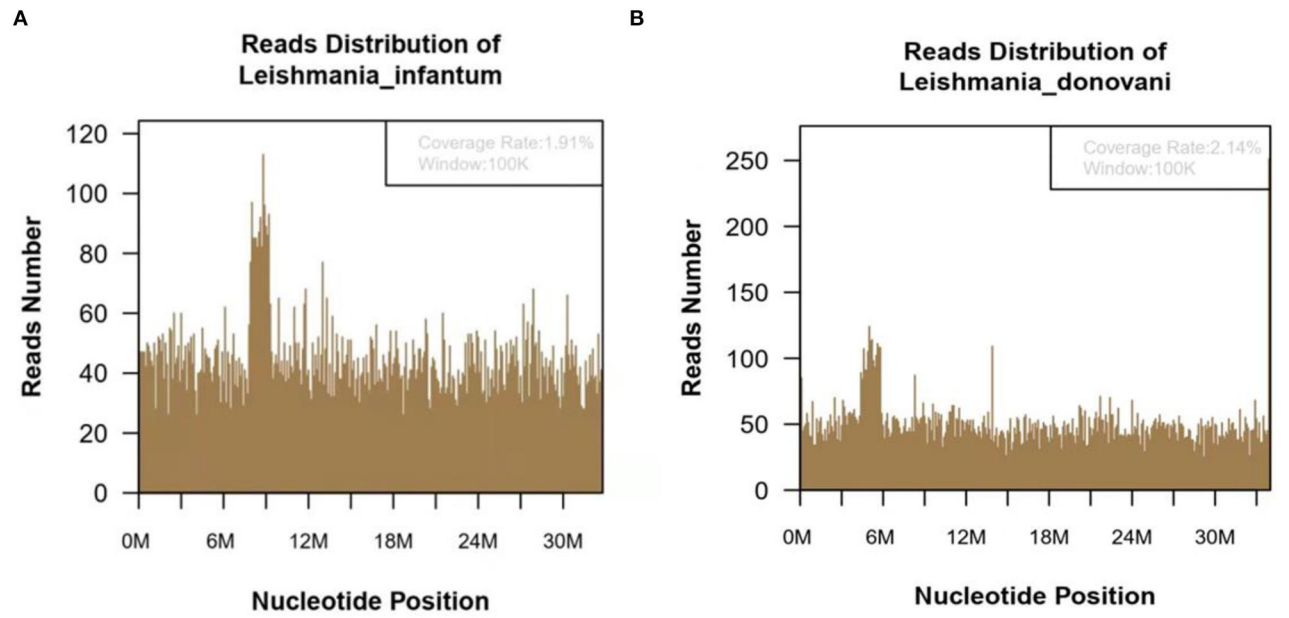

FIGURE 2 | The metagenomic next-generation sequencing (mNGS) of blood sample of 47-year-old kala-azar patient. **(A)** mNGS result showed 118,783 microorganism sequence reads and 14,812 Leishmania Infantum reads, which accounted for 1.91% (626118/32803598) of the whole genome. **(B)** mNGS of blood sample showed a total of 118,783 microorganism sequence reads, and 17,299 reads of *Leishmania Donovani*, accounting for 2.14% (726792/34012130) of the whole genome.

were negative. Abdominal ultrasound showed enlarged liver and spleen (**Figure 1**). Chest and plain abdominal CT: cirrhosis, splenomegaly, portal hypertension with collateral circulation, and peritoneal effusion. The following diagnosis was considered: sepsis, fever of undetermined origin (FUO): infection? The tumor? Child–Pugh B stage of decompensated cirrhosis. An emergency mNGS blood test was performed to diagnose the fever with unknown cause. Even after being treated with moxifloxacin anti-infective therapy, the patient continued to suffer from recurrent fever. The blood mNGS test results on the 4th day of admission detected *Leishmania infantum* and *Leishmania donovani* (**Figure 2**). Suspected diagnosis: kala-azar. One day later, the Centers for Disease Control and Prevention performed an rK39 antibody test and the result appeared positive; therefore, the clinical diagnosis of kala-azar was made, and the patient was subjected to sodium stibogluconate (SSG) treatment. According to the treatment standard of 90–130 mg/kg, a total of 9000 mg SSG was used (the maximum dose was given according to the weight of kg) and then stopped. The SSG was divided into 8 days, 600 mg on the first day and 1,200 mg/d after the first day. During the treatment, the patient persistently showed anemia, thrombocytopenia, and coagulation dysfunction, so repeated transfusion therapy was administered. After 3 days of the treatment, the patient's temperature decreased

and the fever never returned. However, after 10 days of sodium stibogluconate treatment, the patient developed decreased blood pressure and multiple organ failure (progressive deterioration of coagulation, renal function, and liver function and continued thrombocytopenia). Septic shock was considered, and active anti-infection, fluid replenishment, and non-invasive ventilation were arranged. The patient's condition was not alleviated, and his family refused to adopt emergency treatment measures, such as endotracheal intubation, chest compressions, and continuous renal replacement therapy (CRRT). The patient died 18 days after admission.

Case II of a 15-Year-Old Male Patient

Patient 2: Male, 15 years old, a middle-school student. He lived in Chongqing for a long time and was admitted to the emergency fever clinic chamber in January 5th, 2021 due to "fever accompanied with cough for more than 10 days." Novel Coronavirus nucleic acid test was negative. The patient developed fever after catching a cold more than 10 days before admission, with the temperature fluctuating between 37 and 38°C, accompanied by cough, fatigue, chills, and pharyngeal discomfort. The symptoms were not relieved even after "GanKang" was administered. The symptoms aggravated in December 5th, 2020, with the temperature peaking to 41°C and reducing to below 38°C after ibuprofen was administered orally. The hospitalization inspection at the local hospital showed the following: WBC 3.3×10^9/L, Hb 85 g/L, PLT 87×10^9/L. Bone marrow puncture indicated that hematopoietic tissue hyperplasia was active and the proportion of three-line blood cells was roughly normal. Lymphocytes accounted for 9.5%, and atypical lymphocytes were found occasionally. Adenovirus IgM was weakly positive, ferritin: >2,000 ng/ml, and procalcitonin: 4.14 ng/ml. Abdominal ultrasound and CT scan indicated hepatomegaly and splenomegaly. Cerebrospinal fluid: glucose 3.8 mmol/L, chlorine 125 mmol/L, protein 0.28 g/L, and nucleated cells 3×10^6/L. The respiratory tract had 13 types of virus and complete immunophenotyping of leukemia; echocardiography showed no evident abnormalities. After treatment with cefoperazone sulbactam sodium, the symptoms were not significantly relieved, and the diagnosis was not clear, so the patient came to our hospital for further treatment. Vital signs: T: 37.1°C, P: 110/min, R: 19/min, BP: 110/72 mmHg. Hospitalization inspection after admission: Blood routine examination: WBC 4.68×10^9/L, Hb 100 g/L, and RBC3.65×10^{12}/L. Biochemical test: ALT 204 IU/L; AST 176 IU/L; GGT 153 IU/L; GLU tendency for 6.66/L; TG tendency for 2.29/L; 0.30 tendency for HDL – C/L; LDH 889 IU/L; Ferritin: >2,000 ng/ml; PCT: 2.11 ng/ml; CRP: 53.5 mg/L, IL-6 31.58 pg/ml. TORCH + EBV: CMV, HSV, rubella virus, and EBV IgG were all positive. Coombs' test (direct anti-human globulin test): positive, ++. Autoimmune antibody: ANA + 1:100; Anti-jo-1 antibody +; RF 207 IU/ml; HIV, and syphilis tests were negative. Blood culture: no bacterial growth was observed in 5 days. T cell subsets: (–). Chest CT showed no obvious abnormality. Abdominal ultrasound showed that the spleen thickness was ∼6.6 cm intercostal, suggesting splenomegaly (**Figure 3A**). The diagnosis was considered to be: (1) FUO:sepsis with hematological disease? Do not exclude the possibility of parasitic diseases? Hemophilic cell syndrome? Lymphoma? Autoimmune disease? (2) Mild anemia. (3) Splenomegaly. The cause of the fever was unclear, and an mNGS test was performed on the second day after admission to the emergency department. Emergent treatment: Ceftriaxone 2.0ivgtt Qd for 3 days and dexamethasone administered to reduce the fever; however, the patient showed no significant relief of fever. On the third day, the patient was admitted to the department of infectious diseases. On the fourth day, the mNGS test results of the patient showed *Leishmania infantum* (**Figure 4**). CDC was contacted for rK39 antibody test, and the antibody was detected to be positive on the seventh day, which is in accordance with the criteria for clinically diagnosed cases (Aronson et al., 2016). The anti-kala-azar treatment was started and sodium stibogluconate was administered. The patient was given 600 mg SSG daily for 10 consecutive days intravenously, and the drug was discontinued after the patient's symptoms improved significantly. The patient's temperature began to gradually return to normal 3 day later. On the 17th day, the temperature was normal. His spleen retracted, and he was discharged after bone marrow puncture. The patient underwent 3 bone marrow puncture examinations successively. On the 11th day of admission, hematopoietic cells in the bone marrow were actively hyperplasia, and the immunohistochemistry showed scattered lymphocytes and a few suspicious EBER positive cells. On the 17th day, the bone marrow hematopoietic cells were hyperactive. On the 14th day of admission, the spleen was retracted, and the thickness of the spleen was about 5.1 cm (**Figure 3B**). One month after discharge, the follow-up showed that the bone marrow hematopoietic cell hyperplasia was low. The intercostal spleen thickness was ∼4.5 cm (**Figure 3C**). The blood routine and liver function returned to normal.

DISCUSSION

Kala-azar is one of the most neglected infectious diseases globally, with ∼1.5–2 million new cases reported every year. It is endemic in more than 60 countries worldwide, such as the Mediterranean, Middle East, sub-Saharan Africa, southern Europe, India, Pakistan, and China. As its prevention and control were carried out in China, kala-azar has been nearly eliminated, but there is a small-range prevalence in Xinjiang, Gansu, Sichuan, Shaanxi, and Shanxi (Zheng et al., 2020). The first patient, in this case, had a history of epidemic areas in Africa. Therefore, it interfered with the doctors' inquiry about other epidemics and ignored other infectious diseases. The second case was a case who lived in Chongqing city and had a history of Yangquan, Shanxi Province residence. The lack of knowledge of this rare infectious disease among front-line clinicians and the atypical clinical manifestations of kala-azar led to the easy misdiagnosis and missed diagnosis of kala-azar. In addition to the strengthening knowledge dissemination and training on infectious diseases, strengthening clinical etiology detection technology is also one of the main ways to improve the level of diagnosis and treatment of infectious diseases.

FIGURE 3 | Abdominal color ultrasound of 15-year-old patient. **(A)** Examination results on the first day of admission showed that the intercostal spleen thickness was approximately 6.6 cm and parenchymal echo was uniform, indicating splenomegaly. **(B)** On the 14th day of admission, the spleen was retracted, and the thickness of the spleen was about 5.1 cm. **(C)** Follow-up 1 month after discharge, the spleen was retracted, and the thickness was about 4.5 cm.

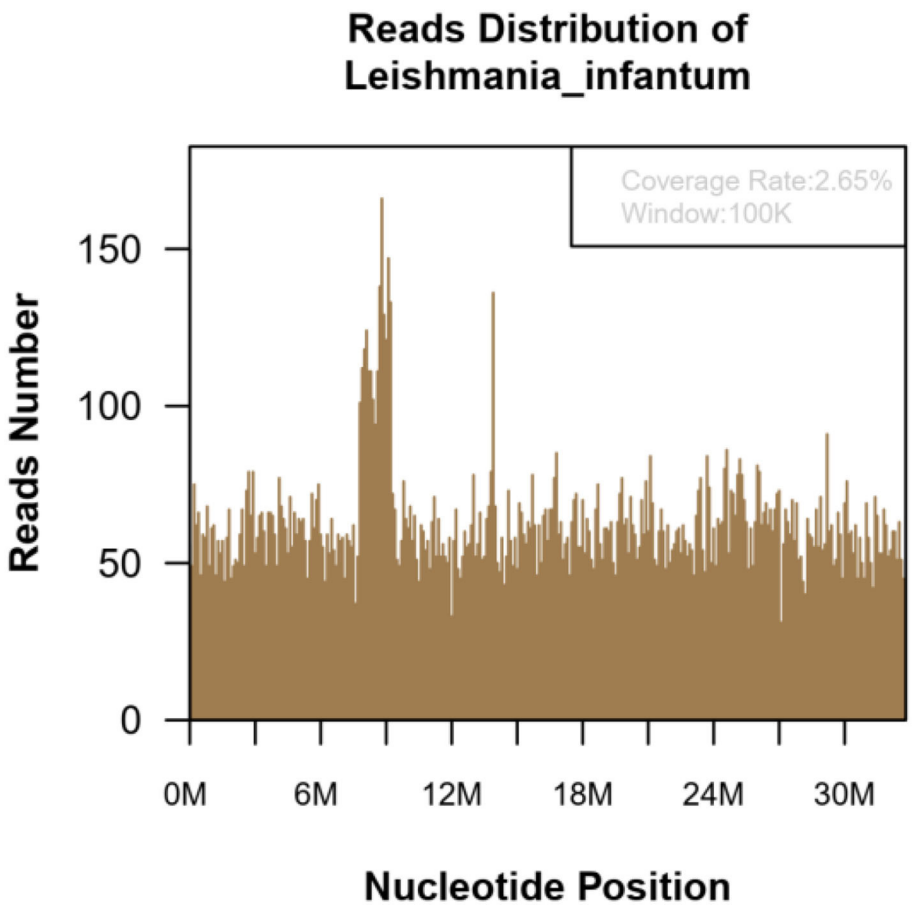

FIGURE 4 | The mNGS of the blood sample of 15-year-old patient. Result showed 139,030 microorganism sequence reads and 20,629 Leishmania Infantum reads, which accounted for 2.65% (869709/32803598) of the whole genome.

The clinical manifestations of kala-azar are complex, and the symptoms overlap with those of severe infections, hematologic diseases, and autoimmune diseases, such as fever, splenomegaly, and cytopenia, which cause great confusion to doctors and are not easy to identify. Kala-azar can hardly achieve self-healing, and the mortality rate can exceed 90% if the treatment is not accepted (Martins-Melo et al., 2014). Clinical studies have reported that the misdiagnosis rate of kala-azar is 84.2%

(Mondal et al., 2010; Copeland and Aronson, 2015). The misdiagnosis might be due to the lack of clinical awareness and attention to kala-azar and insufficient epidemiological history data. Kala-azar is easily misdiagnosed as connective tissue disease, especially systemic lupus erythematosus (Tunccan et al., 2012). The positive rates of ANA and RF in kala-azar are 88 and 63%, respectively (Liberopoulos et al., 2013). The immunologic tests of the two patients in this study were as follows: Coombs' test: positive, ++; ANA +1:100; Anti-jo-1 antibody +; and RF 207 IU/ml. These results are consistent with those obtained previously (Santana et al., 2015). The polyclonal activation of kala-azar B cells is considered the main cause of immunoglobulin and antibody formation (Smelt et al., 2000).

The detection of the kala-azar pathogen is difficult. The clinical diagnosis of kala-azar is mainly achieved by bone marrow smear, histopathological biopsy etiology, and rK39 immunochromatographic strip test, among which the discovery of *Leishmania* parasite in bone marrow, lymph nodes, spleen, skin, and other tissues is considered the golden criterion of diagnosis. The positive rate of bone marrow puncture is 53–86% (Lun et al., 2015). Lymph node biopsy has a sensitivity of 65.1% for kala-azar diagnosis (Reus et al., 2005). The first patient in this study had low platelet count, abnormal coagulation function, and high puncture risk, which limited the bone marrow puncture examination. In the second patient, all three attempts of bone marrow punctures were failed to diagnose *Leishman-Donovan* body, which increased the difficulty in the diagnosis. The detection rate of pathogens in splenic puncture smear is high (Miao et al., 2017), and the risk of splenic puncture is also relatively high. The positive rate of the rK39 immunochromatographic strip test for detecting leishmaniasis antibodies was high, and according to the diagnostic criteria of leishmaniasis, although the suspected cases + immunological test results were clinically diagnosed cases of leishmaniasis, and not confirmed cases, they could still guide clinical treatment. Hospitals that do not have access to rK39 test should contact their local CDC for further testing (The Editorial Committee of Chinese Journal of Infectious Diseases, 2017). Various PCR-based detection methods have shown good application prospects, but currently there is a lack of applicable commercial kits in China, and molecular diagnosis has not been widely carried out (Guo et al., 2020). At present, the emergence and development of second-generation sequencing technology provide convenient diagnoses for rare pathogens. McCarthy et al. (2011) used mNGS for the first time to investigate the populations of *Lutzomyia longipalpis* associated with visceral leishmaniasis, which helps to monitor the occurrence of insect vector-borne infectious diseases. There are a few reports on the detection of *Leishmania* by mNGS in China. In this study, mNGS testing was performed in both patients at an early stage in the emergency department, thus enabling rapid diagnosis. The first patient had a poor prognosis due to time-consuming out-of-hospital diagnosis. The second patient benefited from rapid and accurate early diagnosis in an emergency department and had a good prognosis.

This case study does have some limitations: (1) As this study is a case report, the leishmania was detected by mNGS in two cases, which is not generally representative. The significance of mNGS in the detection and diagnosis of acute infectious diseases needs to be further studied. (2) The rK39 antibody test is highly sensitive to kala-azar diagnosis, but it is not a routine test item for the requisition of CDC application, which limits its clinical use in medical institutions and makes the universal screening of kala-azar unachievable.

Currently, the clinical diagnosis of rare infectious diseases, such as kala-azar, is relatively difficult. The metagenomics sequencing technology, which is a second-generation sequencing technology, has been gradually applied to the pathogen detection of clinical infectious diseases owing to its advantages of being unbiased, fast, and accurate and having wide coverage. Moreover, it has important clinical value for suspicious and complicated infectious diseases. It is helpful for emergency doctors to diagnose and treat this special pathogen early, to advance patient treatment and improve their prognosis. In short, kala-azar requires early stage diagnosis and treatment to achieve a relatively satisfactory prognosis. The mNGS detection is beneficial to the diagnosis and treatment of infectious diseases with unknown causes in the early stage of emergency treatment.

DATA AVAILABILITY STATEMENT

The datasets presented in this study can be found in online repositories. The names of the repository/repositories and accession number(s) can be found below: NCBI - PRJNA814613.

ETHICS STATEMENT

The studies involving human participants were reviewed and approved by Ethical Committee of West China Hospital, Sichuan University. Written informed consent to participate in this study was provided by the participants' legal guardian/next of kin. Written informed consent was obtained from the individual(s), and minor(s)' legal guardian/next of kin, for the publication of any potentially identifiable images or data included in this article.

AUTHOR CONTRIBUTIONS

HG: writing—original draft preparation. TL and JW: writing—review and editing. SZ: idea. All authors read and approved the final manuscript.

ACKNOWLEDGMENTS

We thank the Bullet Edits Limited for the linguistic editing and proofreading of the manuscript.

REFERENCES

Aronson, N., Herwaldt, B. L., Libman, M., Pearson, R., Lopez-Velez, R., Weina, P., et al. (2016). Diagnosis and Treatment of Leishmaniasis: Clinical Practice Guidelines by the Infectious Diseases Society of America (IDSA) and the American Society of Tropical Medicine and Hygiene (ASTMH). *Clin. Infect. Dis.* 63, e202–e264. doi: 10.1093/cid/ciw742

Brown, J. R., Bharucha, T., and Breuer, J. (2018). Encephalitis diagnosis using metagenomics: application of next generation sequencing for undiagnosed cases. *J. Infect.* 76, 225–240. doi: 10.1016/j.jinf.2017.12.014

Copeland, N. K., and Aronson, N. E. (2015). Leishmaniasis: treatment updates and clinical practice guidelines review. *Curr. Opin. Infect. Dis.* 28, 426–437. doi: 10.1097/QCO.0000000000000194

Dujardin, J. C., Campino, L., Canavate, C., Dedet, J. P., Gradoni, L., Soteriadou, K., et al. (2008). Spread of vector-borne diseases and neglect of Leishmaniasis, Europe. *Emerg. Infect. Dis.* 14, 1013–1018. doi: 10.3201/eid1407.071589

Guo, F., Kang, L., and Xu, M. (2020). A case of pediatric visceral leishmaniasis-related hemophagocytic lymphohistiocytosis diagnosed by mNGS. *Int. J. Infect. Dis.* 97, 27–29. doi: 10.1016/j.ijid.2020.05.056

Li, H. (2013). *Aligning Sequence Reads, Clone Sequences and Assembly Contigs With BWA-MEM*. arXiv:1303.3997v2 [q-bio.GN].

Liberopoulos, E., Kei, A., Apostolou, F., and Elisaf, M. (2013). Autoimmune manifestations in patients with visceral leishmaniasis. *J. Microbiol. Immunol. Infect.* 46, 302–305. doi: 10.1016/j.jmii.2012.01.016

Lun, Z. R., Wu, M. S., Chen, Y. F., Wang, J. Y., Zhou, X. N., Liao, L. F., et al. (2015). Visceral leishmaniasis in China: an endemic disease under control. *Clin. Microbiol. Rev.* 28, 987–1004. doi: 10.1128/CMR.00080-14

Martins-Melo, F. R., Lima Mda, S., Ramos, A. N. Jr., Alencar, C. H., and Heukelbach, J. (2014). Mortality and case fatality due to visceral leishmaniasis in Brazil: a nationwide analysis of epidemiology, trends and spatial patterns. *PLoS ONE* 9, e93770. doi: 10.1371/journal.pone.0093770

McCarthy, C. B., Diambra, L. A., and Rivera Pomar, R. V. (2011). Metagenomic analysis of taxa associated with Lutzomyia longipalpis, vector of visceral leishmaniasis, using an unbiased high-throughput approach. *PLoS Negl. Trop. Dis.* 5, e1304. doi: 10.1371/journal.pntd.0001304

Miao, R., Wang, Z., Guo, Q., Wen, Y., Liao, Q., Zhu, Y., et al. (2017). Clinical and epidemiologic features of visceral leishmaniasis in children in Southwestern China: a retrospective analysis from 2001 to 2015. *Pediatr. Infect. Dis. J.* 36, 9–12. doi: 10.1097/INF.0000000000001343

Mondal, S., Bhattacharya, P., and Ali, N. (2010). Current diagnosis and treatment of visceral leishmaniasis. *Expert. Rev. Anti. Infect. Ther.* 8, 919–944. doi: 10.1586/eri.10.78

Rahman, K. M., Olsen, A., Harley, D., Samarawickrema, I. V. M., Butler, C. D., Zahid, K., et al. (2021). Early diagnosis of kala-azar in Bangladesh: findings from a population based mixed methods research informing the post-elimination era. *Parasitol. Int.* 85, 102421. doi: 10.1016/j.parint.2021.102421

Reus, M., Garcia, B., Vazquez, V., Morales, D., Fuster, M., and Sola, J. (2005). Visceral leishmaniasis: diagnosis by ultrasound-guided fine needle aspiration of an axillary node. *Br. J. Radiol.* 78, 158–160. doi: 10.1259/bjr/33263789

Santana, I. U., Dias, B., Nunes, E. A., Rocha, F. A., Silva, F. S. Jr., and Santiago, M. B. (2015). Visceral leishmaniasis mimicking systemic lupus erythematosus: case series and a systematic literature review. *Semin. Arthritis Rheum.* 44, 658–665. doi: 10.1016/j.semarthrit.2014.12.004

Smelt, S. C., Cotterell, S. E., Engwerda, C. R., and Kaye, P. M. (2000). B cell-deficient mice are highly resistant to Leishmania donovani infection, but develop neutrophil-mediated tissue pathology. *J. Immunol.* 164, 3681–3688. doi: 10.4049/jimmunol.164.7.3681

The Editorial Committee of Chinese Journal of Infectious Diseases (2017). Expert consensus on diagnosis and treatment of Leishmania infection in China. *Chin. J. Infect. Dis.* 35, 513–518. doi: 10.3760/cma.j.issn.1000-6680.2017.10.001

Tunccan, O. G., Tufan, A., Telli, G., Akyurek, N., Pamukcuoglu, M., Yilmaz, G., et al. (2012). Visceral leishmaniasis mimicking autoimmune hepatitis, primary biliary cirrhosis, and systemic lupus erythematosus overlap. *Korean J. Parasitol.* 50, 133–136. doi: 10.3347/kjp.2012.50.2.133

Wang, Q., Li, J., Ji, J., Yang, L., Chen, L., Zhou, R., et al. (2018). A case of Naegleria fowleri related primary amoebic meningoencephalitis in China diagnosed by next-generation sequencing. *BMC Infect. Dis.* 18, 349. doi: 10.1186/s12879-018-3261-z

Zheng, C., Wang, L., Li, Y., and Zhou, X. N. (2020). Visceral leishmaniasis in northwest China from 2004 to 2018: a spatio-temporal analysis. *Infect. Dis. Poverty* 9, 165. doi: 10.1186/s40249-020-00782-4

Conflict of Interest: The authors declare that the research was conducted in the absence of any commercial or financial relationships that could be construed as a potential conflict of interest.

frontiers | Frontiers in Microbiology

TYPE Original Research
PUBLISHED 15 September 2022
DOI 10.3389/fmicb.2022.958693

OPEN ACCESS

EDITED BY
Bing Gu,
Guangdong Provincial People's Hospital, China

REVIEWED BY
Mariana Boité,
Oswaldo Cruz Foundation (Fiocruz), Brazil
Greg Matlashewski,
McGill University, Canada

*CORRESPONDENCE
Vanessa Adaui
vanessa.adaui@upc.edu.pe

†PRESENT ADDRESSES
Luis Cabrera-Sosa,
Laboratorio de Malaria: Parásitos y Vectores, Laboratorios de Investigación y Desarrollo, Facultad de Ciencias y Filosofía, Universidad Peruana Cayetano Heredia, Lima, Peru
Jose A. Nakamoto,
Laboratory of Protein Evolution, Department of Experimental Medical Science, Lund University, Lund, Sweden

SPECIALTY SECTION
This article was submitted to Infectious Agents and Disease, a section of the journal Frontiers in Microbiology

RECEIVED 31 May 2022
ACCEPTED 06 July 2022
PUBLISHED 15 September 2022

CITATION
Dueñas E, Nakamoto JA, Cabrera-Sosa L, Huaihua P, Cruz M, Arévalo J, Milón P and Adaui V (2022) Novel CRISPR-based detection of *Leishmania* species. *Front. Microbiol.* 13:958693. doi: 10.3389/fmicb.2022.958693

Novel CRISPR-based detection of *Leishmania* species

Eva Dueñas[1], Jose A. Nakamoto[1†], Luis Cabrera-Sosa[1,2†], Percy Huaihua[3], María Cruz[2,4], Jorge Arévalo[2,3], Pohl Milón[1] and Vanessa Adaui[1,2*]

[1]Laboratory of Biomolecules, Faculty of Health Sciences, Universidad Peruana de Ciencias Aplicadas (UPC), Lima, Peru, [2]Instituto de Medicina Tropical Alexander von Humboldt, Universidad Peruana Cayetano Heredia, Lima, Peru, [3]Laboratorio de Patho-antígenos, Laboratorios de Investigación y Desarrollo, Facultad de Ciencias y Filosofía, Universidad Peruana Cayetano Heredia, Lima, Peru, [4]Hospital Nacional Adolfo Guevara Velasco, Cusco, Peru

Tegumentary leishmaniasis, a disease caused by protozoan parasites of the genus *Leishmania*, is a major public health problem in many regions of Latin America. Its diagnosis is difficult given other conditions resembling leishmaniasis lesions and co-occurring in the same endemic areas. A combination of parasitological and molecular methods leads to accurate diagnosis, with the latter being traditionally performed in centralized reference and research laboratories as they require specialized infrastructure and operators. Clustered regularly interspaced short palindromic repeats/CRISPR-associated protein (CRISPR/Cas) systems have recently driven innovative tools for nucleic acid detection that combine high specificity, sensitivity and speed and are readily adaptable for point-of-care testing. Here, we harnessed the CRISPR-Cas12a system for molecular detection of *Leishmania* spp., emphasizing medically relevant parasite species circulating in Peru and other endemic areas in Latin America, with *Leishmania (Viannia) braziliensis* being the main etiologic agent of cutaneous and mucosal leishmaniasis. We developed two assays targeting multi-copy targets commonly used in the molecular diagnosis of leishmaniasis: the 18S ribosomal RNA gene (18S rDNA), highly conserved across *Leishmania* species, and a region of kinetoplast DNA (kDNA) minicircles conserved in the *L*. (*Viannia*) subgenus. Our CRISPR-based assays were capable of detecting down to 5×10^{-2} (kDNA) or 5×10^{0} (18S rDNA) parasite genome equivalents/reaction with PCR preamplification. The 18S PCR/CRISPR assay achieved pan-*Leishmania* detection, whereas the kDNA PCR/CRISPR assay was specific for *L*. (*Viannia*) detection. No cross-reaction was observed with *Trypanosoma cruzi* strain Y or human DNA. We evaluated the performance of the assays using 49 clinical samples compared to a kDNA real-time PCR assay as the reference test. The kDNA PCR/CRISPR assay performed equally well as the reference test, with positive and negative percent agreement of 100%. The 18S PCR/CRISPR assay had high positive and negative percent agreement of 82.1% and 100%, respectively. The findings support the potential applicability of the newly developed CRISPR-based molecular tools for first-line diagnosis of *Leishmania* infections at the genus and *L*. (*Viannia*) subgenus levels.

KEYWORDS

tegumentary leishmaniasis, *Leishmania*, CRISPR-Cas, nucleic acid detection, molecular diagnostics, kDNA, 18S rDNA, invasive and non-invasive clinical specimens

Introduction

Leishmaniasis is a vector-borne disease of global public health importance caused by intracellular protozoan parasites of the genus *Leishmania*. The disease affects 12 million people spread in 98 countries, with approximately 1.6 million new cases occurring annually (Alvar et al., 2012). In leishmaniasis endemic areas, asymptomatic infections by *Leishmania* are common (representing ~10–60%; Bañuls et al., 2011; Ibarra-Meneses et al., 2022), yet some infected individuals develop a variety of clinical manifestations that affect the skin and/or mucosal tissues (tegumentary leishmaniasis, TL) or internal organs (visceral leishmaniasis, VL) (Burza et al., 2018). In the Americas, TL is widespread, with 56,000 cases reported annually in 18 endemic countries (Pan American Health Organization/World Health Organization, 2020; Ruiz-Postigo et al., 2021). It encompasses skin lesions (96% of reported cases) and mucosal lesions (4% of cases) that can lead to permanent scars and devastating life-threatening mutilation of the nasopharynx, respectively (Pan American Health Organization/World Health Organization, 2019). These phenotypes are caused by different *Leishmania* species and are associated with diverse host–parasite interactions and human host immune responses (Carvalho et al., 2012; Gollob et al., 2014). Among the diverse Neotropical *Leishmania* species of the *Viannia* and *Leishmania* subgenera that circulate in endemic areas, the former are the most frequent cause of TL (Davies et al., 2000; Reithinger et al., 2007; Brito et al., 2009). Particularly, infections with *Leishmania* (*Viannia*) *braziliensis* are predominant and of public health concern because of the associated risk of disease progression from cutaneous to mucosal leishmaniasis (Llanos-Cuentas et al., 1984; Marsden, 1986) and treatment failure (Arevalo et al., 2007; Adaui et al., 2016).

Early and accurate diagnosis of leishmaniasis is critical for its clinical management and timely treatment. Differential diagnosis of TL is challenging due to the clinical pleiomorphism and thus combines clinical characteristics, epidemiological factors, and multiple laboratory diagnostic tests because no perfect reference standard test exists (Adams et al., 2018). Screening for *Leishmania* amastigotes by microscopic examination of Giemsa-stained slide smears of human skin lesions and isolation of parasites from lesions in *in vitro* culture are mainly used for routine diagnosis of TL. However, these methods have suboptimal sensitivity (Weigle et al., 1987, 2002; Faber et al., 2003; Goto and Lindoso, 2010), particularly in chronic skin lesions and mucosal lesions (Weigle et al., 1987, 2002) as they harbor low parasite loads (Gutierrez et al., 1991; Jara et al., 2013). Furthermore, laboratory diagnosis of leishmaniasis remains challenging at health posts or centers that provide primary care in rural areas, where TL is endemic, due to the necessity of resources and infrastructure (Reimão et al., 2020). Molecular methods based on the polymerase chain reaction (PCR), including real-time PCR assays, are accessible only in research and reference laboratories and became increasingly important to complement the conventional parasitological tests. PCR-based nucleic acid amplification techniques (NAATs) provide the most sensitive and specific techniques used for *Leishmania* detection. Often, molecular typing of the infecting parasite species is necessary to guide the selection of the most appropriate treatment or prognosis of the disease (Arevalo et al., 2007; Van der Auwera and Dujardin, 2015; Akhoundi et al., 2017; Moreira et al., 2018; Mesa et al., 2020).

Recent research efforts have been devoted to develop and test molecular methods that have great potential to be further developed into point-of-care (POC) diagnostic tools for leishmaniasis and other neglected tropical diseases (reviewed in Bharadwaj et al., 2021). Among these, isothermal NAATs have attracted attention owing to their operation at a constant temperature (thus requiring minimal laboratory setup) and cost-effectiveness. Several studies that evaluated their diagnostic accuracy for different clinical forms of leishmaniasis reported high sensitivity (Adams et al., 2010, 2018; Mugasa et al., 2010; Saldarriaga et al., 2016; Ibarra-Meneses et al., 2018; Schallig et al., 2019; Cossio et al., 2021; Dixit et al., 2021; Travi et al., 2021). Still, these methods require further development and optimization for POC testing and field validation before their implementation in routine clinical care. Isothermal NAATs may suffer from non-specific amplification that can lead to low specificity, which can impact their applicability (Wang et al., 2015). Another test development concerns the simplified and standardized detection of PCR-amplified DNA of *Leishmania* using an oligochromatographic dipstick format (i.e., the commercially available *Leishmania* OligoC-TesT kit), which showed high diagnostic sensitivity and specificity in clinical samples (Deborggraeve et al., 2008; Espinosa et al., 2009). The advent of user-friendly portable devices such as Palm PCR™ (Kariyawasam et al., 2021), real-time fluorimeters [e.g., for real-time monitoring of the amplification profile of loop-mediated isothermal amplification (LAMP) reactions (Ibarra-Meneses et al., 2018; Dixit et al., 2021)], and the Bento Lab®, a mobile DNA laboratory setup (Kambouris et al., 2020), have opened the possibility to ease implementation of field-applicable molecular methods for use at POC to facilitate early diagnosis of leishmaniasis.

Recently, the clustered regularly interspaced short palindromic repeats (CRISPR)/CRISPR-associated proteins (Cas) technology is revolutionizing the field of nucleic acid detection and

next-generation molecular diagnostics, making possible field-deployable POC testing solutions (Myhrvold et al., 2018; Verosloff et al., 2021). CRISPR-Cas systems, naturally occurring in many bacteria and archaea as adaptive immune systems (Wiedenheft et al., 2012), are aiding in the development of novel nucleic acid detection platforms for major diseases such as cancer (Chen et al., 2018) and infectious diseases (Gootenberg et al., 2017). CRISPR-Cas technology is based on the specificity, programmability, and versatility of Cas effector proteins for nucleic acid sensing. Cas enzymes are easily programmable by the custom design of CRISPR RNAs (crRNAs) to recognize and cleave target DNA or RNA sequences with single-nucleotide specificity (Gootenberg et al., 2017). The most widely used Cas enzymes in nucleic acid detection and diagnostic applications are Cas9, Cas12a, and Cas13a. The latter two exhibit non-sequence-specific collateral (*trans*-cleavage) activity on target recognition. The discovery of the collateral cleavage activity on non-targeted single-stranded DNA (Cas12a) or single-stranded RNA (Cas13a) in solution funneled the development of CRISPR-Cas12a-based (DETECTR, Chen et al., 2018) and –Cas13a-based (SHERLOCK, Gootenberg et al., 2017) methods for *in vitro* nucleic acid detection. By adding quenched fluorescent oligonucleotide reporter probes in the CRISPR reaction mixture, which are cleaved by collateral activity, the released fluorescent signal indicates the presence of the target nucleic acid in a sample. Cas-mediated detection is commonly analyzed *via* fluorescence and lateral-flow readouts. Most CRISPR-based detection platforms function downstream of NAATs, which improves specificity due to crRNA-directed target sequence recognition (Kaminski et al., 2021). The preamplification step using NAATs enriches target molecules and increases the sensitivity of target detection down to attomolar (10^{-18} M) clinically meaningful concentrations (Gootenberg et al., 2017; Chen et al., 2018). Both isothermal (used in most CRISPR-based methods including SHERLOCK and DETECTR) and PCR-based (e.g., used in HOLMES combined with Cas12a-mediated detection, Li et al., 2018) NAATs are employed as preamplification strategies. CRISPR-based methods have been developed and applied to detect pathogens of public health importance, including bacteria [e.g., *Mycobacterium tuberculosis* (Ai et al., 2019; Sam et al., 2021)], viruses [e.g., Zika virus, dengue virus (Gootenberg et al., 2017, 2018; Myhrvold et al., 2018), human papillomavirus (Chen et al., 2018; Gong et al., 2021), SARS-CoV-2 (Broughton et al., 2020; Fozouni et al., 2021; Alcántara et al., 2021a)], fungi (Huang et al., 2021), and protozoa [with a major focus on parasites belonging to the phylum Apicomplexa, such as *Plasmodium* spp. (Lee et al., 2020; Cunningham et al., 2021), *Toxoplasma gondii* (Ma et al., 2021), and *Cryptosporidium parvum* (Yu et al., 2021)]. Concerning trypanosomatid protozoan parasites, a recent study reported a newly developed CRISPR-dCas9-based DNA detection scheme with visual readout *via* DNAzymes (G-quadruplex-hemin complexes) and used spiked-in kinetoplast DNA (kDNA) from *Leishmania* into blood and urine samples as a proof-of-principle (Bengtson et al., 2022).

Here, we aimed to establish a novel method for CRISPR-Cas12a-mediated detection of amplified DNA from human lesion samples derived from patients with suspected cutaneous leishmaniasis (CL). Particularly, we used PCR amplification of multicopy *Leishmania* genetic targets coupled to downstream Cas12a-based detection aiming for high sensitivity and specificity of *Leishmania* detection with potential applicability in the diagnosis of CL in Latin America. To this end, we propose proof-of-concept of two assays, one targeting the conserved 18S ribosomal RNA gene (18S rDNA) for pan-*Leishmania* detection and the other targeting a region of kDNA minicircles conserved among *L.* (*Viannia*) species of medical importance in Latin America. We report the analytical sensitivity and specificity using extracted DNA from *Leishmania* and *Trypanosoma cruzi* reference strains. The assay performance was assessed using a panel of DNA samples from human skin lesion specimens with known diagnosis, wherein assay concordance was analyzed in relation to a previously validated kDNA qPCR assay (Jara et al., 2013).

Materials and methods

Bioinformatics analyses

crRNA selection and template design

For the 18S rDNA gene, crRNA guide sequence candidates were obtained from EuPaGDT[1] (Peng and Tarleton, 2015) based on the *L.* (*V.*) *braziliensis* MHOM/BR/75/M2904 sequence (TriTrypDB ID: LbrM.27.2.208540).[2] The top ten protospacer adjacent motif (PAM) sequences (TTTV for LbCas12a, formerly LbCpf1) at the 5′ end of the target DNA and the 20 nt-long target recognition sequences (i.e., guide sequence) in the crRNA were selected based on the total score and guide RNA efficiency/activity score.

To identify conserved regions in *L.* (*Viannia*) kDNA minicircle sequences, an initial computational alignment included the sequences of 14 *L.* (*V.*) *braziliensis*, 10 *L.* (*V.*) *guyanensis*, 18 *L.* (*V.*) *lainsoni*, and 13 *L.* (*V.*) *panamensis* strains reported in GenBank. A second alignment focused on *L.* (*V.*) *braziliensis* kDNA minicircle sequences (409 sequences reported in GenBank as of June 4, 2020). All alignments were performed locally using the ClustalX package for Ubuntu with default parameters (Larkin et al., 2007). Conserved regions in the *Viannia* subgenus of *Leishmania* were identified with the AliView software (Larsson, 2014). PAM sequences were searched within the conserved regions to identify potential target recognition sites. Sequence alignments are available in Supplementary File S1.

Then, PAM sequences and recognition sites selected for both DNA targets were aligned against available sequences in GenBank of *L.* (*V.*) *braziliensis*, *L.* (*V.*) *guyanensis, L.* (*V.*) *panamensis, L.* (*V.*)

1 http://grna.ctegd.uga.edu/

2 https://tritrypdb.org/tritrypdb/

lainsoni, and *L.* (*L.*) *major* using NCBI BLAST. For the 18S rDNA gene, sequences with less than 100% identity and coverage in any *Leishmania* species were discarded. For kDNA minicircles, sequences with less than 100% identity and coverage in any species belonging to the *L.* (*Viannia*) subgenus were discarded.

In order to minimize the occurrence of cross-reactivity with the human genome, with microorganisms that cause skin lesions other than CL, and phylogenetically related protozoan parasites, filtered PAM sequences and target recognition sites were aligned against available genome sequences in GenBank of *Homo sapiens*, *Trypanosoma cruzi*, *Mycobacterium tuberculosis*, *Mycobacterium leprae*, *Sporothrix schenckii*, *Trypanosoma brucei*, *Blastomyces*, *Plasmodium vivax*, *Plasmodium falciparum*, and *Toxoplasma gondii*. Sequences were ranked by the number of different species of those listed above with at least 75% coincidence in sequence identity and coverage. For each target, the recognition site with the lowest rank was finally chosen.

In addition, a crRNA targeting the human RNase P *POP7* gene reported by Broughton et al. (2020) was used as a control for specimen quality. Double-stranded DNA (dsDNA) templates for crRNA generation through *in vitro* transcription were designed with a T7 promoter sequence (Beckert and Masquida, 2011), followed by the LbCas12a crRNA scaffold (Chen et al., 2018) and the selected target recognition site (as in Alcántara et al., 2021b).

Primer design

For the 18S rDNA gene, primer candidates for PCR preamplification of the target sequences prior to the CRISPR-Cas reaction were designed using the Primer3Plus v.2.4.2 server with the default settings and an average Tm of 60°C (Untergasser et al., 2012).[3] For kDNA minicircles, primer candidates were manually searched (18–22 nt long, average Tm of 60°C) within conserved regions identified previously.

Primer candidates were aligned against the human genome using NCBI BLAST and discarded if they had more than 80% sequence identity and coverage with any human sequence. Self- and hetero-dimer formation were tested using the IDT OligoAnalyzer Tool.[4] Primers with $\Delta G < -7$ kcal/mol in any parameter were discarded. For the RNase P gene, primers reported previously (Curtis et al., 2018; Alcántara et al., 2021a) were selected. Oligonucleotides were ordered from Macrogen Inc. (Seoul, South Korea). All primer and crRNA template sequences used in this study are listed in Supplementary Table S1.

crRNA preparation

crRNAs were prepared from dsDNA templates using the TranscriptAid T7 High Yield Transcription Kit (Thermo Fisher Scientific, Waltham, MA, United States) at 37°C for 3 h. Immediately thereafter, crRNAs were purified using the Direct-zol RNA miniprep kit (Zymo Research, Irvine, CA, United States) with a DNase I digestion in a column step for 15 min at room temperature (RT) and eluted in 80 µl nuclease-free water. Finally, crRNAs were quantified by the NanoDrop One microvolume UV–Vis spectrophotometer (Thermo Fisher Scientific), aliquoted to working volumes (~10 µl) and stored at −80°C (Alcántara et al., 2021b).

DNA samples from reference strains of *Leishmania* spp. and *Trypanosoma cruzi*

Genomic DNA (gDNA) samples extracted from cultured promastigotes of reference strains of *Leishmania* [*L.* (*V.*) *braziliensis* (MHOM/BR/75/M2904, MHOM/PE/91/LC2043 and MHOM/PE/91/LC2177), *L.* (*V.*) *peruviana* (MHOM/PE/90/LCA08, MHOM/PE/90/HB22), *L.* (*V.*) *guyanensis* (IPRN/PE/87/Lp52), *L.* (*V.*) *lainsoni* (MHOM/BR/81/M6426), *L.* (*L.*) *amazonensis* LV79 (MPRO/BR/72/M1841), *L.* (*L.*) *major* (MHOM/SU/73/5-ASKH), *L.* (*L.*) *infantum* (MHOM/TN/80/IPT1), and *L.* (*L.*) *donovani* (MHOM/IN/80/DD8 LEM 703)] analyzed here were retrieved from the DNA biobank of the leishmaniasis research group at the Molecular Epidemiology Unit of the Instituto de Medicina Tropical Alexander von Humboldt (IMTAvH), Universidad Peruana Cayetano Heredia (UPCH) in Lima, Peru. gDNA from the *Trypanosoma cruzi* Y strain (MHOM/BR/00/Y isolate; DTU TcII) was kindly provided by Dr. Manuela Verástegui (Infectious Diseases Research Laboratory, UPCH).

Patient DNA samples

Ethics statement

This study used anonymized stored DNA samples derived from skin lesion specimens from patients who tested positive or negative for *Leishmania* infection by conventional kDNA PCR (see below) and provided written informed consent for future research use of their specimens and clinical data. Patients with clinically suspected CL were recruited at the Hospital Nacional Adolfo Guevara Velasco (HNAGV) in Cusco, a region with endemic transmission of *Leishmania* (*Viannia*) parasites, with higher prevalence of *L.* (*V.*) *braziliensis* followed by *L.* (*V.*) *guyanensis* and *L.* (*V.*) *lainsoni* infections (Lucas et al., 1998; Sandoval-Juárez et al., 2020), during 2019 and 2020 as part of an ongoing collaborative study between the HNAGV and UPCH aimed at developing a rapid lateral flow assay for the diagnosis of TL in primary health care facilities in rural endemic areas in Peru. The protocol and informed consent of that study (registration number: 103155) were approved by the Institutional Review Board of the UPCH (IRB approval letter 063–05-19 dated 01/30/2019, latest renewed on 04/26/2022 with letter R-122-17-22). Written informed consent was obtained from all

3 https://www.bioinformatics.nl/cgi-bin/primer3plus/primer3plus.cgi

4 https://www.idtdna.com/pages/tools/oligoanalyzer

patients prior to enrollment. The activities of HNAGV and UPCH were conducted in compliance with all applicable international regulations governing the protection of human subjects.

Skin sample DNA isolation

DNA was isolated from different human skin lesion specimen types (biopsies, lancet scrapings, cytology brushes, swabs, and filter paper lesion impressions) as previously described (Boggild et al., 2010; Suárez et al., 2015). Samples were processed for DNA isolation using the High Pure PCR Template Preparation Kit (Roche, Mannheim, Germany) according to the manufacturer's instructions. DNA from biopsy specimens was eluted into 150 µl of elution buffer, while for the other specimen types, a 100 µl elution volume was used. The isolated DNA was quantified by fluorometry using the Quant-iT high sensitivity dsDNA assay kit on the Qubit fluorometer (Invitrogen; Thermo Fisher Scientific). The DNA samples were stored at −20°C until further molecular analyses.

Study design: Inter-rater agreement study with a binary outcome

This study was designed to assess the applicability and performance of the newly developed CRISPR-based assays for detection of *Leishmania* DNA in patient samples in comparison to the kDNA qPCR assay (Jara et al., 2013). We had access to a total of 49 DNA samples, collected from patients with PCR-confirmed diagnosis of CL ($n = 36$) or with skin lesions of other etiology (non-CL, $n = 13$). For this fixed sample size, we performed an statistical analysis to calculate the expected lower bound of a one-sided 95% confidence interval for an anticipated value of kappa coefficient of 0.8 between tests, for two raters, assuming a prevalence of 0.75 positive cases and a significance level (alpha) of 5% (using the FixedNBinary function of the R software package "kappaSize" version 1.2; (Rotondi, 2018)). This calculation resulted in a lower limit for kappa of 0.581, which provides confidence in finding at least a moderate (0.4–0.6) or substantial (0.6–0.8) agreement in the concordance analysis.

PCR-based preamplification of target DNA

PCR reactions were performed in a 25-µl reaction mixture consisting of 5 µl of DNA sample, 0.2 µM each target-specific forward and reverse primers (Supplementary Table S1), and 1 × DreamTaq Green PCR master mix (Thermo Scientific). Reactions were performed independently for kDNA, 18S rDNA, and RNase P. Cycling conditions consisted of an initial activation step at 95°C for 2 min followed by 45 cycles of denaturation at 95°C for 20 s, annealing at 60°C (18S rDNA and RNase P) or 61°C (kDNA) for 30 s, and extension at 68°C for 15 s, followed by a final extension step at 68°C for 5 min on the T100™ thermal cycler (Bio-Rad, Hercules, CA, United States). During protocol optimization, PCR products were visualized by 2–3% agarose gel electrophoresis using SYBR Gold staining. A positive control [*L.* (*V.*) *braziliensis* M2904 gDNA, 10^4 parasite genome equivalents/µl], a negative control [human gDNA from peripheral blood mononuclear cells (PBMC) of a healthy donor, 40 ng of input DNA], and two negative amplification controls [i.e., No-Template Control (NTC) reactions: NTC1, kept closed without water addition, and NTC2, made with PCR-grade water as the template replacement] were included in all experiments.

LbCas12a *trans*-cleavage assays

LbCas12a-based detection reactions were performed as described previously (Chen et al., 2018; Broughton et al., 2020) with some modifications (Alcántara et al., 2021a). The recombinant LbCas12a protein was expressed and purified as described (Mendoza-Rojas et al., 2021). A single-stranded DNA (ssDNA) fluorophore quencher (FQ)-labeled reporter probe (5′ Cy3/TTATT/BHQ-2 3′) was selected and synthesized commercially (Macrogen Inc., Seoul, South Korea). The *in vitro* transcribed crRNA was first heated at 65°C for 10 min in a heating block followed by refolding at RT for 10 min. Then, the CRISPR complex was prepared at ten-fold concentration (100 nM LbCas12a, 150 nM crRNA, 2 µM ssDNA-FQ reporter) in Reaction buffer (10 mM Tris–HCl (pH 7.9 at 25°C), 50 mM NaCl, 100 µg/ml BSA, without adding $MgCl_2$ at this step) and incubated at RT for 10 min in the dark. In parallel, 6 µl of PCR-amplified target DNA was diluted in 102 µl of Reaction buffer containing 18 mM $MgCl_2$. Next, 10 µl of the CRISPR complex was mixed with 90 µl of the diluted PCR-amplified DNA in a flat-bottom, black 96-well microplate (Thermo Scientific; Cat. no. 237107). Final concentration of $MgCl_2$ was 15 mM in the 100 µl final volume. Reactions were incubated in a fluorescence plate reader (most measurements used the Synergy™ H1 hybrid multi-mode reader, BioTek Instruments, Winooski, VT, United States; for some experiments, measurements used the Cytation™ 5 Cell Imaging multi-mode reader, BioTek Instruments, see details in the respective figure legends) for 2 h at 25°C. Fluorescence measurements were recorded every minute (excitation wavelength: 520 ± 9 nm, emission wavelength: 570 ± 20 nm) from the top of the wells. The fluorescence gain settings were 120 on the Synergy H1 plate reader and 150 on the Cytation 5 plate reader.

In addition to the PCR controls, a No-Template Control (NTC) of the CRISPR reaction (Reaction buffer containing 15 mM $MgCl_2$ instead of the PCR product) was included. The PCR and CRISPR reaction setups were performed in a unidirectional workflow using separated laboratory work areas for each step to prevent amplicon carryover contamination.

Analytical sensitivity and specificity testing

Serial dilutions of *L.* (*V.*) *braziliensis* M2904 gDNA (extracted from a promastigote culture) to a final range of 5×10^4 to 5×10^{-3} parasite genome equivalents per reaction (encompassing the same range of parasite genome equivalents per reaction of the standard curve used in the kDNA qPCR assay; Jara et al., 2013) were tested as input DNA in PCR reactions to amplify the target gene, followed by LbCas12a-based detection assays as described above. The analytical sensitivity for each target gene was determined based on 3 independent experiments.

The analytical specificity of the PCR/CRISPR assays targeting *Leishmania* kDNA (*Viannia* subgenus) or 18S rDNA was tested using gDNA of laboratory reference strains of New World and Old World *Leishmania* species, and of *T. cruzi*. Target genes were amplified by PCR (using 20–40 ng of input DNA corresponding to 2.35×10^5–4.71×10^5 *Leishmania* genome equivalents) and detected by LbCas12a-based detection assays as described above. Two independent PCR/CRISPR experiments were performed.

Performance evaluation of PCR/CRISPR assays on clinical samples

A total of 49 patient DNA samples extracted from skin lesion specimens described above were tested blindly in groups of ten, plus positive and negative controls. Five µl of 1/10 diluted DNA samples (1–250 ng of input DNA) were subjected to PCR-based amplification of *Leishmania* kDNA and 18S rDNA, and human RNase P gene. The PCR products were then detected by LbCas12a-based detection assays as described above. As a validation, a subset of samples was retested; this corresponded to 13 of 49 samples (26.5%) for kDNA PCR/CRISPR and 14 of 49 samples (28.6%) for 18S PCR/CRISPR.

Conventional kDNA PCR

A qualitative conventional PCR targeting a 70-bp conserved region of *Leishmania* (*Viannia*) kDNA minicircles (Lopez et al., 1993) was performed to detect *Leishmania* infection in clinical samples. The reaction mixture consisted of 0.4 µM of each primer (MP1L and MP3H; Lopez et al., 1993) for the amplification of the kDNA target, 0.4 µM of each primer (HBBL and HBBR; Boggild et al., 2010) for the amplification of the human beta-globin gene as an indicator of specimen adequacy, 0.2 mM dNTPs, 1 × Qiagen PCR buffer, 1.5 mM $MgCl_2$, 1 × Q-Solution, 0.5 U HotStarTaq DNA polymerase (Qiagen, Hilden, Germany), and 5 µl of DNA sample (two reaction tubes were set up in parallel: one with the undiluted DNA sample and the other with 1/10 diluted DNA sample as a technical replicate) in a 25 µl total volume. Cycling conditions were as follows: 5 min at 95°C followed by 40 cycles of 1 min at 94°C, 1 min at 60°C, 1 min at 72°C followed by a final extension step for 10 min at 72°C on the Veriti™ 96-well thermal cycler (Applied Biosystems; Thermo Fisher Scientific). Amplicons were visualized on 3% agarose gels stained with ethidium bromide. Each run included a positive control [DNA isolated from the *L.* (*V.*) *braziliensis* M2904 reference strain, 20 ng of input DNA], a negative control (human gDNA from PBMC of a healthy donor, 10–20 ng of input DNA), and a NTC.

Quantitative real-time PCR

A SYBR Green-based qPCR assay targeting kDNA minicircles, based on the same primer set as for the diagnostic conventional PCR, was performed to detect and quantify *Leishmania* (*Viannia*) parasites in clinical samples, as described previously (Jara et al., 2013). A sample was considered detectable if a sigmoidal amplification curve and Cq value were obtained with a *Leishmania*-specific amplicon in the post-amplification melting curve analysis. The standard curve was prepared using ten-fold serially diluted *L.* (*V.*) *braziliensis* M2904 gDNA corresponding to 5×10^4 to 5×10^{-3} parasite genome equivalents per reaction. In parallel, a qPCR assay detecting the human endogenous retrovirus 3 (*ERV-3*) gene, using the primers reported by Yuan et al. (2001), was used to quantify host cells, as described previously (Jara et al., 2013). The *ERV-3* standard curve was established from DNA extracted from human PBMC and comprised 2×10^4 to 8×10^1 copies/reaction. The *Leishmania* parasite load was calculated as follows: parasite genome equivalents (estimated by kDNA qPCR) normalized to the number of human cells (*ERV-3* average copy number/2) $\times 10^6$, expressed as the number of *Leishmania* parasites per 10^6 human cells. Each run included a positive-control sample (DNA from a biopsy specimen of a patient with confirmed diagnosis of CL), which allowed monitoring the inter-assay variation in quantitative results between runs. In addition, a negative control [DNA from a non-leishmanial (kDNA PCR-negative) skin lesion] and a NTC were included. Standard curve dilution series, controls and clinical samples were tested in duplicate.

Data processing and analysis

Following the LbCas12a-based detection reactions, the raw fluorescence collected data from each well of the assay plate were exported to Microsoft Excel. Based on the fluorescence time-course data gathered during the analytical sensitivity and specificity experiments with DNA samples from reference *Leishmania* strains and controls that were run in parallel, the time point of fluorescence accumulation for data analysis was defined (at 20-min time point for kDNA and at 10-min time point for 18S rDNA). For RNase P, analysis was performed at the 10-min time point as described previously (Broughton et al., 2020).

The raw fluorescence data were normalized by dividing target reaction fluorescence accumulated at the defined time point of the test sample to that of the NTC1 (PCR blank) reaction that was run in parallel on the same Cas12a assay plate. This is referred to as the "fluorescence ratio." In the performance evaluation of the PCR/CRISPR assays with clinical samples, the fluorescence ratios were calculated using the mean of the NTC1 fluorescence values across all runs for a given target. In case of discordant results between the two independent measurements for the subset of clinical samples tested twice (i.e., discordant if one was positive and the other was negative), the sample was retested to confirm the result.

To determine the threshold cutoff value for detection of *Leishmania* in clinical samples by PCR/CRISPR, we calculated the mean and standard deviation of the fluorescence ratio of the negative clinical samples ($n = 10$). We considered positive signal in a reaction as being over three standard deviations higher than the mean fluorescence ratio of the negative samples. As an alternative method to set the detection threshold, we calculated the percentage positivity (PP) of the test samples relative to a positive control [*L.* (*V.*) *braziliensis* M2904 preamplified target DNA from 5×10^4 parasite genome equivalents] that was run in each Cas12a assay plate. This method controls for inter-plate variability of the assay (Wright et al., 1993; Lejon et al., 2006; Zimic et al., 2009). The PP of the test samples was calculated as: PP = (raw fluorescence of the test sample/raw fluorescence of the positive control of the corresponding plate) × 100. Then, the mean PP of the two independent measurements for the subset of retested samples was calculated. Using the PP of the tested samples as the predictor variable, a simple logistic regression was performed to model the *Leishmania* infection status (positive/negative, as determined by kDNA qPCR). Sensitivity, specificity and a receiver operating characteristic (ROC) curve were calculated over the range of cutoff points for the predictor variable (PP). The optimal probability cutoff point for classification (Pr-cutoff/PP) was selected based on the maximization of the Youden's J-index (sensitivity + specificity – 1).

As quality control during CRISPR-Cas assay data analysis, we calculated the mean and standard deviation of the raw fluorescence values of the negative controls examined along with clinical samples across all runs at the 20-, 40-, 60- and 120-min time points. We established the range of acceptable fluorescence values for the negative controls to those that fell within 15% of the mean fluorescence (for each negative control) across all runs. In cases where any of the negative controls was out of the acceptable range, i.e., showing a marked increase in raw fluorescence, the experimental run was considered invalid due to contamination.

The CRISPR-Cas assay data analysis was blinded to the qPCR data and only compared once all samples had been tested. The concordance of the results obtained with kDNA PCR/CRISPR, 18S PCR/CRISPR, or kDNA conventional PCR (routine diagnostic test; Lopez et al., 1993) against the kDNA qPCR reference method was assessed by calculating the positive and negative percent agreement (PPA and NPA, respectively) with Wilson score 95% confidence intervals (CI) using the Analyse-it software add-in for Microsoft Excel.[5] In addition, Cohen's Kappa coefficient was calculated using kDNA qPCR as the reference method (McHugh, 2012).

Graphs, numerical data analyses, and statistical analyses were performed using GraphPad Prism version 9 (GraphPad Software, San Diego, CA, United States). For comparison of the fluorescence ratio data between groups of *L.* (*Viannia*) and *L. (Leishmania)* strains or between assay controls, an unpaired *t*-test was used. Differences with $p < 0.05$ were considered significant. The logistic regression and ROC curve analysis were conducted using Stata version MP 17 (StataCorp, College Station, TX, United States) as well as GraphPad Prism version 9.

Results

Development, optimization and analytical validation of Cas12a-based assays for detection of *Leishmania* spp.

Herein, we sought to develop CRISPR-Cas12a-based assays for genus-specific detection of *Leishmania* spp. and *L.* (*Viannia*) subgenus-specific detection of the species responsible for most cases of cutaneous and mucosal leishmaniasis in Latin America. We chose the widely used multicopy 18S rDNA and kDNA minicircle targets to ensure high sensitivity and to provide proof-of-concept of the applicability of CRISPR-based detection to *Leishmania* spp. in clinical specimens. Each assay starts from extracted DNA and comprises a preamplification step of the target DNA using conventional PCR, followed by Cas12a detection with fluorescent readout on a plate reader (Figure 1). Thus, this test yields qualitative detection of nucleic acids from *Leishmania*. Raw fluorescence values over 2 h were measured to assess the fluorescence change over time for the test samples as compared to the controls. For assay interpretation and reporting results, the fluorescent signal of each sample obtained at a defined time point (20 min for kDNA and 10 min for 18S rDNA; see details below) of the Cas12a reaction was normalized relative to the No-Template Control (NTC) fluorescence value, thereby resulting in a fluorescence ratio.

The highly conserved nature of the 18S rDNA gene was used for the development of a pan-*Leishmania* detection assay using a crRNA directed to a conserved target site across *Leishmania* species (Figures 2A,B and Supplementary File S1). For the kDNA target, we first searched *in silico* for conserved regions in kDNA minicircle sequences among New World *L.* (*Viannia*) species and selected one region

5 https://analyse-it.com/

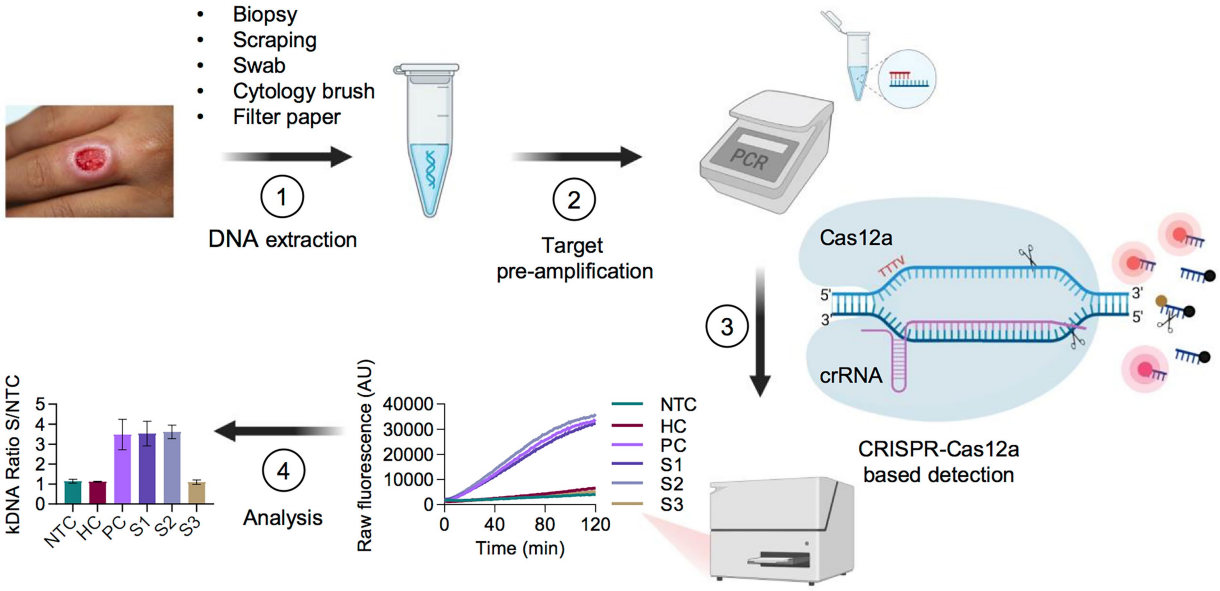

FIGURE 1
Schematic of the PCR coupled CRISPR-Cas12a-based assay workflow for detection of *Leishmania* spp. in clinical samples. **(1)** Skin lesion specimens suggestive of CL are processed for gDNA extraction. **(2)** The isolated DNA is subjected to PCR preamplification using primers targeting *Leishmania* kDNA minicircles or 18S rDNA, or the sample control, human RNase P gene. **(3)** The PCR amplicon is then used as input DNA for Cas12a-based detection guided by a target-specific CRISPR RNA (crRNA). A ternary complex is formed if the target DNA is present in the reaction mixture. Cas12a recognizes a 5′-TTTV-3′ PAM in the target DNA, which results in base pairing between the crRNA guide (spacer) segment and the complementary target DNA. Upon specific target DNA recognition by Cas12a, the activated Cas12a enzyme generates non-sequence-specific cleavage of a single-stranded DNA (ssDNA) reporter probe, thereby producing a fluorescence signal that can be recorded by a fluorescence plate reader. **(4)** Normalized fluorescence readings (test sample/NTC), expressed as a fluorescence ratio, are used to interpret the assay results. As an illustrative example, data shown correspond to the kDNA target and are represented as mean±standard deviation (SD; *n*=2 independent amplification and detection runs). Standardized conditions consisted of ~90-min amplification (45 PCR cycles) and fluorescence signal (LbCas12a detection assay) at 20-min time point for kDNA and at 10-min time point for both 18S rDNA and RNase P. AU, arbitrary units; NTC, no-template control of the Cas12a reaction; HC, human PBMC gDNA from a healthy donor (negative control); PC, *L.* (*V.*) *braziliensis* M2904 gDNA (positive control); Samples S1–S3, DNA from clinical samples. Figure created with BioRender.com.

with a suitable PAM site for Cas12a crRNA design (Figures 2A,B, Supplementary File S1, and Supplementary Figure S1). We designed a kDNA–crRNA, located within minicircle conserved sequence block CSB2 (Supplementary Figure S1), which recognizes a target sequence that is highly conserved among *L.* (*Viannia*) species according to the *in silico* multiple sequence alignments performed (Figure 2B and Supplementary File S1). A careful crRNA selection was carried out for both *Leishmania* target sequences, thereby filtering against the human genome and genomes from related pathogens that co-circulate in leishmaniasis endemic regions and/or cause leishmaniasis-like lesions (Figure 2A).

We then designed PCR primers to amplify genomic segments spanning the selected crRNA target sites (Figure 2C and Supplementary Table S1). For the 18S rDNA target, we designed three forward and three reverse primers to be tested in four primer pairs (sets 1–4, Figure 2C). For the kDNA target, we designed PCR primers located within minicircle conserved sequence blocks CSB1 and CSB3 (kDNA primer set 1, namely primers F1/R, Figure 2C and Supplementary Figure S1). Additionally, we selected a combination of the previously published MP1L primer (Lopez et al., 1993), located immediately upstream of the CSB1, and the designed R primer located within CSB3 (kDNA primer set 2, MP1L/R, Figure 2C and Supplementary Figure S1).

During the optimization of PCR amplification conditions for both *Leishmania* targets, each primer set generated a PCR product of the expected size from genomic DNA of the *L. braziliensis* M2904 reference strain, while not producing an amplified product from the NTC controls (Figure 2D). The standardized conditions consisted of ~90-min amplification (45 PCR cycles), in order to boost the sensitivity of the PCR/CRISPR assays. Two primer pairs (kDNA primer set 2 and 18S primer set 3) produced non-specific PCR products in the negative control with human genomic DNA (Figure 2D). However, these did not generate a signal above the NTC controls in the Cas12a-based detection assay (see below).

For our Cas12a-based assays we used conditions that were previously optimized for viral targets of SARS-CoV-2 (Alcántara et al., 2021a,b), namely 10 nM LbCas12a, 15 nM crRNA, 15 mM $MgCl_2$, and 200 nM of the reporter probe. The Cas12a reaction was incubated at 25°C as previously described (Alcántara et al., 2021a,b). Next, we carried out serial dilutions of *L. braziliensis* M2904 genomic DNA used as template DNA to determine the analytical sensitivity of the PCR-based preamplification with each primer set coupled to Cas12a-based detection. The raw

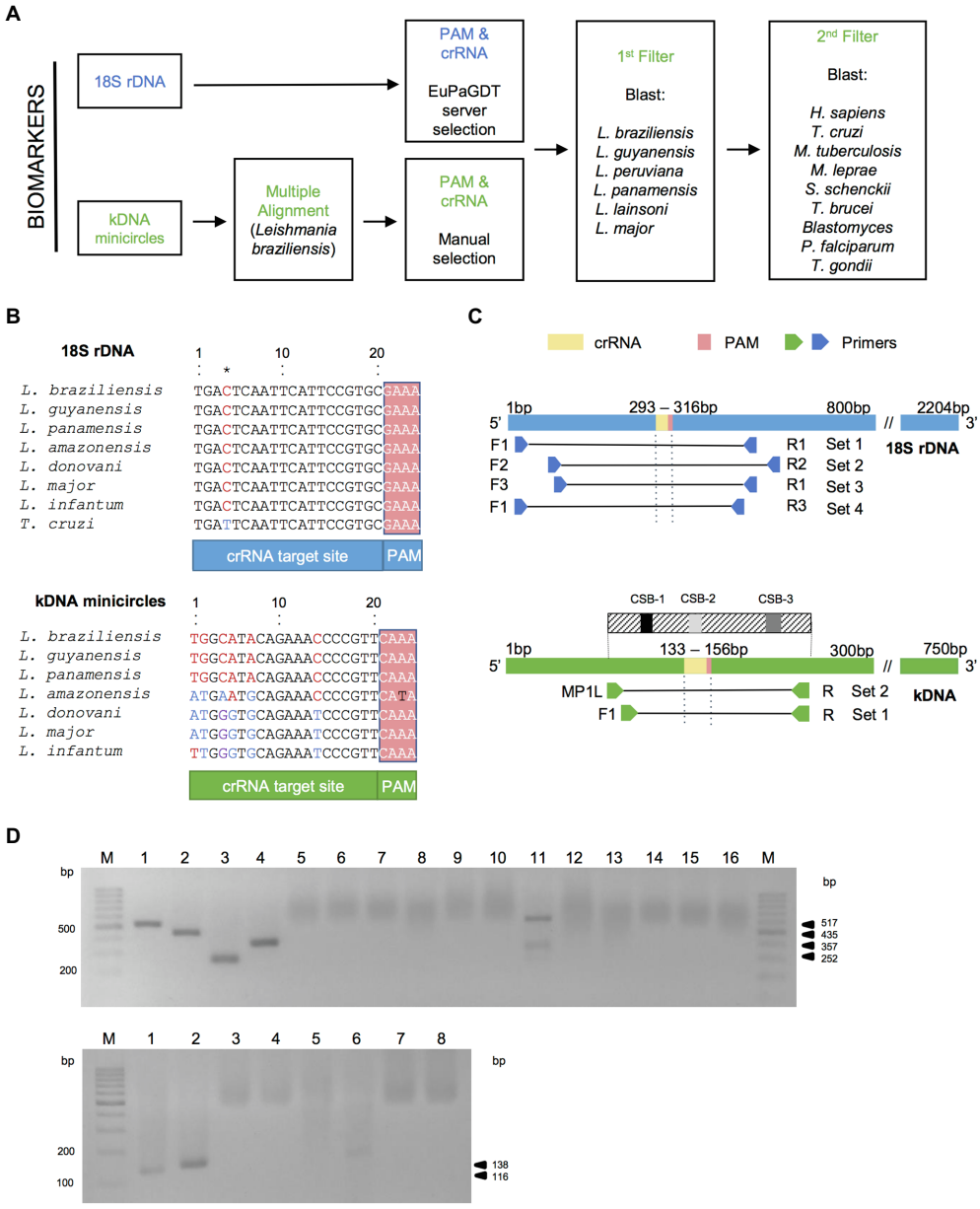

FIGURE 2
Bioinformatics analysis for crRNA and primer sets design. **(A)** Bioinformatics workflow for crRNA filtered selection for *Leishmania* kDNA minicircle and 18S rDNA biomarkers (see "Materials and Methods" for details). **(B)** Alignments of the target DNA sequence (that is complementary to the crRNA guide sequence) and flanking PAM from seven strains representative of different *Leishmania* species for the two targets and the *Trypanosoma cruzi* Y strain for the 18S rDNA target (the kDNA alignment including *T. cruzi* Y strain resulted in a 21bp gap in the crRNA). Aligned sequences of the 18S rDNA gene concerned the strains: *L.* (*V.*) *braziliensis* MHOM/BR/75/M2904 2019 (TriTrypDB ID code: LbrM.27.2.208560), *L.* (*V.*) *guyanensis* MHOM/BR/1975/M4147 (GenBank accession number: X53913), *L.* (*V.*) *panamensis* MHOM/PA/94/PSC-1 (TriTrypDB ID code: LPMP_27rRNA1), *L.* (*L.*) *amazonensis* MHOM/BR/1973/M2269 (TriTrypDB ID code: LAMA_000552800), *L.* (*L.*) *donovani* MHOM/ET/67/HU3 (isolate LV9, TriTrypDB ID code: LdLV9.00.2.200020), *L.* (*L.*) *major* MHOM/IL/80/Friedlin (TriTrypDB ID code: LmjF.27.rRNA.06), *L.* (*L.*) *infantum* MCAN/ES/98/LLM-877 (strain JPCM5, TriTrypDB ID code: LINF_270031400), and *T. cruzi* Y (GenBank accession number: AF301912). The alignment of the nucleotide sequences of the kDNA minicircle target shown here included the strains (GenBank accession numbers are indicated between brackets): *L.* (*V.*) *braziliensis* MHOM/BR/75/M2904 (KY698821), *L.* (*V.*) *guyanensis* MHOM/BR/78/M5378 (KY699068), *L.* (*V.*) *panamensis* MHOM/PA/75/M4037 (AF118474), *L.* (*L.*) *amazonensis* RAT/BR/72/LV78 (KY698896), *L.* (*L.*) *donovani* MHOM/IN/80/DD8 (AF167712), *L.* (*L.*) *major* MHOM/IL/67/LV563 (KM555295), *L.* (*L.*) *infantum* MHOM/FR/91/LEM-2298 (AF190883). Nucleotide positions differing among aligned sequences are highlighted. The 18S rDNA target sequence shows conservation at the *Leishmania* genus level, whereas the selected kDNA minicircle target region is conserved among *L.* (*Viannia*) species. See Supplementary File S1 for all alignments. **(C)** Locations of PCR primer sets that flank the crRNA target site and PAM sequence in the target genomic regions (nucleotide positions are based on the *L.* (*V.*) *braziliensis* M2904 strain). For the kDNA minicircle target, we used PCR primers located within conserved sites CSB1 and CSB3 (see Supplementary Figure S1). **(D)** Agarose gel electrophoresis of PCR products generated with primer sets shown in **(C)**. M, molecular size marker (100bp; GeneRuler, Thermo Scientific). The PCR amplicons (6μl) were mixed with 2μl 6X TriTrack DNA loading dye (Thermo Scientific) plus SYBR Gold solution, loaded onto a 2% agarose gel

(Continued)

FIGURE 2 (Continued)
(18S rDNA) or 3% agarose gel (kDNA), and run in 1X TBE buffer for 1h at 100V. *Upper gel*: PCR products obtained using the 18S primer set 1 (lanes 1, 5, 9, 13), set 2 (lanes 2, 6, 10, 14), set 3 (lanes 3, 7, 11, 15), and set 4 (lanes 4, 8, 12, 16). Lanes 1–4: *L.* (*V.*) *braziliensis* M2904 gDNA (5×10^4 parasite genome equivalents per reaction; positive control). The size of the expected product is 517bp for 18S primer set 1 (lane 1), 435bp for 18S primer set 2 (lane 2), 252bp for 18S primer set 3 (lane 3), and 357bp for 18S primer set 4 (lane 4). Lanes 5–8: no-template control (NTC1). Lanes 9–12: human PBMC gDNA (HC, negative control). The non-specific bands seen in the HC reaction with the 18S primer set 3 (lane 11) did not interfere with the Cas12a assay (see Figures 3B and 4B). Lanes 13–16: NTC2. *Bottom gel*: PCR products obtained using the kDNA primer set 1 (lanes 1, 3, 5, 7) and set 2 (lanes 2, 4, 6, 8). Lanes 1 and 2, *L.* (*V.*) *braziliensis* M2904 gDNA (5×10^4 parasite genome equivalents per reaction; positive control). The size of the expected product is 116bp for kDNA primer set 1 (lane 1) and 138bp for kDNA primer set 2 (lane 2). Lanes 3 and 4, NTC1. Lanes 5 and 6, HC. The non-specific band seen in the HC reaction with the kDNA primer set 2 (lane 6) did not interfere with the Cas12a assay (see Supplementary Figures S2A–D). Lanes 7 and 8, NTC2. Processing of the gel images was performed using the ImageJ software (http://imagej.nih.gov/ij/).

fluorescence curves over 2 h clearly delineated a positive result (i.e., target DNA detected) from a negative one or background with a marked increase in relative fluorescence for both *Leishmania* kDNA (Figure 3A) and 18S rDNA (Figure 3B) targets. For the kDNA target, on the basis of the raw fluorescence curves (Figure 3A) a time point 20 min discriminated between specific and background signal from the human negative control (HC) and NTC controls. Preamplification of the kDNA target with either primer set 1 or set 2 allowed detection of at least 5×10^{-2} parasite genome equivalents/reaction (Figures 3C,D). Moreover, in one out of 3 independent experiments using kDNA primer set 2, detection of 5×10^{-3} parasite genome equivalents/reaction (fluorescence ratio of the Cas12a assay = 3.43) was achieved (Figure 3D). Thus, we found mostly similar analytical sensitivity of the kDNA PCR/CRISPR assay using either kDNA primer set 1 or set 2 coupled to crRNA-guided Cas12a detection as compared to the performance of the kDNA qPCR assay for *Leishmania* DNA detection (Jara et al., 2013).

For the 18S rDNA target, the fluorescence signal of the Cas12a detection assay showed saturation in less than 60 min (Figure 3B); and a time point 10 min allowed us to distinguish between specific and background signal. The Cas12a assay employing preamplified 18S rDNA target with either primer set 2 (Figure 3F), set 3 (Figure 3G) or set 4 (Figure 3H) could detect at least 5×10^0 parasite genome equivalents/reaction, whereas target preamplification with primer set 1 (Figure 3E) resulted in lower detection sensitivity, i.e., of at least 5×10^1 parasite genome equivalents/reaction. Of these evaluated 18S primer sets, we chose primer set 3 out of convenience for further evaluation.

We then evaluated the specificity of our PCR/CRISPR assays with DNA samples from 11 reference strains of various *L.* (*Viannia*) and *L.* (*Leishmania*) species as well as one strain of the phylogenetically closely related *T. cruzi* (Figure 4). For the PCR-based preamplification step, we tested both kDNA primer sets and the 18S primer set 3. For the kDNA target, the crRNA-guided Cas12a detection assay on preamplified target DNA with primer set 1 detected a distinctive fluorescent signal with *L.* (*Viannia*) DNA [fluorescence ratio values at 20-min time point ranging from 1.816 to 2.817; $n = 7$ strains], whereas DNA samples from representative strains of *L.* (*Leishmania*) species (range, 0.827–1.229; $n = 4$ strains) and the *T. cruzi* Y strain (range, 0.892–0.915) did not exhibit signal above the negative control reactions (range, 0.864–1.179) (Figure 4A and associated time course data in Supplementary Figures S3A–D). In contrast, the Cas12a assay on the kDNA target preamplified with primer set 2 detected a comparable signal with any of *Leishmania* DNAs tested from strains belonging to the *L.* (*Viannia*) and *L.* (*Leishmania*) subgenera, while no cross-reaction was observed with *T. cruzi* Y or human DNA (Supplementary Figures S2A–D). Since we were interested in developing a *L.* (*Viannia*)-specific detection assay targeting kDNA minicircles, we selected kDNA primer set 1 for the preamplification step in combination with the examined kDNA-crRNA for subsequent testing of patient samples. For the 18S target, the Cas12a assay employing preamplified target DNA with primer set 3 detected a prominent fluorescent signal with DNA from all tested *Leishmania* species (fluorescence ratio values at 10-min time point ranging from 4.350 to 5.723; $n = 11$ strains), whereas the signal from the *T. cruzi* Y strain DNA (range, 0.885–0.962) could not be distinguished from the negative controls (range, 0.922–1.242) (Figure 4B and associated time course data in Supplementary Figures S3E–H). Therefore, the 18S primer set 3 was further used for the target preamplification step, in conjunction with the designed 18S-crRNA, in the evaluation of clinical samples.

Performance evaluation of PCR/CRISPR assays in clinical samples

We next assessed the applicability of our CRISPR-based assays in clinical samples. We tested extracted DNA from 49 cutaneous lesion specimens from patients with previously confirmed positive (36/49; 73.5%) or negative (13/49; 26.5%) *Leishmania* infection status using the routine kDNA conventional PCR (cPCR) diagnostic test (Figure 5A). These samples were analyzed by the newly developed PCR/CRISPR assays targeting *Leishmania* kDNA and the 18S rDNA gene, as well as the human RNase P gene as a sample control, in parallel with a previously validated kDNA qPCR test (Figure 5A). Of the 49 samples analyzed, the kDNA qPCR test identified 79.6% of samples (39 of 49) as *Leishmania* positive, whereas 20.4% of samples (10 of 49) were negative.

Considering the kDNA qPCR assay as the reference test for *Leishmania* detection, 39 of the 39 qPCR positive samples were also positive with the kDNA PCR/CRISPR assay using a cutoff equal to the mean + 3SD of the fluorescence ratio of 10 negative clinical samples (cutoff = 1.151). Fluorescence ratio

10.3389/fmicb.2022.958693

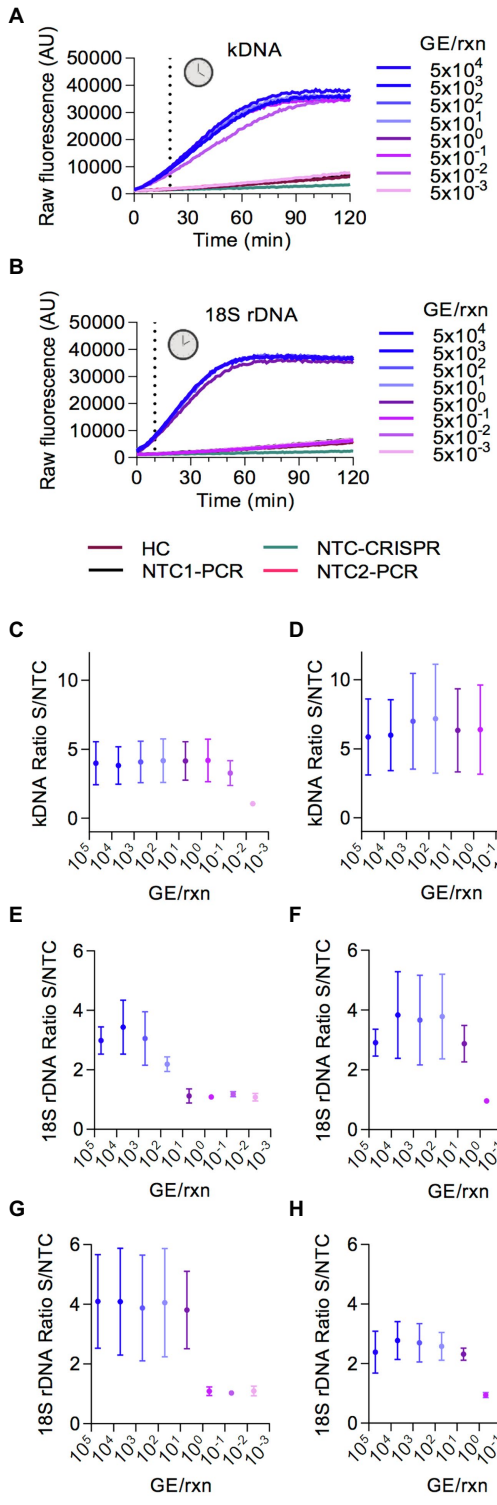

FIGURE 3
Analytical sensitivity of Cas12a-based detection of *L.* (*V.*) *braziliensis* M2904 DNA. Eight serial dilutions of *L.* (*V.*) *braziliensis* M2904 gDNA were subjected to PCR amplification followed by Cas12a-based detection for kDNA and 18S rDNA targets, for determination of the lowest amount of parasite genome equivalents (GE) per reaction that can be consistently detected. Different primer sets (shown in Figure 2C) were evaluated to determine those with the best performance. **(A,B)**

(Continued)

FIGURE 3 (Continued)
Raw fluorescence signal from the Cas12a reaction over 2h on the amplicon generated with the kDNA primer set 1 **(A)** or 18S primer set 3 **(B)**. Data from one experiment are shown, with fluorescence measurements taken on the Synergy H1 plate reader. **(C,D)** Data points depict the fluorescence ratio (fluorescence signal obtained at 20-min time point in the test sample relative to the NTC) from Cas12a reactions on the amplicon generated with the kDNA primer set 1 **(C)** or set 2 **(D)**. Data are represented as mean±SD (n=3 independent amplification and detection runs). The X-axis has a logarithmic scale. **(E–H)** Data points depict the fluorescence ratio (fluorescence signal obtained at 10-min time point in the test sample relative to the NTC) from Cas12a reactions on the amplicon generated with the 18S primer set 1 **(E)**, set 2 **(F)**, set 3 **(G)**, or set 4 **(H)**. Data are represented as mean±SD (n=3 independent amplification and detection runs). The X-axis has a logarithmic scale. In **(C,D,F)**, fluorescence measurements of Cas12a detection runs were taken on the Synergy H1 plate reader (2 runs) and on the Cytation 5 plate reader (one run). In **(E,G)**, one detection run was performed on the Synergy H1 plate reader and 2 detection runs were made on the Cytation 5 plate reader. In **(H)**, all 3 detection runs were conducted on the Cytation 5 plate reader.

values of positive samples by kDNA PCR/CRISPR ranged from 1.91 to 4.49 (Figures 5B,D and Supplementary File S2). Clinical samples that scored positive showed robust fluorescence curves from Cas12a detection of *L.* (*Viannia*) kDNA minicircle molecules (Supplementary Figures S4A,B). Repeated measurements for a subset of clinical samples indicated overall consistent results (Figure 5B and Supplementary File S2). However, two samples (CL-01 and CL-32) out of 13 retested samples showed discordant results (one of two replicates with positive signal in the kDNA Cas12a assay) but were suspected to be negative because both the kDNA cPCR and kDNA qPCR tests identified these samples as negative. To clarify the results, we repeated testing of these samples by kDNA PCR/CRISPR in duplicate, where both samples showed undetectable results (two of two replicates; Supplementary Figures S5A–D).

The 18S PCR/CRISPR assay resulted in 32 of the 39 qPCR positive samples being classified as *Leishmania* positive (using a classification cutoff value of 1.171), with fluorescence ratio values ranging from 2.98 to 7.37 (Figures 5C,D and Supplementary File S2). Positive patient samples exhibited strong fluorescence curves in the Cas12a assay indicating presence of the *Leishmania* 18S rDNA gene (Supplementary Figures S4C,D). Consistent results were obtained upon repeated measuring on a subset of clinical samples (Figure 5C and Supplementary File S2). Discordance between test results (one of two replicates with positive signal in the 18S Cas12a assay) occurred in one sample (CL-41) out of 14 retested samples. That sample had high Cq values (mean Cq of 31.91; Figure 5D) and low parasite load (4.61 parasites per 10^6 human cells; Supplementary File S2) as determined by the kDNA qPCR test. We repeated testing of sample CL-41 by 18S PCR/CRISPR in duplicate, confirming it as negative (two of two replicates; Supplementary Figures S5E,F).

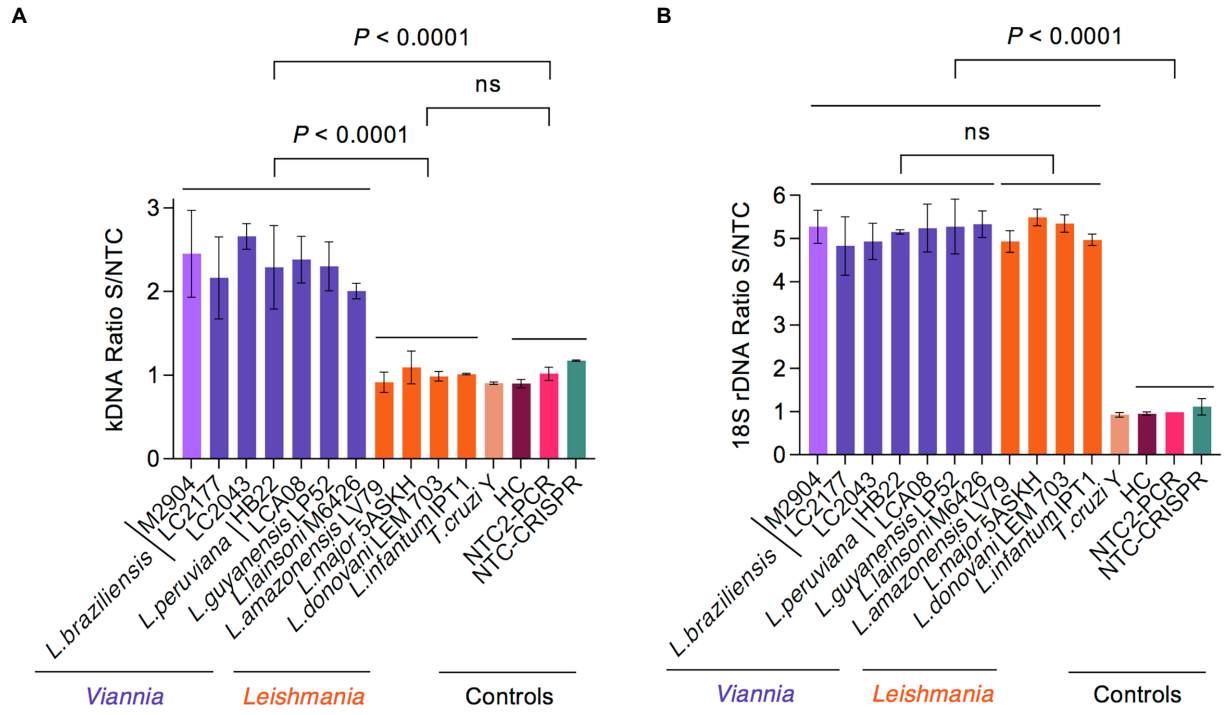

FIGURE 4
Analytical specificity of Cas12a-based detection of *Leishmania* spp. using reference strains. **(A)** The specificity of the kDNA PCR/CRISPR assay was evaluated using gDNA (preamplified with kDNA primer set 1) from 11 *Leishmania* strains (7 of subgenus *Viannia* and 4 of subgenus *Leishmania*) and the *T. cruzi* Y strain. **(B)** The same DNA samples from reference strains as in **(A)** were tested in the specificity assessment of the 18S PCR/CRISPR assay using the 18S primer set 3 in the preamplification step. Bar graphs depict the fluorescence ratio from Cas12a reactions. Data are represented as mean±SD (n=2 independent amplification and detection runs). Statistical comparisons between groups were conducted using an unpaired t-test (two-tailed p values are shown; non-significant p values are indicated by ns). Negative controls included human PBMC gDNA and NTC controls of PCR and CRISPR reactions. Fluorescence measurements of Cas12a detection runs were taken on the Synergy H1 plate reader. See Supplementary Figure S3 for the full time course data.

The human RNase P gene was detected in all 49 clinical samples analyzed by PCR/CRISPR (Figure 5D and Supplementary File S2), thereby confirming the quality of the samples and validating the process of DNA extraction from clinical specimens. Robust fluorescence curves were obtained for the RNase P gene from Cas12a detection (Supplementary Figures S4E,F), with fluorescence ratio values >5 in all cases (Supplementary File S2).

Patient samples detected as *Leishmania* positive in the kDNA and 18S PCR/CRISPR assays showed a large range of Cq values (Figure 6A and Supplementary File S2) and, accordingly, covered a wide range of parasite loads (Figure 6B and Supplementary File S2) as determined by kDNA qPCR. The kDNA PCR/CRISPR assay detected the presence of *Leishmania* kDNA molecules in samples with parasite equivalents/reaction as low as 2.9×10^{-3} (sample CL-43) corresponding to a parasite load of 1 parasite per 10^6 human cells (Figure 6B and Supplementary File S2). The *Leishmania* 18S rDNA target was detected by PCR/CRISPR in samples with parasite equivalents/reaction as low as 5.6×10^{-2} (sample CL-23) corresponding to a parasite load of 42 parasites per 10^6 human cells (Figure 6B and Supplementary File S2). However, not all samples with parasite loads in the range between 35 and 100 parasites per 10^6 human cells were detected by the 18S CRISPR-based assay (Figure 6B and Supplementary File S2). The 18S rDNA gene was consistently detected in samples containing parasite equivalents/reaction of at least 1×10^0 corresponding to a parasite load greater than 10^2 parasites per 10^6 human cells (Figure 6B and Supplementary File S2). As expected, an inverse linear correlation between Cq values and quantified parasite load levels in clinical samples ranging from 1×10^0 to 5.2×10^6 parasites per 10^6 human cells was observed (Figure 6C). Depending on the parasite load of the clinical samples and the analytical sensitivity of the newly developed PCR/CRISPR assays, detection of *Leishmania* target DNA was achieved by PCR/CRISPR in different types of clinical specimens that included invasive sample types (biopsies and lesion scrapings using a sterile lancet) and non-invasive sample types (cytology brushes, swabs, and filter paper lesion impressions; Supplementary File S2). Of the 49 clinical specimens analyzed, the majority were biopsies (n=26; 53.1%), followed by swabs (n=11; 22.4%). The kDNA qPCR test resulted in 84.6% (22/26) of biopsy specimens, 81.8% (9/11) of swab specimens, 60% (3/5) of cytology brush specimens, 100% (4/4) of scraping specimens, and 33.3% (1/3) of filter paper lesion impressions testing positive for *Leishmania* DNA. The kDNA PCR/CRISPR assay

10.3389/fmicb.2022.958693

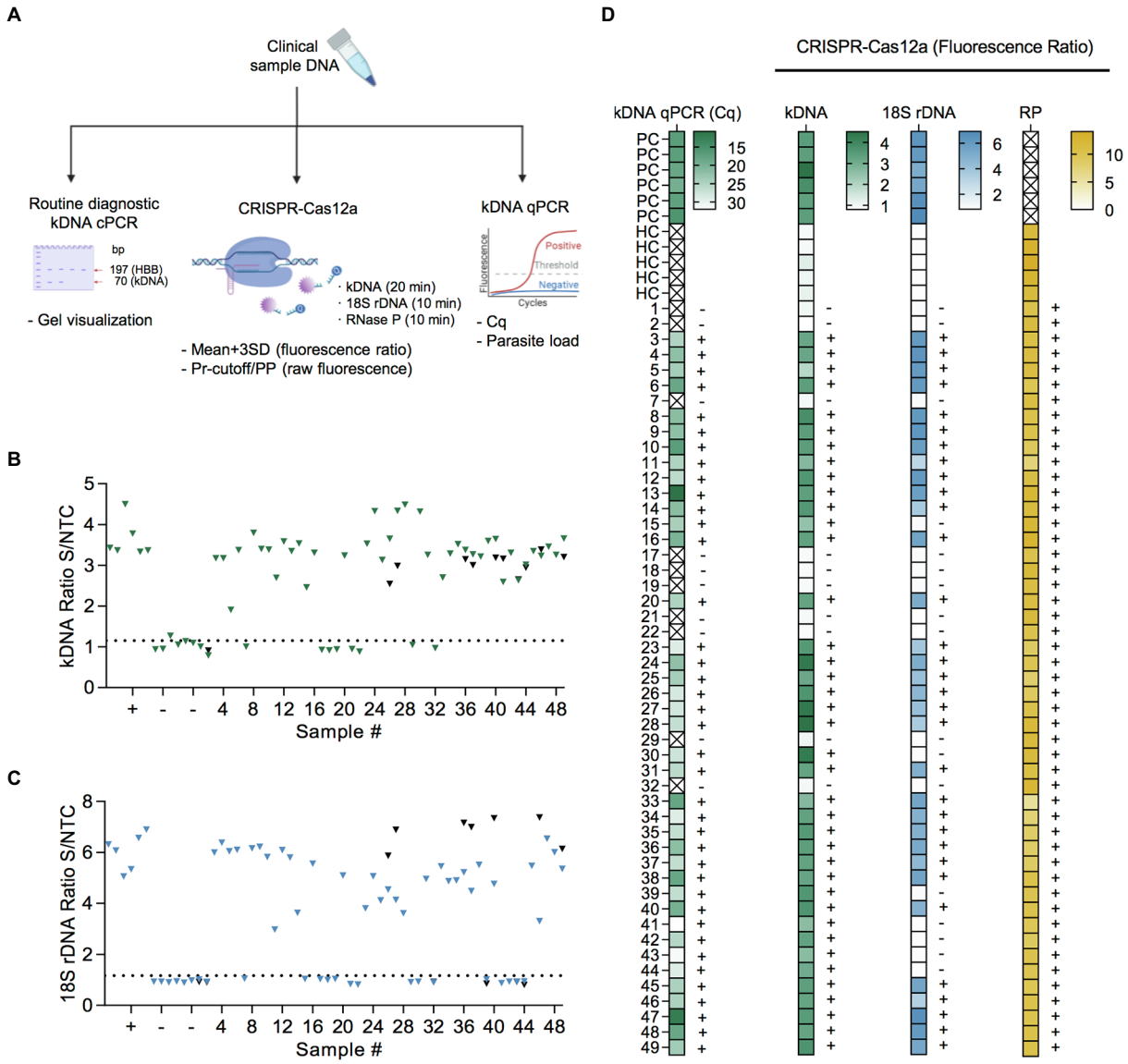

FIGURE 5
Performance evaluation of PCR/CRISPR assays for detection of *Leishmania* DNA targets in clinical samples. **(A)** Sample analysis workflow including molecular analyses (kDNA cPCR, kDNA qPCR, and PCR/CRISPR targeting *Leishmania* kDNA and 18S rDNA or human RNase P gene) and data analysis (see Materials and Methods for more details). Figure created with BioRender.com. **(B,C)** Extracted DNA from 49 clinical samples was subjected to PCR amplification using primers specific to kDNA **(B)** and 18S rDNA **(C)** of *Leishmania*, followed by Cas12a-based detection. Fluorescence measurements were made on the Synergy H1 plate reader. Data shown represent the fluorescence ratio from Cas12a reactions. The dashed lines indicate the positive threshold cutoff value (mean of the fluorescence ratio of negative clinical samples +3SD; n=10) for detection of *Leishmania* targets (cutoff value=1.151 for kDNA and 1.171 for 18S rDNA). +, positive control (*L.* (*V.*) *braziliensis* M2904 gDNA; n=6); –, negative control (human PBMC gDNA; n=6). A subset of clinical samples was retested (black symbols). Full time course data for a group of clinical samples are provided in Supplementary Figure S4. **(D)** Heat maps displaying qPCR and PCR/CRISPR data from clinical samples. *Left panel*, the color scale represents quantification cycle (Cq) values determined by kDNA qPCR. The X mark inside the box symbol indicates that no Cq value was obtained. *Second-fourth panels*, the color scale represents fluorescence ratio values from Cas12a reactions for *Leishmania* kDNA and 18S rDNA targets and the sample control, human RNase P (RP) gene, respectively. The X mark inside the box symbol in the RP gene heatmap indicates not applicable. The detection threshold of the Cas12a assay on the *Leishmania* targets was set as the mean of the fluorescence ratio of negative clinical samples (n=10)+3SD. The positive threshold for the RP gene was set as a fluorescence signal of 5-fold above background (i.e., fluorescence ratio >5; Khan et al., 2021). The test results (+, detected; –, not detected) are indicated on the right side of the heat maps. Samples are coded as 1–49. PC, positive control (*L.* (*V.*) *braziliensis* M2904 gDNA for the PCR/CRISPR assays; DNA from a biopsy specimen positive for *Leishmania* by kDNA cPCR used for the qPCR assay). HC, human PBMC gDNA. See Supplementary File S2 for the complete dataset of this study.

showed 100% concordance with the qPCR test in all specimen types. Of the 39 qPCR positive specimens, *Leishmania* DNA was detected by the 18S PCR/CRISPR assay in 95.5% (21/22) of biopsy specimens, 44.4% (4/9) of swab specimens, 100% (3/3) of cytology brush specimens, and 100% (4/4) of scraping specimens, while no *Leishmania* DNA was detected in the single

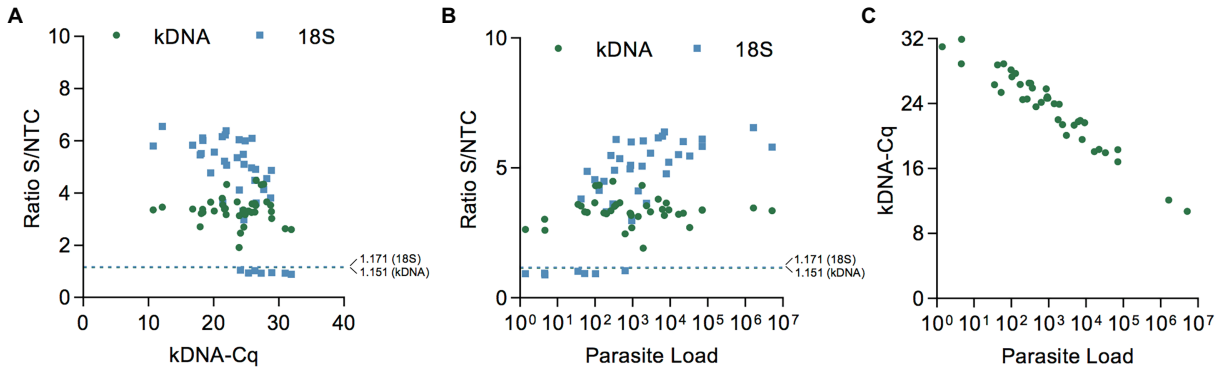

FIGURE 6
Performance evaluation of PCR/CRISPR assays across the range of parasite load levels in clinical samples. **(A,B)** Scatter plot showing the fluorescence ratio from Cas12a reactions for *Leishmania* targets in clinical samples (data shown in Figures 5B,C) versus Cq values determined by kDNA qPCR **(A)** or the parasite load **(B)**. The dashed lines shown indicate the positive threshold cutoff value (mean of the fluorescence ratio of negative clinical samples +3SD; *n*=10) for detection of *Leishmania* targets (cutoff value=1.151 for kDNA and 1.171 for 18S rDNA). **(C)** Scatter plot showing the inverse correlation between Cq values (determined by kDNA qPCR) and the parasite load in clinical samples. The parasite load is expressed as the number of *Leishmania* parasites/10^6 human cells.

filter paper lesion impression sample that tested positive by qPCR.

As an alternative method to analyze the PCR/CRISPR results on clinical samples, we calculated the percentage positivity (PP) for each sample from the raw fluorescence data and performed a statistical analysis to select the optimal Pr-cutoff/PP to discriminate amongst positive and negative results. We considered the verified PCR/CRISPR results on repeat testing. For the kDNA PCR/CRISPR test, a logistic regression could not be fit due to perfect separation. The predictor variable (kDNA PP) predicted the outcome variable (qPCR result, i.e., measurable or not detectable Cq value) perfectly (Figure 7A). Positive samples for *L.* (*Viannia*) kDNA ($n=39$) had a PP > 29.9%, whereas negative samples ($n=10$) showed a PP ≤ 29.9% (Figure 7B). The area under the ROC curve for the kDNA PCR/CRISPR assay was 1 (Figure 7C). Regarding the 18S PCR/CRISPR test results, the sets of sensitivity/specificity and their relationship calculated from the logistic regression model using the 18S PP as the predictor variable are shown in Figure 7D. Classification of samples based on the Pr-cutoff/PP (18.251%) that maximized the Youden's J index resulted in 33 samples (67.3%) identified as *Leishmania* positive and 16 samples (32.7%) as negative (Figure 7E). One sample (CL-30) had a PP = 18.425% and was classified as positive with the Pr-cutoff/PP, whereas this sample was classified as negative with the cutoff equal to the mean + 3SD. That sample CL-30 had a raw fluorescence value (measured in relative fluorescence units, RFU) of 1,118 at the time point 10 min of the Cas12a reaction for the 18S rDNA target, and the fluorescence signal did not show a marked increase over the Cas12a reaction time (RFU at 120 min = 2,892), similarly to the negative control with human gDNA (RFU at 120 min = 2,764) (Supplementary File S2). The 18S PCR/CRISPR assay efficacy, measured by Youden's J index, was 0.846, and the area under the ROC curve was 0.8795 (Figure 7F).

We compared the test performance (considering the verified results on repeat testing) by calculating the positive and negative percent agreement (PPA and NPA, respectively) and Cohen's kappa relative to the kDNA qPCR comparator method (Table 1). The kDNA PCR/CRISPR test correctly identified all 39 samples that had tested positive using the kDNA qPCR test, with 100% PPA (95% CI = 91.0 to 100.0%). Cohen's kappa was 1, consistent with perfect agreement between methods. Using the classification cutoff equal to the mean + 3SD, the 18S PCR/CRISPR test had a PPA of 82.1% (95% CI = 67.3 to 91.0%) and Cohen's kappa was 0.65, which represents a substantial strength of agreement. Based on the Pr-cutoff/PP, the PPA for the 18S PCR/CRISPR test was 84.6% (95% CI = 70.3 to 92.8%) and Cohen's kappa was 0.69. The PPA for the kDNA cPCR test was 92.3% (95% CI = 79.7 to 97.3%) and Cohen's kappa was 0.83, consistent with excellent agreement between the kDNA cPCR and qPCR methods. Keeping in mind the limitation of having analyzed a relatively small sample set, particularly samples that were negative for *Leishmania* infection with the reference test ($n=10$), the NPA of all evaluated tests was 100% (95% CI = 72.2 to 100.0%).

Lastly, we carried out an evaluation of the intermediate precision (within-laboratory reproducibility or inter-assay variability) of measurements across PCR amplification and Cas12a-based detection runs for the positive and negative controls included alongside test samples. While the measurements were performed by a single operator using the same instrument (Synergy H1 plate reader), variable conditions across runs were the time scale (5 months) and reagent batches (i.e., two batches of *in vitro* transcribed crRNAs). For both the kDNA and 18S PCR/CRISPR assays, the time course data of Cas12a reactions showed a steady increase in fluorescence for the positive control (PC), whereas the fluorescence signal remained low in the HC and NTC controls of PCR and CRISPR reactions (Figures 8A,D), as expected. For the kDNA target, the analysis of the PC showed

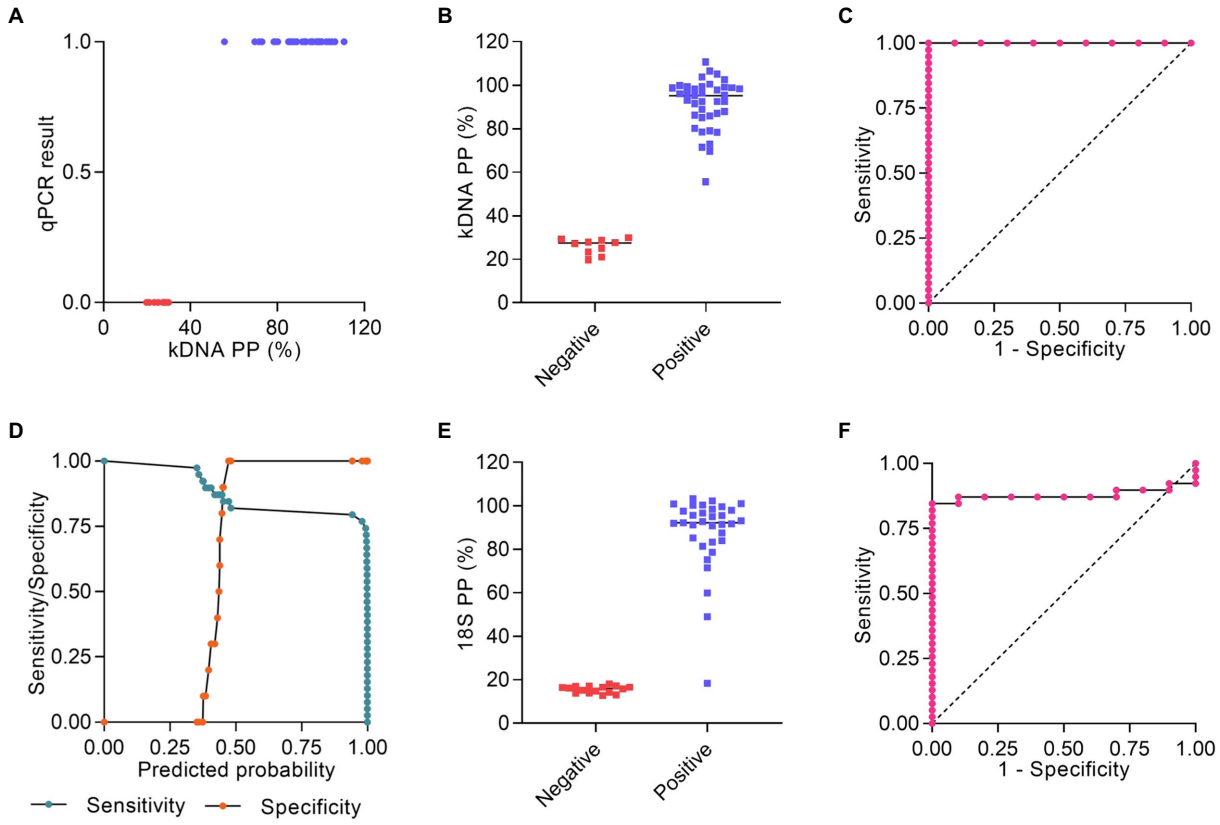

FIGURE 7
Statistical analysis of Cas12a assay results. **(A–C)** Raw fluorescence data of the Cas12a detection assay on the kDNA target using DNA from clinical samples were expressed as percentage positivity (PP) relative to a positive control, which was run in each plate. **(A)** The predictor variable (PP) predicts the outcome variable *Y* (qPCR result) perfectly since PP>29.9% corresponds to *Y*=1 (positive) and PP≤29.9% corresponds to *Y*=0 (negative). **(B)** Plot representing the PP of positive (*n*=39) and negative (*n*=10) results obtained by the kDNA PCR/CRISPR assay in clinical samples. **(C)** ROC curve for the kDNA PCR/CRISPR test, ratio of true positive rate (sensitivity) vs. false positive rate (1-specificity) with area under the ROC curve of 1. **(D–F)** Raw fluorescence data of the Cas12a detection assay on the 18S rDNA target gene using DNA from clinical samples were expressed as PP relative to a positive control, which was run in each plate. **(D)** Sensitivity/specificity analysis vs. predicted probability (i.e., probability cutoff). The probability cutoff point determines the sensitivity (85%) and specificity (100%) of the 18S PCR/CRISPR assay. **(E)** Plot representing the PP (cutoff: 18.251%) of positive (*n*=33) and negative (*n*=16) results obtained by the 18S PCR/CRISPR assay in clinical samples. **(F)** ROC curve for the 18S PCR/CRISPR test, ratio of true positive rate (sensitivity) vs. false positive rate (1-specificity) with area under the ROC curve of 0.8795.

increased variability (standard deviation) of mean raw fluorescence values over the reaction time course across runs ($n=12$; Figure 8A). Normalization of the fluorescence signal relative to the NTC (i.e., fluorescence ratio) showed a similar trend in the overall distribution (spread) of data values (Figure 8B). At the selected 20-min time point of the Cas12a reaction on the kDNA target for data analysis, there was a clear distinction between specific and background signal: the PC showed fluorescence ratio values ranging from 2.08 to 5.71 and a median of 3.48, while the negative controls yielded a maximal fluorescence ratio of 1.28 (Figure 8C). For the 18S rDNA target, raw fluorescence measurements for the PC showed a mostly similar variability over the reaction time course across runs ($n=9$; Figure 8D). The determined fluorescence ratio values for the PC showed less variability at early time points (e.g., at 10 and 20 min) as compared to later time points (40 and 60 min) of the Cas12a reaction employing the 18S-crRNA (Figure 8E). At the selected 10-min time point of the Cas12a reaction on the 18S rDNA target for data analysis, the fluorescence ratio clearly distinguished specific from background signal: the PC showed fluorescence ratio values ranging from 5.00 to 6.92 and a median of 5.67, while the negative controls showed a maximal fluorescence ratio of 1.32 (Figure 8F). Altogether, these data showed that the positive and negative controls provided consistent reference data points in each experiment.

Discussion

Accurate detection of *Leishmania* infections is critically important in the confirmatory diagnosis of leishmaniasis. In the Americas, where tegumentary leishmaniasis is highly endemic, skin lesions suspicious of CL may be caused by other infectious agents like mycobacteria or fungi that are prevalent in the same

10.3389/fmicb.2022.958693

TABLE 1 Concordance analysis of molecular tests compared to the reference kDNA qPCR test for detection of *Leishmania* in clinical samples.

Classification threshold/readout	Test	kDNA qPCR		PPA	NPA	Kappa
		Positive	Negative	% (95% CI)	% (95% CI)	(95% CI)
	kDNA cPCR					
Specific detectable band	Positive	36	0	92.3 (79.7–97.3)	100.0 (72.2–100.0)	0.83 (0.55–1.11)
(gel electrophoresis)	Negative	3	10			
	kDNA PCR/CRISPR					
Mean + 3SD	Positive	39	0	100.0 (91.0–100.0)	100.0 (72.2–100.0)	1.00 (0.72–1.28)
	Negative	0	10			
	18S PCR/CRISPR					
Mean + 3SD	Positive	32	0	82.1 (67.3–91.0)	100.0 (72.2–100.0)	0.65 (0.39–0.91)
	Negative	7	10			
Pr-cutoff/PP	Positive	33	0	84.6 (70.3–92.8)	100.0 (72.2–100.0)	0.69 (0.42–0.96)
	Negative	6	10			
	Total	39	10			

The PPA/NPA agreement measures between the reference method (kDNA qPCR) and any of the other tests, and Wilson score 95% confidence intervals (CI) were calculated using the Analyse-it software for Microsoft Excel. The Kappa coefficient and 95% CIs were calculated as described previously by McHugh (2012) (https://www.ncbi.nlm.nih.gov/pmc/articles/PMC3900052/). PPA, positive percent agreement; NPA, negative percent agreement; SD, standard deviation; Pr-cutoff, probability cutoff; PP, percentage positivity; cPCR, conventional PCR; and qPCR, real-time quantitative PCR.

endemic areas or non-infectious conditions like skin neoplasms (Tirelli et al., 2017). Differential diagnosis of TL requires reliable confirmatory tests that help to guide clinical management and appropriate treatment, to avoid exposing patients to unnecessary and toxic antileishmanial drugs (Burza et al., 2018). In this study, we report the development of two novel CRISPR-Cas12a-based assays for the detection of *Leishmania* spp. in human clinical specimens. We present the analytical validation using laboratory reference strains and the assessment of the performance of the assays in a panel of clinical samples with PCR-predetermined *Leishmania* infection status derived from patients with suspected CL from Cusco, an endemic region where *L.* (*Viannia*) parasites circulate, with predominance of *L.* (*V.*) *braziliensis* and less frequently *L.* (*V.*) *guyanensis* and *L.* (*V.*) *lainsoni* infections (Lucas et al., 1998; Sandoval-Juárez et al., 2020). The choice of the molecular target sequences was based on their multicopy nature, conservation across species of *Leishmania* at the genus level (18S rDNA) to allow pan-*Leishmania* detection or at the *L.* (*Viannia*) subgenus level (kDNA minicircle conserved region) to detect the main parasite species that cause TL in the Americas, and the fact that they are well-validated genetic targets widely used for the molecular diagnosis of leishmaniasis (Van der Auwera and Dujardin, 2015; Akhoundi et al., 2017).

The 18S rDNA locus is a region on chromosomal DNA that is highly conserved across *Leishmania* species (van Eys et al., 1992), present at about 10–170 copies per genome (Leon et al., 1978; Inga et al., 1998), that has been harnessed for the development of *Leishmania* detection assays of high sensitivity (de Paiva Cavalcanti et al., 2013; Adams et al., 2014; León et al., 2017; Filgueira et al., 2020; Rosales-Chilama et al., 2020) as well as for the estimation of parasite loads (Bezerra-Vasconcelos et al., 2011; Filgueira et al., 2020). Here, the estimated analytical sensitivity of our 18S PCR/CRISPR assay with DNA of *L. braziliensis* M2904 culture promastigotes corresponded well with its performance in clinical samples being capable of detecting the equivalent of 1 parasite per reaction. This detection capability of our novel assay is similar to a previously reported 18S qPCR assay (Rosales-Chilama et al., 2020), which was able to detect down to 10^{-1} *L.* (*V.*) *panamensis* promastigotes and 1 intracellular amastigote per reaction. Our assay enabled detection of species of both *L.* (*Leishmania*) and *L.* (*Viannia*) subgenera, with no cross-reaction with *T. cruzi* DNA (Y strain) or human DNA. Due to the high sequence conservation of 18S rDNA throughout the Trypanosomatidae, other non-*Leishmania* trypanosomatids not evaluated here could probably be detected with the 18S PCR/CRISPR assay. A low specificity of the 18S rDNA target was indeed the case with a 18S qPCR assay that was not exclusive for *Leishmania* detection because it showed cross-reactivity with non-*Leishmania* trypanosomatids, including *T. cruzi* (Y strain), *T. rangeli* and lower insect-dwelling trypanomatids (Filgueira et al., 2020).

The minicircles of kinetoplast (mitochondrial) DNA constitute the most widely used genetic target for extremely sensitive *Leishmania* detection (Akhoundi et al., 2017), because they are present in high copy numbers, at about 10,000 copies per cell (Simpson, 1987). qPCR assays that target kDNA minicircles proved highly sensitive and accurate for detection and quantification of *Leishmania* spp. in human clinical specimens (Weirather et al., 2011; Jara et al., 2013). Here, we tested two kDNA primer sets for the preamplification step, because differences in the performance of kDNA primer sets for detection of *Leishmania* spp. have been reported (Weirather et al., 2011) and likely reflect the heterogeneity in minicircle sequence classes

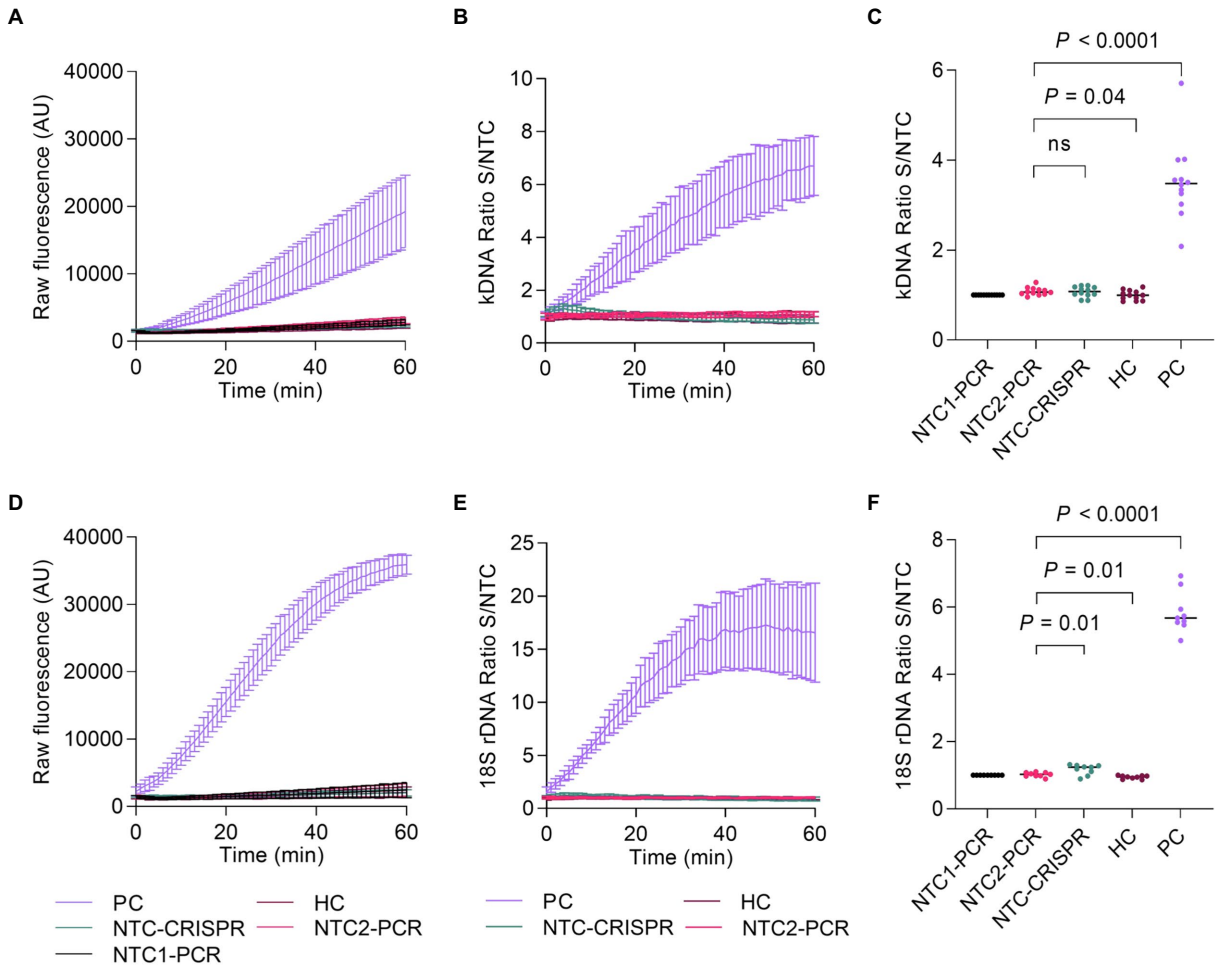

FIGURE 8
Assessment of PCR/CRISPR assay precision for detection of *Leishmania* targets. Measurements in independent experiments of the positive and negative controls (included alongside test samples) allowed to assess the intermediate precision (within-laboratory reproducibility) across PCR amplification and Cas12a-based detection runs. Fluorescence measurements taken on the Synergy H1 plate reader were considered for this analysis. The assays were performed by the same operator over a period of 5 months; two reagent batches of *in vitro* transcribed crRNAs were used. The positive control (PC) consisted of gDNA from *L.* (*V.*) *braziliensis* M2904 (5×10^4 parasite genome equivalents/reaction used as input DNA). The human negative control (HC) consisted of gDNA from PBMC of a healthy donor (40 ng of input DNA). Two NTC reactions were included in PCR runs to monitor for contamination: NTC1, kept closed without water addition [this control served for normalization of raw fluorescence values of the Cas12a reaction, expressed as a fluorescence ratio], and NTC2, made with water instead of the template. NTC-CRISPR, no-template control of the Cas12a reaction. **(A)** Raw fluorescence signal from the Cas12a reaction over 1h for the kDNA target. Mean raw fluorescence values (arbitrary units, AU)±SD are plotted as lines with error bars (n=12). **(B)** The data in **(A)** were normalized to the fluorescence of the NTC1 (PCR blank) and expressed as a fluorescence ratio. **(C)** The normalized data in **(B)** were used for detection analysis at the 20-min time point. **(D)** Raw fluorescence signal from the Cas12a reaction over 1h for the 18S rDNA target. Mean raw fluorescence values (arbitrary units, AU)±SD are plotted as lines with error bars (n=9). **(E)** The data in **(D)** were normalized to the fluorescence of the NTC1 (PCR blank) and expressed as a fluorescence ratio. **(F)** The normalized data in **(E)** were used for detection analysis at the 10-min time point. For **(C,F)**, pairwise comparisons to the NTC2 (PCR blank) were done using an unpaired t-test. Two-tailed p values are shown; non-significant p values (p>0.05) are indicated by ns.

between species and even between strains of the same species (Simpson, 1997; Ceccarelli et al., 2014; Kocher et al., 2018; Camacho et al., 2019). The analytical sensitivity on DNA from *L. braziliensis* promastigotes with either kDNA primer set in combination with the examined kDNA-crRNA reached down to 5×10^{-2} parasite equivalents per reaction, which approximated that of a previously validated kDNA qPCR assay for *L.* (*Viannia*) detection (5×10^{-3} parasite equivalents per reaction; Jara et al., 2013). The combination of the kDNA primer set 1 (PCR preamplification) and the kDNA-crRNA (Cas12a assay) was found to be specific for *L.* (*Viannia*) detection, and thus it was further tested with clinical samples. The kDNA PCR/CRISPR assay did not show cross-reactivity with *T. cruzi* Y strain or human DNA.

The CRISPR-Cas12a-based assays developed here showed good performance in detecting *Leishmania* DNA targets across a wide range of parasite loads in clinical specimens that included both invasive and non-invasive sample types. Remarkably, the

kDNA PCR/CRISPR assay showed perfect agreement with the reference kDNA qPCR assay in classifying the samples with positive (detected) or negative (not detected) *Leishmania* infection status. Of the 39 samples being positive by the kDNA PCR/CRISPR and qPCR assays, 7 samples were negative by the 18S PCR/CRISPR assay, a difference related to the lower copy number of 18S rDNA. These seven samples contained the equivalent of less than one parasite per reaction corresponding to the low range of parasite loads (Figure 6B and Supplementary File S2). An important aspect to remark is that because of the high copy number of kDNA minicircles and therefore the high detection sensitivity achieved with this target, the kDNA PCR/CRISPR assay was more prone to false-positive results. If we would not have carried out assay repeat testing to validate the results, the false positive rate of the kDNA PCR/CRISPR assay was 4.1% (i.e., 2 false positives of 49 patient samples), showing 95.9% accuracy (47/49 test results in agreement with kDNA qPCR results). This drawback with the kDNA target was observed in another study using minicircle kDNA qPCR, in which false-positive reactions were reduced by combining the kDNA target with 18S rDNA in a multiplex probe-based qPCR assay and setting a cutoff Cq value to exclude false-positive samples (Eberhardt et al., 2018). Like our study, the possibility of carryover contamination is a challenge with any of the two-step CRISPR-based detection platforms (Kellner et al., 2019; Nguyen et al., 2022). All these comprise a first step of target preamplification, either by PCR [as in HOLMES (Li et al., 2018)] or isothermal amplification methods [as in SHERLOCK (Gootenberg et al., 2017), DETECTR (Chen et al., 2018), and ENHANCE (Nguyen et al., 2020, 2022)], followed by the CRISPR-based detection reaction. This implies multiple manual operations and opening the lid of the amplification reaction tubes to transfer a volume of preamplified target DNA for the detection phase of the assay, thereby increasing the risk of amplicon carryover contamination. To prevent this, proper laboratory practices and reaction setup must be in place, with physically separated laboratory work areas in which pre- and post-amplification manipulations are performed. As followed here, we recommend processing patient samples in groups of 10–12 per run alongside appropriate negative and positive controls of the amplification and detection reactions to ensure reliability and validity of the assays. The human RNase P gene was used as sample control to verify an efficient DNA extraction and validate true-negative results (i.e., those samples with undetectable *Leishmania* DNA but positive for human RNase P). We also recommend performing two replicate assays to validate the test results in clinical samples as well as performing rigorous data quality control as presented here. Combining preamplification and CRISPR-based detection in a single one-pot assay such as with one-pot SHERLOCK (Gootenberg et al., 2018; Kellner et al., 2019), AIOD-CRISPR (Ding et al., 2020), and other innovative ways (Yin et al., 2020; Wang et al., 2021; Hu et al., 2022) has been shown to be faster, simpler, amenable to large-scale and quantitative applications, and less prone to contamination, albeit with lower sensitivity and a more challenging assay optimization phase than with two-step CRISPR-based assay formats. In fact, a recent study that exploited the Cas13a-based SHERLOCK method to develop an assay for detection of the malaria-causing *Plasmodium* parasites (Cunningham et al., 2021) was unable to replicate the one-pot reaction format previously described for viral targets (Gootenberg et al., 2018), achieving instead the best performance with a two-step reaction format. Another way to greatly reduce carryover contamination is the use of dUTP instead of dTTP in the amplification reaction master mix and treating subsequent reactions with uracil DNA glycosylase (UDG) prior to PCR or isothermal amplification. UDG will degrade dUTP-containing amplicons, thus preventing these molecules to serve as templates (Longo et al., 1990). Integration of LAMP amplification with UDG digestion followed by downstream CRISPR-based detection was successful at lowering the risk of false positives (Qian et al., 2019; Nguyen et al., 2022), though this can result in a higher limit of detection of the method (as found with ENHANCEv2, Nguyen et al., 2022).

This study has a limitation concerning the sample size of tested clinical samples, particularly the small number of samples whose *Leishmania* infection status was negative with the reference qPCR test ($n = 10$). However, this study was designed to provide proof-of-concept of the newly developed CRISPR-based assays for application with patient samples. Keeping in mind the limitation of sample size, we did not calculate estimates of sensitivity and specificity (diagnostic accuracy) and used instead inter-rater agreement measures.

We used standard PCR as the target preamplification strategy to provide proof-of-concept CRISPR-based assays for highly sensitive and specific detection of *Leishmania* infection in clinical specimens. Our assays utilize a detection method similar to HOLMES (a one-HOur Low-cost Multipurpose highly Efficient System), which uses LbCas12a-mediated DNA detection combined with PCR preamplification to achieve high sensitivity (Li et al., 2018). The main differences between our methods concern the PCR amplification cycles (35 cycles for ~45 min in HOLMES vs. 45 cycles for ~90 min in our study) and the incubation temperature of the Cas12a assay (37°C in HOLMES vs. 25°C in our study). Our preliminary assays indicated that shortening the period of PCR preamplification to 35 cycles also enriched the target molecules to enable sufficiently high detection sensitivity, though more evaluations are needed to assess that parameter in the assay performance using clinical samples. While the LbCas12a enzyme displays optimal *trans*-cleavage activity at 37°C (Chen et al., 2018), it is also functional at room temperature (25°C; Ding et al., 2020; Xiong et al., 2020), though with a slower enzyme kinetics at 25°C in a one-pot assay format (Ding et al., 2020) compared to a two-step detection workflow (Xiong et al., 2020). Here, we performed the LbCas12a-based detection assays at 25°C to facilitate further development and adaptation of the assays for POC applicability and observed a good performance (high signal-to-noise ratios).

Nowadays, the PCR technique is widely used in research and reference laboratories in Latin America for molecular diagnosis of

TL (Moreira et al., 2018). Accordingly, our assays in their current format have the potential for widespread application in laboratory settings and reference centers that have the needed infrastructure and resources to perform PCR and analyze Cas12a assay results with a fluorescence plate reader. Further studies are needed to extend the assessment of the analytical and clinical performance of both CRISPR-based assays to different endemic regions across the Americas where different *Leishmania* species and parasite variants circulate. We envisage that our 18S PCR/CRISPR assay would be useful for detection of all medically relevant *Leishmania* species in clinical specimens containing the equivalent of at least 1 parasite/reaction, such as in cutaneous lesions of recent onset (≤3 months) that harbor higher parasite loads than lesions with longer evolution (Weigle et al., 2002; Jara et al., 2013). Furthermore, this novel 18S CRISPR-based assay could be of global applicability if validated on a broader scale in different geographic regions where different forms of leishmaniasis are endemic. The kDNA PCR/CRISPR assay would be a useful addition to specifically detect New World *L.* (*Viannia*) infections, including those at low parasite load levels, as in chronic skin lesions and in mucosal lesions (Jara et al., 2013), which are undetectable by microscopy (Weigle et al., 2002). Both newly developed CRISPR-based assays provide positive or negative results for *Leishmania* DNA detection, but do not enable quantitative applications such as parasite load quantification, as can be determined by real-time qPCR assays (Moreira et al., 2018). Altogether, the results shown here support the potential applicability of the novel 18S and kDNA PCR/CRISPR assays for first-line diagnostic purposes that require detection of *Leishmania* infections at the genus and *L.* (*Viannia*) subgenus levels, respectively.

Several molecular methods that employ different genetic targets have been developed and are in use for molecular detection of *Leishmania*, usually at the genus or subgenus level (Akhoundi et al., 2017). PCR-based methods, particularly real-time qPCR assays, have proved of clinical utility for the detection of *Leishmania* infections and quantification of parasite load in host tissues (Moreira et al., 2018). Many studies report in-house assays using varied protocols involving different types of specimens, which makes it difficult to compare results between different studies. The need for standardization and proper validation of a real-time PCR-based methodology for the molecular diagnosis of TL in the Americas has been underscored (Moreira et al., 2018; Filgueira et al., 2020; Rosales-Chilama et al., 2020) and efforts toward this respect are ongoing (Moreira et al., 2018; Filgueira et al., 2020). This is expected to provide a consensus well-established methodology for broad use at research and reference laboratories across Latin America. There is also the critical need for accessible, sensitive and accurate diagnostic tools that offer easy operation and shorter turnaround time for results to diagnose TL in low-resource settings in endemic regions. CRISPR-based diagnostics has the potential to contribute to this and to become important tools for parasite detection in the clinical and epidemiological context, as illustrated in two recent studies that developed SHERLOCK CRISPR-based assays applied to *Plasmodium* detection and species identification (Lee et al., 2020; Cunningham et al., 2021) as well as drug-resistance genotyping (Cunningham et al., 2021). One advantage of CRISPR-based detection methods over other molecular techniques used in infectious disease diagnosis is the greater flexibility and versatility of the former with respect to simplifying and optimizing the assay workflow as well as adapting it to user-friendly readouts for POC use (at/near the site of patient care), making these tools accessible at the primary health care level in resource-limited settings. In this scenario, our CRISPR-based assays are amenable to further optimization and adaptation to facilitate their use in POC settings. We foresee different options. The assays can be integrated into low-cost and portable PCR (e.g., Bento Lab®, Alcántara et al., 2021a) and fluorescence reader (Katzmeier et al., 2019; Lee et al., 2020; Xiong et al., 2020) devices. A simplified workflow for *Leishmania* detection can be optimized starting from the sample preparation step (e.g., evaluating rapid means to extract nucleic acids with chelating agents to inactivate nucleases), followed by introducing an isothermal preamplification approach coupled to downstream Cas12a-based detection with lateral flow strip readout vs. the use of a handheld fluorimeter. Experimental strategies where *Leishmania* amastigote cells can firstly be enriched from a patient's lesional tissue sample using affinity reagents for cell capture (Chen, 2019; Gray et al., 2020) during the process of sample preparation are worth to be explored for a diagnostic POC test, given the usually low parasite load found in CL lesions.

Concerning the development of CRISPR-based biosensors applied to *Leishmania* DNA detection, in a recently published study, Bengtson et al. describe a newly developed CRISPR-dCas9-based DNA detection scheme targeting *Leishmania* kDNA minicircles and its potential for instrument-free POC diagnosis of VL in endemic, resource-limited settings (Bengtson et al., 2022). This DNA detection system operates entirely at room temperature (23°C) and combines isothermal target amplification by recombinase polymerase amplification and dCas9-based target DNA recognition with a subsequently primed rolling circle amplification (RCA) reaction. The RCA products were designed to fold into G-quadruplex (G4) structures that can associate with hemin to form a peroxidase-mimicking G4 DNAzyme that produces the final colorimetric readout that is visible to the naked eye. This method was combined with instrument-free simplified DNA extraction procedures for blood and urine samples, and it demonstrated to work well for highly sensitive detection of target DNA in simulated patient samples. Notwithstanding that this DNA detection scheme was designed to be directly suited for field use, its performance in clinical samples is not yet determined. Interestingly, Bengtson et al. chose a conserved 23-mer target sequence within kDNA minicircles that has a PAM site for dCas9 binding, which overlaps with our selected Cas12a crRNA target site (Figure 2B). Our chosen target sequence is highly conserved among New World *L.* (*Viannia*) species, whereas the target sequence selected by Bengtson et al. is conserved among some

members of the *L.* (*Leishmania*) subgenus, namely *L.* (*L.*) *donovani*, *L.* (*L.*) *infantum* (both etiologic agents of VL in the Old World), *L.* (*L.*) *infantum* (syn. *L. chagasi*; etiologic agent of VL in the New World), and *L.* (*L.*) *major* (etiologic agent of CL in the Old World), based on *in silico* multiple sequence alignments. While our studies use different CRISPR-based detection approaches, both underscore the great potential of these methods to be adopted for leishmaniasis diagnosis, surveillance and research applications. The performance of the CRISPR-based detection assays/scheme shown in both proof-of-principle studies lays the groundwork for future studies to further develop, adapt and validate these molecular detection systems in clinical and research settings in which the tests are to be used.

Data availability statement

The original contributions presented in the study are included in the article/Supplementary material, further inquiries can be directed to the corresponding author.

Author contributions

ED, PM, and VA designed the study. JN and LC-S performed the bioinformatics analyses. MC recruited patients and carried out sampling of lesions. ED and PH performed the experiments. ED, VA, JN, LC-S, PH, JA, and PM analyzed the data. ED and VA wrote the manuscript with input from all authors. All authors contributed to the article and approved the submitted version.

Funding

This study was supported by ProCiencia, the Peruvian National Council for Science, Technology and Technological Innovation (CONCYTEC)-The World Bank (contracts 036-2019-FONDECYT-BM-INC.INV to VA, JA, and PM, and 095-2018-FONDECYT-BM-IADT-AV to JA). LC-S is supported by a doctoral scholarship of ProCiencia, CONCYTEC in the framework of the project EC-165-2020-FONDECYT-Programa de Doctorado en Ciencias mención Bioquímica y Biología molecular-UPCH. The publication of this article was funded by the Universidad Peruana de Ciencias Aplicadas (internal fund D-027-2020).

Acknowledgments

We thank Roberto Alcántara and Katherin Peñaranda for sharing the CRISPR-Cas12a-based detection assay protocol; Gabriel Mendoza for sharing recombinant LbCas12a; Manuela Verástegui for providing genomic DNA from the *Trypanosoma cruzi* Y strain; Mirko Zimic for advice on the statistical methods to determine the optimal cutoff value (decision threshold) of a diagnostic test; and the Office of Research at the Universidad Peruana de Ciencias Aplicadas for the support provided to carry out this research work.

This manuscript has been released as a preprint at bioRxiv (Dueñas et al., 2022).

Conflict of interest

The authors declare that the research was conducted in the absence of any commercial or financial relationships that could be construed as a potential conflict of interest.

Publisher's note

All claims expressed in this article are solely those of the authors and do not necessarily represent those of their affiliated organizations, or those of the publisher, the editors and the reviewers. Any product that may be evaluated in this article, or claim that may be made by its manufacturer, is not guaranteed or endorsed by the publisher.

Supplementary material

The Supplementary material for this article can be found online at: https://www.frontiersin.org/articles/10.3389/fmicb.2022.958693/full#supplementary-material

References

Adams, E. R., Gomez, M. A., Scheske, L., Rios, R., Marquez, R., Cossio, A., et al. (2014). Sensitive diagnosis of cutaneous leishmaniasis by lesion swab sampling coupled to qPCR. *Parasitology* 141, 1891–1897. doi: 10.1017/S0031182014001280

Adams, E. R., Schoone, G. J., Ageed, A. F., Safi, S. E., and Schallig, H. D. F. H. (2010). Development of a reverse transcriptase loop-mediated isothermal amplification (LAMP) assay for the sensitive detection of *Leishmania* parasites in clinical samples. *Am. J. Trop. Med. Hyg.* 82, 591–596. doi: 10.4269/ajtmh.2010.09-0369

Adams, E. R., Schoone, G., Versteeg, I., Gomez, M. A., Diro, E., Mori, Y., et al. (2018). Development and evaluation of a novel loop-mediated isothermal amplification assay for diagnosis of cutaneous and visceral Leishmaniasis. *J. Clin. Microbiol.* 56, e00386–18. doi: 10.1128/JCM.00386-18

Adaui, V., Lye, L.-F., Akopyants, N. S., Zimic, M., Llanos-Cuentas, A., Garcia, L., et al. (2016). Association of the endobiont double-stranded RNA virus LRV1 with treatment failure for human Leishmaniasis caused by *Leishmania braziliensis* in Peru and Bolivia. *J. Infect. Dis.* 213, 112–121. doi: 10.1093/infdis/jiv354

Ai, J.-W., Zhou, X., Xu, T., Yang, M., Chen, Y., He, G.-Q., et al. (2019). CRISPR-based rapid and ultra-sensitive diagnostic test for *Mycobacterium tuberculosis*. *Emerg. Microbes Infect.* 8, 1361–1369. doi: 10.1080/22221751.2019.1664939

Akhoundi, M., Downing, T., Votýpka, J., Kuhls, K., Lukeš, J., Cannet, A., et al. (2017). *Leishmania* infections: molecular targets and diagnosis. *Mol. Asp. Med.* 57, 1–29. doi: 10.1016/j.mam.2016.11.012

Alcántara, R., Peñaranda, K., Mendoza-Rojas, G., Nakamoto, J. A., Dueñas, E., Alvarez, D., et al. (2021b). UnCovid: a versatile, low-cost, and open-source protocol for SARS-CoV-2 RNA detection. *STAR Protoc.* 2:100878. doi: 10.1016/j.xpro.2021.100878

Alcántara, R., Peñaranda, K., Mendoza-Rojas, G., Nakamoto, J. A., Martins-Luna, J., Del Valle-Mendoza, J., et al. (2021a). Unlocking SARS-CoV-2 detection in low- and middle-income countries. *Cell Rep. Methods* 1, 100093. doi: 10.1016/j.crmeth.2021.100093

Alvar, J., Vélez, I. D., Bern, C., Herrero, M., Desjeux, P., Cano, J., et al. (2012). Leishmaniasis worldwide and global estimates of its incidence. *PLoS One* 7:e35671. doi: 10.1371/journal.pone.0035671

Arevalo, J., Ramirez, L., Adaui, V., Zimic, M., Tulliano, G., Miranda-Verástegui, C., et al. (2007). Influence of *Leishmania (Viannia)* species on the response to antimonial treatment in patients with American Tegumentary Leishmaniasis. *J. Infect. Dis.* 195, 1846–1851. doi: 10.1086/518041

Bañuls, A. L., Bastien, P., Pomares, C., Arevalo, J., Fisa, R., and Hide, M. (2011). Clinical pleiomorphism in human leishmaniases, with special mention of asymptomatic infection. *Clin. Microbiol. Infect.* 17, 1451–1461. doi: 10.1111/j.1469-0691.2011.03640.x

Beckert, B., and Masquida, B. (2011). Synthesis of RNA by In vitro transcription. *Methods Mol. Biol.* 703, 29–41. doi: 10.1007/978-1-59745-248-9_3

Bengtson, M., Bharadwaj, M., Franch, O., van der Torre, J., Meerdink, V., Schallig, H., et al. (2022). CRISPR-dCas9 based DNA detection scheme for diagnostics in resource-limited settings. *Nanoscale* 14, 1885–1895. doi: 10.1039/D1NR06557B

Bezerra-Vasconcelos, D. R., Melo, L. M., Albuquerque, É. S., Luciano, M. C. S., and Bevilaqua, C. M. L. (2011). Real-time PCR to assess the *Leishmania* load in *Lutzomyia longipalpis* sand flies: screening of target genes and assessment of quantitative methods. *Exp. Parasitol.* 129, 234–239. doi: 10.1016/j.exppara.2011.08.010

Bharadwaj, M., Bengtson, M., Golverdingen, M., Waling, L., and Dekker, C. (2021). Diagnosing point-of-care diagnostics for neglected tropical diseases. *PLoS Negl. Trop. Dis.* 15:e0009405. doi: 10.1371/journal.pntd.0009405

Boggild, A. K., Valencia, B. M., Espinosa, D., Veland, N., Ramos, A. P., Arevalo, J., et al. (2010). Detection and species identification of *Leishmania* DNA from filter paper lesion impressions for patients with American cutaneous Leishmaniasis. *Clin. Infect. Dis.* 50, e1–e6. doi: 10.1086/648730

Brito, M. E. F., Andrade, M. S., Mendonça, M. G., Silva, C. J., Almeida, E. L., Lima, B. S., et al. (2009). Species diversity of *Leishmania (Viannia)* parasites circulating in an endemic area for cutaneous leishmaniasis located in the Atlantic rainforest region of northeastern Brazil. *Trop. Med. Int. Heal.* 14, 1278–1286. doi: 10.1111/j.1365-3156.2009.02361.x

Broughton, J. P., Deng, X., Yu, G., Fasching, C. L., Servellita, V., Singh, J., et al. (2020). CRISPR–Cas12-based detection of SARS-CoV-2. *Nat. Biotechnol.* 38, 870–874. doi: 10.1038/s41587-020-0513-4

Burza, S., Croft, S. L., and Boelaert, M. (2018). Leishmaniasis. *Lancet* 392, 951–970. doi: 10.1016/S0140-6736(18)31204-2

Camacho, E., Rastrojo, A., Sanchiz, Á., la Fuente, S. G., Aguado, B., and Requena, J. M. (2019). *Leishmania* mitochondrial genomes: Maxicircle structure and heterogeneity of Minicircles. *Genes (Basel)* 10:758. doi: 10.3390/genes10100758

Carvalho, L. P., Passos, S., Schriefer, A., and Carvalho, E. M. (2012). Protective and pathologic immune responses in human tegumentary leishmaniasis. *Front. Immunol.* 3:301. doi: 10.3389/fimmu.2012.00301

Ceccarelli, M., Galluzzi, L., Migliazzo, A., and Magnani, M. (2014). Detection and characterization of *Leishmania* (*Leishmania*) and *Leishmania* (*Viannia*) by SYBR green-based real-time PCR and high resolution melt analysis targeting kinetoplast minicircle DNA. *PLoS One* 9:e88845. doi: 10.1371/journal.pone.0088845

Chen, Y. Y. (2019). Cell fishing with DNA aptamers. *Nat. Biomed. Eng.* 3, 757–758. doi: 10.1038/s41551-019-0438-8

Chen, J. S., Ma, E., Harrington, L. B., Da Costa, M., Tian, X., Palefsky, J. M., et al. (2018). CRISPR-Cas12a target binding unleashes indiscriminate single-stranded DNase activity. *Science* 360, 436–439. doi: 10.1126/science.aar6245

Cossio, A., Jojoa, J., del Castro, M. M., Castillo, R. M., Osorio, L., Shelite, T. R., et al. (2021). Diagnostic performance of a recombinant polymerase amplification test—lateral flow (RPA-LF) for cutaneous leishmaniasis in an endemic setting of Colombia. *PLoS Negl. Trop. Dis.* 15:e0009291. doi: 10.1371/journal.pntd.0009291

Cunningham, C. H., Hennelly, C. M., Lin, J. T., Ubalee, R., Boyce, R. M., Mulogo, E. M., et al. (2021). A novel CRISPR-based malaria diagnostic capable of *plasmodium* detection, species differentiation, and drug-resistance genotyping. *EBioMedicine* 68:103415. doi: 10.1016/j.ebiom.2021.103415

Curtis, K. A., Morrison, D., Rudolph, D. L., Shankar, A., Bloomfield, L. S. P., Switzer, W. M., et al. (2018). A multiplexed RT-LAMP assay for detection of group M HIV-1 in plasma or whole blood. *J. Virol. Methods* 255, 91–97. doi: 10.1016/j.jviromet.2018.02.012

Davies, C. R., Reithinger, R., Campbell-Lendrum, D., Feliciangeli, D., Borges, R., and Rodriguez, N. (2000). The epidemiology and control of leishmaniasis in Andean countries. *Cad. Saude Publica* 16, 925–950. doi: 10.1590/S0102-311X2000000400013

de Paiva Cavalcanti, M., Dantas-Torres, F., da Cunha Gonçalves de Albuquerque, S., Silva de Morais, R. C., de Brito, M. E. F., Otranto, D., et al. (2013). Quantitative real time PCR assays for the detection of *Leishmania* (*Viannia*) *braziliensis* in animals and humans. *Mol. Cell. Probes* 27, 122–128. doi: 10.1016/j.mcp.2013.01.003

Deborggraeve, S., Laurent, T., Espinosa, D., Van der Auwera, G., Mbuchi, M., Wasunna, M., et al. (2008). A simplified and standardized polymerase chain reaction format for the diagnosis of Leishmaniasis. *J. Infect. Dis.* 198, 1565–1572. doi: 10.1086/592509

Ding, X., Yin, K., Li, Z., Lalla, R. V., Ballesteros, E., Sfeir, M. M., et al. (2020). Ultrasensitive and visual detection of SARS-CoV-2 using all-in-one dual CRISPR-Cas12a assay. *Nat. Commun.* 11, 4711. doi: 10.1038/s41467-020-18575-6

Dixit, K. K., Ramesh, V., Gupta, R., Negi, N. S., Singh, R., and Salotra, P. (2021). Real-time Fluorimetry loop-mediated isothermal amplification for diagnosis of Leishmaniasis and as a tool for assessment of cure for post–Kala-Azar dermal Leishmaniasis. *Am. J. Trop. Med. Hyg.* 104, 2097–2107. doi: 10.4269/ajtmh.20-1057

Dueñas, E., Nakamoto, J. A., Cabrera-Sosa, L., Huaihua, P., Cruz, M., Arévalo, J., et al. (2022). Novel CRISPR-based detection of *Leishmania* species. *bioRxiv* [Epub ahead of preprint]. doi: 10.1101/2022.04.29.490093

Eberhardt, E., Van den Kerkhof, M., Bulté, D., Mabille, D., Van Bockstal, L., Monnerat, S., et al. (2018). Evaluation of a Pan-*Leishmania* spliced-leader RNA detection method in human blood and experimentally infected Syrian Golden hamsters. *J. Mol. Diagnostics* 20, 253–263. doi: 10.1016/j.jmoldx.2017.12.003

Espinosa, D., Boggild, A. K., Deborggraeve, S., Laurent, T., Valencia, C., Pacheco, R., et al. (2009). *Leishmania* OligoC-TesT as a simple, rapid, and standardized tool for molecular diagnosis of cutaneous Leishmaniasis in Peru. *J. Clin. Microbiol.* 47, 2560–2563. doi: 10.1128/JCM.00259-09

Faber, W. R., Oskam, L., van Gool, T., Kroong, N. C. M., Knegt-Junk, K. J., Hofwegen, H., et al. (2003). Value of diagnostic techniques for cutaneous leishmaniasis. *J. Am. Acad. Dermatol.* 49, 70–74. doi: 10.1067/mjd.2003.492

Filgueira, C. P. B., Moreira, O. C., Cantanhêde, L. M., de Farias, H. M. T., Porrozzi, R., Britto, C., et al. (2020). Comparison and clinical validation of qPCR assays targeting *Leishmania* 18S rDNA and HSP70 genes in patients with American Tegumentary Leishmaniasis. *PLoS Negl. Trop. Dis.* 14:e0008750. doi: 10.1371/journal.pntd.0008750

Fozouni, P., Son, S., de León, D., Derby, M., Knott, G. J., Gray, C. N., et al. (2021). Amplification-free detection of SARS-CoV-2 with CRISPR-Cas13a and mobile phone microscopy. *Cell* 184, 323–333.e9. doi: 10.1016/j.cell.2020.12.001

Gollob, K. J., Viana, A. G., and Dutra, W. O. (2014). Immunoregulation in human American leishmaniasis: balancing pathology and protection. *Parasite Immunol.* 36, 367–376. doi: 10.1111/pim.12100

Gong, J., Zhang, G., Wang, W., Liang, L., Li, Q., Liu, M., et al. (2021). A simple and rapid diagnostic method for 13 types of high-risk human papillomavirus (HR-HPV) detection using CRISPR-Cas12a technology. *Sci. Rep.* 11, 12800. doi: 10.1038/s41598-021-92329-2

Gootenberg, J. S., Abudayyeh, O. O., Kellner, M. J., Joung, J., Collins, J. J., and Zhang, F. (2018). Multiplexed and portable nucleic acid detection platform with Cas13, Cas12a, and Csm6. *Science* 360, 439–444. doi: 10.1126/science.aaq0179

Gootenberg, J. S., Abudayyeh, O. O., Lee, J. W., Essletzbichler, P., Dy, A. J., Joung, J., et al. (2017). Nucleic acid detection with CRISPR-Cas13a/C2c2. *Science* 356, 438–442. doi: 10.1126/science.aam9321

Goto, H., and Lindoso, J. A. L. (2010). Current diagnosis and treatment of cutaneous and mucocutaneous leishmaniasis. *Expert Rev. Anti-Infect. Ther.* 8, 419–433. doi: 10.1586/eri.10.19

Gray, B. P., Requena, M. D., Nichols, M. D., and Sullenger, B. A. (2020). Aptamers as reversible sorting ligands for preparation of cells in their native state. *Cell Chem. Biol.* 27, 232–244.e7. doi: 10.1016/j.chembiol.2019.12.004

Gutierrez, Y., Salinas, G. H., Palma, G., Valderrama, L. B., Santrich, C. V., and Saravia, N. G. (1991). Correlation between histopathology, immune response, clinical presentation, and evolution in *Leishmania braziliensis* infection. *Am. J. Trop. Med. Hyg.* 45, 281–289. doi: 10.4269/ajtmh.1991.45.281

Hu, F., Liu, Y., Zhao, S., Zhang, Z., Li, X., Peng, N., et al. (2022). A one-pot CRISPR/Cas13a-based contamination-free biosensor for low-cost and rapid nucleic acid diagnostics. *Biosens. Bioelectron.* 202:113994. doi: 10.1016/j.bios.2022.113994

Huang, D., Ni, D., Fang, M., Shi, Z., and Xu, Z. (2021). Microfluidic ruler-readout and CRISPR Cas12a-responded hydrogel-integrated paper-based analytical devices (μReaCH-PAD) for visible quantitative point-of-care testing of invasive fungi. *Anal. Chem*. 93, 16965–16973. doi: 10.1021/acs.analchem.1c04649

Ibarra-Meneses, A. V., Corbeil, A., Wagner, V., Onwuchekwa, C., and Fernandez-Prada, C. (2022). Identification of asymptomatic *Leishmania* infections: a scoping review. *Parasit. Vectors* 15, 5. doi: 10.1186/s13071-021-05129-y

Ibarra-Meneses, A. V., Cruz, I., Chicharro, C., Sánchez, C., Biéler, S., Broger, T., et al. (2018). Evaluation of fluorimetry and direct visualization to interpret results of a loop-mediated isothermal amplification kit to detect *Leishmania* DNA. *Parasit. Vectors* 11, 250. doi: 10.1186/s13071-018-2836-2

Inga, R., De Doncker, S., Gomez, J., Lopez, M., Garcia, R., Le Ray, D., et al. (1998). Relation between variation in copy number of ribosomal RNA encoding genes and size of harbouring chromosomes in *Leishmania* of subgenus Viannia. *Mol. Biochem. Parasitol.* 92, 219–228. doi: 10.1016/s0166-6851(98)00009-7

Jara, M., Adaui, V., Valencia, B. M., Martinez, D., Alba, M., Castrillon, C., et al. (2013). Real-time PCR assay for detection and quantification of *Leishmania* (*Viannia*) organisms in skin and mucosal lesions: exploratory study of parasite load and clinical parameters. *J. Clin. Microbiol.* 51, 1826–1833. doi: 10.1128/JCM.00208-13

Kambouris, M. E., Siamoglou, S., Kordou, Z., Milioni, A., Vassilakis, S., Goudoudaki, S., et al. (2020). Point-of-need molecular processing of biosamples using portable instrumentation to reduce turnaround time. *Biosaf. Heal.* 2, 177–182. doi: 10.1016/j.bsheal.2020.06.001

Kaminski, M. M., Abudayyeh, O. O., Gootenberg, J. S., Zhang, F., and Collins, J. J. (2021). CRISPR-based diagnostics. *Nat. Biomed. Eng.* 5, 643–656. doi: 10.1038/s41551-021-00760-7

Kariyawasam, R., Valencia, B. M., Lau, R., Shao, E., Thompson, C. A., Stevens, M., et al. (2021). Evaluation of a point-of-care molecular detection device for *Leishmania* spp. and intercurrent fungal and mycobacterial organisms in Peruvian patients with cutaneous ulcers. *Infection* 49, 1203–1211. doi: 10.1007/s15010-021-01673-y

Katzmeier, F., Aufinger, L., Dupin, A., Quintero, J., Lenz, M., Bauer, L., et al. (2019). A low-cost fluorescence reader for in vitro transcription and nucleic acid detection with Cas13a. *PLoS One* 14:e0220091. doi: 10.1371/journal.pone.0220091

Kellner, M. J., Koob, J. G., Gootenberg, J. S., Abudayyeh, O. O., and Zhang, F. (2019). SHERLOCK: nucleic acid detection with CRISPR nucleases. *Nat. Protoc.* 14, 2986–3012. doi: 10.1038/s41596-019-0210-2

Khan, W. A., Barney, R. E., and Tsongalis, G. J. (2021). CRISPR-cas13 enzymology rapidly detects SARS-CoV-2 fragments in a clinical setting. *J. Clin. Virol.* 145:105019. doi: 10.1016/j.jcv.2021.105019

Kocher, A., Valière, S., Bañuls, A.-L., and Murienne, J. (2018). High-throughput sequencing of kDNA amplicons for the analysis of *Leishmania* minicircles and identification of Neotropical species. *Parasitology* 145, 585–594. doi: 10.1017/S0031182017002013

Larkin, M. A., Blackshields, G., Brown, N. P., Chenna, R., McGettigan, P. A., McWilliam, H., et al. (2007). Clustal W and Clustal X version 2.0. *Bioinformatics* 23, 2947–2948. doi: 10.1093/bioinformatics/btm404

Larsson, A. (2014). AliView: a fast and lightweight alignment viewer and editor for large datasets. *Bioinformatics* 30, 3276–3278. doi: 10.1093/bioinformatics/btu531

Lee, R. A., Puig, H.De, Nguyen, P. Q., Angenent-Mari, N. M., Donghia, N. M., McGee, J. P., et al. (2020). Ultrasensitive CRISPR-based diagnostic for field-applicable detection of *plasmodium* species in symptomatic and asymptomatic malaria. *Proc. Natl. Acad. Sci.* 117, 25722–25731. doi: 10.1073/pnas.2010196117

Lejon, V., Jamonneau, V., Solano, P., Atchade, P., Mumba, D., Nkoy, N., et al. (2006). Detection of trypanosome-specific antibodies in saliva, towards non-invasive serological diagnosis of sleeping sickness. *Trop. Med. Int. Heal.* 11, 620–627. doi: 10.1111/j.1365-3156.2006.01620.x

Leon, W., Fouts, D. L., and Manning, J. (1978). Sequence arrangement of the 16S and 26S rRNA genes in the pathogenic haemoflagellate *Leishmania donovani*. *Nucleic Acids Res.* 5, 491–504. doi: 10.1093/nar/5.2.491

León, C. M., Muñoz, M., Hernández, C., Ayala, M. S., Flórez, C., Teherán, A., et al. (2017). Analytical performance of four polymerase chain reaction (PCR) and real time PCR (qPCR) assays for the detection of six *Leishmania* species DNA in Colombia. *Front. Microbiol.* 8:1907. doi: 10.3389/fmicb.2017.01907

Li, S.-Y., Cheng, Q.-X., Wang, J.-M., Li, X.-Y., Zhang, Z.-L., Gao, S., et al. (2018). CRISPR-Cas12a-assisted nucleic acid detection. *Cell Discov.* 4, 20. doi: 10.1038/s41421-018-0028-z

Llanos-Cuentas, E. A., Marsden, P. D., Cuba, C. C., Barreto, A. C., and Campos, M. (1984). Possible risk factors in development of mucosal lesions in leishmaniasis. *Lancet* 324, 295. doi: 10.1016/S0140-6736(84)90346-5

Longo, M. C., Berninger, M. S., and Hartley, J. L. (1990). Use of uracil DNA glycosylase to control carry-over contamination in polymerase chain reactions. *Gene* 93, 125–128. doi: 10.1016/0378-1119(90)90145-h

Lopez, M., Inga, R., Cangalaya, M., Echevarria, J., Llanos-Cuentas, A., Orrego, C., et al. (1993). Diagnosis of *Leishmania* using the polymerase chain reaction: a simplified procedure for field work. *Am. J. Trop. Med. Hyg.* 49, 348–356. doi: 10.4269/ajtmh.1993.49.348

Lucas, C. M., Franke, E. D., Cachay, M. I., Tejada, A., Cruz, M. E., Kreutzer, R. D., et al. (1998). Geographic distribution and clinical description of leishmaniasis cases in Peru. *Am. J. Trop. Med. Hyg.* 59, 312–317. doi: 10.4269/ajtmh.1998.59.312

Ma, Q.-N., Wang, M., Zheng, L.-B., Lin, Z.-Q., Ehsan, M., Xiao, X.-X., et al. (2021). RAA-Cas12a-Tg: A nucleic acid detection system for *toxoplasma gondii* based on CRISPR-Cas12a combined with Recombinase-aided amplification (RAA). *Microorganisms* 9, 1644. doi: 10.3390/microorganisms9081644

Marsden, P. D. (1986). Mucosal leishmaniasis ("spundia" Escomel, 1911). *Trans. R. Soc. Trop. Med. Hyg.* 80, 859–876. doi: 10.1016/0035-9203(86)90243-9

McHugh, M. L. (2012). Interrater reliability: the kappa statistic. *Biochem. Med.* 22, 276–282. doi: 10.11613/BM.2012.031

Mendoza-Rojas, G., Sarabia-Vega, V., Sanchez-Castro, A., Tello, L., Cabrera-Sosa, L., Nakamoto, J. A., et al. (2021). A low-cost and open-source protocol to produce key enzymes for molecular detection assays. *STAR Protoc.* 2:100899. doi: 10.1016/j.xpro.2021.100899

Mesa, L. E., Manrique, R., Muskus, C., and Robledo, S. M. (2020). Test accuracy of polymerase chain reaction methods against conventional diagnostic techniques for cutaneous Leishmaniasis (CL) in patients with clinical or epidemiological suspicion of CL: systematic review and meta-analysis. *PLoS Negl. Trop. Dis.* 14:e0007981. doi: 10.1371/journal.pntd.0007981

Moreira, O. C., Yadon, Z. E., and Cupolillo, E. (2018). The applicability of real-time PCR in the diagnostic of cutaneous leishmaniasis and parasite quantification for clinical management: current status and perspectives. *Acta Trop.* 184, 29–37. doi: 10.1016/j.actatropica.2017.09.020

Mugasa, C. M., Laurent, T., Schoone, G. J., Basiye, F. L., Saad, A. A., el Safi, S., et al. (2010). Simplified molecular detection of *Leishmania* parasites in various clinical samples from patients with leishmaniasis. *Parasit. Vectors* 3, 13. doi: 10.1186/1756-3305-3-13

Myhrvold, C., Freije, C. A., Gootenberg, J. S., Abudayyeh, O. O., Metsky, H. C., Durbin, A. F., et al. (2018). Field-deployable viral diagnostics using CRISPR-Cas13. *Science* 360, 444–448. doi: 10.1126/science.aas8836

Nguyen, L. T., Rananaware, S. R., Pizzano, B. L. M., Stone, B. T., and Jain, P. K. (2022). Clinical validation of engineered CRISPR/Cas12a for rapid SARS-CoV-2 detection. *Commun. Med.* 2, 7. doi: 10.1038/s43856-021-00066-4

Nguyen, L. T., Smith, B. M., and Jain, P. K. (2020). Enhancement of trans-cleavage activity of Cas12a with engineered crRNA enables amplified nucleic acid detection. *Nat. Commun.* 11, 4906. doi: 10.1038/s41467-020-18615-1

Pan American Health Organization/World Health Organization. (2019). *Leishmaniases. Epidemiological Report of the Americas, No. 8*. Washington, DC: WHO Regional Office for the Americas.

Pan American Health Organization/World Health Organization. (2020). *Leishmaniases. Epidemiological Report of the Americas, No. 9*. Washington, DC: WHO Regional Office for the Americas.

Peng, D., and Tarleton, R. (2015). EuPaGDT: a web tool tailored to design CRISPR guide RNAs for eukaryotic pathogens. *Microb. Genomics* 1, e000033. doi: 10.1099/mgen.0.000033

Qian, C., Wang, R., Wu, H., Zhang, F., Wu, J., and Wang, L. (2019). Uracil-mediated new Photospacer-adjacent motif of Cas12a to realize visualized DNA detection at the single-copy level free from contamination. *Anal. Chem.* 91, 11362–11366. doi: 10.1021/acs.analchem.9b02554

Reimão, J. Q., Coser, E. M., Lee, M. R., and Coelho, A. C. (2020). Laboratory diagnosis of cutaneous and visceral Leishmaniasis: current and future methods. *Microorganisms* 8, 1632. doi: 10.3390/microorganisms8111632

Reithinger, R., Dujardin, J.-C., Louzir, H., Pirmez, C., Alexander, B., and Brooker, S. (2007). Cutaneous leishmaniasis. *Lancet Infect. Dis.* 7, 581–596. doi: 10.1016/S1473-3099(07)70209-8

Rosales-Chilama, M., Diaz-Moreno, N., Prieto, M. D., Giraldo-Parra, L., Martínez-Valencia, Á. J., and Gomez, M. A. (2020). Comparative assessment of DNA targets and amplification methods for *Leishmania* (*Viannia*) detection in human samples. *Am. J. Trop. Med. Hyg.* 102, 1323–1327. doi: 10.4269/ajtmh.19-0691

Rotondi, M. A. (2018). Sample size estimation functions for studies of interobserver agreement. R package version 1.2. Available at https://CRAN.R-project.org/package=kappaSize. Accessed May 19, 2022.

Ruiz-Postigo, J. A., Jain, S., Mikhailov, A., Maia-Elkhoury, A. N., Valadas, S., Warusavithana, S., et al. (2021). Global leishmaniasis surveillance: 2019-2020, a baseline for the 2030 roadmap. *Wkly Epidemiol. Rec.* 96, 401–419.

Saldarriaga, O. A., Castellanos-Gonzalez, A., Porrozzi, R., Baldeviano, G. C., Lescano, A. G., de Los Santos, M. B., et al. (2016). An innovative field-applicable molecular test to diagnose cutaneous *Leishmania Viannia* spp. infections. *PLoS Negl. Trop. Dis.* 10:e0004638. doi: 10.1371/journal.pntd.0004638

Sam, I. K., Chen, Y., Ma, J., Li, S., Ying, R., Li, L., et al. (2021). TB-QUICK: CRISPR-Cas12b-assisted rapid and sensitive detection of *Mycobacterium tuberculosis*. *J. Infect.* 83, 54–60. doi: 10.1016/j.jinf.2021.04.032

Sandoval-Juárez, A., Minaya-Gómez, G., Rojas-Palomino, N., and Cáceres, O. (2020). Identificación de especies de *Leishmania* en pacientes derivados al Instituto Nacional de Salud del Perú. *Rev. Peru. Med. Exp. Salud Publica* 37, 87–92. doi: 10.17843/rpmesp.2020.371.4514

Schallig, H. D. F. H., Hu, R. V. P., Kent, A. D., van Loenen, M., Menting, S., Picado, A., et al. (2019). Evaluation of point of care tests for the diagnosis of cutaneous leishmaniasis in Suriname. *BMC Infect. Dis.* 19, 25. doi: 10.1186/s12879-018-3634-3

Simpson, L. (1987). The mitochondrial genome of kinetoplastid protozoa: genomic organization, transcription, replication, and evolution. *Annu. Rev. Microbiol.* 41, 363–380. doi: 10.1146/annurev.mi.41.100187.002051

Simpson, L. (1997). The genomic organization of guide RNA genes in kinetoplastid protozoa: several conundrums and their solutions. *Mol. Biochem. Parasitol.* 86, 133–141. doi: 10.1016/s0166-6851(97)00037-6

Suárez, M., Valencia, B. M., Jara, M., Alba, M., Boggild, A. K., Dujardin, J.-C., et al. (2015). Quantification of *Leishmania* (*Viannia*) Kinetoplast DNA in ulcers of cutaneous Leishmaniasis reveals inter-site and inter-sampling variability in parasite load. *PLoS Negl. Trop. Dis.* 9:e0003936. doi: 10.1371/journal.pntd.0003936

Tirelli, F., Vernal, S., and Roselino, A. M. (2017). Final diagnosis of 86 cases included in differential diagnosis of American tegumentary leishmaniasis in a Brazilian sample: a retrospective cross-sectional study. *An. Bras. Dermatol.* 92, 642–648. doi: 10.1590/abd1806-4841.20175794

Travi, B. L., De los Santos, M. B., Shelite, T. R., Santos, R. P., Rosales, L. A., Castellanos-Gonzalez, A., et al. (2021). Diagnostic efficacy of recombinase-polymerase-amplification coupled with lateral flow strip Reading in patients with cutaneous Leishmaniasis from the Amazonas rainforest of Perú. *Vector-Borne Zoonotic Dis.* 21, 941–947. doi: 10.1089/vbz.2021.0038

Untergasser, A., Cutcutache, I., Koressaar, T., Ye, J., Faircloth, B. C., Remm, M., et al. (2012). Primer3—new capabilities and interfaces. *Nucleic Acids Res.* 40, e115. doi: 10.1093/nar/gks596

Van der Auwera, G., and Dujardin, J.-C. (2015). Species typing in dermal Leishmaniasis. *Clin. Microbiol. Rev.* 28, 265–294. doi: 10.1128/CMR.00104-14

van Eys, G. J., Schoone, G. J., Kroon, N. C., and Ebeling, S. B. (1992). Sequence analysis of small subunit ribosomal RNA genes and its use for detection and identification of *Leishmania* parasites. *Mol. Biochem. Parasitol.* 51, 133–142. doi: 10.1016/0166-6851(92)90208-2

Verosloff, M. S., Shapiro, S. J., Hawkins, E. M., Alpay, E., Verma, D., Stanfield, E. G., et al. (2021). CRISPR-Cas enzymes: The toolkit revolutionizing diagnostics. *Biotechnol. J.* 2100304, e2100304. doi: 10.1002/biot.202100304

Wang, D.-G., Brewster, J., Paul, M., and Tomasula, P. (2015). Two methods for increased specificity and sensitivity in loop-mediated isothermal amplification. *Molecules* 20, 6048–6059. doi: 10.3390/molecules20046048

Wang, R., Chen, R., Qian, C., Pang, Y., Wu, J., and Li, F. (2021). Ultrafast visual nucleic acid detection with CRISPR/Cas12a and rapid PCR in single capillary. *Sensors Actuators B Chem.* 326:128618. doi: 10.1016/j.snb.2020.128618

Weigle, K. A., de Dávalos, M., Heredia, P., Molineros, R., Saravia, N. G., and D'Alessandro, A. (1987). Diagnosis of cutaneous and Mucocutaneous Leishmaniasis in Colombia: A comparison of seven methods. *Am. J. Trop. Med. Hyg.* 36, 489–496. doi: 10.4269/ajtmh.1987.36.489

Weigle, K. A., Labrada, L. A., Lozano, C., Santrich, C., and Barker, D. C. (2002). PCR-based diagnosis of acute and chronic cutaneous Leishmaniasis caused by *Leishmania* (*Viannia*). *J. Clin. Microbiol.* 40, 601–606. doi: 10.1128/JCM.40.2.601-606.2002

Weirather, J. L., Jeronimo, S. M. B., Gautam, S., Sundar, S., Kang, M., Kurtz, M. A., et al. (2011). Serial quantitative PCR assay for detection, species discrimination, and quantification of *Leishmania* spp. in human samples. *J. Clin. Microbiol.* 49, 3892–3904. doi: 10.1128/JCM.r00764-11

Wiedenheft, B., Sternberg, S. H., and Doudna, J. A. (2012). RNA-guided genetic silencing systems in bacteria and archaea. *Nature* 482, 331–338. doi: 10.1038/nature10886

Wright, P. F., Nilsson, E., Van Rooij, E. M. A., Lelenta, M., and Jeggo, M. H. (1993). Standardisation and validation of enzyme-linked immunosorbent assay techniques for the detection of antibody in infectious disease diagnosis. *Rev. Sci. Tech.* 12, 435–450. doi: 10.20506/rst.12.2.691

Xiong, Y., Zhang, J., Yang, Z., Mou, Q., Ma, Y., Xiong, Y., et al. (2020). Functional DNA regulated CRISPR-Cas12a sensors for point-of-care diagnostics of non-nucleic-acid targets. *J. Am. Chem. Soc.* 142, 207–213. doi: 10.1021/jacs.9b09211

Yin, K., Ding, X., Li, Z., Zhao, H., Cooper, K., and Liu, C. (2020). Dynamic aqueous multiphase reaction system for one-pot CRISPR-Cas12a-based ultrasensitive and quantitative molecular diagnosis. *Anal. Chem.* 92, 8561–8568. doi: 10.1021/acs.analchem.0c01459

Yu, F., Zhang, K., Wang, Y., Li, D., Cui, Z., Huang, J., et al. (2021). CRISPR/Cas12a-based on-site diagnostics of *Cryptosporidium parvum* IId-subtype-family from human and cattle fecal samples. *Parasit. Vectors* 14, 208. doi: 10.1186/s13071-021-04709-2

Yuan, C. C., Miley, W., and Waters, D. (2001). A quantification of human cells using an ERV-3 real time PCR assay. *J. Virol. Methods* 91, 109–117. doi: 10.1016/S0166-0934(00)00244-5

Zimic, M., Pajuelo, M., Rueda, D., López, C., Arana, Y., Castillo, Y., et al. (2009). Utility of a protein fraction with cathepsin L-like activity purified from cysticercus fluid of *Taenia solium* in the diagnosis of human cysticercosis. *Am. J. Trop. Med. Hyg.* 80, 964–970. doi: 10.4269/ajtmh.2009.80.964

frontiers | Frontiers in Microbiology

TYPE Original Research
PUBLISHED 07 October 2022
DOI 10.3389/fmicb.2022.973996

OPEN ACCESS

EDITED BY
Kamal El Bissati,
The University of Chicago, United States

REVIEWED BY
Rui Pang,
Guangdong Academy of Science, China
Mehdi Soltani,
Murdoch University,
Australia

*CORRESPONDENCE
Yongliang Lou
lyl@wmu.edu.cn
Xingxing Xiao
xiaoxingxing@wmu.edu.cn

†These authors have contributed equally to this work

SPECIALTY SECTION
This article was submitted to Infectious Agents and Disease, a section of the journal Frontiers in Microbiology

RECEIVED 20 June 2022
ACCEPTED 13 September 2022
PUBLISHED 07 October 2022

CITATION
Lin Z, Lu J, Wu S, Lin X, Zheng L, Lou Y and Xiao X (2022) A novel detection method for the pathogenic *Aeromonas hydrophila* expressing *aerA* gene and/or *hlyA* gene based on dualplex RAA and CRISPR/Cas12a.
Front. Microbiol. 13:973996.
doi: 10.3389/fmicb.2022.973996

A novel detection method for the pathogenic *Aeromonas hydrophila* expressing *aerA* gene and/or *hlyA* gene based on dualplex RAA and CRISPR/Cas12a

Ziqin Lin†, Jinfang Lu†, Sihong Wu, Xi Lin, Laibao Zheng, Yongliang Lou* and Xingxing Xiao*

Wenzhou Key Laboratory of Sanitary Microbiology, Key Laboratory of Laboratory Medicine, Ministry of Education, School of Laboratory Medicine and Life Sciences, Wenzhou Medical University, Wenzhou, Zhejiang, China

Aeromonas hydrophila is an emerging waterborne and foodborne pathogen with pathogenicity to humans and warm water fishes, which severely threatens human health, food safety and aquaculture. A novel method for the rapid, accurate, and sensitive detection of pathogenic *A. hydrophila* is still needed to reduce the impact on human health and aquaculture. In this work, we developed a rapid, accurate, sensitive, and visual detection method (dRAA-CRISPR/Cas12a), without elaborate instruments, integrating the dualplex recombinase-assisted amplification (dRAA) assay and CRISPR/Cas12a system to detect pathogenic *A. hydrophila* expressing *aerA* and/or *hlyA* virulence genes. The dRAA-CRISPR/Cas12a method has high sensitivity, which can rapidly detect (about 45min) *A. hydrophila* with the limit of detection in 2 copies of genomic DNA per reaction, and has high specificity for three pathogenic *A. hydrophila* strains (*aerA*$^+$*hlyA*$^-$, *aerA*$^-$*hlyA*$^+$, and *aerA*$^+$*hlyA*$^+$). Moreover, dRAA-CRISPR/Cas12a method shows satisfactory practicability in the analysis of the spiked human blood and stool and fish samples. These results demonstrate that our developed pathogenic *A. hydrophila* detection method, dRAA-CRISPR/Cas12a, is a promising potential method for the early diagnosis of human *A. hydrophila* infection and on-site detection of *A. hydrophila* in food and aquaculture.

KEYWORDS

***Aeromonas hydrophila*, dualplex recombinase-aided amplification assay, CRISPR/Cas12a, detection, diagnosis**

Introduction

Aeromonas hydrophila is a widespread aquatic and zoonotic pathogen (Daskalov, 2006; Li et al., 2011). In animals, *A. hydrophila* mainly causes diseases in aquaculture animals, such as the motile Aeromonas septicemia and red sore disease in warm water fishes (Janda and Abbott, 2010), resulting in huge economic losses and food safety risks. In humans,

A. hydrophila was initially thought to be an opportunistic pathogen for immunocompromised populations (Balsalobre et al., 2009), but a growing body of research indicates that it is an emerging enteric (Özbaş et al., 2000), waterborne (Chauret et al., 2001), and foodborne (Daskalov, 2006) pathogen regardless of the immune status of the host (Balsalobre et al., 2009).

The pathogenicity of *A. hydrophila* is closely related to its production of virulence factors (Janda and Abbott, 2010; Tichoniuk et al., 2010; Li et al., 2011). It has been reported that the pathogenic *A. hydrophila* can survive and multiply in water, soil and various foods (milk, fish, raw meat, etc.) at room temperature and low temperature (Balakrishna et al., 2010; Janda and Abbott, 2010), and produce virulence factors aerolysin and/or hemolysin (Wong et al., 1998; Heuzenroeder et al., 1999; Balakrishna et al., 2010; Janda and Abbott, 2010). Patients infected with *A. hydrophila* can develop sepsis and necrotizing fasciitis, which have an acute onset and rapid progression (Tsai et al., 2015; Sun et al., 2021) and are life-threatening, mainly through ingestion of contaminated water and food and exposed wounds, respectively (Meng et al., 2015); moreover, sepsis can reach a state of systemic toxicity within 24 h (Zhu et al., 2021). In view of these aspects, a rapid, accurate, and sensitive detection method of pathogenic *A. hydrophila* would contribute to improving the treatment and control strategies and then reducing the hazard of this bacterial infection.

Nowadays, many methods can be used for the detection of *A. hydrophila*. The traditional culture method is accurate, but it takes a long time. The biochemical test is complicated, and only typical strains can be detected because of the limited biochemical characteristics (Abbott et al., 2003). Enzyme-linked immunosorbent assay (ELISA; Swain et al., 2003), dot blotting (Longyant et al., 2010), and serotyping (Nielsen et al., 2001) have low diagnostic sensitivity. Over the past decade, a large number of assays based on PCR technology have been developed to detect *A. hydrophila* by targeting virulence gene (Wang et al., 2003; Hussain et al., 2014). However, these methods require professional personnel and specialized equipment and are not suitable for on-site application or resource-constrained areas. In recent years, isothermal nucleic acid amplification technologies, such as recombinase-aided amplification (RAA; Piepenburg et al., 2006; Subsoontorn et al., 2020) and loop-mediated isothermal amplification (Nagamine et al., 2002), have promoted the development of nucleic acid amplification without thermal cyclers. RAA assay that only requires one primer set and can be reacted even at body temperature of operator (Wang et al., 2017) has been used for the detection of pathogens such as *A. hydrophila* (Qu et al., 2021) and *Enterocytozoon hepatopenaei* (Zhou et al., 2020), but this method has low sensitivity (Xiao et al., 2021) and the result is complicated to obtain (Zhou et al., 2020).

Recently, the discovery of the trans-cleavage activity of clustered regularly interspaced short palindromic repeats (CRISPR)-associated protein Cas12a has made the CRISPR/Cas12a system a hot spot in the field of *in vitro* diagnostics (Chen et al., 2018; Li et al., 2018a,b). Chen et al. developed a DETECTR platform, consisting of a RPA assay and the CRISPR/Cas12a system, with aM sensitivity and high specificity to distinguish between HPV16 and HPV18 (Chen et al., 2018). Zhang et al. used PCR assay and CRISPR/Cas12a system to develop an integrated naked-eye detection method for the *tlh* gene of *Vibrio parahaemolyticus* with a detection limit of 1.02×10^2 copies/μl (Zhang et al., 2020). Because of its speed, sensitivity, specificity, and simplicity, DETECTR platform is a promising method to be used for on-site detection, and has been performed to detect pathogens including *Listeria monocytogenes* (Li et al., 2021), *Vibrio vulnificus* (Xiao et al., 2021), and SARS-CoV-2 (Broughton et al., 2020).

The virulence factors play roles through cooperation or alone in the establishment of *A. hydrophila* infection (Nawaz et al., 2010; Li et al., 2011; Nagar et al., 2011; Igbinosa and Okoh, 2013), and the detection methods only targeting one virulence gene of pathogenic *A. hydrophila* always lead to false negative results (Elsheshtawy et al., 2019). Here, a dRAA-CRISPR/Cas12a method targeting *aerA* and *hlyA* genes for the detection of pathogenic *A. hydrophila* without elaborate instruments was developed by integrating dualplex RAA (dRAA) and CRISPR/Cas12a system (Figure 1), and was compared with the dPCR-CRISPR/Cas12a method to investigate their sensitivity in detecting *A. hydrophila* stains and practicability in spiked samples. The whole process only takes 45 min, and the sensitivity is as low as 2 copies per reaction. The dRAA-CRISPR/Cas12a method we developed may be a promising method for rapid, accurate, and sensitive detection of pathogenic *A. hydrophila* in samples from human, fish, and food.

Materials and methods

Bacterial strains

Bacterial strains preserved in our laboratory were used in this study and consisted of eight standard strains and eight isolation strains. The standard strains were *A. hydrophila* (ATCC 7966), *Vibrio vulnificus* (ATCC 27562), *Vibrio alginolyticus* (ATCC 17749), *Vibrio harvey* (ATCC 14126), *Staphylococcus aureus* (ATCC 25923), *Escherichia coli* (ATCC 25922), *Pseudomonas aeruginosa* (ATCC 27853) and *Bacillus cereus* (ATCC 14579). The isolation strains were *A. hydrophila* strain 1, *A. hydrophila* strain 2, *A. hydrophila* strain 3, *A. veronii*, *A. sobria*, *Vibrio parahaemolyticus*, *Edwardsiella piscicida*, and *Salmonella typhimurium*, which were isolated from affected aquatic animal, patients, and environment. The *aerA* and *hlyA* genes expressed in these four *A. hydrophila* strains were detected by dualplex RAA assay, and the results showed that *A. hydrophila* strain 1 (NQ201810) is $aerA^{-}hlyA^{-}$, *A. hydrophila* strain 2 (NQ201906) is $aerA^{+}hlyA^{-}$, *A. hydrophila* strain 3 (AS1.1801) is $aerA^{-}hlyA^{+}$, and *A. hydrophila* strain 4 (ATCC 7966) is $aerA^{+}hlyA^{+}$ (Supplementary Figure S1). Moreover, the expression of *aerA* and *hlyA* genes in *A. veronii* and *A. sobria* was also detected by dualplex RAA assay, and the results showed that these two species of *Aeromonas* are $aerA^{+}hlyA^{-}$ (Supplementary Figure S2).

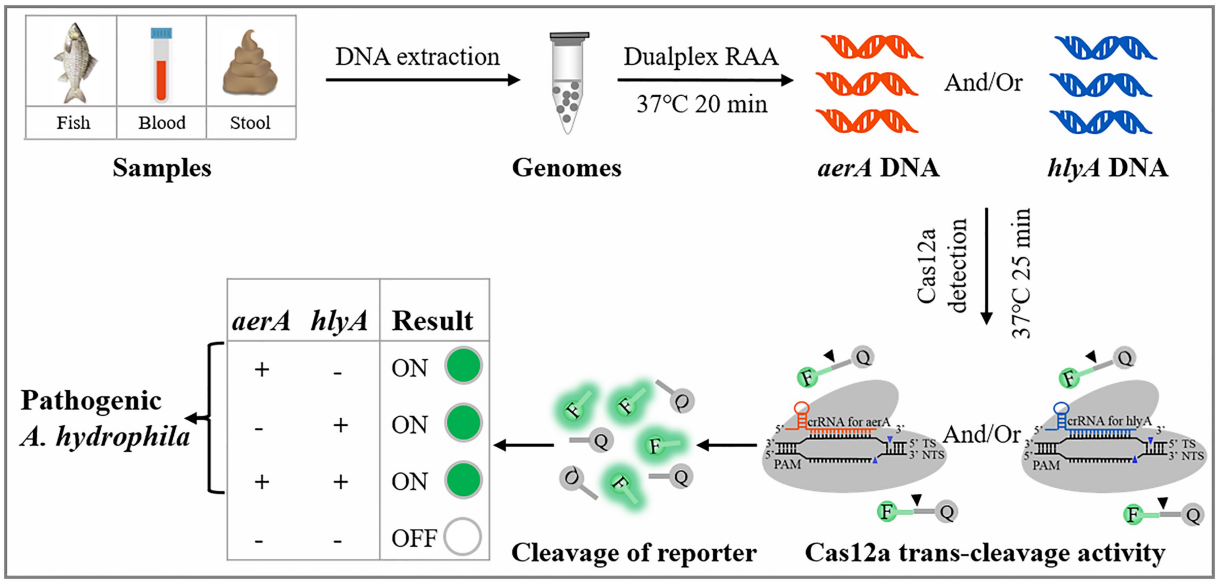

FIGURE 1
Schematic illustration of the developed dRAA-CRISPR/Cas12a method in the detection of *pathogenic Aeromonas hydrophila*.

Genomic DNA extraction

Bacterial strains were inoculated into 2216E broth or LB medium and cultured with shaking at 28°C or 37°C for 12–16 h, and then the genomic DNA of them were extracted by Kit-based and NaOH-based method. The Kit-based method for the extraction of genomic DNA was conducted with a MiniBEST Bacteria Genomic DNA Extraction Kit Ver.3.0 (9,763; TaKaRa Bio Inc., Japan) according to the Kit manual. The NaOH-based method was conducted to extract the genomic DNA of *A. hydrophila* according to the method mentioned in two published papers (Zhang et al., 2020; Xiao et al., 2021). The genomic DNA was stored at −20°C and then used as the templates of RAA and PCR assays.

Nucleic acid preparation

The primer sets for *aerA* (F: 5′-AAGACGGCC ATCAAGGTCAG-3′; R: 5′- ACGAAGGTGTGGTTCCAGT-3′) and *hlyA* (F: 5′-CCGGCATCTCTTTTGATGCG-3′; R: 5′-GGATGTTGACCGAGGAGTCG-3′) were used to amplify the *aerA* gene and *hlyA* gene of *A. hydrophila* by PCR assay respectively, and then the PCR products were sequenced by GENEWIZ (GENEWIZ, China).

Several sequences of *Aeromonas aerA* and *hlyA* genes obtained from GenBank were aligned using the online tool, Clustal Omega. The aligned results and the conserved regions of *A. hydrophila aerA* and *hlyA* genes were shown in Supplementary Figures S4, S5, respectively. The regions of *aerA* and *hlyA* sequences that were highly conserved among *A. hydrophila* were selected as templates for the design of RAA primers, which was conducted with NCBI Primer-BLAST. Five primer sets for *aerA* gene and four primer sets for *hlyA* gene were designed according to the design instruction of RPA primer[1], and the sequences of them were listed in Supplementary Table S1.

According to the complementary pairing characteristics of crRNA with target sequence (Chen et al., 2018), PAM sequences (TTTN) were first found from RAA amplicon of *aerA* or *hlyA*, and then 15–25 bp was selected from the adjacent sequence of PAM as the target sequence. The specific sequences that can distinguish *A. hydrophila* from other pathogens were selected from the candidate target sequences (Supplementary Figures S6, S7), and the crRNA sequence was comprised of the repeat sequence (UAA UUU CUA CUA AGU GUA GAU) and the selected specific sequence. The ssDNA-FQ reporter (5′−/6-FAM/TTATT/ BHQ1/−3′) was used to indicate the existence of the target gene. The crRNA and ssDNA-FQ were purchased from GENEWIZ (GENEWIZ, China).

The genomic DNA of three pathogenic *A. hydrophila* strains (*aerA*$^+$*hlyA*$^-$, *aerA*$^-$*hlyA*$^+$, and *aerA*$^+$*hlyA*$^+$) extracted by Kit-based method were gradiently diluted with 1 × NEB buffer 2.1, and the obtained diluents of *A. hydrophila* genomic DNA with different concentrations (1×10^0 to 1×10^7 copies/μl) were stored at −80°C.

Single and dualplex RAA assay

The RAA Nucleic Acid Amplification Kit (B00000; Jiangsu Qitian Gene Biological Co., China) was employed to conduct

1 https://www.twistdx.co.uk/support/rpa-assay-design/

single and dualplex RAA assay. Single RAA assay was carried out according to the Kit manual. Briefly, 25 µl of buffer V, 16.5 µl of purified water, 2 µl of primer F (10 µm), 2 µl of primer R (10 µm), 2.5 µl of magnesium acetate, and 2 µl of genomic DNA were added to the reaction tube. After being softly vortexed for 8 s, the reaction tube was incubated for 20 min at a 37°C water bath. The procedure for dRAA assay was similar to single RAA assay, and the only difference was that the addition volume of each primer (20 µm) in dRAA assay was 1 µl.

Dualplex RAA-CRISPR/Cas12a assay

The product of dRAA assay was used as the target of CRISPR-Cas12a system. The Cas12a trans-cleavage reaction was performed as follows: 5 µl of 1,000 nm Cas12a (M0653T; New England Biolabs Inc., MA, United States) and 5 µl of 400 nm crRNAmix (crRNA mixture), consisting of crRNA for *aerA* (ACR) and crRNA for *hlyA* (HCR), were preincubated at 37°C for 20 min to form Cas12a-crRNA complex. 10 µl of 1,000 nm ssDNA-FQ, 10 µl of 1 × NEB buffer 2.1, and 2 µl of dRAA product were added to the tube containing 10 µl of Cas12a-crRNA complex. After softly vortexed for 8 s, the tube containing 32 µl of mixture was incubated at 37°C for 35 min. The results can be read with an UV flashlight or a multifunctional microplate reader (λ_{ex}: 485 nm and λ_{em}: 520 nm). In this study, we optimized the concentration of Cas12a, the concentration of ssDNA-FQ, and the Cas12a cleavage time.

Dualplex PCR-CRISPR/Cas12a assay

The procedure for dPCR-CRISPR/Cas12a assay was similar to the dRAA-CRISPR/Cas12a assay. Briefly, dualplex PCR assay was carried out using Phanta® Max Super-Fidelity DNA Polymerase (P505-d1; Vazyme Biotechnology Co. LTD., China) in a 50 µl reaction mixture, containing 25 µl of 2 × Phanta Max Buffer, 1 µl of 10 µm forward and reverse primers (total of 4 µl; Supplementary Table S1), 1 µl of dNTP Mix (10 mm each), 1 U Phanta Max Super-Fidelity DNA Polymerase, 2 µl of genomic DNA, and 17 µl of H_2O. 2 µl of dPCR product was then added to the reaction mixture containing the ssDNA-FQ and Cas12a-crRNA complex.

Spiked sample testing

This experiment was conducted by two operators. Firstly, 15 healthy crucian carps were purchased from supermarket. One operator took out the livers of crucian carp, cut them into small pieces, and then added 20 mg of tissue to the 15 tubes containing 200 µl of 0.5 M NaOH solution at clean workbench. Then, 15 tubes were numbered, and 1×10^3 CFU of *A. hydrophila* were added to some tubes. These tissue samples were grinded with a Disposable Tissue Grinding Pestle (Sangon, China) for 3 min, and upon 20-fold dilution with H_2O, 2 µl of lysate was used as the DNA template for the dRAA assay. Above was the NaOH-based method for the extraction of *A. hydrophila* genomic DNA from spiked fish (Zhang et al., 2020; Xiao et al., 2021; Zhao et al., 2022), and meanwhile, the Kit-based extraction method was also conducted as a comparative test. The other operator who did not know the number of spiked samples performed the dRAA-CRISPR/Cas12a assay.

Application of dRAA-CRISPR/Cas12a assay for human blood and stool specimens

Human blood and stool samples were provided by three healthy volunteers. The spiked samples were prepared by adding 100 µl of human blood or 200 mg of stool into the tubes containing 1×10^3 CFU of *A. hydrophila* (*aerA*$^+$*hlyA*$^+$). The MiniBEST Universal Genomic DNA Extraction Kit (9,765; TaKaRa Bio Inc., Japan) and the TIANamp Stool DNA Kit (DP328; TIANGEN BIOTECH CO. LTD, China) were employed to extract genomic DNA from these spiked samples and samples without *A. hydrophila*, which acted as negative controls. The genomic DNA of these samples were then detected by dRAA-CRISPR/Cas12a assay.

Statistical analysis

Statistical analysis was performed using SPSS 13.0 software (SPSS Inc., Chicago, IL, USA). The data were analyzed by Student's *t* test. $p < 0.05$ (indicated by *) was considered statistically significant.

Results

Screening the RAA primer pairs targeting *aerA* gene and *hlyA* gene

High amplification efficiency of the amplification assay can increase the detection sensitivity of the method (Clementi et al., 1993; Pfaffl, 2004). To obtain the primer pair with high amplification efficiency, we designed five primer pairs and four primer pairs targeting *aerA* gene and *hlyA* gene, respectively, and then screened an optimal primer pair according to the relative intensity of RAA product band for each primer pair. The results showed that all the predicted product bands were clearly distinguishable (Figure 2A). As for the *aerA* gene, the band intensity of the No.5 lane obtained with the primer set AF5 (5′-GCCATCAAGGTCAGCAATTTTGCGTACAAC-3′)/AR5 (5′- CACTTGAACTTGTTCTTGGTGGTCACCTTCTC-3′) was the strongest among the five bands, while as for the *hlyA* gene, it was the No.8 lane obtained with the primer set HF3

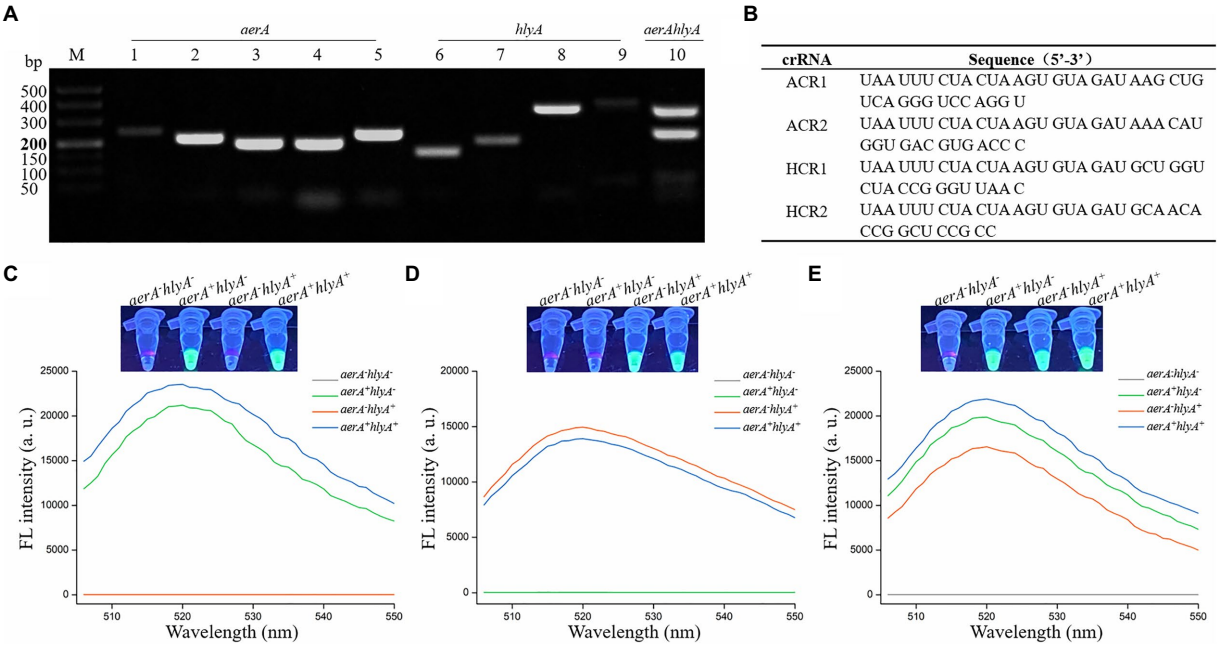

FIGURE 2
Feasibility verification of the dRAA-CRISPR/Cas12a assay in the detection of *Aeromonas hydrophila*. **(A)** Screening the RAA primer pairs. The single and dualplex RAA assays were performed using the genomic DNA extracted from *aerA*$^+$*hlyA*$^+$ *A. hydrophila* strain as the template. Lanes 1–5, screening the primer pair targeting for *aerA* gene. Lanes 6–9, screening the primer pair targeting for *hlyA* gene. Lane 10, feasibility of dRAA assay with the optimal *aerA* and *hlyA* primer pairs. **(B)** Sequences of crRNA used in this study. **(C–E)** Feasibility verification of the dRAA-CRISPR/Cas12a assay using the ACR1 and ACR2 **(C)**, HCR1 and HCR2 **(D)**, and ACR1, ACR2, HCR1 and HCR2 **(E)** in the detection of four *A. hydrophila* strains. Fluorescence signals were read using an UV flashlight (upper) or a multifunctional microplate reader (below).

(5′- CACGTGGCCTTCTACCTCAACGTCAACC-3′)/HR3 (5′-CCTTGGTGTTGGACGCCTCGATGCTGAA-3′). Furthermore, these two primer sets were used to amplify *aerA* gene and *hlyA* gene through dRAA assay, and the result showed that two predicted bands with satisfactory intensity were present at the No.10 lane. Therefore, the RAA primer sets, AF5/AR5 and HF3/HR3, were chosen as the optimal primers for the dRAA reaction, and the amplicon of AF5/AR5 and HF3/HR3 was used to design crRNA for *aerA* and *hlyA*, respectively.

Feasibility verification of the dRAA-CRISPR/Cas12a assay in the detection of *Aeromonas hydrophila*

According to the principle of crRNA design mentioned in Materials and Methods, ACR1 and ACR2, targeting *aerA* gene, and HCR1 and HCR2, targeting *hlyA* gene, were designed, and the sequences of these four crRNAs were listed in Figure 2B. To investigate the validity of the designed crRNA and verify the feasibility of the dRAA-CRISPR/Cas12a method, the dRAA-CRISPR/Cas12a assays for the detection of four *A. hydrophila* strains (*aerA*$^-$*hlyA*$^-$, *aerA*$^+$*hlyA*$^-$, *aerA*$^-$*hlyA*$^+$ and *aerA*$^+$*hlyA*$^+$) were performed using the ACR1 and ACR2 (Figure 2C), HCR1 and HCR2 (Figure 2D), and ACR1, ACR2, HCR1 and HCR2 (Figure 2E), respectively. As shown in Figure 2C, only the genomic DNA samples extracted from *aerA*$^+$*hlyA*$^-$ and *aerA*$^+$*hlyA*$^+$ *A. hydrophila* strains could generate fluorescence signals, indicating that ACR1 and ACR2 were valid and specific crRNAs in the detection of *A. hydrophila* expressing *aerA* gene. Our results also indicated that HCR1 and HCR2 were valid and specific crRNAs in the detection of *A. hydrophila* expressing *hlyA* gene (Figure 2D). Furthermore, as shown in Figure 2E, only the genomic DNA samples extracted from *A. hydrophila* expressing *aerA* and/or *hlyA* genes could generate fluorescence signals, indicating that our developed method, dRAA-CRISPR/Cas12a, using ACR1, ACR2, HCR1 and HCR2 as the crRNAmix could be used to detect the pathogenic *A. hydrophila* expressing *aerA* and/or *hlyA* genes.

Optimization of the conditions of dRAA-CRISPR/Cas12a assay

The concentrations of Cas12a and ssDNA-FQ and the Cas12a cleavage time are related to cleavage efficiency, signal output, and reaction speed of the CRISPR-based detection method (Broughton et al., 2020; Sun et al., 2020; Fu et al., 2022). To achieve an ideal reaction performance, dRAA-CRISPR/Cas12a assay was conducted to optimize the concentration of Cas12a, the concentration of ssDNA-FQ and the Cas12a cleavage time with the *aerA*$^+$*hlyA*$^+$ *A. hydrophila* genomic DNA (1×10^4 copies/μL)

and H_2O as templates. The ratio of the fluorescence intensity triggered by *A. hydrophila* (F) to the fluorescence intensity triggered by H_2O (F_0) was employed to assess the reaction concentrations of Cas12a and ssDNA-FQ. As shown in Figure 3A, both the F and F_0 increased with the increasing of the Cas12a concentrations, and when the Cas12a concentration was 600 nm, the ratio of F/F_0 reached maximum. As shown in Figure 3B, the results indicated that the optimal concentration of ssDNA-FQ was 500 nm. The cleavage time of Cas12a was further explored using the optimized concentrations of Cas12a (600 nm) and ssDNA-FQ (500 nm). The results showed that the increasing of F reached a plateau after 25 min, which indicated that the optimal cleavage time of Cas12a was 25 min. Therefore, the reaction conditions of our developed method, dRAA-CRISPR/Cas12a, were as followed: 20 min of RAA reaction, 5 µl of 600 nm Cas12a, 5 µl of 400 nm crRNAmix, 10 µl of 500 nm ssDNA-FQ, and 25 min of Cas12a cleavage, and in the subsequent experiments, dRAA-CRISPR/Cas12a assays were conducted according to the above conditions.

Sensitivity of dRAA-CRISPR/Cas12a assay for detecting *Aeromonas hydrophila*

To investigate the detection sensitivity of dRAA-CRISPR/Cas12a assay for pathogenic *A. hydrophila*, 2 µl of the genomic DNA with different concentrations (1×10^0–1×10^6 copies /µL) extracted from three *A. hydrophila* strains (*aerA*$^+$*hlyA*$^-$, *aerA*$^-$*hlyA*$^+$ and *aerA*$^+$*hlyA*$^+$) were used as templates to perform the dRAA assay, and then 2 µl of dRAA product was subjected to Cas12a cleavage test. The dPCR-CRISPR/Cas12a assay was conducted as a comparative test. The results of dRAA-CRISPR/Cas12a assays showed that fluorescence signals were detected in all samples except negative control (H_2O; Figure 4A), and the limit of detection (LOD) of dRAA-CRISPR/Cas12a assay for each *A. hydrophila* strain reached 2 copies per reaction, which was in line with the LOD of dPCR-CRISPR/Cas12a assay (Figure 4B). Therefore, our developed detection method, dRAA-CRISPR/Cas12a, showed high sensitivity (2 copies/reaction) for pathogenic *A. hydrophila* expressing *aerA* and/or *hlyA* genes.

Specificity of dRAA-CRISPR/Cas12a assay for detecting *Aeromonas hydrophila*

To evaluate the specificity of dRAA-CRISPR/Cas12a assay in *A. hydrophila* detection, 16 genomic DNA samples extracted from four *A. hydrophila* strains and 12 other strains of waterborne and/or foodborne pathogenic bacteria were used as dRAA templates, and H_2O was used as negative control. As shown in Figure 5, one *A. hydrophila* strain (*aerA*$^-$*hlyA*$^-$) and 12 other bacterial strains did not generate the fluorescence signal, while it was only detected in three *A. hydrophila* strains expressing *aerA* and/or *hlyA* genes, indicating no cross-reactions with non-pathogenic *A. hydrophila* and non-*Aeromonas hydrophila* bacteria of dRAA-CRISPR/Cas12a assay in pathogenic *A. hydrophila* detection. Therefore, our developed detection method, dRAA-CRISPR/Cas12a, showed high specificity for pathogenic *A. hydrophila* expressing *aerA* and/or *hlyA* genes.

Practicability evaluation of the dRAA-CRISPR/Cas12a assay in the detection of spiked samples

Finally, to evaluate the practicability of the dRAA-CRISPR/Cas12a assay, fish and human samples were employed to conduct this experiment by two operators. For fish samples, livers were taken out from 15 healthy crucian carps, nine liver samples (20 mg/sample) were spiked with 1×10^3 CFU of *A. hydrophila*, and then the genomic

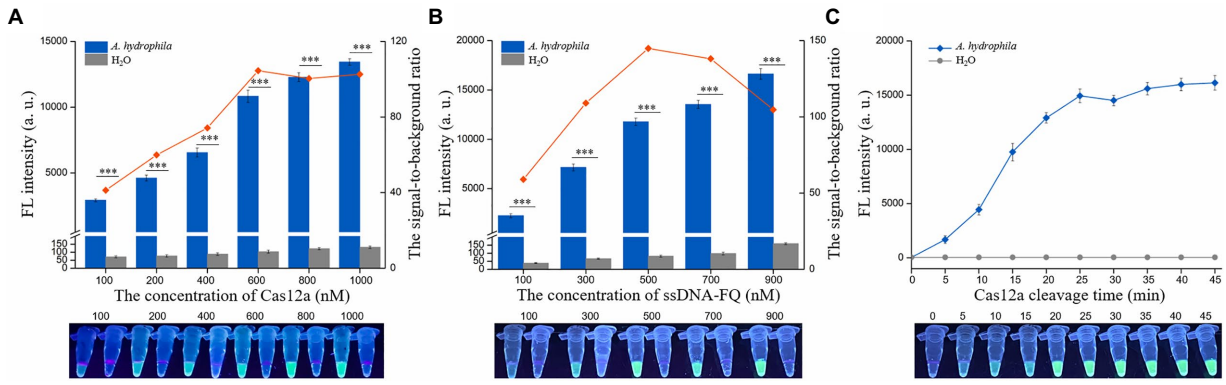

FIGURE 3
Optimization of the conditions of dRAA-CRISPR/Cas12a assay. The dRAA-CRISPR/Cas12a assays were conducted using AF5/AR5 and HF3/HR3 as RAA primer sets, *aerA*$^+$*hlyA*$^+$ *A. hydrophila* genomic DNA (1×10^4 copies/µl) or H_2O as a RAA template, and ACR1, ACR2, HCR1 and HCR2 as crRNAmix to optimize the concentration of Cas12a **(A)** and ssDNA-FQ **(B)** and the cleavage time of Cas12a **(C)**. The results were read using an UV flashlight (below) or a multifunctional microplate reader (upper). **(A,B)** $n=3$ technical replicates; two-tailed Student's *t* test; ***$p<0.001$; bars represent mean±SEM.

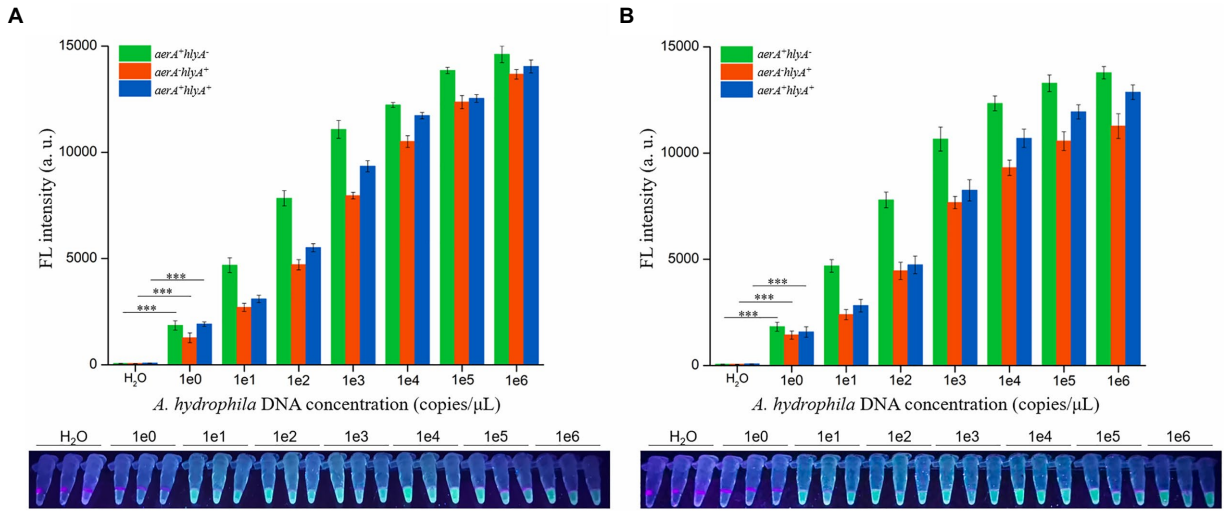

FIGURE 4
Sensitivity evaluation. Sensitivity of dRAA-CRISPR/Cas12a **(A)** and dPCR-CRISPR/Cas12a **(B)** assays were evaluated in the detection of pathogenic *Aeromonas hydrophila*. The different concentrations (1×10^0–1×10^6 copies/μl) of *A. hydrophila* genomic DNA were used as the detection template, and H_2O was used as a negative control. The results were read using an UV flashlight (below) or a multifunctional microplate reader (upper). n=3 technical replicates; two-tailed Student's t test; ***p<0.001, experimental group versus corresponding negative control group (only shown the 1e0 vs. H_2O); bars represent mean±SEM.

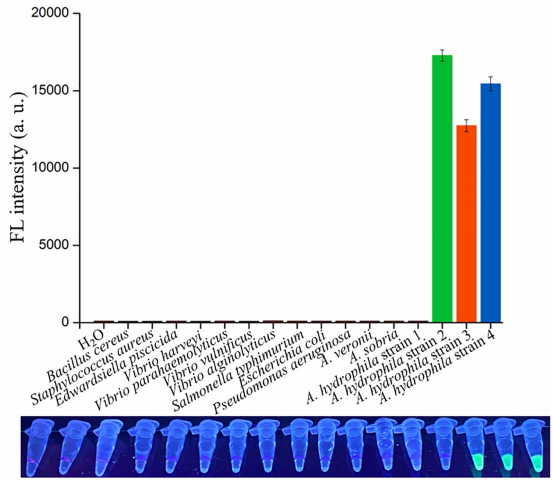

FIGURE 5
Specificity and practicability evaluation of dRAA-CRISPR/Cas12a assay. Specificity evaluation. 16 bacterial strains were employed to evaluate the specificity of dRAA-CRISPR/Cas12a assay in the detection of *A. hydrophila*. *A. hydrophila* strain 1, 2, 3, and 4 were *aerA*$^-$*hlyA*$^-$, *aerA*$^+$*hlyA*$^-$, *aerA*$^-$*hlyA*$^+$, and *aerA*$^+$*hlyA*$^+$, respectively. H_2O was used as a negative control. n=3 technical replicates; bars represent mean±SEM.

DNA was extracted using the NaOH-based method from these 15 liver samples by one operator, while the other one did the dRAA-CRISPR/Cas12a and dPCR-CRISPR/Cas12a assays with these 15 liver samples. The results of dRAA-CRISPR/Cas12a assays showed that only the spiked samples could generate the fluorescence signal (Figure 6A). This result was consistent with the result obtained from dPCR-CRISPR/Cas12a assays (Figures 6B,C). In addition, the genomic DNA extracted from the other 15 liver samples using Kit-based method were detected by dRAA-CRISPR/Cas12a assay, and the same result with Figure 6A was obtained (Supplementary Figure S3). Therefore, these results indicated that our developed method, dRAA-CRISPR/Cas12a, could rapidly and accurately detect *A. hydrophila* from fish samples.

For human samples, blood and stool samples were collected from three healthy volunteers, and some blood and stool were spiked with 1×10^3 CFU of *A. hydrophila* (*aerA*$^+$*hlyA*$^+$). As shown in Figure 6D, only the spiked samples could generate the fluorescence signal. These results indicated that our developed method, dRAA-CRISPR/Cas12a, could be used to detect clinical sepsis and gastroenteritis caused by *A. hydrophila*.

Discussion

Aeromonas hydrophila is an emerging pathogen with pathogenicity to humans and fishes (Tichoniuk et al., 2010; Li et al., 2011). Increasingly, *A. hydrophila* is posing a serious threat to human health, aquaculture and food safety, and foodborne outbreaks of its infection have occurred in many countries (Morena et al., 1993; Krovacek et al., 1995; Zhang et al., 2012; Tsheten et al., 2016). Many studies have reported that the pathogenicity of *A. hydrophila* is determined by multiple virulence factors (Janda and Abbott, 2010; Tichoniuk et al., 2010; Li et al., 2011), and based on this reason, there are many methods targeting one or more virulence genes to detect pathogenic *A. hydrophila* (Tichoniuk et al., 2010; Uma et al., 2010; Li et al., 2011; Elsheshtawy et al., 2019; Qu et al., 2021). However, these methods have some flaws, such as long operation time, low sensitivity, complicated operation, and missed

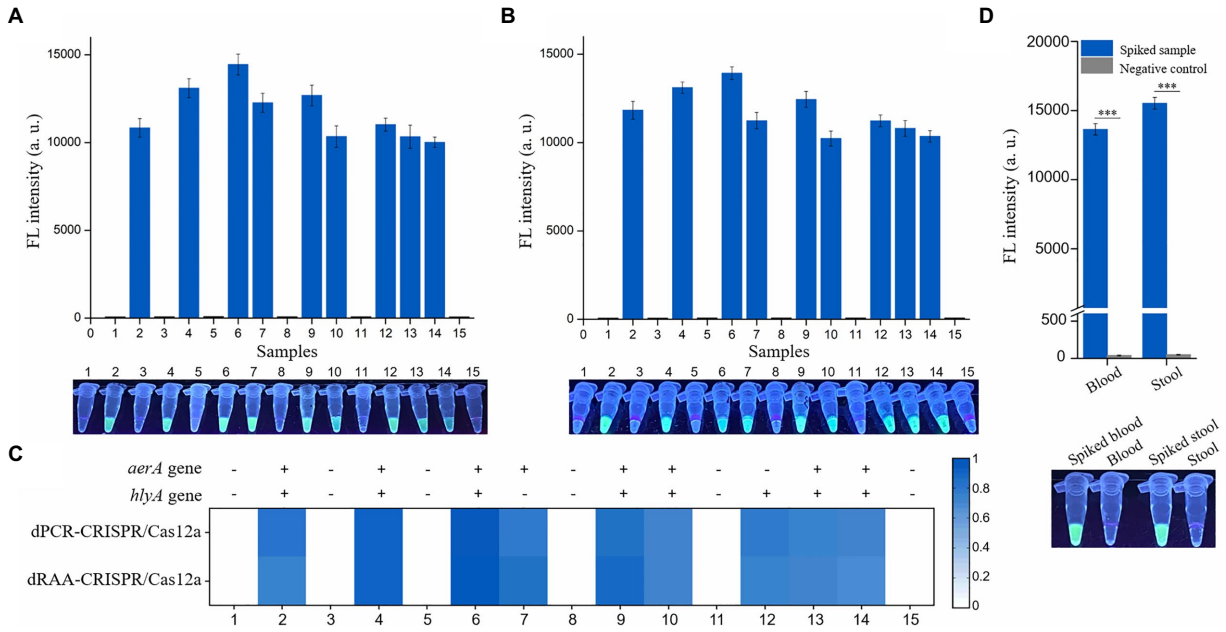

FIGURE 6
Practicability evaluation of the dRAA-CRISPR/Cas12a and dPCR-CRISPR/Cas12a assays in the detection of spiked samples. Six normal liver samples and nine liver samples spiked with 1×10^3CFU of *A. hydrophila* were used to extract genomic DNA according to the NaOH-based method. These genomic DNA samples were detected using dRAA-CRISPR/Cas12a **(A)** and dPCR-CRISPR/Cas12a **(B)** assays. n=3 technical replicates; bars represent mean±SEM. **(C)** Heatmap of the results of the two assays for the detection of *A. hydrophila* from 15 crucian carps. **(D)** Human blood and stool samples were spiked with 1×10^3CFU of *A. hydrophila* (*aerA*$^+$*hlyA*$^+$). Normal blood and stool samples were served as negative controls. The fluorescence signals were read using an UV flashlight (below) or a multifunctional microplate reader (upper). n=3 technical replicates; two-tailed Student's t test; ***p<0.001; bars represent mean±SEM.

detection. In this study, to avoid these flaws, we developed a novel method, dRAA-CRISPR/Cas12a, for the detection of pathogenic *A. hydrophila* targeting *aerA* and *hlyA* genes based on dRAA assay and CRISPR/Cas12a system (Figure 1). This method performed according to our optimized conditions only takes 45 min to obtain the accurate result without an elaborate instrument (Figure 3), and the LOD of it is as low as 2 copies of *A. hydrophila* genomic DNA per reaction (Figure 4A).

The target genes, *aerA* and *hlyA*, encoding aerolysin and hemolysin respectively, of our proposed method are two important virulent genes of *A. hydrophila* (Wong et al., 1998; Biscardi et al., 2002; Ørmen et al., 2003; Janda and Abbott, 2010). Aerolysin and hemolysin are most common in clinical and environmental strains of *A. hydrophila* (Wong et al., 1998; González-Rodríguez et al., 2002; Janda and Abbott, 2010) and play key roles through cooperation or alone in the pathogenicity of it (Biscardi et al., 2002; Singh et al., 2008; Nawaz et al., 2010; Igbinosa and Okoh, 2013). Moreover, the study reported by Heuzenroeder et al. indicated that a method targeting *aerA* and *hlyA* genes was a trustworthy approach to detect pathogenic *A. hydrophila* (Heuzenroeder et al., 1999). Therefore, *aerA* and *hlyA* genes were selected for the detection of pathogenic *A. hydrophila* in this study. Because *aerA* and *hlyA* genes are also present in some other species of *Aeromonas*, the published *aerA* and *hlyA* sequences were downloaded from GenBank and aligned to seek the sequences which are highly conserved in *A. hydrophila* but not in other *Aeromonas* species (Supplementary Figures S4–S7), and based on these sequences, we successfully designed two crRNAs for *aerA* and two crRNAs for *hlyA* (Figures 2B–E). Furthermore, the results of specificity experiment indicated that only three *A. hydrophila* strains expressing *aerA* gene and/or *hlyA* gene could be detected by our developed method, dRAA-CRISPR/Cas12a (Figure 5), which further confirmed the validity of our designed crRNA and RAA primer sets.

In addition, we investigated the sensitivity of dRAA-CRISPR/Cas12a in the detection of three pathogenic *A. hydrophila* strains (*aerA*$^+$*hlyA*$^-$, *aerA*$^-$*hlyA*$^+$ and *aerA*$^+$*hlyA*$^+$), and found that the LOD for each strain reached 2 copies of genomic DNA per reaction (Figure 4A), which was consistent with the results of dPCR-CRISPR/Cas12a (Figure 4B). However, because the samples used to investigate the sensitivity of dRAA-CRISPR/Cas12a were the pure bacteria, the result of this experiment may not reflect the real sensitivity of dRAA-CRISPR/Cas12a in detecting the clinical and environmental samples with a large number of impurities that may influence the amplification efficiency of RAA assay. Finally, we evaluated the practicability of the dRAA-CRISPR/Cas12a assay in the detection of spiked fish samples. Our proposed method dRAA-CRISPR/Cas12a could only detect the presence of *A. hydrophila* from all the spiked liver samples (Figure 6A), and this result completely matched the results got from dPCR-CRISPR/Cas12a assay (Figures 6B,C), indicating that dRAA-CRISPR/Cas12a method is a promising candidate for on-site

A. hydrophila detection in fish samples. Because *A. hydrophila* infection mainly causes sepsis and gastroenteritis in humans (González-Serrano et al., 2002; Zhu et al., 2021), we also performed dRAA-CRISPR/Cas12a method to detect the spiked blood and stool samples, and found that the fluorescence signal could only be detected in spiked blood and stool samples (Figure 6D), indicating that the dRAA-CRISPR/Cas12a method can also be used to diagnose patients infected by *A. hydrophila*.

In conclusion, the dRAA-CRISPR/Cas12a method we developed can rapidly, accurately, and sensitively detect pathogenic *A. hydrophila* expressing *aerA* gene and/or *hlyA* gene, and the results can be read using an UV flashlight. It is very beneficial for early diagnosis and on-site detection of *A. hydrophila* infection especially in resource-poor areas. Apart from dRAA-CRISPR/Cas12a method, dPCR-CRISPR/Cas12a used in this study can also be a candidate to detect *A. hydrophila* in Lab.

Data availability statement

The original contributions presented in the study are included in the article/Supplementary material, further inquiries can be directed to the corresponding authors.

Author contributions

XX and YL conceived and designed the study. XX and ZL wrote the manuscript. ZL, JL, and SW performed the experiments and analyzed the data. XL and LZ reviewed the manuscript. All authors read and approved the submitted version.

Funding

This study was supported by the National Natural Science Foundation of China (grant no. 82002117), the Science and Technology Bureau of Wenzhou (grant no. Y20210109), and the Key Discipline of Zhejiang Province in Medical Technology (First Class, Category A).

Conflict of interest

The authors declare that the research was conducted in the absence of any commercial or financial relationships that could be construed as a potential conflict of interest.

Publisher's note

All claims expressed in this article are solely those of the authors and do not necessarily represent those of their affiliated organizations, or those of the publisher, the editors and the reviewers. Any product that may be evaluated in this article, or claim that may be made by its manufacturer, is not guaranteed or endorsed by the publisher.

Supplementary material

The Supplementary material for this article can be found online at: https://www.frontiersin.org/articles/10.3389/fmicb.2022.973996/full#supplementary-material

References

Abbott, S. L., Cheung, W. K., and Janda, J. M. (2003). The genus *Aeromonas*: biochemical characteristics, atypical reactions, and phenotypic identification schemes. *J. Clin. Microbiol.* 41, 2348–2357. doi: 10.1128/JCM.41.6.2348-2357.2003

Balakrishna, K., Murali, H. S., and Batra, H. V. (2010). Detection of toxigenic strains of *Aeromonas* species in foods by a multiplex PCR assay. *Indian J. Microbiol.* 50, 139–144. doi: 10.1007/s12088-010-0038-5

Balsalobre, L. C., Dropa, M., Matte, G. R., and Matte, M. H. (2009). Molecular detection of enterotoxins in environmental strains of *Aeromonas hydrophila* and *Aeromonas jandaei*. *J. Water Health* 7, 685–691. doi: 10.2166/wh.2009.082

Biscardi, D., Castaldo, A., Gualillo, O., and De Fusco, R. (2002). The occurrence of cytotoxic *Aeromonas hydrophila* strains in Italian mineral and thermal waters. *Sci. Total Environ.* 292, 255–263. doi: 10.1016/s0048-9697(01)01132-9

Broughton, J. P., Deng, X., Yu, G., Fasching, C. L., Servellita, V., Singh, J., et al. (2020). CRISPR-Cas12-based detection of SARS-CoV-2. *Nat. Biotechnol.* 38, 870–874. doi: 10.1038/s41587-020-0513-4

Chauret, C., Volk, C., Creason, R., Jarosh, J., Robinson, J., and Warnes, C. (2001). Detection of *Aeromonas hydrophila* in a drinking-water distribution system: a field and pilot study. *Can. J. Microbiol.* 47, 782–786. doi: 10.1139/w01-070

Chen, J. S., Ma, E., Harrington, L. B., Da Costa, M., Tian, X., Palefsky, J. M., et al. (2018). CRISPR-Cas12a target binding unleashes indiscriminate single-stranded DNase activity. *Science* 360, 436–439. doi: 10.1126/science.aar6245

Clementi, M., Menzo, S., Bagnarelli, P., Manzin, A., Valenza, A., and Varaldo, P. E. (1993). Quantitative PCR and RT-PCR in virology. *PCR Methods Appl.* 2, 191–196. doi: 10.1101/gr.2.3.191

Daskalov, H. (2006). The importance of *Aeromonas hydrophila* in food safety. *Food Control* 17, 474–483. doi: 10.1016/j.foodcont.2005.02.009

Elsheshtawy, A., Yehia, N., Elkemary, M., and Soliman, H. (2019). Direct detection of unamplified *Aeromonas hydrophila* DNA in clinical fish samples using gold nanoparticle probe-based assay. *Aquaculture* 500, 451–457. doi: 10.1016/j.aquaculture.2018.10.046

Fu, X., Sun, J., Ye, Y., Zhang, Y., and Sun, X. (2022). A rapid and ultrasensitive dual detection platform based on Cas12a for simultaneous detection of virulence and resistance genes of drug-resistant salmonella. *Biosens. Bioelectron.* 195:113682. doi: 10.1016/j.bios.2021.113682

González-Rodríguez, M., Santos, J., Otero, A., and García-López, M. (2002). PCR detection of potentially pathogenic aeromonads in raw and cold-smoked freshwater fish. *J. Appl. Microbiol.* 93, 675–680. doi: 10.1046/j.1365-2672.2002.01739.x

González-Serrano, C., Santos, J., García-López, M., and Otero, A. (2002). Virulence markers in *Aeromonas hydrophila* and *Aeromonas veronii* biovar *sobria* isolates from freshwater fish and from a diarrhoea case. *J. Appl. Microbiol.* 93, 414–419. doi: 10.1046/j.1365-2672.2002.01705.x

Heuzenroeder, M. W., Wong, C. Y., and Flower, R. L. (1999). Distribution of two hemolytic toxin genes in clinical and environmental isolates of *Aeromonas* spp.: correlation with virulence in a suckling mouse model. *FEMS Microbiol. Lett.* 174, 131–136. doi: 10.1111/j.1574-6968.1999.tb13559.x

Hussain, I. A., Jeyasekaran, G., Shakila, R. J., Raj, K. T., and Jeevithan, E. (2014). Detection of hemolytic strains of *Aeromonas hydrophila* and *A. sobria* along with other *Aeromonas* spp. from fish and fishery products by multiplex PCR. *J. Food Sci. Technol.* 51, 401–407. doi: 10.1007/s13197-013-1190-9

Igbinosa, I. H., and Okoh, A. I. (2013). Detection and distribution of putative virulence associated genes in *Aeromonas* species from freshwater and wastewater treatment plant. *J. Basic Microbiol.* 53, 895–901. doi: 10.1002/jobm.201200351

Janda, J. M., and Abbott, S. L. (2010). The genus *Aeromonas*: taxonomy, pathogenicity, and infection. *Clin. Microbiol. Rev.* 23, 35–73. doi: 10.1128/CMR.00039-09

Krovacek, K., Dumontet, S., Eriksson, E., and Baloda, S. B. (1995). Isolation, and virulence profiles, of *Aeromonas hydrophila* implicated in an outbreak of food poisoning in Sweden. *Microbiol. Immunol.* 39, 655–661. doi: 10.1111/j.1348-0421.1995.tb03253.x

Li, S. Y., Cheng, Q. X., Liu, J. K., Nie, X. Q., Zhao, G. P., and Wang, J. (2018a). CRISPR-Cas12a has both cis- and trans-cleavage activities on single-stranded DNA. *Cell Res.* 28, 491–493. doi: 10.1038/s41422-018-0022-x

Li, S. Y., Cheng, Q. X., Wang, J. M., Li, X. Y., Zhang, Z. L., Gao, S., et al. (2018b). CRISPR-Cas12a-assisted nucleic acid detection. *Cell Discov.* 4:20. doi: 10.1038/s41421-018-0028-z

Li, J., Ni, X., Liu, Y., and Lu, C. (2011). Detection of three virulence genes alt, ahp and aerA in *Aeromonas hydrophila* and their relationship with actual virulence to zebrafish. *J. Appl. Microbiol.* 110, 823–830. doi: 10.1111/j.1365-2672.2011.04944.x

Li, F., Ye, Q., Chen, M., Zhou, B., Zhang, J., Pang, R., et al. (2021). An ultrasensitive CRISPR/Cas12a based electrochemical biosensor for listeria monocytogenes detection. *Biosens. Bioelectron.* 179:113073. doi: 10.1016/j.bios.2021.113073

Longyant, S., Chaiyasittrakul, K., Rukpratanporn, S., Chaivisuthangkura, P., and Sithigorngul, P. (2010). Simple and direct detection of *Aeromonas hydrophila* infection in the goldfish, *Carassius auratus* (L.), by dot blotting using specific monoclonal antibodies. *J. Fish Dis.* 33, 973–984. doi: 10.1111/j.1365-2761.2010.01197.x

Meng, S., Wang, Y., Wang, Y., Liu, D., and Ye, C. (2015). Development of cross-priming amplification assays for rapid and sensitive detection of *Aeromonas hydrophila*. *Lett. Appl. Microbiol.* 61, 171–178. doi: 10.1111/lam.12439

Morena, M. L., Van, R., Singh, K., Brian, M., Murray, B. E., and Pickering, L. K. (1993). Diarrhea associated with *Aeromonas* species in children in day care centers. *J. Infect. Dis.* 168, 215–218. doi: 10.1093/infdis/168.1.215

Nagamine, K., Hase, T., and Notomi, T. (2002). Accelerated reaction by loop-mediated isothermal amplification using loop primers. *Mol. Cell. Probes* 16, 223–229. doi: 10.1006/mcpr.2002.0415

Nagar, V., Shashidhar, R., and Bandekar, J. R. (2011). Prevalence, characterization, and antimicrobial resistance of *Aeromonas* strains from various retail food products in Mumbai, India. *J. Food Sci.* 76, M486–M492. doi: 10.1111/j.1750-3841.2011.02303.x

Nawaz, M., Khan, S. A., Khan, A. A., Sung, K., Tran, Q., Kerdahi, K., et al. (2010). Detection and characterization of virulence genes and integrons in *Aeromonas veronii* isolated from catfish. *Food Microbiol.* 27, 327–331. doi: 10.1016/j.fm.2009.11.007

Nielsen, M. E., Høi, L., Schmidt, A., Qian, D., Shimada, T., Shen, J., et al. (2001). Is *Aeromonas hydrophila* the dominant motile *Aeromonas* species that causes disease outbreaks in aquaculture production in the Zhejiang Province of China? *Dis. Aquat. Org.* 46, 23–29. doi: 10.3354/dao046023

Ørmen, Ø., Regue, M. Q., Tomás, J. M., and Granum, P. E. (2003). Studies of aerolysin promoters from different *Aeromonas* spp. *Microb. Pathog.* 35, 189–196. doi: 10.1016/s0882-4010(03)00124-4

Özbaş, Z. Y., Lehner, A., and Wagner, M. (2000). Development of a multiplex and semi-nested PCR assay for detection of *Yersinia enterocolitica* and *Aeromonas hydrophila* in raw milk. *Food Microbiol.* 17, 197–203. doi: 10.1006/fmic.1999.0298

Pfaffl, M. W. (2004). Quantification strategies in real-time PCR. *AZ Quantit. PCR* 1, 89–113.

Piepenburg, O., Williams, C. H., Stemple, D. L., and Armes, N. A. (2006). DNA detection using recombination proteins. *PLoS Biol.* 4:e204. doi: 10.1371/journal.pbio.0040204

Qu, Y., Wang, Q., Li, Y., Wang, Y., Yin, J., Ren, Y., et al. (2021). Development of a real-time recombinase polymerase amplification assay for rapid detection of *Aeromonas hydrophila*. *J. Fish Dis.* 44, 469–477. doi: 10.1111/jfd.13291

Singh, V., Rathore, G., Kapoor, D., Mishra, B., and Lakra, W. (2008). Detection of aerolysin gene in *Aeromonas hydrophila* isolated from fish and pond water. *Indian J. Microbiol.* 48, 453–458. doi: 10.1007/s12088-008-0056-8

Subsoontorn, P., Lohitnavy, M., and Kongkaew, C. (2020). The diagnostic accuracy of isothermal nucleic acid point-of-care tests for human coronaviruses: a systematic review and meta-analysis. *Sci. Rep.* 10, 22349–22313. doi: 10.1038/s41598-020-79237-7

Sun, H.-H., He, F., Wang, T., Yin, B.-C., and Ye, B.-C. (2020). A Cas12a-mediated cascade amplification method for microRNA detection. *Analyst* 145, 5547–5552. doi: 10.1039/d0an00370k

Sun, Y., Zhao, Y., Xu, W., Fang, R., Wu, Q., He, H., et al. (2021). Taxonomy, virulence determinants and antimicrobial susceptibility of *Aeromonas* spp. isolated from bacteremia in southeastern China. *Antimicrob. Resist. Infect. Control* 10:43. doi: 10.1186/s13756-021-00911-0

Swain, P., Nayak, S., Sahu, A., Meher, P., and Mishra, B. (2003). High antigenic cross-reaction among the bacterial species responsible for diseases of cultured freshwater fishes and strategies to overcome it for specific serodiagnosis. *Comp. Immunol. Microbiol. Infect. Dis.* 26, 199–211. doi: 10.1016/s0147-9571(02)00059-0

Tichoniuk, M., Gwiazdowska, D., Ligaj, M., and Filipiak, M. (2010). Electrochemical detection of foodborne pathogen *Aeromonas hydrophila* by DNA hybridization biosensor. *Biosens. Bioelectron.* 26, 1618–1623. doi: 10.1016/j.bios.2010.08.030

Tsai, Y. H., Shen, S. H., Yang, T. Y., Chen, P. H., Huang, K. C., and Lee, M. S. (2015). Monomicrobial necrotizing fasciitis caused by *Aeromonas hydrophila* and *Klebsiella pneumoniae*. *Med. Princ. Pract.* 24, 416–423. doi: 10.1159/000431094

Tsheten, T., Tshering, D., Gyem, K., Dorji, S., Wangchuk, S., Tenzin, T., et al. (2016). An outbreak of *Aeromonas hydrophila* food poisoning in deptsang village, Samdrup Jongkhar, Bhutan, 2016. *J. Res. Health. Sci.* 16, 224–227. PMID: 28087856

Uma, A., Rebecca, G., Meena, S., and Saravanabava, K. (2010). PCR detection of putative aerolysin and hemolysin genes in an *Aeromonas hydrophila* isolate from infected Koi carp (*Cyprinus carpio*). *Tamil. J. Vet. Anim. Sci.* 6, 31–33.

Wang, G., Clark, C. G., Liu, C., Pucknell, C., Munro, C. K., Kruk, T. M., et al. (2003). Detection and characterization of the hemolysin genes in *Aeromonas hydrophila* and *Aeromonas sobria* by multiplex PCR. *J. Clin. Microbiol.* 41, 1048–1054. doi: 10.1128/JCM.41.3.1048-1054.2003

Wang, R., Zhang, F., Wang, L., Qian, W., Qian, C., Wu, J., et al. (2017). Instant, visual, and instrument-free method for on-site screening of GTS 40-3-2 soybean based on body-heat triggered recombinase polymerase amplification. *Anal. Chem.* 89, 4413–4418. doi: 10.1021/acs.analchem.7b00964

Wong, C. Y., Heuzenroeder, M. W., and Flower, R. L. (1998). Inactivation of two haemolytic toxin genes in *Aeromonas hydrophila* attenuates virulence in a suckling mouse model. *Microbiology* 144, 291–298. doi: 10.1099/00221287-144-2-291

Xiao, X., Lin, Z., Huang, X., Lu, J., Zhou, Y., Zheng, L., et al. (2021). Rapid and sensitive detection of *Vibrio vulnificus* using CRISPR/Cas12a combined with a recombinase-aided amplification assay. *Front. Microbiol.* 12:767315. doi: 10.3389/fmicb.2021.767315

Zhang, M., Liu, C., Shi, Y., Wu, J., Wu, J., and Chen, H. (2020). Selective endpoint visualized detection of Vibrio parahaemolyticus with CRISPR/Cas12a assisted PCR using thermal cycler for on-site application. *Talanta* 214:120818. doi: 10.1016/j.talanta.2020.120818

Zhang, Q., Shi, G. Q., Tang, G. P., Zou, Z. T., Yao, G. H., and Zeng, G. (2012). A foodborne outbreak of *Aeromonas hydrophila* in a college, Xingyi City, Guizhou, China, 2012. *Western Pac. Surveill Response J.* 3, 39–43. doi: 10.5365/WPSAR.2012.3.4.018

Zhao, G., Wang, J., Yao, C., Xie, P., Li, X., Xu, Z., et al. (2022). Alkaline lysis-recombinase polymerase amplification combined with CRISPR/Cas12a assay for the ultrafast visual identification of pork in meat products. *Food Chem.* 383:132318. doi: 10.1016/j.foodchem.2022.132318

Zhou, S., Wang, M., Liu, M., Jiang, K., Wang, B., and Wang, L. (2020). Rapid detection of *Enterocytozoon hepatopenaei* in shrimp through an isothermal recombinase polymerase amplification assay. *Aquaculture* 521:734987. doi: 10.1016/j.aquaculture.2020.734987

Zhu, G., Zeng, C., Yuan, S., and Li, R. (2021). Emergency amputation necessitated within 24 hours by a human bite: a case report. *J. Int. Med. Res.* 49:3000605211012201. doi: 10.1177/03000605211012201

frontiers | Frontiers in Microbiology

TYPE Review
PUBLISHED 25 October 2022
DOI 10.3389/fmicb.2022.1019876

OPEN ACCESS

EDITED BY
Kamal El Bissati,
The University of Chicago,
United States

REVIEWED BY
Shawn Babiuk,
National Centre for Foreign Animal Disease (NCFAD), Canada
Fangfeng Yuan,
University of Illinois at Urbana-Champaign, United States

*CORRESPONDENCE
Shuangqi Fan
shqfan@scau.edu.cn
Jinding Chen
jdchen@scau.edu.cn

SPECIALTY SECTION
This article was submitted to Infectious Agents and Disease, a section of the journal Frontiers in Microbiology

RECEIVED 15 August 2022
ACCEPTED 30 September 2022
PUBLISHED 25 October 2022

CITATION
Chen W, Wang W, Wang X, Li Z, Wu K, Li X, Li Y, Yi L, Zhao M, Ding H, Fan S and Chen J (2022) Advances in the differential molecular diagnosis of vesicular disease pathogens in swine.
Front. Microbiol. 13:1019876.
doi: 10.3389/fmicb.2022.1019876

Advances in the differential molecular diagnosis of vesicular disease pathogens in swine

Wenxian Chen[1,2], Weijun Wang[1,2], Xinyan Wang[1,2], Zhaoyao Li[1,2], Keke Wu[1,2], Xiaowen Li[1,2], Yuwan Li[1,2,3], Lin Yi[1,2,3], Mingqiu Zhao[1,2,3], Hongxing Ding[1,2,3], Shuangqi Fan[1,2]* and Jinding Chen[1,2]*

[1]College of Veterinary Medicine, South China Agricultural University, Guangzhou, China, [2]Guangdong Laboratory for Lingnan Modern Agriculture, Guangzhou, China, [3]Key Laboratory of Zoonosis Prevention and Control of Guangdong Province, Guangzhou, China

Foot-and-mouth disease virus (FMDV), Senecavirus A (SVA) and swine vesicular disease virus (SVDV) are members of the family Picornaviridae, which can cause similar symptoms - vesicular lesions in the tissues of the mouth, nose, feet, skin and mucous membrane of animals. Rapid and accurate diagnosis of these viruses allows for control measures to prevent the spread of these diseases. Reverse transcription-polymerase chain reaction (RT-PCR) and real-time RT-PCR are traditional and reliable methods for pathogen detection, while their amplification reaction requires a thermocycler. Isothermal amplification methods including loop-mediated isothermal amplification and recombinase polymerase amplification developed in recent years are simple, rapid and do not require specialized equipment, allowing for point of care diagnostics. Luminex technology allows for simultaneous detection of multiple pathogens. CRISPR-Cas diagnostic systems also emerging nucleic acid detection technologies which are very sensitivity and specificity. In this paper, various nucleic acid detection methods aimed at vesicular disease pathogens in swine (including FMDV, SVA and SVDV) are summarized.

KEYWORDS

FMDV, SVA, SVDV, PCR, isothermal amplification, Luminex, CRISPR-Cas, differential diagnosis

Introduction

Picornaviruses are small non-enveloped viruses containing a single-stranded and positive-sense RNA protected by an icosahedral capsid (Holland et al., 1960; Kim et al., 2016). Picornaviruses seriously affect the respiratory system, digestive system and central nervous system, and cause a series of inflammation and lesions in organs and tissues such as heart, liver and skin (Zell, 2018). Picornaviruses are omnipresent and distributed worldwide. Studies have shown that the number of newly identified picornaviruses has increased dramatically over the past decade, and they become important pathogens that

endanger human and animal health (Palmenberg et al., 2009; Lewis-Rogers and Crandall, 2010; Tapparel et al., 2013; Zell, 2018). Foot-and-mouth disease virus (FMDV), Senecavirus A (SVA) and swine vesicular disease virus (SVDV) are members of the family *Picornaviridae*, which can cause similar symptoms - vesicular lesions in the tissues of the mouth, nose, feet, skin and mucous membrane of animals. All three of them can threaten the development of animal industry and national economy.

FMDV, classified into the genus *Aphthovirus* in the family *Picornaviridae*, is still one of the important animal disease pathogens of economic concern (Rodriguez-Habibe et al., 2020; Brown et al., 2021). Based on genetic and antigenic analyzes, FMDVs throughout the world have been geographically divided into seven serotypes (O, A, Asia1, C, SAT1, SAT2, SAT3). FMDV has a broad host range to all cloven-hoofed animals including domestic and wild ruminants and pigs. (Grubman and Baxt, 2004; Rodriguez-Habibe et al., 2020). Animals infected with FMDV often present with symptoms of fever and blisters on the mouth and hooves, with low mortality but high morbidity, leading to production losses. FMDV can contaminate the environment through aerosols and cause long-distance transmission events, so that it complicates the control of Foot-and-mouth disease (FMD) outbreaks (Gloster et al., 2003; Brown et al., 2022).

SVA is the only member of the genus *Senecavirus* in the family *Picornaviridae*, which was discovered in 2002 and once named Seneca Valley virus 001 (SVV-001; Hales et al., 2008). Initially, it was used in different human cancer treatment research as its potent oncolytic activity (Reddy et al., 2007; Burke, 2016). Subsequently, pigs with idiopathic vesicular disease (IVD) like clinical symptom occurred in Canada (Pasma et al., 2008), America (Singh et al., 2012) and Brazil (Leme et al., 2015; Vannucci et al., 2015) were confirmed to be infected with SVA. In 2015, the pathogen of vesicular lesions occurred in a pig farm in Guangdong Province of China was identified as SVA (Wu Q. et al., 2017), and then SVA gradually spread to other provinces in the following years (Liu et al., 2020).

SVDV, the causative agent of Swine vesicular disease (SVD), was first diagnosed in Italy in 1966 (Nardelli et al., 1968). SVDV belongs to the *Enterovirus* genus in the family *Picornaviridae* and was considered to be a porcine variant of human coxsackievirus B5 due to their close serological relationship (Graves, 1973). The disease only affects pigs and does not have a serious impact on production. However, SVD has similar clinical symptoms to FMD, which can pose a threat to international trade (Lin and Kitching, 2000; Dibaba, 2019).

These pathogens are difficult to diagnose clinically due to the similar vesicular lesions observed on infected animals. With the development of biotechnology, molecular biology diagnostic technology is constantly innovating and plays an important role in the diagnosis and differentiation of different viruses. In this paper, we mainly describe available and novel emerging diagnostic methods and multiplex assays for the detection of FMDV, SVA and SVDV. Tables 1–3 summarizes some recent studies on molecular diagnostic assays for the detection of FMDV, SVA and SVDV, respectively.

The Vesicular exanthema of swine virus (VESV, Caliciviridae, Vesivirus) can also cause vesicular disease in pigs. The origin of VES was traced to feeding meat from sea mammals to pigs and was eradicated from California populations in 1956. We also briefly refer to the laboratory diagnosis of VESV in this article.

Diagnostic methods

Reverse transcription-polymerase chain reaction (RT-PCR) assay

RT-PCR, one of the most traditional and common nucleic acid detection methods in the laboratory, is used extensively in various fields such as biology and medicine, microbiology and food based on its characteristics of simple operation, high sensitivity and strong specificity. Currently, multiple RT-PCR assays aimed at different viral targets have been reported and used as diagnostic tests.

FMDV is divided into seven serotypes based on genetic and antigenic analyzes. Meyer et al. designed primers based on the highly conserved regions of the seven FMDV serotypes genome and reported the establishment of a rapid and sensitive FMDV RT-PCR detection method (Meyer et al., 1991). Nishi et al. designed the primer set FM8/9 to amplify 644 bases in the conserved 3D region of all seven FMDV serotypes using RT-PCR assay, which is suitable for FMD diagnosis (Nishi et al., 2019). The study found that the sensitivities of FM8/9 primers were $10^{0.6}$- to $10^{3.8}$-fold higher than 1F/R primers described in the OIE manual (Nishi et al., 2019). There is a lack of cross-immune protection between different FMDV serotypes, and even within the same serotype, there are differences in the antigenicity of different isolates. Thus, it is necessary to develop a rapid detection method for distinguishing FMDV serotypes. FMDV VP1 coding sequences vary considerably among different FMDV serotypes, so that it can be used to RT-PCR assay for FMDV serotyping (Callens and De Clercq, 1997; Le et al., 2011). Even so, important phenotypic traits of FMDV cannot be reflected by relying on the VP1 coding sequence, since the FMDV genome is prone to variation and recombination events can occurr in the non-structural genes of FMDV (Carrillo et al., 2005; Klein et al., 2007; Brito et al., 2018). Xu et al. developed a universal L-P1 RT-PCR for amplifying and sequencing a 3 kb fragment including FMDV leader and capsid-coding region, which can be used for rapid antigenic characterization of FMDV and phylogenetic analyzes, and is expected to be an instructive for vaccine selection during FMDV outbreaks (Xu et al., 2013). A simple, quick and cost-efficient RT-PCR assay suitable for generating genomic sequences of all FMDV serotypes was described, and this approach can amplify the sequence reaching from the IRES to the end of the open reading frame, which can assist in immediate virus genotyping, phylogenetic analysis, and epidemiological studies of FMDV (Dill et al., 2017).

TABLE 1 Molecular diagnostic assays for detection of FMDV infection.

Detection method	Detection serotype	Detection target	Amplification temperature and time	Display of result	Limit of detection	References
RT-PCR	O/A/C/Asia 1 universal	5'UTR	-	Agarose gel electrophoresis	10^{0} to 10^{-2} dilution	Reid et al. (2000)
One-step multiplex RT-PCR	Detection and differentiation of Vietnamese FMDV serotypes O, A, and Asia 1 directly	2B and VP1	-	Agarose gel electrophoresis	O: $10^{2.5}$ $TCID_{50}$/mL Asia1: $10^{3.5}$ $TCID_{50}$/mL A: $10^{1.5}$ $TCID_{50}$/mL	Le et al. (2011)
RT-PCR	7 serotypes are universal	L and P1	-	Agarose gel electrophoresis	10^{-1} to 10^{-3} dilution	Xu et al. (2013)
RT-PCR	7 serotypes are universal	3D	-	Agarose gel electrophoresis	$10^{0.2}$ to $10^{-2.8}$ $TCID_{50}$/mL	Nishi et al. (2019)
Real-time RT-PCR	7 serotypes are universal	3D	-	Fluorescent intensity in real-time thermal cycler	10 and 100 virus genomes/vol tested	Callahan et al. (2002)
Real-time RT-PCR	detection and differentiation of serotype O, A and Asia-1 in the Middle East	VP1	-	Fluorescent intensity in real-time PCR Thermocycler	1.78 to 2.74 copies of in vitro–transcribed FMDV RNA depending on serotypes	Reid et al. (2014)
Real-time RT-PCR	all 7 serotypes	3D and 5'UTR	-	Fluorescent intensity in real-time PCR Thermocycler	The detection limit of RT-qPCR (with tailed primers) targeting 3D and 5′ UTR of FMDV are −0.72 and −0.35 log10 TCID50/mL of FMDV O1 Manisa, respectively	Vandenbussche et al. (2017)
A fully automated cartridge-based real-time RT-PCR diagnostic system	All 7 serotypes	3D	-	Fluorescent intensity in real-time PCR Thermocycler	10^{-5} to 10^{-6} dilution of the FMDV O/UAE 2/2003 stock depending on the nuclei acid extraction kits	Goller et al. (2018)
RRT-PCR	Six serotypes (O, A, Asia 1, SAT 1, 2 and 3)	3D	-	Fluorescent intensity in handheld Biomeme two3™ Real-Time PCR Thermocycler (two3)	10^{-4}, 10^{-3}, 10^{-2}, 10^{-5}, 10^{-3}, and 10^{-3} dilutions of FMDV O, A, Asia 1, SAT 1, SAT 2, and SAT 3 stocks, respectively	Hole and Nfon (2019)
Multiplex real-time RT-PCR	Detection and serotyping of serotype O, A and Asia-1	VP1	-	Fluorescent intensity in real-time PCR detection system	O: 10^{1} $TCID_{50}$/mL A: 10^{1} $TCID_{50}$/mL Asia1: 10^{2} $TCID_{50}$/mL	Lim et al. (2022)
RT-iiPCR	All 7 serotypes	3D	-	Utilizes a commercially available compact, portable POCKIT™ Nuclei Acid Analyzer (GeneReach, USA) for rapid (<2 h) detection	≥9 copies of in vitro–transcribed FMDV O1 Manisa/69 3D RNA	Ambagala et al. (2017)
RT-ddPCR	serotypes O, A, and C	3D	-	PCR amplification of cDNA target in the droplets, the plate containing the droplets was placed in a QX200 droplet reader	$10^{1.4}$ $TCID_{50}$/mL and 26.5 copies of viral RNA	Pinheiro-de-Oliveira et al. (2018)
RT-LAMP	all 7 serotypes	2B	Be performed at 64°C for 45 min and then terminated by heating at 80°C for 10 min.	Agarose gel electrophoresis	10 copies of FMDV RNA per reaction	Chen et al. (2011)

(Continued)

TABLE 1 (Continued)

Detection method	Detection serotype	Detection target	Amplification temperature and time	Display of result	Limit of detection	References
RT-LAMP	Serotyping of serotype O, A and Asia1	P1	Incubation at 63°C for 60 min	Agarose gel electrophoresis	O: 10^{-3} $TCID_{50}$ A: 10^{-5} $TCID_{50}$ Asia1: 10^{-3} $TCID_{50}$	Madhanmohan et al. (2013)
RT-LAMP	Serotype O	VP3	Incubation at 62°C for 40 min and then terminated by heating at 80°C for 5 min	By visual detection of a color change from purple to sky blue due to the presence of the metal ion indicator, HNB.	10^2 $TCID_{50}$/mL and 10^3 copies/μL	Lim D. R. et al. (2018)
RT-LAMP	Serotype A	VP1	Be completed in 40 min at 62°C	By visual detection of a color change from purple to sky blue due to the presence of the metal ion indicator, HNB.	10^2 $TCID_{50}$/mL	Lim D. et al. (2018)
RRT-LAMP	All 7 serotypes	3D	Positive assay signals were generated within 15 min for the lowest concentration of a standard RNA sample at 62°C	Real-time fluorescence values of 6-carboxyfluorescein (FAM)-labeled probe were measured in on-going reactions at the end of each annealing step.	10^2 copies/μL	Lim et al. (2020)
RT-RPA	All 7 serotypes	3D	Incubation at 42°C for 20 min.	Fluorescence detection in the FAM channel (excitation 470 nm and detection 520 nm) was performed in an ESEQuant tubescanner (Qiagen Lake Constance GmbH, Stockach, Germany) at 42°C for 20 min	10^2 RNA molecules	Abd et al. (2013)
RPA-LFD	All 7 serotypes	2B	Incubation at 38°C within 20 min	Be visualized by LFD duplexes labeled with anti-FAM gold conjugates and anti-Biotin antibodies (Milenia Biotec GmbH, Germany)	10 copies of plasmid	Wang H. M. et al. (2018)
RPA-LFD	Differentiate FMDV serotypes A, O or Asia 1, respectively	VP1	Incubation at 38°C for 20 min	Be visualized by LFD	3 copies of plasmid DNA or 50 copies of viral RNA per reaction	Wang H. et al. (2018)
LFS RT-RPA	Serotypes O, A and Asia1	3D	Be performed in a closed fist using body heat for 15 min, and the products were visible on the LFS inspected by the naked eyes within 2 min	Be performed in a closed fist using body heat for 15 min, and the products were visible on the LFS inspected by the naked eyes within 2 min	10^2 copies	Liu et al. (2018)

TABLE 2 Molecular diagnostic assays for detection of SVA infection.

Detection method	Detection target	Amplification temperature and time	Display of result	Limit of detection	References
RT-PCR	VP3/VP1 region	-	Agarose gel electrophoresis	-	Leme et al. (2015)
nest-PCR	VP1	-	Agarose gel electrophoresis	0.0181 ng/μL of cell-cultured SVA isolate	Feronato et al. (2018)
rRT-PCR	3D	-	Fluorescent intensity in real-time PCR detection system	0.79 $TCID_{50}$/mL	Fowler et al. (2017)
TaqMan-based qRT-PCR	VP1	-	Fluorescent intensity in real-time PCR detection system	1.3×10^1 genomic copies/μL	Dall et al. (2017)
Real-time RT-PCR	5' UTR	-	Amplification reactions were performed on an ABI 7500 Fast instrument (Thermo Fisher Scientific).	About 3.5 RNA copies per reaction	Zhang J. et al. (2019)
RT-ddPCR one-step	3D	-	The QX200 droplet reader (BIO-RAD, USA) was used to analyze each droplet individually, which counts positive and negative droplets to establish absolute quantification of samples (concentration).	0.185 $TCID_{50}$ of virus and 0.1 fg of SVA plasmid	Pinheiro-de-Oliveira et al. (2019)
RT-ddPCR	3D	-	After amplification, the droplets from each well of the plate were read individually by a QX200™ Droplet Reader (Bio-Rad), and the data were analyzed with QuantaSoft™ software (Bio-Rad)	1.53 ± 0.22 copies of SVA RNA	Zhang Z. et al. (2019)
RT-iiPCR	3D	-	Be placed into a POCKIT™ Nucleic Acid Analyzer for RT-PCR reaction	7 RNA copies per reaction	Zhang J. et al. (2019)
Real-time RT-LAMP	VP2	Incubation at 63 °C for 1 h.	Be detected a Thermostatic Fluorescence Detector DEAOU-308C	1 $TCID_{50}$/mL	Zeng et al. (2018)
RT-LAMP LFD	3D	Incubation at 61°C for 50 min.	Be visualized by LFD	4.5×10^{-8} ng/μL	Li et al. (2019)
rRT-RAA	VP2	Incubation at 42°C for 30 min	Fluorescence signal was automatically recorded in real-time by CFX96 Bio-Rad real-time PCR instrument.	1.185 $TCID_{50}$	Wang et al. (2021)
RPA-LF	VP1	Incubation at 35°C for 25 min	Be visualized by LFD	15 copies/μL	Wang et al. (2022)

Since 2015, pig-producing countries such as Brazil (Leme et al., 2015), China (Wu Q. et al., 2017), the United States (Canning et al., 2016), Colombia (Sun et al., 2017), Canada (Xu et al., 2017), and Thailand (Saeng-Chuto et al., 2018) have successively reported cases of SVA-VD. SVA seems to be becoming a globally prevalent virus. Several RT-PCR assays based on SVA conserved genome have been established for viral diagnosis and epidemiological investigation of SVA (Laguardia-Nascimento et al., 2016). Leme et al. designed a primer set which can amplify a 542 bp product size of the VP3/VP1 region of SVA genome in RT-PCR assay, and the primer set can be useful in molecular screening of SVA infection and for characterization of the virus (Leme et al., 2015). Wu et al. designed RT-PCR primers for amplification of the whole SVA genome, and firstly carried out complete genome

TABLE 3 Molecular diagnostic assays for detection of SVDV infection.

Detection method	Detection target	Amplification temperature and time	Display of result	Limit of detection	References
RT-PCR	Parts regions of the structural proteins 1C and 1D	-	Agarose gel electrophoresis	100 $TCID_{50}$	Lin et al. (1997)
RT-nPCR	Parts regions of the structural proteins 1C and 2A	-	Agarose gel electrophoresis	0.1 $TCID_{50}$	Lin et al. (1997)
Double PCR	The simultaneous Detection of SVDV and ASFV P72	-	Agarose gel electrophoresis	SVDV: 7.6×10^2 copies/μL ASFV: 1.5×10^5 copies/μL	Peng et al. (2015)
RT-PCR	3D	-	Agarose gel electrophoresis	1 $TCID_{50}$	Pezzoni et al. (2020)
Real-time one-step RT-PCR	2C	-	Fluorescent intensity in real-time PCR detection system	2×10^2 copies/μL	McMenamy et al. (2011)
Real-time RT-PCR	5' UTR	-	Fluorescent intensity in real-time PCR detection system	10^{-6}–10^{-7} dilution of UKG 27/72 SVDV isolates	Reid et al. (2004b)
rtRT-PCR SYBR Green	3D	-	Fluorescent intensity in real-time PCR detection system	10 $TCID_{50}$	Pezzoni et al. (2020)
rtRT-PCR TaqMan Probe	3D	-	Fluorescent intensity in real-time PCR detection system	10 $TCID_{50}$	Pezzoni et al. (2020)
rtRT-PCR based on 2B-IR TaqMan Probe	5' UTR	-	Fluorescent intensity in real-time PCR detection system	10 $TCID_{50}$	Pezzoni et al. (2020)
rtRT-PCR based on 3-IR TaqMan Probe	5' UTR	-	Fluorescent intensity in real-time PCR detection system	1 $TCID_{50}$	Pezzoni et al. (2020)
RT-LAMP	3D	Incubation at 63°C within 30–60 min followed by an inactivation period of 2 min at 80°C	Agarose gel electrophoresis	approximately 50 viral RNA copies per assay	Blomström et al. (2008)

identification, phylogenetic analysis and clinical characterization of SVA that infected pigs with Porcine Idiopathic Vesicular Disease (PIVD) in China (Wu Q. et al., 2017). Transient viremia can be caused in SVA infected animals. In the meanwhile, viral nucleic can be detected in almost all tissues through RT-PCR. However, after viremia disappeared in affected animals, the virus can only be detected in the tonsils and lymph nodes using this method (Houston et al., 2020). A specific nested-PCR assay based on VP1 fragments of SVA genome was established and the limit of detection was 0.0181 ng/μL for the cell-cultured SVA isolate, which is more sensitive than traditional RT-PCR (Feronato et al., 2018).

Italy was the first country to report the outbreak of SVD in1966 and began an eradication program in 1995 (Nardelli et al., 1968; Bellini et al., 2007). So far, SVD monitoring is still ongoing in Italy and no evidence of SVD activity has been found, which indicated the complete SVD virus eradication from the Italian pig industry (Tamba et al., 2020). Whatever, SVDV has clinically similar symptoms with FMDV and affects trade activities such as pork products, as a result, it is necessary yet for diagnosis and surveillance of SVDV. Several RT-PCR assays based on different targets including capsid, VP1, 3BC and 2A genes were reported for SVDV detection and molecular evolution analysis (Marquardt and Ohlinger, 1995; Lin et al., 1997; Zhang et al., 1999). Nielsen et al. depicted a method for rapid sequencing of the SVDV isolates genomes using the Roche GS FLX Sequencing Platform (Nielsen et al., 2014). Vázquez-Calvo et al. designed PCR Primer sets and reported the first complete coding sequence of a Spanish SVDV isolate (SPA/1/'93)(Vazquez-Calvo et al., 2016). A double PCR method was described for detecting ASFV and SVDV (Peng et al., 2015). Pigs infected with SVDV can shed large amounts of the virus through the nose, mouth and feces to contaminate the surrounding environment. Given the absence of clinical signs, feces are the sample of choice for viral testing to identify

subclinical infections (Pezzoni et al., 2020). Sensitive detection methods are necessary due to the low viral content of stool samples. The diagnostic performance of six genomic amplification methods for SVDV detection including RT-PCR, real-time RT-PCR and RT-LAMP assay was evaluated and the result showed that the conventional 3D RT-PCR and the 3D rtRT-PCR using SYBR Green as a detector were still the most sensitive and efficient methods for detecting SVDV in fecal samples (Pezzoni et al., 2020). However, compared with RT-qPCR, the procedure of RT-PCR is more complicated, and agarose gel electrophoresis is required to determine the results of the corresponding samples.

Real-time PCR assay

As the gold standard of laboratory detection, the quantitative real-time reverse transcription PCR (qRT-PCR) assay has been successfully used in the diagnosis of various pathogenic pathogens (Munro et al., 2013; Shi et al., 2016; Fischer et al., 2017; Corman et al., 2020). qRT-PCR allows the quantification of molecular targets in templates by using standard substance. The sample content determination does not need to open the reaction tube, and can be analyzed by the fluorescence signal intensity generated during the qRT-PCR amplification process, avoiding cross-contamination between samples (Galluzzi et al., 2018). qRT-PCR has the advantages of rapidity and sensitivity, and is suitable for different clinical sample types including swabs, sera, vesicular fluid, milk and tissue samples (Burkhalter and Savage, 2017; Fontel et al., 2019; Yeo et al., 2020; Armson et al., 2020a). At present, Real-Time PCR is a commonly used method to detect the pathogens of animal diseases. Usually, the same diagnostic sample is repeated following a positive result to confirm the presence of the disease agent followed by secondary confirmatory testing if the disease is exotic. According to the OIE manual, qRT-PCR amplification of FMDV 3D genome sequence is recommended as a standard method for the viral diagnosis of all FMDV serotypes (Callahan et al., 2002). 5'UTR sequence is also the frequently-used target for FMDV detection (Reid et al., 2002). Both Reid et al. (2014) and Lim et al. (2022) established multiplex real-time RT-PCR based on FMDV VP1 coding region to detect and identify different FMDV serotypes (O, A and Asia). Normally, the FMDV RNA for diagnostic purposes can be harvested from infected animal samples containing blister fluid, blister tissue, serum, milk and swabs of lesion (Armson et al., 2019a; Wong et al., 2020). One study showed that EDTA-stabilized blood samples can be adapted to FMDV detection during FMD outbreak even though the sensitivity of it was 10-fold less than that of serum samples (Fontel et al., 2019). Armson et al. determined the utility of testing pooled milk by rRT-PCR as an alternative approach for FMD surveillance, and proved that pooled milk has potential value as a surveillance sample to reveal subclinical FMD infection (Armson et al., 2020a,b). Yeo et al. amplified the FMDV genomic sequence in meat juice using qRT-PCR and confirmed the presence of FMDV RNA (Yeo et al., 2020). The discovery indicated that meat juice can be used as a good sample type for FMDV detection and play a role in the import and export quarantine of meat products (Yeo et al., 2020). The application of qRT-PCR in low-and middle-income countries (LMICs) was limited because of the complex diagnostic procedures and expensive equipment (Vosloo et al., 2002; Namatovu et al., 2013). Recently, some of the filed-deployable molecular assays for FMD diagnosis were developed and proved the feasibility through research (Howson et al., 2017b, 2018; Hole and Nfon, 2019). Ambagala et al. described a potentially useful field-deployable reverse transcription-insulated isothermal PCR (RT-iiPCR) assay for rapid detection of FMDV in countries with poor equipment conditions (Ambagala et al., 2017). Moreover, a recent study described a portable, handheld real-time PCR platform that can be manipulated via a smartphone app, which has great potential for FMDV detection (Hole and Nfon, 2019).

qRT-PCR enables the fast and accurate diagnosis of any vesicular diseases including SVA, due to the characteristics of high efficiency and sensitivity (Leme et al., 2017). Different qRT-PCR targeting diverse SVA genomic conserved regions (including 3D, VP1 and 5'-UTR) were established for the SVA detection and quantification (Bracht et al., 2016; Gimenez-Lirola et al., 2016; Dall et al., 2017; Fowler et al., 2017; Zhang J. et al. 2019). Joshi et al. utilized real-time reverse transcriptase PCR and virus isolation to screen out the existence of SVA in pigs, mice and houseflies (Joshi et al., 2016). Several researchers detected the viral nucleic acid in tissue, serum, oral swabs and/or rectal swabs from pigs challenged with SVA by qRT-PCR, and found the low viral level in serum, which indicated that SVA can induce transient viremia (Fernandes et al., 2018; Buckley et al., 2021). Moreover, the study suggested that the tonsil may be the main site of SVA replication (Fernandes et al., 2018). Zhang et al. designed primers and probes based on conserved sequences of the viral genome, and established a SVV rRT-PCR targeting the conserved 5'-UTR and a SVV RT-iiPCR targeting the 3D gene, both of which have good consistency in the diagnosis process of clinical samples (Zhang J. et al., 2019).

A variety of real-time quantitative PCR methods have been described for the detection of SVDV (Reid et al., 2004a; Hakhverdyan et al., 2006; Niedbalski, 2009; McMenamy et al., 2011). The use of oral fluid (OF) samples to assess animal group health status has been proposed as an attractive and cost-effective method for disease surveillance, since this approach has no complex collection process and can be operated easily for anyone (Mur et al., 2013; Senthilkumaran et al., 2017). Senthilkumaran et al. utilized a qRT-PCR assay based on SVDV 3D target and an adapted competitive ELISA to detect the levels of viral nucleic acid and antibodies in OF samples (Senthilkumaran et al., 2017). The result showed that the high levels of SVDV RNA could be detected from 1 day post-infection (DPI) to 21 DPI and the antibodies to SVDV could be discovered starting at DPI 6, which indicated the potential value of OF for SVD surveillance (Senthilkumaran et al., 2017). Pezzoni et al. compared the sensitivity of the two real-time RT-PCRs targeted on the 3D region (based on SYBR Green and TaqMan probe detection), and they showed an equivalent

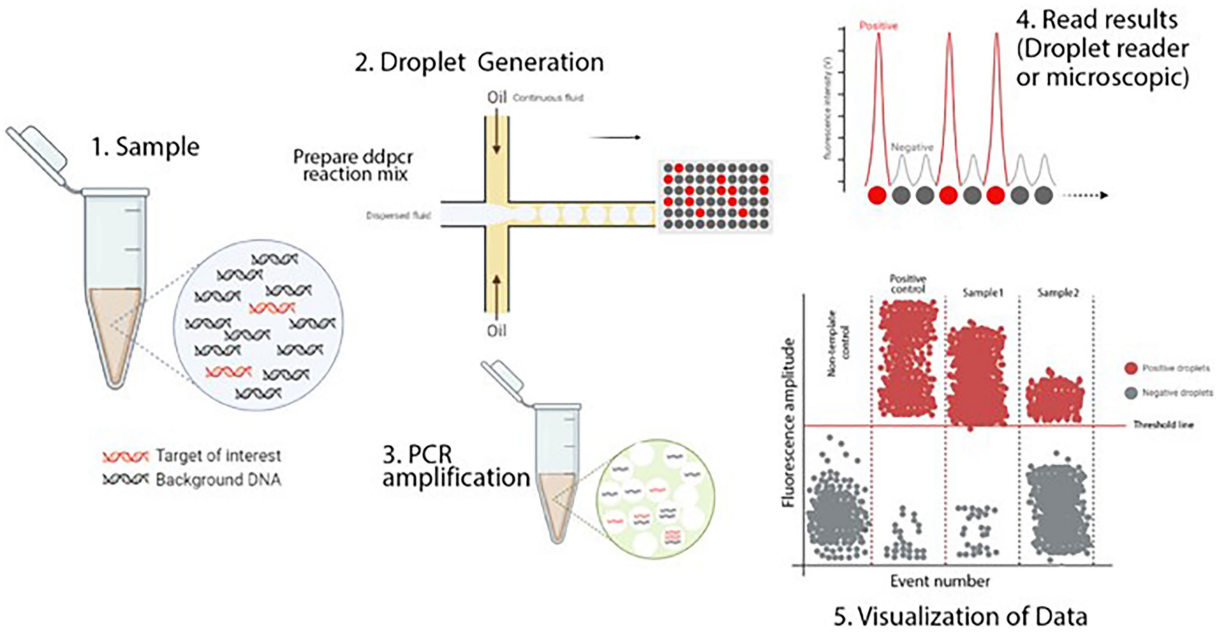

FIGURE 1
Schematic illustration of ddPCR. This figure illustrates the digital PCR droplet principle and how a single sample containing the target sequence is partitioned. PCR amplified produces thousands of copies that can be detected and interpreted by a detection system. In a typical ddPCR workflow, a single sample includes target and nonspecific sequences (DNA or RNA), real-time PCR primers and fluorescent-labeled probes, and standard real-time PCR master mixes. (1) A sample partitioned into thousands of single nanoliter droplets with the generation of water-in-oil emulsions. A proportion of droplets contain no template molecules, while others contain one or more targets. The generation of droplets from the sample is achieved in several ways. Standard methods include T-junction and flow-focusing geometry. Only the flow-focusing geometry is shown here. For more details, see the text. (2) Traditional end-point PCR is then performed to amplify the target sequence. (3) Target sequence droplets exhibit higher fluorescence intensity and are known to be positive droplets. Empty or no targets show low and negative fluorescent intensity. This fluorescence intensity versus time is plotted on a graph. The number of targets per partition will follow the normal Poisson distribution encapsulation of the DNA or RNA that occurs randomly. Various methods can interpret the fluorescent intensity of droplets. The most popular of these is a fluorescent microscope or a droplet reader. (4) The acquired data is visualized in a graph by different software. The threshold value indicates the intensity of fluorescence as the positive particles are separated from the negative. Although this value is set automatically by the software, it can be adjusted manually (Kojabad et al., 2021).

analytical sensitivity, while the diagnostic sensitivity of the 3D rtRT-PCR using SYBR Green as a detector was high than the assay based on TaqMan probe detection (Pezzoni et al., 2020).

Droplet digital PCR

ddPCR is considered a graceful adaptation of the current qPCR format and has the potential application value on virus diagnosis (Jones et al., 2014). Its principle is shown in Figure 1. In ddPCR, the clinical sample is divided into thousands of droplets, each of which contains zero or several copies of the target nucleic acids. Molecular targets of each droplet are amplified by PCR and the fluorescence intensity produced by the reaction products is read after amplification, so as to achieve accurate and absolute quantification of target nucleic acid (Taylor et al., 2017). ddPCR does not depend on the standard calibration curve, and has a strong tolerance to PCR inhibitors so that it can realize the direct quantification of clinical samples including stool, blood, and tissue without nucleic acid purification (Taylor et al., 2017; Sahore et al., 2018). The rise of ddPCR is of great significance for the development of precision virus detection platform and viral diagnosis in the early period of infection. At present, dd-PCR has been widely used in the detection of various pathogens such as Epstein-Barr virus; human cytomegalovirus, human T-cell leukemia virus type 1, respiratory syncytial virus (RSV) and Japanese encephalitis virus (JEV) (Lin et al., 2016; Nicot et al., 2016; Wu X. et al., 2017; Persson et al., 2019). A study reported a RT-ddPCR method for the quantification of foot-and-mouth virus RNA, which is based on an OIE-recognized real-time RT-PCR that detects the 3D-encoding region of FMDV (Pinheiro-de-Oliveira et al., 2018). The assay can detect and quantify three serotypes of FMDV (O, A and C) with high specificity, and can detect at least $10^{1.4}$ $TCID_{50}$/mL of FMDV and 2 fg of the circularized or linearized plasmid with the same analytical sensitivity of RT-qPCR (Pinheiro-de-Oliveira et al., 2018). Besides, T F Pinheiro-de-Oliveira et al. developed a one-step RT-ddPCR method with superior performance to identify SVA in biological samples (Pinheiro-de-Oliveira et al., 2019). Based on the high sensitivity and specificity, the one-step RT-ddPCR can be a useful tool for the prevention and control of vesicular diseases such as SVA (Pinheiro-de-Oliveira et al., 2019). Zhang et al. also

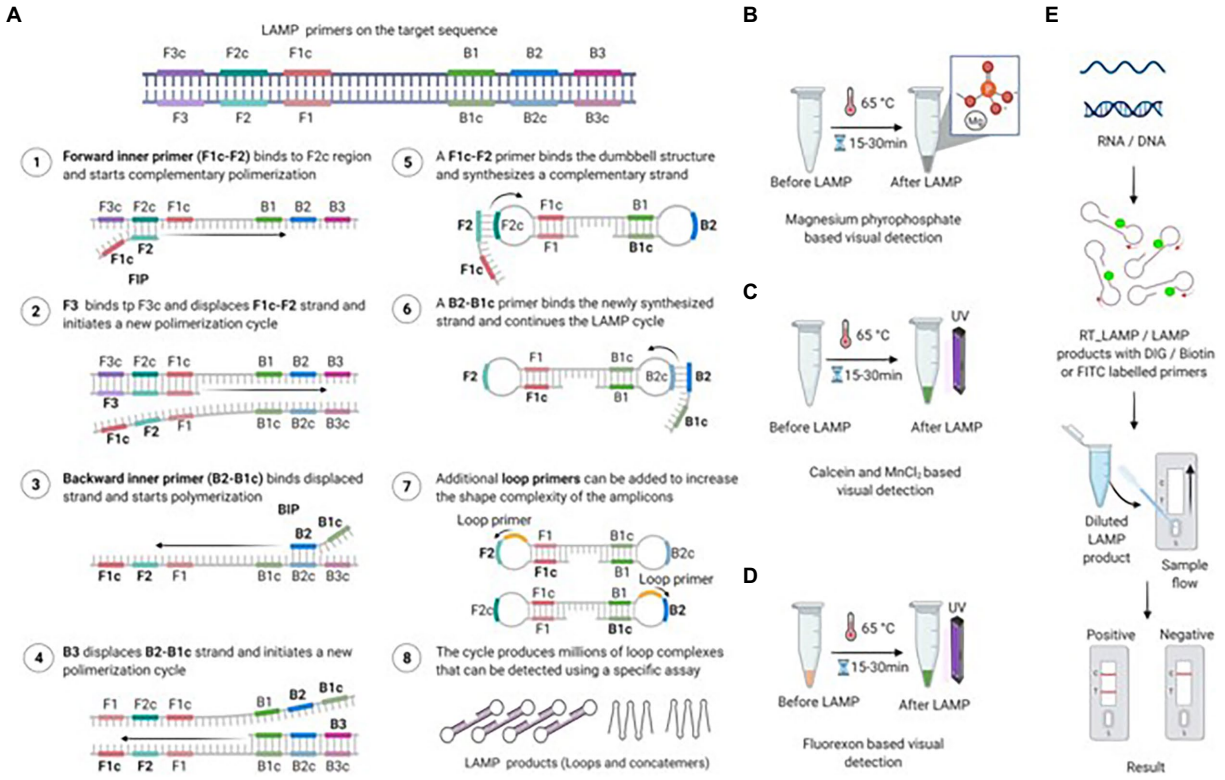

FIGURE 2
Amplification via loop-mediated isothermal amplification (LAMP) and various detection methods. **(A)** Diagramof LAMP primers located on the target sequence and the amplification process. The FIP primer binds to its complementary sequence and begins amplifying the first strand, followed by binding and amplification of the second strand by the F3 primer. The following steps involve the amplification of the FIP-amplified strand by the B3 primer. Finally, FIP and BIP continue the LAMP cycle, resulting in dumbbell-shaped amplicons. A full stepwise description of the individual steps is provided in the figure. **(B)** Magnesium pyrophosphate-based visual detection of the LAMP product. During LAMP, a large amount of pyrophosphate ion is produced as a by-product, which reacts with magnesium provided in the reaction mixture. The resulting product, magnesium pyrophosphate, forms a white precipitate that allows easy visual detection. The turbidity of the final LAMP reaction confirms the presence or absence of the targeted nucleic acid. **(C)** Calcein-based fluorescence detection of the LAMP product. The reaction of the by-product pyrophosphate with magnesium or calcein-manganese aids in the visualization of the LAMP product by producing a precipitate or emitting bright green fluorescence under UV light. Calcein-based fluorescence is enhanced by the presence of magnesium in the reaction mixture. **(D)** Fluorexon-based visual detection of the LAMP product. Upon completion of the LAMP reaction, fluorexon-MnCl turns from orange to green. The resulting green fluorescence is visualized with the naked eye under UV light. **(E)** Lateral flow-based detection of the LAMP product. To visualize LAMP with LFA, the target nucleic acid (RNA/DNA) is amplified via RT-LAMP or LAMP with DIG, biotin, or FITC-labeled primers. The labeled LAMP product is diluted and applied to the lateral flow strip. After 5 to 15min of incubation, the appearance of bands on the test and control lines indicates the presence of the target nucleic acid (Bhat et al., 2022).

established a novel RT-ddPCR assay targeting the conserved SVA polymerase 3D gene, and the detection limit of this assay was 10-fold more sensitive than the RT-rPCR assay (Zhang Z. et al. 2019). Currently, there is no digital PCR reported for SVDV.

ddPCR has the characteristic of accurate quantification and can quantify the mutated target genes by using a small amount of sample, which is important in the detection of rare mutation targets (Huggett and Whale, 2013; Milbury et al., 2014). In addition, it gives great benefits in fast and easy diagnosis for some diseases difficulted to identify accurately due to the high sensitivity and specificity of ddPCR (Li et al., 2018). However, ddPCR is still limited in use even in many modern diagnostic laboratories for routine testing (Liao and Huang, 2017). In terms of technology use, professional personnel is required for ddPCR operations and results reading. Anyhow, as a novel, sensitive, accurate and promising quantitative technique, ddPCR plays an important role in the monitoring of cancer, pathogens, water environment and so on (Li et al., 2018; Postel et al., 2018; Kojabad et al., 2021; Tiwari et al., 2022).

Loop-mediated isothermal amplification

Loop-mediated isothermal amplification (LAMP) is an isothermal amplification approach developed in 2000, and has become the focus of point-of-care (POC) diagnostics due to its simple operation, rapid measurement and high sensitivity of this assay (Notomi et al., 2000). As shown in Figure 2 (Bhat et al., 2022), under the strand displacement activity of the Bst DNA polymerase from *Bacillus stearothermophilus* in 60-65°C, the

target nucleotide was transformed into a stem-loop structure through the exploit of four pairs of primers (outward forward (F3), outward backward (B3), forward inner (FIP), and backward inner (BIP)). Then the stem-loop structure containing multiple initiation sites was used as the template of LAMP reaction for cyclic amplification, and many nucleotide chains with different lengths were generated finally. The results of LAMP assay can be visualized through the following ways (Nie, 2005; Almasi et al., 2014; Mansour et al., 2015; Peng et al., 2021; Bhat et al., 2022), (1) by agarose gel electrophoresis; (2) measuring the fluorescence emitted by SYBR Green or other dyes on a real-time basis; (3) the turbidity of LAMP reaction based on magnesium pyrophosphate; (4) the green fluorescence intensity based on calcein-manganese or fluorexon under UV light; (5) be visualized with a lateral flow device (LFD).

To date, several reverse transcription LAMP (RT-LAMP) assays have been developed that are capable of detecting all seven FMDV serotypes and serotype-specific detection of O, A, C and Asia 1 FMDVs (Lim et al., 2020). Timely diagnosis is essential for the control, monitoring and eradication of FMD. Compared with PCR, LAMP does not require complex temperature cycling conditions and requires less time to perform allowing it to be used for FMDV rapid detection in the field. The use of lyophilized reagents allows for pathogen detection in field environments where equipment conditions are insufficient. Howson et al. described the performance of lyophilized rRT-PCR and RT-LAMP assays to detect FMDV (Howson et al., 2017a). They found that lyophilization greatly improved the storage stability of test reagents without jeopardizing the assays' performance, which further supported the potential on field diagnosis of RT-LAMP assay (Howson et al., 2017a). Recently, Lim et al. developed a probe-based real-time reverse transcription loop-mediated isothermal amplification (RRT-LAMP) assay for rapid and specific detection of FMDV, and the detection limit of the assay was 10^2 copies/μL which is comparable to that achieved by qRT-PCR (Lim et al., 2020). Rapid and accurate detection of SVA is necessary to confirm the disease causing agent, and to initiate the implementation of control processes. Zeng et al. described a real time RT-LAMP targeting the VP1 and VP2 regions of SVA and this assay can detect at least 1 $TCID_{50}$/mL of virus titers (Zeng et al., 2018). Li et al. combined RT-LAMP with a lateral flow dipstick (LFD) for spot rapid diagnosis of SVA (Li et al., 2019). Armson et al. established SVV-1 RT-LAMP assay using lyophilized reagents, which negated the requirement for RNA extraction and the time of sample amplification was reduced within 12 min (Armson et al., 2019b). RT-LAMP technology is also used in the rapid detection of SVDV. Blomström et al. developed a one-step RT-LAMP assay based on the highly conserved 3D polymerase gene to test viral nucleic acid easily and quickly (Blomström et al., 2008).

Unlike PCR assays, LAMP does not require expensive equipment and complex cycling-temperature conditions, and can be easily performed by an untrained person. The designing principle of LAMP primers is a bit complicated. LAMP primers can be designed using the free online software package Primer Explorer version 5[1] or paid software[2] (Bhat et al., 2022). On the whole, LAMP is a potential tool for use of pathogen detection in resource-poor environments.

Recombinase polymerase amplification

RPA was originally developed by Piepenburg and collaborators for the use of human pathogen detections, and was later applied in the diagnosis of different RNA targets (Piepenburg et al., 2006; Silva et al., 2018). Generally speaking, RPA reaction contains 3 main protein components: uvsX recombinase from T4 phage, DNA polymerase, and single-stranded DNA binding protein (SSB). As shown in Figure 3, the recombinase protein can bind with primers to form a complex that can recognize and pair complementary sequences of the template under constant temperature. Then the target nucleic acid is amplified in large quantities under the action of polymerase and binding enzyme. Recombinase-aided amplification (RAA) developed by Qitian (Wuxi, China) has similar amplification rules with RPA while the recombinant enzyme is obtained from *Escherichia coli* (Shen et al., 2019). Similarly, the results of RPA can be visualized by agarose gel electrophoresis while it is easy to appear smeared bands. To avoid this phenomenon, the RPA product can be purified to remove proteins and crowding agents prior to gel electrophoresis (Bhat et al., 2022). In addition, real-time fluorimeter and lateral flow assay can also be used to detect RPA products when using intercalating dyes and specific probes (Daher et al., 2016; Lobato and O'Sullivan, 2018; Powell et al., 2018). A RPA reaction is incubated at a single temperature of 25–42°C without the need for thermocycling, and the time of DNA amplification is usually between 5 and 30 min, which is faster than that of other nucleic acid amplification techniques such as PCR assay (Piepenburg et al., 2006; LaBarre et al., 2011).

RPA has been successfully used to detect several infectious agents, including viruses. Howson et al. defined the relative performance of RT-RPA and RT-LAMP for the detection of FMDV, benchmarked against rRT-PCR (Howson et al., 2017b). They found that RT-LAMP can detect FMDV RNA without RNA extraction, while accurate results by RT-RPA only obtained when using RNA extraction (Howson et al., 2017b). A visible and equipment-free RT-RPA combined with lateral flow strip (LFS RT-RPA) was developed to detect FMDV 3D gene (Liu et al., 2018). The FMDV LFS RT-RPA assay was performed successfully in a closed fist using body heat for 15 min, and the products were visible on the LFS inspected by the naked eyes within 2 min (Liu et al., 2018). Wang et al. established a series of serotype-specific RT-RPA assays combined with LFD to differentiate FMDV serotypes A, O or Asia 1, respectively, and the detection limits of

1 https://primerexplorer.jp/e/

2 www.optigene.co.uk/lamp-designer/

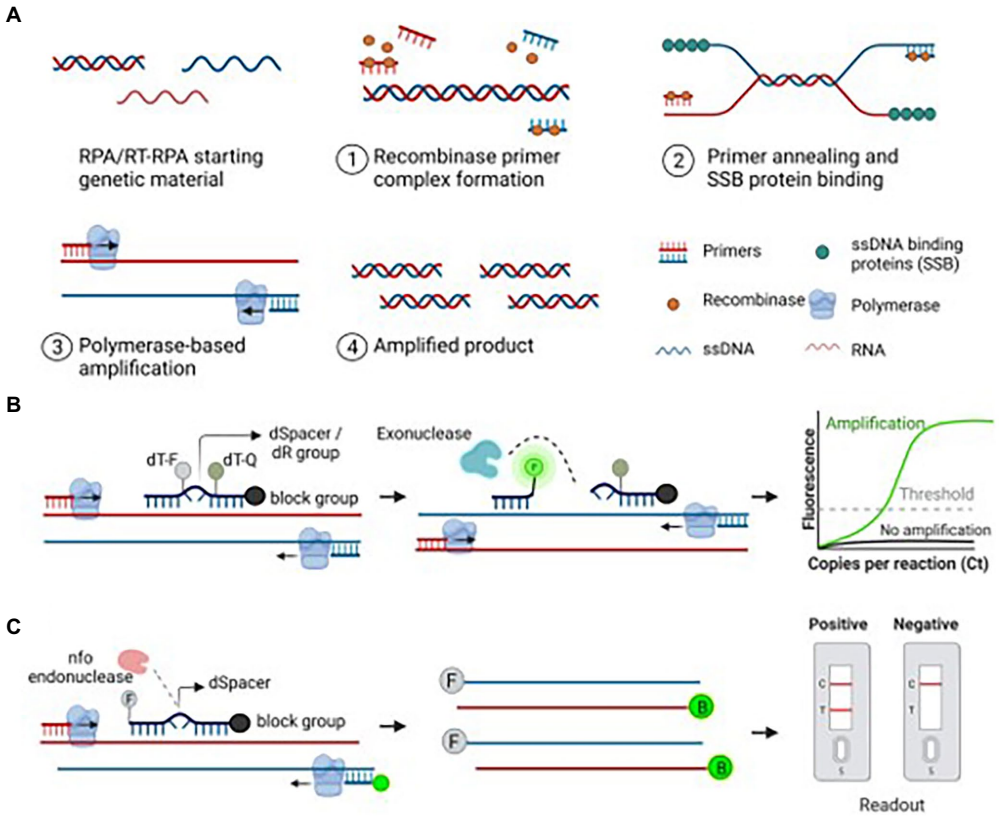

FIGURE 3
Recombinase polymerase amplification (RPA)-based amplification and its detection methods. **(A)** Schematic diagram of the RPA assay. An ideal RPA assay consists of forward and reverse primers, a recombinase protein that helps bind primers to the target nucleic acid, ssDNA-binding proteins to stabilize the ssDNA, and a polymerase to amplify the primer-bound strands. The stepwise amplification process is shown in the figure. **(B)** Exonuclease-based detection of the RPA product. A 46–52bp long Exo probe flanked by a quencher and fluorophore binds to the amplified product. Exo probe contains a THF (tetrahydrofuran) residue known as dSpacer, which is cleaved by the exonuclease, thus releasing the fluorophore from the quencher. The observed fluorescent signal indicates the presence of the target nucleic acid. **(C)** Endonuclease-based detection of the RPA product. A 46–52bp long oligonucleotide probe labeled with FAM or Alexa fluor binds to the target strand. The annealed probe is cleaved by the nfo enzyme, freeing the 3′-OH group of the probe and is used as a primer in the subsequent reactions. The resulting amplicons are produced with FAM and biotin using a biotin-labeled reverse primer. The final RPA product is applied to the LFA strip, and the results are visualized after the appearance of matching lanes (Bhat et al., 2022).

these assays were 3 copies of plasmid DNA or 50 copies of viral RNA per reaction (Wang H. et al., 2018). Wang et al. developed a VP2-based real-time fluorescent reverse transcription RPA (rRT-RPA) assay to rapidly detect SVA, and the detection limit of this assay is 1.185 $TCID_{50}$, which is comparable to that of a previously published rRT-PCR assay (Wang et al., 2021). A simple, rapid and accurate (RPA-LF) diagnostic assay for SVA detection was developed, and the optimal reaction conditions were incubated at 35 °C for 25 min, and the result was visualized directly on the dipstrip (Wang et al., 2022).

Luminex (beads-based technology)

In 2001, Luminex technology, a bead-based detection platform, became the first multi-target detection technology approved by FDA for clinical diagnosis. Luminex has two core technologies including xMAP and xTAG. xMAP, a solution-phase array composed of spectrally distinct microspheres ("beads"), could detect up to 100 targets in a reaction by coupling probes of different targets with microspheres. The TAG sequence is a generic TAG unique to Luminex and consists of 24 bases. The primers with TAG sequence were mixed with nucleic acids for PCR amplification to obtain the target products containing TAG sequence. The TAG sequence specifically combined with the anti-TAG sequence on the beads to acquire a "beads-detector." Then the fluorescence of each microsphere was detected and analyzed by flow cytometry. With the advantages of high throughput, rapidity, sensitivity and accuracy, Luminex technology has been widely used in many fields such as drug development, disease diagnosis and food safety. Wu et al. developed a PCR-based fluorescent Luminex assay for human papillomavirus (HPV) genotyping, and the assay may be used to provide critical clinical information for the early detection of HPV (Oh et al., 2007). A Luminex xTAG multiplex detection method with high sensitivity and specificity, was developed for the

simultaneous detection of 11 porcine viral diarrhea pathogens (Shi et al., 2021). A total of 753 porcine stool specimens from five districts in Shanghai were detected using this assay and the surveillance confirmed that PEDV is still the main pathogen of porcine diarrhea (Shi et al., 2021). Wang et al. reported a multiplex Luminex assay for rapid detection and differentiation of the PRRSV field strains and vaccine strains (Wang et al., 2020b). Compared to RT-qPCR method, Luminex assay can achieve higher strain coverage since only two oligos may be required in the detection system (Wang et al., 2020b). A rapid, highly multiplexed nucleic acid assay employing Luminex™ liquid array technology was developed early for the differential diagnosis of FMDV, SVDV and other vesicular diseases pathogens (Lenhoff et al., 2008). Due to its high-throughput characteristics, Luminex technology enables multiplex detection of pathogens. A variety of commercial kits based on Luminex technology for different pathogens have also been developed, which provides convenience for the rapid diagnosis of different pathogens, especially those with similar symptoms (Krunic et al., 2011; Gray and Coupland, 2014; Glushakova et al., 2019).

CRISPR-Cas technology

In order to deal with the threat of emerging and re-emerging infectious diseases, rapid detection of pathogen specific nucleic acid is essential. As a novel biosensing platform, CRISPR-Cas technology plays a key role in gene editing and molecular diagnosis. The system was originally discovered to resist the invasion of foreign DNA and viruses in bacteria and archaea (Wiedenheft et al., 2012). Subsequently, CRISPR-Cas9 system was developed as a powerful genome engineering tool and applied in various fields, especially in the treatment of genetic diseases, screening and detection of disease-related genes, cancer treatment, transformation of animals and plants, and prevention of pathogenic microorganisms (Yin et al., 2021). Cas12a is a single RNA-guided endonuclease lacking trans-activating crRNA (tracrRNA), which could recognize a T-rich PAM and exert the DNA cleavage activity (Zetsche et al., 2015). Unlike Cas12a, Cas13a targets and cleaves RNA at multiple locations without recognizing PAM (Yin et al., 2021). Intriguingly, both of the two nucleases exhibit collateral, nonspecific activities on random ssDNA or ssRNA respectively upon target recognition, so that they are respectively explored for nucleic acid detection (Yin et al., 2021). Diagnostic tool DETECTOR based on Cas12a (Chen et al., 2018) and SHERLOCK based on Cas13a (Gootenberg et al., 2017) were successively developed for DNA or RNA diagnosis (Figure 4). When the two nucleases recognized the corresponding targets, the trans-cleavage activity of Cas12a and Cas13a was activated to degrade the doubly labeled fluorescent reporter, which could produce fluorescence. CRISPR-Cas systems are developed as novel and powerful diagnostic techniques, and could use different strategies for virus detection including different signal readouts and lateral flow assays (LFA) (Yin et al., 2021). In general, good real-time PCR assays can detect 10 or less genome copies in a sample and the CRISPR-Cas assays can detect at similar levels. Meanwhile, combined with LFA, CRISPR-Cas technology is being developed as a sensitive, specific, rapid molecular diagnostic tool with potential, and shows great advantages in field-deployable detection. Multiple detection methods based on CRISPR-Cas12a/Cas13a were developed for different virus diagnosis such as influenza A viruses (Liu et al., 2019), SARS-CoV-2(Broughton et al., 2020), ASFV (Yang et al., 2022), PRRSV (Chang et al., 2020) and JEV (Xu et al., 2022). Multiplex detection of viruses

Different molecular biological detection methods including those mentioned earlier have played an important role in disease diagnosis and pathogen monitoring. PCR and other amplification reactions using different primer pairs simultaneously can quickly confirm the exact causative agent. Multiple specific primers pairs (including SVA, FMDV, SVDV and VSV) were used to identify SVA as the pathogen of vesicular disease in PIVD piglets from Guangdong and Hubei province, China (Qian et al., 2016; Zhang et al., 2018). However, these primers are reacted in separate tubes, so that it is time consuming, labor intensive and not cost-effective. The advantage of multiplex tests is that they increase the chance of identifying the microbial causes of viral infections and can detect more than one pathogen at a single time point when there are co-infections. Multiplex PCR (mPCR) is a validated strategy for the rapid detection and precise identification of a large number of viruses by incorporating several primers within one reaction tube to amplify genomic fragments of many pathogens. Fernandez et al. established a highly sensitive and specific one-step multiplex RT-PCR assay for the simultaneous and differential detection of FMDV, SVDV and vesicular stomatitis virus (VSV) (Fernandez et al., 2008). Lung et al. developed a multiplex RT-PCR and microarray for the detection/typing of 4 vesicular disease viruses (FMDV, VSV, SVDV, VESV) (Lung et al., 2011). In this study, multiple virus-specific probes for each of the four target viruses and serotype-specific probes for all VSV and FMDV serotypes were identified. Probe redundancy is an important advantage of microarrays over real-time RT-PCR in allowing broader coverage of diverse strains (Erickson et al., 2018). The use of a large number of probes increases the confidence of positive results and also decreases the likelihood of generating false negative results that may occur due to genetic changes resulting from virus evolution. Several other microarray assays have been described recently for the detection of vesicular disease viruses, but only two of these serotyped any viruses: FMDV (Baxi et al., 2006) and VSV (Baner et al., 2007). The assay used padlock probe methodology and both rolling circle amplification and PCR amplification. This assay targeted three vesicular disease viruses (FMDV, VSV and SVDV), but not VESV. Padlock probe technology has the capacity for highly multiplex assays and is promising for the detection and typing of genetically variable RNA viruses because the number of conserved regions on the target needed for amplification and detection is reduced when compared with conventional PCR amplification. The assay as

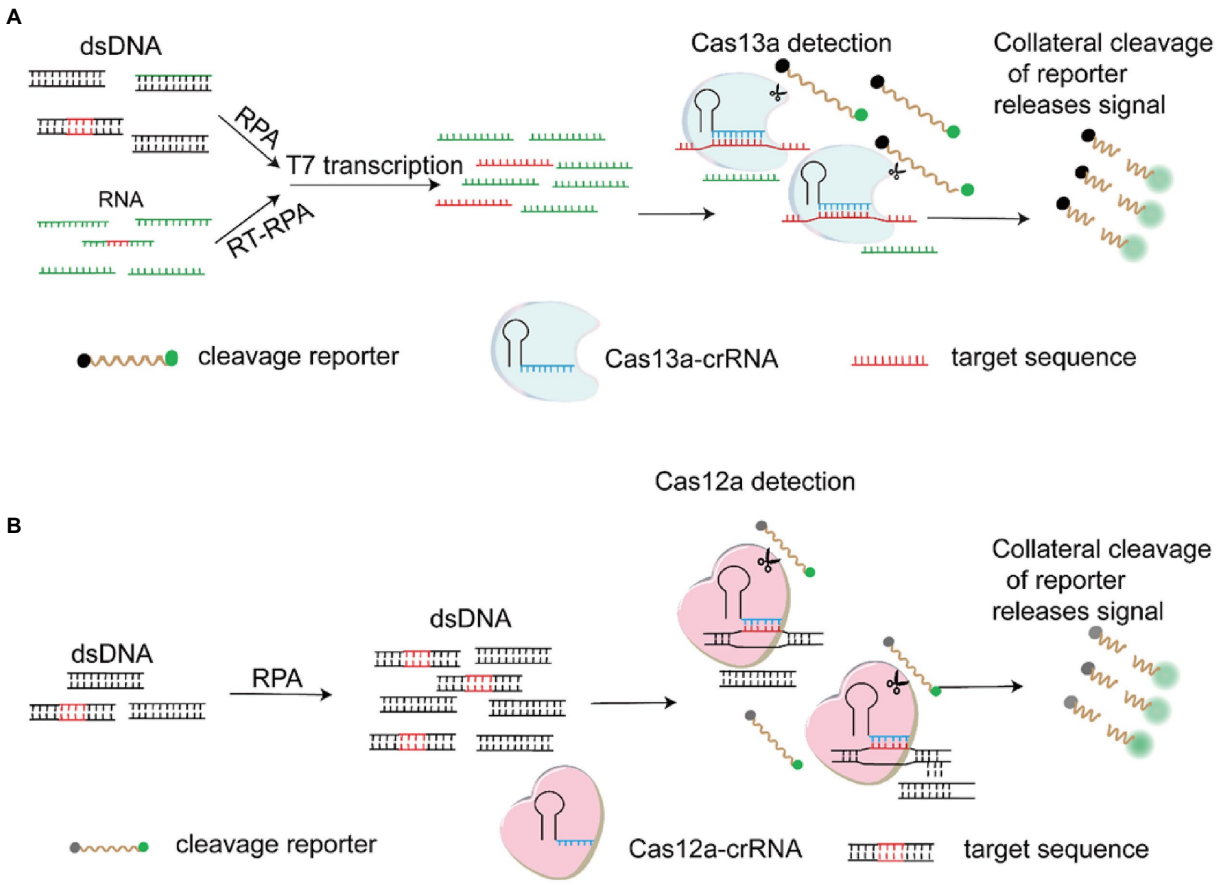

FIGURE 4
Schematic of the SHERLOCK and DETECTR. **(A)** CRISPR-Cas13a based detection (SHERLOCK). Following the RPA (Recombinase Polymerase Amplification) or RT (Reverse Transcription)-RPA, the RNA target recognized by Cas13a-crRNA complex is produced by in vitro transcription of the DNA amplicons. On recognition of the RNA target, the trans-cleavage activity of Cas13a is activated, resulting in the degradation of the doubly labeled fluorescent reporter. **(B)** CRISPR-Cas12a based detection (DETECTR). The RPA amplicon is used directly as the target for the Cas12a-crRNA complex. On the recognition of the DNA target, the trans-cleavage activity of Cas12a is activated, resulting in the degradation of the doubly labeled fluorescent reporter (Yin et al., 2021).

described by Banér et al. had a run time that was comparable to real-time RT-PCR, but required separate addition of several reagents and the assay did not serotype FMDV. Furthermore, the sensitivity of the assay presented here appears to be higher for all three vesicular disease viruses targeted by Baner et al. (2007), although viral strains used for evaluation of the diagnostic sensitivity were different between the two studies. The single virus FMDV serotyping assay developed by Baxi et al. (2006) was expanded in this current work by including a multiplex RT-PCR for four vesicular disease viruses and a microarray that serotypes VSV in addition to FMDV. The additional information obtained regarding the presence or absence of differential pathogens may make the assay an attractive screening tool for vesicular viruses for use on a herd basis. Erickson and the colleagues combined PCR assay with microarray technology to develop a multiplex reverse transcription PCR and automated electronic microarray assay for detection and differentiation of FMDV, SVDV, VESV, CSFV, and ASFV (Erickson et al., 2018). Even though these assays with microarrays have been demonstrated to be effective, these microarrays are not used for diagnostics due to the cost and complexity of them. Shi et al. developed and validated a panel of multiplex real-time assays for simultaneous detection and differentiation of 12 important viruses and viral serotypes (Shi et al., 2016). The newly developed panel of multiplex real-time PCR assays offers a rapid, high-throughput, and reliable screening system for the 12 major viruses including FMDV and SVDV in swine (Shi et al., 2016). Recently, multiplex real-time RT-PCR assays for the detection and differentiation of FMDV and SVA was also developed and evaluated (Wang et al., 2020a).

Concluding remarks

In recent years, with the growth of international trade, the risk of cross-border transmission of certain diseases has increased significantly. In order to prevent the spread of the vital pathogens that could harm economic animals, accurate diagnosis is essential.

The possible disease agent can be determined through the observation of clinical symptoms and pathological changes of sick animals. However, the viruses with similar symptoms could not be distinguished such as FMDV, SVA and SVDV. Virus isolation is time-consuming and requires multiple blind passes of samples to produce usable amounts of infectious material. Further accurate and rapid confirmation of pathogens is required by serological and molecular biological methods. With the development of biotechnology, different molecular diagnostic techniques are constantly developing, which play a significant effect in the pathogen detection of swine vesicular diseases. RT-PCR and real-time RT-PCR are still the most reliable methods for detecting the viruses including FMDV, SVA and SVDV, among which real-time RT-PCR with high sensitivity is regarded as the gold standard. The development of multiplex detection provides a powerful technical means for the diagnosis of pathogens with similar clinical symptoms and the detection of co-infections. The combination of isothermal nucleic acid amplification method and lateral flow test can get rid of the limitation of instruments, save time and effort, and be helpful for rapid and accurate diagnosis on-site. How to improve sensitivity is the key to the development of this technology. Luminex technology has the advantages of high throughput, wide detection range and small sample size. In addition, it is suitable for large-scale screening of clinical samples, especially for the detection of multiple infections. The technology provides a new platform for high-throughput nucleic acid detection, and is widely used in the detection of various infectious diseases. CRISPR-Cas, characterized by sensitivity, specificity and programmability for nucleic acid recognition, has been repurposed for molecular diagnostics, thereby advancing a new path in biosensing. Disease diagnosis is an important part of epidemic prevention and control. New rapid and sensitive detection platforms applicable to the field are required to provide more time-saving and effective means in the outbreak of infectious diseases and minimize economic losses. Surveillance for FMDV and other viruses with similar symptoms including SVA, SVDV and VESV is necessary. The key to field diagnosis is the development of simple, low cost, user friendly, highly sensitive and specific rapid tests. This can be potentially accomplished using inexpensive, portable fluorescent instruments and test strips.

Author contributions

WC: writing—original draft preparation. WW and XW: writing—review and editing. ZL, XL, and KW: conceptualization, supervision, and project administration. YL, LY, MZ, HD, SF, and JC: contributed to both the conception and design of the work. All authors have read and agreed to the published version of the manuscript.

Funding

This work was supported by grants from the National Key R&D Program of China (2021YFD1800300); the Program of National Natural Science Foundation of China (No. 32172824); the Key Research Projects of Universities in Guangdong Province (No. 2019KZDXM026).

Conflict of interest

The authors declare that the research was conducted in the absence of any commercial or financial relationships that could be construed as a potential conflict of interest.

Publisher's note

All claims expressed in this article are solely those of the authors and do not necessarily represent those of their affiliated organizations, or those of the publisher, the editors and the reviewers. Any product that may be evaluated in this article, or claim that may be made by its manufacturer, is not guaranteed or endorsed by the publisher.

References

Abd, E. W. A., El-Deeb, A., El-Tholoth, M., Abd, E. K. H., Ahmed, A., Hassan, S., et al. (2013). A portable reverse transcription recombinase polymerase amplification assay for rapid detection of foot-and-mouth disease virus. *Plos One.* 8:e71642. doi: 10.1371/journal.pone.0071642

Almasi, M. A., Hosseyni-Dehabadi, S. M., and Aghapour-ojaghkandi, M. (2014). Comparison and evaluation of three diagnostic methods for detection of beet curly top virus in sugar beet using different visualizing systems. *Appl. Biochem. Biotechnol.* 173, 1836–1848. doi: 10.1007/s12010-014-0970-7

Ambagala, A., Fisher, M., Goolia, M., Nfon, C., Furukawa-Stoffer, T., Ortega, P. R., et al. (2017). Field-deployable reverse transcription-insulated isothermal pcr (rt-iipcr) assay for rapid and sensitive detection of foot-and-mouth disease virus. *Transbound. Emerg. Dis.* 64, 1610–1623. doi: 10.1111/tbed.12554

Armson, B., Di Nardo, A., Nyaguthii, D. M., Sanz-Bernardo, B., Kitala, P. M., Chepkwony, E., et al. (2020a). Utilizing milk from pooling facilities as a novel approach for foot-and-mouth disease surveillance. *Transbound. Emerg. Dis.* 67, 1532–1542. doi: 10.1111/tbed.13487

Armson, B., Gubbins, S., Mioulet, V., Qasim, I. A., King, D. P., and Lyons, N. A. (2020b). Foot-and-mouth disease surveillance using pooled milk on a large-scale dairy farm in an endemic setting. *Front. Vet. Sci.* 7:264. doi: 10.3389/fvets.2020.00264

Armson, B., Wadsworth, J., Kibona, T., Mshanga, D., Fowler, V. L., Knowles, N. J., et al. (2019a). Opportunities for enhanced surveillance of foot-and-mouth disease in endemic settings using milk samples. *Transbound. Emerg. Dis.* 66, 1405–1410. doi: 10.1111/tbed.13146

Armson, B., Walsh, C., Morant, N., Fowler, V. L., Knowles, N. J., and Clark, D. (2019b). The development of two field-ready reverse transcription loop-mediated isothermal amplification assays for the rapid detection of seneca valley virus 1. *Transbound. Emerg. Dis.* 66, 497–504. doi: 10.1111/tbed.13051

Baner, J., Gyarmati, P., Yacoub, A., Hakhverdyan, M., Stenberg, J., Ericsson, O., et al. (2007). Microarray-based molecular detection of foot-and-mouth disease, vesicular stomatitis and swine vesicular disease viruses, using padlock probes. *J. Virol. Methods.* 143, 200–206. doi: 10.1016/j.jviromet.2007.03.004

Baxi, M. K., Baxi, S., Clavijo, A., Burton, K. M., and Deregt, D. (2006). Microarray-based detection and typing of foot-and-mouth disease virus. *Vet. J.* 172, 473–481. doi: 10.1016/j.tvjl.2005.07.007

Bellini, S., Santucci, U., Zanardi, G., Brocchi, E., and Marabelli, R. (2007). Swine vesicular disease surveillance and eradication activities in Italy. *Rev Sci Tech.* 26, 585–593.

Bhat, A. I., Aman, R., and Mahfouz, M. (2022). Onsite detection of plant viruses using isothermal amplification assays. *Plant Biotechnol. J.* 20, 1859–1873. doi: 10.1111/pbi.13871

Blomström, A., Hakhverdyan, M., Reid, S. M., Dukes, J. P., King, D. P., Belák, S., et al. (2008). A one-step reverse transcriptase loop-mediated isothermal amplification assay for simple and rapid detection of swine vesicular disease virus. *J. Virol. Methods.* 147, 188–193. doi: 10.1016/j.jviromet.2007.08.023

Bracht, A. J., O'Hearn, E. S., Fabian, A. W., Barrette, R. W., and Sayed, A. (2016). Real-time reverse transcription PCR assay for detection of Senecavirus A in swine vesicular diagnostic specimens. *PLoS One.* 11:e146211. doi: 10.1371/journal.pone.0146211

Brito, B., Pauszek, S. J., Hartwig, E. J., Smoliga, G. R., Vu, L. T., Dong, P. V., et al. (2018). A traditional evolutionary history of foot-and-mouth disease viruses in southeast Asia challenged by analyses of non-structural protein coding sequences. *Sci Rep.* 8:6472. doi: 10.1038/s41598-018-24870-6

Broughton, J. P., Deng, X., Yu, G., Fasching, C. L., Servellita, V., Singh, J., et al. (2020). Crispr-cas 12-based detection of SARS-cov-2. *Nat. Biotechnol.* 38, 870–874. doi: 10.1038/s41587-020-0513-4

Brown, V. R., Miller, R. S., McKee, S. C., Ernst, K. H., Didero, N. M., Maison, R. M., et al. (2021). Risks of introduction and economic consequences associated with African swine fever, classical swine fever and foot-and-mouth disease: a review of the literature. *Transbound. Emerg. Dis.* 68, 1910–1965. doi: 10.1111/tbed.13919

Brown, E., Nelson, N., Gubbins, S., and Colenutt, C. (2022). Airborne transmission of foot-and-mouth disease virus: a review of past and present perspectives. *Viruses.* 14. doi: 10.3390/v14051009

Buckley, A. C., Michael, D. D., Faaberg, K. S., Guo, B., Yoon, K., and Lager, K. M. (2021). Comparison of historical and contemporary isolates of Senecavirus A. *Vet. Microbiol.* 253:108946. doi: 10.1016/j.vetmic.2020.108946

Burke, M. J. (2016). Oncolytic Seneca valley virus: past perspectives and future directions. *Oncolytic Virother.* 5, 81–89. doi: 10.2147/OV.S96915

Burkhalter, K. L., and Savage, H. M. (2017). Detection of zika virus in desiccated mosquitoes by real-time reverse transcription PCR and plaque assay. *Emerg. Infect. Dis.* 23, 680–681. doi: 10.3201/eid2304.161772

Callahan, J. D., Brown, F., Osorio, F. A., Sur, J. H., Kramer, E., Long, G. W., et al. (2002). Use of a portable real-time reverse transcriptase-polymerase chain reaction assay for rapid detection of foot-and-mouth disease virus. *J. Am. Vet. Med. Assoc.* 220, 1636–1642. doi: 10.2460/javma.2002.220.1636

Callens, M., and De Clercq, K. (1997). Differentiation of the seven serotypes of foot-and-mouth disease virus by reverse transcriptase polymerase chain reaction. *J. Virol. Methods.* 67, 35–44. doi: 10.1016/s0166-0934(97)00074-8

Canning, P., Canon, A., Bates, J. L., Gerardy, K., Linhares, D. C. L., Piñeyro, P. E., et al. (2016). Neonatal mortality, vesicular lesions and lameness associated with Senecavirus A in a U.S. Sow farm. *Transbound. Emerg. Dis.* 63, 373–378. doi: 10.1111/tbed.12516

Carrillo, C., Tulman, E. R., Delhon, G., Lu, Z., Carreno, A., Vagnozzi, A., et al. (2005). Comparative genomics of foot-and-mouth disease virus. *J. Virol.* 79, 6487–6504. doi: 10.1128/JVI.79.10.6487-6504.2005

Chang, Y., Deng, Y., Li, T., Wang, J., Wang, T., Tan, F., et al. (2020). Visual detection of porcine reproductive and respiratory syndrome virus using CRISPR-Cas 13a. *Transbound. Emerg. Dis.* 67, 564–571. doi: 10.1111/tbed.13368

Chen, J. S., Ma, E., Harrington, L. B., Da, C. M., Tian, X., Palefsky, J. M., et al. (2018). CRISPR-cas12a target binding unleashes indiscriminate single-stranded DNase activity. *Science.* 360, 436–439. doi: 10.1126/science.aar6245

Chen, H., Zhang, J., Liu, Y., and Liu, X. (2011). Detection of foot-and-mouth disease virus RNA by reverse transcription loop-mediated isothermal amplification. *Virol. J.* 8:510. doi: 10.1186/1743-422X-8-510

Corman, V. M., Landt, O., Kaiser, M., Molenkamp, R., Meijer, A., Chu, D. K., et al. (2020). Detection of 2019 novel coronavirus (2019-ncov) by real-time RT-PCR. *Euro Surveill.* 25:2000045. doi: 10.2807/1560-7917.ES.2020.25.3.2000045

Daher, R. K., Stewart, G., Boissinot, M., and Bergeron, M. G. (2016). Recombinase polymerase amplification for diagnostic applications. *Clin. Chem.* 62, 947–958. doi: 10.1373/clinchem.2015.245829

Dall, A. A., Otonel, R., Leme, R. A., Alfieri, A. A., and Alfieri, A. F. (2017). A taqman-based qRT-PCR assay for Senecavirus A detection in tissue samples of neonatal piglets. *Mol Cell Probes.* 33, 28–31. doi: 10.1016/j.mcp.2017.03.002

Dibaba, A. B. (2019). The risk of introduction of swine vesicular disease virus into Kenya via natural sausage casings imported from Italy. *Prev. Vet. Med.* 169:104703. doi: 10.1016/j.prevetmed.2019.104703

Dill, V., Beer, M., and Hoffmann, B. (2017). Simple, quick and cost-efficient: a universal RT-PCR and sequencing strategy for genomic characterisation of foot-and-mouth disease viruses. *J. Virol. Methods.* 246, 58–64. doi: 10.1016/j.jviromet.2017.04.007

Erickson, A., Fisher, M., Furukawa-Stoffer, T., Ambagala, A., Hodko, D., Pasick, J., et al. (2018). A multiplex reverse transcription PCR and automated electronic microarray assay for detection and differentiation of seven viruses affecting swine. *Transbound. Emerg. Dis.* 65, e272–e283. doi: 10.1111/tbed.12749

Fernandes, M., Maggioli, M. F., Joshi, L. R., Clement, T., Faccin, T. C., Rauh, R., et al. (2018). Pathogenicity and cross-reactive immune responses of a historical and a contemporary Senecavirus A strains in pigs. *Virology* 522, 147–157. doi: 10.1016/j.virol.2018.06.003

Fernandez, J., Aguero, M., Romero, L., Sanchez, C., Belak, S., Arias, M., et al. (2008). Rapid and differential diagnosis of foot-and-mouth disease, swine vesicular disease, and vesicular stomatitis by a new multiplex RT-PCR assay. *J. Virol. Methods.* 147, 301–311. doi: 10.1016/j.jviromet.2007.09.010

Feronato, C., Leme, R. A., Diniz, J. A., Agnol, A. M. D., Alfieri, A. F., and Alfieri, A. A. (2018). Development and evaluation of a nested-PCR assay for senecavirus a diagnosis. *Trop. Anim. Health Pro.* 50, 337–344. doi: 10.1007/s11250-017-1436-z

Fischer, C., Torres, M. C., Patel, P., Moreira-Soto, A., Gould, E. A., Charrel, R. N., et al. (2017). Lineage-specific real-time rt-pcr for yellow fever virus outbreak surveillance, Brazil. *Emerg. Infect. Dis.* 23. doi: 10.3201/eid2311.171131

Fontel, K. S., Botner, A., Belsham, G. J., and Lohse, L. (2019). Diagnostic comparison of serum and EDTA-stabilized blood samples for the detection of foot-and-mouth disease virus RNA by RT-qPCR. *J. Virol. Methods.* 270, 120–125. doi: 10.1016/j.jviromet.2019.05.003

Fowler, V. L., Ransburgh, R. H., Poulsen, E. G., Wadsworth, J., King, D. P., Mioulet, V., et al. (2017). Development of a novel real-time RT-PCR assay to detect Seneca valley virus-1 associated with emerging cases of vesicular disease in pigs. *J. Virol. Methods.* 239, 34–37. doi: 10.1016/j.jviromet.2016.10.012

Galluzzi, L., Ceccarelli, M., Diotallevi, A., Menotta, M., and Magnani, M. (2018). Real-time PCR applications for diagnosis of leishmaniasis. *Parasite. Vector.* 11:273. doi: 10.1186/s13071-018-2859-8

Gimenez-Lirola, L. G., Rademacher, C., Linhares, D., Harmon, K., Rotolo, M., Sun, Y., et al. (2016). Serological and molecular detection of senecavirus a associated with an outbreak of swine idiopathic vesicular disease and neonatal mortality. *J. Clin. Microbiol.* 54, 2082–2089. doi: 10.1128/JCM.00710-16

Gloster, J., Champion, H. J., Sorensen, J. H., Mikkelsen, T., Ryall, D. B., Astrup, P., et al. (2003). Airborne transmission of foot-and-mouth disease virus from burnside farm, heddon-on-the-wall, northumberland, during the 2001 epidemic in the United Kingdom. *Vet. Rec.* 152, 525–533. doi: 10.1136/vr.152.17.525

Glushakova, L. G., Alto, B. W., Kim, M. S., Hutter, D., Bradley, A., Bradley, K. M., et al. (2019). Multiplexed kit based on luminex technology and achievements in synthetic biology discriminates zika, chikungunya, and dengue viruses in mosquitoes. *Bmc Infect. Dis.* 19:418. doi: 10.1186/s12879-019-3998-z

Goller, K. V., Dill, V., Madi, M., Martin, P., Van der Stede, Y., Vandenberge, V., et al. (2018). Rapid and simple detection of foot-and-mouth disease virus: evaluation of a cartridge-based molecular detection system for use in basic laboratories. *Transbound. Emerg. Dis.* 65, 578–584. doi: 10.1111/tbed.12744

Gootenberg, J. S., Abudayyeh, O. O., Lee, J. W., Essletzbichler, P., Dy, A. J., Joung, J., et al. (2017). Nucleic acid detection with CRISPR-cas13a/c2c2. *Science.* 356, 438–442. doi: 10.1126/science.aam9321

Graves, J. H. (1973). Serological relationship of swine vesicular disease virus and coxsackie b5 virus. *Nature.* 245, 314–315. doi: 10.1038/245314a0

Gray, J., and Coupland, L. J. (2014). The increasing application of multiplex nucleic acid detection tests to the diagnosis of syndromic infections. *Epidemiol. Infect.* 142, 1–11. doi: 10.1017/S0950268813002367

Grubman, M. J., and Baxt, B. (2004). Foot-and-mouth disease. *Clin. Microbiol. Rev.* 17, 465–493. doi: 10.1128/CMR.17.2.465-493.2004

Hakhverdyan, M., Rasmussen, T. B., Thorén, P., Uttenthal, A., and Belák, S. (2006). Development of a real-time PCR assay based on primer-probe energy transfer for the detection of swine vesicular disease virus. *Arch. Virol.* 151, 2365–2376. doi: 10.1007/s00705-006-0817-9

Hales, L. M., Knowles, N. J., Reddy, P. S., Xu, L., Hay, C., and Hallenbeck, P. L. (2008). Complete genome sequence analysis of seneca valley virus-001, a novel oncolytic picornavirus. *J. Gen. Virol.* 89, 1265–1275. doi: 10.1099/vir.0.83570-0

Hole, K., and Nfon, C. (2019). Foot-and-mouth disease virus detection on a handheld real-time polymerase chain reaction platform. *Transbound. Emerg. Dis.* 66, 1789–1795. doi: 10.1111/tbed.13227

Holland, J. J., Mclaren, L. C., Hoyer, B. H., and Syverton, J. T. (1960). Enteroviral ribonucleic acid. Ii. Biological, physical, and chemical studies. *J. Exp. Med.* 112, 841–864. doi: 10.1084/jem.112.5.841

Houston, E., Temeeyasen, G., and Pineyro, P. E. (2020). Comprehensive review on immunopathogenesis, diagnostic and epidemiology of senecavirus a. *Virus Res.* 286:198038. doi: 10.1016/j.virusres.2020.198038

Howson, E., Armson, B., Lyons, N. A., Chepkwony, E., Kasanga, C. J., Kandusi, S., et al. (2018). Direct detection and characterization of foot-and-mouth disease virus in east Africa using a field-ready real-time PCR platform. *Transbound. Emerg. Dis.* 65, 221–231. doi: 10.1111/tbed.12684

Howson, E., Armson, B., Madi, M., Kasanga, C. J., Kandusi, S., Sallu, R., et al. (2017a). Evaluation of two lyophilized molecular assays to rapidly detect foot-and-mouth disease virus directly from clinical samples in field settings. *Transbound. Emerg. Dis.* 64, 861–871. doi: 10.1111/tbed.12451

Howson, E., Kurosaki, Y., Yasuda, J., Takahashi, M., Goto, H., Gray, A. R., et al. (2017b). Defining the relative performance of isothermal assays that can be used for rapid and sensitive detection of foot-and-mouth disease virus. *J. Virol. Methods.* 249, 102–110. doi: 10.1016/j.jviromet.2017.08.013

Huggett, J. F., and Whale, A. (2013). Digital pcr as a novel technology and its potential implications for molecular diagnostics. *Clin. Chem.* 59, 1691–1693. doi: 10.1373/clinchem.2013.214742

Jones, M., Williams, J., Gartner, K., Phillips, R., Hurst, J., and Frater, J. (2014). Low copy target detection by droplet digital pcr through application of a novel open access bioinformatic pipeline, 'definetherain'. *J. Virol. Methods.* 202, 46–53. doi: 10.1016/j.jviromet.2014.02.020

Joshi, L. R., Mohr, K. A., Clement, T., Hain, K. S., Myers, B., Yaros, J., et al. (2016). Detection of the emerging picornavirus senecavirus a in pigs, mice, and houseflies. *J. Clin. Microbiol.* 54, 1536–1545. doi: 10.1128/JCM.03390-15

Kim, D. S., Son, K. Y., Koo, K. M., Kim, J. Y., Alfajaro, M. M., Park, J. G., et al. (2016). Porcine sapelovirus uses alpha 2, 3-linked sialic acid on GD1a ganglioside as a receptor. *J. Virol.* 90, 4067–4077. doi: 10.1128/JVI.02449-15

Klein, J., Hussain, M., Ahmad, M., Normann, P., Afzal, M., and Alexandersen, S. (2007). Genetic characterisation of the recent foot-and-mouth disease virus subtype A/IRN/2005. *Virol. J.* 4:122. doi: 10.1186/1743-422X-4-122

Kojabad, A. A., Farzanehpour, M., Galeh, H., Dorostkar, R., Jafarpour, A., Bolandian, M., et al. (2021). Droplet digital pcr of viral DNA/RNA, current progress, challenges, and future perspectives. *J. Med. Virol.* 93, 4182–4197. doi: 10.1002/jmv.26846

Krunic, N., Merante, F., Yaghoubian, S., Himsworth, D., and Janeczko, R. (2011). Advances in the diagnosis of respiratory tract infections: role of the luminex xtag respiratory viral panel. *Ann N Y Acad Sci.* 1222, 6–13. doi: 10.1111/j.1749-6632.2011.05964.x

LaBarre, P., Hawkins, K. R., Gerlach, J., Wilmoth, J., Beddoe, A., Singleton, J., et al. (2011). A simple, inexpensive device for nucleic acid amplification without electricity-toward instrument-free molecular diagnostics in low-resource settings. *Plos One.* 6:e19738. doi: 10.1371/journal.pone.0019738

Laguardia-Nascimento, M., Gasparini, M. R., Sales, E. B., Rivetti, A. J., Sousa, N. M., Oliveira, A. M., et al. (2016). Molecular epidemiology of senecavirus a associated with vesicular disease in pigs in Brazil. *Vet. J.* 216, 207–209. doi: 10.1016/j.tvjl.2016.08.013

Le, V. P., Lee, K. N., Nguyen, T., Kim, S. M., Cho, I. S., Van Quyen, D., et al. (2011). Development of one-step multiplex RT-PCR method for simultaneous detection and differentiation of foot-and-mouth disease virus serotypes o, a, and Asia 1 circulating in Vietnam. *J. Virol. Methods.* 175, 101–108. doi: 10.1016/j.jviromet.2011.04.027

Leme, R. A., Alfieri, A. F., and Alfieri, A. A. (2017). Update on senecavirus infection in pigs. *Viruses.* 9. doi: 10.3390/v9070170

Leme, R. A., Zotti, E., Alcântara, B. K., Oliveira, M. V., Freitas, L. A., Alfieri, A. F., et al. (2015). Senecavirus a: an emerging vesicular infection in Brazilian pig herds. *Transbound. Emerg. Dis.* 62, 603–611. doi: 10.1111/tbed.12430

Lenhoff, R. J., Naraghi-Arani, P., Thissen, J. B., Olivas, J., Carillo, A. C., Chinn, C., et al. (2008). Multiplexed molecular assay for rapid exclusion of foot-and-mouth disease. *J. Virol. Methods.* 153, 61–69. doi: 10.1016/j.jviromet.2008.06.015

Lewis-Rogers, N., and Crandall, K. A. (2010). Evolution of *Picornaviridae*: an examination of phylogenetic relationships and cophylogeny. *Mol. Phylogenet. Evol.* 54, 995–1005. doi: 10.1016/j.ympev.2009.10.015

Li, H., Bai, R., Zhao, Z., Tao, L., Ma, M., Ji, Z., et al. (2018). Application of droplet digital PCR to detect the pathogens of infectious diseases. *Biosci Rep.* 38. doi: 10.1042/BSR20181170

Li, J., Liang, W., Xu, S., Shi, J., Zhou, X., Liu, B., et al. (2019). Rapid and sensitive detection of senecavirus a by reverse transcription loop-mediated isothermal amplification combined with a lateral flow dipstick method. *Plos One.* 14:e216245. doi: 10.1371/journal.pone.0216245

Liao, P., and Huang, Y. (2017). Digital PCR: endless frontier of "divide and conquer". *Micromachines (Basel).* 8. doi: 10.3390/mi8080231

Lim, D., Kim, H., Chae, H., Ku, B., Nah, J., Ryoo, S., et al. (2020). Probe-based real-time reverse transcription loop-mediated isothermal amplification (RRT-LAMP) assay for rapid and specific detection of foot-and-mouth disease virus. *Transbound. Emerg. Dis.* 67, 2936–2945. doi: 10.1111/tbed.13669

Lim, D. R., Kim, H. R., Park, M. J., Chae, H. G., Ku, B. K., Nah, J. J., et al. (2018). An improved reverse transcription loop-mediated isothermal amplification assay for sensitive and specific detection of serotype o foot-and-mouth disease virus. *J. Virol. Methods.* 260, 6–13. doi: 10.1016/j.jviromet.2018.06.017

Lim, D., Kim, H., Park, M., Chae, H., Ku, B., Nah, J., et al. (2018). A tailored reverse transcription loop-mediated isothermal amplification for sensitive and specific detection of serotype a foot-and-mouth disease virus circulating in pool 1 region countries. *Transbound. Emerg. Dis.* 65, 1898–1908. doi: 10.1111/tbed.12971

Lim, D., Ryoo, S., Kang, H., Park, H., Hwang, H., Kim, J., et al. (2022). Enhanced detection and serotyping of foot-and-mouth disease virus serotype o, a, and Asia 1 using a novel multiplex real-time RT-PCR. *Transbound. Emerg. Dis.* doi: 10.1111/tbed.14603

Lin, F., and Kitching, R. P. (2000). Swine vesicular disease: an overview. *Vet. J.* 160, 192–201. doi: 10.1053/tvjl.2000.0505

Lin, F., Mackay, D. K., and Knowles, N. J. (1997). Detection of swine vesicular disease virus RNA by reverse transcription-polymerase chain reaction. *J. Virol. Methods.* 65, 111–121. doi: 10.1016/s0166-0934(96)02174-x

Lin, H. T., Okumura, T., Yatsuda, Y., Ito, S., Nakauchi, H., and Otsu, M. (2016). Application of droplet digital pcr for estimating vector copy number states in stem cell gene therapy. *Hum Gene Ther Methods.* 27, 197–208. doi: 10.1089/hgtb.2016.059

Liu, F., Wang, Q., Huang, Y., Wang, N., and Shan, H. (2020). A 5-year review of senecavirus a in china since its emergence in 2015. *Front Vet Sci.* 7:567792. doi: 10.3389/fvets.2020.567792

Liu, L., Wang, J., Zhang, R., Lin, M., Shi, R., Han, Q., et al. (2018). Visual and equipment-free reverse transcription recombinase polymerase amplification method for rapid detection of foot-and-mouth disease virus. *Bmc Vet. Res.* 14:263. doi: 10.1186/s12917-018-1594-x

Liu, Y., Xu, H., Liu, C., Peng, L., Khan, H., Cui, L., et al. (2019). Crispr-cas 13a nanomachine based simple technology for avian influenza a (h7n9) virus on-site detection. *J. Biomed. Nanotechnol.* 15, 790–798. doi: 10.1166/jbn.2019.2742

Lobato, I. M., and O'Sullivan, C. K. (2018). Recombinase polymerase amplification: basics, applications and recent advances. *Trends Analyt Chem.* 98, 19–35. doi: 10.1016/j.trac.2017.10.015

Lung, O., Fisher, M., Beeston, A., Hughes, K. B., Clavijo, A., Goolia, M., et al. (2011). Multiplex RT-PCR detection and microarray typing of vesicular disease viruses. *J. Virol. Methods.* 175, 236–245. doi: 10.1016/j.jviromet.2011.05.023

Madhanmohan, M., Nagendrakumar, S. B., Manikumar, K., Yuvaraj, S., Parida, S., and Srinivasan, V. A. (2013). Development and evaluation of a real-time reverse transcription-loop-mediated isothermal amplification assay for rapid serotyping of foot-and-mouth disease virus. *J. Virol. Methods.* 187, 195–202. doi: 10.1016/j.jviromet.2012.08.015

Mansour, S. M., Ali, H., Chase, C. C., and Cepica, A. (2015). Loop-mediated isothermal amplification for diagnosis of 18 world organization for animal health (oie) notifiable viral diseases of ruminants, swine and poultry. *Anim Health Res Rev.* 16, 89–106. doi: 10.1017/S1466252315000018

Marquardt, O., and Ohlinger, V. F. (1995). Differential diagnosis and genetic analysis of the antigenically related swine vesicular disease virus and coxsackie viruses. *J. Virol. Methods.* 53, 189–199. doi: 10.1016/0166-0934(95)00014-l

McMenamy, M. J., McKillen, J., Reid, S. M., Hjertner, B., King, D. P., Adair, B., et al. (2011). Development of a minor groove binder assay for real-time one-step rt-pcr detection of swine vesicular disease virus. *J. Virol. Methods.* 171, 219–224. doi: 10.1016/j.jviromet.2010.11.001

Meyer, R. F., Brown, C. C., House, C., House, J. A., and Molitor, T. W. (1991). Rapid and sensitive detection of foot-and-mouth disease virus in tissues by enzymatic rna amplification of the polymerase gene. *J. Virol. Methods.* 34, 161–172. doi: 10.1016/0166-0934(91)90096-i

Milbury, C. A., Zhong, Q., Lin, J., Williams, M., Olson, J., Link, D. R., et al. (2014). Determining lower limits of detection of digital PCR assays for cancer-related gene mutations. *Biomol Detect Quantif.* 1, 8–22. doi: 10.1016/j.bdq.2014.08.001

Munro, S. B., Kuypers, J., and Jerome, K. R. (2013). Comparison of a multiplex real-time pcr assay with a multiplex luminex assay for influenza virus detection. *J. Clin. Microbiol.* 51, 1124–1129. doi: 10.1128/JCM.03113-12

Mur, L., Gallardo, C., Soler, A., Zimmermman, J., Pelayo, V., Nieto, R., et al. (2013). Potential use of oral fluid samples for serological diagnosis of African swine fever. *Vet. Microbiol.* 165, 135–139. doi: 10.1016/j.vetmic.2012.12.034

Namatovu, A., Wekesa, S. N., Tjornehoj, K., Dhikusooka, M. T., Muwanika, V. B., Siegsmund, H. R., et al. (2013). Laboratory capacity for diagnosis of foot-and-mouth disease in eastern Africa: implications for the progressive control pathway. *Bmc Vet. Res.* 9:19. doi: 10.1186/1746-6148-9-19

Nardelli, L., Lodetti, E., Gualandi, G. L., Burrows, R., Goodridge, D., Brown, F., et al. (1968). A foot and mouth disease syndrome in pigs caused by an *Enterovirus*. *Nature.* 219, 1275–1276. doi: 10.1038/2191275a0

Nicot, F., Cazabat, M., Lhomme, S., Marion, O., Saune, K., Chiabrando, J., et al. (2016). Quantification of HEV RNA by droplet digital PCR. *Viruses.* 8. doi: 10.3390/v8080233

Nie, X. (2005). Reverse transcription loop-mediated isothermal amplification of DNA for detection of potato virus y. *Plant Dis.* 89, 605–610. doi: 10.1094/PD-89-0605

Niedbalski, W. (2009). Application of real-time reverse transcription polymerase chain reaction for the detection of SVDV. *Pol. J. Vet. Sci.* 12, 119–121.

Nielsen, S. C., Bruhn, C. A., Samaniego, J. A., Wadsworth, J., Knowles, N. J., and Gilbert, M. T. (2014). Near-complete genome sequencing of swine vesicular disease virus using the roche gs flx sequencing platform. *Plos One.* 9:e97180. doi: 10.1371/journal.pone.0097180

Nishi, T., Kanno, T., Shimada, N., Morioka, K., Yamakawa, M., and Fukai, K. (2019). Reverse transcription-PCR using a primer set targeting the 3d region detects foot-and-mouth disease virus with high sensitivity. *Transbound. Emerg. Dis.* 66, 1776–1783. doi: 10.1111/tbed.13202

Notomi, T., Okayama, H., Masubuchi, H., Yonekawa, T., Watanabe, K., Amino, N., et al. (2000). Loop-mediated isothermal amplification of DNA. *Nucleic Acids Res.* 28:E63. doi: 10.1093/nar/28.12.e63

Oh, Y., Bae, S. M., Kim, Y. W., Choi, H. S., Nam, G. H., Han, S. J., et al. (2007). Polymerase chain reaction-based fluorescent Luminex assay to detect the presence of human papillomavirus types. *Cancer Sci.* 98, 549–554. doi: 10.1111/j.1349-7006.2007.00427.x

Palmenberg, A. C., Spiro, D., Kuzmickas, R., Wang, S., Djikeng, A., Rathe, J. A., et al. (2009). Sequencing and analyses of all known human rhinovirus genomes reveal structure and evolution. *Science.* 324, 55–59. doi: 10.1126/science.1165557

Pasma, T., Davidson, S., and Shaw, S. L. (2008). Idiopathic vesicular disease in swine in Manitoba. *Can. Vet. J.* 49, 84–85.

Peng, Q., Ning, J., Xu, Q., Yang, T., Wang, Y., Zheng, T., et al. (2021). Development and application of a reverse transcription loop-mediated isothermal amplification combined with lateral flow dipstick for rapid and visual detection of citrus leaf blotch virus in kiwifruit. *Crop Prot.* 143

Peng, S., Wang, Y., Yang, Z., Yao, X., Hu, L., Chen, P., et al. (2015). A double polymerase chain reaction method for detecting African swine fever and swine vesicular disease virus. *Trop. J. Pharm. Res.* 14

Persson, S., Karlsson, M., Borsch-Reniers, H., Ellstrom, P., Eriksson, R., and Simonsson, M. (2019). Missing the match might not cost you the game: primer-template mismatches studied in different hepatitis a virus variants. *Food Environ. Virol.* 11, 297–308. doi: 10.1007/s12560-019-09387-z

Pezzoni, G., Benedetti, D., Bregoli, A., Barbieri, I., Foglia, E. A., Grazioli, S., et al. (2020). Diagnostic performances of different genome amplification assays for the detection of swine vesicular disease virus in relation to genomic lineages that circulated in Italy. *Viruses.* 12:doi:10.3390/v12111336.

Piepenburg, O., Williams, C. H., Stemple, D. L., and Armes, N. A. (2006). Dna detection using recombination proteins. *Plos Biol.* 4:e204. doi: 10.1371/journal.pbio.0040204

Pinheiro-de-Oliveira, T. F., Fonseca, A. J., Camargos, M. F., Laguardia-Nascimento, M., de Oliveira, A. M., Cottorello, A., et al. (2018). Development of a droplet digital RT-PCR for the quantification of foot-and-mouth virus RNA. *J. Virol. Methods.* 259, 129–134. doi: 10.1016/j.jviromet.2018.06.015

Pinheiro-de-Oliveira, T. F., Fonseca-Junior, A. A., Camargos, M. F., Laguardia-Nascimento, M., Giannattasio-Ferraz, S., Cottorello, A., et al. (2019). Reverse transcriptase droplet digital pcr to identify the emerging vesicular virus senecavirus a in biological samples. *Transbound. Emerg. Dis.* 66, 1360–1369. doi: 10.1111/tbed.13168

Postel, M., Roosen, A., Laurent-Puig, P., Taly, V., and Wang-Renault, S. F. (2018). Droplet-based digital PCR and next generation sequencing for monitoring circulating tumor DNA: a cancer diagnostic perspective. *Expert Rev. Mol. Diagn.* 18, 7–17. doi: 10.1080/14737159.2018.1400384

Powell, M. L., Bowler, F. R., Martinez, A. J., Greenwood, C. J., Armes, N., and Piepenburg, O. (2018). New FPG probe chemistry for direct detection of recombinase polymerase amplification on lateral flow strips. *Anal. Biochem.* 543, 108–115. doi: 10.1016/j.ab.2017.12.003

Qian, S., Fan, W., Qian, P., Chen, H., and Li, X. (2016). Isolation and full-genome sequencing of Seneca valley virus in piglets from China, 2016. *Virol. J.* 13:173. doi: 10.1186/s12985-016-0631-2

Reddy, P. S., Burroughs, K. D., Hales, L. M., Ganesh, S., Jones, B. H., Idamakanti, N., et al. (2007). Seneca valley virus, a systemically deliverable oncolytic picornavirus, and the treatment of neuroendocrine cancers. *J Natl Cancer Inst.* 99, 1623–1633. doi: 10.1093/jnci/djm198

Reid, S. M., Ferris, N. P., Hutchings, G. H., King, D. P., and Alexandersen, S. (2004a). Evaluation of real-time reverse transcription polymerase chain reaction assays for the detection of swine vesicular disease virus. *J. Virol. Methods.* 116, 169–176. doi: 10.1016/j.jviromet.2003.11.007

Reid, S. M., Ferris, N. P., Hutchings, G. H., Samuel, A. R., and Knowles, N. J. (2000). Primary diagnosis of foot-and-mouth disease by reverse transcription polymerase chain reaction. *J. Virol. Methods.* 89, 167–176. doi: 10.1016/s0166-0934(00)00213-5

Reid, S. M., Ferris, N. P., Hutchings, G. H., Zhang, Z., Belsham, G. J., and Alexandersen, S. (2002). Detection of all seven serotypes of foot-and-mouth disease virus by real-time, fluorogenic reverse transcription polymerase chain reaction assay. *J. Virol. Methods.* 105, 67–80. doi: 10.1016/s0166-0934(02)00081-2

Reid, S. M., Mioulet, V., Knowles, N. J., Shirazi, N., Belsham, G. J., and King, D. P. (2014). Development of tailored real-time rt-pcr assays for the detection and differentiation of serotype o, a and asia-1 foot-and-mouth disease virus lineages circulating in the middle east. *J. Virol. Methods.* 207, 146–153. doi: 10.1016/j.jviromet.2014.07.002

Reid, S. M., Paton, D. J., Wilsden, G., Hutchings, G. H., King, D. P., Ferris, N. P., et al. (2004b). Use of automated real-time reverse transcription-polymerase chain reaction (rt-pcr) to monitor experimental swine vesicular disease virus infection in pigs. *J. Comp. Pathol.* 131, 308–317. doi: 10.1016/j.jcpa.2004.05.003

Rodriguez-Habibe, I., Celis-Giraldo, C., Patarroyo, M. E., Avendano, C., and Patarroyo, M. A. (2020). A comprehensive review of the immunological response against foot-and-mouth disease virus infection and its evasion mechanisms. *Vaccines (Basel).* 8. doi: 10.3390/vaccines8040764

Saeng-Chuto, K., Rodtian, P., Temeeyasen, G., Wegner, M., and Nilubol, D. (2018). The first detection of senecavirus a in pigs in Thailand, 2016. *Transbound. Emerg. Dis.* 65, 285–288. doi: 10.1111/tbed.12654

Sahore, V., Doonan, S. R., and Bailey, R. C. (2018). Droplet microfluidics in thermoplastics: device fabrication, droplet generation, and content manipulation using integrated electric and magnetic fields. *Anal Methods.* 10, 4264–4274. doi: 10.1039/C8AY01474D

Senthilkumaran, C., Bittner, H., Ambagala, A., Lung, O., Babiuk, S., Yang, M., et al. (2017). Use of oral fluids for detection of virus and antibodies in pigs infected with swine vesicular disease virus. *Transbound. Emerg. Dis.* 64, 1762–1770. doi: 10.1111/tbed.12563

Shen, X., Qiu, F., Shen, L., Yan, T., Zhao, M., Qi, J., et al. (2019). A rapid and sensitive recombinase aided amplification assay to detect hepatitis b virus without DNA extraction. *Bmc Infect. Dis.* 19:229. doi: 10.1186/s12879-019-3814-9

Shi, Y., Li, B., Tao, J., Cheng, J., and Liu, H. (2021). The complex co-infections of multiple porcine diarrhea viruses in local area based on the Luminex xtag multiplex detection method. *Front Vet Sci.* 8:602866. doi: 10.3389/fvets.2021.602866

Shi, X., Liu, X., Wang, Q., Das, A., Ma, G., Xu, L., et al. (2016). A multiplex real-time pcr panel assay for simultaneous detection and differentiation of 12 common swine viruses. *J. Virol. Methods.* 236, 258–265. doi: 10.1016/j.jviromet.2016.08.005

Silva, G., Oyekanmi, J., Nkere, C. K., Bomer, M., Kumar, P. L., and Seal, S. E. (2018). Rapid detection of potyviruses from crude plant extracts. *Anal. Biochem.* 546, 17–22. doi: 10.1016/j.ab.2018.01.019

Singh, K., Corner, S., Clark, S. G., Scherba, G., and Fredrickson, R. (2012). Seneca valley virus and vesicular lesions in a pig with idiopathic vesicular disease. *Journal of Veterinary Science & Technology.* 3

Sun, D., Vannucci, F., Knutson, T. P., Corzo, C., and Marthaler, D. G. (2017). Emergence and whole-genome sequence of senecavirus a in Colombia. *Transbound. Emerg. Dis.* 64, 1346–1349. doi: 10.1111/tbed.12669

Tamba, M., Plasmati, F., Brocchi, E., and Ruocco, L. (2020). Eradication of swine vesicular disease in italy. *Viruses.* 12. doi: 10.3390/v12111269

Tapparel, C., Siegrist, F., Petty, T. J., and Kaiser, L. (2013). Picornavirus and *Enterovirus* diversity with associated human diseases. *Infect. Genet. Evol.* 14, 282–293. doi: 10.1016/j.meegid.2012.10.016

Taylor, S. C., Laperriere, G., and Germain, H. (2017). Droplet digital PCR versus qPCR for gene expression analysis with low abundant targets: from variable nonsense to publication quality data. *Sci Rep.* 7:2409. doi: 10.1038/s41598-017-02217-x

Tiwari, A., Ahmed, W., Oikarinen, S., Sherchan, S. P., Heikinheimo, A., Jiang, G., et al. (2022). Application of digital PCR for public health-related water quality monitoring. *Sci. Total Environ.* 837:155663. doi: 10.1016/j.scitotenv.2022.155663

Vandenbussche, F., Lefebvre, D. J., De Leeuw, I., Van Borm, S., and De Clercq, K. (2017). Laboratory validation of two real-time rt-pcr methods with 5'-tailed primers for an enhanced detection of foot-and-mouth disease virus. *J. Virol. Methods.* 246, 90–94. doi: 10.1016/j.jviromet.2017.04.014

Vannucci, F. A., Linhares, D. C. L., Barcellos, D. E. S. N., Lam, H. C., Collins, J., and Marthaler, D. (2015). Identification and complete genome of Seneca valley virus in vesicular fluid and sera of pigs affected with idiopathic vesicular disease, Brazil. *Transbound. Emerg. Dis.* 62, 589–593. doi: 10.1111/tbed.12410

Vazquez-Calvo, A., Saiz, J. C., Sobrino, F., and Martin-Acebes, M. A. (2016). First complete coding sequence of a Spanish isolate of swine vesicular disease virus. *Genome Announc.* 4. doi: 10.1128/genomeA.01742-15

Vosloo, W., Bastos, A. D., Sangare, O., Hargreaves, S. K., and Thomson, G. R. (2002). Review of the status and control of foot and mouth disease in sub-Saharan Africa. *Rev Sci Tech.* 21, 437–449. doi: 10.20506/rst.21.3.1349

Wang, Y., Das, A., Zheng, W., Porter, E., Xu, L., Noll, L., et al. (2020a). Development and evaluation of multiplex real-time rt-pcr assays for the detection

and differentiation of foot-and-mouth disease virus and Seneca valley virus 1. *Transbound. Emerg. Dis.* 67, 604–616. doi: 10.1111/tbed.13373

Wang, H., Dong, J., Zhang, T., Wang, F., Yang, R., Zhang, Y., et al. (2022). A novel rapid detection of senecavirus a using recombinase polymerase amplification (RPA) coupled with lateral flow (LF) dipstrip. *Anal. Biochem.* 646:114627. doi: 10.1016/j.ab.2022.114627

Wang, H., Hou, P., Zhao, G., Yu, L., Gao, Y., and He, H. (2018). Development and evaluation of serotype-specific recombinase polymerase amplification combined with lateral flow dipstick assays for the diagnosis of foot-and-mouth disease virus serotype a, o and Asia 1. *Bmc Vet. Res.* 14:359. doi: 10.1186/s12917-018-1644-4

Wang, Y., Yim, I. W., Porter, E., Lu, N., Anderson, J., Noll, L., et al. (2020b). Development of a bead-based assay for detection and differentiation of field strains and four vaccine strains of type 2 porcine reproductive and respiratory syndrome virus (PRRSV-2) in the USA. *Transbound. Emerg. Dis.* 68, 1414–1423. doi: 10.1111/tbed.13808

Wang, H. M., Zhao, G. M., Hou, P. L., Yu, L., He, C. Q., and He, H. B. (2018). Rapid detection of foot-and-mouth disease virus using reverse transcription recombinase polymerase amplification combined with a lateral flow dipstick. *J. Virol. Methods.* 261, 46–50. doi: 10.1016/j.jviromet.2018.07.011

Wang, W., Zhou, L., Ge, X., Han, J., Guo, X., Chen, Y., et al. (2021). Development of a vp 2-based real-time fluorescent reverse transcription recombinase-aided amplification assay to rapidly detect senecavirus a. *Transbound. Emerg. Dis.* doi: 10.1111/tbed.14435

Wiedenheft, B., Sternberg, S. H., and Doudna, J. A. (2012). RNA-guided genetic silencing systems in bacteria and archaea. *Nature* 482, 331–338. doi: 10.1038/nature10886

Wong, C. L., Yong, C. Y., Ong, H. K., Ho, K. L., and Tan, W. S. (2020). Advances in the diagnosis of foot-and-mouth disease. *Front Vet Sci.* 7:477. doi: 10.3389/fvets.2020.00477

Wu, X., Lin, H., Chen, S., Xiao, L., Yang, M., An, W., et al. (2017). Development and application of a reverse transcriptase droplet digital pcr (rt-ddpcr) for sensitive and rapid detection of Japanese encephalitis virus. *J. Virol. Methods.* 248, 166–171. doi: 10.1016/j.jviromet.2017.06.015

Wu, Q., Zhao, X., Bai, Y., Sun, B., Xie, Q., and Ma, J. (2017). The first identification and complete genome of senecavirus a affecting pig with idiopathic vesicular disease in China. *Transbound. Emerg. Dis.* 64, 1633–1640. doi: 10.1111/tbed.12557

Xu, B., Gong, P., Zhang, Y., Wang, Y., Tao, D., Fu, L., et al. (2022). A one-tube rapid visual crispr assay for the field detection of Japanese encephalitis virus. *Virus Res.* 319:198869. doi: 10.1016/j.virusres.2022.198869

Xu, W., Hole, K., Goolia, M., Pickering, B., Salo, T., Lung, O., et al. (2017). Genome wide analysis of the evolution of senecavirus a from swine clinical material and assembly yard environmental samples. *Plos One.* 12:e176964. doi: 10.1371/journal.pone.0176964

Xu, L., Hurtle, W., Rowland, J. M., Casteran, K. A., Bucko, S. M., Grau, F. R., et al. (2013). Development of a universal rt-pcr for amplifying and sequencing the leader and capsid-coding region of foot-and-mouth disease virus. *J. Virol. Methods.* 189, 70–76. doi: 10.1016/j.jviromet.2013.01.009

Yang, B., Shi, Z., Ma, Y., Wang, L., Cao, L., Luo, J., et al. (2022). Lamp assay coupled with crispr/cas 12a system for portable detection of African swine fever virus. *Transbound. Emerg. Dis.* 69, e216–e223. doi: 10.1111/tbed.14285

Yeo, S., Yang, M., Nyachoti, M., Rauh, R., Callahan, J. D., and Nfon, C. (2020). Detection of foot-and-mouth disease virus in swine meat juice. *Pathogens.* 9. doi: 10.3390/pathogens9060424

Yin, L., Man, S., Ye, S., Liu, G., and Ma, L. (2021). CRISPR-Cas based virus detection: recent advances and perspectives. *Biosens. Bioelectron.* 193:113541. doi: 10.1016/j.bios.2021.113541

Zell, R. (2018). *Picornaviridae*-the ever-growing virus family. *Arch. Virol.* 163, 299–317. doi: 10.1007/s00705-017-3614-8

Zeng, F., Cong, F., Liu, X., Lian, Y., Wu, M., Xiao, L., et al. (2018). Development of a real time loop-mediated isothermal amplification method for detection of senecavirus a. *J. Virol. Methods.* 261, 98–103. doi: 10.1016/j.jviromet.2018.08.005

Zetsche, B., Gootenberg, J. S., Abudayyeh, O. O., Slaymaker, I. M., Makarova, K. S., Essletzbichler, P., et al. (2015). CPF 1 is a single rna-guided endonuclease of a class 2 CRISPR-cas system. *Cell.* 163, 759–771. doi: 10.1016/j.cell.2015.09.038

Zhang, G., Haydon, D. T., Knowles, N. J., and McCauley, J. W. (1999). Molecular evolution of swine vesicular disease virus. *The Journal of general virology.* 80, 639–651. doi: 10.1099/0022-1317-80-3-639

Zhang, J., Nfon, C., Tsai, C. F., Lee, C. H., Fredericks, L., Chen, Q., et al. (2019). Development and evaluation of a real-time rt-pcr and a field-deployable rt-insulated isothermal pcr for the detection of Seneca valley virus. *Bmc Vet. Res.* 15:168. doi: 10.1186/s12917-019-1927-4

Zhang, X., Xiao, J., Ba, L., Wang, F., Gao, D., Zhang, J., et al. (2018). Identification and genomic characterization of the emerging senecavirus a in southeast china, 2017. *Transbound. Emerg. Dis.* 65, 297–302. doi: 10.1111/tbed.12750

Zhang, Z., Zhang, Y., Lin, X., Chen, Z., and Wu, S. (2019). Development of a novel reverse transcription droplet digital pcr assay for the sensitive detection of senecavirus a. *Transbound. Emerg. Dis.* 66, 517–525. doi: 10.1111/tbed.13056

frontiers | Frontiers in Microbiology

TYPE Original Research
PUBLISHED 10 November 2022
DOI 10.3389/fmicb.2022.1041789

OPEN ACCESS

EDITED BY
Bing Gu,
Guangdong Provincial People's Hospital, China

REVIEWED BY
Litian Ma,
Fourth Military Medical University, China
Muhammad Akbar Shahid,
Bahauddin Zakariya University, Pakistan
Israel Nissan,
Ministry of Health, Israel

*CORRESPONDENCE
Hongliang Chen
chenhongliang2007@126.com
Shixing Tang
tamgshixing@smu.edu.cn

†These authors have contributed equally to this work

SPECIALTY SECTION
This article was submitted to Infectious Agents and Disease, a section of the journal Frontiers in Microbiology

RECEIVED 11 September 2022
ACCEPTED 31 October 2022
PUBLISHED 10 November 2022

CITATION
Zhao J, Shui J, Luo L, Ao C, Lin H, Liang Y, Wang L, Wang H, Chen H and Tang S (2022) Identification and characterization of mixed infections of *Chlamydia trachomatis via* high-throughput sequencing. *Front. Microbiol.* 13:1041789. doi: 10.3389/fmicb.2022.1041789

Identification and characterization of mixed infections of *Chlamydia trachomatis via* high-throughput sequencing

Jianhui Zhao[1†], Jingwei Shui[1†], Lipei Luo[2†], Cailing Ao[1], Hongqing Lin[1], Yuanhao Liang[1], Li Wang[2], Haiying Wang[1], Hongliang Chen[2*] and Shixing Tang[1*]

[1]Department of Epidemiology, School of Public Health, Southern Medical University, Guangzhou, China, [2]Department of Clinical Microbiology Laboratory, Chenzhou No. 1 People's Hospital, Chenzhou, China

Precise genotyping is necessary to understand epidemiology and clinical manifestations of *Chlamydia trachomatis* infection with different genotypes. Next-generation high-throughput sequencing (NGHTS) has opened new frontiers in microbial genotyping, but has been clinically characterized in only a few settings. This study aimed to determine *C. trachomatis* genotypes in particular mixed-genotype infections and their association with clinical manifestations and to characterize the sensitivity and accuracy of NGHTS. Cervical specimens were collected from 8,087 subjects from physical examination center (PEC), assisted reproductive technology center (ART) and gynecology clinics (GC) of Chenzhou Hospital of China. The overall prevalence of *C. trachomatis* was 3.8% (311/8087) whereas a prevalence of 2.8, 3.7 and 4.8% was found in PEC, ART and GC, respectively. The most frequent three *C. trachomatis* genotypes were E (27.4%, 83/303), F (21.5%, 65/303) and J (18.2%, 55/303). Moreover, NGHTS identified 20 (6.6%, 20/303) mixed-genotype infections of *C. trachomatis*. Genotype G was more often observed in the subjects with pelvic inflammatory disease than genotype E (adjusted *OR*=3.61, 95%*CI*, 1.02–12.8, p=0.046). Mixed-genotype infection was associated with severe vaginal cleanliness (degree IV) with an adjusted *OR* of 5.17 (95%*CI* 1.03–25.9, p=0.046) whereas mixed-genotype infection with large proportion of minor genotypes was associated with cervical squamous intraepithelial lesion (SIL) with an adjusted *OR* of 5.51 (95%*CI* 1.17–26.01, p=0.031). Our results indicated that NGHTS is a feasible tool to identity *C. trachomatis* mixed-genotype infections, which may be associated with worse vaginal cleanliness and cervical SIL.

KEYWORDS

***Chlamydia trachomatis*, next-generation high-throughput sequencing, genotype, mixed-genotype infection, clinical manifestation**

Introduction

Chlamydia trachomatis is one of the most widespread sexually transmitted diseases (Fu et al., 2022). Approximately, 80% of *C. trachomatis* infections are essentially asymptomatic (Marcone et al., 2012). Persistent *C. trachomatis* infection can cause various sequelae such as urethritis, endometritis, pelvic inflammatory disease (PID), tubal factor infertility, and ectopic pregnancy (Woodhall et al., 2018). *C. trachomatis* includes 19 genotypes (Bax et al., 2011). In general, genotype A, B and C are usually associated with trachoma while genotype D-K primarily cause urogenital infection (Bax et al., 2011). In addition, genotype L1-L3 are the agents of lymphogranuloma venereum (Jurstrand et al., 2001).

The *ompA* is one of the most variable genes in the *C. trachomatis* genomes and encodes the main outer membrane protein (MOMP) (Nunes et al., 2009). The *ompA* gene contains four highly polymorphic variable sequences VS1–4, which are separated by five constant sequences CS1–5 (Spaargaren et al., 2005). The most variable and discriminatory nucleotide sequences are found in the VS1 and VS2 regions, which make them the suitable target fragments for *C. trachomatis* genotyping (Spaargaren et al., 2005). However, previous studies showed that the recombination and horizontal gene transfer of *ompA* is a natural phenomenon occurring within some *C. trachomatis* strains (Somboonna et al., 2011; Harris et al., 2012; Matičič et al., 2016). Although the *ompA* gene of *C. trachomatis* is a single copy gene and may have a lower probability of switching compared to the multi-copy genes, e.g., cryptic plasmid (Joseph et al., 2011), it may not always represent the genetic background of the *C. trachomatis*.

At present, the methods for *C. trachomatis* genotyping include Sanger sequencing, polymerase chain reaction-based restriction fragment length polymorphism (PCR-RFLP) (Petrovay et al., 2015; Foschi et al., 2016), hybridization methods (Ruettger et al., 2011; Gharsallah et al., 2012; Martinez et al., 2015; Brasiliense et al., 2016), real-time PCR using fluorescent probes (Jalal et al., 2007), DNA microarray assay (Gallo Vaulet et al., 2016) and whole genome sequencing (WGS; Brown and Christiansen, 2019). Sanger sequencing is the most widely used technique for genotyping, but is not adequate to detect mixed-genotype infections of *C. trachomatis* since it only provides one consensus sequence (Quint et al., 2007; Ruettger et al., 2011; Gharsallah et al., 2012). Although PCR-RFLP, hybridization methods and DNA microarray assay can identify mixed-genotype infections to some extent (Ruettger et al., 2011; Gharsallah et al., 2018), their sensitivity and reliability remain to be improved. In contrast, next-generation high-throughput sequencing (NGHTS) targeting variable regions of *ompA* gene can not only inherit the advantage of *ompA* Sanger sequencing to identify *C. trachomatis* genotypes, but also determine mixed-genotype infections and the proportion of different genotypes in the mixed-genotype infections due to enough sequencing depth and large number of sequencing reads (Kawada et al., 2016), which are more suitable for the detection of co-infections or super-infections of different *C. trachomatis* genotypes.

Indeed, the previous studies of *C. trachomatis*-infected patients or animals have demonstrated the difference of *C. trachomatis* genotypes in virulence and pathogenicity (Ito et al., 1990; Lyons et al., 2004). However, these studies only compared the virulence of different *C. trachomatis* genotypes (Batteiger et al., 1989; Workowski et al., 1994; Ngandjio et al., 2003; Lyons et al., 2004). It remains to elucidate whether mixed-genotype infection of *C. trachomatis* could result in enhanced virulence and may account for divergent clinical outcomes of *C. trachomatis* infection. Few studies have attempted to correlate specific clinical manifestations of genital mixed-genotype infection of *C. trachomatis* in humans because of the technical difficulty to identify mixed-genotype infections (Yan et al., 2018).

In this study, we explored the feasibility of NGHTS to determine *C. trachomatis* genotypes and to identify mixed-genotype infections in a large number of *C. trachomatis*-positive cervical samples in a cross-sectional and observational study. The objective of this study was to characterize the sensitivity and accuracy of NGHTS and to determine *C. trachomatis* genotypes in particular mixed-genotype infections and their association with clinical manifestations.

Materials and methods

Study participants and clinical samples

A total of 8,087 samples of cervical swabs from the physical examination center (PEC), assisted reproductive technology center (ART) and gynecology clinics (GC) of Chenzhou No.1 People's Hospital in Chenzhou of Hunan Province, China were randomly collected and tested for *C. trachomatis* nucleic acid from March 1, 2019 to July 13, 2021. The hospital is the biggest general hospital in Chenzhou and consists of five campuses to cover the whole city and nearby regions. The 2,950 female subjects from PEC were those for routine annual health examinations while the 1,666 female subjects from ART and 3,471 female subjects from GC were those for diagnosis and treatment of infertility and gynecological diseases, respectively. The inclusion criteria were female, and not pregnant. Cervical swab samples were collected using a 200 mm polyethylene Cervix brush device (Hybribio Corp, Guangzhou, China). The specimens were transferred to a tube containing cervical cell preservation solution provided in the kit and stored at −80°C until analysis. For *C. trachomatis* positive subjects, demographic characteristics, antibiotic usage during the previous 3 months, human papillomavirus (HPV) infection, clinical symptoms, vagina cleanliness, cervical abnormalities were retrospectively collected. To detect HPV infection, DNA was extracted from cervical swab samples within 48 h after collection using the QIAamp mini kit (Qiagen, Hilden, Germany). HPV detection and genotyping were performed by using the Hybribio Rapid Geno-Array test kit (Hybribio Corp, Guangdong) based on

the PCR-reverse dot blot hybridization method. The study was conducted in Chenzhou No.1 People's Hospital, China, under the Principles of the Declaration of Helsinki, and was approved by the Ethical Committee of Chenzhou No.1 People's Hospital (CZ/1128). Written informed consent was obtained from all the participants. All the experiments were carried out in the lab certified by the National Center for Clinical Laboratories following the laboratory biosafety guidelines (Burnett et al., 2009).

Clinical manifestations and diagnosis

Asymptomatic *C. trachomatis* infection was defined as positive for *C. trachomatis* nucleic acid without symptoms, such as painful sexual intercourse, abnormal vaginal discharge, urethritis, irregular vaginal bleeding, or bleeding after sexual intercourse and genital warts (Chen et al., 2020). Vaginosis was diagnosed according to Amsel criteria (Carr et al., 1998). There are many methods to evaluate the vaginal microenvironment. In China, the vaginal cleanliness grade is also used to comprehensively evaluate the status of the vaginal microenvironment (Group., C.M.A.O.a.G.B.I.D.C, 2016), and has been widely accepted for gynecological studies (Yue et al., 2015; Yu et al., 2018). Vaginal cleanliness is classified as I, II, III and IV grades according to bacterium vaginae, Coccus, epithelial cell and leukocytes (Supplementary Table S1). Class I and II are considered normal while class III and IV as abnormal (Bao et al., 2015), and Grade IV vaginal cleanliness is regarded as severe vaginal cleanliness. The vaginal cleanliness is characterized by microscopy and bacterial morphology, and cannot identify the specific species of bacterium vaginae. PID is defined as tenderness with adnexal, cervical motion, and uterine tenderness (Dean et al., 1995). Cervicitis is determined by evaluating and scoring the clinical findings at the time of speculum examination. A score of ≥ 3 is defined as cervicitis while ≤ 2 as no cervicitis (Supplementary Table S1; Batteiger et al., 1989). Colposcopy screening is performed using a digital electronic colposcopy (SLC-3000, Philips, Shenzhen, China) following a standard procedure (Chen et al., 2020). According to the standard and terminology of the American Society for Colposcopy and Cervical Pathology (ASCCP) (Khan et al., 2017), colposcopy impression includes benign, low-grade squamous intraepithelial lesion (LSIL), high-grade squamous intraepithelial lesion (HSIL), and cancer. LSIL and HSIL represent Grade 1 (minor) and Grade 2 (major) abnormal colposcopy findings defined by the International Federation for Cervical Pathology and Colposcopy (IFCPC) nomenclature, respectively (Bornstein et al., 2012). The samples for cytology analysis are harvested by using polyethylene cervix brush device and cervical cell preservation solution (Hybribio Corp, Guangzhou, China). Sectioning and staining are conducted in all-in-one machine (Dacheng, Guangzhou, China). The cytology results are plotted in a table and categorized according to the Bethesda system (TBS) (de Oliveira et al., 2020). The following variables are considered: no malignancy, ASC-US, LSIL, ASC-H, HSIL, squamous cell carcinoma, atypical glandular cells (AGC), adenocarcinoma, and other malignant neoplasms.

Detection and genotyping of *Chlamydia trachomatis* by PCR and sanger sequencing

DNA was extracted from the cervical swabs using QIAamp DNA Minikit QIAgen (Qiagen, Hilden, Germany) according to the manufacturer's instructions. The isolated DNA was stored at −80°C until use for PCR and sequencing. A 200 bp conserved cryptic plasmid Pgp2 fragment of *C. trachomatis* was amplified by PCR for diagnosis of *C. trachomatis* infection with the primers of CT-d-F and CT-d-R (Supplementary Table S2). PCR was carried out in 25 µl reaction mixture in a thermal cycler with the following reaction conditions: 95°C for 2 min, followed by 35 cycles of 95°C for 15 s, 55°C for 30 s and 72°C for 40 s with a final elongation at 72°C for 5 min.

For genotyping, *C. trachomatis ompA* fragment VS1–VS4 was first amplified by nested PCR using the outer primers CT1 and CT2 followed by the amplification of a 580 bp VS1–VS2 fragment using the inner primers CT3 and CT4. First round PCR was carried out in 25 µl reaction mixture with the following reaction conditions: 95°C for 5 min, followed by 25 cycles of 95°C for 60 s, 55°C for 60 s and 72°C for 80 s, with a final elongation at 72°C for 10 min. The reaction conditions of the second round PCR were: 95°C for 5 min, followed by 35 cycles of 95°C for 30 s, 55°C for 30 s and 72°C for 30 s, with a final elongation at 72°C for 10 min. All the primer sequences were listed in the Supplementary Table S2. The *C. trachomatis* strain (ATCC VR-348B) was used as positive control and DNase-free water as negative control in PCR. PCR products for *C. trachomatis ompA* gene were sent out for Sanger sequencing in Ruibo Biotech (Guangzhou, China). Genotypes of *C. trachomatis* were determined by BLAST as previously described (Yang et al., 2010).

Identification of mixed-genotype infections of *Chlamydia trachomatis* using NGHTS

For *C. trachomatis* genotyping through NGHTS, a 448 bp fragment of *C. trachomatis ompA* gene VS1–VS2 region was amplified using nested PCR with the following primers (Supplementary Figure S1): outer primes *ompA* CT-HTS-F-outer/CT-HTS-R-outer and inner primers CT-HTS-F-inner/CT-HTS-R-inner with barcode (Supplementary Table S2). The first round PCR was carried out in 25 µl reaction mixture, with 12.5 µl of Phanta® Max Super-Fidelity DNA polymerase (Vazyme Biotech, Nanjing, China), 0.5 µl of forward and reverse primers (10 pmol/ul), and the following reaction conditions: 95°C for 3 min, followed by 25 cycles of 95°C for 15 s, 55°C for 30 s and 72°C for 40 s, with a final elongation at 72°C for 5 min. The second round

PCR was carried out in 50 µl reaction volume with 25 µl of Phanta® Max Super-Fidelity DNA polymerase (Vazyme Biotech, Nanjing, China), 1 µl of forward and reverse primers (10 pmol/ul), and 2 µl first-round PCR product. Thermal cycling consisted of initial denaturation at 95°C for 3 min, followed by 35 cycles of denaturation at 95°C for 15 s, annealing at 55°C for 15 s, and elongation at 72°C for 30 s with final incubation at 72°C for 5 min. The second-round PCR products were purified using universal DNA Purification Kit (TIANGEN Biotech, Beijing, China) according to the manufacturer's manual, and quantified using GENOVA NANO (Bibby Scientific Ltd., Stone, United kingdom). Finally, 10 samples were mixed at 1 µg of purified DNA per sample and confirmed by electrophoresis on 2% agarose gel.

Sequencing libraries were generated using NEB Next® UltraTM DNA Library Prep Kit for Illumina (NEB, Massachusetts, United States) following the manufacturer's recommendations and index codes were added. The library quality was assessed on the Qubit@ 2.0 Fluorometer (Thermo Scientific, Massachusetts, United States) and Agilent Bioanalyzer 2100 system (Agilent Technologies, CA, United States). Finally, the library was sequenced on an Illumina NovaSeq 6000 and 250 bp paired-end reads were generated. To make the analysis results more accurate and reliable, the original data were first spliced and filtered to obtain clean data. The clean data was obtained using fastp software, with the following criterion (Novogene Technology Co., LTD, Beijing, China): when the N in any sequencing read exceeds 10% of the total number of reads, or the number of bases with low quality ($Q \leq 5$) in any sequencing reads exceeds 50% of the total number of reads, or sequencing read contains adapter sequences, these reads are eliminated. Paired-end reads from the original DNA fragments were merged by using the FLASH program, which inputs a fastq library of paired-end reads (reads1 and reads2) in which some of the reads overlap the read generated from the opposite end of the same DNA fragment, and merged the fragments based on the correct overlap between the paired-end reads (Magoč and Salzberg, 2011). The sequences of different samples were extracted based on the specific barcode sequences. Burrows-Wheeler transform (BWA 0.7.17; Li and Durbin, 2009) with the default parameters was used for aligning all the clean sequence data with the reference sequences of *C. trachomatis* genotype A-K and L1-L3. Based on the results of sequence alignment, the genotype of each read was determined and the composition of different genotypes was calculated. The proportion of minor genotype >1% is defined as a mixed-genotype infection (Quer et al., 2015). The genotype with the large proportion is considered to be the major genotype in the case of a mixed-genotype infection identified. The reference sequences used in this study included A/Sa1(M58938), B/ IU1226 (AF063208), C/ TW3 (M17343), D/ UW3 (AE001338), E/Bour (X52557), F/ IC-Cal3 (X52080), G/UW57 (AF063199), H/UW4 (X16007), I/ UW-12 (AF063200), J/UW36 (AF063202), K/UW31 (AF063204), L1/440 (M36533), L2/434 (M14738), and L3/404 (X55700).

Detection limit of NGHTS for identifying mixed genotypes

A 456 bp fragment of the *ompA* gene was amplified from the clinical samples infected with *C. trachomatis* genotype B, D, E, F, G, H, J and K, and cloned into the pUC57 vector (TsingKe Biotech Corp, Beijing, China). The plasmid DNA was purified and quantified using a GENOVA NANO (Bibby Scientific Ltd., Stone, United Kingdom). The DNA copy number was calculated using the following formula: DNA copy number (copy number/µL) = [6.02 × 10^{23} × plasmid concentration (ng/µL) × 10^{-9}]/[DNA in length × 660]. A serial 10-fold diluted plasmid DNAs for *C. trachomatis* genotype B, D, E, F, G, H, J and K were used to determine the low detection limit of NGHTS. Furthermore, the mixtures of different plasmid DNAs of *C. trachomatis* genotype of F/G, E/J and E/F were prepared at the ratio of 50/50, 30/70, 20/80, 10/90, 2.5/97.5, 1/99, and amplified and sequenced to assess the sensitivity and accuracy of NGHTS in distinguishing mixed *C. trachomatis* genotypes.

Amplification of minor genotypes using genotype-specific primers in the samples infected with mixed *Chlamydia trachomatis* genotypes

The genotype-specific primers for minor genotypes were designed using DNASTAR software (DNASTAR Inc., Madison, WI, United States) according to the sequence difference between *C. trachomatis* genotypes (Supplementary Table S3). For the verification of the samples with mixed *C. trachomatis* genotypes, *C. trachomatis ompA* fragment VS1–VS2 was first amplified using the outer primes *ompA* CT-HTS-F-outer/CT-HTS-R-outer followed by the amplification using the sample-genotype-specific primers. For each sample with mixed-genotype infections, the genotype-specific primer was designed to match the sequence of minor genotype but not the major genotype, especially in the 3′ end. The PCR products were detected by electrophoresis on 2% agarose gel and sent to Ruibo Bioteh (Guangzhou, China) for Sanger sequencing. Genotype verification was conducted by using the BLAST program as previously described (Yang et al., 2010).

Detection of bacterial load of *Chlamydia trachomatis*

A real-time quantitative PCR (qPCR) assay was adapted to determine *C. trachomatis* bacterial loads using primers of the *Pgp2* gene (Supplementary Table S2). qPCR was carried out in 20 µl reaction volume with 10 µl of TB Green Fast qPCR Mix (Takara Bio Inc., Shiga, Japan), 0.8 µl of forward and reverse primers (10 pmol/ul), 6.4 µl of H_2O and 2 µl DNA template. The following are the reaction conditions with LightCycler 480 System (Roche Diagnostics GmbH, Mannheim, Germany): 95°C for 30 s,

followed by 40 cycles of 95°C for 30 s, 57°C for 30 s and 72°C for 30 s. The bacterial loads were calculated according to the standard curve.

Statistical analysis

Statistical analysis was done using SPSS 25.0 software (IBM). Continuous variables were presented as mean ± SE and tested by *t*-test whereas categorical variables were expressed as numbers and tested by Chi-square tests. Association of *C. trachomatis* genotype or mixed-genotype with clinical manifestations was explored by multivariate logistic regression analysis and presented as odds ratio (*OR*).

Propensity scores (PS) was calculated using logistic regression with respect to age, clinical departments, antibiotic usage, HPV infection. In addition, PS was adjusted by a standardized mortality ratio weighting (SMRW) method in which a weight of 1 was assigned for cases and a weight of [PS (1 − Pt)]/[(1 − PS) Pt] for controls, respectively. The proportion of treatment (Pt) was calculated by the number of cases / the number of cases plus controls. Different clinical manifestations between *C. trachomatis* genotypes were then compared using the PS-adjusted pseudo-population created by the statistical procedures and presented as adjusted odds ratio (a*OR*).

Results

Performance of NGHTS for identifying mixed genotypes

The schematic diagram of the identification of *C. trachomatis* mixed-genotype infection using NGHTS was shown in Supplementary Figure S2. The nested-PCR to construct NGHTS library was capable of amplifying 10 copies per reaction of the recombinant plasmid DNAs for 8 *C. trachomatis* genotypes (Supplementary Figure S3). To further assess the sensitivity and accuracy of NGHTS in distinguishing mixed *C. trachomatis* genotypes, we prepared a series of plasmid DNA mixtures of two *C. trachomatis* genotypes at the ratio of 1–99, including genotype F and G, J and E as well as E and F. The proportion of different genotypes determined by NGHTS was excellently correlated with the ratio we prepared (Figure 1). For example, when we added 1% of the minor genotype into the mixture, the proportion of the minor genotype determined by NGHTS ranged from 1.11 to 4.69%, suggesting that NGHTS could detect at least 1% of the minor genotype in clinical samples with mixed-genotype infection.

Next, we designed genotype-specific primers to amplify the minor genotypes identified by NGHTS. We found that these genotype-specific primers could specifically amplify the minor genotypes when using plasmid DNAs as templates (Supplementary Figure S4A) and in the samples with mixed genotypes of *C. trachomatis* (Supplementary Figure S4B). We also used PCR products of 7 samples infected with two genotypes to transfect *E. coli* cells. Ten colonies per sample were randomly picked up and sequenced to determine their genotypes of *C. trachomatis*. We found that 5 out of the 7 samples contained the same *C. trachomatis* genotypes as those determined by NGHTS although the proportion of the genotypes were slightly different from the data obtained by NGHTS (Supplementary Table S4). Taken together, our results confirmed the good performance of NGHTS in identifying the composition and proportion of *C. trachomatis* genotypes in the clinical samples.

Prevalence and genotype distribution of *Chlamydia trachomatis* infection

A total of 8,087 participants were tested for *C. trachomatis Pgp2* gene and 311 (3.8, 95% confidence interval [CI] 3.4–4.2%) were found to be positive (Figure 2). The prevalence of *C. trachomatis* infection was 2.8, 3.7 and 4.8% for the participants from PEC, ART and GC, respectively (Figure 2). The *ompA* gene was successfully amplified and sequenced in 97.4% (303/311) *C. trachomatis* pgp2-positive samples, and was classified into 8 *C. trachomatis* genotypes and 3 genogroups proposed by Yuan et al. (1989). The most common three *C. trachomatis* genotypes were E (27.4%, 83/303), F (21.5%, 65/303) and J (18.2%, 55/303, Table 1). Two subjects (0.66%, 2/303) were infected with genotype B (Table 1). For the subjects infected with single *C. trachomatis* genotype, the genotyping results of NGHTS and Sanger sequencing were identical (Supplementary Table S5). For the 8 *C. trachomatis pgp2*-positive samples without genotyping results, both Sanger sequencing primers and NGHTS primers failed to amplify the target *ompA* gene.

Moreover, NGHTS identified 6.6% (20/303) *C. trachomatis* positive samples to be infected with two ($n = 18$) or three ($n = 2$) *C. trachomatis* genotypes (Table 2). The most frequent two genotypes observed in the mixed-genotype infections were F (55.0%, 11/20) and E (50.0%, 10/20), respectively. Co-infection of genotype F and G accounted for 20.0% (4/20) of the samples with mixed genotypes (Table 2). Of note, among the 20 samples infected with mixed *C. trachomatis* genotypes, 10 (50%) samples were dominated by one *C. trachomatis* genotype, i.e., the proportion of the major genotype >90% (Table 2). In addition, we measured the bacterial load of *C. trachomatis* using qPCR in 17 samples with mixed-genotype infections and 232 samples of single-genotype infection. Although the bacterial load was slightly higher in the mixed-genotype infections than in the single-genotype infections, i.e., 1.36×10^5 (IQR: 6.00×10^4, 4.37×10^5) copies/mL vs. 0.85×10^5 (IQR: 1.44×10^4, 3.97×10^5) copies/mL, the difference was not statistically significant ($p = 0.476$).

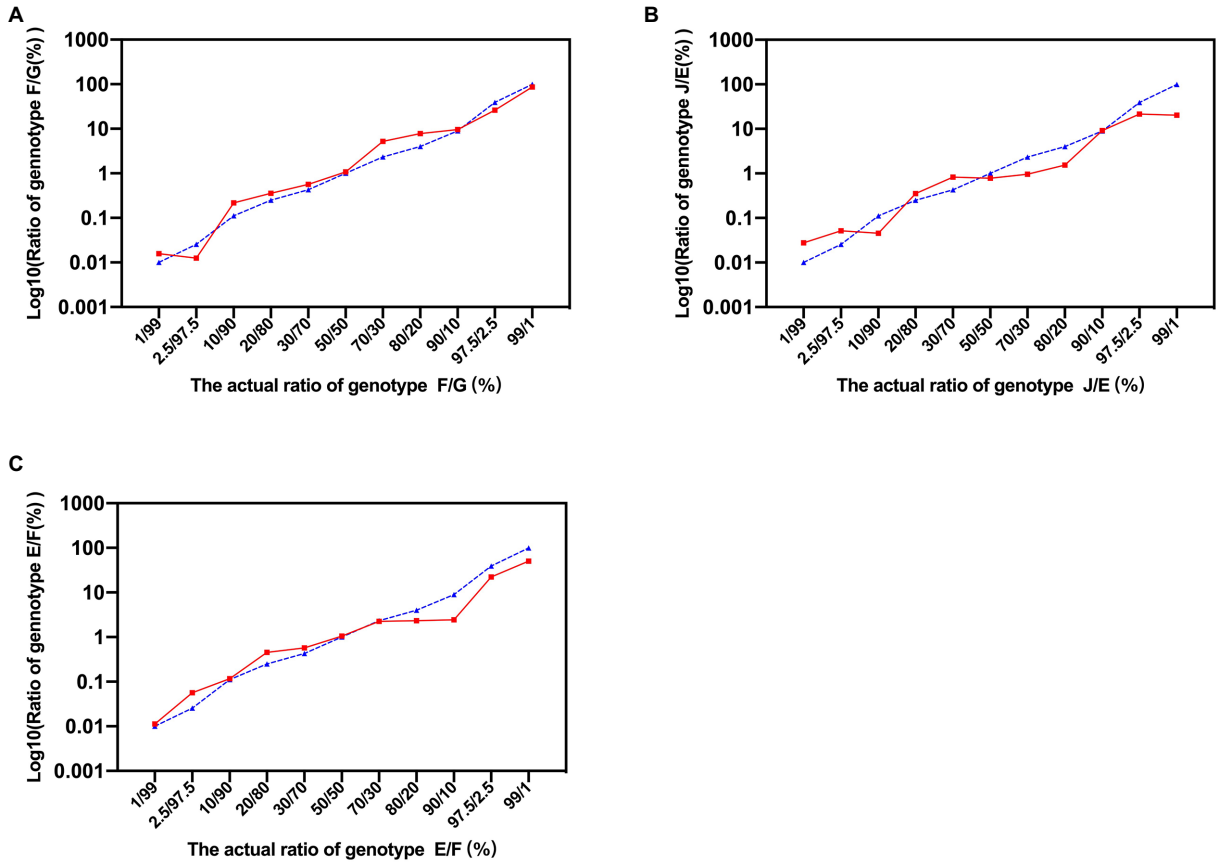

FIGURE 1
Evaluation of next generation high-throughput sequencing (NGHTS) to quantify the composition of different *Chlamydia trachomatis* genotypes. Plasmid DNAs of different *C. trachomatis* genotypes F/G **(A)**, J/E **(B)**, E/F **(C)** were mixed at the ratio of 1–99, and were amplified and sequenced. The blue dash line and solid red line represent the ratios of different *C. trachomatis* genotypes determined by researchers or detected by NGHTS, respectively. The above experiments were repeated twice and the mean values were calculated and presented.

Association between clinical manifestations and *Chlamydia trachomatis* genotypes

For the 303 genotype-defined subjects, no significant difference was observed in terms of age, clinical departments, antibiotic usage and HPV infection ($p > 0.2$, Supplementary Table S6). Similar results were obtained between the subjects with single or mixed-genotype infections ($p > 0.3$, Supplementary Table S6). In our study, 70.1% (218/303) of the participants reported 14 symptoms or signs including vaginosis (38.3%), PID (10.9%) and cervicitis (8.4%; Supplementary Table S7). Of note, only 29.9% (93/311) of subjects were asymptomatic *C. trachomatis* infection. However, the percentage of asymptomatic *C. trachomatis* infection was significantly higher (71.3%) in PEC compared to ART (23.7%) and GC (10.4%, $p < 0.001$, Table 3). Co-infection with HPV increased the risk of symptomatic *C. trachomatis* infection (83.1% vs. 67.2%, $p = 0.01$) and cervical squamous intraepithelial lesion (23.7% vs. 8.5%, $p < 0.001$, Table 3).

In addition, patients from GC were more likely to present with vaginosis (51.8%, $p < 0.001$) and vaginal cleanliness of degree IV (50.7%, $p < 0.001$) compared to the subjects from PEC (16.3% for vaginosis and 12.7% for degree IV) and ART (32.2% for vaginosis and 20.7% for degree IV, Table 3). PID was more often recorded in the patients from ART (33.9%) compared to the subjects from PEC (0%) or GC (8.5%, $p < 0.001$). In our study, PID was also more frequently observed in older subjects ($p = 0.017$) and those with antibiotic usage history ($p = 0.001$). Furthermore, vaginosis was more likely diagnosed in younger women, especially those under 25 years old ($p = 0.03$, Table 3).

The association between *C. trachomatis* genogroup or genotypes and clinical manifestations was analyzed by multivariate logistic regression among 283 subjects infected with single *C. trachomatis* genotype after controlling the parameters of age, clinical departments, antibiotic usage and HPV infection (Table 4). Compared to genotype E, subjects infected with genotype G were more often diagnosed as PID (27.8% vs. 9.6%, OR = 6.06, 95%CI, 1.29–28.5; $p = 0.023$, Table 4) and vagina cleanliness of degree IV (40.0% vs. 27.3%, *OR* = 6.91, 95%*CI*, 1.25–38.1, $p = 0.026$, Table 4). Further analysis of propensity score

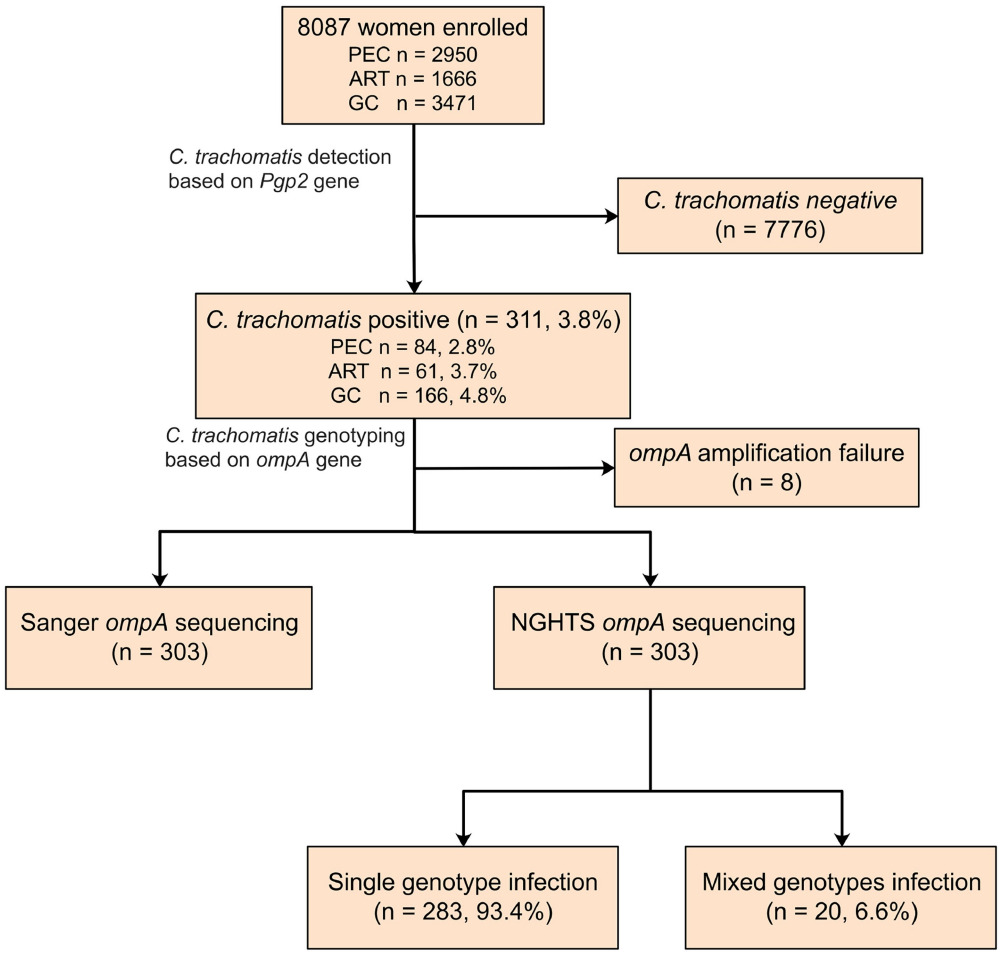

FIGURE 2
Flow chart for detection and genotyping of *C. trachomatis* in an observational study. The subjects were enrolled from physical examination center (PEC), assisted reproductive technology center (ART), or gynecology clinics (GC), respectively in a hospital in Chenzhou, China. They were first screened for *C. trachomatis* nucleic acid by using polymerase chain reaction (PCR) targeting *Pgp2* gene followed by Sanger sequencing or NGHTS to determine genotypes.

TABLE 1 Distribution of *C. trachomatis* genotypes in 303 *C. trachomatis* positive subjects according to *ompA* sequencing results in Chenzhou, China during 2019 and 2021.

Genogroup	Genotype	No. (%) ($N = 303$)
B complex	B	2 (0.66)
	D	40 (13.20)
	E	83 (27.39)
F, G group	F	65 (21.45)
	G	18 (5.94)
C-complex	H	10 (3.30)
	J	55 (18.15)
	K	10 (3.30)
Mixed		20 (6.60)
Total		303 (100.0)

reweighting data using the SMRW method confirmed the association of *C. trachomatis* genotype G infection with PID (a*OR* = 3.61, 95% *CI*, 1.02–12.8, $p = 0.046$, Supplementary Table S8), but not vagina cleanliness of degree IV (a*OR* = 3.00, 95% *CI*, 0.65–13.9, $p = 0.161$, Supplementary Table S8) even though all other parameters were well balanced after weighting (Supplementary Table S9).

Comparison of clinical manifestations between *Chlamydia trachomatis* single and mixed-genotype infections

Although the subjects with *C. trachomatis* single and mixed-genotype infections reported similar symptoms, mixed-genotype infections were more likely to result in worse vagina cleanliness of degree IV (*OR* = 8.61, 95%*CI*, 1.53–48.5; $p = 0.015$, Table 5) than single genotype infections. Further stratified analysis revealed that the occurrence of worse vagina cleanliness and cervical SIL (*OR* = 5.76, 95%*CI*, 1.06–31.20, $p = 0.042$) was mainly observed in the mixed genotype-infected subjects whose minor *C. trachomatis* genotype was ≥10% (Table 5).

TABLE 2 Composition of *C. trachomatis* genotypes in 20 specimens of mixed-genotype infections using high-throughput sequencing in Chenzhou, China during 2019 and 2021.

Ratio of major versus minor genotype	Sample ID	Total sequencing reads	*C. trachomatis* genotypes (reads, %)	
			Major genotype	Minor genotype
≤9	CZ-13154	2865633	**D** 1495589(**52.19**)	**G** 1369971(**47.81**)
	CZ-2906	107674	**D** 57498(**53.40**)	**E** 50172(**46.60**)
	CZ-7399	2114109	**F** 1267351(**59.95**)	**H** 838830(**39.68**)
	CZ-3706	2080328	**J** 1266951(**60.90**)	**E** 804196(**38.66**)
	CZ-8033	1630749	**D** 1023163(**62.74**)	**F** 599935(**36.79**)
	CZ-9288	130285	**D** 90742(**69.65**)	**F** 39218(**30.10**)
	CZ-3612	1695345	**F** 1235996(**72.91**)	**E** 458921(**27.07**)
	CZ-2117	1088398	**E** 882877(**81.12**)	**H** 185179(**17.01**)
				K 14015(**1.29**)
	CZ-2021	191006	**E** 161181(**84.39**)	**J** 26375(**13.81**)
				F 3116(**1.63**)
	CZ-4061	2242349	**J** 1996995(**89.06**)	**F** 245339(**10.94**)
>9	CZ-1761	124818	**D** 116786(**93.57**)	E 8027(**6.43**)
	CZ-29060	79424	**G** 77444(**97.51**)	**F** 1244(**1.57**)
	CZ-1708	1895050	**H** 1848791(**97.56**)	**E** 39242(**2.07**)
	CZ-10505	1729932	**E** 1690609(**97.73**)	**J** 26740(**1.55**)
	CZ-1860	145204	**J** 142371(**98.05**)	**E** 2829(**1.95**)
	CZ-23209	197318	**F** 193812(**98.22**)	**G** 3480(**1.76**)
	CZ-2477	139817	**G** 137418(**98.28**)	**F** 1486(**1.06**)
	CZ-29117	99617	**K** 98083(**98.46**)	**J** 1521(**1.53**)
	CZ-28087	278981	**G** 275295(**98.68**)	**F** 3574(**1.28**)
	CZ-15863	61654	**E** 60889(**98.76**)	**F** 757(**1.23**)

We then conducted propensity score reweighting analysis to balance the factors of age, clinical departments, antibiotic usage, HPV infection and major *C. trachomatis* genotypes (Supplementary Table S10). Further logistic regression analysis confirmed the association of worse vagina cleanliness (a*OR* = 5.17, 95%*CI*, 1.03–25.9, $p = 0.046$) and cervical SIL (a*OR* = 5.51, 95%*CI*, 1.17–26.01, $p = 0.031$) with mixed-genotype infection when compared to single-genotype infection in particular for the mixed-genotype infections in which minor *C. trachomatis* genotype was ≥10% (Table 5). These results indicated that mixed-genotype infections of *C. trachomatis* may be associated with worse vaginal inflammation and cervical squamous intraepithelial lesion.

Discussion

In this study, a prevalence of 3.8% of current *C. trachomatis* infection was documented in the subjects who visited Chenzhou Hospital of China for either annual physical examination, diagnosis or treatment of infertility or gynecological diseases. The predominant *C. trachomatis* genotypes were E, F and J, which are similar to our previous findings (Chen et al., 2020). In addition, genotype B, an ocular genotype to cause ocular infection, was detected in two subjects in our study. However, genotype B ocular strain may be a recombinant strain with a urogenital genomic backbone and ocular genotype B *ompA* insert. Similar findings have been reported in one subject in Zheng et al. study and four subjects in Lesiak-Markowicz et al. study, respectively (Zheng et al., 2007; Lesiak-Markowicz et al., 2019).

In our study, we adapted NGHTS technology to determine *C. trachomatis* genotypes in particular mixed-genotype infections. Our results indicated that both NGHTS and Sanger sequencing correctly identified *C. trachomatis* genotypes in 283 subjects who infected with single genotype of *C. trachomatis*. Moreover, NGHTS was able to identify the presence and proportion of mixed C. *trachomatis* genotypes in 6.6% of *C. trachomatis* positive samples. We further found that mixed-genotype infections were associated with worse vaginal cleanliness and cervical SIL. To the best of our knowledge, this is the first study to assess the feasibility of NGHTS to identify and quantify mixed-genotype infection of *C. trachomatis* in China. Our preliminary results support NGHTS as a simple and useful method for differentiating *C. trachomatis* genotypes and determining mixed-genotype infections.

There are several genotyping methods for *C. trachomatis* including high-resolution multilocus sequence typing (hr-MLST) of multiple genes, and one serovar may consist of several different sequence types (STs) of *C. trachom*atis (Versteeg et al., 2015). However, sequencing of the *ompA* gene is still widely used to determine the serovars or genotypes of *C. trachomatis* and the

TABLE 3 Clinical manifestations of *C. trachomatis*-infected women with respect to age, clinical departments, antibiotic usage and HPV infection.

Manifestations	Age (year)				*p*[a] value	Clinical departments[b]			*p* value	Antibiotic usage (previous 3 months)		*p* value	HPV infection		*p* value
	≤25 *n* = 63	25–35 *n* = 140	35–45 *n* = 58	>45 *n* = 42		PEC *n* = 80	ART *n* = 59	GC *n* = 164		Yes *n* = 14	No *n* = 289		Yes *n* = 71	No *n* = 232	
Asymptomatic (%)															
Yes	20.6	27.9	32.8	40.5	0.15	71.3	23.7	10.4	**<0.001**	7.1	30.1	0.122	16.9	32.8	**0.01**
No	79.4	72.1	67.2	59.5		28.8	76.3	89.6		92.9	69.9		83.1	67.2	
Vaginosis (%)															
Yes	52.4	39.3	29.3	28.6	**0.03**	16.3	32.2	51.8	**<0.001**	57.1	37.7	0.145	45.1	36.6	0.202
No	47.6	60.7	70.7	71.4		83.8	67.8	48.2		42.9	62.3		54.9	63.4	
Pelvic inflammatory disease (%)															
Yes	6.3	14.3	17.2	0.0	**0.017**	0.0	33.9	8.5	**<0.001**	42.9	9.7	**0.001**	8.5	12.1	0.398
No	93.7	85.7	82.8	100.0		100.0	66.1	91.5		57.1	90.3		91.5	87.9	
Cervicitis (%)															
Yes	6.3	7.9	10.3	11.9	0.726	12.5	10.2	6.1	0.218	0.0	9.0	0.493	8.5	8.6	0.964
No	93.7	92.1	89.7	88.1		87.5	89.8	93.9		100.0	91.0		91.5	91.4	
Vagina cleanliness (%)															
I/II	31.6	35.3	41.7	40.6	0.97	46.8	44.8	18.3	**<0.001**	41.7	36.2	0.671	34.6	37.2	0.439
III	36.8	37.3	33.3	31.3		40.5	34.5	31.0		41.7	35.2		30.8	37.2	
IV	31.6	27.5	25.0	28.1		12.7	20.7	50.7		16.7	28.6		34.6	25.6	
Cervical abnormalities (%)[c]															
Benign	76.6	82.8	83.3	86.1	0.792	88.6	83.9	78.1	0.371	87.5	82.0	0.78	62.7	88.3	**<0.001**
ASC-US	10.6	5.2	4.2	2.8		2.5	6.5	7.3		0.0	5.9		13.6	3.2	
SIL	12.8	12.1	12.5	11.1		8.9	9.7	14.6		12.5	12.1		23.7	8.5	

[a]*p* values were calculated using Chi-square tests. Bold *p* value indicate statistically significant, i.e., $p < 0.05$.
[b]PEC, physical examination center; ART, assisted reproductive technology; GC, gynecology clinics.
[c]ASC-US, atypical squamous cells of undetermined significance; SIL, squamous intraepithelial lesion.

results are highly associated with the serotyping methods using a large panel of monoclonal antibodies (Mukherjee et al., 2011). We would like to emphasize that the purpose of our study is to identify mixed infections of *C. trachomatis* and their pathological impact, not to accurately determine the sequence types of *C. trachomatis* in the clinical samples.

Sanger sequencing is a powerful tool for genotyping and has been used to determine *C. trachomatis* genotypes. However, it may not be suitable for identifying mixed-genotype infections of *C. trachomatis* since Sanger sequencing only produces one consensus sequence according to the alignment results of multiple sequencing data and the intensity of sequencing signals at each point; hence, only the dominant genotype sequence could be identified (Gharsallah et al., 2018). Although the mixed-genotype infections can be identified by PCR-RFLP, hybridization methods and DNA microarray assay, these assays are not sensitive enough to identify all the mixed-genotype infections and cannot quantify genotype proportions in mixed-genotype infections. In addition, these assays cannot detect novel mutations or genovariants (Gharsallah et al., 2012). NGHTS has opened a new frontier to characterize the composition of complex populations of microbes and to uncover novel sequences or mutations, and it overcomes the constraints of Sanger sequencing and can achieve greater than 10,000 base pair coverage per sample (Shendure and Ji, 2008). Meanwhile, NGHTS is capable of obtaining tens or even hundreds of thousands of reads simultaneously, and the sensitivity of detecting low-frequency mutation sites and minor sequences has been dramatically enhanced. For example, Quer et al. (2015) have reported that NGHTS is a reliable method for genotyping hepatitis C virus (HCV) and identifying mixed-genotype infections of HCV through a phylogenetic classification of sequencing reads of HCV *NS5B* gene. In our study, we found that NGHTS could readily determine different proportions of *C. trachomatis* genotypes D-K at the ratio of 1:1.1–1:92.7 in clinical samples. In contrast, the detection limit of microarray assay was about 1:5, which lags far behind the detection performance of NGHTS. Although NGHTS methodology is not simple and needs support of research laboratories, we have assessed the possibility of NGHTS in large-scale implementation by labeling primers with different barcode sequences and mixing 10 samples in one NGHTS reaction. Therefore, NGHTS will dramatically improve the efficiency and greatly reduce the cost for identifying *C. trachomatis* genotypes. Additionally, the potential quantitation bias caused by nested-PCR should be taken into account, thus the NGHTS is only a relatively quantitative method.

TABLE 4 Relationships of clinical manifestations to *C. trachomatis* genotypes in 283 women infected with single-genotype of *C. trachomatis*.

Manifestations	*C. trachomatis* genotype ($n = 261$)[a]					*C. trachomatis* genogroup ($n = 283$)		
	E $n = 83$	D $n = 40$	F $n = 65$	G $n = 18$	J $n = 55$	B-complex $n = 125$	F/G group $n = 83$	C-complex $n = 75$
Asymptomatic								
Yes (*n*, %)	22 (26.5)	15 (37.5)	20 (30.8)	6 (33.3)	13 (23.6)	37 (29.6)	26 (31.3)	20 (26.7)
OR (95% *CI*)[b]	Ref[c]	1.58 (0.56–4.51)	0.81 (0.33–1.99)	0.69 (0.18–2.67)	0.78 (0.3–2.05)	Ref	0.7 (0.33–1.51)	0.91 (0.42–2.0)
Vaginosis								
Yes (*n*, %)	33 (39.8)	14 (35.0)	20 (30.8)	5 (27.8)	28 (50.9)	48 (38.4)	25 (30.1)	35 (46.7)
OR (95% *CI*)	Ref	0.87 (0.37–2.06)	0.79 (0.38–1.64)	0.73 (0.22–2.42)	1.75 (0.84–3.66)	Ref	0.8 (0.43–1.51)	1.43 (0.77–2.66)
Pelvic inflammatory disease								
Yes (*n*, %)	8 (9.6)	2 (5.0)	7 (10.8)	5 (27.8)	9 (16.4)	10 (8.0)	12 (14.5)	10 (13.3)
OR (95% *CI*)	Ref	0.32 (0.04–2.41)	1.44 (0.42–4.9)	**6.06 (1.29–28.5)**	1.54 (0.48–4.91)	Ref	2.71 (0.95–7.78)	1.49 (0.52–4.3)
Cervicitis								
Yes (*n*, %)	5 (6.0)	4 (10.0)	8 (12.3)	2 (11.1)	3 (5.5)	9 (7.2)	10 (12.0)	5 (6.7)
OR (95% *CI*)	Ref	1.71 (0.41–7.05)	2.07 (0.63–6.86)	1.88 (0.32–10.9)	0.89 (0.2–3.94)	Ref	1.62 (0.61–4.32)	0.92 (0.29–2.94)
Vagina cleanliness (vs. I/II)								
III (*n*, %)	16 (29.1)	9 (36.0)	17 (37.8)	6 (40.0)	18 (45.0)	26 (31.7)	23 (38.3)	21 (39.6)
OR (95% *CI*)	Ref	1.71 (0.52–5.58)	1.43 (0.56–3.67)	3.16 (0.65–15.32)	2.39 (0.88–6.49)	Ref	1.39 (0.62–3.14)	1.48 (0.64–3.45)
IV (*n*, %)	15 (27.3)	7 (28.0)	9 (20.0)	6 (40.0)	10 (25.0)	22 (26.8)	15 (25.0)	14 (26.4)
OR (95% *CI*)	Ref	2.49 (0.6–10.29)	0.89 (0.28–2.87)	**6.91 (1.25–38.09)**	1.59 (0.49–5.12)	Ref	1.29 (0.49–3.38)	1.18 (0.44–3.15)
Cervical abnormalities (vs. Benign)[d]								
ASC-US (*n*, %)	4 (6.0)	2 (5.7)	1 (1.8)	0	3 (7.7)	6 (5.8)	1 (1.4)	6 (10.7)
OR (95% *CI*)	Ref	0.71 (0.11–4.77)	0.32 (0.03–3.42)	NA[e]	0.84 (0.15–4.73)	Ref	0.31 (0.04–2.81)	1.79 (0.5–6.48)
SIL (*n*, %)	4 (6.0)	6 (17.1)	9 (16.4)	1 (6.7)	4 (10.3)	10 (9.6)	10 (14.3)	6 (10.7)
OR (95% *CI*)	Ref	2.96 (0.71–12.34)	3.44 (0.94–12.58)	1.15 (0.11–11.98)	1.67 (0.38–7.41)	Ref	1.82 (0.68–4.88)	1.21 (0.4–3.69)

[a]Genotypes of < 5% of the total patients were analyzed only in their corresponding genogroups.
[b]Odds ratio (*OR*) was calculated in multivariate logistic regression analysis in which the parameters of age, clinical departments, antibiotic usage and HPV infection were under control. Bold *OR* and a*OR* indicate statistically significant, i.e., $p < 0.05$.
[c]Genotype E and B-complex genogroup were set as reference group, respectively.
[d]ASC-US, atypical squamous cells of undetermined significance; SIL, squamous intraepithelial lesion.
[e]NA, not applicable.

It has been reported that the prevalence of *C. trachomatis* mixed-genotype infection varied from 2 to 19% (Stothard, 2001; Molano et al., 2004; Xiong et al., 2006; Zhang et al., 2012). It remains to elucidate if mixed-genotype infections represent co-infection or superinfection of different *C. trachomatis* genotypes. Hsu et al. (2006) proposed that two separate episodes of *C. trachomatis* infection and the lack of immunological cross protection between *C. trachomatis* genotypes may result in mixed-genotype infections. In our study, *C. trachomatis* genotype E and F were more frequently detected in the mixed-genotype infections (Table 2), which may be due to the extensive distribution of these two genotypes in China. Gallo Vaulet and Gharsallah, et al. also reported that 86.7 and 76.9% of the mixed-genotype infections contained genotype E, respectively (Gallo Vaulet et al., 2016; Gharsallah et al., 2018). Interestingly, we found that genotype G only accounted for 5.94% of the total *C. trachomatis* infections in our study population, but was detected in 25.0% of the mixed-genotype infections. It is unclear if genotype G has weaker immunological cross protection than other *C. trachomatis* genotypes. Furthermore, genotype D was more often detected in the mixed-genotype infections particularly when the proportion of minor *C. trachomatis* genotype was ≥10%. Our results might suggest increased susceptibility of genotype D and G in the co- or super-infection of *C. trachomatis*.

Another important issue is the association between specific clinical manifestations and *C. trachomatis* genotypes or mixed-genotype infections. It has been reported that several *C. trachomatis* genotypes such as F, G and K may result in more severe clinical manifestations (Geisler et al., 2003; Molano et al., 2004; Millman et al., 2006; Gao et al., 2007). In the current study, we also observed that *C. trachomatis* genotype G infection was more prone to PID (Table 4). Our results are consistent with the findings of Gao et al. (2007). Till now, there are few studies to compare the difference of clinical manifestations between single and mixed-genotype infections of *C. trachomatis*. Our preliminary results indicated that mixed-genotype infections may result in worse vaginal cleanliness and cervical SIL (Table 5) while we found no significant difference of vaginal cleanliness among different single-genotype *C. trachomatis* infections, suggesting that co- or super-infection

TABLE 5 Comparison of clinical manifestations between women with *C. trachomatis* single-genotype and mixed-genotype infections.

Manifestations	Single genotype event/*N* (%)	*C. trachomatis* mixed-genotype infection[a]								
		Total (*N* = 20)			Without dominant genotype (*N* = 10)			With dominant genotype (*N* = 10)		
		Event/*N* (%)	*OR*[b] (95% *CI*)	a*OR*[c] (95% *CI*)	Event/*N* (%)	OR (95% CI)	a*OR* (95% *CI*)	Event/*N* (%)	*OR* (95% *CI*)	a*OR* (95% *CI*)
Asymptomatic	83/283 (29.3)	5/20 (25.0)	0.83 (0.24–2.86)	0.80 (0.28–2.28)	1/10 (10.0)	0.67 (0.08–5.64)	0.41 (0.05–3.29)	4/10 (40.0)	0.89 (0.19–4.15)	0.86 (0.24–3.12)
Vaginosis	108/283 (38.2)	9/20 (45.0)	1.52 (0.57–4.03)	1.33 (0.54–3.32)	6/10 (60.0)	1.91 (0.51–7.16)	2.22 (0.61–8.03)	3/10 (30.0)	1.19 (0.27–5.24)	1.21 (0.3–4.78)
Pelvic inflammatory disease	32/283 (11.3)	2/20 (10.0)	0.6 (0.11–3.21)	0.88 (0.20–3.98)	0	NA	NA	2/10 (20.0)	1.3 (0.18–9.19)	1.43 (0.29–6.96)
Cervicitis	24/283 (8.5)	2/20 (10.0)	1.1 (0.23–5.16)	1.20 (0.26–5.49)	1/10 (10.0)	1.5 (0.17–12.92)	1.68 (0.2–14.0)	1/10 (10.0)	0.93 (0.11–8.13)	0.71 (0.09–5.79)
Vagina cleanliness (vs. I/II)										
III	70/195 (35.9)	4/13 (30.8)	2.46 (0.43–14.24)	2.11 (0.37–11.87)	0	NA	NA	4/8 (50.0)	2.69 (0.46–15.78)	2.07 (0.37–11.64)
IV	51/195 (26.2)	7/13 (53.8)	**8.61 (1.53–48.53)**	**5.17 (1.03–25.92)**	5/5 (100.0)	NA[d]	NA	2/8 (25.0)	3.44 (0.43–27.73)	1.41 (0.19–10.35)
Cervical abnormalities (vs. Benign)[e]										
ASC-US	13/230 (5.7)	1/17 (5.9)	1.18 (0.12–11.35)	1.22 (0.15–10.12)	0	NA	NA	1/10 (10.0)	2.14 (0.2–23.5)	1.85 (0.21–15.91)
SIL	26/230 (11.3)	4/17 (23.5)	2.8 (0.75–10.5)	2.44 (0.73–8.13)	3 (42.9)	**5.76 (1.06–31.22)**	**5.51 (1.17–26.01)**	1/10 (10.0)	1.06 (0.11–10.25)	0.92 (0.11–7.64)

[a]Mixed-genotype infections were divided into two groups with or without dominant genotype in which the proportion of minor genotypes was <10% or ≥10%, respectively.
[b]Odds ratio (*OR*) was calculated in multivariate logistic regression analysis in which the parameters of age, clinical departments, antibiotic usage and HPV infection were under control.
[c]adjusted odd ratio (a*OR*) was calculated based on the data of propensity score weighting. Bold *OR* and a*OR* indicate statistically significant, i.e., $p < 0.05$.
[d]NA, not applicable.
[e]ASC-US, atypical squamous cells of undetermined significance; SIL, squamous intraepithelial lesion.

and the interaction of different *C. trachomatis* strains may contribute to stronger inflammatory reactions and worse vaginal or cervical damage (Gharsallah et al., 2012). It has been found that cervical SIL and cervical cancer are related to *C. trachomatis* infection (Smith et al., 2004; Castellsagué et al., 2014) or *C. trachomatis*/HPV co-infection (de Paula et al., 2007; da Silva Barros et al., 2012; de Abreu et al., 2012; Magalhães et al., 2015). Our further analysis indicated that *C. trachomatis* mixed-genotype infection was associated with cervical SIL compared with single-genotype infection even controlling for HPV infection (Table 5). Furthermore, Madeleine et al. (2007) reported that *C. trachomatis* genotypes B, D, E, G, I, and J were associated with squamous cell cancer although this association was not supported by other studies (Smith et al., 2004). We also did not observe the association of different *C. trachomatis* genotypes with SIL (Table 4). Previous studies indicated that *C. trachomatis* could inhibit apoptosis of *C. trachomatis*-infected cells, trigger host DNA damage, and induce cell proliferation (Chumduri et al., 2013). These results support *C. trachomatis* infection as a potential cause of SIL (Kun et al., 2013). Therefore, it is reasonable to speculate that mixed-genotype infection may facilitate *C. trachomatis*-associated effects on the development of cervical SIL due to the synergistic effect of multiple genotype infections. Similar synergistic impact has been observed in HPV mixed-genotype infections in which cervical SIL was significantly more frequent in mixed-genotype HPV infection than in single genotype HPV infection (Bachtiary et al., 2002; Bruno et al., 2020; Oyervides-Muñoz et al., 2020; Kim et al., 2021). Further research did show that tumors caused by mixed-genotype infection of HPV had a higher PD-1 expression in tumor-infiltrating lymphocytes (TILs), which could help cancer cells evade the immune response and progress more quickly (Mendoza et al., 2021). Actually, inflammation *per se* is a risk factor for cell malignant transformation (Greten and Grivennikov, 2019). More severe inflammation caused by mixed-genotype infection of *C. trachomatis* may also play a role in the process of cervical SIL during *C. trachomatis* infection.

In addition, previous studies have revealed high recombination rates among *C. trachomatis* strains, indicating their important role in the evolutionary pathways (Gomes et al., 2007). For example, the recombination event between the MOMP genes of genotype I and H may generate the composite MOMP of Ia variant (Lampe et al., 1993). Clinical strains of *C. trachomatis* have been reported to

be resistant to tetracycline (Jones et al., 1990), macrolides (Misyurina et al., 2004), even multiple antibiotics (Somani et al., 2000). In an *in vitro* study (Suchland et al., 2009), a co-infection model was used to successfully generate tetracycline-resistant *C. trachomatis* L_2 strain from co-infection of tetracycline-resistant *C. suis* R19 and a tetracycline-sensitive L_2 strain. The *ompA* gene of *C. trachomatis* can be inserted into different genomic backbones through potential gene recombination. However, the recombination of *ompA* may happen most likely between L strain and I/J/K strains or between ocular and urogenital branches or between L2b and D-Da strains (Somboonna et al., 2011; Harris et al., 2012; Matičič et al., 2016; Borges et al., 2021). Hadfield et al. (2017) reported that in their comprehensive global genome dynamic analysis of *C. trachomatis*, only serovar D and J appeared in both monophyletic lineage T1 and T2. In addition, recombination did not disrupt the *ompA* gene of the most prevalent genotype E. Furthermore, the *ompA* gene of *C. trachomatis* is a single copy gene and may have a lower probability of switching compared to the multi-copy genes, e.g., cryptic plasmid (Joseph et al., 2011). Dalevi et al. (2002) found that the major factors influencing the structure of the *C. trachomatis* genomes are nucleotide substitutions and deletions, and the frequency of horizontal gene transfer events was low. Although the recombination of the *ompA* gene was mainly reported in case reports, the mixed-genotype infection identified in our study was just based on the *ompA* typing system and did not address the potential recombination of the *ompA* gene. WGS or hr-MLST needs to be performed to address the mixed genotype identified in our study and to identify any potential recombinants arising as a result of mixed infection. Our preliminary results prove the importance of identifying mixed-genotype infections of *C. trachomatis* by using NGHTS as a screening assay. Furthermore, qPCR is more sensitive than conventional PCR in detecting C. trachomatis infection. It is necessary to use qPCR for simultaneous detection to ensure accuracy when NGHTS is used to detect C. trachomatis mixed-genotype infections in clinical samples.

Our study has some limitations. (1) The cross-sectional study cannot determine the cause-effect of mixed-genotype infection of *C. trachomatis* and cervical damage. Our findings should be explained with caution. (2) The number of *C. trachomatis* positive samples is small due to the low prevalence of *C. trachomatis* infection and mixed-genotype infections of *C. trachomatis* although a total of 8,087 clinical samples were screened in our study. However, the sample size of 20 mixed-genotype infections was relatively large compared with previous studies. We also used the propensity scores weighting analysis to ensure the accuracy and reliability of the results. (3) All the subjects were from one hospital and were consecutively recruited from the selected clinics. The selection of the participants may limit the generalizability of the findings. (4) Conventional PCR detection rather than qPCR was used in our study and may underestimate *C. trachomatis* prevalence. The *ompA* target genotyping did not cover the entire *ompA* gene due to the read length limitation of NGHTS. (5) Antibiotic resistance of *C. trachomatis* is an ongoing concern although Hadfield, et al. reported that the comprehensive global genome dynamics of *C. trachomatis* did not show evidence of circulating genomic resistance in *C. trachomatis* (Hadfield et al., 2017). In our study, we did not investigate antibiotic resistance since the purpose of our study was to genotype *C. trachomatis* in the samples analyzed.

We confirmed NGHTS as a useful tool for sensitive and accurate identification of *C. trachomatis* genotypes in particular mixed-genotype infections. Our results revealed the feasibility of NGHTS in characterizing mixed *C. trachomatis* infections and its clinical value. Mixed infections of *C. trachomatis* may associate with worse vaginal cleanliness and cervical SIL. Therefore, NGHTS should be further assessed and implemented as a routine screening assay for diagnosis and genotyping of *C. trachomatis* infections.

Data availability statement

The datasets presented in this study can be found in online repositories. The names of the repository/repositories and accession number(s) can be found at: https://www.ncbi.nlm.nih.gov/, PRJNA786082.

Ethics statement

The studies involving human participants were reviewed and approved by Ethical Committee of Chenzhou No. 1 People's Hospital. The patients/participants provided their written informed consent to participate in this study.

Author contributions

JZ and JS: analysis and interpretation of data, conduction of experiment, and drafting of manuscript. LL: acquisition of data and conduction of experiment. CA, HL, and LW: performed experiment. YL: performed the data analysis. HW: revision of manuscript. ST and HC: conception, design, and finalizing manuscript. All authors read and approved the final manuscript.

Funding

This work was supported by the Bureau of Science and Information Technology of Guangzhou Municipality (grant no. 201704020219), Natural Science Foundation of Hunan Province (grant no. 2021JJ70002) and Bureau of Chenzhou Science and Technology (yfzx201908).

Conflict of interest

The authors declare that the research was conducted in the absence of any commercial or financial relationships that could be construed as a potential conflict of interest.

Publisher's note

Supplementary material

The Supplementary material for this article can be found online at: https://www.frontiersin.org/articles/10.3389/fmicb.2022.1041789/full#supplementary-material

SUPPLEMENTARY FIGURE S1
Reference sequences alignment and primers design for next generation high-throughput sequencing (NGHTS) targets.

SUPPLEMENTARY FIGURE S2
The schematic diagram of the identification of *Chlamydia trachomatis* (*C. trachomatis*) mixed-genotype infection using the next generation high-throughput sequencing (NGHTS) process. PCR, polymerase chain reaction; BWA, Burrows-Wheeler transform.

SUPPLEMENTARY FIGURE S3
Low detection limit of high-throughput sequencing primers for different *Chlamydia trachomatis* genotypes.

SUPPLEMENTARY FIGURE S4
Verification of genotype-specific primers for amplifying minor *Chlamydia trachomatis* (*C. trachomatis*) genotypes from mixed-genotype infections of *C. trachomatis*. **(A)** Genotype-specific primers can specifically amplify minor *C. trachomatis* genotypes when using plasmid DNAs of mixed-genotypes of *C. trachomatis* as templates. **(B)** The minor genotypes were specifically amplified from the samples of mixed-genotype infections by using genotype-specific primers. NC, negative control; +, PCR positive; -, PCR negative.

References

Bachtiary, B., Obermair, A., Dreier, B., Birner, P., Breitenecker, G., Knocke, T., et al. (2002). Impact of multiple HPV infection on response to treatment and survival in patients receiving radical radiotherapy for cervical cancer. *Int. J. Cancer* 102, 237–243. doi: 10.1002/ijc.10708

Bao, Y., Hu, M., Gao, G., Huang, J., and Zhang, Z. (2015). Multivariate analysis for pelvic floor dysfunction. *Zhong Nan Da Xue Xue Bao Yi Xue Ban* 40, 1229–1233. doi: 10.11817/j.issn.1672-7347.2015.11.011

Batteiger, B., Lennington, W., Newhall, W., Katz, B., Morrison, H., and Jones, R. (1989). Correlation of infecting serovar and local inflammation in genital chlamydial infections. *J. Infect. Dis.* 160, 332–336. doi: 10.1093/infdis/160.2.332

Bax, C., Quint, K., Peters, R., Ouburg, S., Oostvogel, P., Mutsaers, J., et al. (2011). Analyses of multiple-site and concurrent *Chlamydia trachomatis* serovar infections, and serovar tissue tropism for urogenital versus rectal specimens in male and female patients. *Sex. Transm. Infect.* 87, 503–507. doi: 10.1136/sti.2010.048173

Borges, V., Isidro, J., Correia, C., Cordeiro, D., Vieira, L., Lodhia, Z., et al. (2021). Transcontinental dissemination of the L2b/D-Da recombinant *Chlamydia trachomatis* lymphogranuloma venereum (LGV) strain: need of broad multi-country molecular surveillance. *Clin. Infect. Dis.* 73, e1004–e1007. doi: 10.1093/cid/ciab067

Bornstein, J., Bentley, J., Bösze, P., Girardi, F., Haefner, H., Menton, M., et al. (2012). 2011 colposcopic terminology of the International Federation for Cervical Pathology and Colposcopy. *Obstet. Gynecol.* 120, 166–172. doi: 10.1097/AOG.0b013e318254f90c

Brasiliense, D. M., Borges Bdo, N., and Ferreira, W. A. (2016). Genotyping and prevalence of *Chlamydia trachomatis* infection among women in Belem, Para, northern Brazil. *J. Infect. Dev. Ctries.* 10, 134–137. doi: 10.3855/jidc.6474

Brown, A. C., and Christiansen, M. T. (2019). Whole-genome sequencing of *Chlamydia trachomatis* directly from human samples. *Methods Mol. Biol.* 2042, 45–67. doi: 10.1007/978-1-4939-9694-0_6

Bruno, M., Scalia, G., Cassaro, N., and Boemi, S. (2020). Multiple HPV 16 infection with two strains: a possible marker of neoplastic progression. *BMC Cancer* 20:444. doi: 10.1186/s12885-020-06946-7

Burnett, L., Lunn, G., and Coico, R. (2009). Biosafety: guidelines for working with pathogenic and infectious microorganisms. *Curr. Protoc. Microbiol.* 13, 111–1114. doi: 10.1002/9780471729259.mc01a01s13

Carr, P., Felsenstein, D., and Friedman, R. (1998). Evaluation and management of vaginitis. *J. Gen. Intern. Med.* 13, 335–346. doi: 10.1046/j.1525-1497.1998.00101.x

Castellsagué, X., Pawlita, M., Roura, E., Margall, N., Waterboer, T., Bosch, F., et al. (2014). Prospective seroepidemiologic study on the role of human papillomavirus and other infections in cervical carcinogenesis: evidence from the EPIC cohort. *Int. J. Cancer* 135, 440–452. doi: 10.1002/ijc.28665

Chen, H., Luo, L., Wen, Y., He, B., Ling, H., Shui, J., et al. (2020). *Chlamydia trachomatis* and human papillomavirus infection in women from southern Hunan Province in China: a large observational study. *Front. Microbiol.* 11:827. doi: 10.3389/fmicb.2020.00827

Chumduri, C., Gurumurthy, R., Zadora, P., Mi, Y., and Meyer, T. (2013). Chlamydia infection promotes host DNA damage and proliferation but impairs the DNA damage response. *Cell Host Microbe* 13, 746–758. doi: 10.1016/j.chom.2013.05.010

da Silva Barros, N., Costa, M., Alves, R., Villa, L., Derchain, S., Zeferino, L., et al. (2012). Association of HPV infection and *Chlamydia trachomatis* seropositivity in cases of cervical neoplasia in Midwest Brazil. *J. Med. Virol.* 84, 1143–1150. doi: 10.1002/jmv.23312

Dalevi, D. A., Eriksen, N., Eriksson, K., and Andersson, S. G. (2002). Measuring genome divergence in bacteria: a case study using chlamydian data. *J. Mol. Evol.* 55, 24–36. doi: 10.1007/s00239-001-0087-9

de Abreu, A., Nogara, P., Souza, R., da Silva, M., Uchimura, N., Zanko, R., et al. (2012). Molecular detection of HPV and *Chlamydia trachomatis* infections in Brazilian women with abnormal cervical cytology. *Am. J. Trop. Med. Hyg.* 87, 1149–1151. doi: 10.4269/ajtmh.2012.12-0287

de Oliveira, A. C. A., Domingues, M. F., Neufeld, P. M., Fleury, M., and Nogueira Neto, J. F. (2020). Comparison between conventional cytology and liquid-based cytology in the tertiary Brazilian navy Hospital in Rio de Janeiro. *Acta Cytol.* 64, 539–546. doi: 10.1159/000508018

de Paula, F., Fernandes, A., Carmo, B., Vieira, D., Dutra, M., Santos, C., et al. (2007). Molecular detection of *Chlamydia trachomatis* and HPV infections in cervical samples with normal and abnormal cytopathological findings. *Diagn. Cytopathol.* 35, 198–202. doi: 10.1002/dc.20629

Dean, D., Oudens, E., Bolan, G., Padian, N., and Schachter, J. (1995). Major outer membrane protein variants of *Chlamydia trachomatis* are associated with severe upper genital tract infections and histopathology in San Francisco. *J. Infect. Dis.* 172, 1013–1022. doi: 10.1093/infdis/172.4.1013

Foschi, C., Nardini, P., Banzola, N., D'Antuono, A., Compri, M., Cevenini, R., et al. (2016). *Chlamydia trachomatis* infection prevalence and serovar distribution in a high-density urban area in the north of Italy. *J. Med. Microbiol.* 65, 510–520. doi: 10.1099/jmm.0.000261

Fu, L., Sun, Y., Han, M., Wang, B., Xiao, F., Zhou, Y., et al. (2022). Incidence trends of five common sexually transmitted infections excluding HIV from 1990 to 2019 at the global, regional, and National Levels: results from the global burden of disease study 2019. *Front. Med. (Lausanne)* 9:851635. doi: 10.3389/fmed.2022.851635

Gallo Vaulet, L., Entrocassi, C., Portu, A. I., Castro, E., Di Bartolomeo, S., Ruettger, A., et al. (2016). High frequency of *Chlamydia trachomatis* mixed infections detected by microarray assay in south American samples. *PLoS One* 11:e0153511. doi: 10.1371/journal.pone.0153511

Gao, X., Chen, X. S., Yin, Y. P., Zhong, M. Y., Shi, M. Q., Wei, W. H., et al. (2007). Distribution study of *Chlamydia trachomatis* serovars among high-risk women in China performed using PCR-restriction fragment length polymorphism genotyping. *J. Clin. Microbiol.* 45, 1185–1189. doi: 10.1128/jcm.02076-06

Geisler, W. M., Suchland, R. J., Whittington, W. L., and Stamm, W. E. (2003). The relationship of serovar to clinical manifestations of urogenital *Chlamydia trachomatis* infection. *Sex. Transm. Dis.* 30, 160–165. doi: 10.1097/00007435-200302000-00013

Gharsallah, H., Frikha-Gargouri, O., Besbes, F., Sellami, H., and Hammami, A. (2012). Development and application of an in-house reverse hybridization method for *Chlamydia trachomatis* genotyping. *J. Appl. Microbiol.* 113, 846–855. doi: 10.1111/j.1365-2672.2012.05375.x

Gharsallah, H., Frikha-Gargouri, O., Bom, R. J., Hammami, A., and Bruisten, S. M. (2018). Comparison of reverse hybridization and ompA sequencing methods

applied on *Chlamydia trachomatis* strains from Tunisia. *Microbiology* 7:e00549. doi: 10.1002/mbo3.549

Gomes, J., Bruno, W., Nunes, A., Santos, N., Florindo, C., Borrego, M., et al. (2007). Evolution of *Chlamydia trachomatis* diversity occurs by widespread interstrain recombination involving hotspots. *Genome Res.* 17, 50–60. doi: 10.1101/gr.5674706

Greten, F., and Grivennikov, S. (2019). Inflammation and cancer: triggers, mechanisms, and consequences. *Immunity* 51, 27–41. doi: 10.1016/j.immuni.2019.06.025

Group., C.M.A.O.a.G.B.I.D.C (2016). Expert consensus on clinical application of vaginal microecosystem assessment. *Chin. J. Obstet. Gynecol.* 51, 721–723.

Hadfield, J., Harris, S. R., Seth-Smith, H. M. B., Parmar, S., Andersson, P., Giffard, P. M., et al. (2017). Comprehensive global genome dynamics of *Chlamydia trachomatis* show ancient diversification followed by contemporary mixing and recent lineage expansion. *Genome Res.* 27, 1220–1229. doi: 10.1101/gr.212647.116

Harris, S. R., Clarke, I. N., Seth-Smith, H. M., Solomon, A. W., Cutcliffe, L. T., Marsh, P., et al. (2012). Whole-genome analysis of diverse *Chlamydia trachomatis* strains identifies phylogenetic relationships masked by current clinical typing. *Nat. Genet.* 44:413-419, s411. doi: 10.1038/ng.2214

Hsu, M. C., Tsai, P. Y., Chen, K. T., Li, L. H., Chiang, C. C., Tsai, J. J., et al. (2006). Genotyping of *Chlamydia trachomatis* from clinical specimens in Taiwan. *J. Med. Microbiol.* 55, 301–308. doi: 10.1099/jmm.0.46262-0

Ito, J. I., Lyons, J. M., and Airo-Brown, L. P. (1990). Variation in virulence among oculogenital serovars of *Chlamydia trachomatis* in experimental genital tract infection. *Infect. Immun.* 58, 2021–2023.

Jalal, H., Stephen, H., Alexander, S., Carne, C., and Sonnex, C. (2007). Development of real-time PCR assays for genotyping of *Chlamydia trachomatis*. *J. Clin. Microbiol.* 45, 2649–2653. doi: 10.1128/JCM.00451-07

Jones, R., Van der Pol, B., Martin, D., and Shepard, M. (1990). Partial characterization of *Chlamydia trachomatis* isolates resistant to multiple antibiotics. *J. Infect. Dis.* 162, 1309–1315. doi: 10.1093/infdis/162.6.1309

Joseph, S. J., Didelot, X., Gandhi, K., Dean, D., and Read, T. D. (2011). Interplay of recombination and selection in the genomes of *Chlamydia trachomatis*. *Biol. Direct* 6:28. doi: 10.1186/1745-6150-6-28

Jurstrand, M., Falk, L., Fredlund, H., Lindberg, M., Olcén, P., Andersson, S., et al. (2001). Characterization of *Chlamydia trachomatis* omp1 genotypes among sexually transmitted disease patients in Sweden. *J. Clin. Microbiol.* 39, 3915–3919. doi: 10.1128/jcm.39.11.3915-3919.2001

Kawada, J., Okuno, Y., Torii, Y., Okada, R., Hayano, S., Ando, S., et al. (2016). Identification of viruses in cases of pediatric acute encephalitis and encephalopathy using next-generation sequencing. *Sci. Rep.* 6:33452. doi: 10.1038/srep33452

Khan, M., Werner, C., Darragh, T., Guido, R., Mathews, C., Moscicki, A., et al. (2017). ASCCP colposcopy standards: role of colposcopy, benefits, potential harms, and terminology for Colposcopic practice. *J. Low. Genit. Tract Dis.* 21, 223–229. doi: 10.1097/lgt.0000000000000338

Kim, M., Park, N., Jeong, J., and Park, J. (2021). Multiple human papilloma virus (HPV) infections are associated with HSIL and persistent HPV infection status in Korean patients. *Viruses* 13:1342. doi: 10.3390/v13071342

Kun, D., Xiang-Lin, C., Ming, Z., and Qi, L. (2013). Chlamydia inhibit host cell apoptosis by inducing Bag-1 via the MAPK/ERK survival pathway. *Apoptosis* 18, 1083–1092. doi: 10.1007/s10495-013-0865-z

Lampe, M., Suchland, R., and Stamm, W. (1993). Nucleotide sequence of the variable domains within the major outer membrane protein gene from serovariants of *Chlamydia trachomatis*. *Infect. Immun.* 61, 213–219. doi: 10.1128/iai.61.1.213-219.1993

Lesiak-Markowicz, I., Schötta, A., Stockinger, H., Stanek, G., and Markowicz, M. (2019). *Chlamydia trachomatis* serovars in urogenital and ocular samples collected 2014-2017 from Austrian patients. *Sci. Rep.* 9:18327. doi: 10.1038/s41598-019-54886-5

Li, H., and Durbin, R. (2009). Fast and accurate short read alignment with burrows-wheeler transform. *Bioinformatics (Oxford, England)* 25, 1754–1760. doi: 10.1093/bioinformatics/btp324

Lyons, J. M., Ito, J. I., and Morré, S. A. (2004). *Chlamydia trachomatis* serovar E isolates from patients with different clinical manifestations have similar courses of infection in a murine model: host factors as major determinants of C trachomatis mediated pathogenesis. *J. Clin. Pathol.* 57, 657–659. doi: 10.1136/jcp.2003.013086

Madeleine, M., Anttila, T., Schwartz, S., Saikku, P., Leinonen, M., Carter, J., et al. (2007). Risk of cervical cancer associated with *Chlamydia trachomatis* antibodies by histology, HPV type and HPV cofactors. *Int. J. Cancer* 120, 650–655. doi: 10.1002/ijc.22325

Magalhães, P., Miranda, C., Lima, É., Moizéis, R., de Lima, D., Cobucci, R., et al. (2015). Genital tract infection with *Chlamydia trachomatis* in women attended at a cervical cancer screening program in northeastern from Brazil. *Arch. Gynecol. Obstet.* 291, 1095–1102. doi: 10.1007/s00404-014-3514-z

Magoč, T., and Salzberg, S. (2011). FLASH: fast length adjustment of short reads to improve genome assemblies. *Bioinformatics* 27, 2957–2963. doi: 10.1093/bioinformatics/btr507

Marcone, V., Recine, N., Gallinelli, C., Nicosia, R., Lichtner, M., Degener, A. M., et al. (2012). Epidemiology of *Chlamydia trachomatis* endocervical infection in a previously unscreened population in Rome, Italy, 2000 to 2009. *Euro Surveill.* 17:20203. doi: 10.2807/ese.17.25.20203-en

Martinez, M. A., Ovalle, A., Camponovo, R., and Vidal, R. (2015). *Chlamydia trachomatis* genovars causing urogenital infections in Santiago. *Chile. Infect Dis (Lond)* 47, 156–160. doi: 10.3109/00365548.2014.977341

Matičič, M., Klavs, I., Videčnik Zorman, J., Vidmar Vovko, D., Kogoj, R., and Keše, D. (2016). Confirmed inguinal lymphogranuloma venereum genovar L2c in a man who had sex with men, Slovenia, 2015. *Euro Surveill.* 21, 2–5. doi: 10.2807/1560-7917.Es.2016.21.5.30129

Mendoza, R., Haidary, T., Gabutan, E., Zhou, Y., Bukhari, Z., Connelly, C., et al. (2021). Mixed and nonvaccine high risk HPV types are associated with higher mortality in Black women with cervical cancer. *Sci. Rep.* 11:14064. doi: 10.1038/s41598-021-93485-1

Millman, K., Black, C. M., Stamm, W. E., Jones, R. B., Hook, E. W., Martin, D. H., et al. (2006). Population-based genetic epidemiologic analysis of *Chlamydia trachomatis* serotypes and lack of association between ompA polymorphisms and clinical phenotypes. *Microbes Infect.* 8, 604–611. doi: 10.1016/j.micinf.2005.08.012

Misyurina, O., Chipitsyna, E., Finashutina, Y., Lazarev, V., Akopian, T., Savicheva, A., et al. (2004). Mutations in a 23S rRNA gene of *Chlamydia trachomatis* associated with resistance to macrolides. *Antimicrob. Agents Chemother.* 48, 1347–1349. doi: 10.1128/aac.48.4.1347-1349.2004

Molano, M., Meijer, C. J. L. M., Morre, S. A., Pol, R., and Van den Brule, A. J. C. (2004). Combination of PCR targeting the VD2 of omp1 and reverse line blot analysis for typing of urogenital *Chlamydia trachomatis* Serovars in cervical scrape specimens. *J. Clin. Microbiol.* 42, 2935–2939. doi: 10.1128/JCM.42.7.2935-2939.2004

Mukherjee, A., Sood, S., Bala, M., Satpathy, G., Mahajan, N., Kapil, A., et al. (2011). The role of a commercial enzyme immuno assay antigen detection system for diagnosis of C. trachomatis in genital swab samples. *Indian J. Med. Microbiol.* 29, 411–413. doi: 10.4103/0255-0857.90180

Ngandjio, A., Clerc, M., Fonkoua, M. C., Thonnon, J., Njock, F., Pouillot, R., et al. (2003). Screening of volunteer students in Yaounde (Cameroon, Central Africa) for *Chlamydia trachomatis* infection and genotyping of isolated C. trachomatis strains. *J. Clin. Microbiol.* 41, 4404–4407. doi: 10.1128/jcm.41.9.4404-4407.2003

Nunes, A., Borrego, M. J., Nunes, B., Florindo, C., and Gomes, J. P. (2009). Evolutionary dynamics of ompA, the gene encoding the *Chlamydia trachomatis* key antigen. *J. Bacteriol.* 191, 7182–7192. doi: 10.1128/jb.00895-09

Oyervides-Muñoz, M., Pérez-Maya, A., Sánchez-Domínguez, C., Berlanga-Garza, A., Antonio-Macedo, M., Valdéz-Chapa, L., et al. (2020). Multiple HPV infections and viral load Association in Persistent Cervical Lesions in Mexican women. *Viruses* 12:40380. doi: 10.3390/v12040380

Petrovay, F., Németh, I., Balázs, A., and Balla, E. (2015). Chlamydial conjunctivitis: prevalence and serovar distribution of *Chlamydia trachomatis* in adults. *J. Med. Microbiol.* 64, 967–970. doi: 10.1099/jmm.0.000115

Quer, J., Gregori, J., Rodríguez-Frias, F., Buti, M., Madejon, A., Perez-del-Pulgar, S., et al. (2015). High-resolution hepatitis C virus subtyping using NS5B deep sequencing and phylogeny, an alternative to current methods. *J. Clin. Microbiol.* 53, 219–226. doi: 10.1128/jcm.02093-14

Quint, K. D., van Doorn, L. J., Kleter, B., de Koning, M. N., van den Munckhof, H. A., Morre, S. A., et al. (2007). A highly sensitive, multiplex broad-spectrum PCR-DNA-enzyme immunoassay and reverse hybridization assay for rapid detection and identification of *Chlamydia trachomatis* serovars. *J. Mol. Diagn.* 9, 631–638. doi: 10.2353/jmoldx.2007.070011

Ruettger, A., Feige, J., Slickers, P., Schubert, E., Morré, S. A., Pannekoek, Y., et al. (2011). Genotyping of *Chlamydia trachomatis* strains from culture and clinical samples using an ompA-based DNA microarray assay. *Mol. Cell. Probes* 25, 19–27. doi: 10.1016/j.mcp.2010.09.004

Shendure, J., and Ji, H. (2008). Next-generation DNA sequencing. *Nat. Biotechnol.* 26, 1135–1145. doi: 10.1038/nbt1486

Smith, J., Bosetti, C., Muñoz, N., Herrero, R., Bosch, F., Eluf-Neto, J., et al. (2004). *Chlamydia trachomatis* and invasive cervical cancer: a pooled analysis of the IARC multicentric case-control study. *Int. J. Cancer* 111, 431–439. doi: 10.1002/ijc.20257

Somani, J., Bhullar, V., Workowski, K., Farshy, C., and Black, C. (2000). Multiple drug-resistant *Chlamydia trachomatis* associated with clinical treatment failure. *J. Infect. Dis.* 181, 1421–1427. doi: 10.1086/315372

Somboonna, N., Wan, R., Ojcius, D. M., Pettengill, M. A., Joseph, S. J., Chang, A., et al. (2011). Hypervirulent *Chlamydia trachomatis* clinical strain is a recombinant between lymphogranuloma venereum (L(2)) and D lineages. *mBio* 2:e00045-11. doi: 10.1128/mBio.00045-11

Spaargaren, J., Fennema, H. S., Morré, S. A., de Vries, H. J., and Coutinho, R. A. (2005). New lymphogranuloma venereum *Chlamydia trachomatis* variant, Amsterdam. *Emerg. Infect. Dis.* 11, 1090–1092. doi: 10.3201/eid1107.040883

Stothard, D. R. (2001). Use of a reverse dot blot procedure to identify the presence of multiple Serovars in *Chlamydia trachomatis* urogenital infection. *J. Clin. Microbiol.* 39, 2655–2659. doi: 10.1128/JCM.39.7.2655-2659.2001

Suchland, R., Sandoz, K., Jeffrey, B., Stamm, W., and Rockey, D. (2009). Horizontal transfer of tetracycline resistance among chlamydia spp. in vitro. *Antimicrob. Agents Chemother.* 53, 4604–4611. doi: 10.1128/aac.00477-09

Versteeg, B., Dubbink, J. H., Bruisten, S. M., McIntyre, J. A., Morré, S. A., and Peters, R. P. (2015). High-resolution multilocus sequence typing reveals novel urogenital *Chlamydia trachomatis* strains in women in Mopani district, South Africa. *Sex Transm Infect* 91, 510–512. doi: 10.1136/sextrans-2014-051998

Woodhall, S., Gorwitz, R., Migchelsen, S., Gottlieb, S., Horner, P., Geisler, W., et al. (2018). Advancing the public health applications of *Chlamydia trachomatis* serology. *Lancet Infect. Dis.* 18, e399–e407. doi: 10.1016/s1473-3099(18)30159-2

Workowski, K., Stevens, C., Suchland, R., Holmes, K., Eschenbach, D., Pettinger, M., et al. (1994). Clinical manifestations of genital infection due to *Chlamydia trachomatis* in women: differences related to serovar. *Clin. Infect. Dis.* 19, 756–760. doi: 10.1093/clinids/19.4.756

Xiong, L., Kong, F., Zhou, H., and Gilbert, G. L. (2006). Use of PCR and reverse line blot hybridization assay for rapid simultaneous detection and Serovar identification of *Chlamydia trachomatis*. *J. Clin. Microbiol.* 44, 1413–1418. doi: 10.1128/JCM.44.4.1413-1418.2006

Yan, Y., Yuanfang, Z., Yon, X., Li-kuan, X., Jun, W., Yan, Z., et al. (2018). Genotype analysis of *Chlamydia trachomatis* infection in pregnant women and neonates. *Chin J Obstet Gynecol* 53, 319–322.

Yang, B., Zheng, H., Feng, Z., Xue, Y., Wu, X., Huang, J., et al. (2010). The prevalence and distribution of *Chlamydia trachomatis* genotypes among sexually transmitted disease clinic patients in Guangzhou, China, 2005-2008. *Jpn. J. Infect. Dis.* 63, 342–345.

Yu, F., Tang, Y. T., Hu, Z. Q., and Lin, X. N. (2018). Analysis of the vaginal microecological status and genital tract infection characteristics of 751 pregnant women. *Med. Sci. Monit.* 24, 5338–5345. doi: 10.12659/msm.909051

Yuan, Y., Zhang, Y., Watkins, N., and Caldwell, H. (1989). Nucleotide and deduced amino acid sequences for the four variable domains of the major outer membrane proteins of the 15 *Chlamydia trachomatis* serovars. *Infect. Immun.* 57, 1040–1049. doi: 10.1128/iai.57.4.1040-1049.1989

Yue, X. A., Chen, P., Tang, Y., Wu, X., and Hu, Z. (2015). The dynamic changes of vaginal microecosystem in patients with recurrent vulvovaginal candidiasis: a retrospective study of 800 patients. *Arch. Gynecol. Obstet.* 292, 1285–1294. doi: 10.1007/s00404-015-3774-2

Zhang, J. J., Zhao, G. L., Wang, F., Hong, F. C., Luo, Z. Z., Lan, L. N., et al. (2012). Molecular epidemiology of genital *Chlamydia trachomatis* infection in Shenzhen, China. *Sex Transm Infect* 88, 272–277. doi: 10.1136/sextrans-2011-050163

Zheng, H., Jiang, L., Fang, D., Xue, Y., Wu, Y., Huang, J., et al. (2007). Application of an oligonucleotide array assay for rapid detecting and genotyping of *Chlamydia trachomatis* from urogenital specimens. *Diagn. Microbiol. Infect. Dis.* 57, 1–6. doi: 10.1016/j.diagmicrobio.2006.05.007

frontiers | Frontiers in Microbiology

TYPE Original Research
PUBLISHED 17 November 2022
DOI 10.3389/fmicb.2022.1028988

OPEN ACCESS

EDITED BY
Kamal El Bissati,
The University of Chicago,
United States

REVIEWED BY
Nadim Sharif,
Jahangirnagar University,
Bangladesh
Marianna Marangi,
University of Foggia,
Italy

*CORRESPONDENCE
Aldo Ummarino
aummarino@scienzebiomediche.it

†These authors have contributed equally to this work

SPECIALTY SECTION
This article was submitted to Infectious Agents and Disease, a section of the journal Frontiers in Microbiology

RECEIVED 26 August 2022
ACCEPTED 31 October 2022
PUBLISHED 17 November 2022

CITATION
Ummarino A, Caputo M, Tucci FA, Pezzicoli G, Piepoli A, Gentile A, Latiano T, Panza A, Calà N, Ceglia AP, Pistoio G, Troiano V, Pucatti M, Latiano A, Andriulli A, Tucci A and Palmieri O (2022) A PCR-based method for the diagnosis of *Enterobius vermicularis* in stool samples, specifically designed for clinical application. *Front. Microbiol.* 13:1028988. doi: 10.3389/fmicb.2022.1028988

A PCR-based method for the diagnosis of *Enterobius vermicularis* in stool samples, specifically designed for clinical application

Aldo Ummarino[1]*, Michele Caputo[1], Francesco Antonio Tucci[1], Gaetano Pezzicoli[1], Ada Piepoli[2], Annamaria Gentile[2], Tiziana Latiano[2], Anna Panza[2], Nicholas Calà[1], Antonio Pio Ceglia[1], Giovanni Pistoio[1], Vincenzo Troiano[1], Michela Pucatti[1], Anna Latiano[2], Angelo Andriulli[2], Antonio Tucci[1†] and Orazio Palmieri[2†]

[1]Agorà Biomedical Sciences, Etromapmacs Pole, Lesina (FG), Italy, [2]Gastroenterology Unit, Fondazione IRCCS "Casa Sollievo Della Sofferenza" Hospital, Viale Cappuccini, Italy

Background: *Enterobius vermicularis* (*E. vermicularis*) is a nematode that infects up to 200 million people worldwide, despite effective medications being available. Conventional diagnostic tests are hindered by low sensitivity and poor patient compliance. Furthermore, no biomolecular techniques are available for clinical application. The aim of this study was to develop a procedure specifically designed for clinical application to detect *E. vermicularis* by means of PCR.

Materials and methods: Two subject groups were taken into account: a group of 27 infected patients and a control group of 27 healthy subjects. A nested-PCR was performed on fecal samples to detect *E. vermicularis*. Due to the intrinsic difficulties of the fecal matrix, several countermeasures were adopted to ensure the efficient performance of the method: (a) a large amount of feces for the extraction process (20g instead of 200mg); (b) a combination of chemical and physical treatments to grind the fecal matrix; (c) an additional purification process for the negative samples after the first nested-PCR; and (d) the selection of a very specific target region for the PCR.

Results: Due to the lack of overlap with other organisms, a sequence of the 5S ribosomal DNA (rDNA) spacer region including the tract SL1 was chosen to design appropriate external and internal primers. The first nested-PCR detected *E.vermicularis* in 19/27 samples from infected patients. After further purification, 5/8 of the negative samples resulted positive at the second PCR. Conversely, all the samples from healthy controls resulted negative to both PCRs. Sensitivity and specificity of the method were, respectively, 88.9% and 100%.

Conclusion: The results prove the high diagnostic accuracy of the proposed method, addressing and overcoming the challenges posed by both

conventional tests and PCR-based approaches. Therefore, the method can be proposed for clinical application.

KEYWORDS

***Enterobiasis vermicularis*, PCR, stool (DNA) test, pinworm infection, ribosomal DNA–rDNA**

Importance

The authors of this study have designed a method to detect pinworms in human stool samples, specifically for clinical application. The purpose of this method is (a) to help clinicians in the diagnosis and cure of patients with suspected *E. vermicularis* infection, (b) to assess the real epidemiology in the general population and in specific subgroups of subjects, (c) to determine the pathogenetic role of the parasite in some gastrointestinal disorders (opening unexpected clinico-pathological scenarios), and (d) to provide significant support in the extraction and purification of nucleic acids from the feces to other diagnostic methods of parasite detection.

Introduction

Enterobius vermicularis (*E. vermicularis*), commonly referred to as "pinworm," is a nematode infecting the human intestine. Affecting up to 200 million people worldwide (Panidis et al., 2011), this parasite is widespread all over the world (Gutierrez, 2000), and pinworm infection is the most common infection among helminths in Western Europe and United States (Burkhart and Burkhart, 2005).

Enterobiasis is typically associated with anal itch. However, the infection may also occur in the absence of clinical symptoms and, in a relevant percentage of cases, it can manifest with abdominal pain and/or altered bowel habits, also with no itch (Brewster, 1989; Wu et al., 2000; Brown, 2006; Jardine et al., 2006; Rajamanickam et al., 2009).

The high prevalence of *E. vermicularis* infection suggests its potential involvement in the pathogenesis of different conditions. Indeed, abdominal discomfort or pain and altered bowel habits are highly frequent symptoms in irritable bowel syndrome (IBS). In addition, the eradication of the parasite in patients with both IBS and evidence of *E. vermicularis* infection has cured the symptoms in some cases (Wu et al., 2000; Petro et al., 2005).

Similarly, the pathogenesis of recurrent abdominal pain in children is unclear, and intestinal infection by nematodes has often been considered in this setting (Jardine et al., 2006).

Infection by *E. vermicularis* has finally been held responsible for the peripheral eosinophilia in some patients with no clear underlying causes (Schroeder et al., 2019), as well as for several cases of misdiagnosed acute appendicitis (Panidis et al., 2011; Risio et al., 2016; Dunphy et al., 2017; Sosin et al., 2019).

Unfortunately, the lack of reliable tests for parasite detection does not allow neither for the estimation of the exact role of *E. vermicularis* in all these conditions nor for the actual infection prevalence.

The only two currently available diagnostic tests (adhesive tape test and parasitological test) are, in fact, characterized by low sensitivity, which may drop to 5–15% (Cook, 1994; Jardine et al., 2006). Consequently, infection by *E. vermicularis* remains undetected in a relevant number of cases and enterobiasis control remains difficult, despite the availability of medications for decades (Wendt et al., 2019).

This bottleneck could be eliminated through the use of a high sensitivity diagnostic molecular biology technique. The PCR (Polymerase Chain Reaction) may be taken into consideration, provided that the parasite detection is performed in stool samples, as they represent the main and most practical biological source material available for clinical practice.

However, designing such a test is hindered by the difficult matrix of feces, known for the presence of many PCR inhibitors (Rossen et al., 1992; Tebbe and Vahjen, 1993; Abu Al-Soud and Rådström, 2000; Morin et al., 2001; Mavziutov et al., 2003; Eggert et al., 2005). For this reason, adequate DNA extraction and purification methods are highly necessary.

To date, several reports (Liu et al., 1995; Blouin, 2002; Iñiguez et al., 2002; Floyd et al., 2005; Nakano et al., 2006; Leles et al., 2009; Khouja et al., 2010; Piperaki et al., 2011; Zelck et al., 2011; Ferrero et al., 2013; Ngui et al., 2014; Sow et al., 2017; Tomanakan et al., 2018; Köller et al., 2020; Medkour et al., 2020) have taken into account the use of PCR for the characterization of *E. vermicularis* (Table 1). However, almost none of the studies were specifically designed to develop a diagnostic method for clinical application. As a matter of fact, these studies were carried out with philological, taxonomic, or archeological purposes, with target regions intentionally not highly specific (e.g., mitochondrial DNA). On the contrary, for diagnostic purposes, high conservation in the species is desirable.

In addition, the PCR assays of these investigations often rely on worm and egg isolation, which are difficult to obtain from infected patients, thus unlikely to be recommended for clinical practice.

Finally, no validation tests confirming the diagnostic validity of the methods implemented were included in these reports. In particular, the assessment with a negative control group was missing in almost all cases or was not adequate (Sow et al., 2017).

The purpose of the present study was to develop a PCR based method to detect *E. vermicularis* in stool samples for clinical

TABLE 1 Studies that used the PCR analysis for the characterization of *E. vermicularis*.

Article	Aim of the study	DNA source	Target sequence	Control group
Tomanakan et al. (2018)	To analyzes the genetic diversity of *E. vermicularis*.	Eggs	cox1, ITS2	no
Zelck et al. (2011)	To perform a genetical characterization of pinworms from different regions of Germany.	Worms	ITS1, ITS2, 18S, 5.8S	no
Piperaki et al. (2011)	To investigate the genetic variation within *E. vermicularis* in humans.	Eggs	cox1	no
Medkour et al. (2020)	To perform a survey of parasites using a fast-typing technique by PCR in feces, to assess potential zoonotic transmission.	Feces	5S rDNA region	no
Ferrero et al. (2013)	To perform a genetic study of pinworms in Denmark with DNA extracted from individual eggs.	Eggs	cox1	no
Iñiguez et al. (2002)	To investigate the genetic variation within *E. vermicularis* in humans.	Feces	SL1	no
Liu et al. (1995)	Case report of a hemorrhagic eosinophilic enterocolitis associated with *E. vermicularis*.	Worms	28S rDNA, 5SrDNA spacer region	no
Floyd et al. (2005)	To design PCR primers to amplify a c. 1 kb fragment of the 18S ribosomal DNA gene (specific to the phylum Nematoda).	Worms	18s rRNA gene	no
Leles et al. (2009)	To introduce a method that would allow molecular diagnosis of *Ascaris* sp. from feces as an alternative source of *Ascaris* sp. material.	Feces, eggs	ITS1, mtDNA (citocrome B gene)	no
Khouja et al. (2010)	To determine the presence of Giardia cysts and Cryptosporidium oocysts in raw and treated wastewater, and to sequence-characterize samples.	Wastewater	SSU rDNA	no
Sow et al. (2017)	To compare the performance of real-time PCR assays to microscopic examination for detection of intestinal parasites.	Feces	5S rDNA	yes*
Blouin (2002)	To compare DNA sequence divergence at ITS-1 and ITS-2 with divergence at mitochondrial cox1 or nad4 loci.	Worms	ITS1, ITS2, cox1	no
Nakano et al. (2006)	To analyze sequences of cox1 gene, ITS2 and 5S rDNA of *E. vermicularis* from chimpanzees and to compare them with those of pinworm eggs from humans.	Worms, eggs	cox1	no
Köller et al. (2020)	To assess and compare the performance of different diagnostic qPCR approaches for human parasites and microsporidia in stool samples without a gold standard.	Feces	Cox1, 28S rDNA, 18S rDNA	no
Ngui et al. (2014)	Case report of an invasive *E. vermicularis* infection in a fallopian tube.	Tissue sections	5-subunit rDNA (5S rDNA)	no

*Subjects included in the control group having only a negative parasitological test (which is notorious for having a very low sensitivity).

application, overcoming the limitations of the conventional tests (low sensitivity and poor patient compliance) and those of the other molecular approaches.

Materials and methods

Study population

Two different groups of subjects were tested: patients with *E. vermicularis* infection and healthy patients.

Patients with *Enterobius vermicularis* infection

Twenty-seven patients (13 males, 14 females; 38 ± 19 years, m ± SD, all Caucasians) with proven infection were included. The criteria used to determine the presence of pinworms were: (1) evidence of the parasite in the feces (evaluated by stereomicroscopic identification) and (2) evidence of characteristic pinworm eggs on adhesive tapes (identified by light microscopy). Patients who met one or both criteria were considered positive to *E. vermicularis* infection. All these patients manifested anal itch as the main symptom of the infection.

Healthy controls

Twenty-seven age and sex matched subjects (13 males, 14 females; 39 ± 14 years, m ± SD, all Caucasians) were chosen for the control group. The study inclusion criteria were: (1) no evidence of *E. vermicularis* in both adhesive tape test and parasitological analysis; (2) no reported evidence of worms in feces; (3) absence of anal itch; (4) no past history of previous *E. vermicularis* infection; (5) no family history of *E. vermicularis* infection; (6) absence of abdominal discomfort (pain, meteorism, etc.); (7) absence of altered bowel habits; and (8) no promiscuity with children (primary school teachers, pediatricians, baby sitters, nannies, etc. were excluded).

Ethical approval

All procedures were carried out in accordance with the ethical standards of the Institutional Committee *Casa Sollievo della Sofferenza Hospital* (132 CE/2015), and with the 1964 Declaration of

Helsinki declaration and its subsequent amendments or comparable ethical standards. Informed consent was signed by all participants.

Stool samples

The entire sample processing workflow is shown in Figure 1. A stool sample of about 20 g was obtained from each subject of both groups. The samples were collected in sterile containers and stored at −20°C, until processing.

Sample preparation

Four aliquots of 5 g were obtained from each defrosted stool sample. Each aliquot was transferred in a 15 ml tube containing a mix of zirconia beads (25 of 2.0 mm diameter and 3 of 5.0 mm diameter).

Five milliliters of buffer ASL (QIAamp DNA Stool Mini Kit, Qiagen, Hilden, Germany) were added to each tube. Then, all tubes were subjected to a grinding process, using Precellys Evolution Homogenizer (Bertin Instruments, Montigny-le-Bretonneux, France).

A set of 3 cycles of 30 s each, at 9,600 rpm, was carried out, with a resting time of 1 min at room temperature between each cycle. The resulting homogenate, together with the beads, was transferred into four 50 ml tubes and a further 40 ml of buffer ASL was added to each of them.

The samples were then vortexed for 10 s, incubated at room temperature for 4 min, vortexed for 10 s, and finally centrifuged for 3 min at 4,500 rpm.

Subsequently, the supernatant was transferred into a new 50 ml tube and vortexed for 10 s. Then, 1.2 ml of the supernatant were taken from each of the four 50 ml tubes and transferred into four 1.5 ml eppendorf tubes (for DNA extraction and purification).

DNA extraction and purification

Isolation of DNA was performed using QIAamp Stool Mini Kit (Qiagen, Hilden, Germany), according to the "Stool Pathogen Detection" manufacturer's protocol with the following modifications: (1) the first five steps of the procedure were replaced by the chemo-physical grinding process as described in paragraph "Sample preparation" of the manufacturer's protocol; (2) the final elution step was performed using half of the suggested buffer volume to increase the DNA final concentration.

The four final eluates obtained from each patient/control were mixed in a single tube, resulting in a cumulative volume of 400 µl.

This pooled eluate was, then, equally divided into two separate 1.5 ml eppendorf tubes. The first tube was used for PCR assay. The second tube, instead, was stored at −20°C, and reserved for further DNA purification to be applied to the samples negative to the PCR assay. Geneclean II Kit (MP Biomedicals, Qbiogene, Inc., Carlsbad,

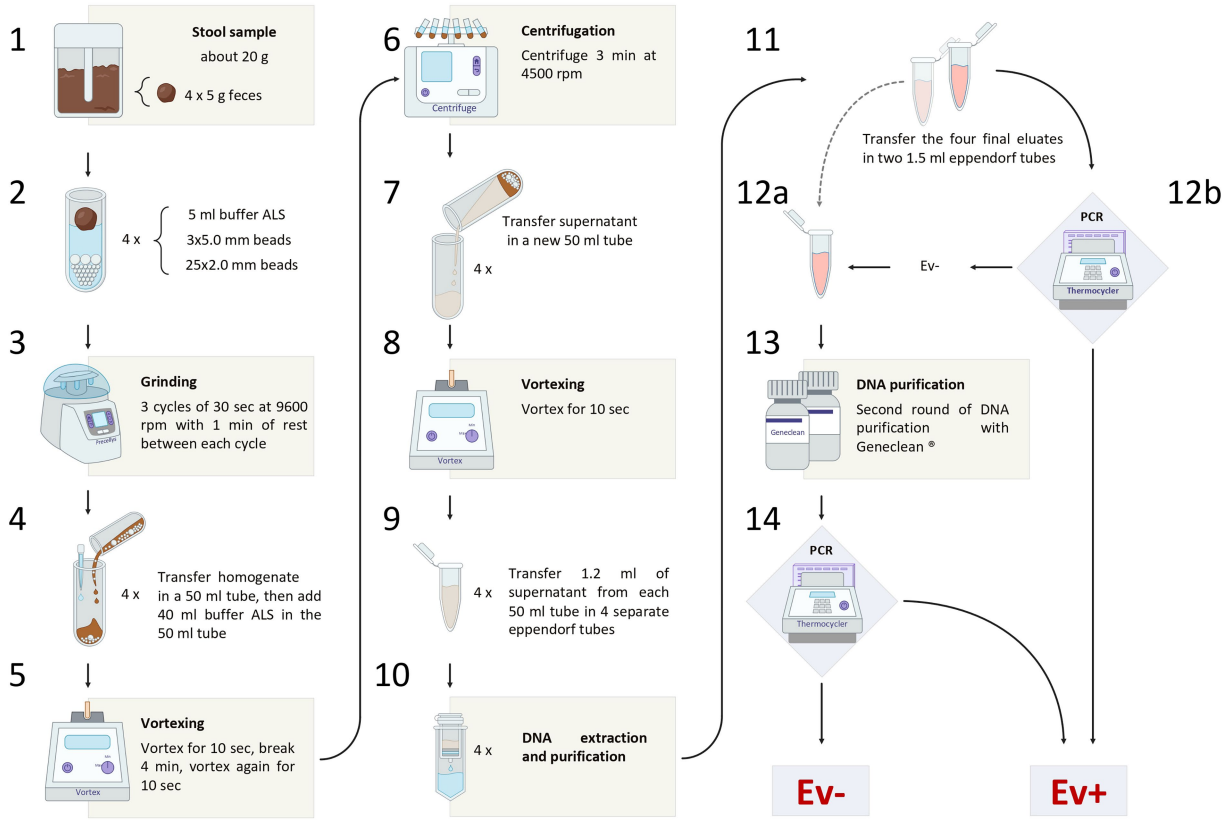

FIGURE 1
The figure shows the entire sample processing workflow, from the sample collection to the final diagnosis of *Enterobius vermicularis* infection.

California, United States) was used in this process, according to the manufacturer's protocol. Thereafter, these samples were retested by PCR assay.

Target sequence

The 5S ribosomal DNA (rDNA) spacer region has been chosen as target DNA for the identification of *E. vermicularis*.

The rDNA is organized into two distinct multigene families, a major and a minor one. The genes of both families are arranged in tandemly repeated clusters containing coding regions, non-transcribed spacer regions (NTS), external, as well as internal spacer regions (ETS and ITS; Figure 2; Richard et al., 2008; Madani et al., 2019; Potapova and Gerton, 2019).

In contrast with the great variability of the spacer regions in other species, *E. vermicularis* shows a highly conserved 5S spacer region (Liu et al., 1996; Iñiguez et al., 2002). This uncommon behavior is due to the selective evolutionary pressure exerted by the spliced leader 1 (SL1) sequence (accession number: AY234778.1),[1] present in this region, which plays a functional role in the trans-splicing process (Sturm et al., 1999; Xu et al., 2000; Nilsen, 2001; Iñiguez et al., 2006). For this reason, the 5S spacer region spanning over the SL1 subregion was considered as the best target sequence for the purposes of this research study. An 839 bp segment of the 5S spacer region encompassing the entire SL1 was retrieved from the *National Center for Biotechnology Information* (NCBI) database (accession number: AY682469.2)[2] and analyzed using *Standard Nucleotide BLAST*[3] to minimize overlaps with other organisms.

Primer design

Primer3plus software (version: Primer3-web 4.0.0)[4] was employed to build the first set of primer (external). Primers were chosen based on the best settings for a low probability of primer-dimer/hairpin formation, the proper GC content, and the adequate annealing temperature.

The second set of primers (internal) was chosen by considering different options within the product sequence of the 1° round of amplification.

In both cases, the sequences identified by the primers were subjected to further analysis with *Align sequences nucleotide BLAST* (see footnote 3), to verify the specificity of the sequence for the DNA of *E. vermicularis* and the possible overlaps with other organisms.

Nested PCR

PCR reactions were carried out in a final volume of 50 µl containing GeneAmp 1× Buffer II (10 mM Tris–HCl, pH 8.3; 50 mM KCl), 1.5 mM $MgCl_2$, 1.5 U of AmpliTaq Gold DNA polymerase (Applied Biosystems), 22.5 pM of each primer, 20 mM of dNTPs (Promega, Madison, WI, United States), and 5 µl of extracted DNA.

1 http://www.ncbi.nlm.nih.gov/nuccore/AY234778.1

2 http://www.ncbi.nlm.nih.gov/nuccore/AY682469.2

3 https://blast.ncbi.nlm.nih.gov/

4 https://primer3.ut.ee/

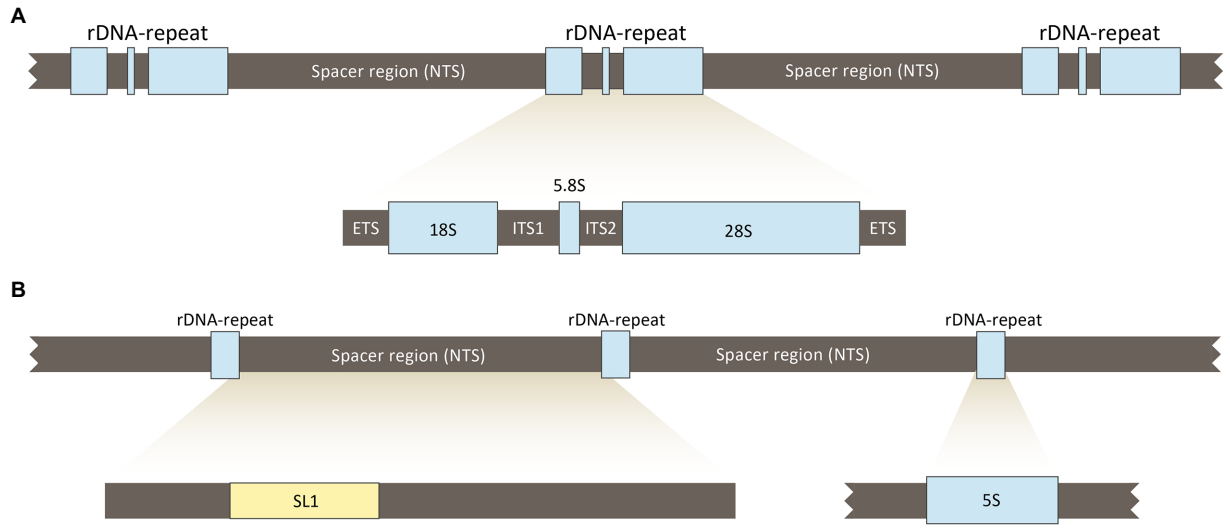

FIGURE 2
The major and minor multigene families of the ribosomal DNA (rDNA) of *Enterobius vermicularis*. In **(A)** is reported the major family; it is arranged in tandemly repeated clusters (r-DNA-repeat), separated by non-transcribed spacer regions (NTS). In **(B)** is reported the minor gene family; it is also organized in tandem repeated clusters (r-DNA-repeat), separated by non-transcribed spacer regions (NTS). ETS, external transcribed spacers region; ITS, internal transcribed spacers region.

Reactions were performed with initial denaturation at 94°C for 5 min, followed by 40 cycles at 94°C for 1 min, annealing at 56°C for 1 min, and extension at 72°C for 1 min. Final extension was 72°C for 10 min. External primers were used for the first round of amplification, while internal primers for nested PCR starting from 5 µl of the product of the first round and in the same thermocycling conditions.

Five microliters of the product of both the first and the second rounds of PCR were run on a 2% agarose gel containing ethidium bromide and exposed to UV light to visualize DNA bands.

Two electrophoresis markers were used: pGem DNA Marker (Promega, Madison, WI, United States) and 50 bp DNA ladder (Invitrogen, Carlsbad, CA, United States), with two different size scales (36–2,645 bp for pGem and 50–800 bp for 50 bp DNA ladder), to better assess the molecular weight of the amplified sequence.

A positive and negative control was included in each round of the nested PCR experiment.

Positive and negative control

Two positive controls were obtained by isolating eggs from adhesive tapes of infected patients. Specifically, a small portion (3 mm × 3 mm) of the tape containing eggs, confirmed under microscopic observation, was directly dipped into 100 µl of 0.02 N NaOH solution. As a matter of fact, through this procedure eggs are removed from the adhesive surface of the tape (H. Hasegawa, personal communication, April 20, 2010). Finally, the eggs were subjected to heat shock, consisting of 10 min immersion in 95°C water, followed by 3 min at-80°C. The obtained DNA was stored at −20°C until PCR procedure.

The negative control was obtained by adding 5 µl of ultra-sterile water to the complete PCR mixture.

Sequencing of PCR products

Amplicons from positive controls were Sanger-sequenced to verify the correspondence with the sequences selected *in silico*. Briefly, PCR products were sequentially purified by GeneClean kit and a vacuum system (Millipore, Bedford, MA, United States), according to the manufacturer's recommendation.

Purified DNA was then resuspended in 25 µl of dH_2O and run on 2% agarose gel. Amplicons were sequenced from both ends using an aliquot (3.2 pM) of the PCR reaction primers relying on the BigDye Terminator Cycle Sequencing Kit v. 1.1 (Thermo Fisher Scientific, Somerset, NJ, United States). After purification by using Centri-Sep columns (Princeton separations, Adelphia, NJ, United States), sequencing reactions were loaded on 3500 DX Genetic Analyzer capillaries (Applied Biosystems, Foster City, CA, United States) and analyzed using the Sequencing Analysis software v5.4 (Applied Biosystems, Foster City, CA, United States). The electropherogram results were expressed as the percentage of homology (%). The forward and reverse sequences obtained from each sample were assembled in one sequence using the CAP3 algorithm as implemented in SnapGene software v6.1 (Dotmatics, Boston, MA, United States). Discrepancies between forward and reverse sequences due to poor-quality base calls were manually curated and resolved. The sequences from both the controls were submitted to *NCBI GenBank* (accession numbers: OP650208, OP650209) through the BankIt submission tool and are publicly available.

Results

Target sequence

The analysis of *E. vermicularis* SL1 of the 5S spacer region performed by using the Nucleotide Blast tool in the NCBI database showed that all the records with the highest alignment score with the query sequence (bars in red) corresponded to different *E. vermicularis* sequencings, as expected (Figure 3). However, there were other bars with a lower alignment score (in green) that did not account for *E. vermicularis* and aligned with the middle part of the query sequence in the middle tract, leaving two segments, at both the ends, still highly specific for *E. vermicularis*. The first tract corresponds to nucleotides 1–223 (223 bp) and the second one to nucleotides 341–839 (499 bp) of the 5S spacer region.

This analysis highlighted two candidate regions highly conserved and specific. The first sequence was chosen as target sequence since it partially spanned over the SL1 region and thus is more likely to be conserved within the species.

Primer design

The analysis with *Primer3plus* software was performed using the nucleotides 1–310 of *E. vermicularis* spacer region to provide some spanning around the target sequence and to allow for the design of two couples of nested primers. The software generated 10 different options of external primers (Figure 4). Five couples (first, second, fourth, sixth, and seventh) were discarded as they did not include the SL1 sequence. Among the remaining ones, the tenth couple were chosen because it picked the shorter segment (182 bp, nucleotides 82–263) including the SL1 sequence (Figure 4).

These primers were named "Ev_ext_fw" and "Ev_ext_rv" and their target sequence was further analyzed in the NCBI database, confirming their specificity exclusively for *E. vermicularis* with high alignment scores (Figure 5A).

Next, an inner tract of 116 bp (nucleotides 116–231) was chosen within the amplicon of the first round of amplification to design the second internal set of primers and named them "Ev_int_fw" and "Ev_int_rv." Also in this case, the analysis in the NCBI database confirmed the specificity of the sequence obtained only

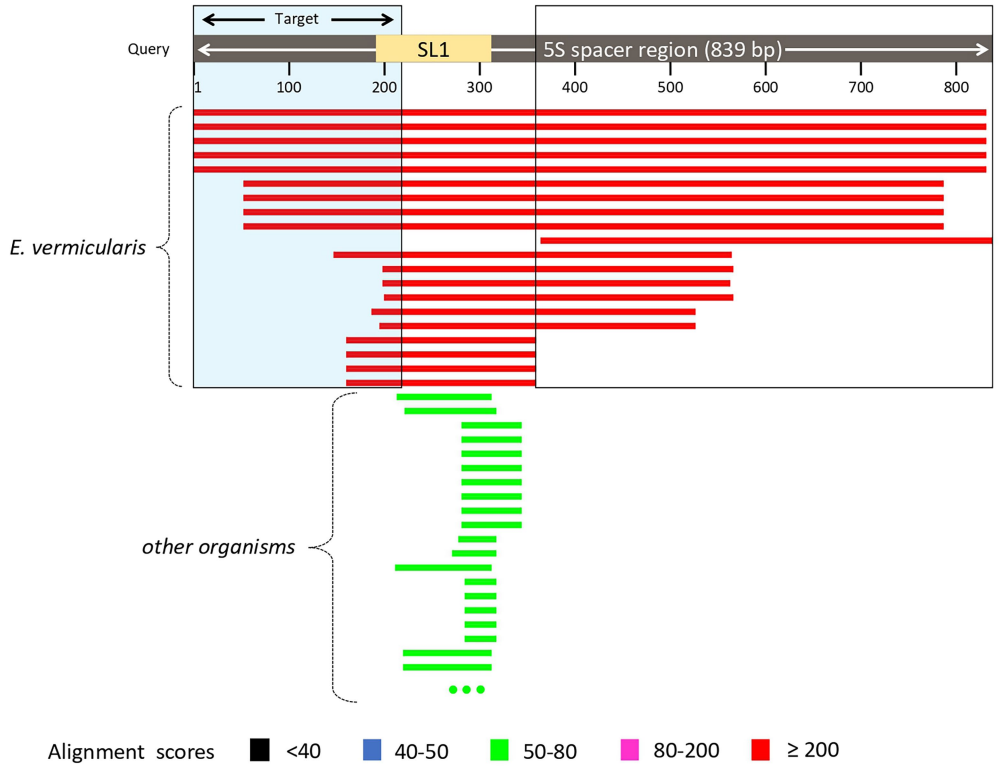

FIGURE 3
Analysis of *Enterobius vermicularis* SL1 of the 5S spacer region using the Nucleotide Blast tool. The records with the highest alignment score with the query sequence (bars in red) corresponded to different *E. vermicularis* isolates, while those with the lower alignment score (in green), correspond to other organisms. The two segments at both the ends are highly specific for *E. vermicularis*. The first tract corresponds to nucleotides 1–223 (223bp) and the second one to nucleotides 341–839 (499bp) of the 5S spacer region.

for *E. vermicularis* (Figure 5B). The sequences and the characteristics of the primers are summarized in Figure 6 and Table 2.

Positive controls and sequencing of the PCR products

The nested PCR on the two positive controls obtained from *E. vermicularis* eggs and subsequent agarose gel electrophoresis led to the display of three different bands. The 182 bp upper band is to be traced to the primer's excess of the first round of amplification; the 116 bp middle band is consequent to the nested PCR; and the lower band is due to dimer primers (Figure 7).

The amplicons obtained after the first round of amplification were Sanger-sequenced with both the forward and reverse primers. We compared the assembled sequences obtained demonstrating a 100% homology with those predicted *in silico* for both samples (Table 3).

Nested PCR in the study population

Enterobius vermicularis was detected by nested PCR in 19 of the 27 extracted DNA samples from infected patients. Among the eight negative patients, the further purification process with GeneClean yielded five additional positive results. Overall, 24 of the 27 infected patients (88.9%) resulted positive with the applied procedures. In healthy controls, nested PCR did not show any evidence of the *E. vermicularis* genome, both in extracted and further purified DNA samples (Figure 8).

Hence, the sensitivity and specificity of the proposed method were 88.9% and 100%, respectively.

Discussion

Intestinal infection by *E. vermicularis* is one of the most common helminth infections in the world, with up to 200 million infections estimated worldwide (Panidis et al., 2011). Enterobiasis may occur silently, but may often manifest with anal itch and, in some cases, with abdominal pain/discomfort, or altered bowel habits (Brewster, 1989; Wu et al., 2000; Arca et al., 2004; Brown, 2006; Jardine et al., 2006; Rajamanickam et al., 2009). This raises the question on the role of the parasite in recurrent abdominal pain in children and in irritable bowel syndrome.

However, due to the low sensitivity of the tests currently available in clinical laboratories (adhesive tape test and parasitological test; Cook, 1994; Jardine et al., 2006; Remm and Remm, 2009), the actual role of the pinworms in the pathogenesis

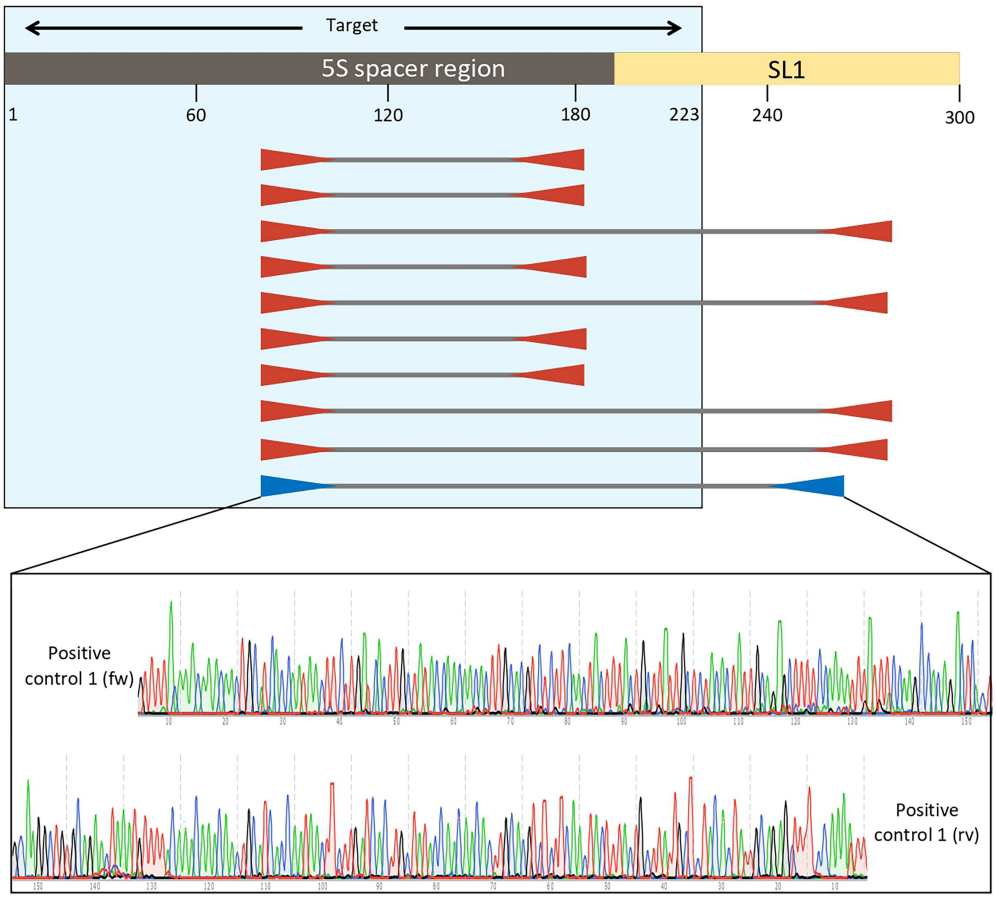

FIGURE 4
Analysis with *Primer3plus* software using the nucleotides 1–310 of *Enterobius vermicularis* spacer region. The software generates 10 different options of external primers. The couples first, second, fourth, sixth, and seventh do not include the SL1 sequence, while the others do. Among the latter, the tenth couple was chosen for the external primers because it picked the shorter tract (181bp, nucleotides 82–263) including the target sequence. Assembled reads from Sanger sequencing of the positive control 1 showing perfect homology with the expected *E. vermicularis* amplicon with the selected pairs of primers.

of these conditions cannot be assessed. For this reason, patients with symptoms caused by the parasite and negative to the relative clinical tests have no access to the medications to treat their condition.

In this study, a PCR-based assay for the diagnosis of enterobiasis, specifically designed for clinical application, has been introduced. One of the major difficulties encountered in the development of such an approach was the DNA isolation and purification from fecal samples. Due to the high amount of PCR inhibitors in the fecal matrix and to the very low amount of the parasite DNA in feces (Monteiro et al., 1997; Abu Al-Soud and Rådström, 2000), the development of a reliable DNA isolation procedure has been quite challenging. Appropriate countermeasures have been adopted to overcome the above limitations and the approach here developed represents one of the most remarkable findings of the authors' work. Three strategies have been adopted: (a) the use of a large amount of feces for the extraction process (20 g instead of the 200 mg commonly processed in stool PCR testing), (b) the use of a combination of chemical and physical treatments to thoroughly grind the complex fecal matrix; and (c) the adjunct of an additional purification process for the samples resulted negative after the first nested PCR. In our experience, the integration of the three procedures above reported is mandatory for a proper diagnostic tool for the detection of parasites in stool samples.

The choice of using stools as a DNA source for the PCR analysis is the distinctive feature of this study compared to most of the previous studies. Indeed, almost all the PCR reports on *E. vermicularis* employed pinworms or their eggs as source material (Table 1), as these studies were essentially driven by philological, taxonomic, or archeological purposes. However, by doing so, the issue of DNA extraction from feces was simply disregarded resulting in a serious methodological problem. On the other hand, a diagnostic test intended for clinical use based on worm and egg isolation would entail the same as the adhesive tape test. Therefore, the choice of using fecal samples, in our study, is to be considered the most appropriate and in line with the purposes of clinical application, since it requires only a simple stool sample, which is easily obtainable for patients.

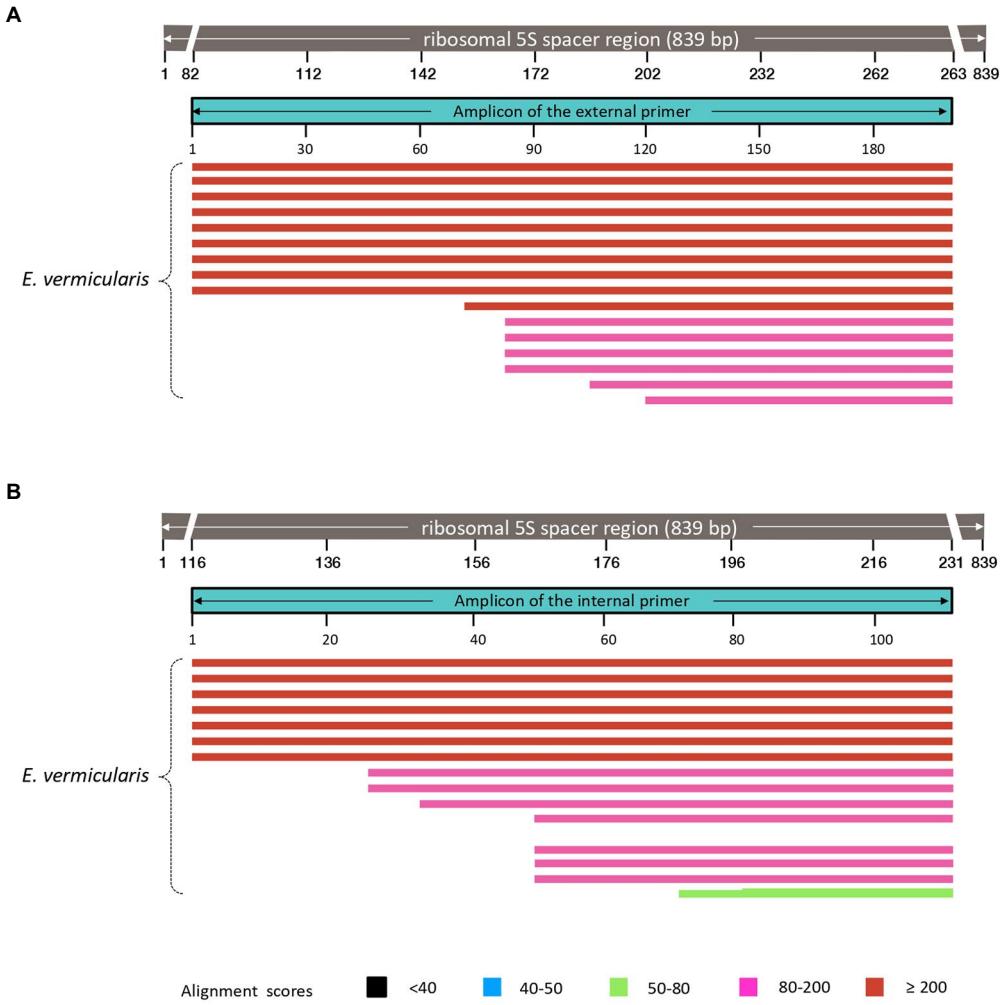

FIGURE 5
Analysis of the sequences obtained using our primers in the NCBI database. Both external **(A)**, and internal **(B)**, primers select DNA sequences highly specific for *Enterobius vermicularis*, with no cross-reaction with other organisms.

In addition to that, further clarification is needed with reference to the choice of the target region. The DNA regions commonly targeted for PCR investigations on parasites are essentially two: the mitochondrial DNA (mtDNA) and the ribosomal DNA (rDNA). Since the former is characterized by a high variability, the focus of this study was on DNA coding for ribosomal subunits, largely conserved and remarkably similar in organisms of the same species. In addition, most of the previous reports, designed for phylogenetic, taxonomic, or archeological purposes, did not prevent cross-reactions with other nematodes (which were even sought in some cases). The primers adopted in the aforementioned studies are, often, general nematode primers, since the aim of these investigations was to evaluate the parasite genetic variability of the parasite and its evolutionary significance within the nematode phylogenetic framework. In contrast, since the test outcome affects both clinical interpretation and therapeutic approach, for clinical purposes a high degree of specificity is required for clinical purposes. For this reason, in the present study, careful attention was paid to the selection of the target sequence. After several investigations, a region of the 5S rDNA spanning over the SL1 subregion was chosen, which proved to be an appropriate solution. As a matter of fact, the simulation analysis performed on Nucleotide BLAST software demonstrated that the high specificity of the target sequence chosen to detect *E. vermicularis*, showing no overlap with sequences of other organisms. Furthermore, the designed primers proved to be reliable and effective in amplifying the target sequence. The performance tests carried out on the software platform and corroborated by the *in vitro* molecular analysis confirm that the sequences of the PCR products (both after the first and the nested PCR) are highly specific and exclusive for *E. vermicularis*. These outcomes are in line with the design philosophy and further support the results obtained in the subject groups investigated. The high positivity rate in the positive control group (88.9%) and the complete absence of *E. vermicularis* positivity among the negative controls (100%),

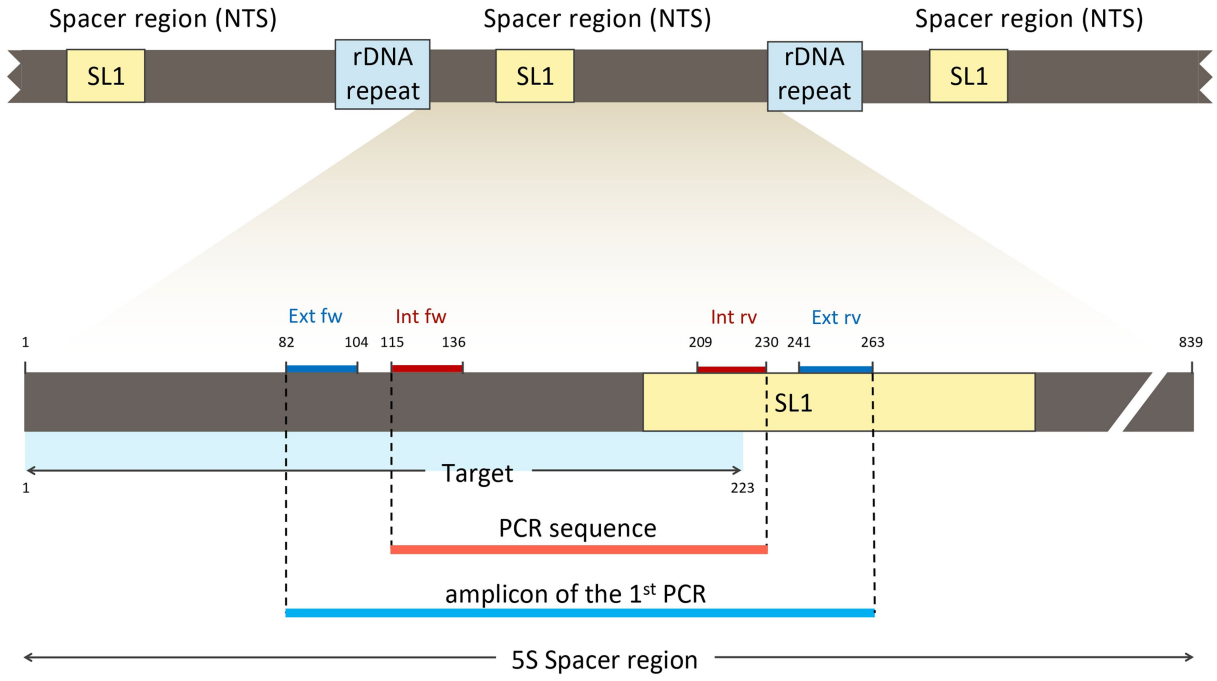

FIGURE 6
Location of the external (Ext fw and Ext rv) and internal primers (Int fw and Int rv) in relation to the SL1 region and the target sequence.

TABLE 2 External (ext) and internal (int) primers used for the nested PCR.

Primer	Sequence (5' ➔ 3')	Length (bp)	GC content (%)	Melting temperature (°C)
Ev_ext_fw	ACAGTGCAAGGCTGTGCAGAACT	23	52.1	69.4
Ev_ext_rv	ACATCAGTGAGTCTGTGGCTTGGA	24	50	69.2
Ev_int_fw	CAAACAAACAACTGCATCACCA	22	40.9	65.7
Ev_int_rv	TGGAAAAGCTCTGCAATAGTGT	22	40.9	62.6

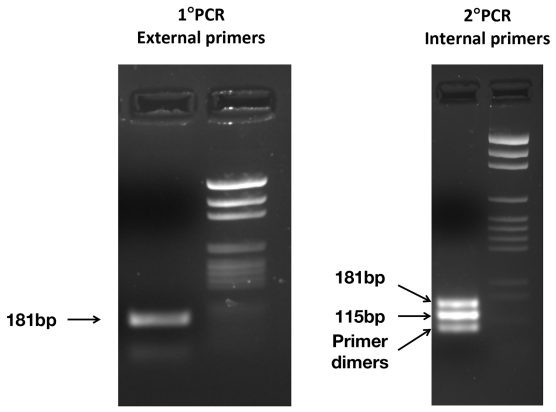

FIGURE 7
Electrophoresis of the PCR products was obtained after the first PCR (left panel) and the nested PCR (right panel) carried out on one positive control. In the left panel, one band of 181bp is observed, on the right panel three bands: 182 and 116bp from the nested PCR, while the lower band from primer dimers.

strongly support high specificity, and the overall high diagnostic accuracy of the method. The implementation of a rigorously selected and sex-age matched negative control group in the study significantly contributed to the accuracy and robustness of the results. In all the previous studies reported in literature (Table 1), the assessment in a negative control group was missing in nearly all cases, or, when present, the same was not adequate (i.e., the report of Sow D. et al. that included a negative control group of unselected subjects with only a negative parasitological test, which is notorious characterized by low sensitivity; Sow et al., 2017). However, although rigorous, the authors are aware that the number of subjects enrolled in this study is limited and they think that further investigations in bigger cohorts are needed to corroborate their data. To the authors' best knowledge, there is only one kit available to diagnose *E. vermicularis* infestation through real-time PCR (RT-PCR) on feces (AmpliTest *Enterobius vermicularis*, Amplicon, Wroclaw, Poland). However, up to date, no specific data have been reported, no validation tests have been presented, and no publications have been

TABLE 3 Assembled sequences obtained from DNA sequencing of the amplicons of the first PCR of two different positive controls (CTR1 and CTR2) and comparison with the expected sequence.

Sample	Reference sequence (182 bp)	Sequence obtained after sequencing	% query cover (% homology)
CTR1	ACAGTGCAAGGCTGTGCAGAACTAA	GCAAGGCTGTGCAGAACTAAAT	95%
(*172 bp*)	ATGTTTTACAAACAAACAACTG	GTTTTACAAACAAACAACTGCA	(100%)
	CATCACCAATAACTTCTTGATCACTT	TCACCAATAACTTCTTGATCACT	
	GCTATACCAACAACACTTGCAC	TGCTATACCAACAACACTTGCAC	
	GTCTCTTCAACTACTTTACTGCTTATT	GTCTCTTCAACTACTTTACTGCTT	
	GCTCTACACTATTGCAGAGCTT	ATTGCTCTACACTATTGCAGAGCT	
	TTCCAAAATTTATTTCCAAG	TTTCCAAAATTTATTTCCAAGCCA	
	CCACAGACTCACTGATGT	CAGACTCACT	
CTR2		GGCTGTGCAGAACTAAATGTTTTA	95%
(*173 bp*)		CAAACAAACAACTGCATCACCAAT	(100%)
		AACTTCTTGATCACTTGCTATACCA	
		ACAACACTTGCACGTCTCTTCAACT	
		ACTTTACTGCTTATTGCTCTACACTA	
		TTGCAGAGCTTTTCCAAAATTTATTT	
		CCAAGCCACAGACTCACTGATGT	

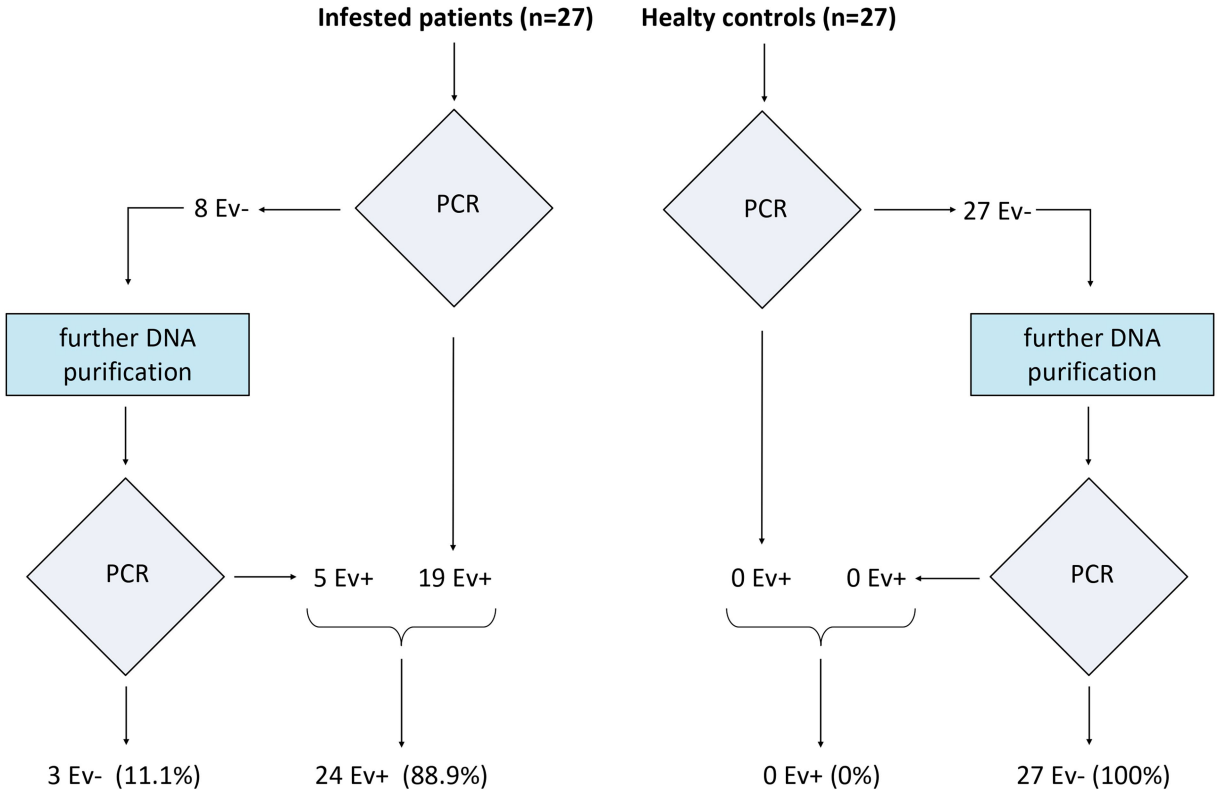

FIGURE 8
Nested PCR in the study population. On the left are reported the results in the infested patients, while on the right there are those in healthy controls.

published in the literature regarding this kit. Another kit (Allplex™ GI-Helminth assay) is also available for helminths detection through PCR, but a recent publication demonstrated low specificity (36% of false negative results in the cohort investigated) in the diagnosis of *E. vermicularis* in stool samples (Autier et al., 2021).

Currently, the scotch tape technique is considered the gold standard for *E. vermicularis* detection. However, it is widely known that, when it comes to very high diagnostic specificity, its sensitivity is very low (Cook, 1994; Jardine et al., 2006; Remm and Remm, 2009) and up to three tests in three different consecutive days are required to increase the chances of confirming the diagnosis (Wendt et al., 2019). This lack of sensitivity is due to the parasite vital cycle, which inhabits the terminal ileum-cecum-appendix region and only occasionally migrates into the rectum, laying eggs in the perianal region.

A similar scenario occurred in the recent past with *Helicobacter pylori* (*H. pylori*). In the last decade of 1900 and in the first decade thereafter, the gold standard for the diagnosis of the infection was the microbial culture (Mégraud, 1995). As with the scotch test, microbial culture reported high specificity but a low sensitivity. For years, the same was considered the reference (gold standard) for the diagnosis. However, it has been later replaced by the urea breath test, which is more sensitive and only slightly less specific (Pohl et al., 2019).

With regard to *E. vermicularis* there is the need for a specific and sensitive method, and, showing 88.9% sensitivity and 100% specificity, the method implemented in the present study seems to meet this condition. Certainly, it has two undeniable intrinsic limits: complexity and costs. However, if on the one hand, these limits cannot be underestimated, on the other hand, they are justified by the constraints of the research implementing a method with not only a high sensitivity and diagnostic specificity, but also non-invasive and easy to perform on patients. The collection of 20 g of feces (less than a plum) for a patient does not represent a difficulty, in light of the small amount considered, and it can easily fit in a normal container for feces or urine.

As for its complexity, as in the case of *H. pylori*, new methods are usually initially complicated, and then progressively simplified and economized (i.e., the first devices for the urea breath test were cumbersome, complex, very expensive, and used radioactive reagents; the current ones are small, simple, cheap, and do not use radioactive components). Therefore, the authors believe that further investigations will lead to a simplified, more affordable, and improved method compared to the procedure described in the present study.

However, regardless of possible future developments, this research is undoubtedly to be credited for: (1) the design of a method to detect *E. vermicularis*, easy to perform on patients; (2) the identification of a highly specific target region for *E. vermicularis* preventing cross-reactions with other nematodes; (3) the development of a strategy for the isolation and purification of DNA parasite from difficult fecal matrix; (4) the implementation of a diagnostic method characterized not only by a good specificity, but also by a high sensitivity; and (5) the validation of the proposed method with a carefully selected sample of positive and (especially) negative controls.

In light of these considerations, a relevant impact of the findings reported on future research is to be hypothesized. Firstly, the proposed method, if validated in larger cohorts of patients and simplified in the procedure, could access clinical practice as the main tool for the diagnosis of *E. vermicularis,* thus becoming the gold standard. This would help the clinicians to correctly interpret, and consequently treat, symptom profiles in patients with suspected enterobiasis.

Secondly, such a test could be used to assess the actual prevalence of *E. vermicularis* in the general population and in specific subgroups of subjects.

Thirdly, the new diagnostic tool could be used to determine the pathogenetic role of the parasite in some gastrointestinal disorders (such as irritable bowel syndrome and recurrent abdominal pain in children) and may even open unexpected clinico-pathological scenarios.

Finally, the nucleic acid isolation and purification processes developed for the detection of *E. vermicularis* can be taken from other diagnostic methods for the detection of other parasites in feces.

Data availability statement

The original contributions presented in the study are included in the article/Supplementary material, further inquiries can be directed to the corresponding author.

Ethics statement

The studies involving human participants were reviewed and approved by Casa Sollievo della Sofferenza Hospital (132 CE/2015). The patients/participants provided their written informed consent to participate in this study.

Author contributions

AU performed most of the experiments, wrote part of the manuscript, and contributed to the overall organization of the paper. MC, GiP, TL, APa, NC, AC, GaP, VT, MP, and AG contributed to the experiments, especially in the extraction of the DNA from the human specimens, in the PCR assays, and in the sequencing reactions. FAT contributed to the graphics and to the manuscript. APi, AA, AL, OP, and AT supervised the writing of the manuscript and edited the materials overall. All authors contributed to the article and approved the submitted version.

Funding

This work has been funded by Italian Ministry of Health, Ricerca Corrente program 2022–2024 to Gastroenterology

Unit, Fondazione IRCCS "Casa Sollievo della Sofferenza" Hospital. Agorà Biomedical Sciences is a no-profit association committed to scientific research. Fundings for this manuscript came from the voluntary donations to the association.

Acknowledgments

We thank Patrizia Bubici, Angela Calà, Concetta Caputo, Lucia Cicculli, Maria Grazia Giovanditti, Rossella Giovanditti, and Nicola Persiani for the help in the sampling process. Finally, we would like to thank Federico Ummarino for the precious support during all the years of this research and Julia Maria Scilabra for her language polishing work.

Conflict of interest

The authors declare that the research was conducted in the absence of any commercial or financial relationships that could be construed as a potential conflict of interest.

Publisher's note

All claims expressed in this article are solely those of the authors and do not necessarily represent those of their affiliated organizations, or those of the publisher, the editors and the reviewers. Any product that may be evaluated in this article, or claim that may be made by its manufacturer, is not guaranteed or endorsed by the publisher.

References

Abu Al-Soud, W., and Rådström, P. (2000). Effects of amplification facilitators on diagnostic PCR in the presence of blood, feces, and meat. *J. Clin. Microbiol.* 38, 4463–4470. doi: 10.1128/JCM.38.12.4463-4470.2000

Arca, M. J., Gates, R. L., Groner, J. I., Hammond, S., and Caniano, D. A. (2004). Clinical manifestations of appendiceal pinworms in children: an institutional experience and a review of the literature. *Pediatr. Surg. Int.* 20, 372–375. doi: 10.1007/s00383-004-1151-5

Autier, B., Gangneux, J.-P., and Robert-Gangneux, F. (2021). Evaluation of the Allplex TM GI-helminth(I) assay, the first marketed multiplex PCR for helminth diagnosis. *Parasite* 28:33. doi: 10.1051/parasite/2021034

Blouin, M. S. (2002). Molecular prospecting for cryptic species of nematodes: mitochondrial DNA versus internal transcribed spacer. *Int. J. Parasitol.* 32, 527–531. doi: 10.1016/s0020-7519(01)00357-5

Brewster, D. H. (1989). Enterobius vermicularis: a possible cause of intestinal colic? *J. R. Coll. Gen. Pract.* 39, 387–388.

Brown, M. D. (2006). Images in clinical medicine. *Enterobius vermicularis*. *N. Engl. J. Med.* 354:e12. doi: 10.1056/NEJMicm040931

Burkhart, C. N., and Burkhart, C. G. (2005). Assessment of frequency, transmission, and genitourinary complications of enterobiasis (pinworms). *Int. J. Dermatol.* 44, 837–840. doi: 10.1111/j.1365-4632.2004.02332.x

Cook, G. C. (1994). Enterobius vermicularis infection. *Gut* 35, 1159–1162. doi: 10.1136/gut.35.9.1159

Dunphy, L., Clark, Z., and Raja, M. H. (2017). Enterobius vermicularis (pinworm) infestation in a child presenting with symptoms of acute appendicitis: a wriggly tale! *BMJ Case Rep.* 2017. doi: 10.1136/bcr-2017-220473

Eggert, L. S., Maldonado, J. E., and Fleischer, R. C. (2005). Nucleic acid isolation from ecological samples--animal scat and other associated materials. *Methods Enzymol.* 395, 73–87. doi: 10.1016/S0076-6879(05)95006-4

Ferrero, M. R., Röser, D., Nielsen, H. V., Olsen, A., and Nejsum, P. (2013). Genetic variation in mitochondrial DNA among Enterobius vermicularis in Denmark. *Parasitology* 140, 109–114. doi: 10.1017/S0031182012001308

Floyd, R. M., Rogers, A. D., Lambshead, P. J. D., and Smith, C. R. (2005). Nematode-specific PCR primers for the 18S small subunit rRNA gene. *Mol. Ecol. Notes* 5, 611–612. doi: 10.1111/j.1471-8286.2005.01009.x

Gutierrez, Y. (2000). *Diagnostic Pathology of Parasitic Infections With Clinical Correlations*. Oxford, UK: Oxford University Press.

Iñiguez, A. M., Reinhard, K., Carvalho Gonçalves, M. L., Ferreira, L. F., Araújo, A., and Paulo Vicente, A. C. (2006). SL1 RNA gene recovery from Enterobius vermicularis ancient DNA in pre-Columbian human coprolites. *Int. J. Parasitol.* 36, 1419–1425. doi: 10.1016/j.ijpara.2006.07.005

Iñiguez, A. M., Vicente, A. C. P., Araújo, A., Ferreira, L. F., and Reinhard, K. J. (2002). Enterobius vermicularis: specific detection by amplification of an internal region of 5S ribosomal RNA intergenic spacer and trans-splicing leader RNA analysis. E. vermicularis: specific detection by PCR and SL1 RNA analysis. *Exp. Parasitol.* 102, 218–222. doi: 10.1016/s0014-4894(03)00059-6

Jardine, M., Kokai, G. K., and Dalzell, A. M. (2006). Enterobius vermicularis and colitis in children. *J. Pediatr. Gastroenterol. Nutr.* 43, 610–612. doi: 10.1097/01.mpg.0000243425.01593.58

Khouja, L. B. A., Cama, V., and Xiao, L. (2010). Parasitic contamination in wastewater and sludge samples in Tunisia using three different detection techniques. *Parasitol. Res.* 107, 109–116. doi: 10.1007/s00436-010-1844-8

Köller, T., Hahn, A., Altangerel, E., Verweij, J. J., Landt, O., Kann, S., et al. (2020). Comparison of commercial and in-house real-time PCR platforms for 15 parasites and microsporidia in human stool samples without a gold standard. *Acta Trop.* 207:105516. doi: 10.1016/j.actatropica.2020.105516

Leles, D., Araújo, A., Vicente, A. C. P., and Iñiguez, A. M. (2009). Molecular diagnosis of ascariasis from human feces and description of a new Ascaris sp. genotype in Brazil. *Vet. Parasitol.* 163, 167–170. doi: 10.1016/j.vetpar.2009.03.050

Liu, L. X., Blaxter, M. L., and Shi, A. (1996). The 5S ribosomal RNA intergenic region of parasitic nematodes: variation in size and presence of SL1 RNA. *Mol. Biochem. Parasitol.* 83, 235–239. doi: 10.1016/s0166-6851(96)02753-3

Liu, L. X., Chi, J., Upton, M. P., and Ash, L. R. (1995). Eosinophilic colitis associated with larvae of the pinworm Enterobius vermicularis. *Lancet Lond. Engl.* 346, 410–412. doi: 10.1016/s0140-6736(95)92782-4

Madani, M., Ward, L., Vierstraete, A., De Boer, S. H., and Moens, M. (2019). The ribosomal intergenic spacer (IGS) in the potato and tobacco cyst nematodes, Globodera pallida, G. rostochiensis and G. tabacum. *Mol. Cell. Probes* 48:101441. doi: 10.1016/j.mcp.2019.101441

Mavziutov, A. R., Bondarenko, V. M., and Latkin, A. T. (2003). Inhibitors of the polymerase chain reaction. *Zh. Mikrobiol. Epidemiol. Immunobiol.*, 93–98.

Medkour, H., Amona, I., Laidoudi, Y., Davoust, B., Bitam, I., Levasseur, A., et al. (2020). Parasitic infections in African humans and non-human primates. *Pathog. Basel Switz.* 9:E561. doi: 10.3390/pathogens9070561

Mégraud, F. (1995). Diagnosis of helicobacter pylori. *Baillieres Clin. Gastroenterol.* 9, 507–518. doi: 10.1016/0950-3528(95)90045-4

Monteiro, L., Bonnemaison, D., Vekris, A., Petry, K. G., Bonnet, J., Vidal, R., et al. (1997). Complex polysaccharides as PCR inhibitors in feces: helicobacter pylori model. *J. Clin. Microbiol.* 35, 995–998. doi: 10.1128/jcm.35.4.995-998.1997

Morin, P. A., Chambers, K. E., Boesch, C., and Vigilant, L. (2001). Quantitative polymerase chain reaction analysis of DNA from noninvasive samples for accurate microsatellite genotyping of wild chimpanzees (pan troglodytes verus). *Mol. Ecol.* 10, 1835–1844. doi: 10.1046/j.0962-1083.2001.01308.x

Nakano, T., Okamoto, M., Ikeda, Y., and Hasegawa, H. (2006). Mitochondrial cytochrome c oxidase subunit 1 gene and nuclear rDNA regions of Enterobius vermicularis parasitic in captive chimpanzees with special reference to its relationship with pinworms in humans. *Parasitol. Res.* 100, 51–57. doi: 10.1007/s00436-006-0238-4

Ngui, R., Ravindran, S., Ong, D. B. L., Chow, T. K., Low, K. P., Nureena, Z. S., et al. (2014). Enterobius vermicularis salpingitis seen in the setting of ectopic pregnancy in a Malaysian patient. *J. Clin. Microbiol.* 52, 3468–3470. doi: 10.1128/JCM.01191-14

Nilsen, T. W. (2001). Evolutionary origin of SL-addition trans-splicing: still an enigma. *Trends Genet.* 17, 678–680. doi: 10.1016/S0168-9525(01)02499-4

Panidis, S., Paramythiotis, D., Panagiotou, D., Batsis, G., Salonikidis, S., Kaloutsi, V., et al. (2011). Acute appendicitis secondary to Enterobius vermicularis

infection in a middle-aged man: a case report. *J. Med. Case Rep.* 5:559. doi: 10.1186/1752-1947-5-559

Petro, M., Iavu, K., and Minocha, A. (2005). Unusual endoscopic and microscopic view of Enterobius vermicularis: a case report with a review of the literature. *South. Med. J.* 98, 927–929. doi: 10.1097/01.SMJ.0000163347.53138.B1

Piperaki, E.-T., Spanakos, G., Patsantara, G., Vassalou, E., Vakalis, N., and Tsakris, A. (2011). Characterization of Enterobius vermicularis in a human population, employing a molecular-based method from adhesive tape samples. *Mol. Cell. Probes* 25, 121–125. doi: 10.1016/j.mcp.2011.03.005

Pohl, D., Keller, P. M., Bordier, V., and Wagner, K. (2019). Review of current diagnostic methods and advances in helicobacter pylori diagnostics in the era of next generation sequencing. *World J. Gastroenterol.* 25, 4629–4660. doi: 10.3748/wjg.v25.i32.4629

Potapova, T. A., and Gerton, J. L. (2019). Ribosomal DNA and the nucleolus in the context of genome organization. *Chromosom. Res.* 27, 109–127. doi: 10.1007/s10577-018-9600-5

Rajamanickam, A., Usmani, A., Suri, S., and Dimov, V. (2009). Chronic diarrhea and abdominal pain: pin the pinworm. *J. Hosp. Med.* 4, 137–139. doi: 10.1002/jhm.322

Remm, M., and Remm, K. (2009). Effectiveness of repeated examination to diagnose enterobiasis in nursery school groups. *Kor. J. Parasitol.* 47, 235–241. doi: 10.3347/kjp.2009.47.3.235

Richard, G.-F., Kerrest, A., and Dujon, B. (2008). Comparative genomics and molecular dynamics of DNA repeats in eukaryotes. *Microbiol. Mol. Biol. Rev.* 72, 686–727. doi: 10.1128/MMBR.00011-08

Risio, D., Rendine, A., Napolitano, L., and Schiavone, C. (2016). Appendicitis by Enterobius vermicularis presenting with recurrent abdominal pain and eosinophilia a case report. *Ann. Ital. Chir.*:87

Rossen, L., Nørskov, P., Holmstrøm, K., and Rasmussen, O. F. (1992). Inhibition of PCR by components of food samples, microbial diagnostic assays and DNA-extraction solutions. *Int. J. Food Microbiol.* 17, 37–45. doi: 10.1016/0168-1605(92)90017-W

Schroeder, J. C., Jones, D., and Maranich, A. (2019). Peripheral eosinophilia found in pediatric Enterobius vermicularis infections. *Clin. Pediatr.* 58, 13–16. doi: 10.1177/0009922818805193

Sosin, M., Kent, J. R., and Chahine, A. A. (2019). Enterobius vermicularis Appendiceal colic. *J. Laparoendosc. Adv. Surg. Tech. A* 29, 717–719. doi: 10.1089/lap.2018.0693

Sow, D., Parola, P., Sylla, K., Ndiaye, M., Delaunay, P., Halfon, P., et al. (2017). Performance of real-time polymerase chain reaction assays for the detection of 20 gastrointestinal parasites in clinical samples from Senegal. *Am. J. Trop. Med. Hyg.* 97, 173–182. doi: 10.4269/ajtmh.16-0781

Sturm, N. R., Yu, M. C., and Campbell, D. A. (1999). Transcription termination and 3′-end processing of the spliced leader RNA in Kinetoplastids. *Mol. Cell. Biol.* 19, 1595–1604. doi: 10.1128/MCB.19.2.1595

Tebbe, C. C., and Vahjen, W. (1993). Interference of humic acids and DNA extracted directly from soil in detection and transformation of recombinant DNA from bacteria and a yeast. *Appl. Environ. Microbiol.* 59, 2657–2665. doi: 10.1128/aem.59.8.2657-2665.1993

Tomanakan, K., Sanpool, O., Chamavit, P., Lulitanond, V., Intapan, P. M., and Maleewong, W. (2018). Genetic variation of Enterobius vermicularis among schoolchildren in Thailand. *J. Helminthol.* 94:e7. doi: 10.1017/S0022149X18000962

Wendt, S., Trawinski, H., Schubert, S., Rodloff, A. C., Mössner, J., and Lübbert, C. (2019). The diagnosis and treatment of pinworm infection. *Dtsch. Arztebl. Int.* 116, 213–219. doi: 10.3238/arztebl.2019.0213

Wu, M. L., Kuksuk, L. K., and Olinger, E. J. (2000). Enterobius vermicularis. *Arch. Pathol. Lab. Med.* 124, 647–648. doi: 10.1043/0003-9985(2000)124<0647:EV>2.0.CO;2

Xu, M. Q., Paulus, H., and Chong, S. (2000). Fusions to self-splicing inteins for protein purification. *Methods Enzymol.* 326, 376–418. doi: 10.1016/s0076-6879(00)26066-7

Zelck, U. E., Ralf, B., and Michael, W. (2011). Molecular phylogenetic analysis of Enterobius vermicularis and development of an 18S ribosomal DNA-targeted diagnostic PCR. *J. Clin. Microbiol.* 49, 1602–1604. doi: 10.1128/JCM.02454-10

frontiers | Frontiers in Microbiology

TYPE Original Research
PUBLISHED 17 November 2022
DOI 10.3389/fmicb.2022.991703

OPEN ACCESS

EDITED BY
Kamal El Bissati,
The University of Chicago,
United States

REVIEWED BY
Jianping Xu,
McMaster University,
Canada
Tiago Alexandre Cocio,
University of São Paulo, Brazil
Tania C. Sorrell,
The University of Sydney, Australia

*CORRESPONDENCE
Yunsong Yu
yvys119@zju.edu.cn
Yan Jiang
jiangy@zju.edu.cn

†These authors have contributed equally to this work and share first authorship

SPECIALTY SECTION
This article was submitted to Infectious Agents and Disease, a section of the journal Frontiers in Microbiology

RECEIVED 11 July 2022
ACCEPTED 31 October 2022
PUBLISHED 17 November 2022

CITATION
Zhang J, Wang Z, Chen Y, Zhou Z, Yang Q, Fu Y, Zhao F, Li X, Chen Q, Fang L, Jiang Y and Yu Y (2022) Antifungal susceptibility and molecular characteristics of *Cryptococcus* spp. based on whole-genome sequencing in Zhejiang Province, China.
Front. Microbiol. 13:991703.
doi: 10.3389/fmicb.2022.991703

Antifungal susceptibility and molecular characteristics of *Cryptococcus* spp. based on whole-genome sequencing in Zhejiang Province, China

Junli Zhang[1,2†], Zhengan Wang[1,2†], Yan Chen[1,2], Zhihui Zhou[1,2], Qing Yang[3], Ying Fu[2,4], Feng Zhao[2,4], Xi Li[5], Qiong Chen[6], Li Fang[1,2], Yan Jiang[1,2*] and Yunsong Yu[1,2*]

[1]Department of Infectious Diseases, Sir Run Run Shaw Hospital, Zhejiang University School of Medicine, Hangzhou, China, [2]Key Laboratory of Microbial Technology and Bioinformatics of Zhejiang Province, Hangzhou, China, [3]Department of Clinical Laboratory, The First Affiliated Hospital, Zhejiang University School of Medicine, Hangzhou, China, [4]Department of Clinical Laboratory, Sir Run Run Shaw Hospital, Zhejiang University School of Medicine, Hangzhou, China, [5]Department of Clinical Laboratory, Zhejiang Provincial People's Hospital, Hangzhou, China, [6]Department of Clinical Laboratory, Affiliated Hangzhou First People's Hospital, Zhejiang University School of Medicine, Hangzhou, China

Cryptococcus spp. is a complex species that often causes cryptococcosis, which is one of the most common opportunistic infections in adults living with HIV and has very high morbidity and mortality rates. This study aimed to investigate the antifungal susceptibility profiles and epidemiological characteristics of the *Cryptococcus neoformans* species complex (CNSC) and the *Cryptococcus gattii* species complex (CGSC) in Zhejiang Province, China. A total of 177 CNSC and 3 CGSC isolates were collected, and antifungal susceptibility was tested by FUNGUS 3 and verified with an E-test. Moreover, multiple classification methods and genomic analyses were performed. The majority of the isolates (96.11%) were *C. neoformans* (formerly *C. neoformans* var. *grubii*) (ST5-VNI-A-α). Our study highlights that most of the patients with cryptococcosis were non-HIV patients in China, and nearly half of them did not have underlying diseases that led to immune insufficiency. Most of the *Cryptococcus* spp. isolates in this study were sensitive to common antifungal drugs. Two 5-flucytosine (5-FC)-resistant strains were identified, and *FUR1* mutation was detected in the 5-FC-resistant isolates. Typing based on whole-genome sequencing (WGS) showed better discrimination than that achieved with multilocus sequence typing (MLST) and indicated a clear population structure. A phylogenetic analysis based on WGS included more genomic information than traditional classification methods.

KEYWORDS

***Cryptococcus neoformans*, *Cryptococcus gattii*, antifungal susceptibility testing, multilocus sequence typing (MLST), mating type (MAT), genotype, whole-genome sequencing (WGS)**

Introduction

Cryptococcosis is primarily caused by infection with the *Cryptococcus neoformans* species complex (CNSC) or *Cryptococcus gattii* species complex (CGSC). CNSC has been classified as *C. neoformans* (serotype A, formerly *C. neoformans* var. *grubii*) which includes four genotypes: VNI, VNII, VNBI, and VNBII, *C. deneoformans* (serotype D, genotype VNIV, formerly *C. neoformans var. neoformans*) and *C. neoformans* × *C. deneoformans hybrid* (serotype AD, genotype VNIII). *C. gattii* was classified into distinct species, including *C. gattii* (genotype VGI, formerly *C. neoformans* var. *gattii*), *C. deuterogattii* (VGII), *C. bacillisporus* (VGIII), *C. decagattii* (VGIIIc/VGIV hybrid), *C. tetragattii* (VGIV) and other unnamed species (VGV), which can be classified into serotypes B or C (Hagen et al., 2015; Kwon-Chung et al., 2017; Montoya et al., 2021). *Cryptococcus* spp. often causes clinical invasive fungal diseases (IFDs), such as cryptococcal meningitis/meningoencephalitis (CM), pulmonary cryptococcosis and cryptococcal sepsis, and among these, CM is the most common and serious type of cryptococcosis. It is estimated that 223,100 cases of cryptococcal meningitis are reported worldwide every year (Rajasingham et al., 2017). Cryptococcosis is known as one of the most common opportunistic infections in adults living with HIV (Rajasingham et al., 2017), but it also occurs in non-HIV populations with underlying diseases, such as diabetes, chronic liver disease, kidney disease, lung disease, malignancies, long-term steroid therapy or solid organ transplants, that may affect the immune status (Xiaobo Feng et al., 2008; Liaw et al., 2010; Zhu et al., 2010; Williamson et al., 2017).

For the clinical treatment of cryptococcosis, particularly CM, the combination of amphotericin B (AMB) and 5-flucytosine (5-FC) followed by fluconazole (FLC) maintenance therapy is recommended (Perfect et al., 2010; Liu et al., 2018). Although research on antifungal drug resistance is important, there is no defined clinical breakpoint (CBP) for antifungal agents except AMB (resistant if MIC >1 mg/L). The epidemiological cut-off values (ECOFFs) indicated in the European Committee on Antimicrobial Susceptibility Testing (2022) guidelines for wild-type (WT) *C. neoformans* are defined as MIC ≤1 mg/L for AMB and MIC ≤0.5 mg/L for posaconazole and voriconazole, and no ECOFFs for other antifungal agents have been established. For *C. gattii*, the ECOFFs are 0.5 mg/L and 1 mg/L for AMB and posaconazole, respectively, no ECOFFs have been indicated for other antifungal agents, and no CBPs have been reported for any antifungal agents (European Committee on Antimicrobial Susceptibility Testing, 2022). It is very important to further study the mechanisms of resistance to these drugs because this resistance increases the failure rate of induction treatment (Perfect et al., 2010; May et al., 2016). Further studies are needed to aid the establishment of cryptococcal CBPs in the future.

Several molecular typing systems have been applied for *Cryptococcus* spp. The commonly used methods include genotype (Meyer et al., 2009), serotype (T G Mitchell JRP., 1995), and mating type (Chaturvedi et al., 2000) analyses. The genotype can be determined with many methods. In this study, we used two band-based methods, M13-based PCR fingerprinting (FP) and URA5-RFLP analysis, and two sequence-based methods, MLST and whole-genome sequencing (WGS). The serotype and mating type can be identified by target sequencing using PCR. MLST (Meyer et al., 2009) provides high discriminatory power, has good repeatability across different laboratories, and is inexpensive. Thus, MLST is a major and important method for strain typing in epidemiological studies of *Cryptococcus* spp. (Meyer et al., 2009). However, the MLST system (Meyer et al., 2009) is not suitable for the molecular typing of hybrids because it fails to amplify certain alleles (Li et al., 2012; Samarasinghe and Xu, 2018; Cogliati et al., 2020). To overcome this problem, new primers were designed to enable the typing of AD hybrids in 2020 (Cogliati et al., 2020).

Multilocus sequence typing was used to determine the internal 469 ~ 723-bp nucleotide sequence of seven housekeeping genes for further typing (Meyer et al., 2009). ST5/VNI is the major molecular type of CNSC in China. Its appearance suggests low genetic diversity because the current genotyping method covers few genes, but the genomes of *Cryptococcus neoformans* var. *neoformans JEC21* and *Cryptococcus gattii WM276* are 18.57 Mb and 18.4 Mb, respectively, and include 14 chromosomes (Loftus et al., 2005; D'Souza et al., 2011). Previous analysis showed that ST5 has different subtypes, which was observed following the detection of single nucleotide polymorphism (SNPs) variants (Zhou et al., 2022), and WGS can further be used to analyse resistance mechanisms and simultaneously acquire other typing features (Zang et al., 2022; Zhou et al., 2022). Considering the complexity of *Cryptococcus* spp. genomes and the development of genome sequencing technology, typing based on WGS has achieved great success in the discrimination of species (Firacative et al., 2016; Wongsuk et al., 2020) and may further reveal the evolutionary relationship and population structure of *Cryptococcus* spp. isolates.

In previous studies of *Cryptococcus* spp. in Zhejiang, 98.1% (51/52) of cryptococcemia isolates were identified as *C. neoformans* var. *grubii* ST5-VNI-α. Most patients (64.80–71.4%) with cryptococcosis were not infected with HIV, according to data from a general hospital in Zhejiang Province, which is also a designated HIV hospital (Fang et al., 2020; Zhao et al., 2021). To collect more strains to further and more comprehensively explore the clinical characteristics, drug susceptibility and molecular characteristics of *Cryptococcus* spp. in Zhejiang Province, we collected all preserved strains of clinically isolated *Cryptococcus* spp. in 4 hospitals in Zhejiang Province from 2012 to 2018, and antimicrobial susceptibility testing (AST), molecular typing, and genomic analysis were performed.

Results

Isolates and clinical information collection

In total, 180 nonrepetitive isolates were collected from four hospitals (99, 64, 14, and 3 from each hospital) in Zhejiang

Province in China, and these included 177 CNSC isolates and three CGSC isolates. All 180 patients were diagnosed as exhibiting positive *Cryptococcus* spp. culture; among these, 68.33% (123/180), 16.67% (30/180) and 13.89% (25/180) were diagnosed with cryptococcal meningitis, pulmonary cryptococcosis and sepsis, respectively, and 1 patient diagnosed with soft tissue infection and 1 patient diagnosed with abdominal infection were also observed. Correspondingly, 123 strains, which included 3 isolates of CGSC, were isolated from the cerebrospinal fluid, and 30, 25, one and one strains were isolated from lung-related specimens, blood culture, skin-soft tissue, and ascites, respectively.

The patients were classified into three groups based on immune status: HIV-associated (12.78%, 23/180), non-HIV but with underlying diseases that may influence the immune system (45.55%, 82/180), and non-HIV and without underlying diseases (41.67%, 75/180). The number of HIV-related cases of infection was lower than the number of cases observed in the other two groups, as shown in Figure 1. Pearson correlation analysis was performed to assess the increasing trend of each group over time. No statistical significance was observed in each group ($p > 0.5$).

Molecular typing

Among 177 CNSC isolates, 173 were *C. neoformans* represented by the genotype VNI, serotype A, and MAT α. Another 4 isolates of CNSC were AD hybrids: RM007 was a hybrid of VNIII-AD, MAT α/a; ZY056 and SR017 were hybrids of VNIII-AD-α; and SR008 was also an AD-MAT α hybrid. Notably, the genotypes of SR008 that were observed using the two genotyping methods were inconsistent; VNIII was genotyped by M13-based PCR fingerprinting (FP), whereas the result of URA5-RFLP was VNIV. The genotyping electrophoresis diagrams of 4 AD hybrids and four reference strains are shown in Supplementary Figures S1A,B. Three isolates of CGSC exhibited the same mating type, MAT α, but different genotypes, including VGI ($n = 1$) and VGII ($n = 2$).

Through MLST typing, 173 isolates of *C. neoformans* were identified into 5 STs: ST5 was the predominant ST ($n = 155$), followed by ST31 ($n = 8$), ST79 ($n = 5$), ST81 ($n = 3$) and ST359 ($n = 2$). The CGSC isolates ($n = 3$) included three STs, namely, ST215 (RM009 VGI, from Taizhou), ST328 (ZY002 VGII, from Shaoxing) and the novel ST577 (SR06 1 VGII, from Taizhou). However, this approach failed to type the 4 AD hybrids even with the newly designed primers (Cogliati et al., 2020). Specifically, 12 ATs, including GPDVNIV 4, PLBVNIV 2, LACVNI 2, IGSVNI 1, IGSVNIV 2, and CAP59VNI 1, could not be amplified.

The phylogenetic tree obtained based on WGS grouped the 180 isolates distinctly, which indicated that the CNSCs and CGSCs belonged to two major clusters (Figure 2). Furthermore, CNSCs were classified into three subclusters: the ST5 cluster, ST31 cluster and hybrid cluster. The ST5 cluster included 165 isolates with sequence types that included ST5, ST79, ST81, and ST359 was the dominant cluster with genotype VNI, serotype A, and MAT α and was persistent during the time period in the study region, indicating its wide and continuous epidemic spread. The ST31 cluster contained 8

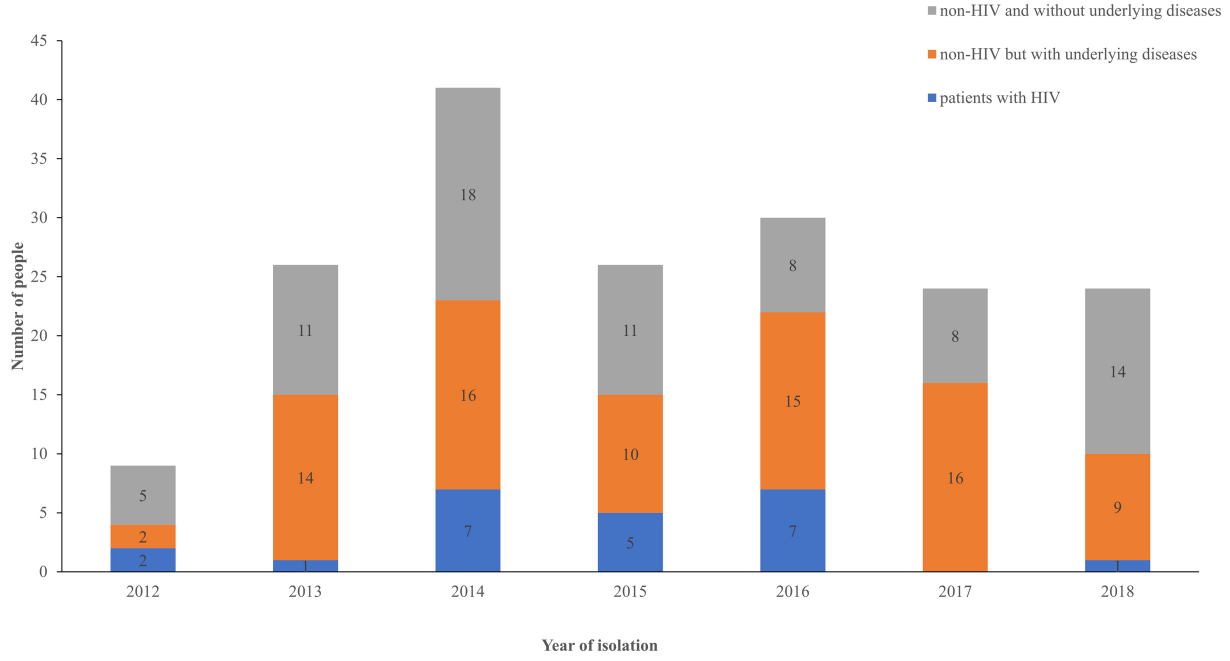

FIGURE 1
Distribution of patients among the three groups over time. Blue, HIV group; orange, non-HIV group with underlying diseases; gray, non-HIV group without underlying diseases.

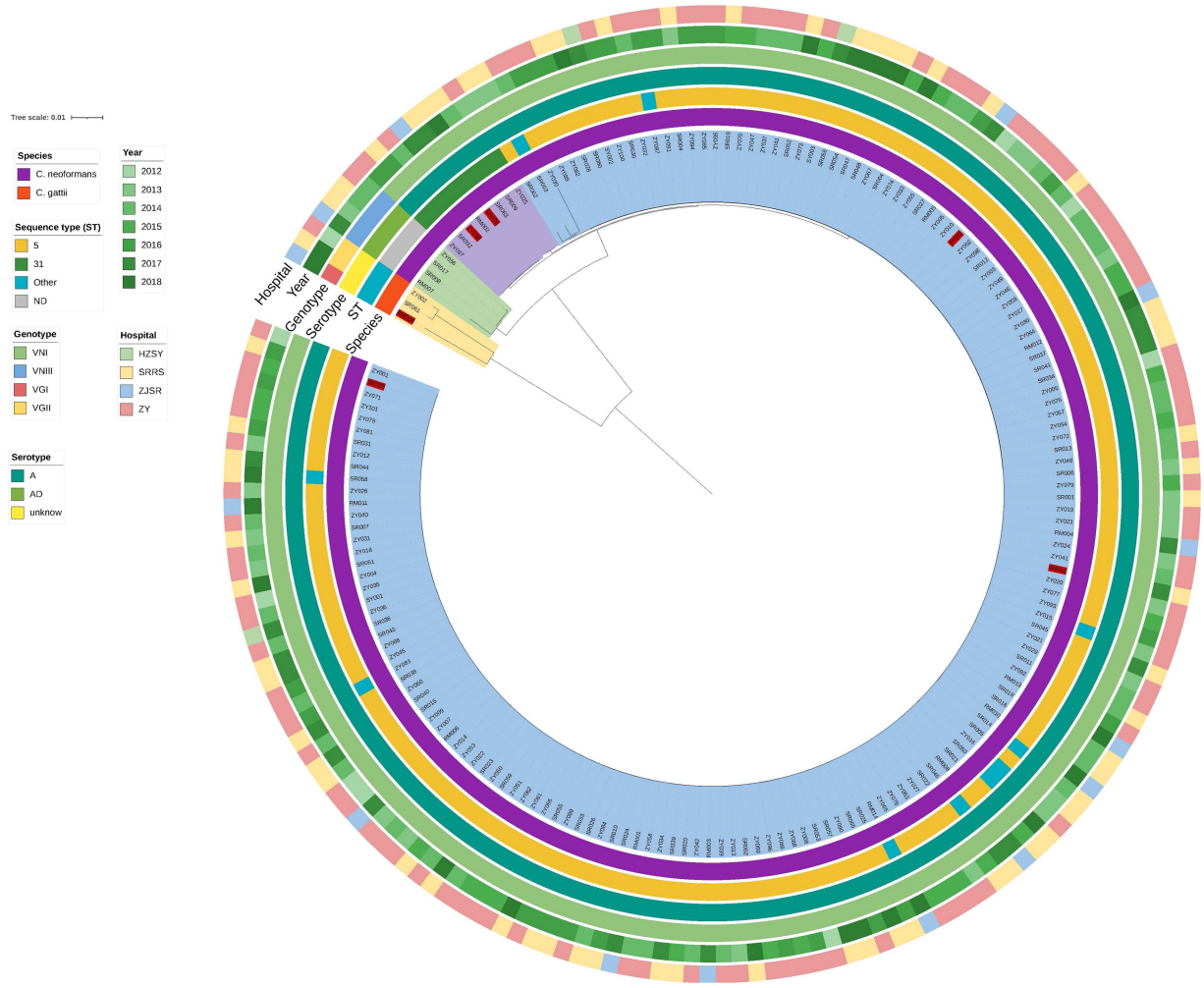

FIGURE 2
Phylogenetic tree of 180 isolates based on WGS. The innermost circle is the phylogenetic tree based on WGS. All strains were classified into two large clusters. The cluster indicated in yellow (corresponding to the bright orange of the "species" in the first circle) represents the CGSCs, and the other (corresponding to the dark purple of the "species") represents *C. neoformans*. The red labelled strains represent strains with high MICs. The second, third, and fourth circles correspond to the sequence type (ST), genotype and serotype, respectively. The cluster of CGSCs contains three strains, RM009-ST215-VGI-α, SR061-ST552-VGII-α, and ZY002-ST328-VGII-α, and these molecular types were significantly different from *C. neoformans*. In the *C. neoformans* cluster, the strains were divided into three clusters (green, purple, and blue); the cluster indicated in green had four hybrids, RM007-VNIII-AαDa, ZY056, SR008, and SR017, which were all VNIII-AD-α; the cluster indicated in purple had 8 strains, all of which were ST31-VNI-A-α; the large cluster, which is represented in blue, had 165 strains, including ST5 (n=155, the dominant ST), ST79 (n=5), ST81 (n=3), and ST359 (n=2), all of which were VNI-A-MAT α. The isolation year (the fifth circle) and hospital (the sixth circle) showed a scattered distribution, and no significant difference in the corresponding strain species was detected.

ST31 isolates. The phylogenetic tree grouped the AD hybrid isolates well, although MLST typing failed. The hybrid isolates were substantially different from those in the other two clusters. Among the hybrid clusters, three strains with the same mating type were closer to each other than to isolate RM007, which had a mating type of a/α (the other 179 strains in this study were all MAT α).

Antimicrobial susceptibility testing and drug resistance mechanism

Only a few strains with high MICs were detected. The MIC range, geometric mean (GM), MIC50 and MIC90 of 5 common antifungal agents are shown in Table 1. Although no AMB-resistant strains were found, 6 isolates with high MICs (Table 2), 2 for 5-FC and 4 for azoles, were identified. Among isolates with high MICs for azoles, 1 isolate had high MICs for all 3 drugs and belonged to cluster 31 (FLC 16 mg/L, ITR 1.5 mg/L, and VRC 0.64 mg/L), 1 isolate had high MICs for FLC (16 mg/L) and ITR (1 mg/L) and belonged to cluster 5, and the other 2 isolates with high MICs (16 mg/L and 24 mg/L) for FLC belonged to clusters 5 and 31 (Figure 2). Two strains had high MICs for 5-FC, with MICs greater than 32 mg/L. RM009 is a type of *C. gattii* (ST215, VGI, MAT α), and ZY011 is a type of *C. neoformans* var. *grubii* (ST5, VNI, MAT α).

The potential drug resistance mechanism was explored. However, no mutation in the *ERG11* gene was observed in strains with high MICs for azoles after comparison with the sequence of the reference gene from H99 (*ERG11*, JQ044790, CNAG_00040). To determine the mechanism underlying 5-FC resistance, mutations in genes belonging to the *FCY2-FCY1-FUR1* pathway were detected. Regarding RM009, there were 5 synonymous mutations in the *FCY2* and *FCY3* genes, 4 synonymous mutations and 2 meaningful mutations (T54C (Ser-Gly) and G460A (Ser-Phe)) in the *FCY1* gene, and 3 synonymous mutations in the *FUR1* gene. Another strain, ZY011 (*C. neoformans*-ST5-VNI-A-α), exhibited no mutations in the *FCY2-4* and *FCY1* genes after comparison with the sequence of the reference gene from strain H99 (VNI, ST2, serotype A), but the sequence alignment of the *FUR1* gene was significantly different from the reference sequence, which lacked approximately 200 bp. This missing region started at the 206th amino acid (Figure 3A). The sequence integrity was verified by PCR and Sanger sequencing. The missing region is close to the 5-fluorouracil (5-FU) binding site and may influence the binding of 5-FU and mediate the increase in the MIC for 5-FC (Figure 3B).

Discussion

As revealed by previous studies (Zhu et al., 2010; Fang et al., 2020; Fu et al., 2020; Zhou et al., 2020; Zhao et al., 2021), there are many more non-HIV patients in China than in other countries. In our study, we observed the same phenomenon: the proportion of patients with HIV was 12.78%. This finding may be due to the lower prevalence of HIV infection and the implementation of primary FLC prophylaxis in patients with CD4 counts <100 cells/μL in China (Organization WH, 2011; Parkes-Ratanshi et al., 2011; Oladele et al., 2017; Williamson et al., 2017). More importantly, this phenomenon indicates the importance of monitoring non-HIV-associated cryptococcosis even in apparently immunocompetent individuals (Williamson et al., 2017). In the United States, 20% of HIV-negative patients have no underlying conditions, such as a history of steroid therapy or malignant tumours (Williamson et al., 2017). Among non-HIV patients in this study, the presence of diseases affecting the immune system did not appear to increase the risk of *Cryptococcus* spp. infection since the proportions of patients with and without underlying diseases were nearly equal (45.55% vs. 41.67%). CNS-related infections were the main type of disease observed among HIV-negative patients (67.52%, 106/157). We reviewed the previous reports of Chinese researchers (Zhu et al., 2010) reported the clinical characteristics of 154 patients with cryptococcal meningitis over a 10-year period, the major of patients (66.9%) were otherwise apparently healthy and only 33.1% patients had predisposition factors (Zhu et al., 2010), there are also more reports from China that about 60% of cryptococcosis were from immunocompetent individuals, it is speculated that Chinese population might be more susceptible to cryptococcal infections than other ethnic groups (Fang et al., 2015).

In previous *Cryptococcus* spp. studies, many typing methods, such as RAPD, PCR fingerprinting, AFLP, MLMT, and MLST, have been employed and have mainly focused on genotyping (Hong et al., 2021). Due to their variable discrimination power, each of these methods has expanded knowledge regarding the genomic diversity of *Cryptococcus* spp. (Meyer et al., 2009; Hagen et al., 2015; Hong et al., 2021). We used band-based methods with the molecular types VNI–VNIV, VNB of CNSC and VGI-VGV of CGSC to assess this type of genomic diversity. With the development of sequencing technology, sequence base typing methods have provided more discriminatory power, repeatability and comparability. Thus, MLST and WGS are becoming increasingly popular. Using the MLST system, we identified lineages using sequence types. However, because MLST only includes the analysis of seven housekeeping genes, MLST may provide unilateral results, unlike WGS typing. Genome analysis in eukaryotes, including assembly, annotation, SNP calling, and

TABLE 1 Antifungal susceptibilities of five antifungal agents.

Antifungal agent	Range (μg/mL)	GM (μg/mL)	MIC50 (μg/mL)	MIC90 (μg/mL)
Amphotericin B	0.38–0.75	0.562	0.5	0.5
5-Flucytosine	0.064 – >32	3.574	4	4
Fluconazole	0.125–24	2.765	2	8
Voriconazole	0.016–0.64	0.124	0.13	0.5
Itraconazole	<0.125–1.5	0.192	0.13	0.25

GM, geometric mean of MICs.

TABLE 2 General information of 6 isolates with high MICs.

Identification number	Species	Year	ST	Genotype	MAT	5-FC	AMB	FCA	ITR	VRC
RM009	*C. gattii*	2018	ST215	VGI	α	>32	<0.5	2	0.25	0.125
ZY011	*C. neoformans*	2013	ST5	VNI	α	>32	<0.5	4	<0.125	<0.06
SR042	*C. neoformans*	2017	ST5	VNI	α	4	<0.5	24	0.5	0.047
ZY038	*C. neoformans*	2014	ST31	VNI	α	4	<0.5	16	0.5	0.5
SR029	*C. neoformans*	2016	ST5	VNI	α	4	<0.5	16	1	0.5
SR035	*C. neoformans*	2017	ST31	VNI	α	4	<0.5	16	1.5	0.64

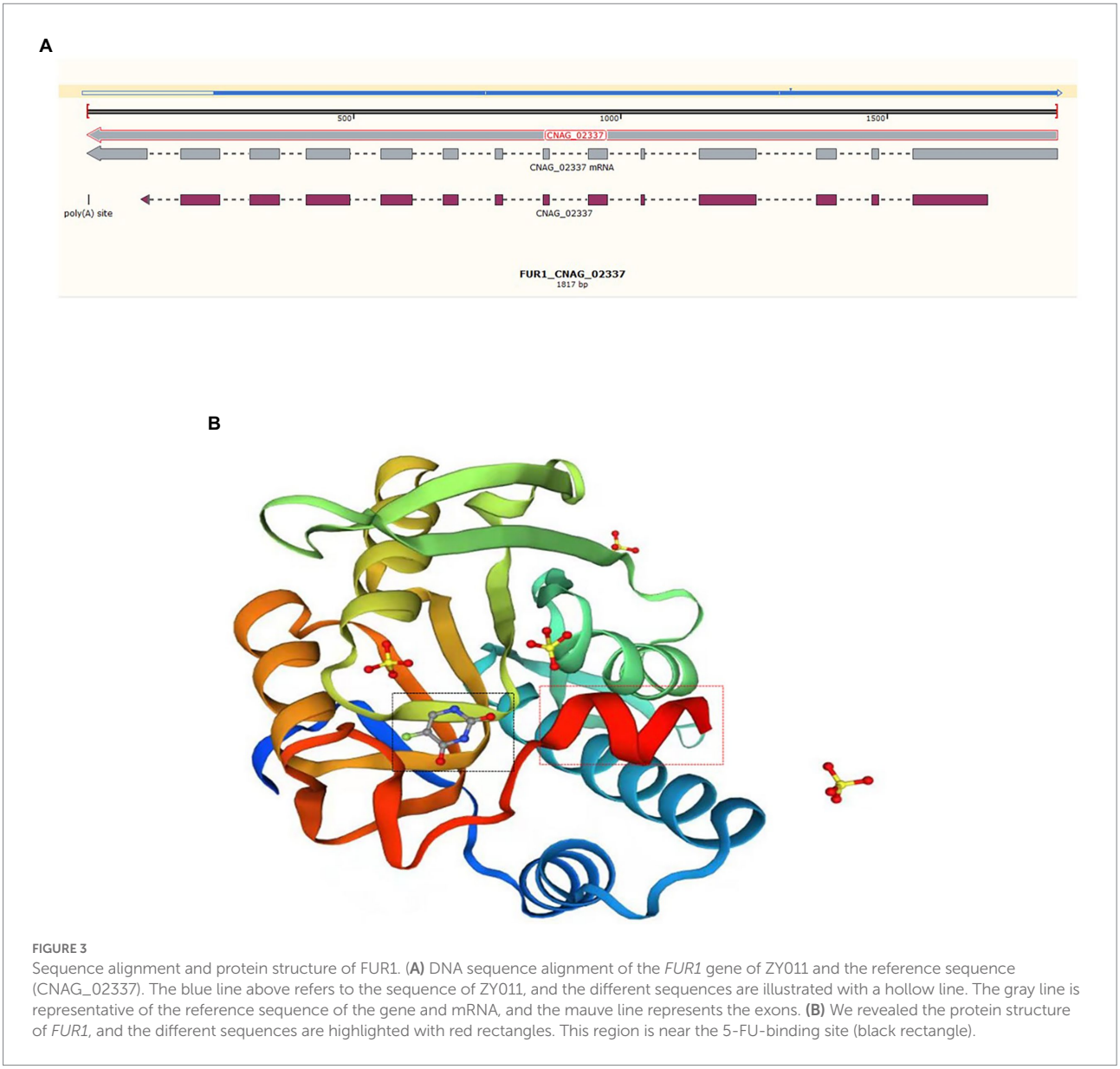

FIGURE 3
Sequence alignment and protein structure of FUR1. **(A)** DNA sequence alignment of the *FUR1* gene of ZY011 and the reference sequence (CNAG_02337). The blue line above refers to the sequence of ZY011, and the different sequences are illustrated with a hollow line. The gray line is representative of the reference sequence of the gene and mRNA, and the mauve line represents the exons. **(B)** We revealed the protein structure of *FUR1*, and the different sequences are highlighted with red rectangles. This region is near the 5-FU-binding site (black rectangle).

phylogenetic tree reconstruction, is extremely difficult and requires expert bioinformatic knowledge and high-performance computers (Desjardins et al., 2017). In our study, we proved that even with roughly processed genomes, the results presented real genomic diversity and were clearly distinguished at the species level and lineage level. Using genome assemblies, Mashtree was used to reconstruct the phylogenetic tree efficiently. Not only can CNSCs and CGSCs be clearly distinguished, but subclusters in the major cluster can also be classified, as reported by Ziyi Zhou et al. in 2022 in a study that showed that ST5 has different subtypes based on the detection of single nucleotide polymorphism (SNPs) variants (Zhou et al., 2022), and the ST5 cluster and ST31 cluster can be roughly considered CC5 and CC31 (Fan et al., 2016; Cogliati et al., 2019; Thanh et al., 2019). Furthermore, the relationship between AD hybrids and other CCs could be clearly distinguished. These results improved the typing methods and revealed the biodiversity of *Cryptococcus* spp. in China (Zang et al., 2022; Zhou et al., 2022).

The latest research has shown that the nonsusceptibility rate (intermediate and resistant) of *Cryptococcus* spp. with FLC reached 25.9% (Simwami et al., 2011), which was significantly higher than the value reported 9 years ago (9.5%) (Wang et al., 2012; Xiao et al., 2018). This finding raises concerns about the increased drug resistance rate. Mutation of the *ERG11* gene is the most common mechanism underlying azole resistance. It has been reported that the G484S, Y145F and G470R mutations of *ERG11* are related to azole resistance (Rodero et al., 2003; Sionov et al., 2012; Gago et al., 2017; Zhang et al., 2019). However, no mutation was found in *ERG11* in these high-MIC strains in our study.

In particular, two strains with high MICs of 5-FC (>32 mg/L) were found in this study: 1 strain of *C. gattii* and 1 strain of *C. neoformans*. To date, the drug resistance rate of 5-FC with

Cryptococcus spp. is 1–25% (Cuenca-Estrella, 2001; Govender et al., 2011; Espinel-Ingroff et al., 2012; Chang et al., 2021). The metabolic pathway of *FCY2-FCY1-FUR1* is related to 5-FC biochemical reactions and may cause 5-FC resistance due to its mutations. The heterozygous G/T mutation at position 145 of the *FCY2* gene and the nonsense mutation C505T have been reported. In addition, the T26C point mutation of the *FCY1* gene leads to a change in the protein (M9T), which can lead to cross-resistance to 5-FC and FLC (Papon et al., 2007; Florent et al., 2009). Considering the mutations identified in the *C. gattii* isolate RM009, we assumed that the two nonsynonymous mutations in the *FCY1* gene may be responsible for 5-FC resistance, but this finding needs further research. There were substantial differences regarding the *C. neoformans* isolate (ZY011); no exon mutation was found in the *FCY2-4* and *FCY1* genes, but the sequence of the *FUR1* gene was significantly different from the reference sequence. The identical sequence ended in an exon sequence, and because there were no other ways to identify the sequence of mRNA or protein, we could not predict the actual change in this gene. Considering that the changed region is near the 5-FU-binding site, mutations in the *FUR1* gene may cause the binding of pyrimidines to be blocked or inefficient, which may be the main factor underlying resistance.

The MICs of the 5 anti-cryptococcal drugs in this study were generally not high, there was no amphotericin B-resistant strain, most of the *Cryptococcus* spp. strains were sensitive to azoles, the MICs of several NWTs were generally not high, only two 5-FC-resistant strains were identified, these provides a more detailed reference for the empirical therapy of cryptococcosis, and our study supplements the available information regarding cryptococcal infections in Zhejiang Province for the global fungal database. These findings prove that simply processed genome sequences also provide convincing evidence of lineages.

Conclusion

In mainland China, the non-HIV population is the most commonly susceptible to cryptococcosis, and *Cryptococcus neoformans* (ST5-VNI-A-α) is the predominant pathogen. The isolated hybrids and CGSCs were rare; of particular interest, three strains of *C. gattii*, which are rare in the clinic, all caused meningitis and occurred in younger patients without underlying diseases. Phylogenetic analysis based on WGS is not band-based, covers more genomic information and therefore shows higher discriminatory power than traditional typing methods. Anti-cryptococcal drug-resistant isolates were rare, but isolates with high MICs were identified. Mutations in *FCY2-FCY1-FUR1* were detected in the 5-FC-resistant isolate, and this finding deserves further study.

Limitations

However, there are also some limitations in this study. First, data may be outdated or incomplete because many data were collected retrospectively through electronic medical records. Second, the proportion of HIV in underlying diseases would be biased in that only one of the four hospitals in the study is a designated hospital for HIV treatment. Third, due to the limitation of diagnosis methods and the lack of understanding of cryptococcosis in early years, not all *Cryptococcus* spp. strains in four hospitals were collected at the same time, resulting in sample bias. A better epidemiological investigation design is needed in the future.

Materials and methods

Ethics statement

The study was approved by the ethics review board (found in Supplementary material).

Isolate collection

Isolates of CNSC and CGSC from four hospitals were collected between 2012 and 2018. All isolates were identified by matrix-assisted laser desorption/ionization time-of-flight mass spectrometry (MALDI-TOF MS). Clinical information, such as age, sex and underlying diseases, was collected by reviewing the patients' electronic medical records. Based on this information, all cases were classified into three groups: (Kwon-Chung et al., 2017) HIV-associated (Hagen et al., 2015) non-HIV but with underlying diseases that may influence the immune status, and (Montoya et al., 2021) non-HIV and without underlying diseases. The following circumstances were considered underlying diseases: receipt of solid organ transplantation, connective tissue disease, aggressive cancer treatment, use of immunosuppressants or glucocorticoids, malignancies, haematologic malignancies, cirrhosis, diabetes mellitus, and uraemia (Zhu et al., 2010; Williamson et al., 2017; Beardsley et al., 2019). The risk level of HBV reactivation is moderate or high when treat with medium (10–20 mg/day) or high dose (≥20 mg/day) prednisone for ≥4 weeks, medium (10–20 mg/day) or high dose (≥20 mg/day) for ≥4 weeks (Lau et al., 2021), and prednisone therapy ≥7.5 mg/day were associated with a higher herpes zoster risk (Pappas et al., 2015). In the present study, patients receiving continuous glucocorticoids therapy that due to connective tissue diseases were included in the glucocorticoid group (excluding glucocorticoid containing chemotherapy); All patients with diabetes were type 2 diabetes. The "non-HIV but without underlying disease" group included patients who had no disease or some diseases that were well controlled, such as gout, hypertension, chronic hepatitis B, chronic kidney disease, and anaemia.

Further statistical analysis was performed, and the results are expressed as the means ± standard deviations.

Reference strains

Eight reference strains were used as controls: WM148 (VNI, serotype A, MATα), WM626 (VNII, serotype A, MATα), WM628

(VNIII, serotype AD, MATα/a), WM629 (VNIV, serotype D, MATα), WM179 (VGI, serotype B, MATα), WM178 (VGII, serotype B, MATα), WM161 (VGIII, serotype B, MATα) and WM779 (VGIV, serotype C, MATα) (Meyer et al., 2009).

DNA extraction

Genomic DNA was extracted from the collected isolates with ZR Fungal/Bacterial DNA Kits (catalogue no. D6005, The Epigenetics Company) according to the manufacturer's recommendations. The extracted DNA was used for MLST, genotype, serotype and next-generation sequencing analyses.

Molecular typing

The genotypes were verified using two methods, M13-based PCR fingerprinting (FP) and URA5-RFLP analysis, according to previously described protocols (Meyer et al., 2009). The serotype and mating type were determined by PCR, and the six related primer pairs of *C. neoformans* were used to determine the strain serotype and mating type according to previously described protocols (Chaturvedi et al., 2000; Dou et al., 2015; Wu et al., 2015).

Genomic analysis

Next,-generation sequencing of the strains was performed on the Illumina HiSeq X Ten platform. The raw genomic sequence data passed a quality control assessment, as demonstrated using fastqc (Andrews, 2010) and multiqc (Ewels et al., 2016). Genomes were then assembled using Shovill (Seemann et al., 2019, unpublished)[1] with an average depth of 77.1. Utilizing the whole-genome sequence, a mash distance-based phylogenetic analysis was performed with Mashtree (Katz et al., 2019), and the results were visualized using the iTOL web service.[2]

ST type was determined by screening the genome data from each isolate on Cryptococcus spp. MLST database.[3] The alleles that could not be matched were verified using the consensus ISHAM protocol by PCR and by sequencing seven loci: *CAP59*, *IGS1*, *GPD1*, *LAC1*, *PLB1*, *SOD1*, and *URA5* (Meyer et al., 2009; Hagen et al., 2015; Cogliati et al., 2020).

In vitro antimicrobial susceptibility testing

The AST of 5 common antifungal agents, including amphotericin B (AMB), 5-flucytosine (5-FC), fluconazole (FLC), itraconazole (ITR), and voriconazole (VRC), was performed using an ATB FUNGUS 3 kit (bioMérieux, France). If the MICs were abnormally high or exhibited strong trailing growth, they were then verified using an E-test (bioMérieux). The preliminary determination of drug sensitivity was based on the Fungus 3 kit instructions and the CBPs of *Candida* spp. recommended by CLSI/NCCLS and the literature (CLSI, 2008; Tewari et al., 2012; Bongomin et al., 2018; Breakpoint Tables for Interpretation of MICs for Antifungal Agents, 2020). Quality control was performed using *Candida parapsilosis* (ATCC 22019) and *Candida krusei* (ATCC 6258) (Torres-Rodriguez and Alvarado-Ramirez, 2007; Performance Standards for Antifungal Susceptibility of Testing Yeasts, 2018).

To explore the possible drug resistance mechanism, the *ERG11* sequences of the high-MIC strains were compared with the reference sequences (*ERG11*, JQ44790, CNAG_00040) using BLAST.[4] The changes in the metabolic pathway of *FCY2-FCY1-FUR1* were responsible for 5-FC resistance. Among *C. neoformans* isolates, pathway-related genes were compared with the reference gene of strain H99 (*FCY1* CNAG_00613, *FCY2* CNAG_01681, *FCY3* CNAG_04982, *FCY4* CNAG_04276, *FUR1* CNAG_02337). For *C. gattii* isolates, we used E566 (VGI, serotype B) as the reference genome. The missing sequence of the *FUR1* gene was verified by PCR and Sanger sequencing with the primers F-TGGATGAGATCATATGCCTG and R-GATTGCT GATTGGAAGGAC.

Data availability statement

The datasets presented in this study can be found in online repositories. The names of the repository/repositories and accession number(s) can be found in the article/Supplementary material.

Author contributions

YY, YJ, and ZZ: conceptualization. JZ, QY, YF, FZ, XL, and LF: data curation. JZ and ZZ: formal analysis. YY: funding acquisition. JZ, ZW, and LF: investigation. YC, YJ, and YY: methodology. JZ, ZW, and YY: project administration. ZZ, QY, YF, FZ, QC, and LF: resources. ZW, YC, XL, and YJ: software. YJ: supervision. JZ and ZW: validation and visualization. JZ: writing—original draft. ZW, YJ, and YY: writing—review and editing. All authors contributed to the article and approved the submitted version.

Funding

This research was funded by the clinical research project of Zhejiang Provincial Department of Health (grant number

1 Seemann, T., Edwards, R., Da Silva, A., and Kiil, K. Shovill. (2019) (unpublished).

2 https://itol.embl.de/

3 www.mycologylab.net

4 https://blast.ncbi.nlm.nih.gov/Blast.cgi

2018ZD030) and General Research Plan for Medical and Health of Zhejiang Province (Class A) (grant number 2020KY604).

Acknowledgments

We thank Wanqing Liao for providing the standard strains of *Cryptococcus* spp. and Ying Zhang for providing the quality control strains of AST.

Conflict of interest

The authors declare that the research was conducted in the absence of any commercial or financial relationships that could be construed as a potential conflict of interest.

Publisher's note

Supplementary material

The Supplementary material for this article can be found online at: https://www.frontiersin.org/articles/10.3389/fmicb.2022.991703/full#supplementary-material

References

Andrews, S. *Fast QC: A quality control tool for high throughput sequence data*. Babraham Bioinformatics, Babraham Institute, Cambridge, United Kingdom. (2010).

Beardsley, J., Sorrell, T. C., and Chen, S. C. (2019). Central nervous system Cryptococcal infections in non-HIV infected patients. *J. Fungi* 5: 71. doi: 10.3390/jof5030071

Bongomin, F., Oladele, R. O., Gago, S., Moore, C. B., and Richardson, M. D. (2018). A systematic review of fluconazole resistance in clinical isolates of Cryptococcus species. *Mycoses* 61, 290–297. doi: 10.1111/myc.12747

Breakpoint Tables for Interpretation of MICs for Antifungal Agents. (2020). The European Committee on Antimicrobial Susceptibility Testing. Breakpoint tables for interpretation of MICs for antifungal agents, version 10.0. Available online at: http://www.eucast.org/astoffungi/clinicalbreakpointsforantifungals/.

Chang, Y. C., Lamichhane, A. K., Cai, H., Walter, P. J., Bennett, J. E., and Kwon-Chung, K. J. (2021). Moderate levels of 5-fluorocytosine cause the emergence of high frequency resistance in cryptococci. *Nat. Commun.* 12:3418. doi: 10.1038/s41467-021-23745-1

Chaturvedi, S., Fan, B. R. J., McClelland, C. M., Wickes, B. L., and Chaturvedi, V. (2000). Direct PCR of Cryptococcus neoformans MATα and MATa pheromones to determine mating type, Ploidy, and variety: a tool for epidemiological and molecular pathogenesis studies. *J. Clin. Microbiol.* 38, 2007–2009. doi: 10.1128/JCM.38.5.2007-2009.2000

CLSI. *Reference method for broth dilution antifungal susceptibility testing of yeasts; approved standard-third edition*. CLSI document M27-A3. Wayne, PA: Clinical and Laboratory Standards Institute. (2008).

Cogliati, M., Desnos-Ollivier, M., McCormick-Smith, I., Rickerts, V., Ferreira-Paim, K., Meyer, W., et al. (2019). Genotypes and population genetics of *Cryptococcus neoformans* and *Cryptococcus gattii* species complexes in Europe and the mediterranean area. *Fungal Genet. Biol.* 129, 16–29. doi: 10.1016/j.fgb.2019.04.001

Cogliati, M., Roger, F., Meyer, W., Robert, V., and Bertout, S. (2020). New multilocus sequence typing primers to enable genotyping of AD hybrids within the Cryptococcus neoformans species complex. *Med. Mycol.* 58, 1005–1009. doi: 10.1093/mmy/myaa047

Cuenca-Estrella, M. T. M. D., Mellado, E., and Rodríguez-Tudela, J. L. (2001). Flucytosine primary resistance in Candida species and Cryptococcus neoformans. *Eur. J. Clin. Microbiol. Infect. Dis.* 20, 276–279. doi: 10.1007/PL00011265

Desjardins, C. A., Giamberardino, C., Sykes, S. M., Yu, C. H., Tenor, J. L., Chen, Y., et al. (2017). Population genomics and the evolution of virulence in the fungal pathogen *Cryptococcus neoformans*. *Genome Res.* 27, 1207–1219. doi: 10.1101/gr.218727.116

Dou, H. T. Y. X., Wang, H. Z., and Li, T. S. (2015). Molecular epidemiology of *Cryptococcus neoformans* and *Cryptococcus gattii* in China between 2007 and 2013 using multilocus sequence typing and the Diversi lab system. *Eur. J. Clin. Microbiol. Infect. Dis.* 34, 753–762. doi: 10.1007/s10096-014-2289-2

D'Souza, C. A., Kronstad, J. W., Taylor, G., Warren, R., Yuen, M., Hu, G., et al. (2011). Genome variation in *Cryptococcus gattii*, an emerging pathogen of immunocompetent hosts. *MBio* 2, e00342–e00310. doi: 10.1128/mBio.00342-10

Espinel-Ingroff, A., Aller, A. I., Canton, E., Castanon-Olivares, L. R., Chowdhary, A., Cordoba, S., et al. (2012). *Cryptococcus neoformans-Cryptococcus gattii* species complex: an international study of wild-type susceptibility endpoint distributions and epidemiological cutoff values for fluconazole, itraconazole, posaconazole, and voriconazole. *Antimicrob. Agents Chemother.* 56, 5898–5906. doi: 10.1128/AAC.01115-12

European Committee on Antimicrobial Susceptibility Testing. (2022). Overview of antifungal ECOFFs and clinical breakpoints for yeasts, moulds and dermatophytes using the EUCAST E.Def 7.3, E.Def 9.4 and E.Def 11.0 procedures. Version 3. Available at: http://www.eucast.org.

Ewels, P., Magnusson, M., Lundin, S., and Käller, M. J. B. (2016). Multi QC: summarize analysis results for multiple tools and samples in a single report, *J. Bioinform.* 32, 3047–3048. doi: 10.1093/bioinformatics/btw354

Fan, X., Xiao, M., Chen, S., Kong, F., Dou, H. T., Wang, H., et al. (2016). Predominance of *Cryptococcus neoformans* var. grubii multilocus sequence type 5 and emergence of isolates with non-wild-type minimum inhibitory concentrations to fluconazole: a multi-Centre study in China. *Clin. Microbiol. Infect.* 22:887.e1-.e9. doi: 10.1016/j.cmi.2016.07.008

Fang, W., Fa, Z., and Liao, W. (2015). Epidemiology of Cryptococcus and cryptococcosis in China. *Fungal Genet. Biol.* 78, 7–15. doi: 10.1016/j.fgb.2014.10.017

Fang, L. F., Zhang, P. P., Wang, J., Yang, Q., and Qu, T. T. (2020). Clinical and microbiological characteristics of cryptococcosis at an university hospital in China from 2013 to 2017. *Braz. J. Infect. Dis.* 24, 7–12. doi: 10.1016/j.bjid.2019.11.004

Firacative, C., Roe, C. C., Malik, R., Ferreira-Paim, K., Escandon, P., Sykes, J. E., et al. (2016). MLST and whole-genome-based population analysis of *Cryptococcus gattii* VGIII links clinical, veterinary and environmental strains, and reveals divergent serotype specific sub-populations and distant ancestors. *PLoS Negl. Trop. Dis.* 10:e0004861. doi: 10.1371/journal.pntd.0004861

Florent, M., Noel, T., Ruprich-Robert, G., Da Silva, B., Fitton-Ouhabi, V., Chastin, C., et al. (2009). Nonsense and missense mutations in FCY2 and FCY1 genes are responsible for flucytosine resistance and flucytosine-fluconazole cross-resistance in clinical isolates of *Candida lusitaniae*. *Antimicrob. Agents Chemother.* 53, 2982–2990. doi: 10.1128/AAC.00880-08

Fu, Y., Xu, M., Zhou, H., Yao, Y., Zhou, J., and Pan, Z. (2020). Microbiological and clinical characteristics of cryptococcemia: a retrospective analysis of 85 cases in a Chinese hospital. *Med. Mycol.* 58, 478–484. doi: 10.1093/mmy/myz089

Gago, S., Serrano, C., Alastruey-Izquierdo, A., Cuesta, I., Martin-Mazuelos, E., Aller, A. I., et al. (2017). Molecular identification, antifungal resistance and virulence of *Cryptococcus neoformans* and *Cryptococcus deneoformans* isolated in Seville, Spain. *Mycoses.* 60, 40–50. doi: 10.1111/myc.12543

Govender, N. P., Patel, J., van Wyk, M., Chiller, T. M., and Lockhart, S. R. (2011). Group for Enteric R, et al. trends in antifungal drug susceptibility of *Cryptococcus neoformans* isolates obtained through population-based surveillance in South Africa in 2002–2003 and 2007–2008. *Antimicrob. Agents Chemother.* 55, 2606–2611. doi: 10.1128/AAC.00048-11

Hagen, F., Khayhan, K., Theelen, B., Kolecka, A., Polacheck, I., Sionov, E., et al. (2015). Recognition of seven species in the *Cryptococcus gattii/Cryptococcus*

neoformans species complex. *Fungal Genet. Biol.* 78, 16–48. doi: 10.1016/j.fgb.2015.02.009

Hong, N., Chen, M., and Xu, J. (2021). Molecular markers reveal epidemiological patterns and evolutionary histories of the human pathogenic Cryptococcus. *Front. Cell. Infect. Microbiol.* 11:683670. doi: 10.3389/fcimb.2021.683670

Katz, L. S., Griswold, T., Morrison, S. S., Caravas, J. A., Zhang, S., den Bakker, H. C., et al. (2019). Mashtree: a rapid comparison of whole genome sequence files. *J. Open Source Softw*. 4:1762. doi: 10.21105/joss.01762

Kwon-Chung, K. J., Bennett, J. E., Wickes, B. L., Meyer, W., Cuomo, C. A., Wollenburg, K. R., et al. (2017). The case for adopting the "species complex" nomenclature for the etiologic agents of cryptococcosis. *mSphere.* 2: e00357–16. doi: 10.1128/mSphere.00357-16

Lau, G., Yu, M. L., Wong, G., Thompson, A., Ghazinian, H., Hou, J. L., et al. (2021). APASL clinical practice guideline on hepatitis B reactivation related to the use of immunosuppressive therapy. *Hepatol. Int.* 15, 1031–1048. doi: 10.1007/s12072-021-10239-x

Li, W., Averette, A. F., Desnos-Ollivier, M., Ni, M., Dromer, F., and Heitman, J. (2012). Genetic diversity and genomic plasticity of Cryptococcus neoformans AD hybrid strains. *G3* 2, 83–97. doi: 10.1534/g3.111.001255

Liaw, S. J., Wu, H. C., and Hsueh, P. R. (2010). Microbiological characteristics of clinical isolates of Cryptococcus neoformans in Taiwan: serotypes, mating types, molecular types, virulence factors, and antifungal susceptibility. *Clin. Microbiol. Infect.* 16, 696–703. doi: 10.1111/j.1469-0691.2009.02930.x

Liu, Z. Y., Wang, G. Q., Zhu, L. P., Lyu, X. J., Zhang, Q. Q., Yu, Y. S., et al. (2018). Expert consensus on the diagnosis and treatment of cryptococcal meningitis. *Zhonghua Nei Ke Za Zhi* 57, 317–323. doi: 10.3760/cma.j.issn.0578-1426.2018.05.003

Loftus, B. J., Fung, E., Roncaglia, P., Rowley, D., Amedeo, P., Bruno, D., et al. (2005). The genome of the basidiomycetous yeast and human pathogen *Cryptococcus neoformans*. *Science* 307, 1321–1324. doi: 10.1126/science.1103773

May, R. C., Stone, N. R., Wiesner, D. L., Bicanic, T., and Nielsen, K. (2016). Cryptococcus: from environmental saprophyte to global pathogen. *Nat. Rev. Microbiol.* 14, 106–117. doi: 10.1038/nrmicro.2015.6

Meyer, W., Aanensen, D. M., Boekhout, T., Cogliati, M., Diaz, M. R., Esposto, M. C., et al. (2009). Consensus multi-locus sequence typing scheme for *Cryptococcus neoformans* and *Cryptococcus gattii*. *Med. Mycol.* 47, 561–570. doi: 10.1080/13693780902953886

Montoya, M. C., Magwene, P. M., and Perfect, J. R. (2021). Associations between Cryptococcus genotypes, phenotypes, and clinical parameters of human disease: A Review. *J. Fungi* 7: 260. doi: 10.3390/jof7040260

Oladele, R. O., Bongomin, F., Gago, S., and Denning, D. W. (2017). HIV-associated Cryptococcal disease in resource-limited settings: a case for "prevention is better than cure"? *J. Fungi* 3: 67. doi: 10.3390/jof3040067

Organization WH. (2011). *Rapid advice: Diagnosis, prevention and management of cryptococcal disease in HIV-infected adults, adolescents and children*. Geneva: World Health Organization. Available online at: https://appswhoint/iris/handle/10665/44786.

Papon, N., Noel, T., Florent, M., Gibot-Leclerc, S., Jean, D., Chastin, C., et al. (2007). Molecular mechanism of flucytosine resistance in *Candida lusitaniae*: contribution of the FCY2, FCY1, and FUR1 genes to 5-fluorouracil and fluconazole cross-resistance. *Antimicrob. Agents Chemother.* 51, 369–371. doi: 10.1128/AAC.00824-06

Pappas, D. A., Hooper, M. M., Kremer, J. M., Reed, G., Shan, Y., Wenkert, D., et al. (2015). Herpes zoster reactivation in patients with rheumatoid arthritis: analysis of disease characteristics and disease-modifying Antirheumatic drugs. *Arthritis Care Res.* 67, 1671–1678. doi: 10.1002/acr.22628

Parkes-Ratanshi, R., Wakeham, K., Levin, J., Namusoke, D., Whitworth, J., Coutinho, A., et al. (2011). Primary prophylaxis of cryptococcal disease with fluconazole in HIV-positive Ugandan adults: a double-blind, randomized, placebo-controlled trial. *Lancet Infect. Dis.* 11, 933–941. doi: 10.1016/S1473-3099(11)70245-6

Perfect, J. R., Dismukes, W. E., Dromer, F., Goldman, D. L., Graybill, J. R., Hamill, R. J., et al. (2010). Clinical practice guidelines for the management of cryptococcal disease: 2010 update by the infectious diseases society of america. *Clin. Infect. Dis.* 50, 291–322. doi: 10.1086/649858

Performance Standards for Antifungal Susceptibility of Testing Yeasts. *Performance standards for antifungal susceptibility of testing yeasts*. Clinical and Laboratory Standards Institute, Wayne, PA. (2018).

Rajasingham, R., Smith, R. M., Park, B. J., Jarvis, J. N., Govender, N. P., Chiller, T. M., et al. (2017). Global burden of disease of HIV-associated cryptococcal meningitis: an updated analysis. *Lancet Infect. Dis.* 17, 873–881. doi: 10.1016/S1473-3099(17)30243-8

Rodero, L., Mellado, E., Rodriguez, A. C., Salve, A., Guelfand, L., Cahn, P., et al. (2003). G484S amino acid substitution in lanosterol 14-alpha demethylase (ERG11) is related to fluconazole resistance in a recurrent Cryptococcus neoformans clinical isolate. *Antimicrob. Agents Chemother.* 47, 3653–3656. doi: 10.1128/AAC.47.11.3653-3656.2003

Samarasinghe, H., and Xu, J. (2018). Hybrids and hybridization in the *Cryptococcus neoformans* and *Cryptococcus gattii* species complexes. *Infect. Genet. Evol.* 66, 245–255. doi: 10.1016/j.meegid.2018.10.011

Simwami, S. P., Khayhan, K., Henk, D. A., Aanensen, D. M., Boekhout, T., Hagen, F., et al. (2011). Low diversity *Cryptococcus neoformans* variety *Grubii multilocus* sequence types from Thailand are consistent with an ancestral African origin. *PLoS Pathog.* 7:e1001343. doi: 10.1371/journal.ppat.1001343

Sionov, E., Chang, Y. C., Garraffo, H. M., Dolan, M. A., Ghannoum, M. A., and Kwon-Chung, K. J. (2012). Identification of a Cryptococcus neoformans cytochrome P 450 lanosterol 14alpha-demethylase (erg 11) residue critical for differential susceptibility between fluconazole/voriconazole and itraconazole/posaconazole. *Antimicrob. Agents Chemother.* 56, 1162–1169. doi: 10.1128/AAC.05502-11

T G Mitchell JRP., (1995). Cryptococcosis in the era of AIDS--100 years after the discovery of *Cryptococcus neoformans*. *Clin. Microbiol. Rev.* 8, 515–548. doi: 10.1128/CMR.8.4.515

Tewari, A., Behera, B., Mathur, P., and Xess, I. (2012). Comparative analysis of the Vitek 2 antifungal susceptibility system and E-test with the CLSI M27-A3 broth microdilution method for susceptibility testing of Indian clinical isolates of Cryptococcus neoformans. *Mycopathologia* 173, 427–433. doi: 10.1007/s11046-012-9528-9

Thanh, L. T., Phan, T. H., Rattanavong, S., Nguyen, T. M., Van Duong, A., Dacon, C., et al. (2019). Multilocus sequence typing of *Cryptococcus neoformans* var. Grubii from Laos in a regional and global context. *Med. Mycol.* 57, 557–565. doi: 10.1093/mmy/myy105

Torres-Rodriguez, J. M., and Alvarado-Ramirez, E. (2007). *In vitro* susceptibilities to yeasts using the ATB FUNGUS 2 method, compared with Sensititre yeast one and standard CLSI (NCCLS) M27-A2 methods. *J. Antimicrob. Chemother.* 60, 658–661. doi: 10.1093/jac/dkm247

Wang, H., Xiao, M., Chen, S. C., Kong, F., Sun, Z. Y., Liao, K., et al. (2012). *In vitro* susceptibilities of yeast species to fluconazole and voriconazole as determined by the 2010 National China Hospital Invasive Fungal Surveillance net (CHIF-NET) study. *J. Clin. Microbiol.* 50, 3952–3959. doi: 10.1128/JCM.01130-12

Williamson, P. R., Jarvis, J. N., Panackal, A. A., Fisher, M. C., Molloy, S. F., Loyse, A., et al. (2017). Cryptococcal meningitis: epidemiology, immunology, diagnosis and therapy. *Nat. Rev. Neurol.* 13, 13–24. doi: 10.1038/nrneurol.2016.167

Wongsuk, T., Homkaew, A., Faksri, K., and Thongnak, C. (2020). Multi-locus sequence typing and whole genome sequence analysis of *Cryptococcus neoformans* isolated from clinical specimens in Vajira hospital, Bangkok, Thailand. *Mycopathologia* 185, 503–514. doi: 10.1007/s11046-020-00456-7

Wu, S. Y., Lei, Y., Kang, M., Xiao, Y. L., and Chen, Z. X. (2015). Molecular characterization of clinical *Cryptococcus neoformans* and *Cryptococcus gattii* isolates from Sichuan province. *China. Mycoses.* 58, 280–287. doi: 10.1111/myc.12312

Xiao, M., Chen, S. C., Kong, F., Fan, X., Cheng, J. W., Hou, X., et al. (2018). Five-year China hospital invasive fungal surveillance net (CHIF-NET) study of invasive fungal infections caused by non-candidal yeasts: species distribution and azole susceptibility. *Infect. Drug Resist.* 11, 1659–1667. doi: 10.2147/IDR.S173805

Xiaobo Feng, Z. Y., Ren, D., Liao, W., and Jingsong, W. (2008). Genotypeandmating typeanalysis of Cryptococcusneoformans and Cryptococcusgattii isolates from China thatmainlyoriginated fromnon-HIV-infectedpatients. *FEMS Yeast Res.* 8, 930–938. doi: 10.1111/j.1567-1364.2008.00422.x

Zang, X., Ke, W., Wang, L., Wu, H., Huang, Y., Deng, H., et al. (2022). Molecular epidemiology and microbiological characteristics of *Cryptococcus gattii* VGII isolates from China. *PLoS Negl. Trop. Dis.* 16:e0010078. doi: 10.1371/journal.pntd.0010078

Zhang, J., Li, L., Lv, Q., Yan, L., Wang, Y., and Jiang, Y. (2019). The fungal CYP51s: their functions, structures, related drug resistance, and inhibitors. *Front. Microbiol.* 10:691. doi: 10.3389/fmicb.2019.00691

Zhao, H., Zhou, M., Zheng, Q., Zhu, M., Yang, Z., Hu, C., et al. (2021). Clinical features and outcomes of Cryptococcemia patients with and without HIV infection. *Mycoses* 64, 656–667. doi: 10.1111/myc.13261

Zhou, L. H., Jiang, Y. K., Li, R. Y., Huang, L. P., Yip, C. W., Denning, D. W., et al. (2020). Risk-based estimate of human fungal disease burden, China. *Emerg Infect Dis.* 26, 2137–2147. doi: 10.3201/eid2609.200016

Zhou, Z., Zhu, C., Ip, M., Liu, M., Zhu, Z., Liu, R., et al. (2022). Molecular epidemiology and antifungal resistance of Cryptococcus neoformans from human immunodeficiency virus-negative and human immunodeficiency virus-positive patients in eastern China. *Front. Microbiol.* 13:942940. doi: 10.3389/fmicb.2022.942940

Zhu, L. P., Wu, J. Q., Xu, B., Ou, X. T., Zhang, Q. Q., and Weng, X. H. (2010). Cryptococcal meningitis in non-HIV-infected patients in a Chinese tertiary care hospital, 1997–2007. *Med. Mycol.* 48, 570–579. doi: 10.3109/13693780903437876

frontiers | Frontiers in Microbiology

TYPE Original Research
PUBLISHED 17 November 2022
DOI 10.3389/fmicb.2022.1030242

OPEN ACCESS

EDITED BY
Bing Gu,
Guangdong Provincial People's Hospital, China

REVIEWED BY
Litian Ma,
Fourth Military Medical University, China
Hillary Crandall,
The University of Utah, United States
Mary Slack,
Griffith University, Australia

*CORRESPONDENCE
Hans-Christian Slotved
hcs@ssi.dk

SPECIALTY SECTION
This article was submitted to Infectious Agents and Disease, a section of the journal Frontiers in Microbiology

RECEIVED 28 August 2022
ACCEPTED 24 October 2022
PUBLISHED 17 November 2022

CITATION
Slotved H-C, Johannesen TB, Stegger M and Fuursted K (2022) Evaluation of molecular typing for national surveillance of invasive clinical *Haemophilus influenzae* isolates from Denmark. *Front. Microbiol.* 13:1030242. doi: 10.3389/fmicb.2022.1030242

Evaluation of molecular typing for national surveillance of invasive clinical *Haemophilus influenzae* isolates from Denmark

Hans-Christian Slotved*, Thor Bech Johannesen, Marc Stegger and Kurt Fuursted

Department of Bacteria, Parasites and Fungi, Statens Serum Institut, Copenhagen, Denmark

H*aemophilus influenzae* is a gram-negative coccobacillus known to cause respiratory and invasive infections. It can possess a polysaccharide capsule that can be categorized into six different serotypes (i.e., Hia, Hib, Hic, Hid, Hie, and Hif) and non-encapsulated strains that are defined as non-typeable. Furthermore, *H. influenzae* can be characterized into eight biotypes (I–VIII). Traditionally, isolates have been serotyped and biotyped using phenotypic methods; however, these methods are not always reliable. In this study, we evaluate the use of whole-genome sequencing (WGS) for national surveillance and characterization of clinical Danish *H. influenzae* isolates. In Denmark, all clinical invasive isolates between 2014 and 2021 have been serotyped using a traditional phenotypic latex agglutination test as well as *in silico* serotyped using the *in silico* programs "hinfluenzae_capsule_characterization" and "hicap" to compare the subsequent serotypes. Moreover, isolates were also biotyped using a phenotypic enzyme test and the genomic data for the detection of the genes encoding ornithine, tryptophan, and urease. The results showed a 99–100% concordance between the two genotypic approaches and the phenotypic serotyping, respectively. The biotyping showed a 95% concordance between genotyping and phenotyping. In conclusion, our results show that in a clinical surveillance setting, *in silico* serotyping and WGS-based biotyping are a robust and reliable approach for typing clinical *H. influenzae* isolates.

KEYWORDS

Denmark, capsular genes, genotyping, serotyping, *Haemophilus influenzae*

Introduction

Haemophilus influenzae is a gram-negative coccobacillus that can cause respiratory infections as well as invasive infections such as septicemia and meningitis (Nørskov-Lauritsen et al., 2021). It is categorized into six serotypes (i.e., Hia, Hib, Hic, Hid, Hie, and Hif) according to the polysaccharide capsule, as well as non-encapsulated strains that are referred to as non-typeable *H. influenzae* (non-cap) (Potts et al., 2019). In the pre-vaccine era, *H. influenzae* serotype b (Hib) was a frequent cause of bacterial meningitis among young children (Bijlmer, 1991; Nørskov-Lauritsen, 2014; Jalalvand and Riesbeck, 2018), but after the introduction of Hib vaccines in the 1980s, the numbers diminished dramatically worldwide (Morris et al., 2008; Nørskov-Lauritsen, 2014). The Hib vaccine was introduced into the Danish immunization program in 1993 as a part of the diphtheria-tetanus-pertussis-polio combination vaccine recommended at 3, 5, and 12 months of age, with high vaccination coverage of 96% (12-month vaccination; [1]accessed 17 December 2021), and it has been estimated to have an effectiveness of more than 97% for the prevention of Hib-related meningitis ([2]accessed 29 November 2021).

Haemophilus influenzae has traditionally been serotyped by phenotypic methods and PCR (Potts et al., 2019; Watts and Holt, 2019). Recently, two *in silico* approaches using whole-genome sequencing (WGS), "hinfluenzae_capsule_characterization" (Potts et al., 2019) and "hicap" (Watts and Holt, 2019), have been described that allow easier serotyping.

Haemophilus influenzae can furthermore be characterized based on eight biotypes defined by the presence and absence of the three enzymes, namely, tryptophanase (indole production), urease, and ornithine decarboxylase (Nørskov-Lauritsen, 2014).

In this study, we evaluated the use of two different *in silico* serotyping programs based on WGS for national surveillance of invasive clinical *H. influenzae* isolates from Denmark received between 2014 and 2021. Additionally, we investigated the clonal relatedness to serotype and biotype.

Materials and methods

Clinical isolates

Since October 2007, surveillance of invasive Hib infections in Denmark has included mandatory submission of isolates to the Neisseria and Streptococcus Reference Laboratory (NSR) at Statens Serum Institut (SSI) following an executive order (BEK nr 1102 of 20/09/2007), and although the surveillance specifies only Hib, the reference laboratory receives the majority of invasive *H. influenzae* isolates from all Danish regional laboratories of clinical microbiology.

All isolates were from invasive cases from mainland Denmark. An invasive case was defined as the presence of invasive *H. influenzae* in a patient who had a positive culture result for *H. influenzae* from cerebrospinal fluid (CSF), blood, or other normally sterile sites.

Data on serotypes and sample sites on all clinical *H. influenzae* isolates between 2014 and 2021 were retrieved from the Danish laboratory surveillance system at the Neisseria and Streptococcus Reference Laboratory (**Figure 1**). The WGS and phenotyping were performed on isolates consecutively when received during the study period. All isolates were grown on chocolate plates for both DNA preparation and phenotyping.

Species identification of *Haemophilus influenzae* isolates

The identification of *H. influenzae* was performed as previously described (Kilian, 1976; Fuursted et al., 2016). Briefly, species identification was performed on strains transferred directly from bacterial colonies using matrix-assisted laser desorption/ionization time-of-flight mass spectrometry (MALDI-TOF MS) (Bruker Daltonics; Compass 1.4, Version 3.4, Build 3.4.76.0). Species identification was based on the standard MALDI-TOF score value [Biotyper database version MBT 6903 MSP Library (#1829023)] and confirmed with WGS data using KmerFinder.[3]

Phenotypic biotyping

From 2014 to 2019, the *H. influenzae* isolates were typed phenotypically into eight biotypes based on their variable production of tryptophanase (indole production), urease, and ornithine decarboxylase (ODC), as described in other studies (Kilian et al., 1979; Nørskov-Lauritsen, 2014). Phenotypic biotyping was not performed on the 2020–2021 isolates.

Serotyping

The isolates were serotyped using latex agglutination test (SSI Diagnostica, Denmark) specific for *H. influenzae* covering all six known serotypes (i.e., Hia, Hib, Hic, Hid, Hie, and Hif).

1 https://statistik.ssi.dk//sygdomsdata#!/?vaccination=3&sex=3&landsdel=100&xaxis=Cohort&show=Graph&datatype=Vaccination

2 https://www.ssi.dk/vaccinationer/boernevaccination/sygdomsforekomst-foer-og-efter-vaccination

3 https://cge.food.dtu.dk/services/KmerFinder/

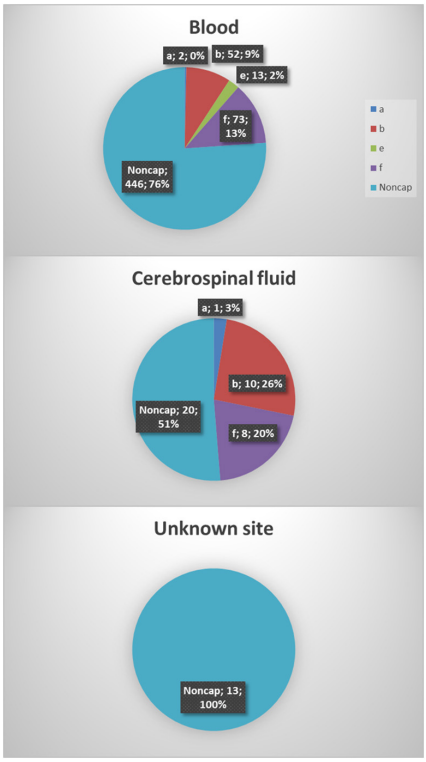

FIGURE 1
A total of six hundred thirty-eight *Haemophilus influenzae* isolates were included in the study. The majority of the isolates were from blood samples (91.8%, 586), 6.1% (39) were from cerebrospinal fluid, and information on the origin of 2% (13) of isolates was not available.

Whole-genome sequencing and assembly

Whole-genome sequencing was performed as previously described (Fuursted et al., 2016; Slotved et al., 2021). Briefly, genomic DNA was extracted using a DNeasy Blood & Tissue Kit (QIAGEN, Hilden, Germany), and fragment libraries were constructed using a Nextera XT Kit (Illumina, San Diego, CA, USA) followed by either 150 or 250 bp paired-end sequencing on either the MiSeq or NextSeq 550 platform (Illumina, San Diego, CA, USA), respectively, according to the manufacturer's instructions. The paired-end data were *de novo* assembled using the SKESA assembler (SKESA version 2.2) (Souvorov et al., 2018).

The genomic sequence data for the 638 clinical isolates have been deposited at the European Nucleotide Archive (ENA) under project no. PRJEB56415.

Genotyping

Genotyping was performed on all isolates using two *in silico* serotyping programs (Potts et al., 2019; Watts and Holt, 2019) with default parameters. The version used for the *in silico* program "hinfluenzae_capsule_characterization" was from the GitHub site: https://github.com/Vikash84/hinfluenzae_capsule_characterization, accessed 07-10-2022. The version used for the *in silico* program "hicap" was the version hicap 1.0.3: https://anaconda.org/bioconda/hicap, accessed 07-10-2022.

For isolates with deviations in phenotype/genotype, the genotype was additionally verified using BLASTN (BLAST 2.9.0 + version) using the sequences as described by Maaroufi et al. (2007) against the assembled genomes.

For the molecular detection of the biotype genes, partial sequences were used from the *H. influenzae* reference genome Rd KW20 (GenBank accession ID L42023); gene HI_0590 (1308 bp), gene HI_1389.1 (1434 bp), and gene HI_0535 (786 bp).

Multilocus sequence typing and phylogenetic analysis

Multilocus sequence typing was performed by uploading the assembled genomes to the PubMLST database (see text footnote 3, accessed 08-02-2022) to identify sequence types (ST) and corresponding clonal complexes (CC) for all isolates. STs sharing at least six of seven allelic variants were grouped into CCs (Shabayek and Spellerberg, 2018).

A phylogenetic tree was created based on single-nucleotide polymorphisms (SNPs) detected in the core genome of the isolate collection. SNPs were identified using NASP (Sahl et al., 2016) with BWAmem for mapping against the chromosome of *H. influenzae* isolate Rd KW20 (GenBank accession ID L42023), and GATK was set to remove positions with less than 10-fold depth and 90% unambiguous variant calls after removal of duplicated regions in the reference using NUCmer. The resulting SNP matrix was purged for recombination using Gubbins (Croucher et al., 2015). The phylogenetic tree was generated using a maximum-likelihood approach with IQ-TREE (Nguyen et al., 2015)[4] and ModelFinder as implemented with 100 bootstraps before visualization using iTOL version 6 (Letunic and Bork, 2021).

Ethical considerations

The data and samples from patients were collected routinely for national surveillance purposes; therefore, no ethical approval or informed consent from patients or guardians was required. The study was approved by the Danish Data Protection Agency (record number 2007-41-0229). For further details on SSI's

4 http://www.iqtree.org/

TABLE 1 List of isolates with divergent phenotype/genotype for serotype or biotype and missing values.

Isolate number	Phenotype	The *in silico* program "hicap" (Watts and Holt, 2019)	The *in silico* program "hinfluenzae _capsule _characterization" (Potts et al., 2019)	Biotype	Biotype (Genotype)	Biotype (Genotype retest)[c]	MLST
HINF-2014-1112	f	f*	Non-cap [f backbone: fcs2 fragmented (82.66% cov)]	I	I	ND	124
HINF-2015-1428	a	a*	Found genes for serotypes a,b, possible contamination[b]	II	II	ND	2053
HINF-2016-1709	Non-cap	Non-cap	Non-cap	III	II	II	46
HINF-2016-1715	f	f	f	II	I	I	124
HINF-2017-1785	e	e	E	I	V	I	386
HINF-2017-1788	Non-cap	Non-cap	Non-cap	III	VII	II	134
HINF-2017-1789	Non-cap	Non-cap	Non-cap	II	VII	II	57
HINF-2017-1793	Non-cap	Non-cap	Non-cap	II	VIII	II	199
HINF-2017-1802	Non-cap	Non-cap	Non-cap	III	II	II	142
HINF-2017-1808	Non-cap	Non-cap	Non-cap	III	VII	II	145
HINF-2017-1815	Non-cap	Non-cap	Non-cap	III	VIII	III	146
HINF-2017-1828	a	a*	Found genes for serotypes a,b, possible contamination[b]	II	VII	II	56
HINF-2017-1838	Non-cap	Non-cap	Non-cap	III	II	II	422
HINF-2017-1840	f	f	f	I	IV	I	124
HINF-2017-1851	Non-cap	Non-cap	Non-cap	II	VIII	II	136
HINF-2017-1917	e	e	e	III	IV	IV	18
HINF-2018-1932	Non-cap	Non-cap	Non-cap	IV	III	III	165
HINF-2018-1948	b	b	b	I	II	II	709
HINF-2018-1979	Non-cap	Non-cap	Non-cap	III	II	II	183
HINF-2018-1986	Non-cap	Non-cap	Non-cap	II	VIII	II	389
HINF-2018-1987	Non-cap	Non-cap	Non-cap	III	II	II	411
HINF-2018-2029	a	a*	Found genes for serotypes a,b, possible contamination[b]	III	II	II	2057
HINF-2018-2048	b	b*	Non-cap [b backbone: bexB fragmented (89.85% cov)]	I	I	I	Novel
HINF-2019-2063	f	f	f	II	I	I	124
HINF-2019-2079	Non-cap	Non-cap	Non-cap	IV	III	III	165
HINF-2019-2094	Non-cap	Non-cap	Non-cap	I	II	II	103
HINF-2019-2107	Non-cap	Non-cap	Non-cap	VII	V	V	1238
HINF-2019-2113	Non-cap	Non-cap	Non-cap	IV	I	I	Novel
HINF-2019-2195	Non-cap	Non-cap	Non-cap	I	II	II	3
HINF-2019-2210	Non-cap	Non-cap	Non-cap	II	III	III	107
HINF-2021-0022	Non-cap	Non-cap	Non-cap	ND	V	V	210
HINF-2021-0033	f	f*	Non-cap [f backbone: fcs1 fragmented (94.34% cov)]	ND	I	I	124
HINF-2021-0050	e	e*	e	ND	IV	IV	18
HINF-2021-0067	e	e*	e	ND	I	I	386
HINF-NML-07-01	d	d*	Found genes for serotypes d,e, possible contamination[b]	ND	IV	I	47
HINF-NML-21-007	c	c*	Found genes for serotypes f,c, possible contamination[b]	ND	II	II	9
HINF-REF4914	d	d*	Found genes for serotypes d,e, possible contamination[b]	ND	IV	I	47

ND, not done. *Confirmed using the PCR sequences from Maaroufi et al. (2007). [b]Contamination as defined by *in silico* 2 (Potts et al., 2019). [c]Using a coverage of 85% and an identity of 85%.

10.3389/fmicb.2022.1030242

TABLE 2 A total of eight hundred seventy-five invasive cases of *Haemophilus influenzae* were reported in Denmark from 2014 to 2021.

2014–2021	Phenotype	Genotype
Serotype		
A	3	3
b	62	62
c	0	0
d	0	0
e	13	13
f	81	81
Non-cap	479	479
Total	638 (72.9%)	638 (72.9%)

Of these, 638 isolates were tested both with phenotypic and molecular serotyping methods according to the *in silico* program "hicap" (Watts and Holt, 2019).

TABLE 3 A total of seven hundred and thirteen invasive cases of *Haemophilus influenzae* were reported in Denmark from 2014 to 2019.

2014–2019	Phenotype	Genotype
Biotypes		
I	165	162
II	209	218
III	117	111
IV	13	13
V	21	23
VI	4	5
VII	2	1
VIII	0	0
Total	533 (74.8%)	533 (74.8%)

Of these, 533 isolates were tested both with phenotypic and molecular methods.

permission to present and publish epidemiological data, see[5] accessed 30-06-2022,[6] accessed 30–06–2022). All presented data were anonymized.

Results

Characterization of the clinical isolates

Between 2014 and 2021, eight hundred seventy-five invasive *H. influenzae* isolates were received, and 638 (72.9%) of those isolates had both phenotypic and genotypic available data and were included in the study. All serotypes were represented except for serotypes c and d. One reference strain for Hic and two for Hid were included in the testing of capsular genes but not included in the clinical data (**Table 1**). The majority of the isolates were from blood cultures (91.8%), whereas 39 (6.1%) were from cerebrospinal fluid samples. No clinical information was available for the remaining 13 (2.0%) isolates (**Figure 1**).

The overall material included 159 (24.9%) typeable and 479 (75.1%) non-typeable isolates (refer to **Tables 2**, **3**).

Serotyping of the isolates

Across the collection, 638 (100%) and 632 (99.1%) isolates showed concordance between the phenotype and the *in silico* approaches developed by Watts and Holt (2019) and Potts et al., 2019; **Tables 1**, **2**. One serotype b and two serotype f isolates were typed as non-cap isolates, while three isolates were labeled as contaminated due to matches against capsular genes for several *H. influenzae* serotypes (refer to **Table 1**). The Hic and Hid reference isolates were correctly identified with the Watts and Holt *in silico* method, while the Potts et al. *in silico* method described them as contaminated although detecting possible capsular genes of serotype c and serotype d, respectively (**Table 1**).

In our reference laboratory, the Watts and Holt *in silico* method was chosen as the reference method. Therefore, we did not perform a second WGS test of all the isolates (six isolates in total) showing contaminating results with the Potts et al. *in silico* method (Potts et al., 2019) (**Table 1**). This might have improved the typing results of the six isolates when using the Potts et al. (2019) *in silico* method.

Biotyping

The most common biotypes were biotype II (39%), I (31%), and III (22%), but all biotypes except for biotype VIII were observed. Of the 533 isolates (2014–2019) tested for both phenotype and genotype, 506 (94.9%) isolates showed concordance, while 27 (5.1%) isolates showed divergent biotypes (**Tables 1**, **3**).

By lowering the coverage and identity to 85 and 85% when blasting for biotype sequences, it was possible to obtain complete concordance for both phenotype and genotype for eight of the 17 isolates with divergent biotypes (**Table 1**). Unfortunately, we were not able to retest the phenotype of the remaining 19 isolates, and we could therefore not rule out the possibility of diverting the biotype due to laboratory mistakes. The biotypes were not linked to a specific serotype, and each biotype was found to cover both capsular and non-capsular isolates (**Figure 2**).

Multilocus sequence typing types and phylogenetic tree

The capsular *H. influenzae* (a–f) were all distributed among six different clonal complexes (**Table 4**) as follows: ST23

5 https://en.ssi.dk/research

6 https://en.ssi.dk/about-us

FIGURE 2
Phylogenetic tree of all isolates. For each isolate, data are presented for the serotype (genotype with color), biotype (biotype with color), and clonal complex. Isolate Hinf Rd KW20 (GenBank nb. L42023) was used as a reference strain in the SNP alignment. Scale bar indicate substitutions per side.

complex (ST56, ST2053, and ST2057), ST6 complex (ST6, ST95, ST190, ST206, ST709, and ST1448), ST18 complex (ST18, ST122, and ST386), and ST124 complex (ST124, ST598, and ST1739).

The dominant ST types were ST6 (21 isolates), ST190 (28 isolates), and ST709 (six isolates), all of serotype b. ST18 consisted of 13 serotype e isolates, whereas ST124 consisted of 76 serotype f isolates. Finally, the four ST1739 were all serotype f. The reference strain serotype c belonged to the ST7 complex (ST9), and the two serotype d isolates belonged to the ST10 complex (ST47).

The *H. influenzae* non-cap isolates had 131 different STs, including 40 novel STs. The dominant STs for non-cap were ST103 (n = 29), ST12 (n = 15), and ST159 (n = 13), whereas novel STs were observed for 40 non-cap isolates (**Table 5**). None of the non-cap isolates were found to be clonal nor related phylogenetically to any of the capsular *H. influenzae* isolates.

Phylogenetic analysis of all isolates (**Figure 1**) shows that all clinical isolates with a capsule clustered both according to serotype and clonal complex. The biotype did not show any type-specific clustering.

Discussion

The characterization of *H. influenzae* isolates has traditionally been based on phenotypic methods (Kilian, 1976; Kilian et al., 1979; Nørskov-Lauritsen, 2014). With the introduction of the Hib vaccine four decades ago, the importance of *H. influenzae* capsular serotype distribution has increased due to continued monitoring of vaccine efficacy (Satola et al., 2007).

Serotyping of *H. influenzae* isolates has for many years mainly been based on slide agglutination serotyping that detects the expressed capsule (Satola et al., 2007; Potts et al.,

TABLE 4 Sequence type and clonal complex found among the *Haemophilus influenzae* isolates with a capsule.

ST	Clonal complex	A	B	C	D	E	F	Non-cap
56	ST-23 complex	1						0
2053	ST-23 complex	1						0
2057	ST-23 complex	1						0
6	ST-6 complex		21					0
95	ST-6 complex		1					0
190	ST-6 complex		28					0
206	ST-6 complex		1					0
709	ST-6 complex		6					0
1448	ST-6 complex		1					0
Novel	ST-6 complex		4					0
9	ST-7 complex			1				0
47	ST-10 complex				2			0
18	ST-18 complex					8		0
122	ST-18 complex					1		0
386	ST-18 complex					2		0
Novel	ST-18 complex					2		0
124	ST-124 complex						76	0
598	ST-124 complex						1	0
1739	ST-124 complex						4	0

2019); however, the slide agglutination serotyping is not always considered reliable, and false-positive Hib designations have been reported (Maaroufi et al., 2007; Satola et al., 2007; Nørskov-Lauritsen, 2014; Potts et al., 2019). With the description of the capsular gene sequences and the development of molecular typing methods, new PCR and WGS-based procedures for *H. influenzae* serotyping have been presented (Maaroufi et al., 2007; Satola et al., 2007; Nørskov-Lauritsen, 2014; Potts et al., 2019; Watts and Holt, 2019). In the study by Potts et al. (2019), 675 invasive isolates were collected from surveillance programs from 27 states in the United States, and 13 isolates of other origins were compared between the *in silico* program "hinfluenzae_capsule_characterization" described serotypes and the serotype results obtained by both PCR and slide agglutination tests. They found that the WGS serotyping method was 99.9% concordant with the slide agglutination tests and completely concordant with RT-PCR. Watts and Holt (2019) tested the *in silico* program "hicap" using 41 publicly available isolate WGS sequences. In 40 of the 41 isolates (98%), they obtained the correct serotype. The difference between the two *in silico* approaches is that the *in silico* program "hicap" uses Prodigal (Hyatt et al., 2010) to identify open reading frames (ORFs) in genomic assemblies and BLAST (Camacho et al., 2009) to identify capsule genes based on a custom reference database. The serotype is then predicted based on the detection of capsule genes. The approach by Potts et al. (2019) performs BLAST directly on the genome assemblies and then parses the identified cap genes for truncations and internal stop codons before predicting a serotype, rather than using external software for gene prediction.

This study, representing 73% of all clinical isolates from 2014 to 2021 from Denmark, found 100% concordance between the capsular genotype and the phenotype (slide agglutination test). This is comparable to the observations by Potts et al. (2019) and Watts and Holt (2019). This is the first study to show that *in silico* serotyping programs are feasible in a national *H. influenzae* surveillance program with the notion that the Hib vaccine efficacy depends on the phenotypic expression of the Hib polysaccharide and not the presence of the capsular sequences.

As a complementary approach to capsular serotyping, a biotyping setup has been described by Kilian in 1976 (Kilian, 1976; Kilian et al., 1979; Nørskov-Lauritsen, 2014). The system is based on eight biotypes defined by variations in the production of tryptophanase (indole production), urease, and ornithine decarboxylase (ODC) (Nørskov-Lauritsen, 2014). However, because the biotype is not related to the capsular serotype and therefore not considered an important part of the efficacy monitoring of the Hib vaccine in Denmark, phenotypic biotyping has not been performed since 2019. However, comparing the phenotypic biotype with the molecular biotype obtained from isolates sampled from 2014 to 2019 did show a high concordance between phenotypic and molecular biotyping. In total, 27 isolates (5.1%) showed diverging biotypes. Adjusting the percentage of coverage and identity could improve the concordance between phenotypic and molecular biotyping (**Table 1**). However, there was a mixture of capsular *H. influenzae* isolates and non-cap *H. influenzae* isolates among each of the specifically detected biotypes (**Figure 2**).

While the isolates expressing a capsule could be linked to a specific CC, this was not the case for the non-cap *H. influenzae* isolates, which exhibited a broad diversity of ST types (**Tables 4**, **5**, and **Figure 2**). Although the ST types in this study could be used to differentiate the capsular *H. influenzae* isolates from the non-cap isolates, it has previously been shown that MLST is not optimal for the identification of capsular *H. influenzae* isolates (Potts et al., 2019). However, we found that the MLST type can indicate the correct identification of the genotype because the capsular isolates appear to be part of only six clonal complexes (**Table 4**). Therefore, this can, in a national routine *H. influenzae* surveillance program for monitoring the effect of the Hib vaccine, be used as an additional confirmation of correct capsule identification, in that non-cap ST types belonging within these six CC or capsular isolates not belonging to these six CC, will need further evaluation before final capsule reporting.

Based on the results of this study, we recommend a workflow using genotyping either based on PCR (Maaroufi et al., 2007; Satola et al., 2007) or WGS (Potts et al., 2019; Watts and Holt, 2019). Because of the use of the Hib vaccine, we additionally suggest confirming the expression of the Hib capsule using a

TABLE 5 Sequence types for *Haemophilus influenzae* non-cap isolates.

ST	Non-cap	ST	Non-cap	ST	Non-cap	ST	Non-cap	ST	Non-cap	ST	Non-cap
2	2	146	2	266	5	567	3	1041	1	1850	1
3	10	147	8	276	4	582	2	1054	1	1904	2
11	4	155	7	311	1	589	1	1069	1	2031	2
12	15	156	1	334	2	597	5	1076	1	2156	1
13	1	159	13	348	2	608	1	1144	1	2332	2
14	5	160	3	349	2	634	3	1170	1	2333	2
34	5	161	1	351	2	652	6	1198	1	2519	1
41	6	165	12	367	10	653	1	1202	1	Novel	40
43	3	176	1	368	3	690	1	1215	1		
46	1	180	2	388	5	697	4	1218	4		
57	10	183	5	389	3	804	1	1220	1		
84	7	187	1	393	5	835	5	1238	1		
98	1	196	1	408	4	836	4	1379	1		
103	29	199	6	409	2	838	1	1382	1		
105	7	200	2	411	3	841	1	1401	2		
107	12	201	2	422	2	914	1	1426	1		
113	2	203	3	425	12	925	1	1497	2		
134	11	208	1	427	2	932	1	1521	1		
136	2	210	4	436	4	943	1	1524	2		
139	7	241	1	472	6	946	3	1591	2		
142	4	245	4	474	2	949	1	1714	1		
143	7	249	1	485	1	958	1	1727	1		
145	11	253	1	524	1	990	1	1773	1		
		262	1	531	2	995	2	1780	2		
		264	1	556	2	1034	11	1834	1		

latex agglutination test for vaccine surveillance. As an additional verification of the serotype, we propose MLST typing as clinical capsular isolates appear to cluster in specific clonal complexes (**Tables 4**, **5**), although the MLST itself cannot be used for serotype identification (Potts et al., 2019).

The weakness of this study is that by only looking at clinical isolates, the tested isolates representing all six serotypes are not equally distributed but dominated by serotypes f, b, and e (**Table 2**), while only a limited number of isolates with serotype a were detected, and none with serotype c and serotype d. The strength of the study is that the evaluation is based on clinical isolates received from Danish regional laboratories of clinical microbiology, and all the tested isolates showed a strong correlation between the results obtained with genotyping vs. phenotyping, in line with observations in other studies (Potts et al., 2019; Watts and Holt, 2019).

In conclusion, our study showed that there is a complete concordance between phenotypic serotyping and molecular-based methods for Danish clinical *H. influenzae* isolates. The concordance is 100% for both the described *in silico* serotyping methods, replacing laborious phenotypic methods with WGS-based *in silico* approaches in a clinical setting. In addition, biotyping shows a high concordance between molecular and phenotypic methods. Furthermore, in our Danish routine laboratory where epidemiological surveillance of *H. influenzae* for monitoring the effect of the Hib vaccine is an important routine task, the MLST type can be used as an indication of whether an isolated expresses a capsule or not. In that, all capsular-defined isolates in this study belonged to one of six clonal complexes depending on their capsule.

Data availability statement

The datasets presented in this study can be found in the online repository at the European Nucleotide Archive (ENA) under project no. PRJEB56415.

Author contributions

H-CS and KF designed the study, analyzed the data, and drafted the manuscript. All authors performed the genomic

analyses and reviewed the data, contributed to the manuscript, and critically revised the manuscript, and have approved the final manuscript.

Acknowledgments

Mikkel Benjamin Nielsen and Nadia Xenia Olsen are acknowledged for their skillful laboratory work and input to this study. We acknowledge the Danish departments of clinical microbiology for submitting *Haemophilus influenzae* isolates for national surveillance throughout the study period. This study is a part of the national surveillance program for severe *H. influenzae* infections.

Conflict of interest

The authors declare that the research was conducted in the absence of any commercial or financial relationships that could be construed as a potential conflict of interest.

Publisher's note

References

Bijlmer, H. A. (1991). World-wide epidemiology of *Haemophilus influenzae* meningitis; industrialized versus non-industrialized countries. *Vaccine* 9(Suppl. 1), S5-S9; discussion S25. doi: 10.1016/0264-410x(91)90172-3

Camacho, C., Coulouris, G., Avagyan, V., Ma, N., Papadopoulos, J., Bealer, K., et al. (2009). BLAST+: Architecture and applications. *BMC Bioinformatics* 10:421. doi: 10.1186/1471-2105-10-421

Croucher, N. J., Page, A. J., Connor, T. R., Delaney, A. J., Keane, J. A., Bentley, S. D., et al. (2015). Rapid phylogenetic analysis of large samples of recombinant bacterial whole genome sequences using gubbins. *Nucleic Acids Res.* 43:e15. doi: 10.1093/nar/gku1196

Fuursted, K., Hartmeyer, G. N., Stegger, M., Andersen, P. S., and Justesen, U. S. (2016). Molecular characterisation of the clonal emergence of high-level ciprofloxacin-monoresistant *Haemophilus influenzae* in the Region of Southern Denmark. *J. Glob. Antimicrob. Resist.* 5, 67–70. doi: 10.1016/j.jgar.2015.12.004

Hyatt, D., Chen, G. L., LoCascio, P. F., Land, M. L., Larimer, F. W., and Hauser, L. J. (2010). Prodigal: Prokaryotic gene recognition and translation initiation site identification. *BMC Bioinformatics* 11:119. doi: 10.1186/1471-2105-11-119

Jalalvand, F., and Riesbeck, K. (2018). Update on non-typeable *Haemophilus influenzae*-mediated disease and vaccine development. *Expert Rev. Vaccines* 17, 503–512. doi: 10.1080/14760584.2018.1484286

Kilian, M. (1976). A taxonomic study of the genus *Haemophilus*, with the proposal of a new species. *J. Gen. Microbiol.* 93, 9–62. doi: 10.1099/00221287-93-1-9

Kilian, M., Sørensen, I., and Frederiksen, W. (1979). Biochemical characteristics of 130 recent isolates from *Haemophilus influenzae* meningitis. *J. Clin. Microbiol.* 9, 409–412. doi: 10.1128/jcm.9.3.409-412.1979

Letunic, I., and Bork, P. (2021). Interactive tree of life (iTOL) v5: An online tool for phylogenetic tree display and annotation. *Nucleic Acids Res.* 49, W293–W296. doi: 10.1093/nar/gkab301

Maaroufi, Y., De Bruyne, J.-M., Heymans, C., and Crokaert, F. (2007). Real-time PCR for determining capsular serotypes of *Haemophilus influenzae*. *J. Clin. Microbiol.* 45, 2305–2308. doi: 10.1128/JCM.00102-07

Morris, S. K., Moss, W. J., and Halsey, N. (2008). *Haemophilus influenzae* type b conjugate vaccine use and effectiveness. *Lancet Infect. Dis.* 8, 435–443. doi: 10.1016/S1473-3099(08)70152-X

Nguyen, L. T., Schmidt, H. A., Von Haeseler, A., and Minh, B. Q. (2015). IQ-TREE: A fast and effective stochastic algorithm for estimating maximum-likelihood phylogenies. *Mol. Biol. Evol.* 32, 268–274. doi: 10.1093/molbev/msu300

Nørskov-Lauritsen, N. (2014). Classification, identification, and clinical significance of *Haemophilus* and *Aggregatibacter* species with host specificity for humans. *Clin. Microbiol. Rev.* 27, 214–240. doi: 10.1128/CMR.00103-13

Nørskov-Lauritsen, N., Pedersen, N., Lam, J. U. H., Nielsen, H. L., Kobel, C. M., Hansen, D. S., et al. (2021). *Haemophilus influenzae* one day in Denmark: Prevalence, circulating clones, and dismal resistance to aminopenicillins. *Eur. J. Clin. Microbiol. Infect. Dis.* 40, 2077–2085. doi: 10.1007/s10096-021-04247-w

Potts, C. C., Topaz, N., Rodriguez-Rivera, L. D., Hu, F., Chang, H.-Y., Whaley, M. J., et al. (2019). Genomic characterization of *Haemophilus influenzae*: A focus on the capsule locus. *BMC Genomics* 20:733. doi: 10.1186/s12864-019-6145-8

Sahl, J. W., Lemmer, D., Travis, J., Schupp, J. M., Gillece, J. D., Aziz, M., et al. (2016). NASP: An accurate, rapid method for the identification of SNPs in WGS datasets that supports flexible input and output formats. *Microb. Genom.* 2:e000074. doi: 10.1099/mgen.0.000074

Satola, S. W., Collins, J. T., Napier, R., and Farley, M. M. (2007). Capsule gene analysis of invasive *Haemophilus influenzae*: Accuracy of serotyping and prevalence of IS1016 among nontypeable isolates. *J. Clin. Microbiol.* 45, 3230–3238. doi: 10.1128/JCM.00794-07

Shabayek, S., and Spellerberg, B. (2018). Group B streptococcal colonization. Molecular Characteristics, and Epidemiology. *Front. Microbiol.* 9:437. doi: 10.3389/fmicb.2018.00437

Slotved, H. C., Fuursted, K., Kavalari, I. D., and Hoffmann, S. (2021). Molecular identification of invasive non-typeable group B *Streptococcus* isolates from Denmark (2015 to 2017). *Front. Cell. Infect. Microbiol.* 11:571901. doi: 10.3389/fcimb.2021.571901

Souvorov, A., Agarwala, R., and Lipman, D. J. (2018). SKESA: Strategic k-mer extension for scrupulous assemblies. *Genome Biol.* 19:153. doi: 10.1186/s13059-018-1540-z

Watts, S. C., and Holt, K. E. (2019). HICAP: In silico serotyping of the *haemophilus influenzae* capsule locus. *J. Clin. Microbiol* 57, e190–e119. doi: 10.1128/JCM.00190-19

frontiers | Frontiers in Microbiology

TYPE Original Research
PUBLISHED 17 November 2022
DOI 10.3389/fmicb.2022.1037343

OPEN ACCESS

EDITED BY
Bing Gu,
Guangdong Provincial People's Hospital,
China

REVIEWED BY
Jens Andre Hammerl,
Bundesinstitut für Risikobewertung,
Germany
Junliang Yin,
Yangtze University,
China

*CORRESPONDENCE
Jiahong Wu
657490050@qq.com
Yu Wang
wangzhongyuwy@163.com.

†These authors have contributed equally to this work

SPECIALTY SECTION
This article was submitted to Infectious Agents and Disease, a section of the journal Frontiers in Microbiology

RECEIVED 05 September 2022
ACCEPTED 24 October 2022
PUBLISHED 17 November 2022

CITATION
Cheng J, Zhou Y, Zhao X, Lu J, Wu J and Wang Y (2022) Development and clinical application of a endonuclease restriction real-time loop-mediated isothermal amplification (ERT-LAMP) assay for rapid detection of *Haemophilus influenzae*. *Front. Microbiol.* 13:1037343. doi: 10.3389/fmicb.2022.1037343

Development and clinical application of a endonuclease restriction real-time loop-mediated isothermal amplification (ERT-LAMP) assay for rapid detection of *Haemophilus influenzae*

Jinzhi Cheng[1†], Yuhong Zhou[2†], Xue Zhao[3], Jingrun Lu[3], Jiahong Wu[1*] and Yu Wang[3*]

[1]School of Basic Medical Sciences, Guizhou Medical University, Guiyang, China, [2]School of Public Health, The Key Laboratory of Environmental Pollution Monitoring and Disease Control, Ministry of Education, Guizhou Medical University, Guiyang, China, [3]Department of Clinical Laboratory, The First People's Hospital of Guiyang, Guiyang, Guizhou, China

Haemophilus influenzae is a main human pathogen that results in a series of diseases in children and adults, such as pneumonia, bacteremia, and meningitis. Although there are many detection methods, they cannot meet the requirements of an early diagnosis. For the prevention and control of *H. influenzae* infection, quick, sensitive, and particular diagnostics are crucial. Loop-mediated isothermal amplification (LAMP) coupled with restricted endonuclease digestion and real-time fluorescence (*H. influenzae*-ERT-LAMP) detection was employed to diagnose *H. influenzae*. *H. influenzae*-ERT-LAMP combines LAMP amplification, restriction endonuclease cleavage, and real-time fluorescence identification into a single-pot reaction, allowing for the rapid identification of *H. influenzae* in 40 min. The outer membrane protein (OMP) P6 gene of *H. influenzae* was employed to build a sequence of *H. influenzae*-ERT-LAMP primers. The limit of detection (LoD) of *H. influenzae*-ERT-LAMP test was 40fg of genomic DNA per reaction, and the non-*H. influenzae* templates did not provide positive outcomes. To investigate the applicability of *H. influenzae*-ERT-LAMP method in clinical sample detection, 30 sputum specimens were obtained from individuals suspected of being infected with *H. influenzae*. *H. influenzae*-ERT-LAMP outcomes were in total agreement with LAMP-LFB and PCR. The *H. influenzae*-ERT-LAMP assay provides rapid, accurate, and sensitive detection making it a promising screening strategy in clinical and basic lab settings.

KEYWORDS

***Haemophilus influenzae*, loop-mediated isothermal amplification, restriction endonuclease digestion, real-time fluorescence detection, *H. influenzae*-ERT-LAMP**

Introduction

One of the primary pathogens of community-acquired respiratory airway infection in children is the gram-negative bacteria *Haemophilus influenzae*, which is often detected in the upper respiratory airways of healthy children and adults (Wang et al., 2008), predominantly leads to significant meningitis, epiglottitis, bacteremia, and pneumonia (Shah et al., 2021). However, the infection rate of *H. influenzae* type b (Hib) decreased after introducing the Hib vaccine, which reveals its effectiveness, but other non-Hib-causing invasive infections and antibiotic resistance are increasing (Wen et al., 2020). Therefore, for the early stage of *H. influenzae*, rapid and accurate identification is very necessary for disease prevention and control.

Fastidious in its requirements, *H. influenzae* needs NAD and an iron supply from hemoglobin, hematin, or hemin (Tristram et al., 2007). The morphology of *H. influenzae* colonies is difficult to differentiate from other spp. of *Haemophilus*, such as *Haemophilus parainfluenzae* (*H. parainfluenzae*). Moreover, traditional identification methods, such as population morphology, basic growth analysis, and serological determination, are also very time-consuming and complex, but they are still used in most laboratories (Tristram et al., 2007). As a result, cultivating and identifying in the clinic takes more time and effort. Rapid, sensitive, and specific methods must be established to obtain the fast and accurate identification of *H. influenzae*.

With the progression of molecular procedures, polymerase chain reaction (PCR) and PCR-based tests (e.g., single PCR, multiplex PCR, real-time PCR, and GeneXpert techniques) have been employed for the identification of *H. influenzae* (Van Ketel et al., 1990). Although these approaches have excellent analytical abilities, the necessities for special equipment, expensive reagents, and long testing procedures limit their application in nursing points and basic laboratories.

Loop-mediated isothermal amplification (LAMP) has been employed for the identification of *H. influenzae* in order to overcome the limitations of PCR technology (Kim et al., 2011; Diallo et al., 2021). LAMP requires four or two loop primers, which recognize six or eight or both regions on target profiles; nucleic acid amplification can be achieved with high efficiency using this method; it has been performed in recognition of many pathogens, like bacteria, viruses, fungi, and emerging/remerging infective agents (Notomi et al., 2000; Takano et al., 2019; Wang et al., 2021). Recently, there are several ways to identify LAMP amplification products, including using a specific fluorescent dye for dsDNA, electrophoresis of amplicons, turbidity due to magnesium pyrophosphate, nanoparticle-based lateral flow biosensor (LFB) and metal ion indicators (Wang et al., 2017). However, the judgment of outcome subjectivity, post-detection procedures require time, real-time detection cannot be achieved, and carryover contamination is a major problem with LAMP reactions (Iseki et al., 2007; Aonuma et al., 2010; Liang et al., 2012). Opening reaction tubes is unrecommended by a manufacturer of LAMP kits, or it requires separate equipment and facilities, further reducing the accuracy. This study introduces a novel endonuclease restriction real-time LAMP assay combined with real-time fluorescence detection. Then, the optimal reaction conditions, specificity, sensitivity and practicability of *H. influenzae*-ERT-LAMP assay were validated using strain pure cultures and clinical samples.

Materials and methods

Reagents and instruments

TianJin HuiDeXin Biotech Co., Ltd. (Tianjin, China) provided the DNA isothermal amplification kits, Nb.*BsrDI*, a polymer nanoparticle-based LFB, and visual detection reagent (VDR), while Baitaike Biotech Co., Ltd. provided the genomic DNA kit for nucleic acid sorting and purification (Beijing, China). Nano-Drop ND-2000 (Beijing, China) was employed to measure the purity and quantity of nucleic acid in A260/280.

Design of *Haemophilus influenzae*-ERT-LAMP primers

A set of *H. influenzae*-ERT-LAMP primers was formed depending on the ERT-LAMP technology pathway using PrimerExplorer V5[1] depending on the *H. influenzae* OMP P6 gene (Wang et al., 2016). A blast analysis showed that *H. influenzae*-ERT-LAMP primers are specific for *H. influenzae.* The dark quenchers employed were Black Hole Quencher-1, and the fluorophores utilized were FAM, which was monitored in real-time by the *H. influenzae*-ERT-LAMP system. The primers data (sequence, length, and alteration) is illustrated in Figure 1 and Table 1, and the length of the targeted sequence was 238 bp. All primers (HPLC purification level) were synthesized and purified by Tsingke Biotech Co., Ltd. (Kunming, China).

Strains of bacteria and DNA preparation

This investigation included 20 clinically sorted strains, 3 *H. influenzae* strains, and 17 non-*H. influenzae* strains were employed, along with laboratory bacteria, reference strains (ATCC10211), and other strains (Table 2). All strains were employed to enrich and obtain genomic DNA templates (DNA minikits; Baitaike, Beijing, China). In order to utilize the obtained genomic templates, they were examined using an ultraviolet spectrophotometer (NanoDrop ND-2000, Beijing, China) at A260/280 and preserved at 20°C.

1 https://primerexplorer.jp

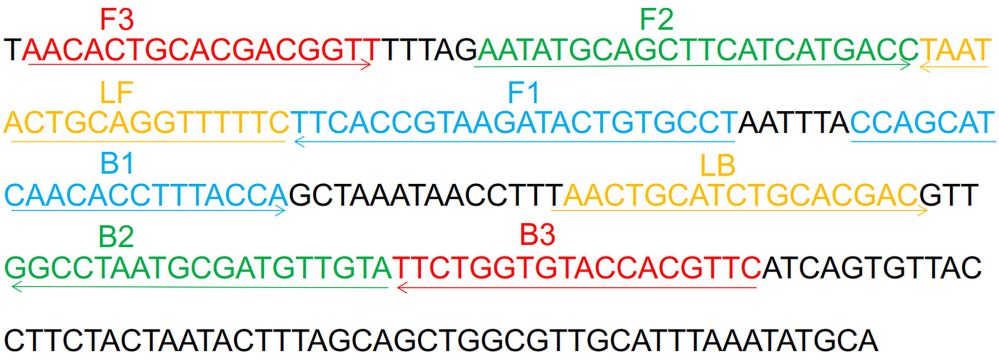

FIGURE 1
Sequence and location of OMP P6 gene used to design *Haemophilus influenzae*-ERT-LAMP primers. The nucleotide sequences of the sense strand of OMP P6 are listed. Right arrows and left arrows indicate sense and complementary sequences that are used.

TABLE 1 Primers used in this study.

Assay type	Primers name[a]	Sequences and modifications (5′-3′)[b]	Length[c]	Gene
ERT-LAMP	F3	AACACTGCACGACGGTT	17 nt	OMPP6
	B3	GAACGTGGTACACCAGAA	18 nt	
	EFIP	5'-FAM-TGCAATGAGGCACAGT(BHQ1)ATCTTACGGTGAA-AATATGCAGCTTCATCATGACC-3'	51 mer	
	BIP	CCAGCATCAACACCTTTACCA-TACAACATCGCATTAGGCC	41 mer	
	LF	GAAAAACCTGCAGTATTA	18 nt	
	LB	AACTGCATCTGCACGAC	17 nt	
LAMP	F3	AACACTGCACGACGGTT	17 nt	
	B3	GAACGTGGTACACCAGAA	18 nt	
	FIP	AGGCACAGTATCTTACGGTGAA-AATATGCAGCTTCATCATGACC	45 mer	
	FIP*	biotin-AGGCACAGTATCTTACGGTGAA-AATATGCAGCTTCATCATGACC	45 mer	
	BIP	CCAGCATCAACACCTTTACCA-TACAACATCGCATTAGGCC	41 mer	
	LF	GAAAAACCTGCAGTATTA	18 nt	
	LF*	FAM-GAAAAACCTGCAGTATTA	18 nt	
	LB	AACTGCATCTGCACGAC	17 nt	
PCR	Hi-PCR-F	AACTTTTGGCGGTTACTCTG	20 nt	
	Hi-PCR-R	CTA ACACTGCACGACGGTTT	20 nt	

[a]FIP*, 5′-labeled with biotin when used in the LAMP-LFB assay; LF*, 5′-labeled with FAM when used in the LAMP-LFB assay; B, backward; BIP, backward inner primer; EFIP, new forward inner primer; F, forward; FIP, forward inner primer; LB, loop backward; LF, loop forward. [b]FAM, 6-carboxy-fluorescein; BHQ1, black hole quencher 1. [c]mer:monomeric; nt: nucleitide.

The standard *Haemophilus influenzae*-ERT-LAMP, LAMP-LFB and PCR reaction

To assess the feasibility of *H. influenzae*-ERT-LAMP primers, *H. influenzae*-ERT-LAMP amplification combinations were carried out in the last volume of 25 μl that included 0.4 μM EFIP primers, 0.4 μM BIP primers, 0.2 μM each LF and LB primers, 0.1 μM each F3 and B3 primers, 12.5 μl 2× reaction mix, 1 μl of *Bst* DNA polymerase, 1 μl of Nb.*BsrDI* endonuclease, 1 μl DNA model and double distilled water (ddH_2O) were added to 25 μl. Applied Biosystems Co., Ltd.'s ABI 7500 real-time fluorescence PCR system, Eiken Chemical Co., Ltd.'s LA-500 real-time turbidity system, and agarose gel electrophoresis were utilized to evaluate the LAMP reactions and to optimize the amplification settings (such as the assay's time and temperature). Utilizing ABI 7500 real-time system, the PCR parameters of holding phase at 65°C for 60 s, 40 rounds of denaturation at 65°C for 10 s, and extension at 65°C for 40 s were employed to observe the *H. influenzae*-ERT-LAMP combinations. FAM channels were employed to record fluorescence measurements concurrently.

The standard LAMP-LFB reaction was performed in a mixture of 25 μl (Wang et al., 2017). The reaction system was 25 μl and included a 2× reaction mix of 12.5 μl, 0.4 μM each FIP* and BIP primers, 0.2 M each of LF* and LB primers, 0.1 μM each of F3 and B3 primers, 1 μl (8 U) of *Bst* DNA polymerase,

TABLE 2 The pathogen used in this study.

Bacteria species	Strain no. (source of strain)[a]	No. of strains	*Haemophilus influenzae*-ERT-LAMP[b]
Haemophilus influenzae	ATCC10211	1	P
Haemophilus influenzae	Isolated strains(GFPH)	3	P
Salmonella	ATCC14028	1	N
Staphylococcus aureus	ATCC29213	1	N
Pseudomonas aeruginosa	ATCC27853	1	N
Candida albicans	ATCC10231	1	N
Escherichia coli	ATCC25922	1	N
Enterococcus faecalis	ATCC29212	1	N
Streptococcus pneumoniae	ATCC49619	1	N
Neisseria meningitidis	ATCC13090	1	N
Vibrio cholerae	ATCC14731	1	N
Staphylococcus epidermidis	Isolated strains(GFPH)	1	N
Enterococcus faecium	Isolated strains(GFPH)	1	N
Viridans streptococcus	Isolated strains(GFPH)	1	N
Proteusbacillus Vulgaris	Isolated strains(GFPH)	1	N
Acinetobacter baumannii	Isolated strains(GFPH)	1	N
Candida tropicalis	Isolated strains(GFPH)	1	N
Candida parapsilosis	Isolated strains(GFPH)	1	N
Stenotrophomonas maltophilia	Isolated strains(GFPH)	1	N

[a]GFPH, The First People's Hospital of Guiyang; ATCC, American Type Culture Collection. [b]P, positive; N, negative. Only genomic DNA templates from *H. influenzae* could be detected by ERT-LAMP assay, indicating the extremely high specificity of the method.

1 µl of DNA template, and ddH_2O were supplemented to 25 µl. In order to terminate the amplification response, it was incubated at 80°C for 5 min after 40 min at 65°C. LFB was employed to track all LAMP-LFB outcomes. In the LFB test, both CL and TL simultaneously emerged, indicating positive findings, while in the case of negative amplification, only CL was visible.

PCR amplification reaction combinations were performed in a 25 µl reaction volume, including 12.5 µl Premix Taq (TaKaRa), Hi-PCR-F primers 0.5 µl and Hi-PCR-R 0.5 µl, 1 µl of DNA template and ddH_2O were added to 25 µl. To detect *H. influenzae*, the reaction environments were adapted to use 35 cycles, each relating 30 s denaturation at 94°C, 30 s of annealing at 50°C, and 30 s of addition at 72°C. Following the last cycle, all reactions were preserved for a further 10 min at 72°C. Our findings were displayed by resolution in agarose gel electrophoresis followed by ethidium bromide staining.

Sensitivity and specificity of the *Haemophilus influenzae*-ERT-LAMP assay

To optimize the *H. influenzae*-ERT-LAMP test and examine the detection limit, 238 bp of the *H. influenzae* OMP P6 gene was chemically synthesized and cloned into pUC57 plasmid (herein referred to as pUC57-Hi-OMP P6 DNA) by Tsingke Biotech Co., Ltd. (Kunming, China), which contained the amplification target of *H. influenzae*-ERT-LAMP primers. The pUC57-Hi-OMP P6 DNA was used as a template for optimizing the H. influenzae-ERT-LAMP system and for the determination of sensitivity. The initial concentrations of pUC57-Hi-OMP P6 DNA were 4 µg, then ten-fold serial dilutions (400 pg, 40 pg, 4 pg, 400 fg, 40 fg, 4 fg, and 400 ag) of pUC57-Hi-OMP P6 DNA were arranged. The consecutive dilutions of pUC57-Hi-OMP P6 DNA were employed for identifying the limit of detection (LoD) of *H. influenzae*-ERT-LAMP, and a volume of 1 µl of these profiles were employed for *H. influenzae*-ERT-LAMP reactions.

For the *H. influenzae*-ERT-LAMP specificity examination, the *H. influenzae*-ERT-LAMP reaction was carried out in the environment illustrated above with pure genomic models from different strains (Table 2). Each specimen was examined separately at least twice.

Applicability of the *Haemophilus influenzae*-ERT-LAMP assay to clinical samples

To evaluate the feasibility of *H. influenzae*-ERT-LAMP test in clinical specimen identification, we obtained 30 specimens of individuals who were suspected of infecting with *H. influenzae* at *the First People's Hospital of Guiyang*. All sputum samples were confirmed as *H. influenzae* using LAMP-LFB and PCR. The gathering and examination of these DNA templates were authorized by *the First People's Hospital of Guiyang* (Ethical approval No.G2020-S001).

Results

Confirmation of *H. influenzae*-ERT-LAMP products

Haemophilus influenzae-ERT-LAMP method combines isothermal amplification, restriction endonuclease digestion, and real-time fluorescence detection in a single reaction vessel based on the standard (Iseki et al., 2007; Wang et al., 2016). Examine the reliability of the ERT-LAMP primers for the H. influenzae test (Table 1). Employing pUC57-Hi-OMP P6 DNA as a template, *H. influenzae*-ERT-LAMP combinations were run for 40 min at a fixed temperature of 65°C. Next, real-time fluorescence PCR and

agarose gel electrophoresis were employed to verify amplification results. Figure 2A shows that the quenching production was detected utilizing a 7,500 real-time PCR system as a strong rise in FAM signals in the positive findings but not in the negative or blank controls. The *H. influenzae*-ERT-LAMP products were then electrophoresed to confirm that the anticipated ladder bands were present (Figure 2B).

Hence, the ERT-LAMP primers for OMP P6 gene recognition in the present research effectively established the *H. influenzae*-ERT-LAMP assay. Also, the best reaction temperature for *H. influenzae*-ERT-LAMP was established, with 67°C being the highest possible option for *H. influenzae*-ERT-LAMP reaction (Supplementary Figure S1).

Evaluation of sensitivity of the *Haemophilus influenzae*-ERT-LAMP assay

Ten-fold serial dilutions of pUC57-Hi-OMP P6 DNA, from 400 pg to 400 ag copies per 1 µl, were employed to detect the sensitivity of *H. influenzae*-ERT-LAMP test. Quenching production can be observed as a vigorous rise in FAM signals, and positive amplification can be noticed in about 40 min. The LoD of *H. influenzae*-ERT-LAMP test for identifying pUC57-Hi-OMP P6 DNA was 40 fg of genomic DNA per tube (Figure 3).

Analytical specificity of the *Haemophilus influenzae*-ERT-LAMP assay

In this investigation, the specificity of *H. influenzae*-ERT-LAMP test was assessed with the genomic templates obtained from the reference strains ATCC10211, 3 *H. infuenzae* strains, and 17 *non-H. infuenzae* bacterial pathogens (Table 2). Figure 4 reveals that the positive outcomes were particularly yielded with the genomic DNA from *H. infuenzae*, while the negative outcomes were identified with *non-H. infuenzae* strains. These outcomes revealed that the *H. influenzae*-ERT-LAMP test defined here was definite to target sequence detection.

Evaluation of the *Haemophilus influenzae*-ERT-LAMP assay by using clinical sample

To define the applied application of novel *H. influenzae*-ERT-LAMP detection of *H. influenzae* in a clinical sample, 30 sputum samples were divided into three equal parts and then simultaneously detected using the *H. influenzae*-ERT-LAMP, LAMP-LFB assay, and PCR assays. Of the 30 sputum samples, 6 samples were *H. influenzae* positive (Table 3). *H. influenzae*-ERT-LAMP results (Figure 5) showed completely in accordance with the LAMP-LFB (Figure 6) and PCR asssy (Figure 7). These

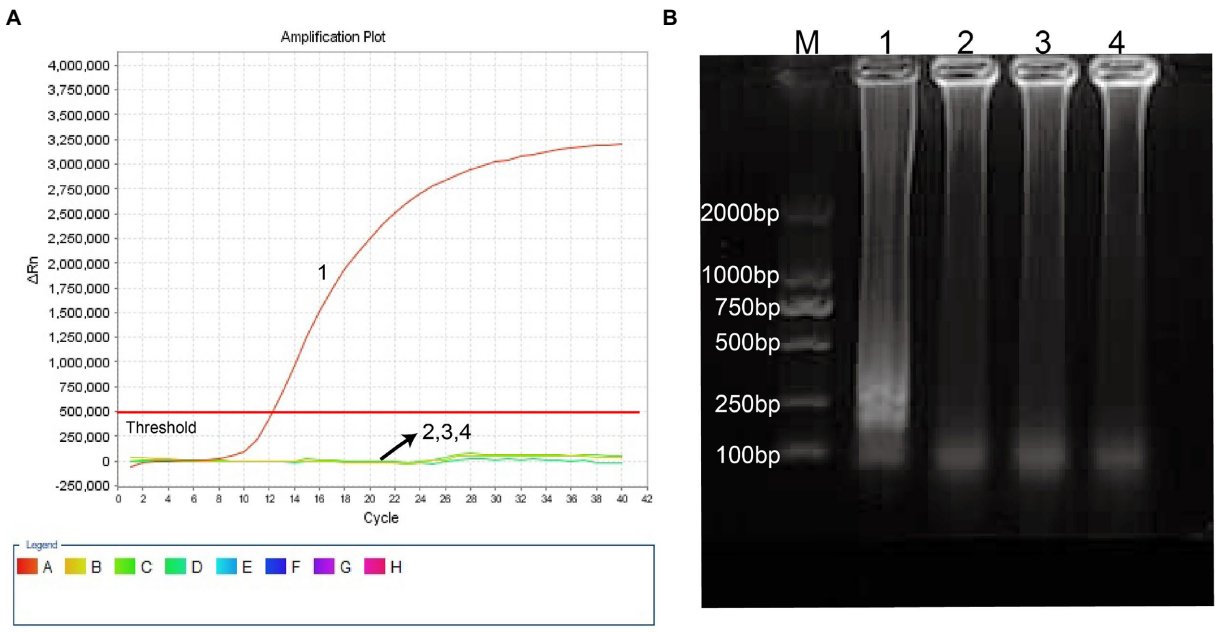

FIGURE 2
Identification and confirmation of *H. influenzae*-ERT-LAMP products. **(A)** the *H. influenzae*-ERT-LAMP was analyzed by means of real-time format, and the figures were obtained from FAM (labeling EFIP of P6 gene sequence) channels. Signals A1 indicate pUC57-Hi-OMP P6 DNA in FAM channels and signals A2, A3 and A4 indicate negative control (*Candida albicans*), negative control (*Escherichia coli*) and blank control (double-distilled water, DW). **(B)** agarose gel electrophoresis applied to *H. influenzae*-ERT-LAMP products; lane BM, DL 2000bp DNA markers, lane B1 positive *H. influenzae*-ERT-LAMP products, lane B2, B3 and B4 indicate negative control (*Candida albicans*), negative control (*Escherichia coli*) and blank control (DW).

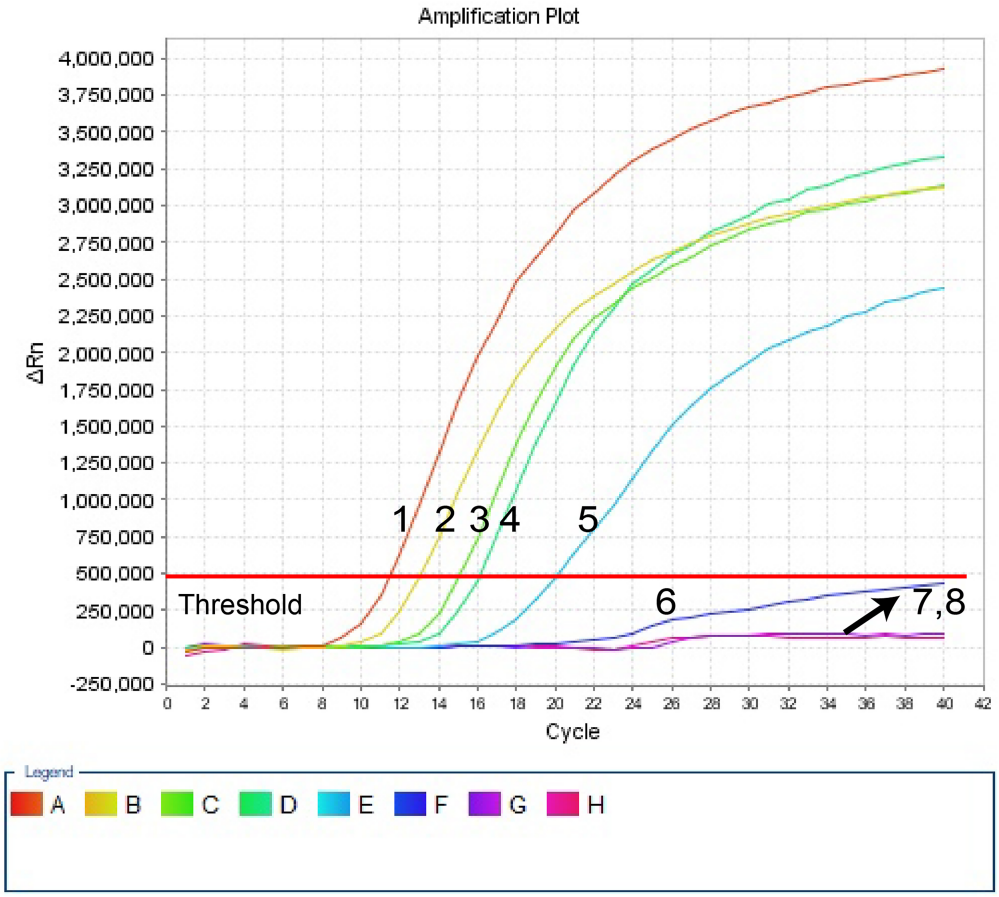

FIGURE 3
Sensitivity of *H. influenzae*-ERT-LAMP assay. Signals 1–7 indicate a series of dilutions (400 pg, 40 pg, 4 pg, 400 fg, 40 fg, 4 fg, 400 ag) of pUC57-Hi-OMP P6 DNA and a blank control (DW) were operated according to standard *H. influenzae*-ERT-LAMP reactions.

outcomes demonstrated that the *H. influenzae*-ERT-LAMP assay offers a rapid, reliable, and sensitive recognition of *H. influenzae*, which can be employed as a possible screening method for *H. influenzae* in the clinical and basic laboratory environment.

Discussion

The World Health Organization (WHO) closely monitors *H. influenzae*, which mostly impacts children under five and people over 65 years of age. It is alleged to be the second most prevalent bacterial infection causing pneumonia in Chinese children (Heliodoro et al., 2020). Hib vaccine is a beneficial and affordable intervention to protect children in mainland China against pneumonia, meningitis, and other illnesses that can be prevented by vaccination (Ning et al., 2018). Non-typeable *H. influenzae* (NTHi) strains have been a worldwide issue since the Hib vaccine was developed since they mostly induce the upper respiratory tract, otitis media, and severe invasive illness (Li et al., 2020). Therefore, it is crucial to distinguish *H. influenzae* quickly, accurately, and sensitively from other pathogenic respiratory tract organisms in order to stop and manage *H. influenzae* outbreaks. Traditional detection techniques, such as population morphology, basic growth analysis, and serological testing, often fall short of the time and sensitivity required for rapid detection.

Herein, we document the new *H. influenzae*-ERT-LAMP chemistry, which successfully combined the conventional LAMP chemistry and restriction endonuclease digestion with fluorescent reporter dye in real-time for checking the result of LAMP products during each amplification cycle, was developed and assessed for nucleic acid examination of clinical samples. Previous studies have demonstrated that *H. influenzae* OMP P6 gene, which is a highly conserved gene and has become a potential vaccine component and is more suitable for the identification of *H. influenzae* than other genes (Murphy et al., 1986; Nelson et al., 1991; Karalus and Murphy, 1999). Therefore, OMP P6 gene was chosen as the target gene for rapid diagnosis of *H. influenzae*.

In our study, *H. influenzae*-ERT-LAMP only needs a reasonably simple fluorescent tool to preserve a fixed temperature for 40 min (Figure 3). As compared to *H. influenzae* LAMP techniques used in previous studies, the *H. influenzae*-ERT-LAMP method detected *Haemophilus influenzae* results in real-time by

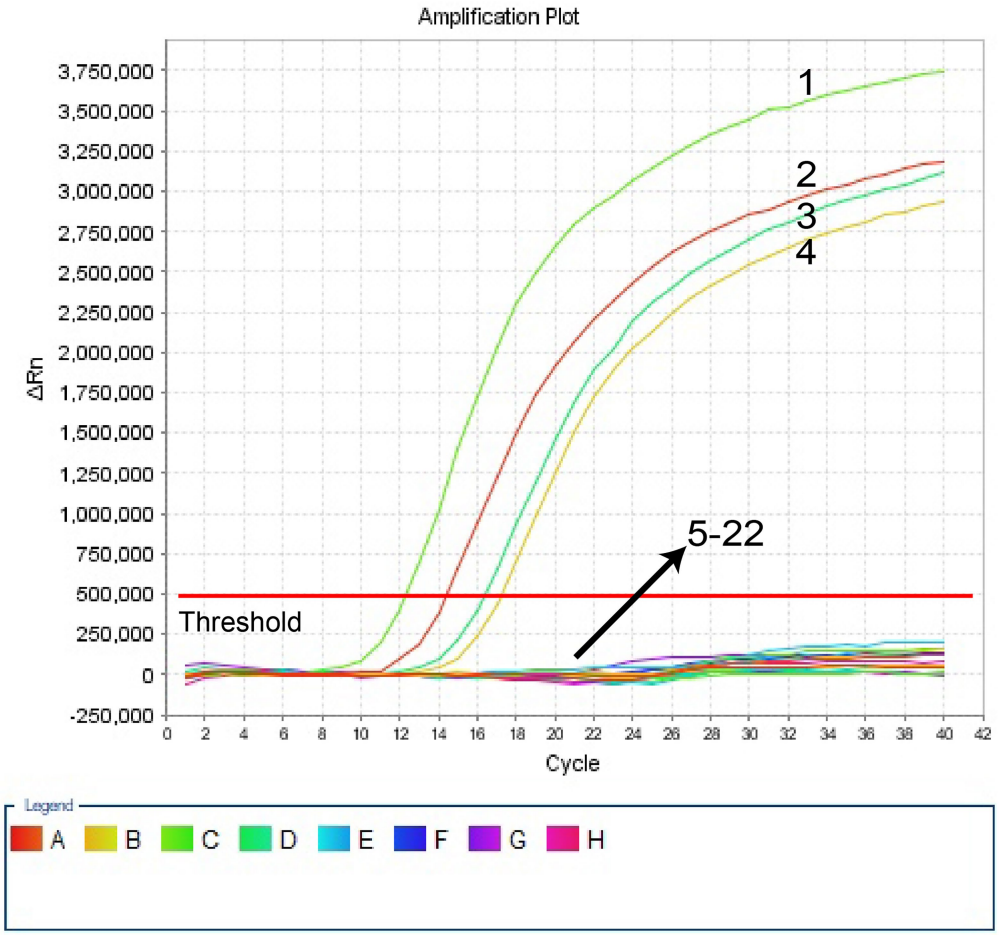

FIGURE 4
Specificity of *H. influenzae*-ERT-LAMP detection for different strains. The *H. influenzae*-ERT-LAMP amplifications were performed using different genomic DNA templates and were monitored by means of real-time detection. Signals 1, Positive control (*H. influenzae* ATCC10211), signals 2–4, *H. influenzae* isolated strains; signals 5, *Salmonella* ATCC14028; signals 6, *Staphylococcus aureus* ATCC29213 signals 7, *Pseudomonas aeruginosa* ATCC27853; signals 8, *Candida albicans* ATCC10231; signals 9, *Escherichia coli* ATCC25922; signals 10, *Enterococcus faecalis* ATCC29212; signals 11, *Streptococcus pneumoniae* ATCC49619; signals 12, *Neisseria meningitidis* ATCC13090; signals 13, *Vibrio cholerae* ATCC14731; signals 14, *Staphylococcus epidermidis* isolated strains; signals 15, *Enterococcus faecium* isolated strains; signals 16, *Viridans streptococcus* isolated strains; signals 17, *Proteusbacillus Vulgaris* isolated strains; signals 18, *Acinetobacter baumannii* isolated strains; signals 19, *Candida tropicalis* isolated strains; signals 20, *Candida parapsilosis* isolated strains; signals 21, *Stenotrophomonas maltophilia* isolated strains; signals 22, a blank control (DW).

TABLE 3 Comparison of *H. influenzae*-ERT-LAMP, LAMP-LFB, and PCR Assays for the Detection of *H. influenzae*.

Detection method[a]	Sputum samples ($n = 30$)		Time consumption (minutes)
	Positive	Negative	
H. influenzae-ERT-LAMP	6	24	40
LAMP-LFB	6	24	45
PCR	6	24	180

[a]*H. influenzae*-ERT-LAMP, *H. influenzae* endonuclease restriction real-time loop-mediated isothermal amplification.

real-time fluorescence examination, which excludes the requests of particular reagents (e.g., pH indicators), complicated processes (e.g., electrophoresis) and costly devices (e.g., real-time turbidity; Cao et al., 2022). Furthermore, carryover contamination is effectively avoided by closing the *H. influenzae*-ERT-LAMP reaction tubes during the experiment. However, due to the need for COVID-19 detection, PCR laboratories have been established in all hospitals above the second level of Chinese mainland, and *H. influenzae*-ERT-LAMP assay has a good prospect of popularization and application (Wang et al., 2021).

The whole procedure of *H. influenzae*-ERT-LAMP recognition, containing genomic DNA template development (20 min) and ERT-LAMP reaction (40 min), was completed within 60 min, improving the usage of a temperature-modulating device, and does not need more agarose gel identification or pyrosequencing. In addition, *H. influenzae*-ERT-LAMP has a high sensitivity. The LoD of *H. influenzae*-ERT-LAMP assay was 40 fg of each genomic DNA per reaction and 1–1,000 times more than that of the PCR method (Falla et al., 1994; Corless et al., 2001; Tian et al., 2012). It can amplify the targets at the LoD level in a shorter time, thus considerably reducing the total test time (Table 3).

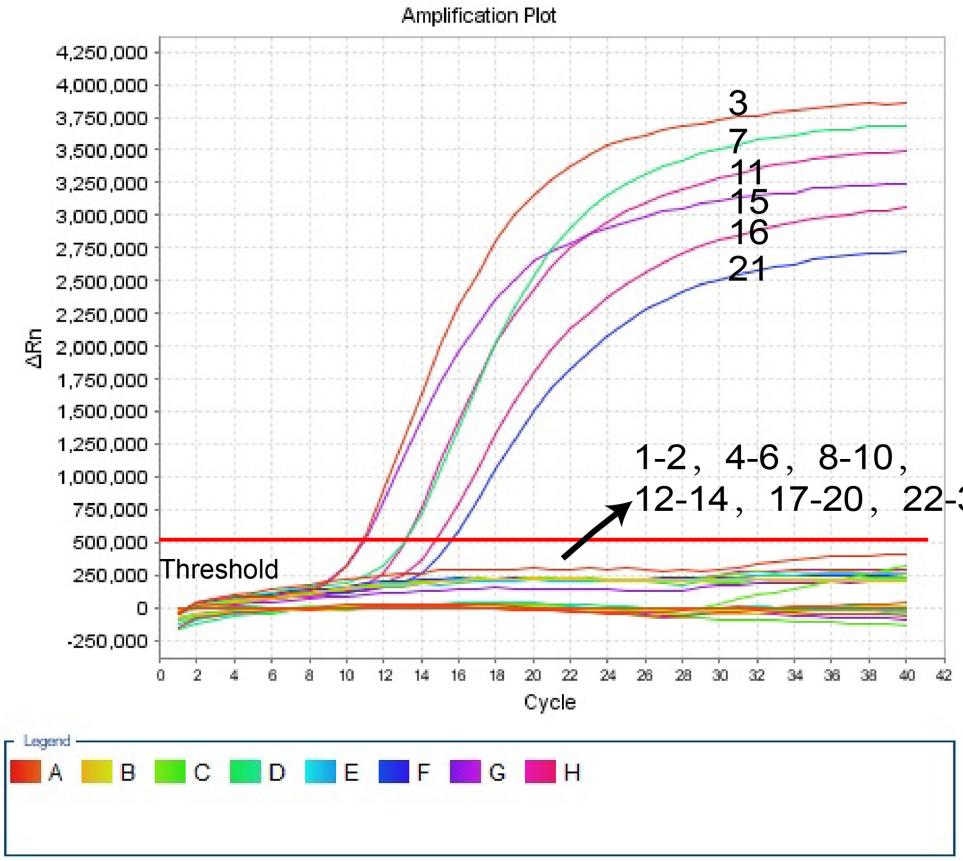

FIGURE 5
The *H. influenzae*-ERT-LAMP assay for detecting *H. influenzae* in clinical samples. Signals 3, 7, 11, 15, 16, 21 indicate *H. influenzae* in clinical samples in FAM channels. Signals 1–2, 4–6, 8–10, 12–14, 17–20, 22–30 represented the negative results.

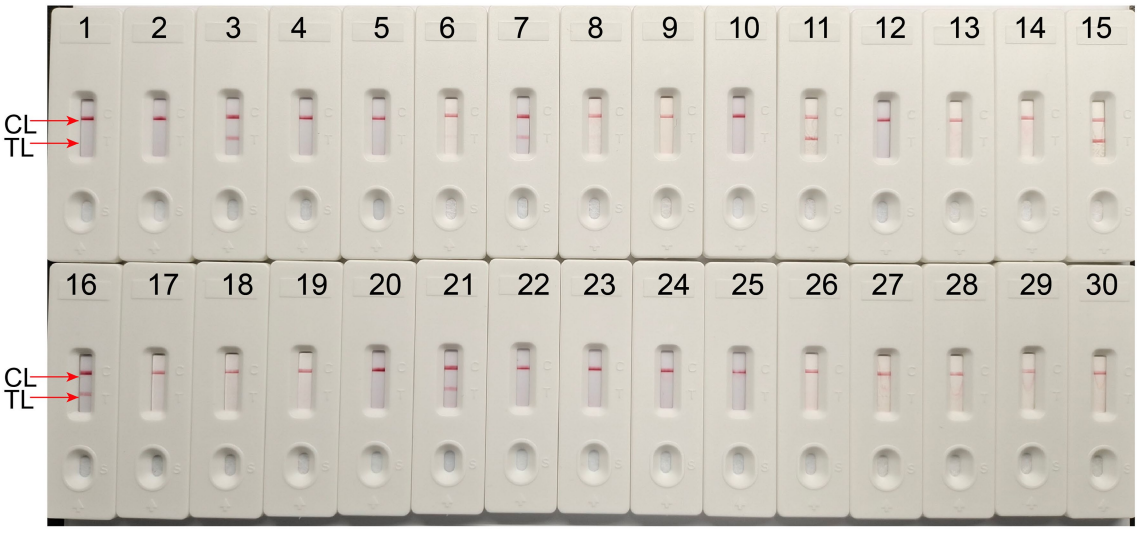

FIGURE 6
The LAMP-LFB assay for detecting *H. influenzae* in clinical samples. Later flow biosensor was applied for detecting LAMP amplicons. The numbers 3, 7, 11, 15, 16, 21 represented the positive results. 1–2, 4–6, 8–10, 12–14, 17–20, 22–30 represented the negative results.

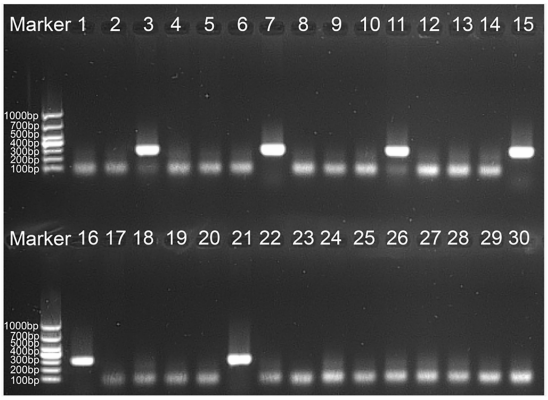

FIGURE 7
The PCR assay for detecting *H. influenzae* in clinical samples. The numbers 3, 7, 11, 15, 16, 21 represented the positive results. 1–2, 4–6, 8–10, 12–14, 17–20, 22–30 represented the negative results.

In addition to high sensitivity, *H. influenzae*-ERT-LAMP test is highly specific. For *the H. influenzae*-ERT-LAMP assay specificity test, positive findings were reported for *H. influenzae* samples; however, non-*H. influenzae* strains did not produce any positive amplifications (Figure 4). Furthermore, the unique *H. influenzae*-ERT-LAMP test proposed here can accurately distinguish target sequences with elevated specificity, perform in a single isothermal amplification stage, and provide interpretable data (Wang et al., 2016). For a further detailed evaluation of the practicality of *H. influenzae*-ERT-LAMP method to target pathogens, 30 clinical sputum samples were randomly tested using *H. influenzae*-ERT-LAMP, LAMP-LFB detection, and PCR, respectively. *H. influenzae*-ERT-LAMP assay showed elevated specificity for *H. influenzae* strains in sputum samples, consistent with the LAMP-LFB and PCR method (Table 3). Based on these characteristics, *H. influenzae*-ERT-LAMP procedure is technically simple, quick, and low cost, delivering applied solutions for medical and disease control laboratories, particularly in reduced resource parameters.

Conclusion

We concluded that *H. influenzae*-ERT-LAMP assay targeted the OMP P6 gene of *H. infuenzae* and was effectively designed in the present study. In the application and assessment procedure, *H. influenzae*-ERT-LAMP method showed good specificity and sensitivity by detecting reference strains and clinical samples. Therefore, the *H. influenzae*-ERT-LAMP assay provides a novel choice for reliable, quick and simple detection of *H. influenzae*.

Data availability statement

The original contributions presented in the study are included in the article/Supplementary material, further inquiries can be directed to the corresponding author.

Ethics statement

The investigation was authorized by the Human Ethics Committee of *the First People's Hospital of Guiyang* (Approval No. G2020-S001) and acts following the Declaration of Helsinki. Prior to receiving the samples/isolates and performing the research, the monitoring stations erased all identifying information from the individuals suspected of being infected with *H. influenzae*. The Human Ethics Committee of t*he First People's Hospital in Guiyang* waived the patient's informed consent.

Author contributions

JC, YZ, and YW conceived and designed the experiments. YZ, XZ, JC, and JL performed the experiments. YZ, YW, XZ, and JW analyzed the data. XZ, JC, and YW wrote the paper. All authors contributed to the article and approved the submitted version.

Funding

This study was supported by Zhu ke he tong [2020]-10-6, [2019] Zhu wei jian ke ji he tong zi di 001 and Zhu ke he tong [2021]-43-25 from the Science and Technology Department of Guiyang city of Guizhou Province, and grant (Qian Ke He Zhi Cheng [2021] Yi Ban 440) from Science and Technology Department of Guizhou Province.

Conflict of interest

The authors declare that the research was conducted in the absence of any commercial or financial relationships that could be construed as a potential conflict of interest.

Publisher's note

All claims expressed in this article are solely those of the authors and do not necessarily represent those of their affiliated organizations, or those of the publisher, the editors and the reviewers. Any product that may be evaluated in this article, or claim that may be made by its manufacturer, is not guaranteed or endorsed by the publisher.

Supplementary material

The Supplementary material for this article can be found online at: https://www.frontiersin.org/articles/10.3389/fmicb.2022.1037343/full#supplementary-material

References

Aonuma, H., Yoshimura, A., Kobayashi, T., Okado, K., Badolo, A., Nelson, B., et al. (2010). A single fluorescence-based LAMP reaction for identifying multiple parasites in mosquitoes. *Exp. Parasitol.* 125, 179–183. doi: 10.1016/j.exppara.2009.12.023

Cao, Q., Liang, S., Lin, F., Cao, J., Wang, L., Li, H., et al. (2022). Detection of *Haemophilus influenzae* by loop-mediated isothermal amplification coupled with nanoparticle-based lateral flow biosensor assay. *BMC Microbiol.* 22:123. doi: 10.1186/s12866-022-02547-5

Corless, C. E., Guiver, M., Borrow, R., Edwards-Jones, V., Fox, A. J., and Kaczmarski, E. B. (2001). Simultaneous detection of *Neisseria meningitidis, Haemophilus influenzae*, and *Streptococcus pneumoniae* in suspected cases of meningitis and septicemia using real-time PCR. *J. Clin. Microbiol.* 39, 1553–1558. doi: 10.1128/JCM.39.4.1553-1558.2001

Diallo, K., Feteh, V. F., Ibe, L., Antonio, M., Caugant, D. A., Du Plessis, M., et al. (2021). Molecular diagnostic assays for the detection of common bacterial meningitis pathogens: a narrative review. *EBioMedicine* 65:103274. doi: 10.1016/j.ebiom.2021.103274

Falla, T. J., Crook, D. W., Brophy, L. N., Maskell, D., Kroll, J. S., and Moxon, E. R. (1994). PCR for capsular typing of *Haemophilus influenzae*. *J. Clin. Microbiol.* 32, 2382–2386. doi: 10.1128/jcm.32.10.2382-2386.1994

Heliodoro, C. I. M., Bettencourt, C. R., and Bajanca-Lavado, M. P. (2020). Molecular epidemiology of invasive *Haemophilus influenzae* disease in Portugal: an update of the post-vaccine period, 2011-2018. *Eur. J. Clin. Microbiol. Infect. Dis.* 39, 1471–1480. doi: 10.1007/s10096-020-03865-0

Iseki, H., Alhassan, A., Ohta, N., Thekisoe, O. M., Yokoyama, N., Inoue, N., et al. (2007). Development of a multiplex loop-mediated isothermal amplification (mLAMP) method for the simultaneous detection of bovine *Babesia parasites*. *J. Microbiol. Methods* 71, 281–287. doi: 10.1016/j.mimet.2007.09.019

Karalus, R. J., and Murphy, T. F. (1999). Purification and characterization of outer membrane protein P6, a vaccine antigen of non-typeable *Haemophilus influenzae*. *FEMS Immunol. Med. Microbiol.* 26, 159–166. doi: 10.1111/j.1574-695X.1999.tb01384.x

Kim, D. W., Kilgore, P. E., Kim, E. J., Kim, S. A., Anh, D. D., and Seki, M. (2011). Loop-mediated isothermal amplification assay for detection of *Haemophilus influenzae* type b in cerebrospinal fluid. *J. Clin. Microbiol.* 49, 3621–3626. doi: 10.1128/JCM.00515-11

Li, X. X., Xiao, S. Z., Gu, F. F., He, W. P., Ni, Y. X., and Han, L. Z. (2020). Molecular epidemiology and antimicrobial resistance of *Haemophilus influenzae* in adult patients in Shanghai, China. *Front. Public Health* 8:95. doi: 10.3389/fpubh.2020.00095

Liang, C., Chu, Y., Cheng, S., Wu, H., Kajiyama, T., Kambara, H., et al. (2012). Multiplex loop-mediated isothermal amplification detection by sequence-based barcodes coupled with nicking endonuclease-mediated pyrosequencing. *Anal. Chem.* 84, 3758–3763. doi: 10.1021/ac3003825

Murphy, T. F., Bartos, L. C., Campagnari, A. A., Nelson, M. B., and Apicella, M. A. (1986). Antigenic characterization of the P6 protein of nontypable *Haemophilus influenzae*. *Infect. Immun.* 54, 774–779. doi: 10.1128/iai.54.3.774-779.1986

Nelson, M. B., Munson, R. S. Jr., Apicella, M. A., Sikkema, D. J., Molleston, J. P., and Murphy, T. F. (1991). Molecular conservation of the P6 outer membrane protein among strains of *Haemophilus influenzae*: analysis of antigenic determinants, gene sequences, and restriction fragment length polymorphisms. *Infect. Immun.* 59, 2658–2663. doi: 10.1128/iai.59.8.2658-2663.1991

Ning, G., Yin, Z., Li, Y., Wang, H., and Yang, W. (2018). Cost-effectiveness of the *Haemophilus influenzae* type b vaccine for infants in mainland China. *Hum. Vaccin. Immunother.* 14, 36–44. doi: 10.1080/21645515.2017.1385687

Notomi, T., Okayama, H., Masubuchi, H., Yonekawa, T., Watanabe, K., Amino, N., et al. (2000). Loop-mediated isothermal amplification of DNA. *Nucleic Acids Res.* 28:E63. doi: 10.1093/nar/28.12.e63

Shah, S., Shah, P., and Green, J. (2021). *Haemophilus influenzae* purulent pericarditis in an immunocompetent individual. *J. Commun. Hosp. Intern. Med. Perspect.* 11, 96–98. doi: 10.1080/20009666.2020.1835213

Takano, C., Kuramochi, Y., Seki, M., Kim, D. W., Omagari, D., Sasano, M., et al. (2019). Molecular serotype-specific identification of *Streptococcus pneumoniae* using loop-mediated isothermal amplification. *Sci. Rep.* 9:19823. doi: 10.1038/s41598-019-56225-0

Tian, G. Z., Zhang, L. J., Wang, X. L., Zhang, L., Li, S. F., Gu, C. M., et al. (2012). Rapid detection of *Haemophilus influenzae* and *Haemophilus parainfluenzae* in nasopharyngeal swabs by multiplex PCR. *Biomed. Environ. Sci.* 25, 367–371. doi: 10.3967/0895-3988.2012.03.016

Tristram, S., Jacobs, M. R., and Appelbaum, P. C. (2007). Antimicrobial resistance in *Haemophilus influenzae*. *Clin. Microbiol. Rev.* 20, 368–389. doi: 10.1128/CMR.00040-06

Van Ketel, R. J., De Wever, B., and Van Alphen, L. (1990). Detection of *Haemophilus influenzae* in cerebrospinal fluids by polymerase chain reaction DNA amplification. *J. Med. Microbiol.* 33, 271–276. doi: 10.1099/00222615-33-4-271

Wang, Y., Li, H., Wang, Y., Zhang, L., Xu, J., and Ye, C. (2017). Loop-mediated isothermal amplification label-based gold nanoparticles lateral flow biosensor for detection of *Enterococcus faecalis* and *Staphylococcus aureus*. *Front. Microbiol.* 8:192. doi: 10.3389/fmicb.2017.00192

Wang, Y., Wang, X., Chen, H., Han, L., Wang, L., Chen, T., et al. (2021). A novel real-time reverse transcription loop-mediated isothermal amplification detection platform: application to diagnosis of COVID-19. *Front. Bioeng. Biotechnol.* 9:748746. doi: 10.3389/fbioe.2021.748746

Wang, Y., Wang, Y., Zhang, L., Li, M., Luo, L., Liu, D., et al. (2016). Endonuclease restriction-mediated real-time polymerase chain reaction: a novel technique for rapid, sensitive and quantitative detection of nucleic-acid sequence. *Front. Microbiol.* 7:1104. doi: 10.3389/fmicb.2016.01104

Wang, A., Yu, S., Yao, K., Zhang, W., Yuan, L., Wang, Y., et al. (2008). Antimicrobial susceptibility of *Haemophilus influenzae* strains and antibiotics usage patterns in pediatric outpatients: results from a children's hospital in China (2000–2004). *Pediatr. Pulmonol.* 43, 457–462. doi: 10.1002/ppul.20789

Wen, S., Feng, D., Chen, D., Yang, L., and Xu, Z. (2020). Molecular epidemiology and evolution of *Haemophilus influenzae*. *Infect. Genet. Evol.* 80:104205. doi: 10.1016/j.meegid.2020.104205

frontiers | Frontiers in Microbiology

TYPE Original Research
PUBLISHED 04 January 2023
DOI 10.3389/fmicb.2022.1013617

OPEN ACCESS

EDITED BY
Kamal El Bissati,
The University of Chicago,
United States

REVIEWED BY
Helen Roberts,
Department for Environment,
Food and Rural Affairs, United Kingdom
Geng Meng,
China Agricultural University,
China

*CORRESPONDENCE
Guoping Liu
✉ guoping.liu@yangtzeu.edu.cn
Liwei Guo
✉ guolw@yangtzeu.edu.cn

†These authors have contributed equally to this work

SPECIALTY SECTION
This article was submitted to Infectious Agents and Disease, a section of the journal Frontiers in Microbiology

RECEIVED 07 August 2022
ACCEPTED 09 December 2022
PUBLISHED 04 January 2023

CITATION
Li C, Liu G, Tong K, Wang Y, Li T, Tan X, Yang J, Yang X, Guo L and Zeng J (2023) Pathogenic ecological characteristics of PCV2 in large-scale pig farms in China affected by African swine fever in the surroundings from 2018 to 2021. *Front. Microbiol.* 13:1013617. doi: 10.3389/fmicb.2022.1013617

Pathogenic ecological characteristics of PCV2 in large-scale pig farms in China affected by African swine fever in the surroundings from 2018 to 2021

Chunqi Li[1†], Guoping Liu[1,2*†], Ke Tong[1†], Yan Wang[1†], Tong Li[1], Xu Tan[1], Jie Yang[1], Xiaolin Yang[1,2], Liwei Guo[1,2*] and Jianguo Zeng[3]

[1]College of Animal Science, Yangtze University, Jingzhou, China, [2]Hubei Institute of Cross Biological Health Industry Technology, Jingzhou, China, [3]Hunan Key Laboratory of Traditional Chinese Veterinary Medicine, Hunan Agricultural University, Changsha, Hunan, China

Porcine circovirus type 2 (PCV2) has been identified as the causal agent of postweaning multisystemic wasting syndrome (PMWS), an economically important multifactorial disease of the swine industry worldwide. This research designed a dual nested polymerase chain reaction (PCR) detection method to simultaneously monitor porcine circovirus type 2 (PCV2) and PCV3. The limit of detection (LoD) of sensitivity for PCV2 and PCV3 was ten copies/mL for both viruses. There was no cross-reaction with any other porcine pathogens tested and no non-specific amplification. The coincidence and repetition rates were both 100%. Through the systematic and clinical sampling, 15,130 samples collected from 30 large-scale pig farms in eight provinces in China (including Hubei, Hunan, Henan, Jiangxi, Shanxi, Guangdong, Hainan, and Heilongjiang) were subjected to early warning surveillance and/or clinical diagnosis. These results revealed that the overall positive rates of PCV3 and PCV2 were 0 and 28.29%, respectively, with the lowest level recorded in Jiangxi province. The highest carrying rate was observed in Hainan province. Pigs at different ages displayed varying carrying rates for PCV: fattening pigs and gilts had the highest and the lowest carrying rates for PCV, respectively. In addition, the excretion rates for PCV of colostrum, semen, and nasal, anal, and vulval swabs were tested. The colostrum, anal swabs, and semen had higher excretion rates for PCV; these were followed by the vulval and nasal swabs that had excretion rates for PCV. Furthermore, a high blood virus-carrying rate was detected in moribund pigs, especially in pigs with fever and red skin. As to the virus-carrying rate in the pig organs received from clinical necropsy, the highest rate was found in placental tissue, followed by the kidneys, and the virus also was detected in lymphoid organs, liver, stomach, and intestines. The PCV2-positive samples were sequenced to reveal the molecular epidemic dynamics of PCV2. The results indicated four major branches, namely, PCV2a, PCV2b, PCV2c, and PCV2d, concerning PCV2 molecular epidemiology in China, with PCV2a, PCV2b, and PCV2d dominating. In conclusion, the results obtained in this study elucidated the molecular epidemiology, transmission, and positive

blood samples of PCV and provided new ideas for developing comprehensive PCV control technologies to begin eliminating the disease caused by PCV by cleaning pig farms.

KEYWORDS

PCV2, PCV3, dual nested PCR, molecular epidemiology, positive rate of blood samples, excretion rate for PCV

1. Introduction

Porcine circovirus (PCV), a member of the Circoviridae family, is one of the smallest DNA viruses discovered in vertebrates to date (Tischer et al., 1982). It has three serotypes: PCV1, PCV2, and the newly reported PCV3 (Opriessnig et al., 2007; Palinski et al., 2017). PCV1, a contaminant from porcine kidney cell lines, is apathogenic in pigs but can generate serum antibodies (Magar et al., 2000). PCV2 is pathogenic and primarily produces immunosuppression in animals. PCV2 is one of the world's most severe infectious swine diseases. It is the major pathogen involved in postweaning multisystemic wasting syndrome (PMWS) (Palinski et al., 2017) and porcine dermatitis and nephropathy syndrome (PDNS; Allan et al., 2000). PCV2 can infect pigs at any age, but five to 16-week-old pigs are more prone to PMWS (Segales et al., 2005), while fattening pigs (16–22 weeks old) often suffer from a respiratory disease syndrome.

The emerging PCV3 serotype is associated with porcine dermatitis, nephrotic syndrome, and reproductive failure, as well as cardiac and multisystem inflammation, but its pathogenic mechanism remains unclear. PCV3 was first reported in the United States and was related to porcine dermatitis, nephrotic syndrome, and abortion in sows. Sows infected with PCV3 exhibit signs of anorexia, multifocal papules and spots, and superficial dermatitis, in addition to decreased production performance (Opriessnig et al., 2007). Infected pregnant sows suffer reproductive disorders, giving birth to weak, stillborn, and mummified fetuses or weak piglets that die in acutely severe cases, with fetuses of different gestational ages at risk of abortion (Sanchez et al., 2001). Due to the low viral load observed in pigs subclinically infected with PCV2, traditional polymerase chain reactions (PCR) yield poor sensitivity, and infections are often missed. Currently, research related to PCV3 is still in its infancy, and effective prevention and control measures are lacking. Therefore, the pathogenic ecology of PCV3 should be systematically explored as a matter of urgency.

Since 3 August, 2018, when the first case of African swine fever was reported in Shenyang province, China, this viral disease has been successively reported in all provinces and posed a grave threat to the pig industry in China (Ge et al., 2018). To control African swine fever, an effective and readily accessible comprehensive technical system has been established in China by pooling information from across the country and beyond. The system includes management, production, and technical aspects that provide early warning, upgrade of facility biosecurity, strengthening of biosecurity and management, control of risks, adjustment of control modes for major diseases at pig farms, and rapid decontamination techniques in emergency situations.

To respond to African swine fever, basic vaccines, including the vaccine of PCV, have almost all ceased on many large-scale farms to control the risk of possibly importing or cross-infection of the disease due to personnel contact with pigs. Thus, the once well-controlled PCV disease has made a comeback, and whether the impact of circovirus on pigs has been aggravated because of this, and whether the molecular characteristics of circoviruses have changed are all presently unknown due to a lack of published literature. Therefore, systematic sampling and evaluation of PCV backgrounds should be conducted, and the positive blood samples status of pigs, distribution of PCV in organs, excretion for PCV of pigs, and molecular epidemic characteristics of the pathogen need to be investigated.

Considering the current situation, a dual nested PCR protocol with excellent sensitivity, good specificity, and the ability to sequence positive samples efficiently while monitoring both PCV2 and PCV3 was constructed in this study. The dual nested PCR protocol was utilized to systematically assess samples from 30 large-scale pig farms, each containing more than 500 sows, in eight provinces in China to clarify the epidemic status, transmission characteristics, and molecular epidemic characteristics of PCV diseases. This study provided systematic support for controlling and eliminating the diseases caused by PCV due to the effects of African swine fever.

2. Materials and methods

2.1. Nested PCR establishment

2.1.1. Viruses and plasmids

The pathogens PCV2, classical swine fever virus (CSFV), porcine parvovirus (PPV), pseudorabies virus (PRV), and porcine respiratory and reproductive syndrome virus (PRRSV) were identified and maintained in our laboratory. PCV3 and the other plasmids used in this study were constructed and preserved within the severe disease early warning and decontamination team laboratory. A spectrophotometer was used to measure the

standard plasmid concentrations. The copy number was calculated based on the following formula: copies/mL = (6.02 × 10(23) copies/mol) × (concentration)/(MW g/mol; Trottier et al., 2002).

2.1.2. Main reagents and primers

Commercially available premix Taq MIX and nucleic acid extraction kits (Tiangen, China), DL2000 Marker and nucleic acid dyes (Solarbio, China), PCV2 enzyme-linked immunosorbent assay (ELISA) detection kits (MEDIAN, Korea), Quantitative PCR (qPCR) detection kits for PCV2 (IDEXX, United States) and PCV3 (IDEXX, USA), and African Swine fever virus real-time PCR detection kit (NECVB, Harbin, China) were acquired. Two pairs of specific primers for PCV 2 and two pairs of specific primers for PCV 3 were designed based on the nucleotide sequence of the Cap protein ORF 2 using Oligo 6.0 and Primer 5.0 software after referring to PCV 2 and PCV 3 gene sequences and the relevant literature. They were synthesized by Sangon Biotech (Shanghai, China) and stored at −20°C. The sequences are shown in Supplementary Table S1.

2.1.3. Optimization of dual nested PCR

Between 0.5 ~ 1.5 μl of primers in 0.5 μl increments were used. The optimal reaction system and optimal reaction program were selected, and two rounds of PCR reactions were performed. The 25 μl PCR reaction contained 12.5 μl of 2 × Taq Mix, 1 μl of PCV2 and PCV3 upstream and downstream primers (10 μmol/l), respectively (the first round was O-F, O-R as Outside-Forward, Outside-Reverse; the second round was I-F, I-R as Inside-Forward, Inside-Reverse), 8.5 μl of ddH2O, and 1 μl of the template, and the first amplification product was used as the template for the second reaction. The amplified products from the two reactions were detected following electrophoresis using 1% agarose gels.

2.1.4. Specificity and sensitivity tests for the dual nested PCR and its coincidence rate

Using the genomes of CSFV, PPV, PRV, PRRSV, *Escherichia coli*, and *Staphylococcus aureus* as templates and recombinant plasmids as controls, the four pairs of primers, PCV2-O-F and PCV2-O-R, PCV3-O-F and PCV3-O-R, PCV2-I-F and PCV2-I-R, and PCV3-I-F, and PCV3-I-R, used in the nested PCR were tested for specificity. In addition, the concentration of the PCV2 genome-wide positive control and recombinant plasmid pMD20-T-PCV3 was determined, followed by a copy number calculation. Next, the plasmids were diluted 10-fold, and the plasmids in each dilution were used as the template for the first PCR amplification with the primers, PCV2-O-F, PCV2-O-R, PCV3-O-F, and PCV3-O-R. The resulting products were used as the template of the corresponding gradient for the second PCR amplification using primers PCV2-I-F, PCV2-I-R, PCV3-I-F, and PCV3-I-R. The products from both the first and second amplification were detected using 1.0% agarose gels, and the smallest detectable number of copies was calculated. On this basis, the PCV2 genome-wide positive controls with copy numbers of 10^5, 10^4, 10^3, 10^2, 10^1, and 10^0, and PCV3 plasmid controls and the same batch of clinical samples collected in Hubei were tested using the established nested PCR, quantitative fluorescence PCR, and conventional PCR. And ELISA was used to test these clinical samples. The test results were used to validate the coincidence rate of the nested PCR.

2.2. Detection of African swine fever virus in the environment around pig farms

From 2018 to 2021, we collected 2056 environmental samples within 3 kilometers around 30 pig farms in eight provinces on a quarterly basis, including soil, water, vehicles, people, and articles. The collected environmental samples were tested with the African Swine fever virus real-time PCR detection kit (NECVB, Harbin, China) according to the manufacturer's instructions.

2.3. Application of dual nested PCR

The dual nested PCR established in this study was used for clinical testing of 15,130 clinical samples from 30 large-scale pig farms (breeding stock >500 sows) in eight provinces, including Hubei, Hunan, Henan, Jiangxi, Shanxi, Guangdong, Hainan, and Heilongjiang provinces (Figure 1) or during the evaluation of early warning surveillance of systematic sampling as per the sampling procedures. In addition, an analysis was conducted on the prevalence and characteristics of PCV, specifically, the virus-carrying rate in the blood and organs, excretion for PCV in semen, colostrum, and saliva, as well as nasal, anal, and vulva swabs, and genetic characteristics of the pathogen, in some areas of China.

An epidemiological survey was performed on pigs without apparent clinical signs (Figure 2). Specifically, semen from boars and nasal, anal, and vulval swabs and colostrum from pregnant sows were systematically collected in a standardized manner. DNA was obtained from samples taken from the nose, anus, and vulva from offspring at different ages, including 30–50 days, 50–70 days, 70–90 days, and over 90 days. A total of 12,691 samples were obtained throughout the study. Furthermore, organ examination was carried out on pigs with suspected clinical signs that included anorexia, redness of the conjunctiva, pale skin, lethargy, and skin disease, as well as sows with reproductive disorders and weak piglets with congenital tremors. Samples were harvested from the heart, cerebrospinal fluid, intestines, lung, liver, spleen, kidney, afterbirth, stomach, and lymph nodes. A total of 2,194 samples were obtained *via* necropsy from 300 pigs.

Samples were collected using a standardized protocol and stored in a closed low-temperature styrofoam box at 4°C, then

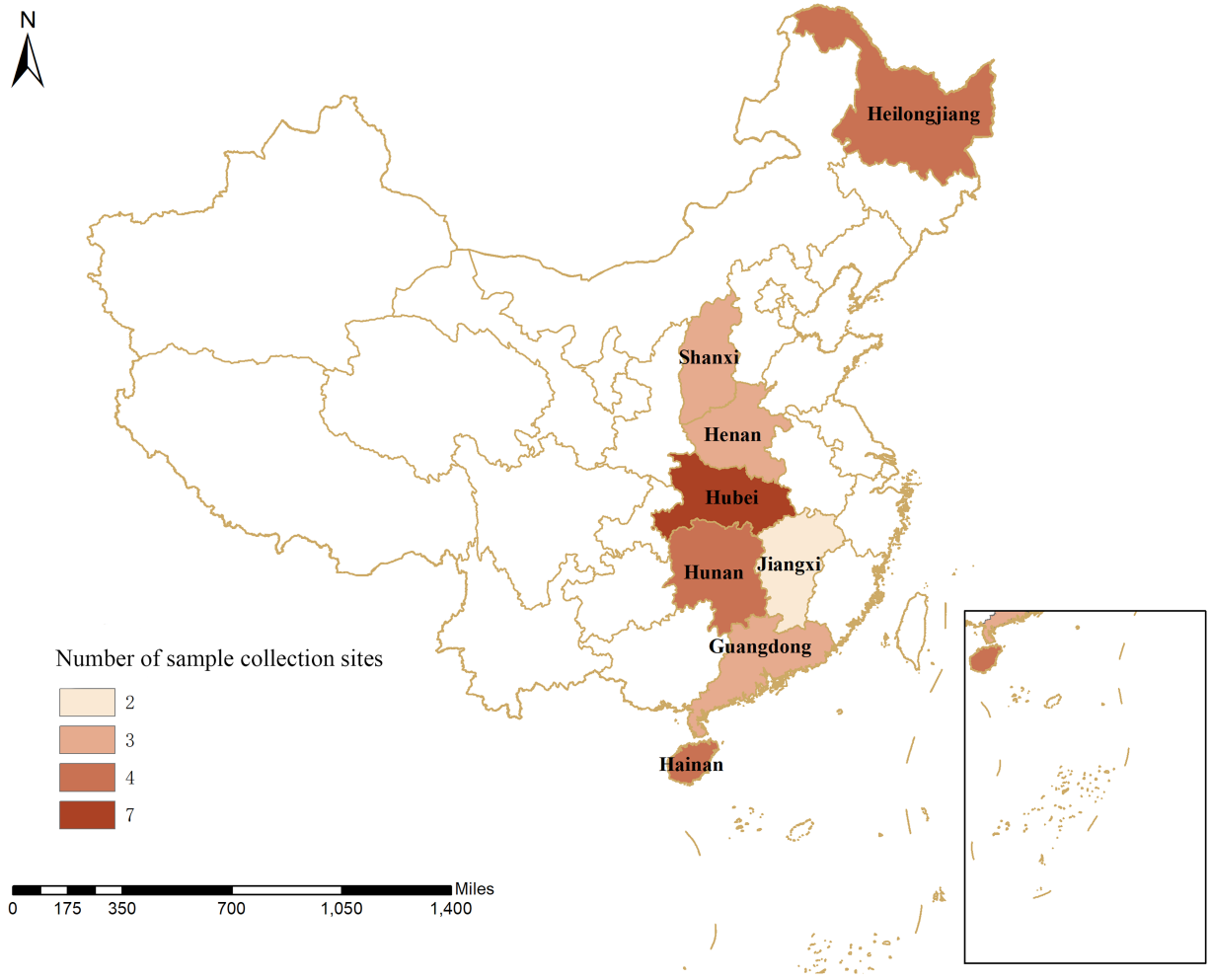

FIGURE 1
Geographical distribution of sample collection from 30 pig farms in eight provinces in China. The numbers show the distribution of pigs on the farms within the provinces in China.

transported to the laboratory within 1–2 h for subsequent processing. The swabs (semen or colostrum) were placed in a 5 ml Eppendorf (Ep) tube and soaked in an appropriate amount of normal saline, followed by 30 s of vortexing. The supernatant was retrieved, placed on a shaker for 30 min, transferred to a 2 ml Ep tube, completely homogenized, and centrifuged. The supernatant was harvested for subsequent DNA extraction. Fresh tissues were collected from the junction between healthy and diseased sites. Then, blood and connective tissues were removed with sterile medical gauze, and the samples were cut into small pieces on ice. The tissue pieces were transferred into a pre-cooled homogenizer, mixed with a homogenization buffer composed of 0.25 mmol/l sucrose, 25 mmol/l Tris–HCl (pH 7.5), 25 mmol/l NaCl, and 25 mmol/l $MgCl_2$ at 10 ml/g. The homogenate was placed on a shaker for 30 min and then homogenized. Following centrifugation at 12,000 r/min for 5 min, the supernatant was collected. All positive samples were sent to Wuhan Sangon for sequencing.

3. Results

3.1. Establishment of dual nested PCR

3.1.1. Optimization of the reaction conditions

The optimized PCR conditions, including annealing temperatures (56°C and 58°C) and template and primer volumes for the four pairs of primers for dual nested PCR, were used with the specific dual nested PCR reaction conditions. After optimizing the dual nested PCR conditions for PCV2 and PCV3, there were distinct target bands that did not produce heterobands. The optimal conditions for the dual nested PCR are listed in Supplementary Table S2.

3.1.2. Specificity test

The genomes of CSFV, PPV, PRV, PRRSV, *Escherichia coli*, and *Staphylococcus aureus* were extracted as templates for the specificity test using the four pairs of primers (PCV2-O-F and

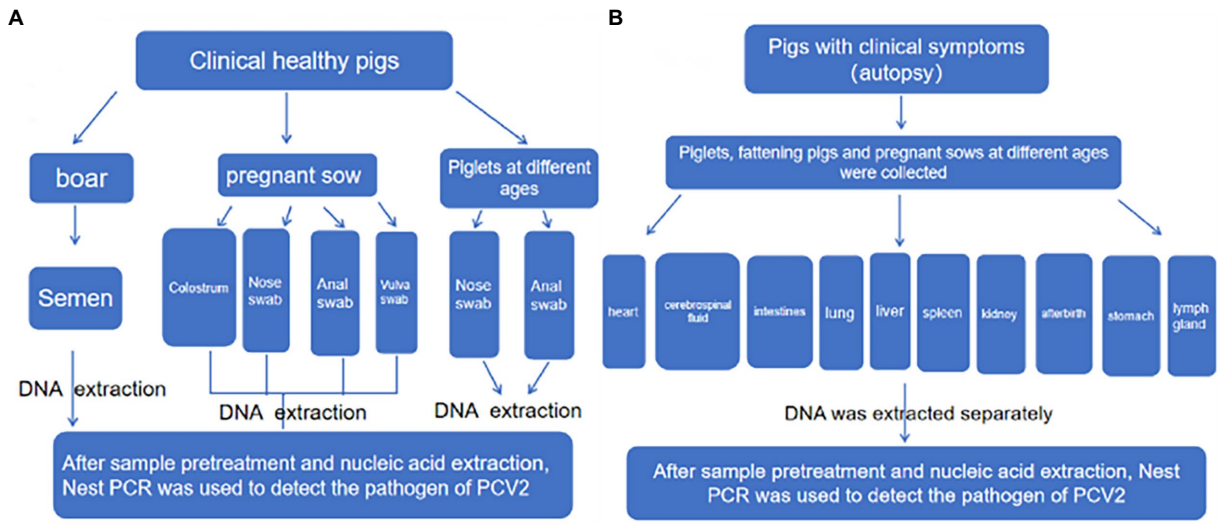

FIGURE 2
Sampling scheme diagram. **(A)** Clinically healthy pigs. **(B)** Piglets at different ages.

PCV2-O-R, PCV3-O-F and PCV3-O-R, PCV2-I-F and PCV2-I-R, and PCV3-I-F and PCV3-I-R), which were used in the dual nested PCR. As shown in Supplementary Figure S1(A) PCV2 and PCV3 exhibited no cross-reactions with these other viruses. No heterobands or dimers were present, indicating that the four pairs of primers had good specificity.

3.1.3. Sensitivity test (dual nested PCR)

Different gradients of the PCV2 whole-genome template and PCV3 recombinant plasmid were amplified using the specific primers, and the virus concentrations were detected concomitantly. The limit of detection (LoD) for PCV2 and PCV3 was ten copies/mL, and the number of copies of PCV2 and PCV3 dilution gradients was 1×10^{9}, 1×10^{8}, 1×10^{7}, 1×10^{6}, 1×10^{5}, 1×10^{4}, 1×10^{3}, 1×10^{2}, 1×10^{1}, and 1×10^{0}, in sequence. As shown in Supplementary Figure S1(B), the LoD of PCV2 and PCV3 detected after two amplifications using the dual nested PCR was ten copies/mL, two to three orders of magnitude higher than that obtained by the current detection method. Regarding interference from other pathogens, the amplified bands exhibited no changes (Supplementary Figure S1(C)).

3.1.4. Coincidence rate and repeatability test

To confirm the coincidence rate of the dual nested PCR, the same batch of clinical samples (including 150 serum samples: 103 PCV2-positive samples and 0 PCV3-positive samples) were tested separately using the dual nested PCR established in this study, a commercial ELISA kit for PCV2, and a fluorescence quantitative PCR detection kit for PCV2 and PCV3 (IDEXX). The test results were compared (Supplementary Table S3) to validate the coincidence rate of the dual nested PCR. Each sample was analyzed in triplicate, and the results were consistent between the three runs, with a repetition rate of 100%. The results demonstrated that the coincidence rate of the dual nested PCR was 100%, and the LoD for PCV2 and PCV3 was ten copies/mL. In addition, there were no false positives or false negatives indicated by the dual nested PCR, according to the sequencing results. In the other conventional methods, the coincidence rate was low. The LoD for PCV2 was 1×10^{5}–1×10^{1}, and no PCV3 was detected. The LoD for the positive plasmids also was ten copies/mL. In addition to the low coincidence rate, virus-negative samples were more likely to test as false positive *via* ELISA and qPCR, which could lead to an incorrect diagnosis.

3.2. Correlation analysis between ASFV and PCV2

The test results showed that 510 samples were positive for ASFV. We used JMP software to analyze the positive rate of ASFV and the positive rate of the PCV2, and the partial correlation reached 0.6, indicating that ASFV and the PCV2 had better correlation (Supplementary Table S4).

3.3. Epidemic research based on dual nested PCR

3.3.1. Prevalence of PCV2 in eight provinces of China

A total of 15,130 clinical samples, including whole blood, colostrum, and semen, as well as nasal, vulval, and anal swabs, were collected from pigs at different ages from eight provinces (Table 1). PCV2 showed a positive rate of 25.61% (599/2,344), 33.64% (529/1,801), 16.79% (391/2,329), 8.31% (133/1,600), 20.30% (307/1,512), 22.63% (415/1,834), 42.36% (726/1,799), and

TABLE 1 Prevalence of Porcine Circovirus type 2 in surveillance samples from eight provinces.

Province	Tested samples	Positive samples	Positive rate(%)	The infection type	Infection pattern	Infection rate(%)
Hubei	2,344	599	25.61% (599/2344)	A single infection	PCV2	3.83% (579/15130) ab
					PCV3	0% (0/15130) c
Hunan	1801	529	33.64% (529/1801)	Double infection	PCV2 + PRRSV	21.28% (3,219/15130) g
Henan	2,329	391	16.79% (391/2329)		PCV2 + PRV	6.10% (923/15130) h
Jiangxi	1,600	133	8.31% (133/1600)		PCV2 + PPV	4.17% (631/15130) b
Shanxi	1,512	307	20.30% (307/1512)	Triple infection	PCV2 + PRRSV+PRV	7.06% (1,068/15130) i
Guangdong	1834	415	22.63% (415/1834)		PCV2 + PRRSV+PPV	3.55% (537/15130) a
Hainan	1799	762	42.36% (762/1799)		PCV2 + PRV + PPV	0.23% (35/15130) j
Heilongjiang	1911	501	26.22% (501/1911)	Multiple infection	PCV2 + PRRSV+PRV + PPV	0.09% (13/15130) k

15,130 clinical samples were collected from eight provinces. Blood and colostrum as well as nasal, vulva, and anal swabs were collected from pigs of different ages and stages of development. The test results showed single infections, double infections, and multiple mixed infections. The SPSS 24.0 chi-square test was used to analyze the differences between the detection results in samples with mixed infections from different regions and from other diseases. $p < 0.05$ was considered significant.

26.22% (501/1,911) in Hubei, Hunan, Henan, Jiangxi, Shanxi, Guangdong, Hainan, and Heilongjiang provinces, respectively. Thus, the positive rate of PCV2 ranged from 8.31 to 42.36%, averaging 24.04% (3,637/15,130), which was highest in Hainan (42.36%, 762/1,799), followed by Hunan, Heilongjiang, Guangdong, Hubei, Shanxi, and Henan provinces, with Jiangxi province exhibiting the lowest rate (8.31%, 133/1,600). The detection results of the mixed infection indicated that the single infection rate of PCV2 was relatively low (3.83%), while the remaining samples exhibited a double or triple mixed infection at 31.55 and 10.61% for all samples, respectively. In the double infection samples, PCV2 + PRRSV, PCV2 + PRV, and PCV2 + PPV were the predominant types observed, with positive rates of 21.28, 6.1, and 4.17% of all samples, respectively, while PCV2 + PRRSV+PRV and PCV2 + PRRSV+PPV were most prevalent in the triple infection samples, with positive rates of 7.06 and 3.55% of all samples, respectively. Other types of mixed infection were rare. This indicated that in some regions of the eight provinces in China, PCV2 was widely prevalent in large-scale pig farms, while the positive rates of mixed infection occurred to varying extents and indicated significant differences ($p < 0.05$; Table 1).

3.3.2. PCV2 Infection in pigs at different ages

Among the 8,675 blood samples from the eight provinces, PCV2 infection was detected in pigs at different ages, indicating that PCV2 could infect pigs at all ages ($p < 0.05$, Figure 3). Specifically, the PCV2-positive rate was highest in fattening pigs (65.01%), followed by nursing pigs (58.26%), then suckling piglets (12.05%), while it was relatively low in multiparous sows (10.42%), primiparous sows (7.91%), and gilts (6.87%; Figure 3). These results demonstrated that infection occurred in pigs at different ages, with significant differences in the positive rates observed. The highest infection rate was detected in fattening pigs aged over 130 days old.

TABLE 2 Distribution of PCV2 in different organs.

Organ Type	Number of samples	Positive number	Positive rate
Heart	71	10	14.08%
Cerebrospinal fluid	36	4	11.11%
Intestines	66	9	13.64%
Lung	71	9	12.68%
Liver	71	17	23.94%
Spleen	71	16	22.54%
Kidney	61	21	34.43%
Afterbirth	12	5	41.67%
Stomach	71	6	8.45%
Lymph gland	19	6	31.58%
Blood	245	50	20.41%

A total of 794 clinically suspected samples were necropsied, and the overall positive rate of PCV2 was 19.43%. PCV2 was detected in all tissue and organ types submitted for inspection.

3.3.3. PCV2 Infection in pigs with different clinical signs

Blood samples collected from pigs with different clinical signs from the pig farms were sent for PCV2 pathogenic surveillance (Table 2). The results showed that the detection rate for positive blood samples was 27.81%. PCV2 had a positive rate of 58.79% in the blood samples from nursing pigs and fattening pigs that presented with red and cyanotic skin, which was the highest positive rate detected in blood. Pregnant sows with lochia, premature delivery, and abortion ranked second for positive in blood (28.92%). Thereafter, the detection rates of positive blood samples were seen in moribund weak piglets among suckling piglets, nursing piglets, and sows with loss of appetite, moribund defective pigs among fattening pigs, and moribund nursing or suckling piglets with diarrhea at rates of 27.91, 22.09, 16.67, and

13.19%, respectively. Positive blood samples also were detected in a few moribund stiff piglets among nursing piglets or piglets that had died of encephalitis, with positive rates of 1.67 and 1.96%, respectively.

3.3.4. PCV2 Infection In different tissues and organs of pigs

The samples that tested positive for PCV2 accounted for 19.43% of the 794 samples retrieved following necropsy (Table 3). PCV2 was detected in all the tissue and organ types submitted for inspection. The highest positive rate was present in afterbirth (in 41.67% of the infected animals with an afterbirth sample collected), followed by the kidney (34.43%), lymph nodes (31.58%), liver (23.94%), spleen (22.54%), heart (14.08%), intestines (13.64%), lung (12.68%), and stomach (8.45%). The examined blood samples exhibited a total positive rate for PCV2 of 20.41%. It should be noted that PCV2 also was detected in cerebrospinal fluid, with a positive rate of 11.11% (4/36).

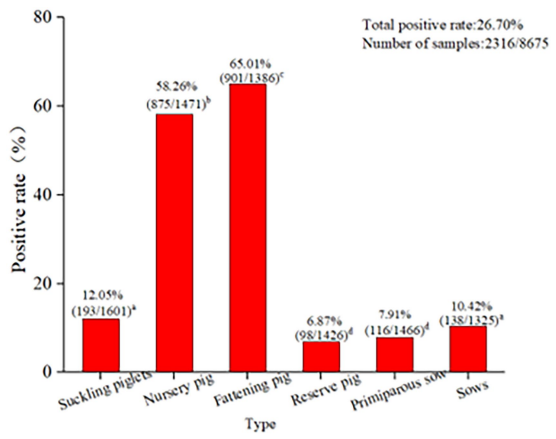

FIGURE 3
PCV2 infection in pigs at different ages in eight provinces. The PCV2 infection in pigs at different ages indicated that PCV2 was able to infect pigs of all ages. The positive rate of PCV2 in finishing pigs (65.01%) was the highest, followed by nursing pigs (58.26%) and lactating pigs (12.05%). The positive rates of economic sows, gilts, and primiparous sows were 10.42, 6.87, and 7.91%, respectively. The test results for PCV2 infection in pigs at different ages in the eight provinces were analyzed using the SPSS 24.0 chi-square test. $p<0.05$ was considered significant.

3.3.5. Excretion ways for PCV2

These results indicated that PCV2 could be passed through colostrum, semen, nose, anus, and vulva, and still showed a high positive rate. The positive rates observed in colostrum, semen, and anal swabs were relatively similar at 26.65, 22.71, and 25.30%, respectively (Figure 4A). However, the rates for the nasal and vulvar swabs were lower at 12.81 and 15.47%, respectively (Figure 4A). Although the way of excreting PCV2 in various provinces and regions was similar, notable differences were found in the excretion rate for PCV2 in the different growth stages of pigs. According to the statistical analysis (Figure 4B), the positive rates for colostrum were lowest in Jiangxi province (7.35%) and the highest in Hainan province (56.69%), and for semen, the lowest rate was in Henan province (0%) and the highest in Guangdong province (46.35%). The positive rates detected in the anus, nose, and vulva ranged from 9.26–47.79%, 7.74–22.02%, and 2.67–36.84%, respectively, with the lowest in Henan, Jiangxi, and Shanxi provinces and the highest in Guangdong, Hainan, and Hunan provinces.

3.3.6. Sequence analysis of PCV2

The variation within the PCV2 Cap protein allowed changes in viral immunogenicity and cell tropism, resulting in differences in virulence. The analysis completed on the Cap amino acid sequences revealed several amino acid variations in the Cap protein (Table 4). Specifically, the PCV2 strains in the genotype PCV2a, PCV2b, PCV2c, and PCV2d harbored ten unique amino acid mutations, respectively. These amino acid loci were highly variable, and amino acids changed from hydrophobic to hydrophilic, with the potential to cause changes in the antigenicity of PCV strains.

The positive products from the Hubei, Hunan, Henan, Jiangxi, Shanxi, Guangdong, Hainan, and Heilongjiang provinces were purified and sequenced. Twenty-four isolates with gene sequences were obtained and compared to the sequences from domestic

TABLE 3 Distribution of different viremias.

Sample Type	Age Stage	Clinical Signs	Tested samples	Positive samples	Positive rate
Whole blood	Suckling piglets	Weak piglet death	129	36	27.91%
	Suckling and nursing piglets	Piglet diarrhea	91	12	13.19%
	Nursing piglets	Piglets died of encephalitis	51	1	1.96%
	Nursing piglets	Dead stiff pig	60	1	1.67%
	Nursing and fattening pigs	Dead pigs with red and cyanotic skin	165	97	58.79%
	Fattening pigs	Residual pig death	54	9	16.67%
	Nursing piglets and sow	Emaciation and loss of appetite	86	19	22.09%
	Pregnant sows	Reproductive disorder	166	48	28.92%

Collection of blood from pigs with different clinical signs in pig farms for PCV2 etiological monitoring.

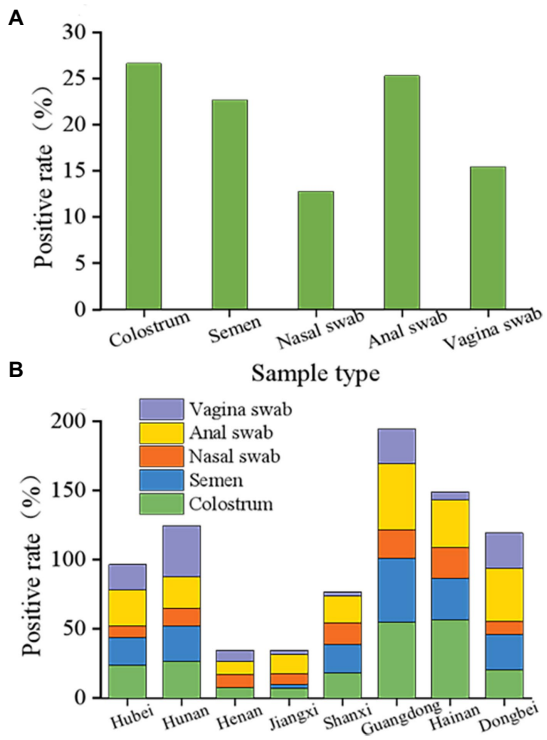

FIGURE 4
Overall status of porcine circovirus type 2 excretion. **(A)** Overall elimination of PCV2 in different organs of pigs in eight provinces. PCV2 is detoxified through colostrum, semen, nose, anus, and vulva and still showed a high positive rate following immunization with the ring vaccine. The positive rates of colostrum, semen, and anal swabs were similar, 26.65, 22.71, and 25.30%, respectively. Nasal swabs and vulvar swabs were recorded as 12.81 and 15.47%, respectively. **(B)** Different excretion pathways of pigs in the eight provinces. Among them, the positive range of colostrum was 7.35 to 56.69%, and the positive rate of colostrum from Jiangxi province was the lowest at 7.35%. The positive colostrum rate in Hainan province was the highest at 56.69%. The lowest semen-positive rate was 0 in Henan province, while the highest was observed in Guangdong province at 46.35%. The detection rates in the anus, nose, and vulva were 9.26 to 47.79%, 7.74 to 22.02%, and 2.67 to 36.84%, and the lowest detection rates were in the Henan, Shanxi, and Jiangxi provinces. The provinces with the highest detection rates were Guangdong, Hainan, and Hunan.

reference strains accessed on MEGA 5.0. According to the phylogenetic comparative analysis, the homology (95.36 to 99.95%) was ascertained between isolates and the classical strains (Supplementary Figure S2(A)). The sequence homology of PCV2 varied in different regions and showed the most similarity between Guangdong01 and Henan02 (99.95% homology) and the largest difference between Henan03 and Hubei03 (95.36% homology). In addition, a homology of 95.46 to 99.98% was validated between the 24 isolates and foreign strains, which revealed the largest variation was between Shanxi03 and JX535286 (95.51% homology), and Hubei01 and KM245558.GX (95.46% homology).

Four genotypes were identified in the 24 isolates, including PCV2a (37.50%), PCV2b (29.17%), PCV2c (0.083%), and PCV2d (25.00%). The epidemic strains were distributed slightly differently in the various regions, with PCV2d (3/5) and PCV2b (2/5) present in Hubei province, PCV2c and PCV2d in Hunan province, PCV2a in Jiangxi and Heilongjiang provinces, PCV2b in Shanxi and Hainan provinces, PCV2a and PCV2d in Guangdong province, and PCV2a (3) in Henan province. As shown in Supplementary Figure S2(B), a phylogenetic tree of PCV2 was constructed, and the data indicated that the sequences were primarily divided into four branches, which belonged to reference strains, PCV2a, PCV2b, PCV2c, and PCV2d. Shanxi01 and Shanxi02 were similar to Hunan02, revealing close homology.

4. Discussion

4.1. The high sensitivity of dual nested PCR

In this study, four pairs of detection primers were designed *via* encoding the PCV2 and PCV3 Cap proteins and optimizing the conditions required for the analysis. The findings revealed that the dual nested PCR constructed showed good specificity when detecting PCV2 and PCV3, with repeatability and coincidence rates of 100%, and they showed no cross-reaction with CSFV, PPV, PRV, or PRRSV. The LoD for both PCV2 and PCV3 was ten

TABLE 4 Amino acid substitutions in the putative Cap protein.

Classic strains	Position	PCV2a	PCV2b	PCV2c	PCV2d
PCV2a-HBxz (GenBank: FJ870968.1)	70(D)	G(2)/L(1)/T(1)	S(2)/L(1)/A(1)	*(2)	L(2)/S(1)/I(1)
	73(R)	N(3)/F(2)	H(2)/*p*(1)/D(1)	L(1)	R(1)/D(1)/H(1)/*F*(1)
	103(V)	A(9)	D(3)	A(2)	H(2)
PCV2b-ZD-1-CHN-2014-PCV2 (GenBank: KU041849.1)	106(W/F)	Q(9)	H(2)	Q(2)	H(2)
	112(T)	*p*(9)	K(3)	*p*(2)	*p*(6)
Pcv2c-DK1980PMWSfree (GenBank: EU148503.1)	115(D)	A(1)	A(1)	S(2)	A(2)
	145(S)	E(1)	E(4)	G(2)	E(2)
	178(N)	R(2)	R(4)	Q(2)	R(3)
Pcv2d-ChenZ-2-1 (GenBank: MH718995.1)	205(S)	A(9)	D(3)	A(2)	A(6)
	211(Y)	V(1)	V(4)	L(2)	V(3)

copies/mL. Therefore, the detection method developed in this study exhibited a relatively high sensitivity compared to the methods in previous reports. The sensitivity of this assay was 2.9 copies for the PCV2 plasmid and 22.5 copies for the PCV3 plasmid (Li et al., 2018). In comparison, the detection limit for ddPCR was two copies/μL for PCV2 and 1 copy/μL for PCV3. The detection limits of another experimental method for PCV2 and PCV3 were ten and one copies/μL (Cao et al., 2021). Therefore, the present method provided favorable anti-interference, specificity, and repeatability and is applicable to clinical or normal diagnosis and detection, early warning, and surveillance of PCV2 and PCV3. Based on a comparative analysis, the previous methods are less sensitive than the current constructed method. The nested PCR could simultaneously detect PCV2 and PCV3 and promptly enabled gene sequencing to be performed following the presence of positive results. This enabled precise assessment of the epidemic situations relating to PCV2 and PCV3 in pig farms facing the current pressure from African swine fever, saving etiological confirmation time and reducing costs.

4.2. PCV prevalence under the pressure of African swine fever

Circovirus disease was once prevalent in large-scale pig farms in China (Shuai et al., 2007; Wang et al., 2009; Guo et al., 2019), but its incidence gradually declined with the implementation of prevention and control measures. Nevertheless, in order to prevent the infection of African swine fever virus, which first appeared in 2018, disease prevention and environmental management in China's pig industry have been significantly improved. Since the infection with the African swine fever virus, some pig farms have not even performed basic immunization due to the need for safe production. In these cases, the large pig farming industry in China may face large-scale economic losses once the infection of circovirus disease appears.

Therefore, because epidemiological surveys on the infection and transmission of PCV remain inconclusive, it is critical to comprehensively and systematically explore the pathogenic ecological characteristics of PCV2 and PCV3 under the effect of African swine fever. In this study, the etiology of PCV in clinical samples sent from large-scale pig farms in several regions of China was detected *via* dual nested PCR. The results indicated no PCV3-positive samples (positive rate: 0%), which was inconsistent with the detection rate of PCV3 (2.96 to 37.96%) in various domestic regions previously reported by others in China (Fu et al., 2018; Ha et al., 2018; Wen et al., 2018; Fang et al., 2019). However, it is noteworthy that such research was carried out prior to the appearance of African swine fever in China. This suggests that the infection of PCV3 in pigs results from using porcine plasma protein or contamination of feed raw materials that might be more strictly controlled following the appearance of African swine fever. The use of porcine plasma protein is prohibited by national regulations, and feed is produced at high temperatures during different periods (Trudeau et al., 2017). Therefore, we speculated that PCV3 might not be widely prevalent in some regions of China due to the current pressure of African swine fever. Nonetheless, a more comprehensive evaluation is needed, particularly in Hebei and Fujian provinces, where numerous cases have been reported. Thus, providing a more thorough and precise basic databank could help reveal the underlying cause(s) of PCV3 transmission or infection in large-scale pig farms in China. In this study, the results revealed that the overall positive rate of PCV2 in some regions of China was 24.04% (3,637/15,130). Specifically, PCV2 showed positive rates of 25.61% (599/2,344), 33.64% (529/1,801), 16.79% (391/2,329), 8.31% (133/1,600), 20.30% (307/1,512), 22.63% (415/1,834), 42.36% (726/1,799), and 26.22% (501/1,911) in Hubei, Hunan, Henan, Jiangxi, Shanxi, Guangdong, Hainan, and Heilongjiang provinces, respectively. Therefore, PCV2 infections exist, to a varying extent, in these regions of China, with notable regional differences. Hainan province was affected the most (42.36%). In general, the differences appear to be linked to feeding density, minimal environment control, biosafety levels, feeding management protocols as well as disease prevention and control procedures of the pig farms; geographical environment and natural climate may also be influencing factors (Lim et al., 2011).

4.3. The influence of geographical location on PCV prevalence

Hainan province is an island located in the southernmost region of China. The high infection rate (42.36%) of PCV2 in Hainan province could be attributed to intensive pig farms with insect vectors that frequently spread viral diseases, the open design of production and breeding buildings, and the large temperature differences between day and night. While Jiangxi province, located in the central China, has a low positive rate of PCV2 (8.31%). These results indicate that due to the pressures of African swine fever, changes in the pig industry promoted the transformation and upgrading of large-scale pig breeding facilities and equipment. In addition, biosafety-related facility upgrades and awareness increased. Finally, improved and refined health and production management to an even greater extent took place. Thus, all of these changes could have reduced the spread of PCV2.

4.4. The transmission pathways of PCV2

The surveillance results from the eight provinces revealed that compared with the numbers observed after African swine fever first appeared, the positive rate of PCV2 was higher prior to the appearance of African swine fever. This result provisionally suggests that biosafety measures, upgrading facilities, and reductions in pig population density might decrease the horizontal transmission of PCV and could contribute to the lower positive rate of PCV2 in Jiangxi province compared to the other provinces.

However, gilts, primiparous sows, multiparous sows, lactating pigs, nursing pigs, and fattening pigs exhibited a distinct upward trend in their PCV2-carrying rate. Overall, the PCV2-carrying rate was significantly lower in sows and suckling piglets than that observed in nursing and fattening pigs. Both the vertical transmission in pigs and the horizontal transmission between pigs were present.

Furthermore, the excretion rates for PCV2 in pigs in the presence of African swine fever were systematically analyzed in this study. The overall data from the eight provinces indicated that despite the gradual upgrades made in biosafety measures, the virus was still excreted *via* different pathways. Colostrum showed a mean excretion rate of 26.65% for PCV. The fact that the virus can be excreted from the colostrum implies that infection of the digestive tract may occur in suckling pigs in the delivery room. As the infection becomes progressively more severe, some suckling pigs, after weaning (or in the delivery room), will suffer from viremia, PMWS, or even acute and chronic death in severe cases. In addition, there may be mixed infections present with epidemic diarrhea, which produces delivery room diarrhea syndrome (Jung et al., 2006; Opriessnig et al., 2011; Tzika, 2017), which consequently causes severe losses to farms.

Notably, infected sows may not be viremic, but their colostrum can still contain virus, which suggests that the virus may enter the mammary glands *via* other body fluids or pathways (Gerber et al., 2011). In this study, the results showed that the anus (25.30%) and colostrum (26.65%) were comparable with respect to the excretion rate for PCV, indicating that circovirus can be excreted through the feces and also suggesting that the digestive tract is vulnerable to circovirus. Thus, the gastrointestinal infection pathway has been elucidated *via* colostrum and anal excretion for PCV, which emphasizes the importance of horizontal transmission in certain circumstances (Patterson and Opriessnig, 2010; Rose et al., 2012).

The circovirus detected in nasal swabs partially reflects the horizontal transmission ability of the virus in the respiratory tract. Due to the presence of African swine fever, a potential downward trend was observed in the horizontal transmission ability of circovirus in the respiratory tract. The positive rate of nasal swabs (12.81%) was lower than that of vulvar swabs (15.47%), indicating that the horizontal transmission ability of circovirus in the respiratory tract was lower than in the reproductive tract and much lower than in the digestive tract, which is inconsistent with our traditional understanding (Rose et al., 2012).

Furthermore, it is important to note that the overall circovirus-carrying rate in semen was relatively high (22.71%), greatly affecting the ability to control viral infection when breeding. If a negative pathogen outcome cannot be guaranteed in semen, the reproductive system of sows bred with circovirus-positive semen may become readily infected. The fact that a boar may be mated with 50 or more sows further expands the infection capacity with the potential to cause an explosive spread of PCV2. Concerning the comparison of horizontal transmission, the data obtained from specific background values systemically made at the early warning level revealed that the infection rate of PCV2 was relatively high in regions with high pathogen-carrying rates in semen, and the opposite results occurred in areas with a low semen pathogen-carrying rate.

4.5. Analysis of clinical signs in pigs infected with PCV2

The issues of how many pigs were affected clinically by PCV2 under the pressure of African swine fever, as well as whether the numbers changed before and after the initial reports of African swine fever, were explored in this study. The results revealed that the highest positive rate was detected in afterbirth (41.67%), and a lower positive rate was discovered in offspring pigs. Therefore, testing positive for the virus in the afterbirth is not equivalent to offspring infection, and appropriate prevention and control strategies are able to block the passage of the afterbirth virus infection to offspring pigs. This might be explained by the idea that the high afterbirth detection rate might be related to insemination with virus-positive semen, allowing the pathogen to settle and multiply in the reproductive system after the reproductive tract was infected *via* the semen (Gava et al., 2008; Grasland et al., 2008; Dissertations and Gradworks, 2009; Opriessnig et al., 2011).

The kidney also showed a high positive rate for PCV2, which is consistent with previous reports (Kleymann et al., 2020), and high levels of PCV can induce PDNS. In addition, a high positive rate also was observed in immune organs such as the liver, spleen, and lymph nodes, which is associated with the frequent invasion of immune organs by PCV2 (Shi et al., 2021), and viremia may occur in severe cases (Correa-Fiz et al., 2020; Lopez-Lorenzo et al., 2021). PCV2 also was detected in the intestines and stomach, which is indicative of gastrointestinal infection with circovirus, and agrees with recent reports (Liu et al., 2019; Yang et al., 2020). The relatively high positive rate observed in the coronary sulcus tissues is basically identical to clinical observations, which helps provide evidence of sudden unexplained death in some pigs (Mikami et al., 2005). Nonetheless, there have been no previous reports concerning this condition thus far.

PCV2-positive outcomes occurred in cerebrospinal fluid, and research into PCV2 invasion of brain tissues has been reported in the literature, but the mechanism of action is unclear (Tummaruk and Pearodwong, 2016). Circovirus detection suggested that after the appearance of African swine fever, a series of comprehensive prevention and control measures (e.g., biosafety, disease prevention and control methods, closed management of pigs, and frequent disinfection of pigs) formulated by farms might cause variations in levels of circovirus, facilitate the ability of the pathogen to break through the blood–brain barrier. This variation might enhance pathogen virulence, posing severe threats to pigs, and deserves closer attention.

To further elucidate circovirus-induced viremia in pigs with clinical signs and moribund states or reproductive disorders,

blood samples were collected before on-site necropsy for viremia detection. The results revealed that the detection rate was 27.81% (223/802) in all pigs. This suggested a relatively high incidence rate of circovirus-induced viremia in pigs with clinical signs and in a moribund state at the pig farms. Thus, under the novel pressures encountered by the presence of African swine fever, the ability of circovirus to induce viremia might be enhanced. In this study, systematic analysis was carried out on pigs with clinical signs and those prone to viremia. The results confirmed that the highest detection rate of viremia was discovered in nursing and fattening pigs with red and cyanotic skin and the appearance of a sudden moribund state, yielding a 58.79% (97/165) infection rate. Thus, it may be concluded that PCV2-induced viremia could be the primary cause of red and cyanotic skin and sudden death in nursing and fattening pigs.

Among nursing pigs and sows with emaciation, loss of appetite, and low-grade fever, those with chronic subclinical signs that turned into an acute moribund state showed a viremia rate of up to 22.09% (19/86), suggesting that circovirus-induced viremia might be one of the causes of death of the affected pigs. Among suckling piglets, moribund weak piglets showed a relatively high detection rate of viremia, which may be attributed to congenital infection with circovirus, oral infection (including from colostrum), infection from polluted environments, and accumulation of virus load. Among fattening pigs, the relatively high detection rate of viremia was found in diseased pigs that died. The reason might be because chronic pathogen infections lead to reduced resistance in the diseased pigs and increase in the carrying rate of PCV in infected tissues. Additionally, diarrhea might occur when the accumulative infection load is excessive in the digestive tract or when mixed infections occur, similar to the porcine epidemic diarrhea virus (PEDV), leading to dehydration or multiple organ failure and resulting in death.

Stiff piglets that appeared among nursing piglets or piglets that died of encephalitis showed a relatively lower detection rate of viremia, suggesting that stiff piglets may have some tolerance to viremia, and after the viremia disappears, they die of organ failure (Opriessnig and Langohr, 2013). Also, the detection rate of encephalitis-induced viremia was unexpectedly low, while the detection rate in cerebrospinal fluid was much higher than that of encephalitis-induced viremia, indicating that PCV2 possibly infects pigs by breaking through the meningeal barrier but not through the blood circulation.

Prior to the reports of African swine fever in China, PCV2 was often found in combination with several other pathogens (e.g., PRRSV, PRV, CSFV, and PEDV), producing mixed infections. Since African swine fever appeared, reports have indicated extremely low single infection rates of PCV2 [1.91% (289/15,130)]. Notably, mixed infections were predominant in the present study, particularly PCV2 with PRRSV, which is consistent with current reports. However, the proportion of mixed infections has shown a downward trend, and the double infection rate is 10.63% currently. Furthermore, some changes have taken place in the types of mixed infections that are observed. For example, there was a high proportion of mixed infections with PPV, especially double mixed infections with PCV (2.08%). This might be attributed to the situation that when the market for pig industry flourished, the prevention of PPV in numerous gilts was not systematic, and production was carried out without necessary and sufficient immunization. Compared with the reports in Shandong and Hebei provinces, PEDV also showed a notably lower rate of mixed infections (0.96%), revealing the drastically declining incidence of diarrhea under the influence of the industry's general emphasis on biosafety.

4.6. Sequential evolution of PCV2 in eight provinces of China

In addition, in the present study, the positive samples were sequenced and analyzed to elucidate the prevalence of PCV2 strains in some regions in China. In this study, the homology was 95.36 to 100% between the 24 isolates and 95.46 to 99.98% between the isolates and the foreign reference strains. Therefore, the overall variation range in this study was small, which was inconsistent with the published literature (Park et al., 2013). The results of gene clustering showed that nine strains belonged to PCV2a, seven strains belonged to PCV2b, two strains belonged to PCV2c, and six strains belonged to PCV2d. However, PCV2e was not detected at all in the study, although it has been detected in lung samples in pigs in Guangdong and Jiangxi (Liu et al., 2018; Xu et al., 2022) Overall, the circovirus epidemic gene clusters varied between the provinces, showing regional characteristics, which might be correlated with the provenance and breeding environment in the different provinces, as well as improvements in biosafety systems. Due to the presence of African swine fever, the interaction between pigs among different provinces has declined, and closed-loop production has been emphasized.

A note of caution should be made that PCV2c appeared in Hunan and Heilongjiang provinces which had not been documented previously. The pigs testing positive for PCV2c were all Danish pigs, suggesting that PCV2c may have been introduced *via* importation into China since the prevalence of PCV2c has been reported in Europe for a long time (Xiao et al., 2015). These conditions make the prevention and control of circovirus more complex.

According to previous reports, there have been many PCV2 genotypes in China, with PCV2a, PCV2b, and PCV2d as the predominant genotypes (Guo et al., 2010; Zhao et al., 2010; Wei et al., 2012; Huang et al., 2021). However, the new gene cluster PCV2c must be noted by the industry. Variations in the PCV2 Cap protein allow for changes in viral immunogenicity and cell tropism, leading to variations in virulence. The analysis of the amino acid sequences of Cap revealed several amino acid variations in the Cap protein. Based on epidemiological investigations, four gene clusters, PCV2a, PCV2b, PCV2c, and PCV2d (Xiao et al., 2015; Franzo et al., 2016), were detected *as per*

the gene-specific locus standard (Wei et al., 2013; Wu et al., 2019), with loci 86 to 91 as the specific sequence loci for Cap protein typing: TNKISI in PCV2a, SNPRSV in PCV2b, EGAQTP in PCV2c, and SLPNTV in PCV2d. PCV2e was not detected, which was inconsistent with the results presented in other studies (Liu et al., 2018; Tsai et al., 2019; Kang et al., 2022).

In addition, the molecular epidemiological investigation showed that new amino acid mutations were detected. For instance, the loci 70(D), 73(R), and 178(N) in PCV2a were separately replaced by G (2)/L(1)/T(1), N(3)/*F*(2), and R(2), which was different from the mutations of 73(R) to (L) and 178(N) to S(1) reported by Wei et al. (2013). In PCV2b, 57(I) and 210(E) served as specific loci in addition to the basic specific loci 86–91 (Wei et al., 2013). This study showed that 178(N) mutated to R(4), which was inconsistent with the mutation of 178(N) to D(1) described in another report (Wen-fang et al., 2020), and there were no mutations at these two amino acid positions.

The locus 70(D) of PCV2c was deleted in the sequences of the two strains isolated in this study, which has not been reported in other studies (Xiao et al., 2015; Franzo et al., 2016; Liu et al., 2016). In PCV2d, besides the above-mentioned specific loci, 53(I), 68(N), 215(I), and 234(K) also acted as specific loci (Wen-fang et al., 2020), and these amino acid positions were not mutated. Moreover, the amino acid mutations in PCV2a, PCV2b, PCV2c, and PCV2d, shown in Table 4, have not been reported in the literature as being related to PCV2. Notably, the unique glycosylation locus 143–145 (NYS) of the Cap protein experienced point mutations at 145 (S) in this study. Mutations were observed in the amino acid sequences in some of the strains, which are possibly implicated in virulence differences between the different strains. These results had not been reported in the relevant PCV2 literature prior to the onset of African swine fever, possibly implying that PCV2 exhibits more variability after the onset of African swine fever. The above amino acid loci were highly variable, allowing the amino acids to change from hydrophobic to hydrophilic, with the potential to cause changes in the antigenicity of the PCV strains. Furthermore, whether the variation of these antigens is correlated with the enhanced ability of PCV2 to break through the meningeal barrier, thus inducing viremia as well as the emergence of novel gene cluster PCV2c, needs to be investigated and validated in future research.

5. Conclusion

Two reasons may explain the increase of porcine circovirus disease in China. First, the prevention and control measures of PCV are weakened due to the prevention and control of African swine fever. Second, the biosafety facilities in some pig farms are backward due to the different geographical location and economic development. In addition, we found that PCV2a, pcv2b, PCV2c, and PCV2d are still prevalent in Hubei, Hunan, Henan, Jiangxi, Shanxi, Guangdong, Hainan, and Heilongjiang provinces of China, and can be transmitted both horizontally and vertically.

Data availability statement

The original contributions presented in the study are included in the article/supplementary material, further inquiries can be directed to the corresponding authors.

Author contributions

CL, GL, and KT provided conceptualization, methodology, writing, reviewing, and editing. XT, CL, and YW provided investigation and data analysis. JY and TL provided methodology and investigation. KT and TL provided visualization. GL and LG provided project administration and manuscript checking. XY and JZ provided supervision and visualization. All authors contributed to the manuscript and approved the submitted version.

Funding

This research was funded by the Cooperative Innovation Center for Sustainable Pig Production of Huazhong Agricultural University and the National Natural Science Foundation of China, Grant No. 31602099, and Hubei GONGFU Farming Co. Ltd., Grant No. 34120015.

Acknowledgments

The authors would like to thank EditSprings (https://www.editsprings.cn/) for the expert linguistic services provided.

Conflict of interest

The authors declare that the research was conducted in the absence of any commercial or financial relationships that could be construed as a potential conflict of interest.

Publisher's note

Supplementary material

The Supplementary material for this article can be found online at: https://www.frontiersin.org/articles/10.3389/fmicb.2022.1013617/full#supplementary-material

References

Allan, G. M., McNeilly, E., Kennedy, S., Meehan, B., Moffett, D., Malone, F., et al. (2000). PCV-2-associated PDNS in Northern Ireland in 1990. Porcine dermatitis and nephropathy syndrome. *Vet. Rec.* 146, 711–712. PMID: 10887989

Cao, F., Luan, X., Wang, W., Li, Y., and Li, J. (2021). Establishment and application of dual TaqMan fluorescence quantitative polymerase chain reaction (PCR) for the detection of porcine Circovirus types 2 and 3. Research Square[Preprint]. Available at: https://doi.org/10.21203/rs.3.rs-319924/v1 (Accessed March 18, 2021).

Correa-Fiz, F., Franzo, G., Llorens, A., Huerta, E., Sibila, M., Kekarainen, T., et al. (2020). Porcine circovirus 2 (PCV2) population study in experimentally infected pigs developing PCV2-systemic disease or a subclinical infection. *Sci. Rep.* 10:17747. doi: 10.1038/s41598-020-74627-3

Dissertations, D. M. J., and Gradworks, T. (2009). Vertical transmission of porcine circovirus type 2 in breeding herds. [master's thesis]. [Ames (IA)]: University of ChicagoIowa State University.

Fang, Q., Ji, C., Feng, Y., Qin, Y., Dong, Q., Wu, G., et al. (2019). Prevalence and genetic characterization of porcine Circovirus type 3 in Guangxi Province from 2009 to 2017. *Pak. Vet. J.* 39, 459–462. doi: 10.29261/pakvetj/2019.008

Franzo, G., Cortey, M., Segales, J., Hughes, J., and Drigo, M. (2016). Phylodynamic analysis of porcine circovirus type 2 reveals global waves of emerging genotypes and the circulation of recombinant forms. *Mol. Phylogenet. Evol.* 100, 269–280. doi: 10.1016/j.ympev.2016.04.028

Fu, X., Fang, B., Ma, J., Liu, Y., Bu, D., Zhou, P., et al. (2018). Insights into the epidemic characteristics and evolutionary history of the novel porcine circovirus type 3 in southern China. *Transbound. Emerg. Dis.* 65, e296–e303. doi: 10.1111/tbed.12752

Gava, D., Zanella, E. L., Morés, N., and Ciacci-Zanella, J. R. (2008). Transmission of porcine circovirus 2 (PCV2) by semen and viral distribution in different piglet tissues. *Pesquisa Veterinária Brasileira* 28, 70–76. doi: 10.1590/s0100-736x2008000100011

Ge, S., Li, J., Fan, X., Liu, F., Li, L., Wang, Q., et al. (2018). Molecular characterization of African swine fever virus, China, 2018. *Emerg. Infect. Dis.* 24, 2131–2133. doi: 10.3201/eid2411.181274

Gerber, P. F., Garrocho, F. M., Lana, A. M. Q., and Lobato, Z. I. P. (2011). Serum antibodies and shedding of infectious porcine circovirus 2 into colostrum and milk of vaccinated and unvaccinated naturally infected sows. *Vet. J.* 188, 240–242. doi: 10.1016/j.tvjl.2010.03.023

Grasland, B., Blanchard, P., Jan, B., and Oger, A. (2008). *Transmission of porcine circovirus of type 2 (PCV2) with semen*. Congress of the International Pig Veterinary Society.

Guo, Z., Li, X., Deng, R., and Zhang, G. (2019). Detection and genetic characteristics of porcine circovirus 3 based on oral fluids from asymptomatic pigs in Central China. *BMC Vet. Res.* 15:200. doi: 10.1186/s12917-019-1952-3

Guo, L. J., Lu, Y. H., Wei, Y. W., Huang, L. P., and Liu, C. M. (2010). Porcine circovirus type 2 (PCV2): genetic variation and newly emerging genotypes in China. *Virol. J.* 7:273. doi: 10.1186/1743-422x-7-273

Ha, Z., Xie, C.-Z., Li, J.-F., Wen, S.-B., Zhang, K.-L., Nan, F.-L., et al. (2018). Molecular detection and genomic characterization of porcine circovirus 3 in pigs from Northeast China. *BMC Vet. Res.* 14:321. doi: 10.1186/s12917-018-1634-6

Huang, Y., Chen, X., Long, Y., Yang, L., Song, W., Liu, J., et al. (2021). Epidemiological analysis from 2018 to 2020 in China and prevention strategy of porcine Circovirus type 2. *Front. Vet. Sci.* 8:753297. doi: 10.3389/fvets.2021.753297

Jung, K., Kim, J., Ha, Y., Choi, C., and Chae, C. (2006). The effects of transplacental porcine circovirus type 2 infection on porcine epidemic diarrhoea virus-induced enteritis in preweaning piglets. *Vet. J.* 171, 445–450. doi: 10.1016/j.tvjl.2005.02.016

Kang, L., Wahaab, A., Shi, K., Mustafa, B. E., Zhang, Y., Zhang, J., et al. (2022). Molecular epidemic characteristics and genetic evolution of porcine Circovirus type 2 (PCV2) in swine herds of Shanghai, China. *Viruses-Basel* 14:289. doi: 10.3390/v14020289

Kleymann, A., Soto, E., Illanes, O., Malik, Y. S., Fuentealba, C., and Ghosh, S. (2020). High rates of detection and complete genomic analysis of porcine circovirus 2 (PCV2) in the Lesser Antilles island of St. Kitts: identification of PCV2b-PCV2d recombinants. *Transbound. Emerg. Dis.* 67, 2282–2289. doi: 10.1111/tbed.13583

Li, X., Qiao, M., Sun, M., and Tian, K. (2018). A duplex real-time PCR assay for the simultaneous detection of porcine Circovirus 2 and Circovirus 3. *Virol. Sin.* 33, 181–186. doi: 10.1007/s12250-018-0025-2

Lim, K., Lee, H.-J., and Yang, S. (2011). A study on the tourism resources and contents of Hainan Island in China. *J. Assoc. Korean Photo Geogr.* 21, 1–11. doi: 10.35149/jakpg.2011.21.4.001

Liu, G. P., Jiang, Y. H., Opriessnig, T., Gu, K. D., Zhang, H. L., and Yang, Z. Q. (2019). Detection and differentiation of five diarrhea related pig viruses utilizing a multiplex PCR assay. *J. Virol. Methods* 263, 32–37. doi: 10.1016/j.jviromet.2018.10.009

Liu, X., Wang, F.-X., Zhu, H.-W., Sun, N., and Wu, H. (2016). Phylogenetic analysis of porcine circovirus type 2 (PCV2) isolates from China with high homology to PCV2c. *Arch. Virol.* 161, 1591–1599. doi: 10.1007/s00705-016-2823-x

Liu, J., Wei, C., Dai, A., Lin, Z., Fan, K., Fan, J., et al. (2018). Detection of PCV2e strains in Southeast China. *Peerj* 6:e4476. doi: 10.7717/peerj.4476

Lopez-Lorenzo, G., Lopez-Novo, C., Prieto, A., Diaz, P., Panadero, R., Rodriguez-Vega, V., et al. (2021). Monitoring of porcine circovirus type 2 infection through air and surface samples in vaccinated and unvaccinated fattening farms. *Transbound. Emerg. Dis.* 69, 1108–1117. doi: 10.1111/tbed.14069

Magar, R., Muller, P., and Larochelle, R. (2000). Retrospective serological survey of antibodies to porcine circovirus type 1 and type 2. *Can. J. Vet. Res.* 64, 184–186. PMID: 10935885

Mikami, O., Nakajima, H., Kawashima, K., Yoshii, M., and Nakajima, Y. (2005). Nonsuppurative myocarditis caused by porcine circovirus type 2 in a weak-born piglet. *J. Vet. Med. Sci.* 67, 735–738. doi: 10.1292/jvms.67.735

Opriessnig, T., and Langohr, I. (2013). Current state of knowledge on porcine Circovirus type 2-associated lesions. *Vet. Pathol.* 50, 23–38. doi: 10.1177/0300985812450726

Opriessnig, T., Madson, D. M., Schalk, S., Brockmeier, S., Shen, H. G., Beach, N. M., et al. (2011). Porcine circovirus type 2 (PCV2) vaccination is effective in reducing disease and PCV2 shedding in semen of boars concurrently infected with PCV2 and mycoplasma hyopneumoniae. 76, 351–360. doi: 10.1016/j.theriogenology.2011.02.014,

Opriessnig, T., Meng, X.-J., and Halbur, P. G. (2007). Porcine circovirus type 2 associated disease: update on current terminology, clinical manifestations, pathogenesis, diagnosis, and intervention strategies. *J. Vet. Diagn. Invest.* 19, 591–615. doi: 10.1177/104063870701900601

Palinski, R., Pineyro, P., Shang, P., Yuan, F., Guo, R., Fang, Y., et al. (2017). A novel porcine Circovirus distantly related to known Circoviruses is associated with porcine dermatitis and nephropathy syndrome and reproductive failure. *J. Virol.* 91, 01879–01816. doi: 10.1128/jvi.01879-16

Park, C., Oh, Y., Seo, H. W., Han, K., and Chae, C. (2013). Comparative effects of vaccination against porcine Circovirus type 2 (PCV2) and porcine reproductive and respiratory syndrome virus (PRRSV) in a PCV2-PRRSV challenge model. *Clin. Vaccine Immunol.* 20, 369–376. doi: 10.1128/CVI.00497-12

Patterson, A. R., and Opriessnig, T. (2010). Epidemiology and horizontal transmission of porcine circovirus type 2 (PCV2). *Anim. Health Res. Rev.* 11, 217–234. doi: 10.1017/s1466252310000162

Rose, N., Opriessnig, T., Grasland, B., and Jestin, A. (2012). Epidemiology and transmission of porcine circovirus type 2 (PCV2). *Virus Res.* 164, 78–89. doi: 10.1016/j.virusres.2011.12.002

Sanchez, R. E., Nauwynck, H. J., McNeilly, F., Allan, G. M., and Pensaert, M. B. (2001). Porcine circovirus 2 infection in swine foetuses inoculated at different stages of gestation. *Vet. Microbiol.* 83, 169–176. doi: 10.1016/s0378-1135(01)00425-4

Segales, J., Calsamiglia, M., Olvera, A., Sibila, M., Badiella, L., and Domingo, M. (2005). Quantification of porcine circovirus type 2 (PCV2) DNA in serum and tonsillar, nasal, tracheo-bronchial, urinary and faecal swabs of pigs with and without postweaning multisystemic wasting syndrome (PMWS). *Vet. Microbiol.* 111, 223–229. doi: 10.1016/j.vetmic.2005.10.008

Shi, R., Hou, L., and Liu, J. (2021). Host immune response to infection with porcine circoviruses. *Anim. Dis.* 1:10. doi: 10.1186/s44149-021-00027-3

Shuai, J., Wei, W., Li, X., Chen, N., Zhang, Z., Chen, X., et al. (2007). Genetic characterization of porcine circovirus type 2 (PCV2) from pigs in high-seroprevalence areas in southeastern China. *Virus Genes* 35, 619–627. doi: 10.1007/s11262-007-0121-0

Tischer, I., Gelderblom, H., Vettermann, W., and Koch, M. A. (1982). A very small porcine virus with circular single-stranded DNA. *Nature* 295, 64–66. doi: 10.1038/295064a0

Trottier, M., Schlitt, B. P., and Lipton, H. L. (2002). Enhanced detection of Theiler's virus RNA copy equivalents in the mouse central nervous system by real-time RT-PCR. *J. Virol. Methods* 103, 89–99. doi: 10.1016/s0166-0934(02)00021-6

Trudeau, M. P., Verma, H., Urriola, P. E., Sampedro, F., Shurson, G. C., and Goyal, S. M. (2017). Survival of porcine epidemic diarrhea virus (PEDV) in thermally treated feed ingredients and on surfaces. *Porcine Health Manag.* 3:17. doi: 10.1186/s40813-017-0064-3

Tsai, G.-T., Lin, Y.-C., Lin, W.-H., Lin, J.-H., Chiou, M.-T., Liu, H.-F., et al. (2019). Phylogeographic and genetic characterization of porcine circovirus type 2 in Taiwan from 2001-2017. *Sci. Rep.* 9:10782. doi: 10.1038/s41598-019-47209-1

Tummaruk, P., and Pearodwong, P. (2016). Porcine circovirus type 2 expression in the brain of neonatal piglets with congenital tremor. *Comp. Clin. Pathol.* 25, 727–732. doi: 10.1007/s00580-016-2256-7

Tzika, E. D. (2017). Update on syndromes and clinical problems associated with porcine circovirus type 2 infection. 56, 256–268. doi: 10.12681/JHVMS.15086

Wang, F., Guo, X., Ge, X., Wang, Z., Chen, Y., Cha, Z., et al. (2009). Genetic variation analysis of Chinese strains of porcine circovirus type 2. *Virus Res.* 145, 151–156. doi: 10.1016/j.virusres.2009.05.015

Wei, W.-K., Zhai, S.-L., Chen, S.-N., Zhang, J.-W., Wei, Z.-Z., Long, J.-X., et al. (2012). Dissection of the possible routes on porcine Circoviruses infecting human. *J. Anim. Vet. Adv.* 11, 1281–1286. doi: 10.3923/javaa.2012.1281.1286

Wei, C., Zhang, M., Chen, Y., Xie, J., Huang, Z., Zhu, W., et al. (2013). Genetic evolution and phylogenetic analysis of porcine circovirus type 2 infections in southern China from 2011 to 2012. *Infect. Genet. Evol.* 17, 87–92. doi: 10.1016/j.meegid.2013.03.041

Wen, S., Sun, W., Li, Z., Zhuang, X., Zhao, G., Xie, C., et al. (2018). The detection of porcine circovirus 3 in Guangxi. *China. Trans. Emerg. Dis.* 65, 27–31. doi: 10.1111/tbed.12754

Wen-fang, D., Wen-bo, S., Xing-xing, H., Shuang, J., Xiang-hong, C., Hong-yan, Y., et al. (2020). Molecular epidemiological analysis of porcine CIRCOVIRUS virus type 2 in Central China during 2017-2018. *Chin. J.f Anim. Infect. Dis.* 28, 32–38. Available at: https://kns.cnki.net/kcms/detail/31.2031.s.20190109.1640.030.html

Wu, M., Jiang, Y., Ao, C., Yu, X., Ku, X., Chen, F., et al. (2019). Epidemiological Investi gation and genetic variation analysisis of PCV2 in Jinhua, Zhe jiang. *Chin. J. Vet.* 39, 1890–1896. doi: 10.16303/j.cnki.1005-4545.2019.10.02

Xiao, C.-T., Halbur, P. G., and Opriessnig, T. (2015). Global molecular genetic analysis of porcine circovirus type 2 (PCV2) sequences confirms the presence of four main PCV2 genotypes and reveals a rapid increase of PCV2d. *J. Gen. Virol.* 96, 1830–1841. doi: 10.1099/vir.0.000100

Xu, Q., Zhang, Y., Sun, W., Chen, H., Zhu, D., Lu, C., et al. (2022). Epidemiology and genetic diversity of PCV2 reveals that PCV2e is an emerging genotype in Southern China: a preliminary study. *Viruses* 14:724. doi: 10.3390/v14040724

Yang, G., Yan, Y. L., Zhang, L., Ruan, Z., Hu, X. Q., Zhang, S., et al. (2020). Porcine circovirus type 2 (PCV2) and campylobacter infection induce diarrhea in piglets: microbial dysbiosis and intestinal disorder. *Anim. Nutrit.* 6, 362–371. doi: 10.1016/j.aninu.2020.05.003

Zhao, G. H., Cheng, W., Zhang, P. J., Han, Y. S., and Chen, D. K. (2010). Novel genotypes of type 2 porcine Circovirus (PCV2) in PMWS pigs in China between 2008 and 2009. *J. Anim. Vet. Adv.* 9, 3083–3091. doi: 10.3923/javaa.2010.3083.3091

Frontiers in Microbiology

Explores the habitable world and the potential of microbial life

The largest and most cited microbiology journal which advances our understanding of the role microbes play in addressing global challenges such as healthcare, food security, and climate change.

Discover the latest Research Topics

See more →

Frontiers

Avenue du Tribunal-Fédéral 34
1005 Lausanne, Switzerland
frontiersin.org

Contact us

+41 (0)21 510 17 00
frontiersin.org/about/contact